BONE DIAGENESIS: THE MYSTERIES OF THE PETROUS PYRAMID

IOANNIS KONTOPOULOS

PhD

UNIVERSITY OF YORK
ARCHAEOLOGY
DECEMBER 2018

‘What the caterpillar calls the end of the world, the master calls a butterfly’

Richard Bach, 1977

ABSTRACT

The discovery of petrous bone as an excellent repository for ancient biomolecules has been a turning point in biomolecular archaeology, especially in the recovery of ancient genomes. Although the information extracted by the biochemical analyses of petrous bone can be valuable, the processes are destructive, expensive and time-consuming, while excessive and uncontrolled sampling could result in loss of this valuable resource for future research.

This study reports on the histological (optical microscopy), physical (FTIR-ATR), elemental (CN), biomechanical (nanoindentation) and biochemical (collagen and DNA analysis) preservation of 272 bones spanning from c. 10.000 BC to c. 1850 AD, including 108 petrous bones. Through the combined application of a number of diagenetic parameters (general histological index; infrared splitting factor; carbonate/phosphate ratio; amide/phosphate ratio; col wt. %; % C, % N and C/N of whole bone and collagen; hardness, elastic modulus, % endogenous DNA), new insights into petrous bone micromorphological and diagenetic characteristics, inter-site, intra-site, intra-individual and intra-bone diagenetic variability, and new evidence to enhance successful screening of archaeological bone prior to aDNA and collagen analysis is presented.

Specifically, the petrous bone microstructure consists of highly osteocytic woven and lamellar-like tissues, and osteons occur in at least two directions (transverse and longitudinal). Despite its stunning micromorphological characteristics, the biomechanical properties and diagenetic characteristics of petrous bone do not differ significantly from those of long bones. Inter-site and intra-site diagenetic variability is mostly affected by the site hydrology, while different types of burials can influence the microenvironment conditions and leave distinctive marks on bone histology. No intra-individual patterns, which could also favour the gut origin of microbial attack in bone, or intra-bone variability are observed in any of the diagenetic parameters. Screening archaeological bone for collagen preservation can be enhanced using the % C of whole bone which is equally strong as % N of whole bone collagen predictor, while the IRSF (< 3.7) and C/P (> 0.15) indices can distinguish bones containing >1 % endogenous DNA with a success rate of c. 85 % as bioapatite preservation is associated with loss of DNA.

CONTENTS

LIST OF TABLES

Appendix A

LIST OF FIGURES

Chapter 2 – Bone biology

Chapter 3 - Bone diagenesis: A review of current research

Chapter 4 – Materials and Methods

Chapter 5 – Results and Discussion

Appendix B

ACKNOWLEDGEMENTS

My PhD has been an amazing journey and I gratefully acknowledge the funding received from Onassis Foundation, Leventis Foundation and the Greek Archaeological Committee UK (GACUK) that made it much easier and pleasant. I am grateful to my supervisors Professor Matthew Collins and Dr. Kirsty Penkman for guidance and support throughout. Particularly, I would like to express my sincere gratitude to Matthew for his enthusiasm, motivation, and advice on research as well as on my career, and for helping me to grow as a research scientist. Not to mention the new BioArCh 'toys'. I am also grateful to Kirsty for her detailed and constant feedback, insightful comments and criticism, punctuality and encouragement. A very big thank you to both does not do it justice.

Besides my supervisors, I would like to thank the rest of my thesis advisory panel (TAP), Dr. Kevin Walsh and Dr. Michelle Alexander for their helpful suggestions and advice. My sincere thanks also go to all our collaborators. Particularly, I thank Prof. Dan Bradley (Trinity College Dublin), Prof. Joachim Burger (University of Mainz), Dr. Morten Allentoft (University of Copenhagen), Dr. Christina Papageorgopoulou (Democritus University of Thrace), Dr. Martina Unterländer, Dr. Amelie Scheu, Dr. Victoria Mullin, Laura Winkelbach and Henrik Hansen for providing the genetic data. Further, I am indebted to the archaeologists, biological anthropologists, curators and relevant authorities that granted access to sample collections. Specifically, I thank Prof. Adamantios Sampson (University of the Aegean), Prof. Ioannis Liritzis (University of the Aegean), Dr. Elena Kranioti (University of Edinburgh), Dr. Chaido Koukouli-Chrysanthaki (Serres Ephorate of Antiquities), Dr. Georgios Kazantzis, Dr. Marilena Chovalopoulou, Andreas Bertsatos, the Ephorate of Palaeoanthropology and Speleology (Greece), the Ephorates of Antiquities in Boeotia and Serres (Greece), the Greek Ministry of Culture and Sports, Prof. Niels Lynnerup (University of Copenhagen) and the Danish National Museum, Dr. Anita Radini, Prof. Jacqui Mulville (Cardiff University), Dr. Ingrid Mainland (University of the Highlands and Islands), Dr. David Allen, Dr. Katrien Van de Vijver, Bart Robberechts, and the Archaeology department of the city council of Mechelen (Belgium) for giving us access to the material used in this study.

I am also grateful to Dr. Graeme McAllister (University of York) for the elemental analysis, Dr. Henrik Birkendal (Aarhus University) for the 3D reconstruction of the synchrotron micro-CT images, and Prof. Peter Zioupos (Cranfield University) for nanoindentation and the two modern human samples (NHS REC approval 10/H0107/14) which were used as references with the kind permission of the Department of Biology Ethics Committee (BEC) of the University of York. I also thank my fellow BioArCh mates for all the moments and fun we have had throughout these years. Of course, I could not forget the fantastic BioArCh lab manager, Matthew Von Tersch, for his precious help and funny moments in the lab.

Words can not express how grateful I am to my mother and father for all the support and sacrifices they have made all these years. At last, I do not know how to thank Kelly enough for constantly enlightening and adding colour to my life, and for giving me so much happiness with the arrival of our little baby boy Ektoras!

DECLARATION

I declare that this thesis is a presentation of original work and I am the sole author. This work has not previously been presented for an award at this, or any other, University. All sources are acknowledged as References. This thesis is the original work of the author.

Aspects of this thesis have been published or under review:

- Kendall C., Eriksen A. M., Kontopoulos I., Collins M. J., and Turner-Walker G. (2018). Diagenesis of archaeological bone and tooth. *Palaeogeography, palaeoclimatology, palaeoecology*, 491, pp.21–37. [Online]. Available at: doi:10.1016/j.palaeo.2017.11.041.
- Kontopoulos I., Presslee S., Penkman K., and Collins M.J. (2018). Preparation of bone powder for FTIR-ATR analysis: The particle size effect. *Vibrational spectroscopy*, 99, pp.167–177. [Online]. Available at: doi:10.1016/j.vibspec.2018.09.004.
- Kontopoulos, I., Penkman, K., McAllister, G. D., Lynnerup, N., Damgaard, P. B., Hansen, H. B., Allentoft, M. E., and Collins, M. J. (2019). Petrous bone diagenesis: A multi-analytical approach. *Palaeogeography, palaeoclimatology, palaeoecology*. Special issue: Advances in the study of diagenesis of fossil and subfossil bones and teeth.
- Kontopoulos, I., Penkman, K., Liritzis, I., and Collins M. J. (under review). Bone diagenesis in a Mycenaean secondary burial (Kastrouli, Greece). *Archaeological and Anthropological Sciences*.

CHAPTER 1: INTRODUCTION

The information that can be extracted from the analysis of histology, bioapatite (BAp), collagen, and ancient DNA (aDNA) preserved within archaeological bone has shaped the way we interpret the past (e.g. Bentley 2006; Brown and Barnes 2015; Buckley et al. 2009; Cappellini et al. 2018; Colonese et al. 2015; Hendy et al. 2018; Katzenberg 2008; Lee-Thorp 2008; Orlando and Cooper 2014). Bone histology can be used for the study of the age-at-death, pathology and to distinguish between human and non-human or burned and unburned bone (e.g. Assis, Santos and Keenleyside 2016; Cattaneo et al. 1999; Cuijpers 2006; De Boer, Van der Merwe and Maat 2013; Dominguez and Crowder 2012; Hanson and Cain 2007; Mulhern and Ubelaker 2001; Stout and Teitelbaum 1976). Bioapatite is important in archaeological research for the study of past human and animal movement (phosphate), dietary habits (carbonate) and environments (phosphate and carbonate) (e.g. Hedges 2003; King, Tayles and Gordon 2011; Lee-Thorp and van der Merwe 1991; Wright and Schwarcz 1996). Bone collagen is used to determine chronological age (i.e. ^{14}C dating), past lifeways (e.g. palaeodietary reconstruction, weaning practices), taxonomic identification, and occasionally for screening (e.g. amino acid racemization) (e.g. Ambrose 1991; Asara et al. 2007; Buckley et al. 2009; Collins et al. 2009; DeNiro and Weiner 1988; Douka et al. 2017; Poinar et al. 1996; Van Klinken 1999), while aDNA can offer unique insights into the genetic change through time for the study of evolutionary and ecological processes (e.g. Orlando and Cooper 2014).

The post-mortem preservation of bone is affected by the complexity of diagenesis, a universal phenomenon controlled by the interplay between biological, chemical and physical processes (e.g. Kendall et al. 2018). The microbial attack of the composite, the chemical deterioration of the inorganic matter (dissolution/recrystallization), and the chemical and biological deterioration of the organic matter alter the microstructure and the biogenic chemical signals of bone post-mortem (Collins et al. 2002; Kendall et al. 2018). Microbial activity can modify bone microstructure (Bell 2012; Hackett 1981; Hedges, Millard and Pike 1995; Turner-Walker and Jans 2008) and in addition to the apparent modifications in bone histology, microbial attack can also enzymatically degrade collagen using collagenases. Temperature also has a profound effect on collagen degradation (Collins et al. 2002; Kendall et al. 2018 Fig.7). Any collagen preserved in archaeological bone can be protected by the bioapatite crystals (BAp) (Grupe 1995), however, post-mortem changes of the mineral phase can expose collagen to chemical hydrolysis (Collins et al. 2002; High et al. 2015).

Such a reorganization or growth of BAp crystals occurs through dissolution and recrystallization when the conditions of the burial environment are greatly under-saturated, primarily due to active

hydrology (recharging with fresh water) or pH (Berna, Matthews and Weiner 2004; Hedges 2002; Hedges and Millard 1995; High et al. 2015; Piepenbrink 1989) and it leads to a considerable loss of DNA (Allentoft et al. 2012; Götherström et al. 2002; Lindahl 1993; Parsons and Weedn 2006). Identifying the diagenetic pathway each bone has followed post-mortem can therefore offer a unique insight into the preservation potential of archaeological bone, in different burial environments and across timescales which are of great importance to archaeological, anthropological and forensic research.

The recent discovery that the petrous bone (a massive portion of the endocranial aspect of the temporal bone) is an excellent repository for long term DNA survival (Gamba et al. 2014; Hansen et al. 2017; Pinhasi et al. 2015) represents a major breakthrough in aDNA research, as the expense of genome sequencing can often be prohibitive due to the low abundance of endogenous DNA (e.g. Green et al. 2010). Collagen extracted from petrous bone has also been identified as a potential indicator of fetal and early years diet (Jørkov, Heinemeier and Lynnerup 2009), as ossification of the petrous pyramid is mainly completed *in utero* (Jeffery and Spoor 2004; Sørensen 1994; Richard et al. 2010). Similarly, through strontium isotope analysis, petrous bone can potentially provide information on the geographic area in which individuals had spent their childhood (Harvig et al. 2014), complementing strontium analyses of teeth. However, although the information extracted by the biochemical analyses of petrous bone can be valuable, the processes are destructive, expensive and time-consuming, while excessive and uncontrolled sampling could result in loss of this valuable resource for future research.

This thesis is the first study to present evidence on the micromorphological and diagenetic characteristics of archaeological petrous bone. This research project has three primary aims:

1. to understand to what extent petrous bone can constitute a reservoir of surviving biomolecules,
2. to provide new data for the successful screening of archaeological bone prior to collagen and DNA analyses, and
3. to provide a foundation for future investigations to further explore bone diagenesis.

To achieve this, the following objectives were undertaken:

1. Examination of the micromorphological characteristics of the petrous bone, as one of the least accessible areas of the skull and possibly densest part of the skeleton.
2. Comparison of the diagenetic characteristics of the petrous bone compared to other skeletal elements, in order to unveil if the petrous bone is the most effective skeletal element for sampling for collagen and DNA analyses.

3. Assessment of inter-site, intra-site, intra-individual and intra-bone variations to reveal the preservation potential of archaeological bone in different environments and micro-environment conditions.
4. Assessment of the relationship between different diagenetic parameters and the survival of collagen and DNA in archaeological bone, in order to identify reliable screening techniques for collagen and aDNA.

The thesis consists of six chapters and three appendices (tables, figures, and papers produced by this PhD research). **Chapter 2** provides the background information on bone biology from the micro- to the nano-level that is necessary for an understanding of bone diagenesis. A thorough synthesis of the different diagenetic pathways in which bone can be changed post-mortem, highlighting the research that has attempted to explain bone diagenetic processes using a range of analytical techniques is outlined in **Chapter 3**. Sections of this chapter have been published in Kendall C., Eriksen A. M., Kontopoulos I., Collins M. J., and Turner-Walker G. (2018). Diagenesis of archaeological bone and tooth. *Palaeogeography, palaeoclimatology, palaeoecology*, 491, pp.21–37. [Online]. Available at: doi:10.1016/j.palaeo.2017.11.041.

Chapter 4 provides some general information on the samples that were drawn from several geographic regions (Belgium, Britain, Central Asia, Denmark, Germany, Greece, Jordan) and a variety of depositional environments (coastal and inland open-air sites, caves) ranging from the Mesolithic (~10.000 BC) to post-medieval assemblages (1850 AD). The details on the techniques and methodological approaches applied in this study, and a practical guide to petrous bone sampling are also provided. This research employs analytical techniques which have been commonly used in past studies (histology, collagen analysis, elemental analysis, endogenous DNA content), new developments building upon existing knowledge (FTIR-ATR using a newly developed protocol by Kontopoulos I., Presslee S., Penkman K., and Collins M.J. (2018). Preparation of bone powder for FTIR-ATR analysis: The particle size effect. *Vibrational spectroscopy*, 99, pp.167–177), and novel approaches to bone diagenesis which can potentially provide useful additional data (2^{nd} derivative analysis of mid-IR spectra, nano-indentation, synchrotron micro-CT).

Chapter 5 builds on the work developed in this study and published in the following papers:

- Kontopoulos I., Presslee S., Penkman K., and Collins M.J. (2018). Preparation of bone powder for FTIR-ATR analysis: The particle size effect. *Vibrational spectroscopy*, 99, pp.167–177. [Online]. Available at: doi:10.1016/j.vibspec.2018.09.004.
- Kontopoulos, I., Penkman, K., McAllister, G. D., Lynnerup, N., Damgaard, P. B., Hansen, H. B., Allentoft, M. E., and Collins, M. J. (2019). Petrous bone diagenesis: A multi-analytical approach. *Palaeogeography, palaeoclimatology, palaeoecology*. Special issue: Advances in the study of diagenesis of fossil and subfossil bones and teeth.

- Kontopoulos, I., Penkman, K., Liritzis, I., and Collins M. J. (under review). Bone diagenesis in a Mycenaean secondary burial (Kastrouli, Greece). *Archaeological and Anthropological Sciences*.

It is divided into subsections that present the results and discuss the preservation of bone histology, bioapatite (BAp), collagen, and DNA in petrous versus other bones. New data on inter-site, intra-site, intra-individual, and intra-bone variability is also explored and put into context, while new screening methods for collagen and DNA are proposed. **Chapter 6** summarizes the key findings of this research project, with a focus on the petrous bone micromorphological and diagenetic characteristics, and the relationship between histological modifications, bioapatite recrystallization/dissolution, collagen degradation, and DNA decay. The limitations of the current techniques are highlighted and potential routes for future research are proposed.

CHAPTER 2: BONE BIOLOGY

Mammalian bone is a highly specialized, complex tissue with a hierarchical structure (**Figure 2.1**) and its function in all vertebrates is the mechanical support, locomotion, protection and activity as a metabolic reservoir. The formation of the skeleton initiates *in utero* via two different processes: a) endochondral and b) intramembranous ossification, while postnatally bone remodelling and resorption occur by the collective action of three main types of cells (osteoblasts, osteocytes, and osteoclasts).

Bone nanostructure contains both inorganic and organic components. The organic matter/osteoid (approximately 20-30 % by dry weight or 30-45 % by volume) is consisted of 90 % collagen (mainly type I collagen), while the remaining is type V collagen, trace amounts of collagen types II, III, XI, XIII, and non-collagenous proteins. The inorganic content (bioapatite crystals) covers approximately 60-70 % by dry weight or 30-45 % by volume, while the remaining is water, lipids and other complex macromolecules.

At the next hierarchical level (microstructure), the production of a collagen-bioapatite composite structure (biomineralization) results in two histological types of bone, the woven or immature and the lamellar or mature bone that display distinct structural motifs. Morphologically (i.e. macrostructure), bones exhibit two different types of tissue: a) cortical and b) cancellous, and are distinguished in long (e.g. humerus, femur), short (e.g. metacarpals), flat (e.g. scapula, parietal), and irregular (e.g. vertebrae) bones with different physical characteristics.

This chapter deals with bone formation and structural characteristics, with the sections being arranged accordingly, commencing with ossification processes and continuing with bone's hierarchical structure from the nano (collagen and bioapatite) to the macro (whole bone) level.

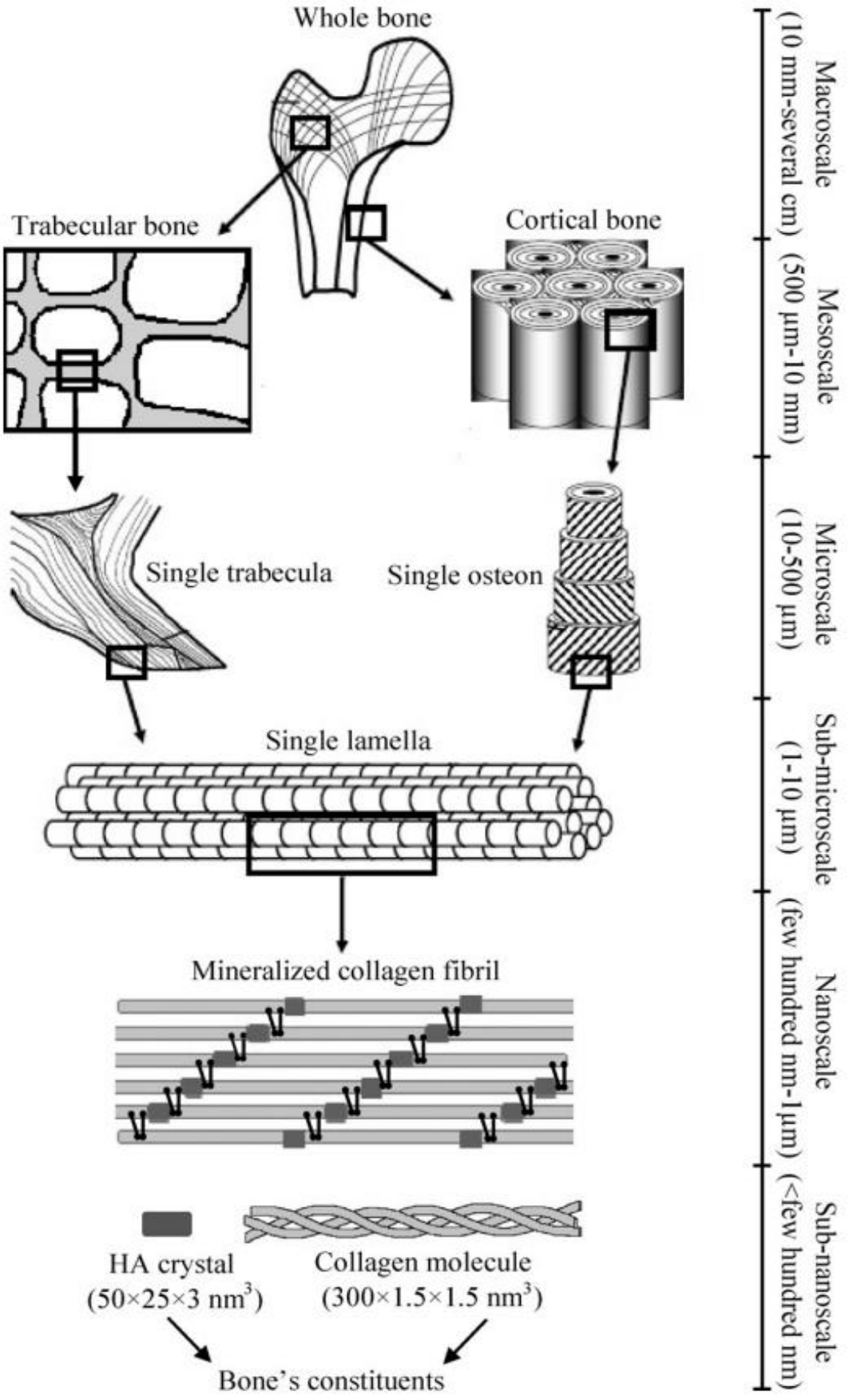

Figure 2.1. The hierarchical structure of bone from the nano- to the macro-scale (Hamed and Jasiuk 2012).

2.1.1. BONE CELLS

OSTEOBLASTS

Osteoblasts are the bone-forming cells that synthesize the organic components of the bone and contribute to the composition of the inorganic component during bone formation and remodelling (Ortner and Turner-Walker 2002; Ross and Pawlina 2011). They are mononuclear cells that differentiate from the osteoprogenitor cells which derive from the primitive mesenchymal stem cells (MSC) found in bone marrow (**Figure 2.2**; Ducy, Schinke and Karsenty 2000; Stevens and Lowe 2005). They are typical protein producing cells that secrete the osteoid, the initial unmineralized bone consisted of type I collagen embedded in a non-collagenous, calcium-binding gel (Ross and Pawlina 2011; Stevens and Lowe 2005). When fully active, osteoblasts are recognized by their cuboidal or polygonal shape (**Figure 2.2**) and they live for about 6 months (Ortner and Turner-Walker 2002; Ross and Pawlina 2011; Stevens and Lowe 2005). When active bone formation ceases, osteoblasts turn into bone lining cells (**Figure 2.2**) that enclose the bone surface and prevent bone resorption (Ortner and Turner-Walker 2002).

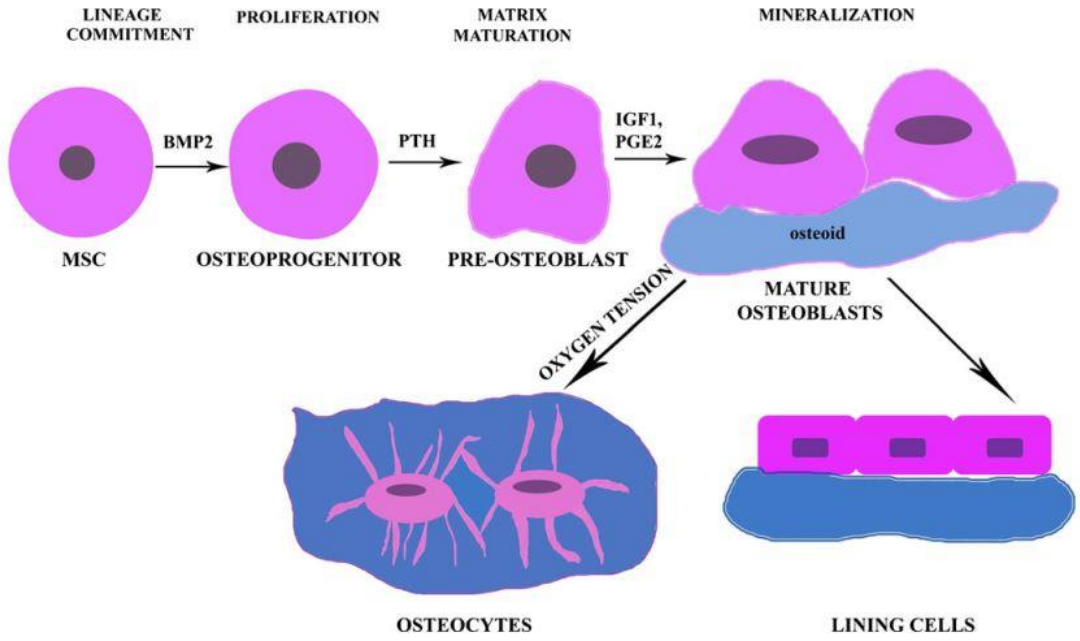

Figure 2.2. Osteoblast formation, maturation, and transformation into osteocytes and bone lining cells (Titorencu et al. 2014).

OSTEOCYTES

Osteocytes are inactive osteoblasts that have completed the producing of the osteoid (Stevens and Lowe 2005; White, Black and Folkens 2012). They are trapped within the mineralized matrix (**Figure 2.2**) and comprise about the 90% of bone cells (Ortner and Turner-Walker 2002). They are smaller than osteoblasts and they reside in oval shape depressions in the bone matrix called lacunae (**Figure 2.3**; Ortner and Turner-Walker 2002; Ross and Pawlina 2011). Their cytoplasmic

extensions travel through very fine channels called canaliculi that allow osteocytes to communicate with each other (**Figure 2.3**), with each osteocyte having around 50-70 such channels (Ortner and Turner-Walker 2002; Ross and Pawlina 2011). Canaliculi are generally aligned perpendicular to the lamellar boundary plane (Reznikov, Shahar and Weiner 2014a). Osteocytes are involved in the physiological activities of bone (e.g. mineralization/mineral control) and the secondary mineralization which is a much slower process than primary mineralization due to the smaller number of cells present in the tissue (Ortner and Turner-Walker 2002; Teti and Zallone 2009). Osteocytes also regulate the flow of calcium and phosphorus and can live for several years (Ortner and Turner-Walker 2002).

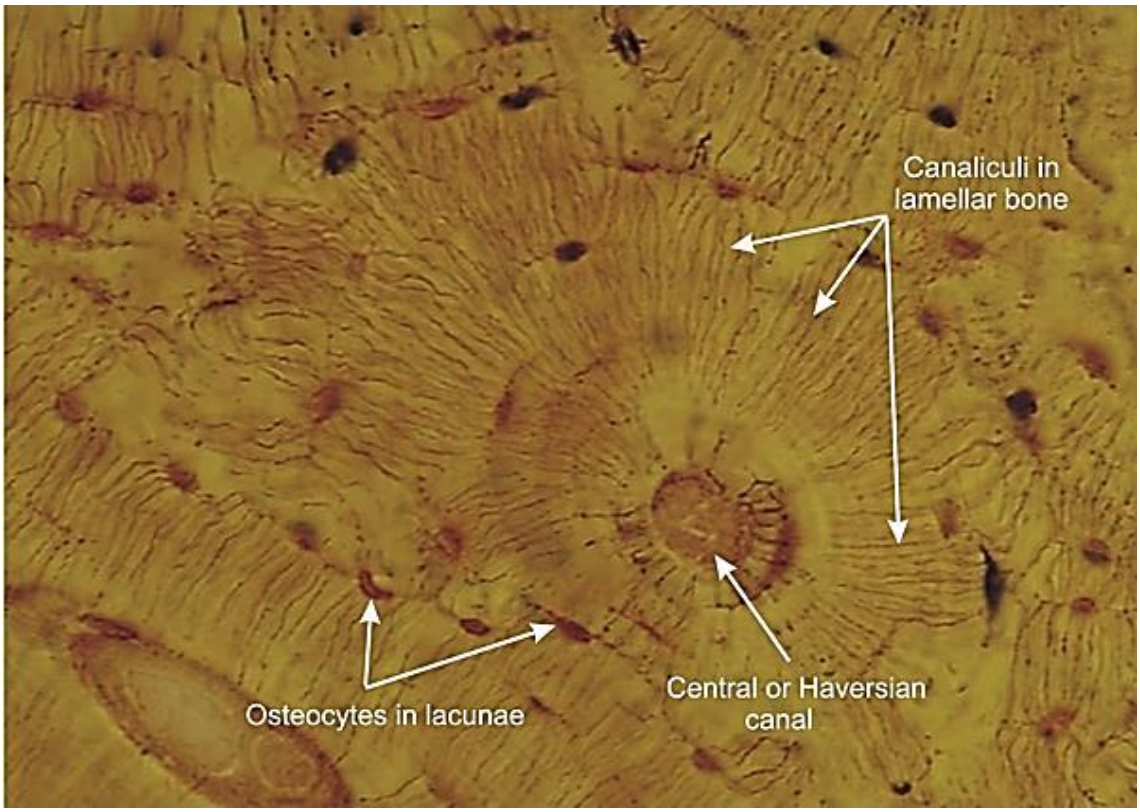

Figure 2.3. Osteocyte lacunae and canaliculi in human compact bone (magnification x1200) (Clermont, Lalli and Bencsath-Makkai 2013).

They have a flattened, almond-like appearance and their average size differs between species (e.g. in human cortical tissue is about 18.9 ± 4.9 μm in length, 9.2 ± 2.1 μm in width and 4.8 ± 1.1 μm in depth) (Ardizzoni 2001; Dong et al. 2014; Hannah et al. 2010; Noble 2008). The lacunar size and number decrease significantly towards the Haversian canal in osteons and with increasing age, while the lacunar shape and density can also vary within the same skeletal element (Ardizzoni 2001; Busse et al. 2010; Carter et al. 2013; Hannah et al. 2010). More specifically, in a study by Carter et al. (2013) the anterior and posterior regions exhibited a lower number and more elongated lacunae comparing to lateral and medial tissues in normal human femora (Carter et al. 2013). However, no volume or orientation related differences between the different regions have been identified (Carter et al. 2013).

OSTEOCLASTS

Osteoclasts are tissue-specific macrophage polykaryons that derive from the merging of blood-borne mononuclear macrophage precursors that derive from haematopoietic stem cells (**Figure 2.4**; Boyle, Simonet and Lacey 2003; Ortner and Turner-Walker 2002). They are very large, bone-resorbing cells, identified on surfaces when calcified bone tissue is being remodelled or removed (Ortner and Turner-Walker 2002). When osteoclast activity is triggered (e.g. receptor activator nuclear factor/RANK-induced signalling, hormonal control), osteoclasts often cluster together and create resorption cavities called Howship lacunae (Asagiri and Takayanagi 2007; Ortner and Turner-Walker 2002).

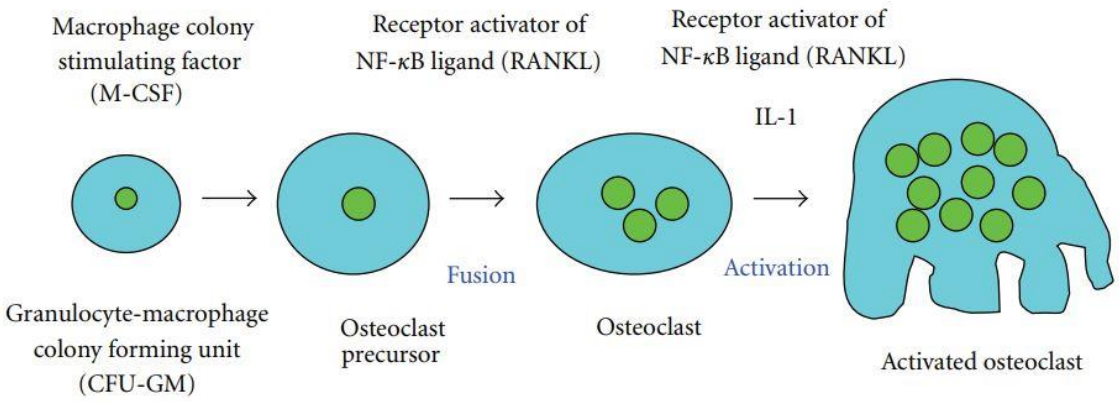

Figure 2.4. Osteoclast formation and activity (Senba, Kawai and Mori 2012).

Osteoclasts have developed a very efficient mechanism to dissolve bioapatite crystals and degrade the organic phase in bone (Väänänen et al. 2000). Bone resorption requires migration of the osteoclast to the site of interest, its attachment to bone, polarization and formation of new membrane domains, dissolution of bioapatite and degradation of organic matrix, removal of degradation products from the Howship lacunae, followed either by the apoptosis of the osteoclasts or their return to the non-resorbing stage (Asagiri and Takayanagi 2007; Väänänen et al. 2000).

2.1.2. OSSIFICATION

Ossification (osteogenesis or simply bone formation) is the process of formation of new bone by osteoblasts. Most bones in the human skeleton develop by endochondral ossification in which a cartilage that precedes bone is gradually ossified (Mackie et al. 2008; Ross and Pawlina 2011; Schwartz 2007). Bone formation occurs from primary and secondary ossification centres that transform cartilage into bone after osteoid secretion and mineralization (Mackie et al. 2008; Stevens and Lowe 2005). A hyaline cartilage is formed in the shape of the desired bone through condensation of mesenchymal cells (Schwartz 2007). Once formed, the mesenchymal cells differentiate into chondrocytes and after proliferation, round proliferating chondrocytes become

flattened, undergo hypertrophy (a dramatic increase in their volume accompanied by extracellular matrix secretion) and eventually die (apoptosis or autophagy) (**Figure 2.5**; Gerber and Ferrara 2000; Mackie et al. 2008).

Cartilage is gradually invaded first at its centre and later at its ends by a mixture of cells that establish the primary and secondary ossification centres, respectively (**Figure 2.5**; Kini and Nandeesh 2012; Mackie et al. 2008). It is progressively eroded by osteoclasts and bone is laid down by osteoblasts to replace the lost cartilage in the embryonic and foetal life (Scheuer and Black 2000). Endochondral ossification, thus, requires a temporal and spatial balance between extracellular matrix deposition and degradation, chondrocyte proliferation and apoptosis plus vascularisation and mineralisation. Disruption of any part of this chain can lead to a spectrum of skeletal defects that ranges from mild to lethal and from rare to common pathologies (e.g. osteogenesis imperfecta).

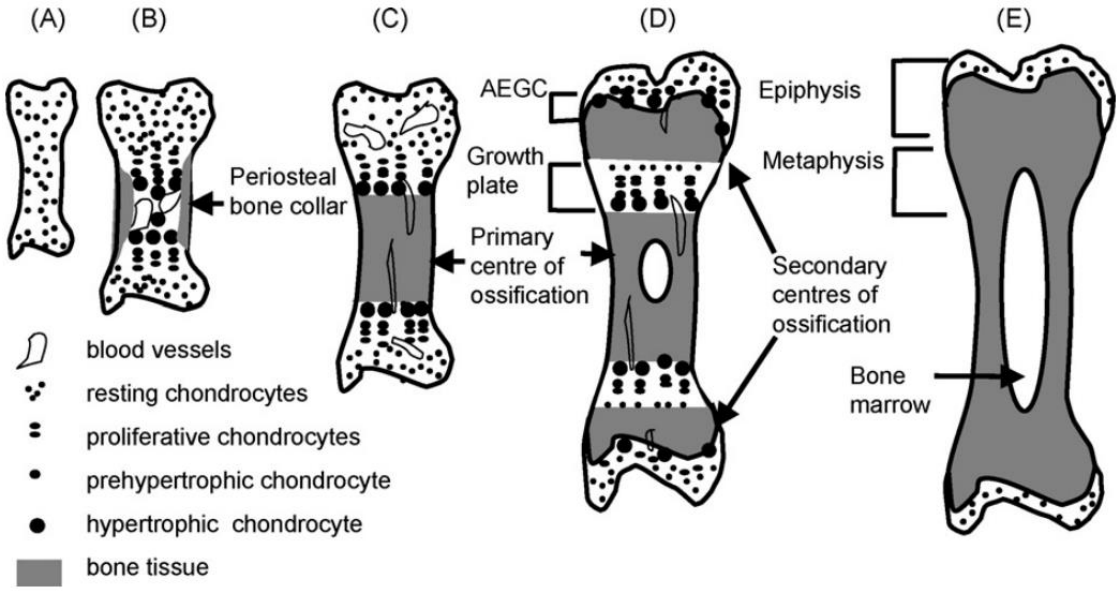

Figure 2.5. Endochondral ossification. Ossification initiates with a cartilage model (A) that ends with the fusion of the epiphyseal and metaphyseal bone in adult bone (E) (Mackie et al. 2008).

Intramembranous ossification occurs by apposition of tissues within an embryonic connective tissue membrane in the formation of the cranial vault, vertebrae, mandible and clavicle (Kini and Nandeesh 2012; Ross and Pawlina 2011; Stevens and Lowe 2005). Unlike endochondral ossification, bone tissue is directly laid down into the primitive connective tissue without any intermediate step (no cartilage present). During this process, the mesenchymal cells commence bone formation when they replicate and cluster together (Scheuer and Black 2000). After this phase, mesenchymal cells differentiate into osteoprogenitor cells which then turn into osteoblasts (Kini and Nandeesh 2012; Scheuer and Black 2000). Then the osteoblasts create an extracellular matrix which is later mineralized. The only difference between the two types of osteogenesis is

the environment in which the development occurs and not the type of tissue as the outcome is the same (Scheuer and Black 2000).

Bone is a dynamic tissue and it remodels in response to the mechanical demands placed upon it as well as hormonal factors (e.g. parathyroid hormone, leptin) (Ducy, Schinke and Karsenty 2000). Bone remodelling is, thus, the dynamic physiologic process by which bone mass is maintained constant throughout adult life in vertebrates (Ducy, Schinke and Karsenty 2000). It consists of two phases that occur simultaneously at multiple locations in the skeleton (**Figure 2.6**): a) resorption (i.e. osteoclast activity) and b) synthesis (i.e. osteoblast activity) of tissue that continue throughout life but at a much slower rate (Ducy, Schinke and Karsenty 2000; Ortner and Turner-Walker 2002). Thus, bone remodelling (or turnover) occurs on a continuous basis to replace dead cells or repair damaged cells associated with ageing, pathology, fracture, or to cope with increased physical activity (Ortner and Turner-Walker 2002). Nevertheless, while skeletal mass increases rapidly during the growth period, it decreases slowly throughout the rest of life. Therefore there is a reduction in the amount of cancellous bone and a decrease in the thickness of cortical bone which clearly affects bone's density, structure and subsequently, post-mortem survival.

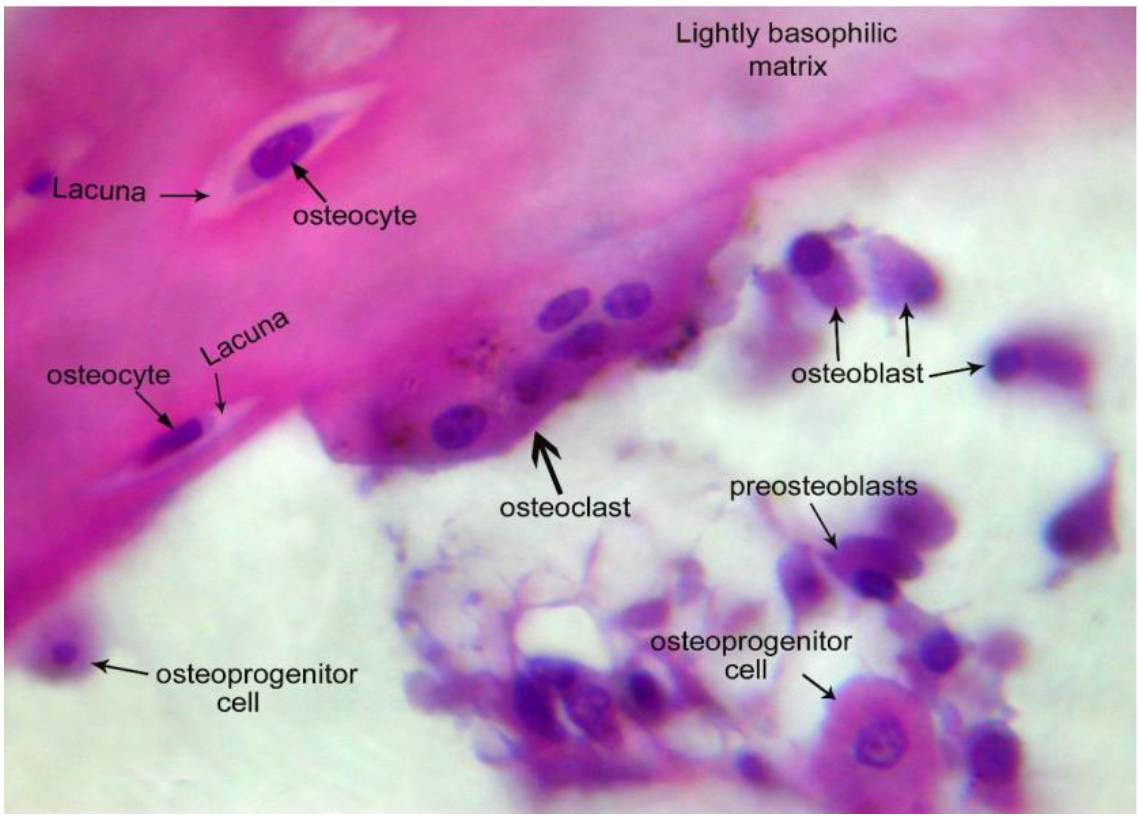

Figure 2.6. Histological section of bony trabeculae of adult male goat showing bone remodelling. The osteoprogenitor cells turn into pre-osteoblasts and these into osteoblasts. Osteoblasts trapped in bone matrix are now osteocytes residing in lacunae. Notice the simultaneous osteoclast activity at the surface of bone (Moussa and Nasr 2012).

2.2.1. NANOSTRUCTURE

ORGANIC COMPONENT

The collagen family (28 types) represents the most abundant proteins in bone extracellular matrix. The shape and mechanical properties of bone depend upon the collagen framework which is mainly (c. 90 %) constituted by type I collagen (Currey 2003; Gelse, Pöschl and Aigner 2003; Keene and Sakai 1991). Each collagen I molecule (tropocollagen) is characterized by a right-handed triple helix of three polypeptide α chains held together by hydrogen bonds and staggered by one residue relative to each other (Hofmann, Fietzek and Kühn 1978; Petruska and Hodge 1964). This triple helix consists of two identical α1(I) chains and one similar but genetically distinct α2(I) chain (polyproline II helices) that intertwine to form a trimeric coiled structure (**Figure 2.7**; Hofmann, Fietzek and Kühn 1978; van der Rest and Garrone 1991).

The α-chains are comprised of left-handed helices and in the α1 chain, 1011 of the 1052 amino acids consist of triplets of residues (Petruska and Hodge 1964; Piez and Miller 1974). Glycine, which is the smallest amino acid, is found every third position of the polypeptide chains resulting in a Gly-Xaa-Yaa motif that is characteristic of all collagens (Petruska and Hodge 1964; Hofmann, Fietzek and Kühn 1978). About 30 % of the X and Y positions are occupied by proline and hydroxyproline (van der Rest and Garrone 1991). The glycine residues of the α-chains are always positioned in the centre of the triple helix, while the side chains of the X and Y amino acids occupy the outer (surface) positions of the protein that allows a close packing of the molecule along the central axis (Gelse, Pöschl and Aigner 2003; van der Rest and Garrone 1991). The other amino acids are not considered critical to the molecular structure and usually, they are available for the interactions that direct molecular packing (Piez and Miller 1974). The residue-to-residue axial distance is c. 0.28 nm at an angular separation of 108° (Ottani et al. 2002; Piez and Miller 1974).

The α-chains are initially bordered by carboxy- and amino-terminal propeptides (procollagen molecule) which are followed by C- and N-telopeptides that are crucial in the formation of the intermolecular cross-links, stabilize the fibrils and increase their tensile strength (Ricard-Blum and Ruggiero 2005; Ricard-Blum 2011; Veis 1997). The N-terminal has 16 residues and the C-terminal has 25 residues with a different kind of sequence (Piez and Miller 1974). These procollagen molecules are secreted from the cells in the extracellular matrix and peptidases cleave off the terminal propeptides during maturation to leave tropocollagen, a single collagen molecule (Ricard-Blum and Ruggiero 2005; Ricard-Blum 2011).

Tropocollagen molecules, which are 300 nm in length and about 1.5 nm in diameter, are staggered every 67 nm (*D*-band periodicity) with a gap region of c. 40 nm between two consecutive

molecules to form the highly ordered fibrils with their axes parallel to the fibril direction (**Figure 2.7**; Gautieri et al. 2011; Petruska and Hodge 1964; Piez and Miller 1974). Fibrils can have a length of up to c. 1 mm and a diameter of 100-500 nm (Gautieri et al. 2011). At the next hierarchical level collagen fibrils form collagen fibres with the aid of cross-linking molecules (**Figure 2.7**).

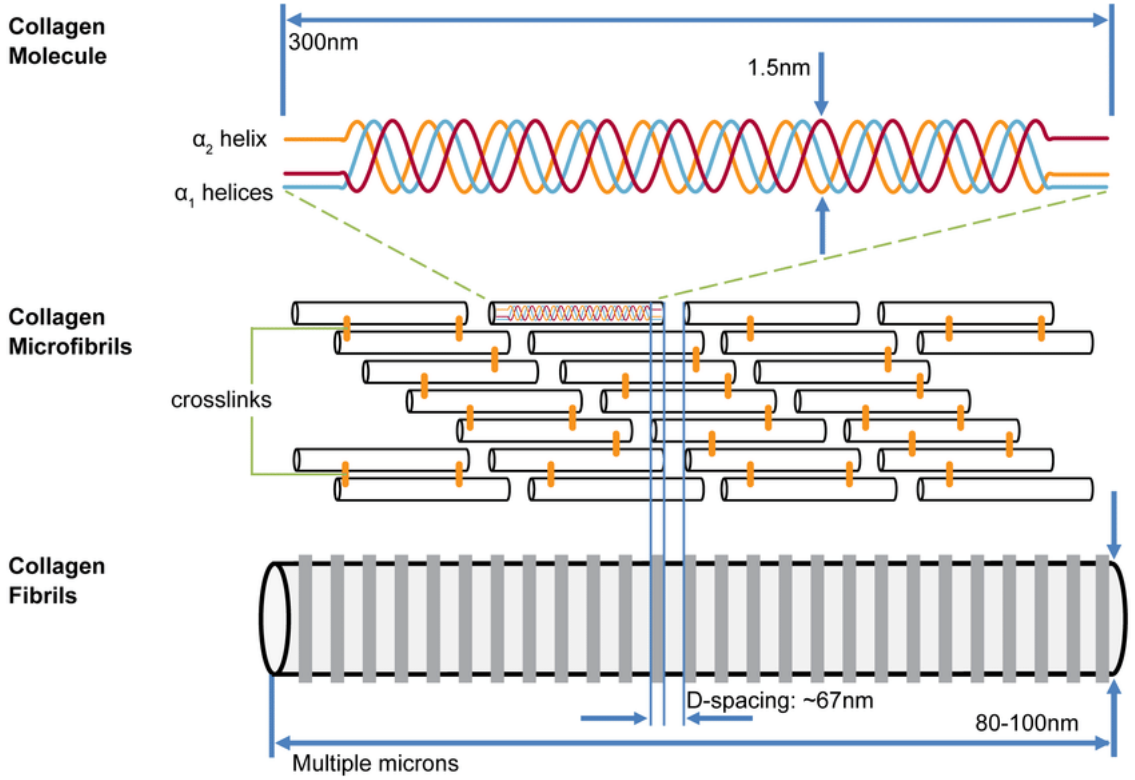

Figure 2.7. The supramolecular assembly of the collagen fibrils in the characteristic quarter-staggered form. The collagen molecules aggregate both in lateral and longitudinal directions to form fibrils (Canelón and Wallace 2016).

The characteristics of collagen are in part controlled by post-translational modifications (PTMs) such as hydroxylation, oxidation, glycosylation, and cross-linking (Ottani et al. 2002; Saito and Marumo 2015). Collagen cross-links in bone (cross-links are tissue-specific) are covalent linkages formed at specific telopeptide and helical residues (e.g. lysine, hydroxylysine and histidine) between the non-helical domains and the helical domain of adjacent collagen molecules (Ricard-Blum 2011; Saito and Marumo 2015). The specific chemistry of the cross-link formed is dependent on the location and hydroxylation of lysine residues. In newly synthesized collagens, cross-links (aldimines and keto-imines) are reducible and bifunctional, and they quickly mature into non-reducible trifunctional cross-links (pyridinoline, deoxypyridinoline, pyrrole in bone) (Ricard-Blum 2011). Bone and dentin have two major bifunctional Hyl aldehyde-derived cross-links, dehydro-dihydroxylysinonorleucine (deH-DHLNL) and dehydro-hydroxylysinonorleucine (deH-HLNL) and their trifunctional mature forms, pyridinoline (Pyr) and pyrrole cross-links (Saito and Marumo 2015; Veis 1997), with other major cross-links found in type I collagen being

the (4) dehydrohistidinohydroxymerodesmosine (deH-HHMD), (5) deoxypyridinoline (lysyl analog of Pyr, d-Pyr), and (6) histidinohydroxylysinonorleucine (HHL) (Eyre 1987, 1995; Light and Bailey 1985).

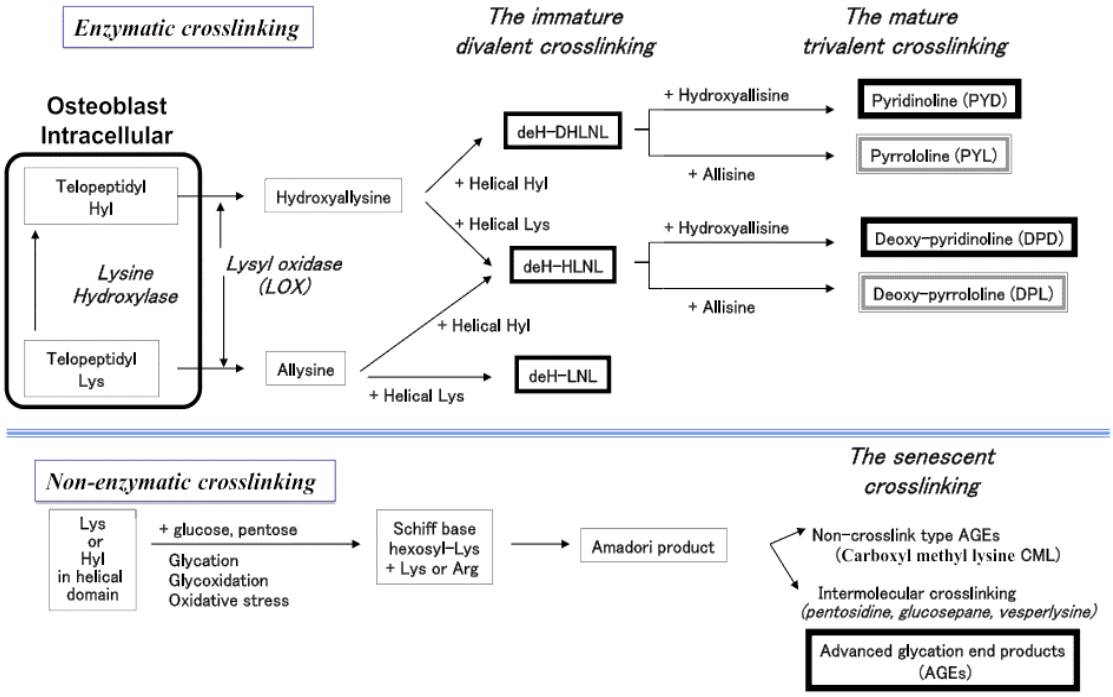

Figure 2.8. The enzymatic (immature and mature) and non-enzymatic cross link formation in collagen (Saito and Marumo 2015).

Collagen cross-linking can be divided into a) enzymatic (lysyl hydroxylase- and lysyl oxidase-mediated) cross-links and b) non-enzymatic (glycation- or oxidation-induced) cross-links (**Figure 2.8**; (Saito and Marumo 2015). Enzymatic and non-enzymatic crosslinks are determinants of the tensile strength, toughness, and post-yield properties in bone (Saito and Marumo 2015). Divalent immature (enzymatic) cross-linking, which is the predominant type of cross-link in bone collagen, seems to maintain the mechanical properties of bone (Saito and Marumo 2010). Aging and pathological conditions (e.g. osteoporosis) have been found to have significant effects on the biomechanical properties (i.e. elastic modulus and tensile strength) of collagen (Burr 2002; Leng et al. 2013; Wang et al. 2002) primarily accompanied by a decrease in enzymatic (immature) divalent cross-links (Nyman et al. 2006; Oxlund, Mosekilde and Ortoft 1996). Advanced glycation end products (AGEs, non-enzymatic cross-links) are generally thought to deteriorate the biological and mechanical functions of bone, although the effects of AGEs on osteoclastic bone resorption remain controversial (Saito and Marumo 2010). While AGEs are formed spontaneously by non-enzymatic glycation or oxidation, there are numerous sources of AGEs and unknown pathways leading to AGEs formation *in vivo* (Saito and Marumo 2010).

Biologic apatite (BAp) is a non-stoichiometric, disordered, nanocrystalline analogue of geologic bioapatite (Cho, Wu and Ackerman 2003; Meneghini et al. 2003). It is a carbonated calcium-deficient phosphate mineral and it is represented by the formula (Ca^{2+}, Na^{+}, Mg^{2+}, [])$_{10}$ (PO_4^{3-}, HPO_4^{3-}, CO_3^{2-})$_6$ (OH^-, F^-, Cl^-, CO_3^{2-}, O, [])$_2$ that accounts for the possible inclusion of various ions (Skinner 2013). Bone mineral is mainly consisted of Ca^{2+} (40 wt. %), PO_4^{3-} (18 wt. %), CO_3^{2-} (4–7 wt. %), minor elements such as Mg^{2+} or Na^{+}, and various trace elements (e.g. Sr^{2+}, Ba^{2+}, F^-, Cl^-), although its composition may vary depending on species, age, pathology, etc. (Antonakos, Liarokapis and Leventouri 2007; Bala, Farlay and Boivin 2013; Boskey 2003; LeGeros et al. 1967, 1969; Skinner 2013; Posner 1985).

The first-formed mineral phase of the mature crystalline mineral is an amorphous (or spherical) calcium phosphate (ACP) phase (Mahamid et al. 2008, 2010). A recent discovery by Mahamid et al. (2011) of a non-crystalline calcium phosphate precursor phase with a low Ca/P ratio concentrated in intracellular vesicles within bone-lining cells revealed the existence of intracellular 'reservoirs' of a mineral precursor. This observation shows that during bone formation the continuous layers of osteoblasts possibly prevent direct access of ions from the body fluids to the mineralizing bone surface (Gay, Gilman and Sugiyama 2000). As a result, the amorphous calcium phosphate (ACP) phase utilizes the bone-lining cells as an intermediate (Mahamid et al. 2010, 2011). However, the translocation process of the intracellular ACP phase into the extracellular mineralizing matrix and its transformation through osteoblast activity is still unclear (Gay, Gilman and Sugiyama 2000; Mahamid et al. 2010, 2011).

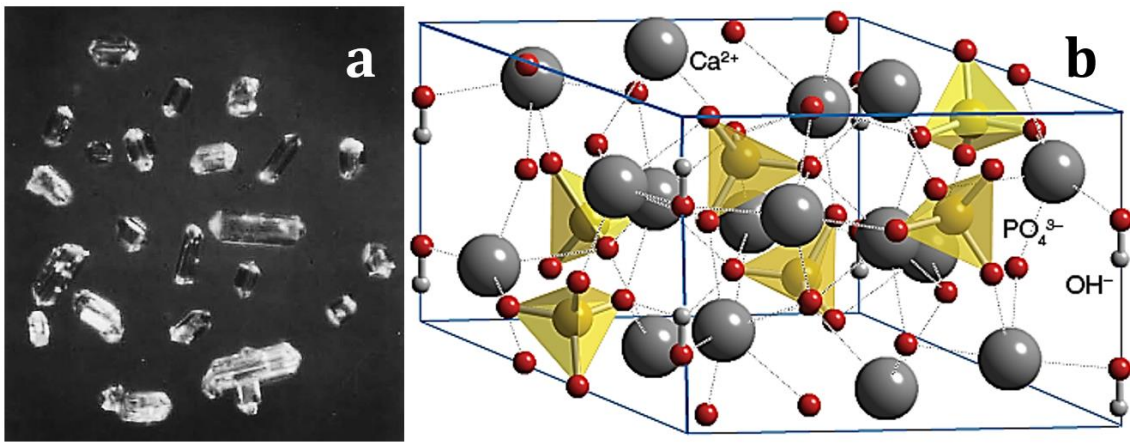

Figure 2.9. (a) Hydroxyapatite crystal hexagonal morphology, and (b) distribution of atoms in the unit cell (adapted from Skinner 2013(a) and Greeves 2018 (b)).

BAp has a hexagonal ($P6_3/m$) crystal system (**Figure 2.9**) with a longer c-axis perpendicular to three equivalent α-axis (α_1, α_2, α_3) at angles 120° to each other (LeGeros 1981; Weiner and Traub 1992). The size of the plate-like crystals is assumed to be around 10-50 nm × 5-25 nm × 2–10 nm; thus, they have a high surface area/mass ratio and high degree of lattice strain (Burger et al.

2008; Dalconi et al. 2003; Rubin et al. 2003; Weiner and Price 1986; Weiner and Traub 1992; Yerramshetty and Akkus 2008). Crystals are also comprised of two components: a) the apatite core, and b) the hydrated layer that surrounds the core (**Figure 2.10a**; Bala, Farlay and Boivin 2013; Neuman and Neuman 1953). BAp crystals can increase in size by secondary nucleation (i.e. each crystal can serve as a branch point for nucleation of additional crystals *in vivo*), by merging of crystals, and/or by ionic exchange with the surrounding environment (**Figure 2.10b**; Boskey 2003; Rey et al. 2007).

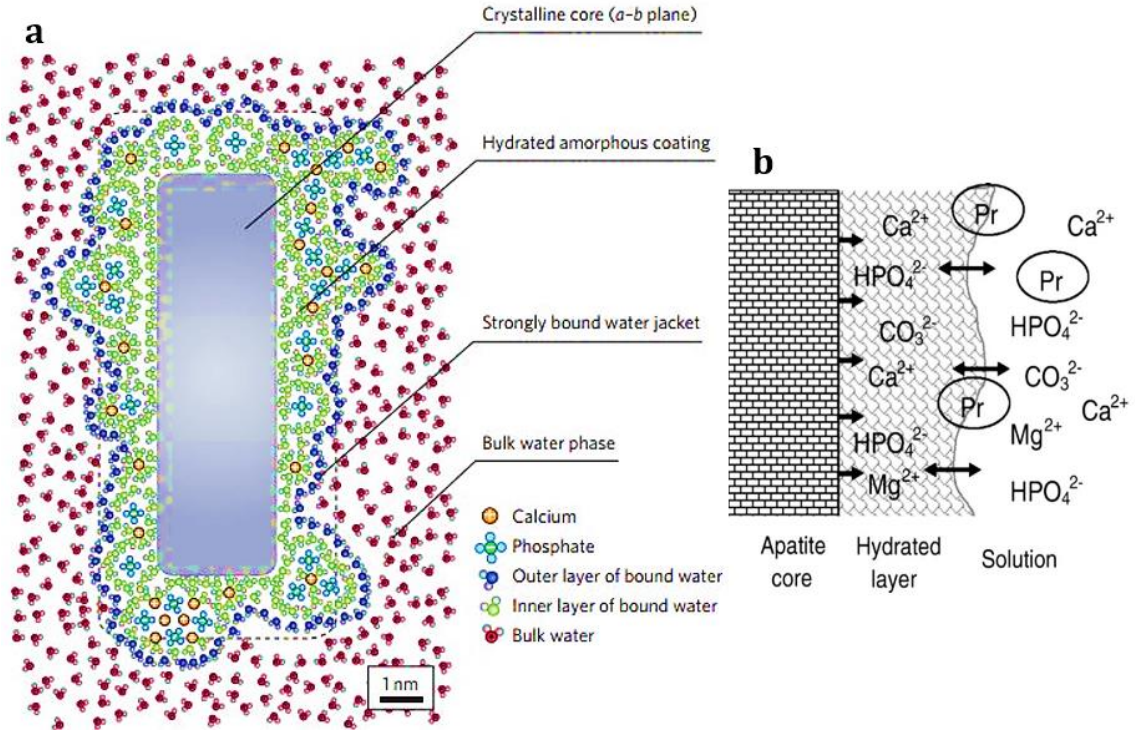

Figure 2.10. (a) The two components of the BAp crystals that interact *in vivo* (adapted from Duer and Veis, 2013), and (b) the apatite core-hydrated layer-surrounding environment ionic exchange (adapted from Rey et al. 2007).

The high BAp crystal surface area (c. 100–200 m^2/g) allows the interaction between the ions of the fragile hydrated layer and these of the apatite core, while the hydration layer seeks to reach equilibrium with its surrounding medium (**Figure 2.10b**) (Boivin and Meunier 2003; Rey et al. 2007; Wang et al. 2013; Weiner and Price 1986). The ionic exchanges can be distinguished into two different groups: a) the iso-ionic, and b) the hetero-ionic (Boivin and Meunier 2003; Neuman and Neuman 1953). The former (iso-ionic) take place when ions from the hydrated layer substitute similar ones inside the core of the crystal (Boivin and Meunier 2003; Neuman and Neuman 1953). The hetero-ionic substitutions occur when ions on the crystal surface are replaced by different ions from the surrounding environment that are normally absent from bone mineral (Boivin and Meunier 2003; Neuman and Neuman 1953). Thus, interaction with water is an essential component of the minerals' milieu (Boivin and Meunier 2003; Wang et al. 2013).

Because of the differences in size (ionic radius) between the different ions, these ionic exchanges may lead to changes in shape, size, unit cell levels, and structure of the crystal (Boivin and Meunier 2003). For instance, the carbonate ions may substitute either the hydroxyl site (A-type) or the phosphate tetrahedron (B-type), and vice versa (Antonakos, Liarokapis and Leventouri 2007; LeGeros 1981; Rey et al. 1989). Type B substitutions predominate in bone as type A substitutions require high temperatures (i.e. 900-1000° C) and exclusion of water (Antonakos, Liarokapis and Leventouri 2007; LeGeros 1965; LeGeros et al. 1969; Rey et al. 1989). Additionally, the incorporation of CO_3^{2-} into the bone apatite crystal limits the OH^- concentrations (Pasteris et al. 2004; Rey et al. 1989). However, these modes of carbonate substitution and the degree of hydroxylation have been debated for several decades (e.g. Antonakos, Liarokapis and Leventouri 2007; LeGeros 1965; LeGeros et al. 1967; Pasteris et al. 2004; Rey et al. 1989). The exact location of the carbonate ions in the crystal structure (e.g. vacant phosphate ion site, phosphate tetrahedron mirror plane) in fact is still unknown (Leventouri 2006), while the BAp crystals are also considered to be deficient in or devoid of OH^- (Pasteris et al. 2004; Wopenka and Pasteris 2005).

The ionic substitutions affect the shape and size of the crystals by changing the lattice's α- and c-axes, and subsequently, the physicochemical properties of the crystal (LeGeros 1965, 1981; LeGeros et al. 1967, 1969). CO_3^{2-} to PO_4^{3-} substitution leads to a contraction of the unit cell as carbonate is smaller than phosphate, whereas a carbonate-to-hydroxyl substitution results to an expansion of the unit cell as CO_3^{2-} is larger than OH^- (LeGeros et al. 1969). The level of ionic substitutions is also strongly related to formation, growth, maturation and dissolution/recrystallization (Bala, Farlay and Boivin 2013; Meneghini et al. 2003). During normal mineralization of bone, crystallinity and maturity usually evolve concomitantly and are well-correlated (Bala, Farlay and Boivin 2013). Crystallinity reflects the size and perfection of the crystal lattice (i.e., atomic order/disorder) which are affected by both extrinsic and intrinsic factors (e.g. organic matrix, distribution of non-collagenous proteins acting in the formation and growth of the crystals, environment, diet, aging, bone remodelling, pathologies, and medication) (Bala, Farlay and Boivin 2013; Boskey 2003). Mineral maturity, on the other hand, reflects the conversion of non apatitic precursors into apatitic mineral (Bala, Farlay and Boivin 2013). Reduction of the hydrated layer and a more stoichiometric structure is related to maturation of the inorganic content in bone and maturity of the mineral phase is also related with the number of carbonate substitutions in bioapatite crystals (Figueiredo, Gamelas and Martins 2012).

ORGANIC-INORGANIC COMPOSITE

The production of a collagen-bioapatite composite structure is a complex phenomenon of high interest that has been extensively studied using various techniques which can provide insights into bone structure and organization at different length scales (for a review of techniques see Georgiadis, Müller and Schneider 2016). Bone mineralization includes the cell-mediated

deposition of crystalline material between the collagen fibrils (inter-fibrillar spaces) or on the surfaces of collagen fibrils (intra-fibrillar spaces) (**Figure 2.11**), with the orientation (crystal c-axis aligned with fibril long axis) and size of BAp crystals controlled by the fibril structure and organization (Boskey 2003; Reznikov, Shahar and Weiner 2014b; Su et al. 2003; Weiner and Price 1986; Weiner and Traub 1992). Although bioapatite crystals probably are initially deposited in the intra-fibrillar regions (i.e. gap zones) of collagen (Nair et al. 2013) and then in the inter-fibrillar spaces (**Figure 2.11**) the exact mechanisms of biomineralization and BAp crystals' arrangement are still unclear (Duer and Veis 2013; Landis 1995; Rubin et al. 2003; Stock 2015; Wang and Nilsen-Hamilton 2013).

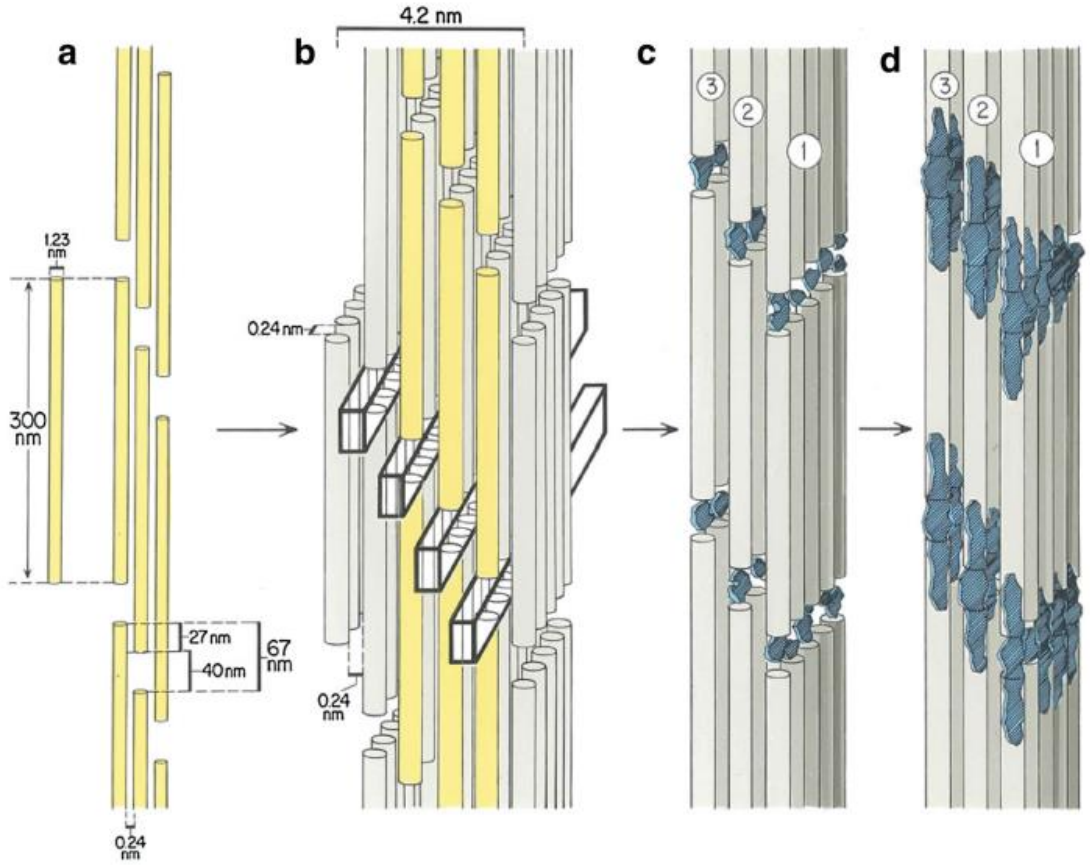

Figure 2.11. (a) Mineralization of closely packed collagen molecules by bioapatite crystals (b; blue) that nucleate mainly in the collagen gaps (c) and grow preferentially in their crystal axis direction (d) (Landis and Jacquet 2013).

Mineralization of the newly deposited organic matrix by secondary nucleation (i.e., the crystals act as nucleation sites for the newer ones) initiates 5–10 days after deposition and results in a mineral content of 50–70 % of the maximum level (Bala, Farlay and Boivin 2013). After this stage that lasts for a few days or weeks until mineralization rate decreases considerably, secondary mineralization begins (Bala, Farlay and Boivin 2013; Boivin and Meunier 2003). During this phase there is a slow increase in crystal number, size, and/or perfection until mineralization is

complete (i.e. 90–95% of the expected maximum level) (Bala, Farlay and Boivin 2013; Boivin and Meunier 2003).

In mammalian skeletal tissues the relative amounts of the mineral, organic and water fractions can vary between species (Currey 1999; Zioupos, Currey and Casinos 2000). When the organic matrix is reinforced with mineral particles, the resulting composite increases in strength and becomes capable of bearing weight (i.e. tension, compression and shear forces; Currey 1999). Bone mineral gives strength and stiffness, while collagen gives toughness (Burr 2002). The mechanical properties of bone are related to this bond between the mineral (degree of mineralization) and organic phases (Currey 1999; Posner 1985), although the collagen-mineral relationship is still unclear (e.g. Weiner and Price 1986).

DNA

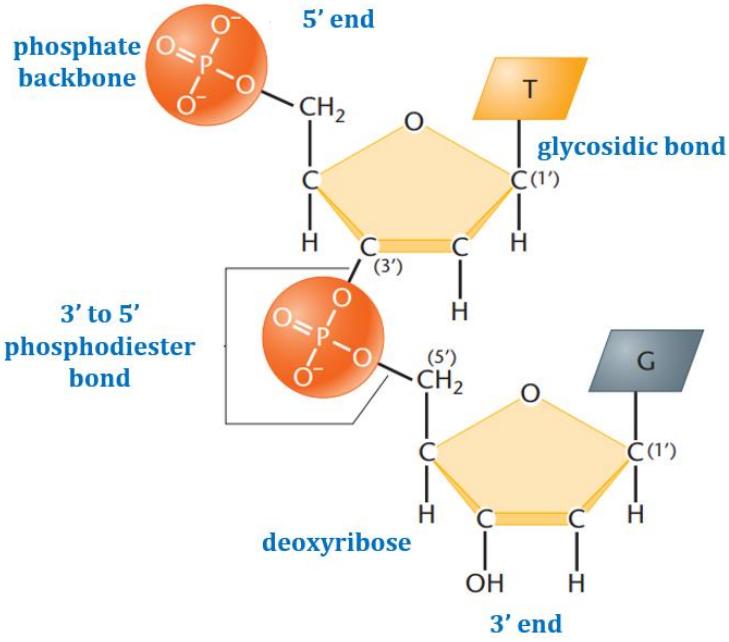

Figure 2.12. The three elements of the DNA nucleotide subunits composed of a five-carbon sugar deoxyribose, a phosphate group, and a purine (bicycle adenine and guanine) or pyrimidine (monocyclic cytosine and thymine) nitrogenous base (adapted from Klug et al. 2012).

DNA (deoxyribonucleic acid) is a linear polymer made up of a fixed backbone that is built of repeating sugar (deoxyribose)-phosphate units covalently bound between the 5′-position of one sugar and the 3′-position of the next, forming a 3′,5′-phosphodiester bond (**Figure 2.12**; Watson and Crick 1953). The four planar bases (i.e. adenine (A), cytosine (C), guanine (G), and thymine (T)) are heterocyclic (carbon- and nitrogen-containing) aromatic rings covalently bind (glycosidic or glycosylic bond) to the 1′-position of a deoxyribose ring to form nucleosides (**Figure 2.12**; Turner et al. 2005). When a nucleoside is bound covalently with one or more phosphate groups to the 3′-, 5′-position it is called nucleotide, and if the sugar is deoxyribose, then the compound is

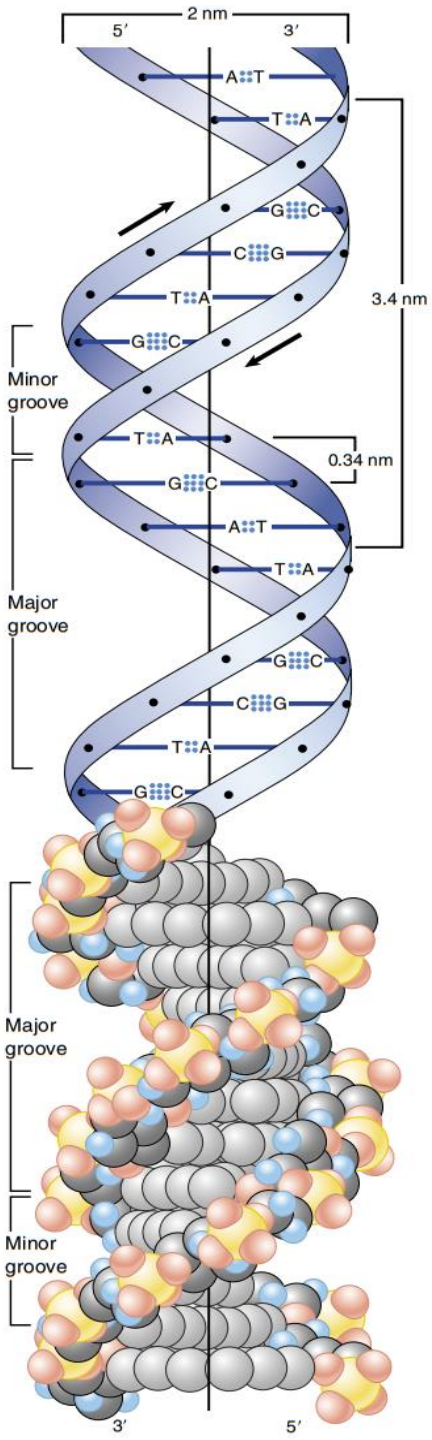

Figure 2.13. The 3D structure of DNA (Raven et al. 2016).

termed deoxynucleotide (Turner et al. 2005). Therefore, a nucleotide in DNA consists of a sugar (deoxyribose), one of four bases (cytosine (C), thymine (T), adenine (A), guanine (G)), and a phosphate (**Figure 2.12**).

The base pairs (bp) attach to the 1′-position of each sugar (**Figure 2.12**) in any order along a DNA strand with a 0.34 nm space between them (Raven et al. 2016; Turner et al. 2005). They are held together by hydrogen bonds (Watson and Crick 1953) which are much weaker than covalent bonds (e.g. carbon-carbon or carbon-nitrogen bonds) that define the structures of the bases themselves (Berg et al. 2015). Hydrogen bonds are weak enough to be reversibly broken in biochemical processes, yet they are strong enough when form simultaneously to help stabilize specific structures such as the double helix (Berg et al. 2015). This right-handed double helix of 2 nm diameter is formed when two intertwined single strands of DNA are combined with the sugar-phosphate backbone on the outside and the bases on the inside (**Figure 2.13**; Watson and Crick 1953). One chain of the DNA molecule may have any conceivable base sequence, but this sequence completely determines the sequence of its partner in the duplex (adenine pairs with thymine (A-T) and guanine pairs with cytosine (G-C) (Watson and Crick 1953). The exact sequence of bases (i.e. gene) along a DNA strand constitutes the genetic information, hence the instructions for assembling proteins that compose the synthesis of other biomolecules that form cells and ultimately organisms (Berg et al. 2015; Cooper 2011).

DNA was initially considered as an extremely stable molecule due to this valuable genetic information that must be retained in cells. However, DNA chemical stability and decay of primary structure are affected *in vivo* by hydrolysis, temperature, pH and active oxygen (**Figure 2.14**; Lindahl 1993). DNA molecules are prone to depurination even under physiological conditions (i.e. c. 37° C and c. 7.4 pH) as the labile glycosidic bonds break and release the purine residues adenine and guanine, followed by chain rupture at the weakened abasic sites, rather than by direct

cleavage of phosphodiester bonds between two intact nucleotides (Lindahl and Nyberg 1972; Lindahl 1993). The rate of depurination is temperature sensitive and increases with increasing temperature, while there is no repair system (Lindahl 1996). Hydrolytic deamination of cytosine to uracil has also been shown to occur at a significant rate in DNA under similar conditions, while deamination of purines is a minor reaction (Lindahl 1993, 1996). In strong acid and elevated temperatures (e.g. 100 °C) nucleic acids are completely hydrolysed to their components (bases, sugar and phosphate) (Turner et al. 2005). Alkaline environments have less severe effects on DNA structure such as denaturing of DNA due to cleavage of hydrogen bonding between the base pairs that can result to the breaking of the double-stranded structure of DNA (Turner et al. 2005). Ultraviolet light and ionizing radiation can also damage intracellular DNA, while oxidatively generated base lesions (**Figure 2.14**) can occur by active oxygen during normal metabolism with DNA pyrimidines being particularly sensitive to ring saturation, fragmentation, and condensation (Cadet and Wagner 2013; 1996).

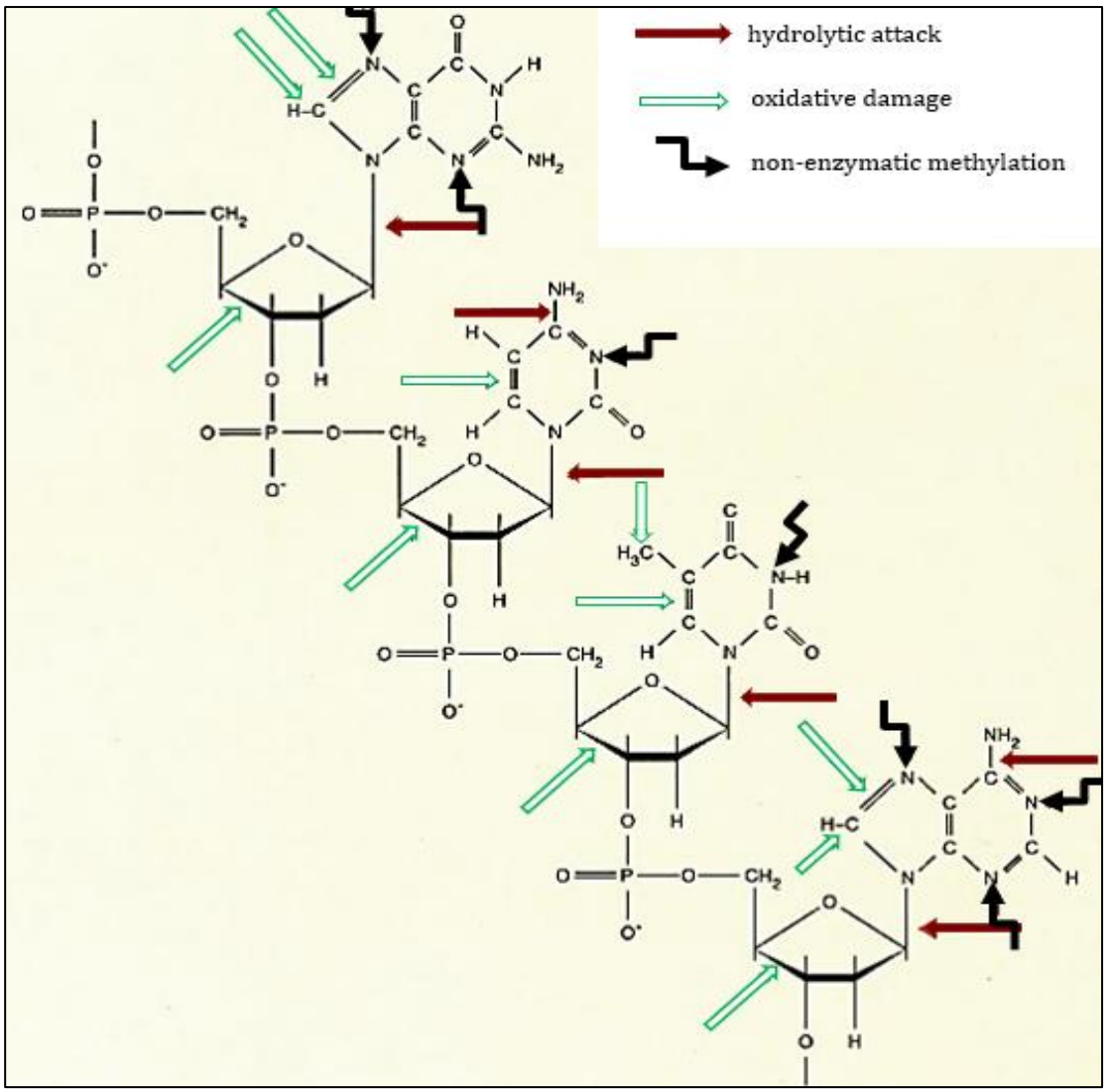

Figure 2.14. Major sites of hydrolytic attack indicated by black arrows (adapted from Lindahl 1993).

2.2.2. MICROSTRUCTURE

Bone exhibits two varieties of tissue with distinct microstructural characteristics: a) woven, primary, or immature; and b) lamellar, secondary, or mature (**Figure 2.15**; Smith 1960), while fibrolamellar tissue (i.e. plexiform) is a combination of lamellar and parallel fibred tissue (Reznikov, Shahar and Weiner 2014a; Weiner and Wagner 1998) typically found in long bones of large and medium-sized mammals (e.g. cow, pig and sheep; Martiniaková et al. 2006, 2007; Mulhern and Ubelaker 2001). During the formation of the skeletal tissues woven bone appears first. It is a temporary, premature form of bone tissue which is produced *in utero* during the initial growth of foetuses and infants and it is later replaced by lamellar tissue (Currey 2002; White, Black and Folkens 2012). Woven bone also appears in sites of fracture repair and in bone tumours as a response to trauma or pathologies in adult individuals, which explains why it is formed more rapidly than lamellar bone (Currey 2002; Ross and Pawlina 2011; White, Black and Folkens 2012). It has a fibrous appearance without lamellae and more osteocytes per unit area which are randomly arranged compared to lamellar bone (**Figure 2.15**; Ross and Pawlina 2011; Weiner and Wagner 1998; White, Black and Folkens 2012).

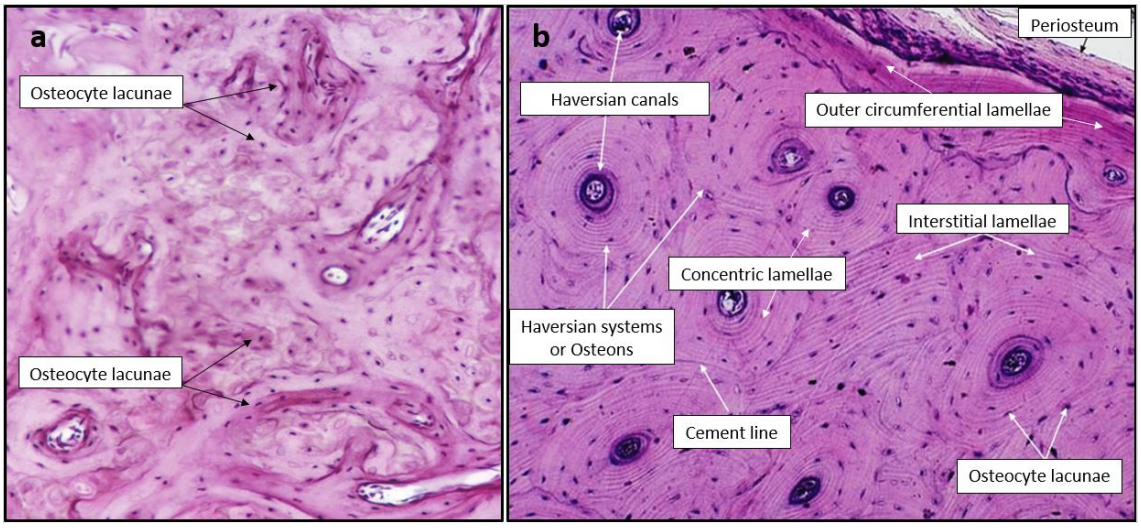

Figure 2.15. Transverse histological sections of human bone. (a) Woven tissue with amorphous appearance and several osteocytes; (b) lamellar tissue (×300 magnification) with parallel (outer circumferential and interstitial lamellae) or concentric layers (Haversian systems or osteons) containing osteocyte lacunae. Notice the cement line at the periphery of osteons (adapted from Memorang 2018 (a) and Clermont, Lalli and Bencsath-Makkai 2013 (b)).

Mammalian adult bone is primarily lamellar with collagen fibres arranged in discrete layers (lamellae) either parallel to each other (interstitial and circumferential lamellae) or concentrically organized (osteons or Haversian systems) around vascular canals (**Figure 2.15**; Smith 1960). Circumferential lamellae are a series of lamellae which are found in periosteal and endosteal regions with a large radius of curvature parallel to the forming surfaces of bone (**Figure 2.15b**; Crescimanno and Stout 2012; Reznikov, Shahar and Weiner 2014a). Osteons have a series of concentric lamellae and cover roughly half the area of mesosteal (mid-cortical) bone with the

other half filled by interstitial lamellae (**Figure 2.15b**; Burr, Schaffler and Frederickson 1988; Crescimanno and Stout 2012; Ross and Pawlina 2011; Schaffler, Burr and Frederickson 1987; Schwartz 2007; Skedros et al. 2005). They are distinguished into primary and secondary, with primary osteons appearing as islands with lamellar bone surrounding them and a lack of distinct mineralized interface at the outermost lamella (i.e. cement line; Schwartz 2007). During the first stage of their formation, tubular cavities within the bone are created by the absorption of the tissue surrounding pre-existing vascular canals in primary osteons (Smith 1960). Next, an appositional growth of new bone occurs at the walls of the cavities until a canal (Haversian) of definitive size is reformed (Smith 1960).

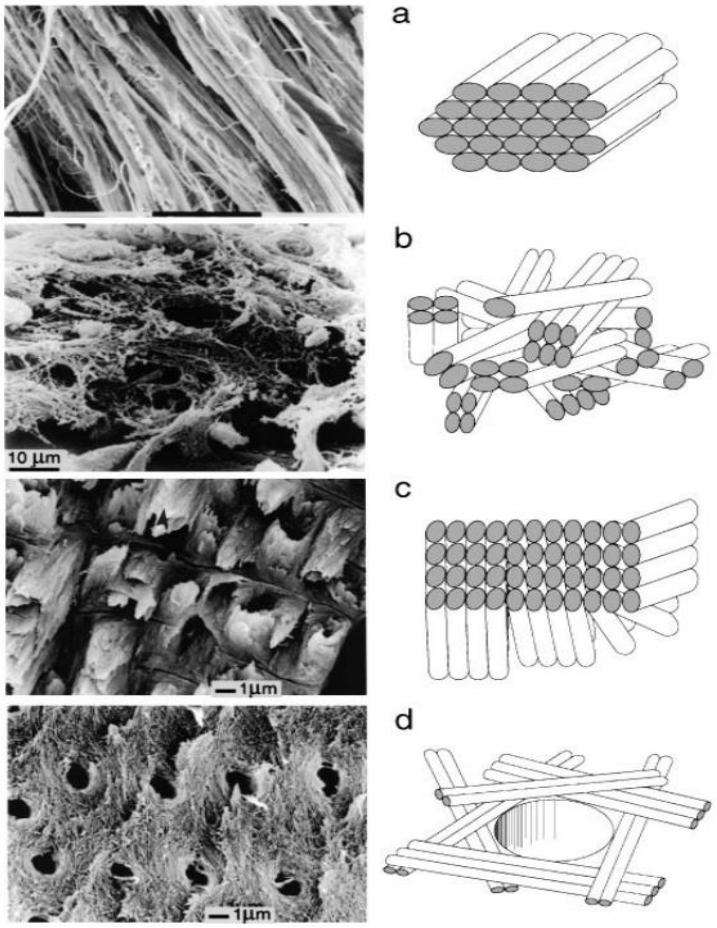

Figure 2.16. The four most common collagen fibril organization patterns. (a) parallel collagen fibrils commonly found in bovids (mineralized turkey tendon); (b) woven fibres with fibril bundles showing different orientations (human foetus femur); (c) plywood-like structure of lamellar bone (baboon tibia); (d) radial fibril arrays with collagen fibrils in one plane (human dentin) (Weiner and Wagner 1998).

The secondary (mature) osteons have an average diameter of about 200-300 µm and an average length of 3-5 mm, although their size and number can vary between and within skeletal elements as well as species (Cattaneo et al. 1999; Martiniaková et al. 2006, 2007; Mulhern and Ubelaker 2001; Van Oers et al. 2008; Urbanová and Novotný 2004; White, Black and Folkens 2012; Lander, Brits and Hosie 2014). These units are demarcated by the cement line that distinguishes them from the surrounding tissues (**Figure 2.15b**; Smith 1960). Any subsequent secondary osteons are developed in relation to the vascular canals of similar pre-existing secondary osteons (Smith 1960). As more and more secondary osteons are formed the amount of woven-fibred bone, primary osteons and surface bone is progressively reduced (Smith 1960). Additional transverse/oblique canals (i.e. Volkmann's canals) link the Haversian canals to create a network that transfers the nutrients to the cells (Schwartz 2007; White, Black and Folkens 2012).

While the circumferential and osteonal lamellar structures are the products of different processes, modelling and remodelling, no differences have been observed in their structures (Reznikov, Shahar and Weiner 2014b). All lamellae in mature bone contain regularly arranged osteocyte lacunae (**Figure 2.15b**) interconnected with a well-organized canalicular network compared to randomly and denser organized lacunae interconnected with more sparse and irregular canaliculi in woven tissue (**Figure 2.15a**; Kollmannsberger et al. 2017; Ross and Pawlina 2011). Lamellae have an average width of 3-4 μm (although it can vary between species) and each lamella has collagen fibres parallel to each other but in successive lamellae the collagen fibres are oriented in different directions (plywood appearance) giving strength to the structure (**Figure 2.16**; Almany Magal et al. 2014; Giraud-Guille 1988; Reznikov, Shahar and Weiner 2014a; Weiner and Wagner 1998). Fibrils parallel to the bone long axis are laid down first, whereas in trabecular bone the collagen fibril orientation is characterized by only two alternating components. In the first one, the collagen fibrils are aligned with the long axis of the trabecula, whereas in the second fibrils are oblique to the long axis of the trabecula either at 60–70° or 30–40° (Reznikov et al. 2015; Weiner, Traub and Wagner 1999). The collagen fibrils in woven tissue are arranged into bundles with up to 30 μm diameter that are loosely packed and poorly oriented (**Figure 2.16b**), particularly in the case of the small-diameter bundles (Ross and Pawlina 2011; Weiner and Wagner 1998; White,Black and Folkens 2012). The collagen microfibres are irregular in thickness and do not have the linear orientation observed in the later stages of formation (Ortner and Turner-Walker 2002).

2.2.3. MACROSTRUCTURE

Cortical or compact bone (*substantia compacta*) is an anisotropic, dense, hard, solid, mass, and represents approximately the 80% of the skeletal mass. It forms a rigid outer wall on the shafts of long bones (thinner in articular regions than mid-diaphysis) and external surfaces that resists deformations (**Figure 2.17**; White, Black and Folkens 2012). Trabecular or cancellous bone is spongy bone (*substantia spongiosa*) that represents the remaining 20% of the skeletal mass. It consists of thin plates that form a loose mesh in the inner parts of bone (**Figure 2.17**; Martin et al. 2015). It is more lightweight, and it is found in flat bones sandwiched between compact bone, in the ends of long bones and in irregular bones (White, Black and Folkens 2012). In living bone, the pores are filled with red marrow which is gradually replaced by the yellow marrow in later stages of growth and adulthood (Ross and Pawlina 2011; White, Black and Folkens 2012). The trabeculae are about 200 μm thick and they have a variable arrangement (Martin et al. 2015). Both cortical and trabecular human bone are composed of lamellar tissue, with the unidirectional fibril bundles showing a variety of alternating orientations in lamellae and a generally aligned orientation with the long axis of the individual strut in trabecular lamellae (Reznikov, Shahar and Weiner 2014a).

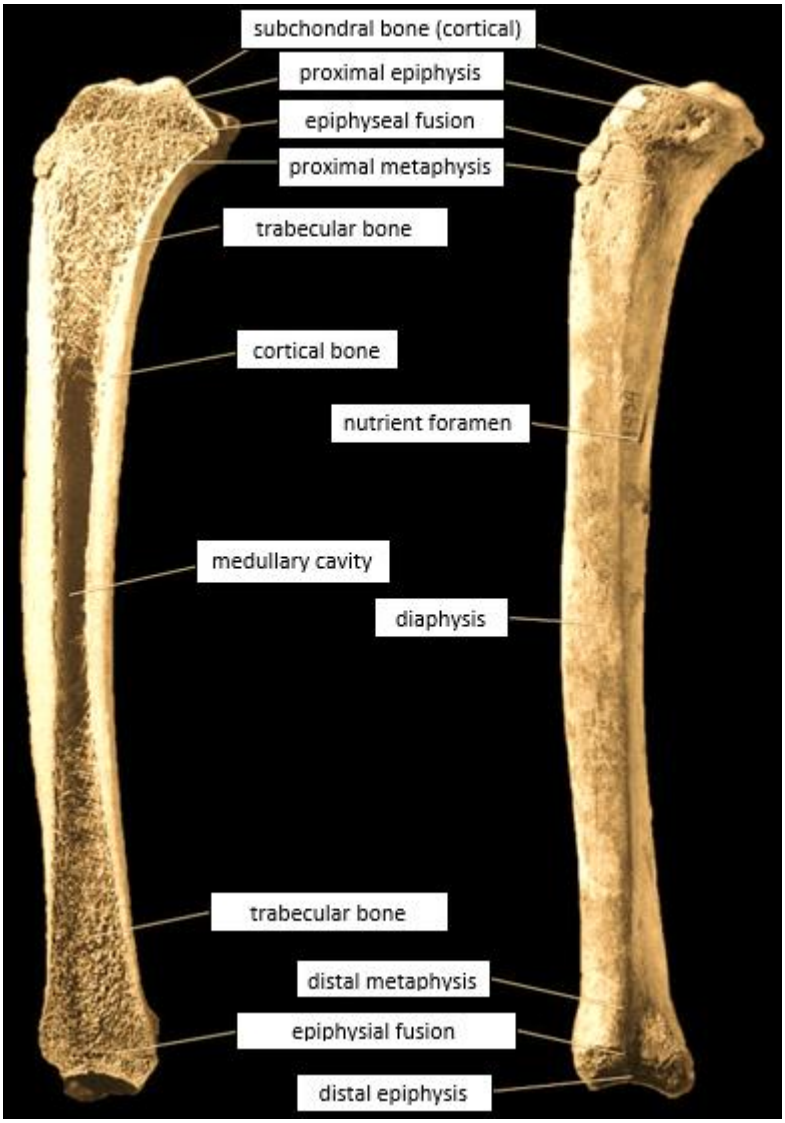

Figure 2.17. Bone macrostructure (adapted from White, Black and Folkens 2012).

The human petrous bone is a pyramid-shaped, massive portion of the endocranial aspect of the temporal bone (**Figure 2.18**) and projects antero-medially to separate the temporal and occipital lobes of the brain (White, Black and Folkens 2012). It is comprised of the middle and inner ear, with the outer ear partly located out of the skull (pinna) and partly penetrating the skull for 2-3 cm, i.e. external auditory meatus (**Figure 2.19a**; Green 1976; Luce 2013; Moller 2000; Yost 1994). The middle ear is a bony cavity of around 2 cm^3 volume that contains the tympanic membrane and the ear ossicles (malleus, incus, stapes) which transport vibrations from the cone-shaped tympanic membrane to the oval window (**Figure 2.19a**; Green 1976; Moller 2000; Yost 1994).

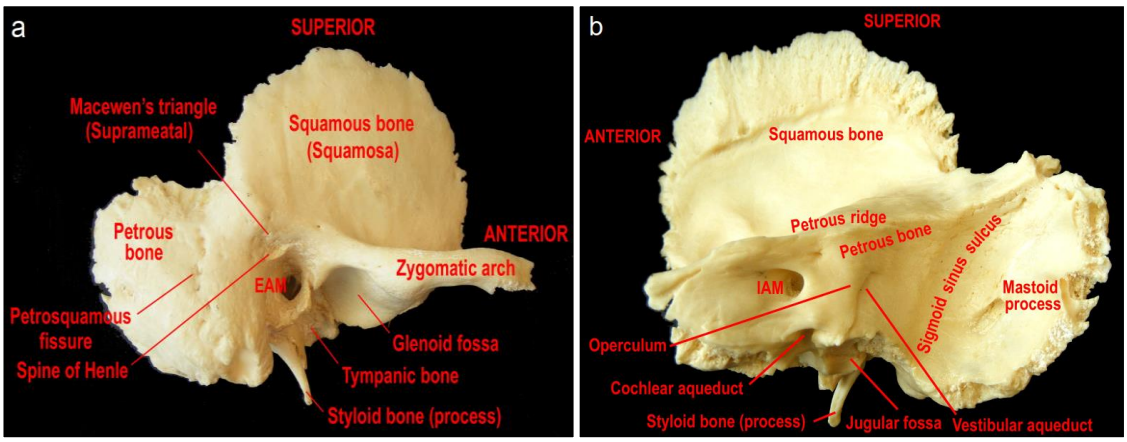

Figure 2.18. Right temporal bone. (a) lateral view with the anterior towards the right and superior up; (b) medial view with the anterior towards the left and superior up. EAM: external auditory meatus; IAM: internal auditory meatus (adapted from Bohne and Militchin 2012).

The inner ear cavity (**Figure 2.19**) is approximately 2 cm long and houses the three main components of the bony labyrinth: (a) the cochlea which is a coiled bony tube resembling a snail shell; (b) the vestibule; and (c) the three semi-circular canals (Green 1976; Yost 1994; Moller 2000). The cochlea is situated at the antero-lateral extension of the internal auditory canal, and if uncoiled, it would be around 3.5 cm in length (**Figure 2.19b**; Green 1976). The vestibule is approximately 4 mm in diameter and connects the cochlea with the semi-circular canals (**Figure 2.19a**) which are orthogonally-oriented and each of them (i.e. lateral, posterior, superior) is around 1 mm in diameter (Moller 2000).

Blood and nervous supply to the inner ear is carried out through the internal auditory canal that carries the facial and cochlear nerves (**Figure 2.19a**) as well as the internal auditory artery (IAA) that branches to the antcrior vestibular, cochlear and vestibulocochlear (Mazzoni 1972). Blood supply to the inner ear comes only from the IAA artery with no collateral supply (Green 1976; Mazzoni 1972). The internal carotid artery, the middle meningeal artery (internally) and the middle temporal artery (externally) contribute to the blood supply of the petrous bone (**Figure 2.19b**).

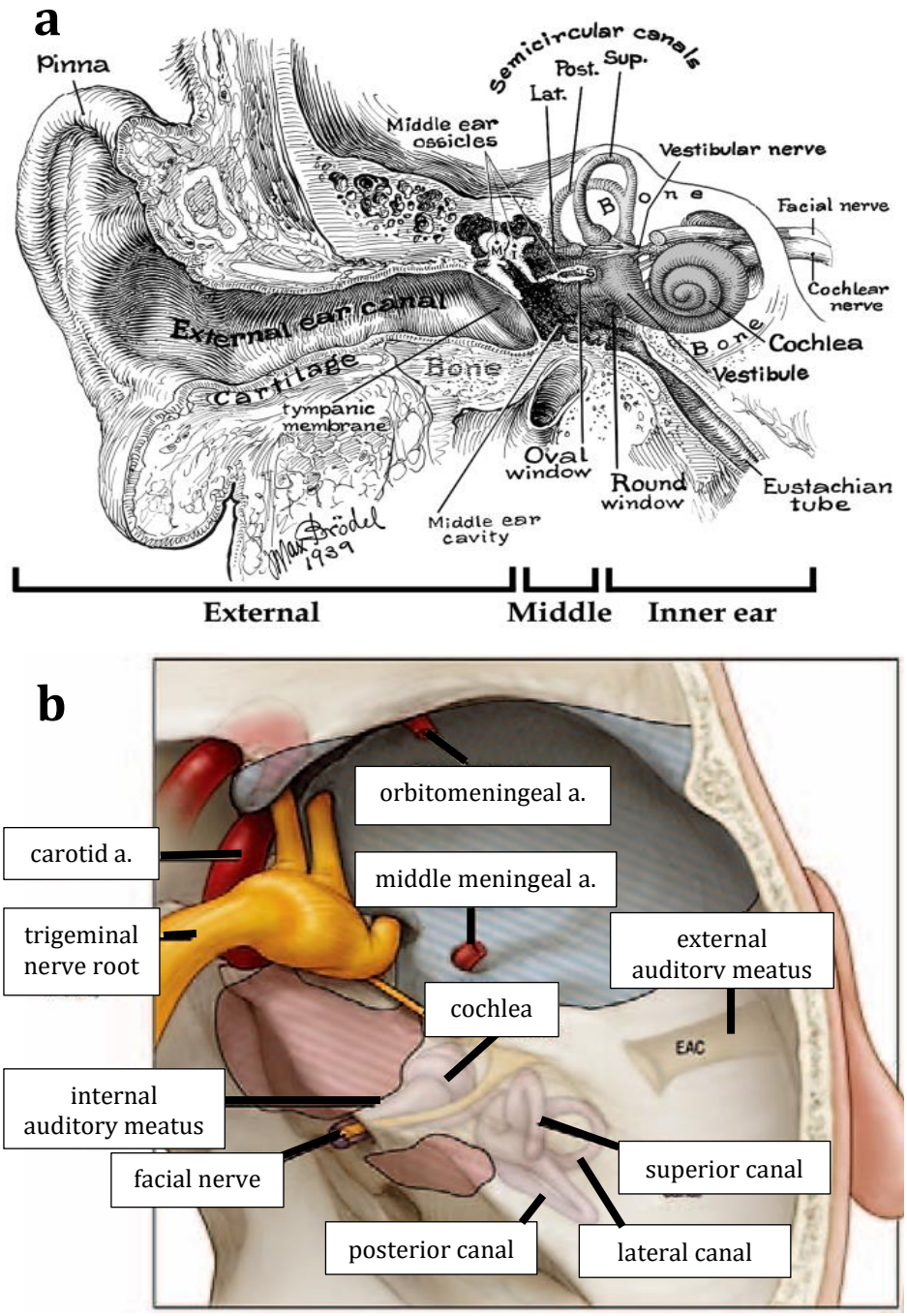

Figure 2.19. Anterior (a) and superior (b) view of the petrous bone (adapted from Bohne and Militchin 2012 (a) and Sun et al. 2018 (b)).

The bony capsule surrounding the membranous labyrinth develops predominantly by endochondral ossification similarly to long bones, but unlike long bones the petrous bone reaches adult size *in utero* (Eby and Nadol 1986; Nemzek et al. 1996; Richard et al. 2010). Development begins at 21 to 24 days of gestation and each part follows distinct growth rates (Jeffery and Spoor 2004). Formation of the membranous semicircular canals begins at 7-8 gestational weeks with the superior developing first, followed by the posterior and the lateral (Nemzek et al. 1996). The semicircular canals have attained adult size at 24-25 weeks or earlier (Jeffery and Spoor 2004; Richard et al. 2010). A progressive torsion of each semicircular canal was also observed during

fetal development (Richard et al. 2010). The cochlea has achieved about half of its size at 8-11 weeks, and the full adult configuration has been completed until 24-26 weeks (Jeffery and Spoor 2004; Nemzek et al. 1996; Richard et al. 2010). The oval window and the vestibule develop until gestational weeks 35 and 39, respectively (Richard et al. 2010). Although the subcomponents of the inner ear have attained their adult size by 5-6 prenatal months (e.g. Jeffery and Spoor 2004), an increase in the overall size of petrous bone throughout fetal life and infancy (**Figure 2.20**) has been reported by other researcher (Fazekas and Kósa 1978; Nagaoka and Kawakubo 2015).

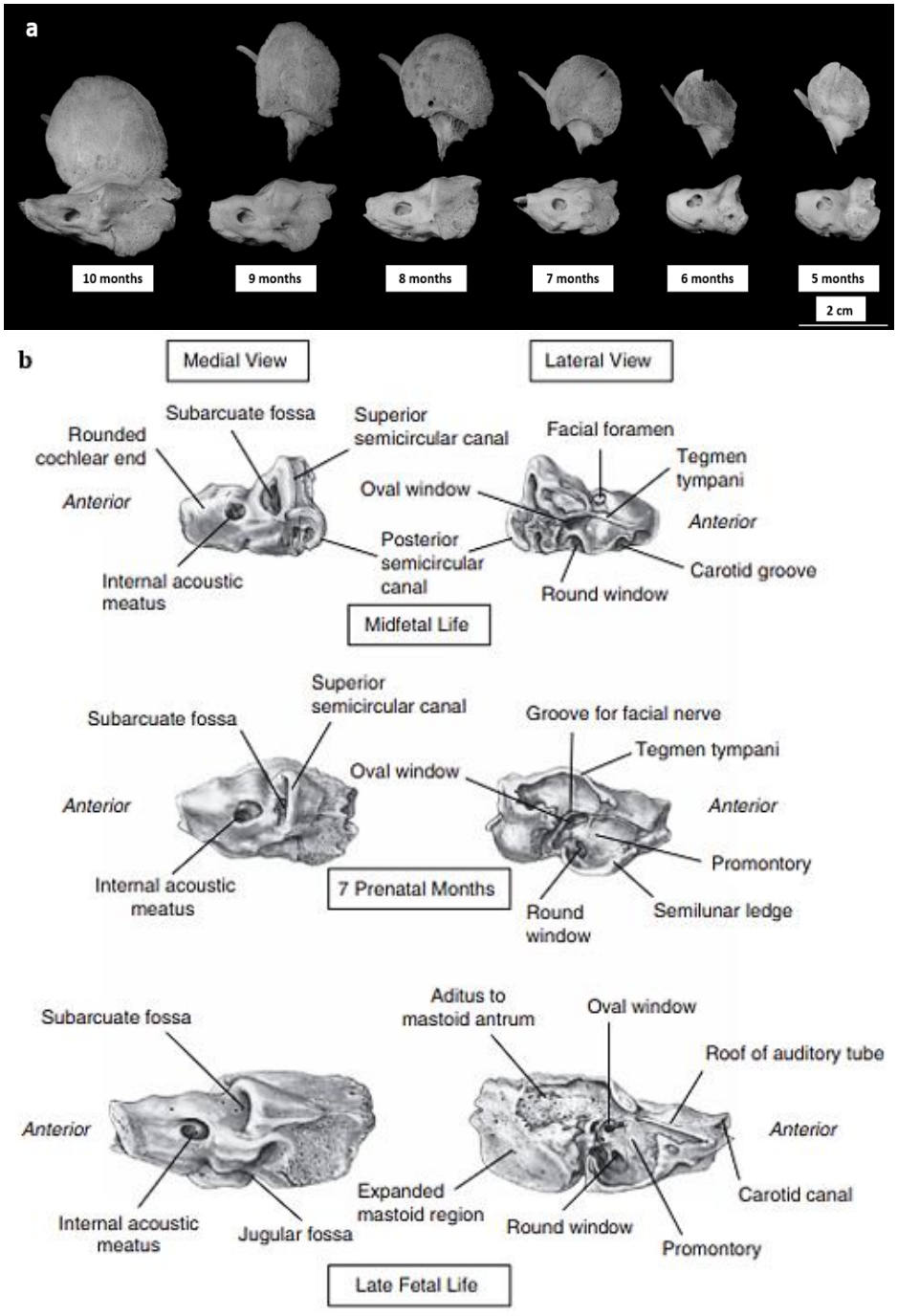

Figure 2.20. Age related changes to the right petrous pyramid (adapted from Nagaoka and Kawakubo 2015 (a) and Schaefer, Black and Scheuer 2009 (b)).

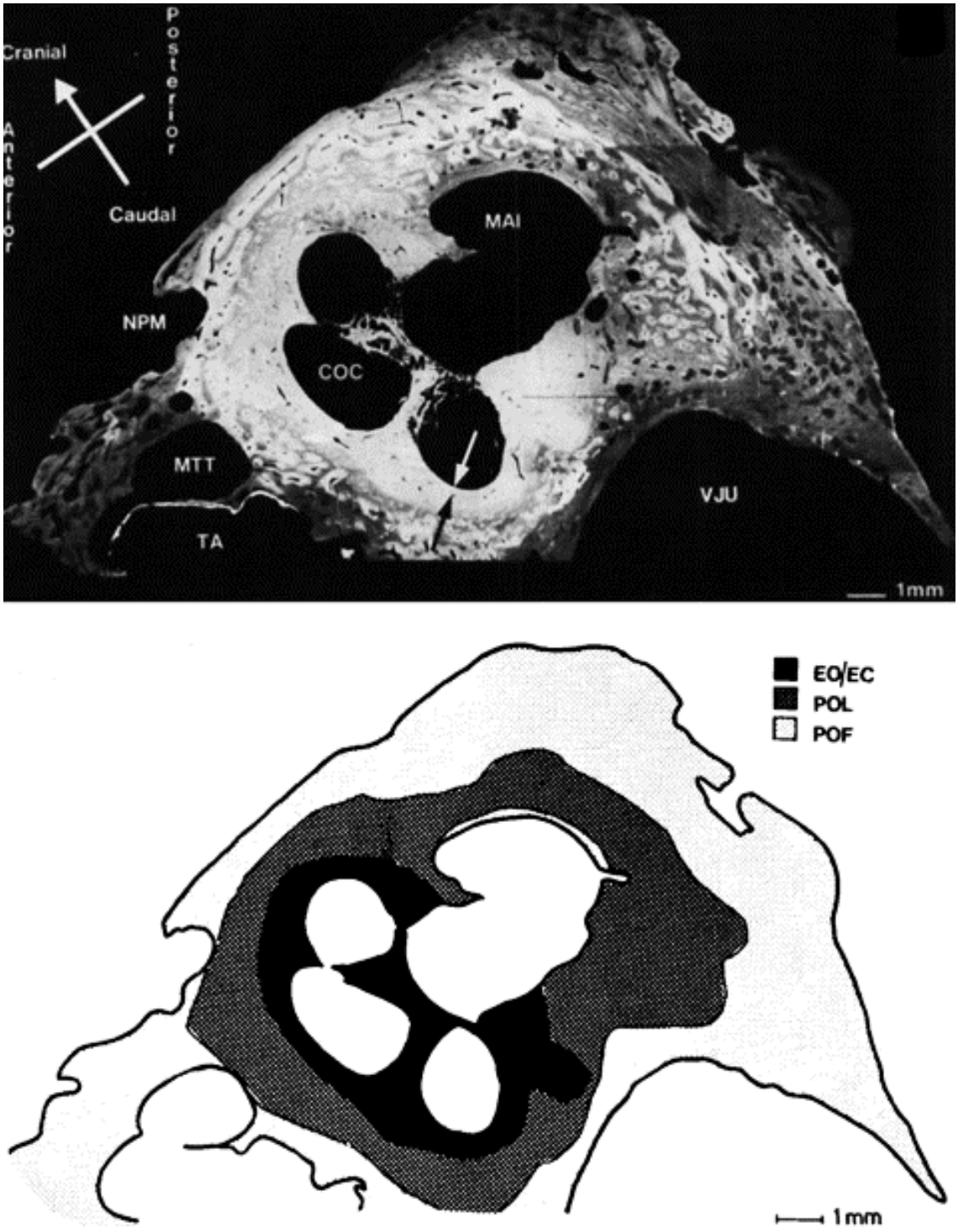

Figure 2.21. Longitudinal section of the left petrous bone of a 74-year-old man within the area of the cochlea microradiogram (top) and schematic distribution of the different tissue layers (bottom). The arrows mark the borders of the endosteal layer. EO=endosteal, POL=inner periosteal layer, POF=outer periosteal layer, COC=cochlea, MAI=internal acoustic meatus (adapted from Doden and Halves 1984).

A lack of remodelling in petrous bone has been noted both in humans (Doden and Halves 1984; Frisch et al. 2000; Jeffery and Spoor 2004) and cetaceans (e.g. de Buffrenil, Dabin and Zylberberg 2004). The high number of viable osteocytes in the inner ear possibly inhibits osteoclast maturation and activation through the secretion of the anti-resorptive osteoprotegerin (OPG) and seems to serve as a pool throughout life (Bloch and Sørensen 2010; Bloch, Kristensen and

Sørensen 2012). Petrous bone's *sui generis* nature is also manifested by three tissue zones that differ compared to long bones (Doden and Halves 1984). These include: a) an outer periosteal; b) an endosteal that surrounds the canals and cochlear surfaces; and c) an inner periosteal that can replace both the outer periosteal and endosteal tissues (**Figure 2.21**).

The outer periosteal tissue is considered less mineralized *in vivo* and has its collagen fibres arranged parallel to the bone's surface (Doden and Halves 1984). Contrariwise, the inner periosteal tissue has randomly oriented collagen fibres and two different degrees of mineralization (Doden and Halves 1984) linked to different concentrations of Ca, P, Sr and Mg (Katić et al. 1991). In dolphins, the collagen matrix is composed of very thin fibrils of 10-30 nm diameter, arranged in a dramatically reduced network compared to normal bone that gives plenty of room to bioapatite crystals, thus increases hardness (de Buffrenil, Dabin and Zylberberg 2004). Such a scenario has been also confirmed by Zioupos et al. (1997) who found increased hardness and Young's modulus in whale's tympanic bulla (c. 83 % mineral) accompanied by low bending strength. As seen in **Figure 2.22**, only the extreme case of the Mesoplodon rostrum (c. 96 % mineral) which is near the endpoint of mineralization process and tooth enamel present higher hardness (Waters 1980). Unfortunately, the mechanical properties of the human petrous bone are still unknown.

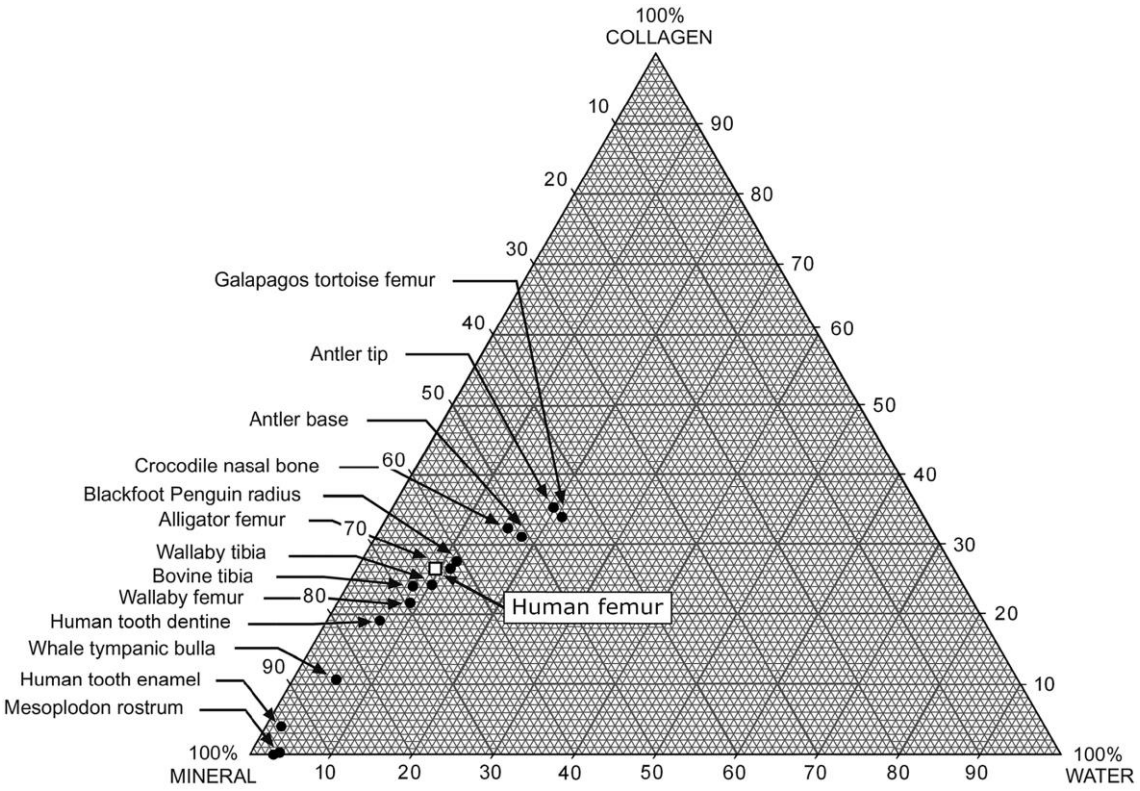

Figure 2.22. Species and skeletal element variation in mineral, organic and water fractions (Kendall et al. 2018).

CHAPTER 3: BONE DIAGENESIS - A REVIEW OF CURRENT RESEARCH

The preservation of biomolecules into archaeological and geological timescales within bone has been the focus of a great number of studies over the past few decades. However, post-mortem degradation of bone is a very complex process and while some bones can be well-preserved, others can rapidly degrade. This chapter reviews the main diagenetic pathways responsible for the post-depositional modifications in bone, a process known as diagenesis. Sections of this chapter have been published in Kendall, C., Eriksen, A. M., Kontopoulos, I., Collins, M. J., and Turner-Walker, G. (2018), Diagenesis of archaeological bone and tooth. *Palaeogeography, palaeoclimatology, palaeoecology,* 491, 21-37. 10.1016/j.palaeo.2017.11.041.

3.1. PRESERVATION OF MICROSTRUCTURE

The use of histology for the study of archaeological bone has changed the way archaeologists and anthropologists interpret osteological data. Histological analysis of thin or thick bone sections can provide valuable information on the age-at-death, pathology, past human lifestyles (e.g. socio-economic groups), distinction between human and non-human and/or burned and unburned bone, and diagenesis (Assis, Santos and Keenleyside 2016; Bell, Skinner and Jones 1996; Blumenschine et al. 2007; Cattaneo et al. 1999; Cuijpers and Lauwerier 2008; De Boer and Maat 2012; Domínguez-Rodrigo and Barba 2006; Garland 1989; Grupe and Garland 1993; Hanson and Cain 2007; Mulhern and Ubelaker 2001; Miszkiewicz and Mahoney 2016; Stout 1978; Stout and Teitelbaum 1976; Turner-Walker and Mays 2008).

Histotaphonomy is the investigation of bone diagenesis at the microstructural level and it is widely applied for the study of the microstructural changes caused by various physical, chemical and biological processes post-mortem (Bell 1990, 2012; Bell and Elkerton 2008; Turner-Walker and Jans 2008). These histomorphological modifications are the product of the attack by bacteria, fungi, presence of algae, collagen degradation, and deterioration of bioapatite (Collins et al. 2002; Hedges 2002). For that reason, bone histology is currently a fundamental method used for the better understanding of the diagenetic histories of skeletal remains (Booth 2016; Booth, Chamberlain and Parker Pearson 2015; Hedges, Millard and Pike 1995; Hollund et al. 2012; Jans et al. 2004; Turner-Walker 2008).

The usefulness of histology for the investigation of microstructural changes present in skeletal remains has been attested by the study of samples from many different environments across the world (Booth 2016; Hollund et al. 2012; Jans et al. 2004; Nielsen-Marsh and Hedges 2000a; Smith et al. 2007). The application of optical microscopy and scanning electron microscopy

(SEM)/backscattered electron (BSE) can provide a wealth of information for the better understanding of histotaphonomy, while transmission electron microscopy (TEM), confocal microscopy and synchrotron micro-computed tomography have been occasionally applied (Ascenzi and Silvestrini 1984; Booth 2016; Fernandez-Jalvo et al. 2010; Hollund et al. 2012; Koon, Nicholson and Collins 2003; 2010; Maggiano et al. 2006; Pesquero et al. 2015; Reiche et al. 2011).

Depending on the nature of the study, preparation of thin sections is usually required (Garland 1989; Grupe and Garland 1993; Turner-Walker and Mays 2008). Preparation of thin sections of embedded specimens in synthetic resin using a microtome or grinder to achieve the desired thickness is the most common methods used in palaeohistology (Booth 2016; Garland 1989; Turner-Walker and Jans 2008). However, some of the reasons palaeohistology remained underdeveloped for several decades is its destructive nature and the fragility of archaeological and fossil bone that make thin sectioning very challenging (Assis, Santos and Keenleyside 2016).

Methodological approaches have significantly improved throughout the last decades and improvements in instrumentation now allows thin sectioning of undecalcified specimens of archaeological origins without embedding them in resins (De Boer and Maat 2012; Kontopoulos, Nystrom and White 2016). Recently, micro-computed tomography (micro-CT) has been proposed as a non-destructive alternative to histology for the examination of post-mortem microstructural changes in archaeological bone (Booth, Redfern and Gowland 2016; Dal Sasso et al. 2014). Nevertheless, micro-CT can be less suitable for the study of bone diagenesis as samples need to be around 1 cm in diameter (less-destructive but not non-destructive) to visualize diagenetic alterations, while there is also a lack of information regarding staining and inclusions (Booth, Redfern and Gowland 2016).

3.1.1. MICROBIAL ACTIVITY, GENERALIZED DESTRUCTION, CRACKING, INCLUSIONS

Microbial activity is commonly identified in archaeological bone (Jans et al. 2004) and it is manifested by microscopic focal destruction (MFD) sites consisted of foci either rounded, branched or interlinked that vary from few microns to hundreds of microns in diameter (Bell 1990; Garland 1989; Hackett 1981). The different types of microbial attack have been successfully presented by Hackett (1981) who provided the first description of MFD and introduced a qualitative method for the evaluation and classification of the microstructural alterations observed in bone (**Figure 3.1**). These include one type of fungal tunnelling (i.e. Wedl), and three types of bacterial tunnelling (i.e. non-Wedl): a) linear longitudinal; b) budded; and c) lamellate) based on the shape, size, abundance, distribution, demineralization, and mineral redeposition/cuffing (Hackett 1981). Although distinction between the different types of bacterial tunnelling is often possible, occasionally categorizing tunnels can be challenging due to the

gradual progression of modifications (Hackett 1981; Pesquero et al. 2015) and similarities with pathological modifications in bone microstructure (Bell 1990; Piepenbrink 1986).

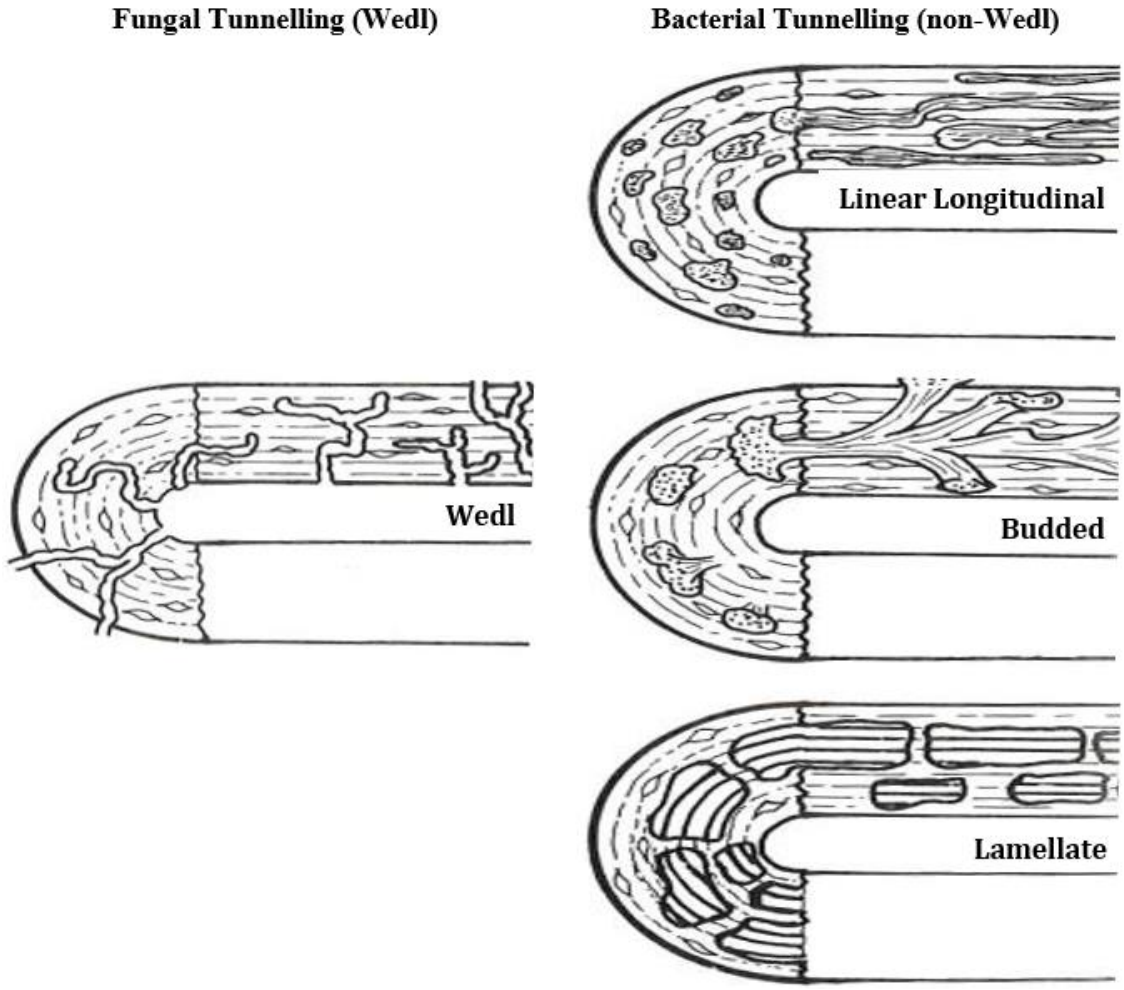

Figure 3.1. *Types of microbial tunnelling* – Schematic representation of MFD at the transverse (semicircle) and longitudinal (rectangle) levels (adapted from Hackett 1981).

Wedl tunnels are considered to be produced by the lytic action of fungi (Bell 1990; Hackett 1981; Marchiafava, Bonucci and Ascenzi 1974; Wedl 1864). Although the way fungi produce tunnelling is not clear, the attack of the inorganic and organic content of bone by enzymes located inside and outside the fungus membrane is the most likely scenario (Marchiafava, Bonucci and Ascenzi 1974). In transverse bone sections, these appear as branched, almost empty canals of 5-10 μm in diameter (**Figure 3.1**; Hackett 1981). Fungal action is not accompanied by remineralization around the edges of the foci (i.e. no cuffing) and it often has ill-defined outline under plane polarized light (**Figure 3.2**; Hackett 1981).

The histological analysis of fragments of human vertebrae, autoclaved fragments (i.e. 100 or 200 for 20 min.) of human vertebrae and rat bone fragments buried in flower pots with garden soil for 45 days at 20° C, has shown that fungi of the *mucor* species can be responsible for microboring of bone to utilize the tissue for energy (Marchiafava, Bonucci and Ascenzi 1974). The process that Marchiafava et al. (1974) followed, however, may have altered the mineral-protein bond and

may have resulted in a bone more susceptible to microbial attack (Turner-Walker 2012). Furthermore, it is not clear which specimens displayed these modifications and there are no accompanying images to show their appearance and characteristics (Turner-Walker 2012). Further studies have also identified other species such as *Ascomycota*, *Chytridiomycota*, *Stachybotrys*, *Crysosporium*, and *Cladosporium* that can dissolve and degrade the bone tissue (Keenan, Engel and Elsey 2013; Piepenbrink 1989), although their amount can vary significantly in different skeletal elements (Keenan, Engel and Elsey 2013).

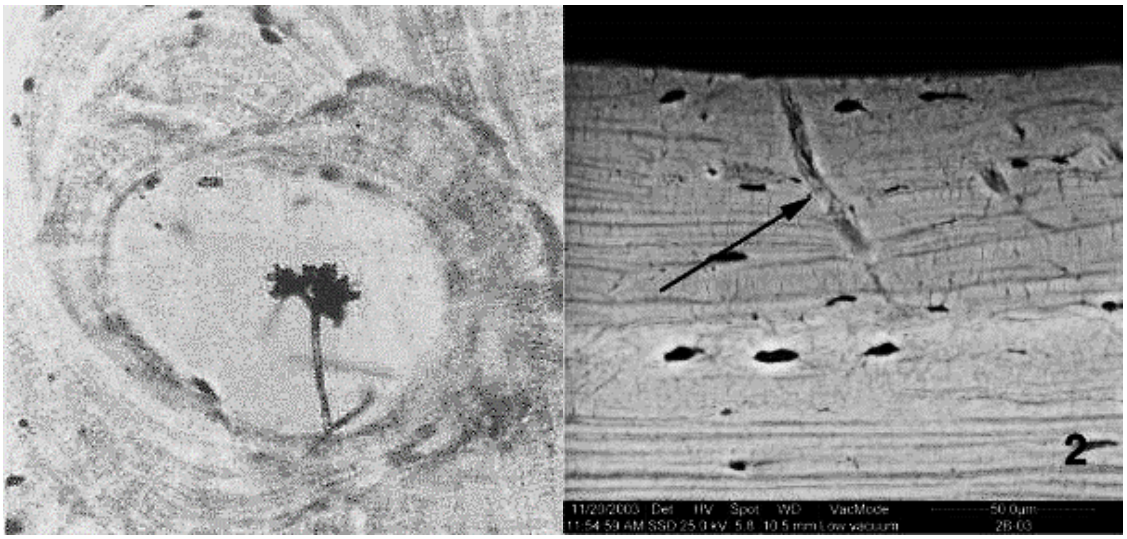

Figure 3.2. *Fungal tunnelling* – **Left**: Thin section of a human femur exhibiting Wedl tunnelling after inoculation with *Stachybotrys* (Piepenbrink, 1989). **Right**: SEM microphotograph showing fungal attack (black arrow) with tunnels penetrating the bone from the periosteal surface (Fernandez-Jalvo et al. 2010).

Regarding bacterial (non-Wedl) tunnelling in transverse sections, the majority of the MFD are usually in the form of linear longitudinal and budded tunnelling, and only a small number demonstrates lamellate (Jans et al. 2004). Linear longitudinal tunnels appear as small rounded opaque foci ranging from 5-10 μm to 50 μm in diameter, while budded tunnels appear as dark frond-like tunnels around 30 μm or wider (**Figure 3.3**; Hackett 1981). A hypermineralized tissue (or cuffing) characterized by increased Ca and P concentrations (Pesquero et al. 2015) usually surrounds these foci (**Figure 3.3**). This is formed through redeposition of mineral and waste products by the micro-organisms which create these foci (Hackett 1981; Garland 1989). It usually ranges from 3 to 6 μm, surrounding mostly the smaller non-Wedl MFD, and when present, it usually inhibits further expansion of the MFD (Hackett 1981).

Linear-longitudinal and budded tunnels are usually found inside osteons and their expansion outside the osteon is also hindered by the presence of the cement line (Hackett 1981). Cement lines usually remain distinct, except in cases where degradation is very advanced (Hanson and Buikstra 1987). Although small areas of unaltered bone can be found next to bacterial degraded areas that are surrounded by hyper-mineralized rims (**Figure 3.3**), tunnels do not enter the area of another tunnel, regardless the density of MFD which can vary even within small regions of bone

tissue (Hackett 1981; Jackes et al. 2001; Piepenbrink 1986). Both types create branched tunnels parallel to each other that travel for few hundreds of microns along the longitudinal axis of bone (**Figure 3.3**; Jackes et al. 2001; Kontopoulos, Nystrom and White 2016), and this indicates that bacteria follow the orientation of the collagen fibres in different parts of the bone to exploit weak, less mineralized tissues (Turner-Walker 2008).

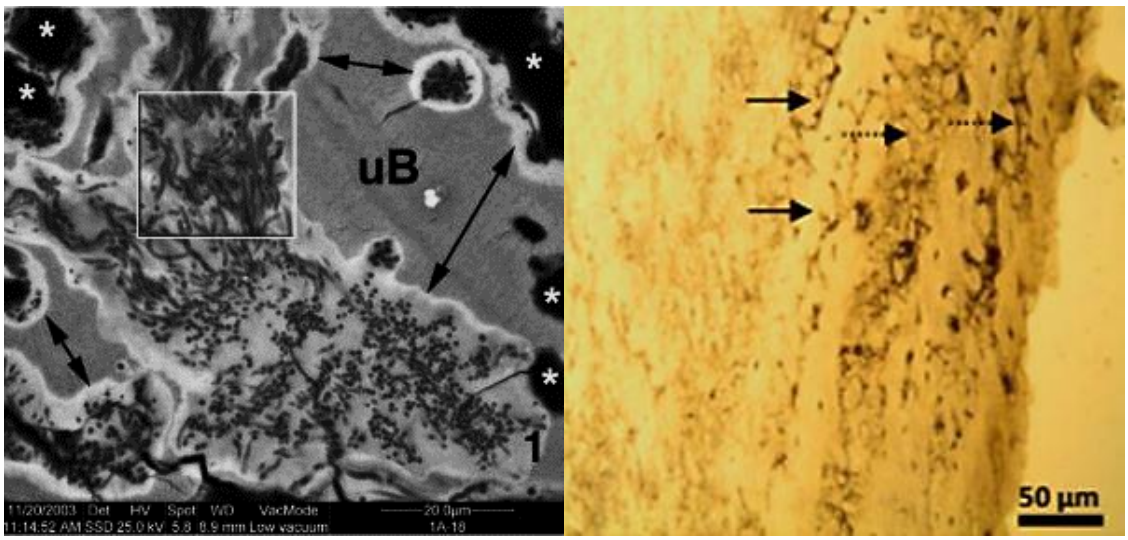

Figure 3.3. **Left image** - *Non-Wedl MFD and hypermineralized rims*: Bacterial colonies in adult sheep's tibia characterized by small pores of 0.1-2 µm in diameter surrounded by cuffing (double-headed black arrows) next to unaffected bone (uB). Black holes (white asterisks) represent non-Wedl MFD (Fernandez-Jalvo et al. 2010).
Right image - *Linear Longitudinal and Budded foci* – Longitudinal section of *sus scrofa* bone with linear longitudinal (black arrow) and budded (dotted black arrows) tunnels travelling along the longitudinal axis in the periosteal/sub-periosteal area. Some dark inclusions within the tunnels observed (Kontopoulos, Nystrom and White 2016).

Lamellate foci are large tunnels that can even reach a size of 60 µm x 250 µm in transverse sections, and contrary to the other two non-Wedl tunnels they can cross the cement lines of the osteons (Hackett 1981). They are produced by denaturing alternate lamellae which often makes difficult the distinction of different foci (Hackett 1981). They are visible in plane polarized light mainly as bright features, whereas in cross-polarized images the birefringent rims surrounding the lamellate foci can be seen due to the survival of collagen fibres (**Figure 3.4**; Hackett 1981). The rims usually disappear when the foci increase in size from mono-lamellate to poly-lamellate, although cuffing may be displayed in some specimens (Hackett 1981). Lamellate tunnelling is usually observed in samples that come from large and densely occupied cemeteries (Jans et al. 2004), and they frequently demonstrate a mosaic pattern (**Figure 3.4**) when packed (Hackett 1981). In longitudinal sections, a similar to transverse rectangular appearance is observed outlined by the rims (Hackett 1981).

The inoculation and incubation of bone specimens with different bacterial colonies (e.g. *Bacillus subtilis, Pseudomonas fluorescens, Clostridium sporogens, pefringens and septicum*) has proved that MFD are the product of the activity of certain bacterial species (Balzer et al. 1997; Jackes et

al. 2001). Specimens incubated with *P. intermedia*, *C. perfringens* and *C. septicum* demonstrated no histological changes, contrariwise to specimens with *C. sporogens* or *C. histolyticum* (Dixon, Dawson and Taylor 2008; Jackes et al. 2001), while *Proteobacteria* (20-35%), *Actinobacteria* (2-11%), *Bacteroidetes* (2-11%) and *Firmicutes* (1-10%) have been recognized in the bacterial communities, although many intra-individual variations may exist (Keenan, Engel and Elsey 2013). The different bacterial species cause different modifications, but they all excrete collagenases to digest the bone organic matter (Jackes et al. 2001).

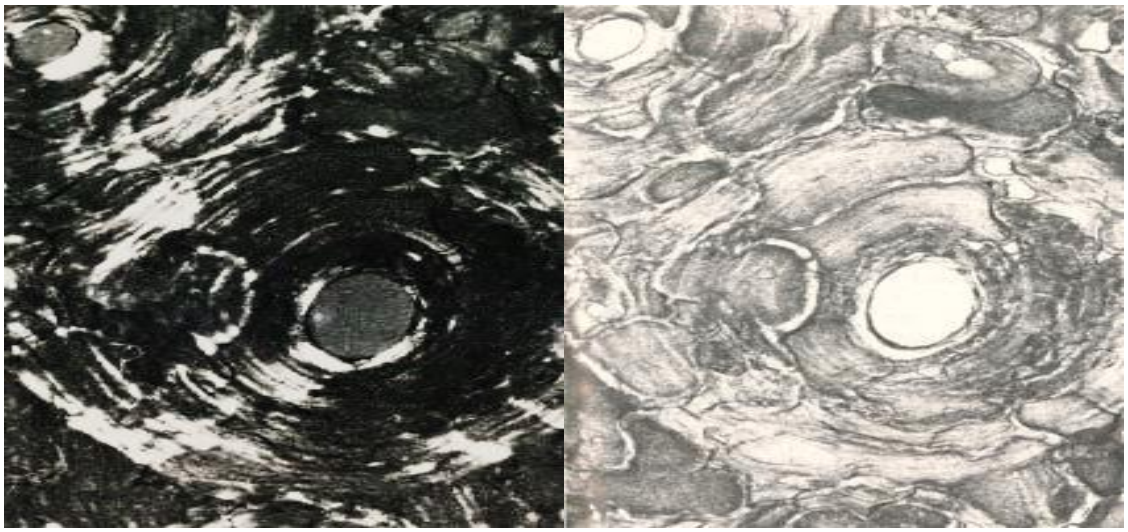

Figure 3.4. *Lamellate foci* – The characteristic mosaic pattern observed in plane polarized light (left) and survival of birefringence in some areas of the section (right) (adapted from Hackett 1981).

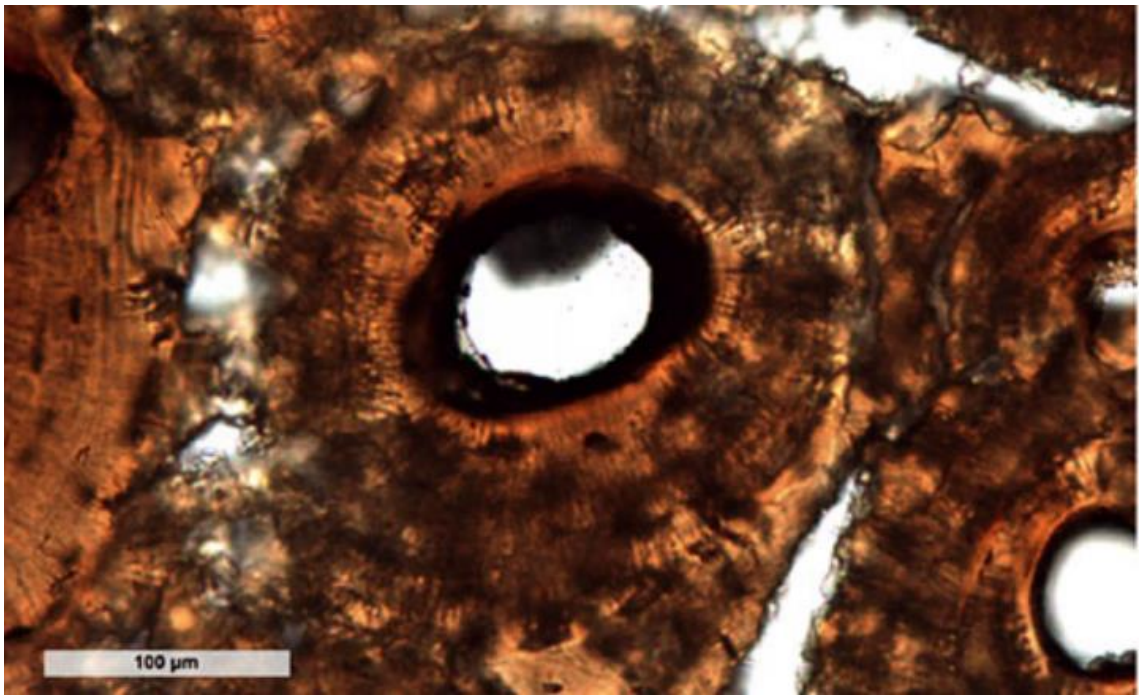

Figure 3.5. *Generalized destruction* – Bone micro-morphology displays an amorphous appearance and cracks with no features such as lamellae and osteocyte lacunae retained (Tjelldén et al. 2018).

Generalized destruction (**Figure 3.5**) is opposed to focal destruction and represents the degradation of extended areas of bone tissue that do not retain any histological features (Garland 1989). Bone appears amorphous (e.g. no lamellae) and the sections as disintegrated, dark areas under plane polarized light, even though some morphological features might be still recognized (Garland 1989). In crossed polarized light, there is considerable reduction in birefringence in the amorphous areas (Garland 1989). This loss of the histological features and the reduced birefringence in generalized destruction areas is assumed to be caused due to the loss of the organic content (Collins et al. 2002; Jackes et al. 2001; Tjelldén et al. 2018).

Other features can be classified into inclusions and infiltrations (Garland 1989). Archaeological bone may be filled with detrital or other exogenous material that penetrates the pores and trabecular spaces (Bodzioch and Kowal-Linka 2012). Inclusions are described as exogenous material incorporated into the bone spaces (Haversian canals, osteocyte lacunae, canaliculi or trabecular bone) and are distinguished into biological (e.g. fungi, hyphae, bacteria) and mineral inclusions (Garland 1989). Similarly, infiltrations may replace osseous material, and these can be identified as stained sites with granular appearance (Garland 1989). Generally, stained bone tissues from humic acids or other exogenous material are considered resistant to microbial attack, although they usually display reduced birefringence (Hedges 2002; Hollund et al. 2012).

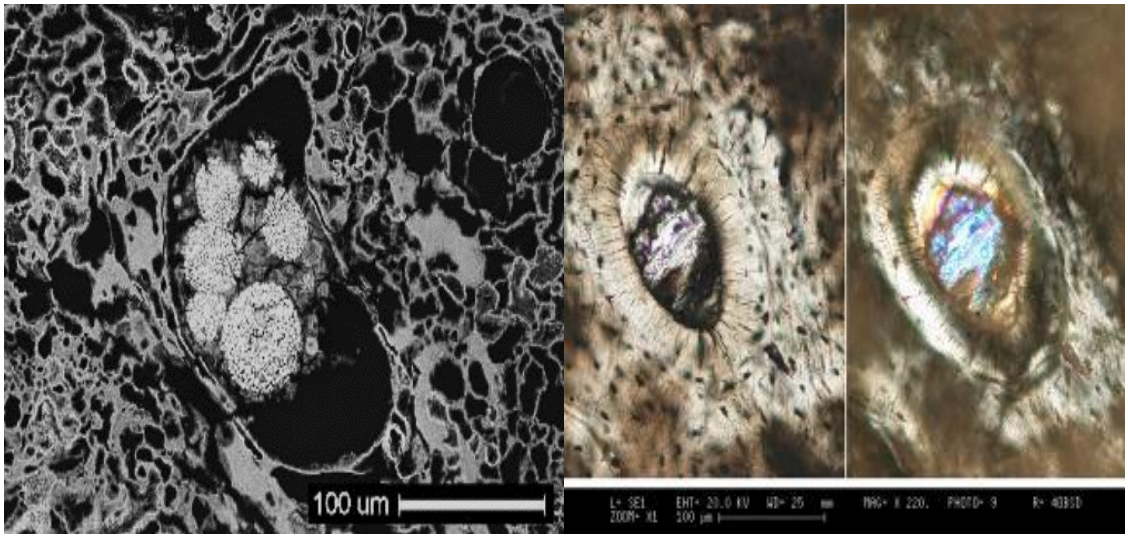

Figure 3.6. *Inclusions* – SEM images of framboidal pyrite in pore spaces (left; Turner-Walker 2008) and magnesium phosphate inclusions in Haversian canals (right; Zangarini, Trombino and Cattaneo 2016).

Iron-rich inclusions (e.g. framboidal pyrite) have been documented in bone as 1-10 μm spherical aggregates that gradually develop to massive, crystalline pyrite (**Figure 3.6**; Hollund et al. 2012; Pesquero et al. 2015; Pfretzschner 2004; Turner-Walker 1999). They primarily fill up osteocyte lacunae and canaliculi without damaging the bone, while at the same time they can block the path to other exogenous substances (Pfretzschner 2004; Turner-Walker 1999). Early diagenetic pyrite can be also found in Haversian canals but usually, it does not fill the whole cross section due to

the larger volume of these cavities (Pfretzschner 2004). Iron oxides are also probably responsible for the orange/brown staining observed in the surrounding areas (Bodzioch and Kowal-Linka 2012; Hollund et al. 2012).

Magnesium phosphate crystallizations can be observed within bone Haversian canals or fissures (**Figure 3.6**) as early as few weeks post-mortem probably due to the permeation of the soft tissue decomposition fluids (Zangarini, Trombino and Cattaneo 2016). Metal oxides and sulphur trioxide may also be noticed in subsequent early diagenetic stages following soft tissue decomposition (Zangarini, Trombino and Cattaneo 2016). This inclusion may colour bone tissues violet-blue and are considered as evidence of early vivianite formation in bone buried in anoxic or organic rich environments (Zangarini, Trombino and Cattaneo 2016).

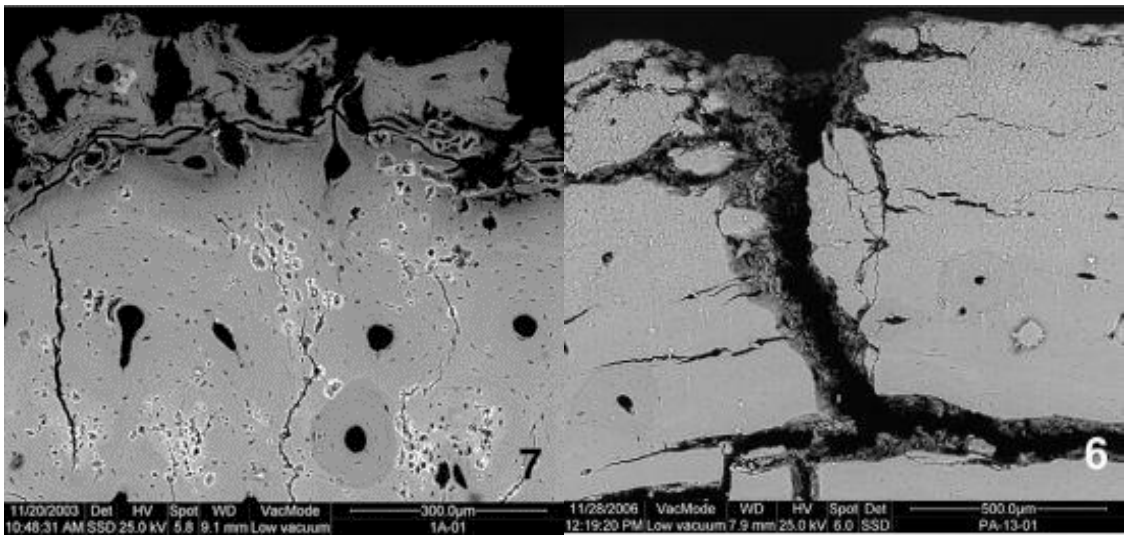

Figure 3.7. *Cracking* – SEM microphotographs of bone sections mounted in resin and polished. Sheep's tibia showing micro-cracking (left) and radio-ulna displaying cracking and micro-cracking (right). The latter specimen was covered by moss and lichen that penetrated the bone (Fernandez-Jalvo et al. 2010).

Manganese oxides can also occupy the open spaces (i.e. canaliculi, osteocyte lacunae and cracks) in bone since early diagenetic stages, while calcite usually precipitates in later diagenetic stages (Dal Sasso et al. 2014; Hollund et al. 2012; Pfretzschner 2004). This assumption was based on observations which shows manganese oxides adhering to the surfaces of the spaces and calcite filling the remaining areas, although pyrolusite (MnO_2) has also been recognized in fossilized dinosaur bones from China (Dal Sasso et al. 2014; Pfretzschner and Tütken 2011).

Cracks and micro-cracks play an important role in bone diagenesis by opening new pathways through the bone matrix (**Figure 3.7**) that increase the leaching of the already degraded collagen and enhance the exchange of ions between water and bioapatite crystals (Pfretzschner 2004). They can be observed in samples covered by moss, algae or lichens as they use microstructural features to penetrate the bone tissue (Fernandez-Jalvo et al. 2010). Cracking close or within osteons relate to changes in density, collagen degradation and mineral dissolution, and they may appear even in

early diagenetic stages (Bell 1990; Pfretzschner and Tütken 2011). Radial micro-cracks (**Figure 3.8B**) that cross the osteon boundaries due to water uptake and swelling can be observed in secondary osteons of specimens buried in aquatic environments (Pfretzschner and Tütken 2011).

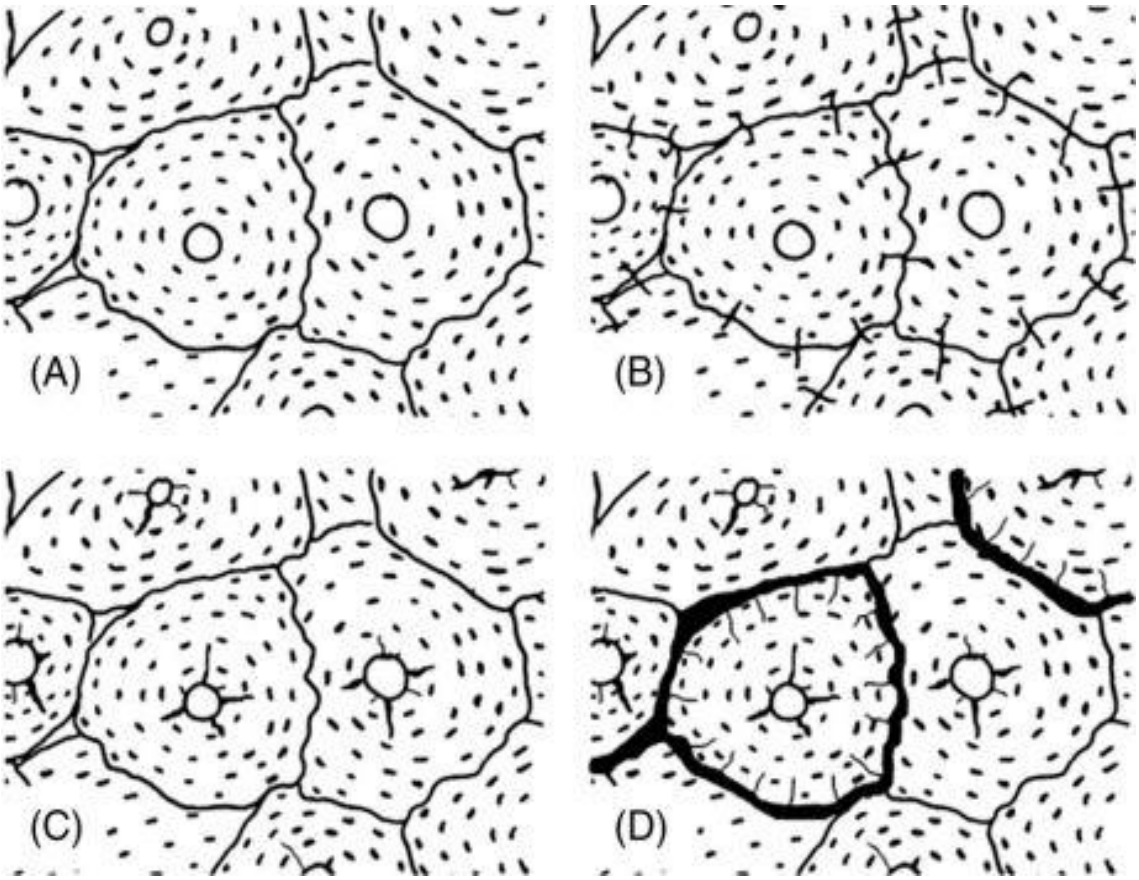

Figure 3.8. *Microcracking types* – Schematic representation of the different microcracking types observed in archaeological and fossil bone: (A) normal bone, (B) radial, (C) central, and (D) peripheral microcracks (Pfretzschner and Tütken 2011).

Desiccation can also lead to cracking as collagen loses water which results to a volume decrease that causes shrinkage and eventually cracking (Pfretzschner and Tütken 2011). Cracks may appear on the walls of Haversian canals and radiate outwards for short distances (i.e. central cracks) or they might be observed at the inner side of cement lines in secondary osteons (i.e. peripheral cracks) without spreading outside osteonal margins though (**Figure 3.8C-D**; Pfretzschner and Tütken 2011). Cracking can also be attributed to physical stresses during sample preparation, e.g. grinding, thin-sectioning, high vacuum of the SEM or even storage (Dal Sasso et al. 2014; Turner-Walker 2012; Lander, Brits and Hosie 2014).

3.1.2. HISTOLOGICAL INDICES

The Oxford Histological Index (OHI) was coined by Hedges, Millard and Pike (1995) for the quantification of the histological changes in archaeological bone using optical microscopy (i.e. plane polarized light) and/or SEM/BSE. It categorizes specimens into six groups (**Figure 3.9**)

based on their percentage of intact histology and the presence of MFD (Hedges, Millard and Pike 1995). Very well-preserved bone should display microstructural features such as lamellae, osteocytes, canaliculi and Haversian canals at least across 95% of a section to be assigned an OHI value of 5 (**Figure 3.10**; Hedges, Millard and Pike 1995). Conversely, all these features should be absent across the 95% of a section (**Figure 3.10**) to be characterized as poorly preserved and receive an OHI value of 0 (Hedges, Millard and Pike 1995).

Millard (2001, p.640)

Index	Approx. % of intact bone	Description
0	<5	No original features identifiable, except that Haversian canals may be present
1	<15	Haversian canals present, small areas of well-preserved bone, or lamellar structure is preserved by the pattern of destructive foci
2	<50	Some lamellate structure is preserved between destructive foci
3	>50	Some osteocyte lacunae preserved
4	>85	Bone is fairly well preserved, with minor amounts of destructive foci
5	>95	Very well preserved, virtually indistinguishable from fresh bone

Figure 3.9. The OHI as modified by Millard (2001) to include the 33-67% range which was overlooked in Hedges, Millard and Pike (1995).

The OHI is the primary tool used for the quantitative assessment of histological sections for the study of bone diagenesis (Booth, Redfern and Gowland 2016; Jans et al. 2004; Nielsen-Marsh and Hedges 2000a; Smith et al. 2007), while the general histological index (GHI) introduced by Hollund et al. (2012) can be used as analogous to the OHI as described by Millard (2001). The latter includes generalized destruction, cracking, and staining in the assessment (Hollund et al. 2012). However, limitations of both indices include the difficulty to estimate the degree of alterations on a spatial scale larger than this of the field of view and the inter-observer error (Hedges, Millard and Pike 1995).

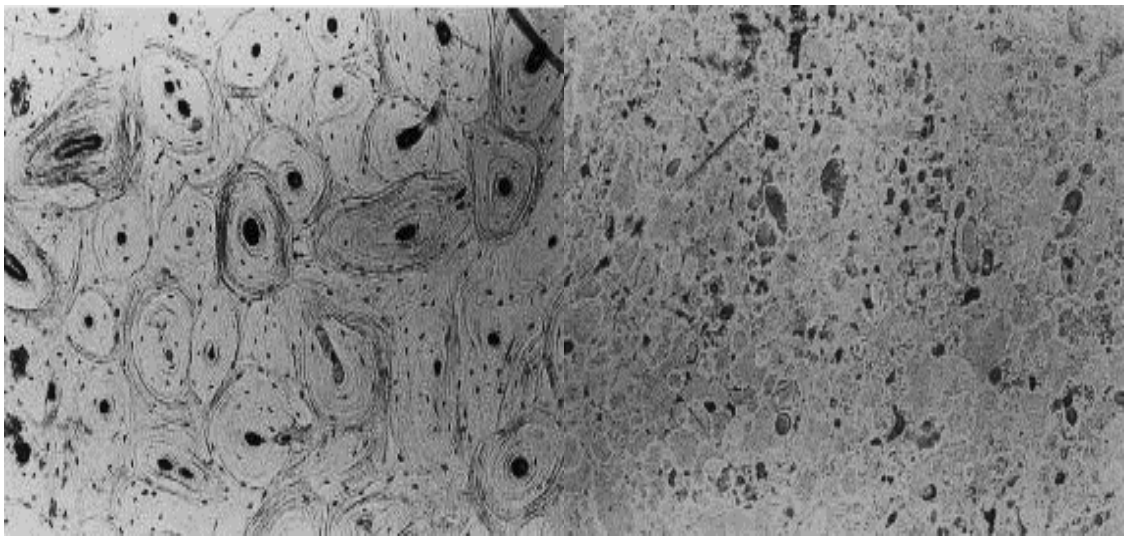

Figure 3.10. *OHI Classification* – Images of specimens showing an OHI value of 5 with very good preservation, virtually indistinguishable from fresh bone (left) and an OHI value of 0 with no original features identifiable (right) (Hedges, Millard and Pike 1995).

Additionally, although the unaltered regions of bone with an OHI value of 4 or 5 are assumed to contain well-preserved collagen, specimens displaying extensive microbial attack may retain variable quantities of collagen which makes OHI usually a poor predictor of collagen preservation (e.g. Hedges, Millard and Pike 1995; Smith et al. 2007). Bone can preserve its histological integrity without preserving its collagen content which is an indication of protein loss due to hydrolysis (Collins et al. 2002; Hedges, Millard and Pike 1995). The 'Apigliano style degradation' is such an atypical diagenetic pattern, for instance, is characterized by such a loss of collagen but no microbial attack accompanied by increased crystallinity, resembling fossilization (Jans et al. 2004; Smith et al. 2002). Preservation of small areas of bone within a poorly-preserved specimen could also potentially explain the often weak OHI-collagen relationship.

The relationship between histological and endogenous DNA preservation in archaeological bone although claimed strong by Hollund et al. (2016) the low number of samples examined in this study hinders further assumptions. Additionally, the relationship between OHI-DNA in the outer and middle cortical areas within the same specimens was actually weak (R^2=0.35), and samples that displayed an OHI of 5 had endogenous DNA percentages varying from 31.71 to 0.64. Thus, it is obvious that there was neither strong relationship nor pattern identified by Hollund et al. (2016).

A different approach for the assessment of collagen preservation in bone can be the collagen birefringence (**Figure 3.11**; Garland 1989). For the quantification of birefringence, Jans et al. (2002) introduced the Birefringence Index (BI) which classifies samples based on the intensity of birefringence into three categories (i.e. in normal=1, reduced=0.5 and absent=0). While theoretically a combined use of the OHI and BI can make histological data comparable, practically BI has little to offer as all samples that display collagen degradation to some extent receive a BI value of 0.5. This issue does not allow an accurate evaluation of histological preservation and its relationship with the surviving biomolecules. Further, it cannot be used to estimate the % collagen retained and the degree of alterations of the bioapatite crystals as in Jans et al. (2002).

Jans et al. (2002) also introduced the Cracking Index (CI) for the quantification of micro-fissures in bone sections under plane polarized images by counting the osteons with and without fissures (Jans et al. 2002). This approach has similar limitations with the OHI as it is difficult to assess the changes on a spatial scale larger than this of the field of view. However, OHI shows linear relationship with small porosity (0.01-0.1 μm) and cracking, and inverse relationship with medium porosity (0.11-8.5 μm) are considered typical effects of microbial activity (Hedges, Millard and Pike 1995; Smith et al. 2007), while it shows no correlation with macroscopic preservation (e.g. Kontopoulos, Nystrom and White 2016).

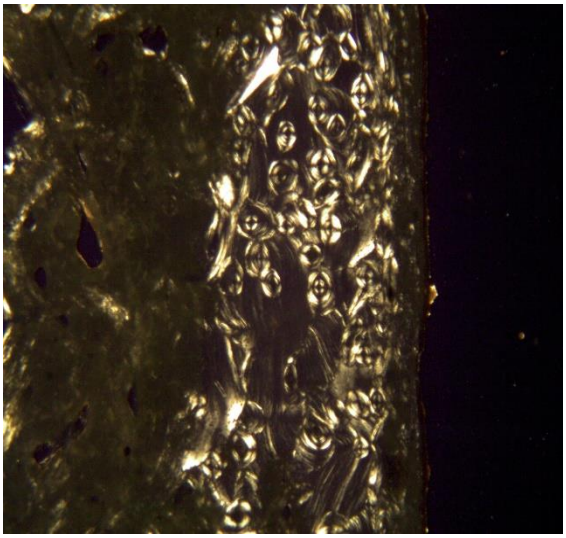

Figure 3.11. *Collagen Birefringence* – Cross polarized image of a thin section from a human tibia displaying areas with normal (white) and reduced (dark) birefringence (taken by the author).

3.1.3. ORIGINS AND PROGRESSION OF MICROBIAL ACTIVITY

One of the main problems in histotaphonomy is to understand if the microstructural alterations are the result of one single, early diagenetic event or diachronic. Microbial attack is assumed to start with few discrete foci (**Figure 3.12**; i.e. enlarged osteocyte lacunae) that gradually merge to form larger foci, and in later stages MFD can cover even the entire cross section (Bell, Skinner and Jones 1996; Hanson and Buikstra 1987; Kontopoulos, Nystrom and White 2016; White and Booth 2014). Nevertheless, the origins of bacteria responsible for the histological alterations is still on debate (Bell 2012; Kendall et al. 2018). Gut bacteria, which are probably formed at or soon after birth, could certainly be the cause of those initial modifications as they can transmigrate via the vascular network to all major internal organs within few hours after death depending on the environment (Bell, Skinner and Jones 1996; Booth 2016; Booth and Madgwick 2016; Hollund et al. 2012; White and Booth 2014). In such case, bacterial attack in archaeological bone would be predominantly related with soft tissue decomposition (Bell 2012; Booth 2016; White and Booth 2014).

The presence of linear longitudinal and budded tunnels in a 1-1.5 Ma hominin mandible from a palaeokarst cave in Swartkrans (South Africa) represents one of the earliest evidences of MFD (Grine et al. 2015). The fact that MFD were mainly concentrated around Haversian canals closer to the endosteal area led Grine et al. (2015) to the assumption that it was at least partially intact after death and microbial attack originated from the endogenous bacterial populations (Grine et al. 2015). Booth, Redfern and Gowland (2016) have also argued that the limited bioerosion in approximately half of the Romano-British neonatal femora examined should be considered as evidence of undeveloped gut microbial communities and this evidence could be used for the discrimination between stillborn from short-lived infants. Indeed, this observation would be important for the study of demography, funerary treatments and infanticide in the archaeological

record (Booth, Redfern and Gowland 2016); however, the number of individuals examined in this study is very small to allow any further assumptions. Furthermore, only two neonatal specimens displayed well-preserved histological structure with an OHI of 5 compared to three stillborn/preterm infants, while one stillborn/preterm infant and one neonatal specimen exhibited an OHI of 0 (Booth, Redfern and Gowland 2016). Additional evidence on possible differences in histological preservation between disarticulated and articulated skeletal remains that could support a gut origin of microbial attack is poor as preservation can be variable (Booth and Madgwick 2016).

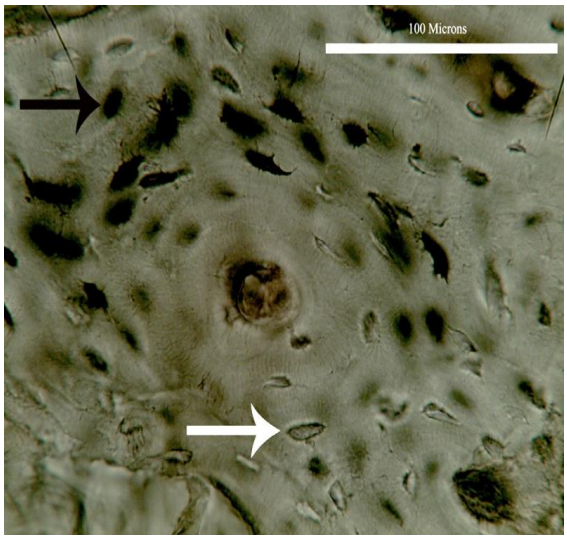

Figure 3.12. *Initiation of microbial attack* – Plane polarized image of a human femoral thin section from Riseholme at one-year post-mortem displaying enlarged osteocyte lacunae (black arrow) and typical osteocyte lacunae (white arrow) that possibly shows early microbial activity (White and Booth 2014).

Currently, only some differences between human and animal bones with respect to the presence of bacterial activity (Jans et al. 2004) could be considered as an attestation of the relationship between MFD and anaerobic gut bacteria. The rationale behind this relationship is that dismemberment and/or defleshing can limit exposure of animal bones to putrefaction and prevent them from the endogenous gut bacteria (Jans et al. 2004). However, the histological analysis of a small number of animal specimens (goat, pig, bovine) from the 13th-15th century site of Hôtel de Mongelas in Paris (France) which were probably food waste as suggested by the cut marks (i.e. no endogenous microbiota available for micro-boring) clearly showed that the defleshed animal bones can clearly contain MFD (Müller et al. 2011).

Therefore, a diametrically opposite theory to gut microbiota-MFD relationship supports an initiation of microbial attack at the point of, or after skeletonization by soil microorganisms who can access bone through the empty Haversian canals and attack its endosteal and periosteal areas (Bell, Skinner and Jones 1996; Hackett 1981; Turner-Walker 2008). Hedges (2002) argues that there is little evidence to suggest a difference in histological preservation in fleshed vs de-fleshed bone or cooked vs uncooked bone. A comparative study performed by Nielsen-Marsh and Hedges

(2000a) on human and animal bones for the effects of differential treatment (e.g. fleshed human vs defleshed animal bones, cooking) indicated that there is no significant variation in histological preservation between those two groups oppositely to Jans et al. (2004) and Booth and Madgwick (2016) arguments. Regarding boiling, it causes no alterations in microstructure although protein loss and crystallinity increase have been noted (Roberts et al. 2002). The loss of organic content could thus make animal remains less attractive to soil microbes (Roberts et al. 2002).

Histological examination of bones from approximately 100 animal carcasses exposed on the ground surface during a 30-year long experiment in Neuadd (Wales) demonstrated that MFD, when present, were mostly found across periosteal and endosteal areas (thus soil bacteria) but not associated with vascular canals (Fernandez-Jalvo et al. 2010). Recent experimental studies with pig carcasses showed that there is a relationship between osteocyte lacunae, canaliculi, and bacterial activity during early diagenetic stages which could possibly explain such an appearance of MFD in different areas of bone not close to Haversian canals (White and Booth 2014). Lastly, the association between skeletal elements and their proximity to internal organs was only observed for the ilium and the atlas (i.e. gut and brain, respectively; Kontopoulos, Nystrom and White 2016).

With reference to chronological age, this seems not to be strongly related to histological preservation as prehistoric samples can be better preserved than historical specimens, while samples from the same chronological period and site may display highly variable diagenetic alterations (Booth 2016; Jans et al. 2002, 2004; Turner-Walker 2008). This assumption is also based on the analysis of 8-40 ka old specimens that showed no relationship between histological preservation and time post-mortem (Hedges, Millard and Pike 1995). Moreover, several forensic specimens from terrestrial burial environments which were examined by Bell et al. (1996) ranging from 1 to 83 years post-mortem have shown no relationship between microbial attack and post-mortem intervals. Additional evidence from the microscopic examination of a set of human skeletal remains from twenty court cases found in different places (open air, buried, indoors) and burial environments (inside metal boxes or bags, scattered or buried) by Cappella et al. (2015) also supports the absence of such a relationship between histological integrity and post-mortem interval. The distinction between archaeological and forensic bones using microscopic analysis was very challenging, even though the different cases were radiocarbon dated with dates ranging from post-1950 to around AD 1000 (Cappella et al. 2015).

Regarding the time span of microbial activity within bone, it is believed that probably most microstructural modifications occur during the first 500 years post-mortem (Hedges, Millard and Pike 1995; Hedges 2002; Pfretzschner 2004). It is likely that microstructure is not further affected in specimens of few thousand years old, while histological alteration is also likely to go towards completion when it starts (Hedges, Millard and Pike 1995; Hedges 2002). However, bacterial

attack may just stop before affecting the whole bone as seen in experimental (Fernandez-Jalvo et al. 2010) and fossil bone (Grine et al. 2015). The histological examination of a c. 1.5-1.0 Ma hominin mandible from a palaeokarst cave in Swartkrans, South Africa represents an important example of MFD in the palaeontological record with linear longitudinal and budded tunnels that did not expand throughout the bone (Grine et al. 2015). Trueman and Martill (2002) have also argued that any skeletal remains attacked by microbes have limited or no chances to survive in the fossil record. This argument, however, has been discarded by Iliopoulos (2004) who presented some SEM-BSE images of fossil bones from Greece (Upper Miocene) which were extensively bioeroded but survived in the fossil record.

Overall, the initiation and expansion of microbial attack depends upon the access to bone collagen which requires increased porosity and demineralization of bone tissues (Hackett 1981; Hedges 2002; Turner-Walker 2008). The role of vascular canals, osteocyte lacunae and canaliculi in the spread of bacteria and fungi during diagenesis is undeniable (Bell 1990; White and Booth 2014; Yoshino et al. 1991). Experiments on the effects of body decomposition on bone histology have revealed that a spread of bacteria (endogenous and/or exogenous) in early diagenetic stages occurs through vascular canals, canaliculi and osteocyte lacunae (Kontopoulos, Nystrom and White 2016; White and Booth 2014; Yoshino et al. 1991). These bacterial species merge osteocyte lacunae to gradually create larger foci (i.e. linear longitudinal canals and budded). Identifying the species responsible for each MFD type and distinguishing between soil and gut bacteria is not possible at the moment (Bell 2012; Piepenbrink 1989). Consequently, as Garland (1989) highlights, there is a need for further investigations of the unknown effects of soft tissue decomposition, desiccation, and adipocere formation on bone degradation.

3.1.4. BURIAL ENVIRONMENT AND BURIAL PRACTICES

The effects of the burial environment (e.g. oxygen availability, temperature, groundwater, and pH) on the histological integrity of archaeological bone has been noted by several researchers (Bell, Skinner and Jones 1996; Fernandez-Jalvo et al. 2010; Jans et al. 2002; Nielsen-Marsh and Hedges 2000a; Turner-Walker 1999). Thus, the beginning and progression of tunnelling may vary significantly for each specimen, primarily because of the specific conditions of the burial environment and the changes throughout the centuries caused by human or natural processes (Hackett 1981; Turner-Walker 2008; Turner-Walker and Jans 2008).

Skeletonised remains in the tropics degrade much more rapidly than those in temperate zones, which in turn degrade more rapidly than those close to the arctic circle (Fernandez-Jalvo et al. 2010; Kendall et al. 2018). Similarly, deeply buried bones tend to survive for longer than those in shallow burial environments. Part of this is because of temperature but also because oxygen availability, as the soil bacteria responsible for tunnelling in buried bones are evidently aerobic

in their metabolic pathways (Turner-Walker 2008; Turner-Walker and Jans 2008). Water availability and movement within the soil has the most significant effect on the preservation of bone as it controls chemical reactions and microbial metabolism (Hedges, Millard and Pike 1995; Turner-Walker 2008). Specimens recovered from permanently waterlogged environments (anoxic), cave sites and dry sandy deposits above water table demonstrate good histological preservation with limited or no microbial activity (Booth 2016; Hedges 2002; Nielsen-Marsh and Hedges 2000a; Turner-Walker 2008). In contrast, specimens from sites with fluctuations in soil water (e.g. limestone soils, floodplains, coastal sites and sites on river banks) usually display histological modifications as wet and dry cycles in burial environments can damage bone microstructure (Nielsen-Marsh and Hedges 2000a; Turner-Walker 2008).

Soil pH is another factor affecting histological preservation of archaeological bone, primarily because it can lead to the deterioration of the organic and inorganic contents, while it can also favour or inhibit microbial activity (Collins et al. 2002; Hanson and Buikstra 1987). The examination of many thin sections (i.e. 119) from adult human femora from different sites at the Lower Illinois Valley, USA (i.e. AD 180 to AD 1200) by Hanson and Buikstra (1987) supports that histological changes depend on local soil chemistry. Low pH values, for example, can lead to decreased bacterial activity (Jackes et al. 2001) and better preservation of the protein content as seen in archaeological bones from acidic soils (i.e. 5.1 pH) in Puerto Rico (Pestle and Colvard 2012). Additionally, a highly variable state of histological preservation observed in samples from the same burial phases in Khartoum, Sudan indicated that bone diagenesis is also strongly influenced by the burial micro-environment (Dal Sasso et al. 2014).

Except within site variations, intra-individual and within bone variations have been observed in archaeological bone (Garland 1989). Although Booth (2016) and Booth, Redfern and Gowland (2016) report an insignificant intra-individual and within bone variation along the femoral mid-shafts of adult and infant individuals, the presence of intra-individual and within bone (proximal vs distal diaphysis; **Figure 3.13**) variation has been confirmed this time in early diagenetic stages in experimental studies that involved the burial of *sus scrofa* carcasses (Kontopoulos, Nystrom and White 2016). However, no distinct overall pattern was observed (Kontopoulos, Nystrom and White 2016). The skeletal elements should also be expected to degrade at different rates depending on the different sizes and biomechanical characteristics such as porosity and remodelling (Hanson and Buikstra 1987). This should result in intra-individual variations and the microbial activity should be related to intrinsic to the tissue physical and chemical factors (Hanson and Buikstra 1987). Consequently, identifying, quantifying, and comparing patterns of bone degradation can be a very complex process, as each bone may follow a unique diagenetic trajectory.

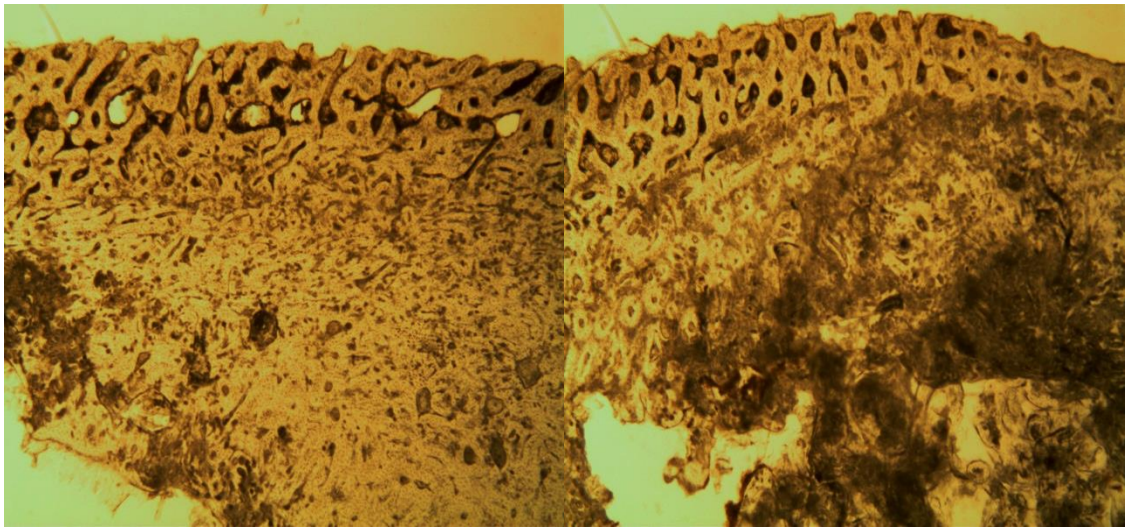

Figure 3.13. *Within bone variation* – Plane polarized image of the right ulna of a *sus scrofa* that shows the variable histological preservation in proximal (left) and distal (right) diaphysis (Kontopoulos 2014).

The death history and the effects of various factors (e.g. season of death, clothing, burial depth, diet and microbiome health) on body decomposition and the preservation of bone are often disregarded in archaeology (Bell 2012; Turner-Walker 2008). As Bell (2012) argues, correlation between peri-mortem history of the body and its post-mortem alterations manifested on the skeletal remains is of major importance because diagenetic change is a matter of whole-body decomposition within its burial environment. Some researchers argue that microscopic evidence can be used for the distinction between different funerary treatments as the alterations caused by anthropogenic processes can be distinguished from those induced by the burial environment (Booth 2016; Booth and Madgwick 2016; Smith et al. 2016). The basis of this assumption is that the exposure of a corpse for longer or prolonged periods of time would result to reduced levels of bone degradation (Booth 2016; Smith et al. 2016). On the contrary, the immediate burial of the bodies would delay skeletonization and would maximize bone degradation (Booth 2016; Smith et al. 2016).

Later prehistoric and historical samples from the British Isles show variability in histological preservation and this has been linked to the different forms of funerary treatments (Booth and Madgwick 2016). Primary burial soon after death assumed to be the cause of low OHI scores accompanying poor histological preservation, whereas good preservation and high OHI values considered indicative of different burial practices (Booth 2016). Yoshino et al. (1991) have reported very limited morphological changes in human bones exposed in open-air for up to 15 years post-mortem with changes mainly observed in periosteal areas. The earliest evidence of MFD in samples buried in soil was 2.5 years post-mortem, although histological changes mainly appeared at approximately 5 years post-mortem and gradually spread to mesosteal areas of bone (Yoshino et al. 1991). The presence of microbial modifications after complete skeletonization led Yoshino et al. (1991) to the conclusion that bone probably degrades when soft tissues have

completely decomposed which supports Turner-Walker's (1999) belief that a rapid burial would initially protect bones from microbial attack.

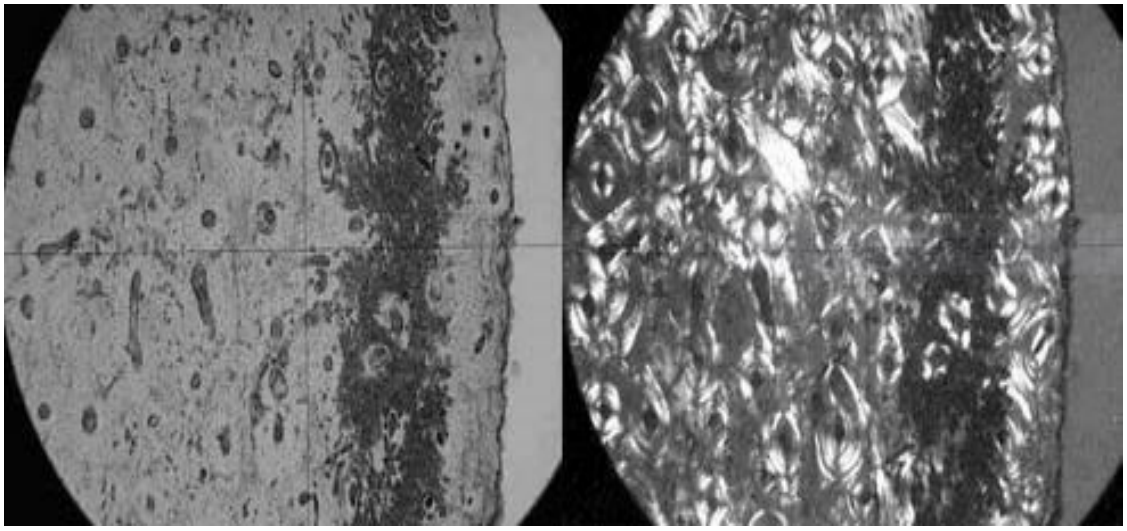

Figure 3.14. '*Mummification*' – Human femur from Cladh Hallan under plane-polarized (left) and cross-polarized (right) light (Parker Pearson et al. 2005).

Limited levels of bacterial activity in specimens from Chalcolithic and Bronze Age Britain have been interpreted as the result of the elimination of the gut microbiota during the removal of the internal organs of the bodies for mummification (**Figure 3.14**; Booth, Chamberlain and Pearson 2015; Parker Pearson et al. 2005). This assumption was supported by the study of two mummified remains from Yemen and Ireland with excellent preservation of the histological features (Booth, Chamberlain and Parker Pearson 2015) with the only modification observed being the enlarged osteocyte lacunae which have been identified as a characteristic alteration during early diagenetic stages (Kontopoulos, Nystrom and White 2016; White and Booth 2014).

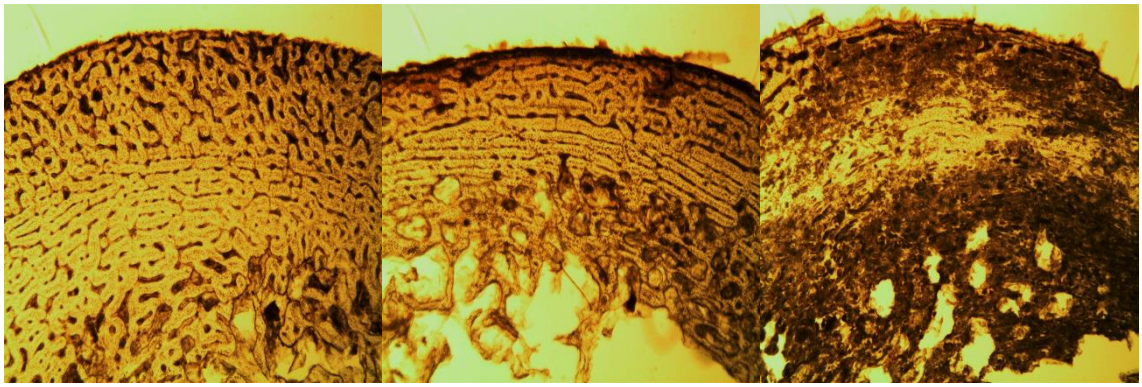

Figure 3.15. *Textile effects* – Plane-polarized images of three individuals covered with a) 100 % cotton textiles (left), b) 79 % cotton textiles (middle), and c) 100 % nylon (right) displaying the variable preservation due to the presence of textiles with different compositions (Kontopoulos, Nystrom and White 2016).

However, several researchers seem not to take into consideration the effects of the micro-environment and other forms of funerary practices (e.g. wrapping) on the variation in bacterial activity. The very tightly flexed position of the individuals from Cladh Hallan (Scotland), for

example, could be also indicative of wrapping/bounding. Although Booth, Redfern and Gowland (2016) argue that wrapping the bodies has no effect on bone degradation, it has been experimentally proved that it affects histological integrity (**Figure 3.15**; Kontopoulos, Nystrom and White 2016). The qualitative data from the histological analysis of thin sections from the mid diaphysis of the left humeri of three *sus scrofa* individuals covered with different fabrics indicated that the composition of the textiles clearly affects bone preservation during the early diagenetic stages (i.e. 6 years post-mortem; Kontopoulos, Nystrom and White 2016). The individual covered with 100% cotton textiles and the individual clothed with 79% cotton, 20% nylon, 1% elastane showed good histological preservation, whereas the individual placed within a rolled-up carpet of 100% nylon exhibited poor histological preservation (**Figure 3.15**; Kontopoulos, Nystrom and White 2016). It is likely that cellulose in some textiles could be used by the soil microorganisms as a source of energy (chemical assimilatory biodeterioration) which could delay or limit microbial invasion into bone (Kontopoulos, Nystrom and White 2016).

3.2. PRESERVATION OF BIOAPATITE

The preservation of bioapatite is important in archaeological research as it can offer valuable information on the movement of past people and animals (phosphate), their dietary habits (carbonate), their environments (phosphate and carbonate) and possibly past funerary practices (Hedges 2003; King, Tayles and Gordon 2011; Lee-Thorp and van der Merwe 1991; Scorrano et al. 2016; Wright and Schwarcz 1996). BAp crystals can survive for long periods of time, however post-mortem changes of biogenic chemical signals have long been recognized as a key issue (Lee–Thorp 2002; Lee-Thorp and van der Merwe 1991; Shin and Hedges 2012; Stiner et al. 2001; Wright and Schwarcz 1996).

Reorganization or growth through dissolution (loss of less stable components) and recrystallization (formation of more stable structure) is necessary for its survival post-mortem (Nielsen-Marsh et al. 2000a; Trueman 2013). Dissolution occurs when conditions are greatly under-saturated, primarily due to active hydrology (recharging with fresh water) or due to a reduction in pH (Hedges 2002; Hedges and Millard 1995; High et al. 2015; Nielsen-Marsh et al. 2000a; Piepenbrink 1989). When the skeletal remains are close to the ground surface (rainwater not yet equilibrated with soil hydroxyapatite), or in highly conductive soils (e.g. sands and gravels, floodplains, etc. with wet and dry cycles) that water never becomes saturated with Ca^{2+} and PO_4^{3-}, water leaches out the mineral phase (Hedges 2002; Nielsen-Marsh et al. 2000a; Turner-Walker 2008).

Soil pH controls the fate of bioapatite as it also dissolves in acidic soils (i.e. increase in H^+ ions), whereas it becomes more stable in more basic soil environments (High et al. 2015; Nielsen-Marsh et al. 2000a). A dissolution of bioapatite in slightly acidic soils can lead to a rise of the soil pH (buffer), while in very acidic environments dissolution leads to a consumption of H^+ ions which does not affect soil pH and results to a significant loss of mass (High et al. 2015; Nielsen-Marsh et al. 2000a). Microbial activity may also lead to mineral dissolution and redistribution of phosphate (Trueman et al. 2004). In such a case, phosphate will be used for the growth of adjacent bioapatite crystals (Trueman et al. 2004).

Recrystallization (isomorphic or heteromorphic) is heavily pH-dependent as bioapatite is more stable in pH around 7.5-8, displays low solubility in slightly alkaline and near neutral environments but gives way to dissolution in pH environments below 6 or over 9 (Berna, Matthews and Weiner 2004; Hedges and Millard 1995; Keenan and Engel 2017; Nielsen-Marsh et al. 2000a; Turner-Walker 2008). Thus, in alkaline to neutral soil pH, bone apatite will undergo recrystallization with bioapatite being recrystallized into authigenic apatite (Berna, Matthews and Weiner 2004). This pH range is called the ‘recrystallization window’ (Berna, Matthews and Weiner 2004). The pH of the groundwater, which can vary from 2.8 to 10, also controls the ions available for exchange with bioapatite (Nielsen-Marsh et al. 2000a; Turner-Walker 2008).

Recrystallization of bone also depends on the hydrological conditions of the burial environment (Hedges and Millard 1995; Piepenbrink 1989; Trueman et al. 2008). The thin nature of the crystals makes them unstable as many atoms can be disordered because of their proximity to the surface (Berna, Matthews and Weiner 2004; Stathopoulou et al. 2008). Cations incorporated into the bone-water system during passage of pore waters may be either adsorbed onto exposed bone crystallites (i.e. labile) or incorporated into authigenic minerals (i.e. structural) (Trueman et al. 2004). Thus, the interaction of the groundwater with the hydrated layer leads to the incorporation of diverse labile and reactive ions (e.g. HPO_4^{2-}, PO_4^{3-}, CO_3^{2-}, Ca^{2+}, Mg^{2+}), which may in turn substitute other ions into the core domain (**Figure 3.16**; Figueiredo, Gamelas and Martins 2012; Lee-Thorp and van der Merwe 1991; Stathopoulou et al. 2008; Trueman, Privat and Field 2008; Trueman 2013). The longer the bone is exposed on the conditions of the burial environment, the greater is its dependency on external sources of phosphate (i.e. authigenic minerals) to fill in the pore space initially occupied by the organic component (Trueman et al. 2004). This means that the newly formed crystals may incorporate any ions present in pore waters. For instance, Na^{+} and Mg^{2+} may substitute Ca^{2+} ions, HPO_4^{2-} ions may substitute PO_4^{3-} ions, while halides (e.g. F^{-} and Cl^{-}) may substitute OH^{-} (Figueiredo, Gamelas and Martins 2012; Stathopoulou et al. 2008).

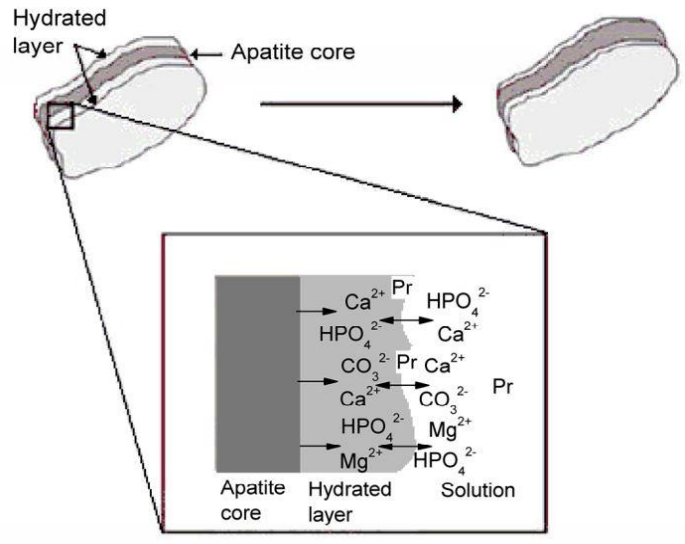

Figure 3.16. *Bioapatite crystal* – Ionic exchange between the crystal and its surrounding environment. (Figueiredo, Gamelas and Martins 2012).

Identification of the changes in the bioapatite crystals can, therefore, provide evidence for the preservation state of bone and the reasons that lead to these modifications in the inorganic component of bone (King, Tayles and Gordon 2011). Until today, no reliable method has been recommended for screening archaeological bones to predict the likely preservation of *in vivo* biochemical signatures of bioapatite (Trueman et al. 2004, 2008). Consequently, understanding the nature of alterations can provide valuable information for the immediate depositional environment or important biological and archaeological information.

3.2.1. CRYSTALLINITY

Bone recrystallization increases crystallinity (i.e. crystal size and lattice perfection) and promotes the formation of a more stable mineral phase usually characterized by lower carbonate content (Salesse et al. 2014). The increase in average and maximum crystal length may be due to an increase the size of the larger crystals at the expense of the smaller ones (i.e. Ostwald ripening), dissolution of the smaller crystals, or both (Nielsen-Marsh et al. 2000a; Reiche, Vignaud and Menu 2002; Stiner et al. 2001; Trueman 2013; Trueman et al. 2004, 2008; Weiner and Bar-Yosef 1990; Wright and Schwarcz 1996). The high degree of disorder is responsible for the promotion of diagenetic modifications in bioapatite (Trueman 2013). Thus, BAp crystals become more ordered post-mortem as the disordered phases are less energetically stable (Asscher et al. 2011; Trueman 2013). Although there is a loss of the smaller, less ordered phases post-mortem, it is not clear if there is a loss of the more disordered phases that results to a more ordered crystal (Trueman 2013).

FOURIER TRANSFORM INFRARED (FTIR) SPECTROSCOPY

The infrared splitting factor (IRSF) can be used as a semi-quantitative index to assess bone mineral preservation (Hollund et al. 2013; Nielsen-Marsh et al. 2000a; Surovell and Stiner 2001; Trueman et al. 2004; 2008; Weiner and Bar-Yosef 1990; Wright and Schwarcz 1996). It is a measure of the structural order (i.e. homogeneity) within the crystal lattice and the increase in their size (Termine and Posner 1966; Surovell and Stiner 2001; Trueman, Privat and Field 2008). The larger and/or more ordered the crystals, the higher the IRSF value (Surovell and Stiner 2001; Trueman et al. 2004; Weiner and Bar-Yosef 1990). Therefore, IRSF can be used as a proxy for diagenetic changes in bioapatite crystals and it can provide a sound estimate of the degree of diagenesis (Berna, Matthews and Weiner 2004; Trueman et al. 2004; 2008).

To estimate the IRSF, the summing heights of the peaks at c. 605 and c. 565 cm^{-1} are divided by this at c. 590 cm^{-1} at the triply degenerate asymmetric v_4 PO_4^{3-} bending (**Figure 3.17**; Weiner and Bar-Yosef 1990). Baseline correction is also necessary to measure the height of the peaks at around 605 cm^{-1} and 565 cm^{-1}, and this of the trough between them at about 590 cm^{-1} (Weiner and Bar-Yosef 1990). The equation of the IRSF is expressed as:

$$IRSF= (565_{ht}+605_{ht})/590$$ (Weiner and Bar-Yosef 1990).

Although IRSF has been used to measure indirectly the mean crystal length (Trueman et al. 2004) some studies argue that there is no clear relationship between IRSF and mean crystal size (Reiche, Vignaud and Menu 2002). Weiner and Bar-Yosef (1990) and Lebon et al. (2010) also argue that IRSF cannot be used as an indisputable means for the assessment of bone preservation. The distinction betweeen exogenous (i.e. authigenic) and mildly altered biogenic bioapatite cannot be achieved as they often exhibit similar IRSF values (Trueman, Privat and Field 2008). Thomspon

et al. (2009) have also reported that IRSF values greatly vary depending on the region of bone examined, while it is not a reliable method to screen bone mineral for isotopic studies (Trueman, Privat and Field 2008).

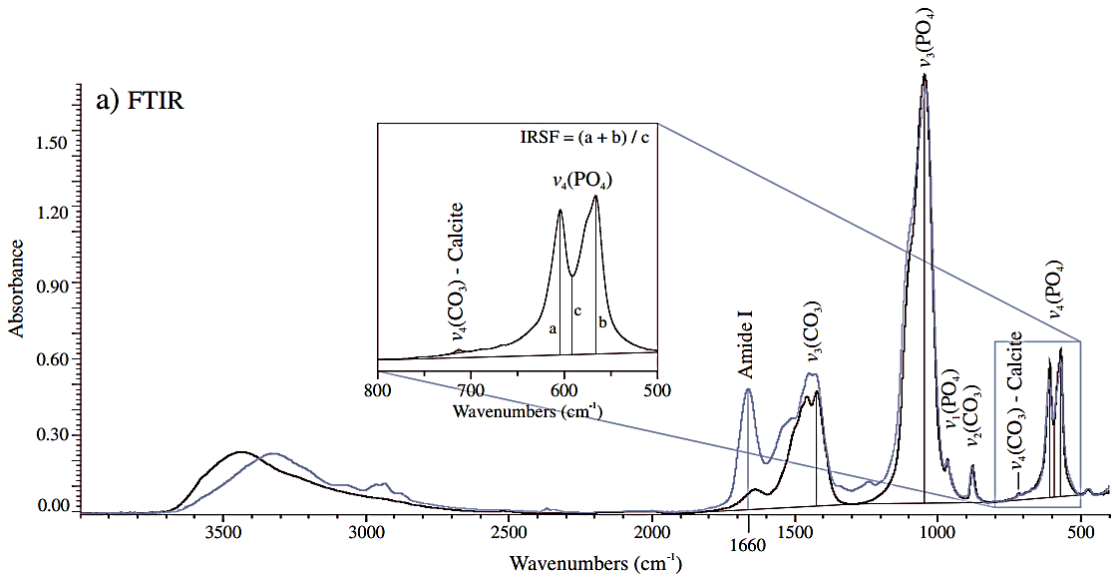

Figure 3.17. *FTIR Spectra* – Graph with the mid-IR spectra of archaeological bone (black) and modern bone (light grey) showing the phosphate, carbonate and amide peaks (Dal Sasso et al. 2016).

Besides the changes in crystal size, diagenesis also alters the atomic disorder of the bone mineral (Asscher et al. 2011) which is also affected by grinding during sample preparation that changes the distribution of different crystal particle sizes within the samples (Kontopoulos et al. 2018; Trueman 2013). Past studies have tried to investigate the effect of sample preparation methods on bone IRSF values, with a decrease in IRSF reported with more intensive pulverization (Surovell and Stiner 2001). Surrovel and Stiner (2001) argue that grinding may introduce variations in crystallinity that may mask the original signal due to structural changes caused to the BAp crystals. They propose two possibilities that could explain the phenomenon: a) changes are primarily caused by the particle separation of bone mineral of differing crystallinity (separation hypothesis), or b) grinding affects the bioapatite crystal structure (destruction hypothesis), and subsequently, the mid-IR spectra.

Overall, it has been argued that there seems to be a destruction of BAp crystals during grinding, although when there is no control, or grinding is excessive, it is difficult to differentiate between the actual bone crystallinity from that introduced during sample preparation (Surovell and Stiner 2001). Hollund et al. (2013) also observed significant preparation-based differences (i.e. drilling and grinding with and without sieving) between IRSF, C/P and Am/P values. The grinding effect was more evident in samples of higher crystallinity, so Hollund et al. (2013) proposed drilling bone without sieving as an alternative to the Surovell and Stiner (2001) preparation method.

Asscher et al. (2011) and Asscher, Weiner and Boaretto (2011) tried to explore the effects of grinding on bone and tooth, and decouple it from the atomic disorder effect, to better assess the preservation state of archaeological/fossil bone. They compared the IRSF values of samples repeatedly ground for variable amounts of time and plotted them against the full width at half maximum (FWHM) of the main v_3 phosphate asymmetric stretching mode at c. 1035 cm^{-1}. As the narrower the FWHM, the smaller the particle size, from the relationship observed, it was shown that grinding (i.e. particle size) affects both the short (IRSF) and long (FWHM at 1010 cm^{-1}) range order of bone (**Figure 3.18**). Thus, the use of the grinding curve approach can increase the sensitivity of FTIR for monitoring diagenesis (slopes of the grinding curves are steeper and shorter with poorer preservation), as compared to the IRSF alone, and it can also allow the identification of differences in crystal size/atomic order of different animal species and hard tissues (i.e. bone, dentine and enamel mineral; **Figure 3.18**).

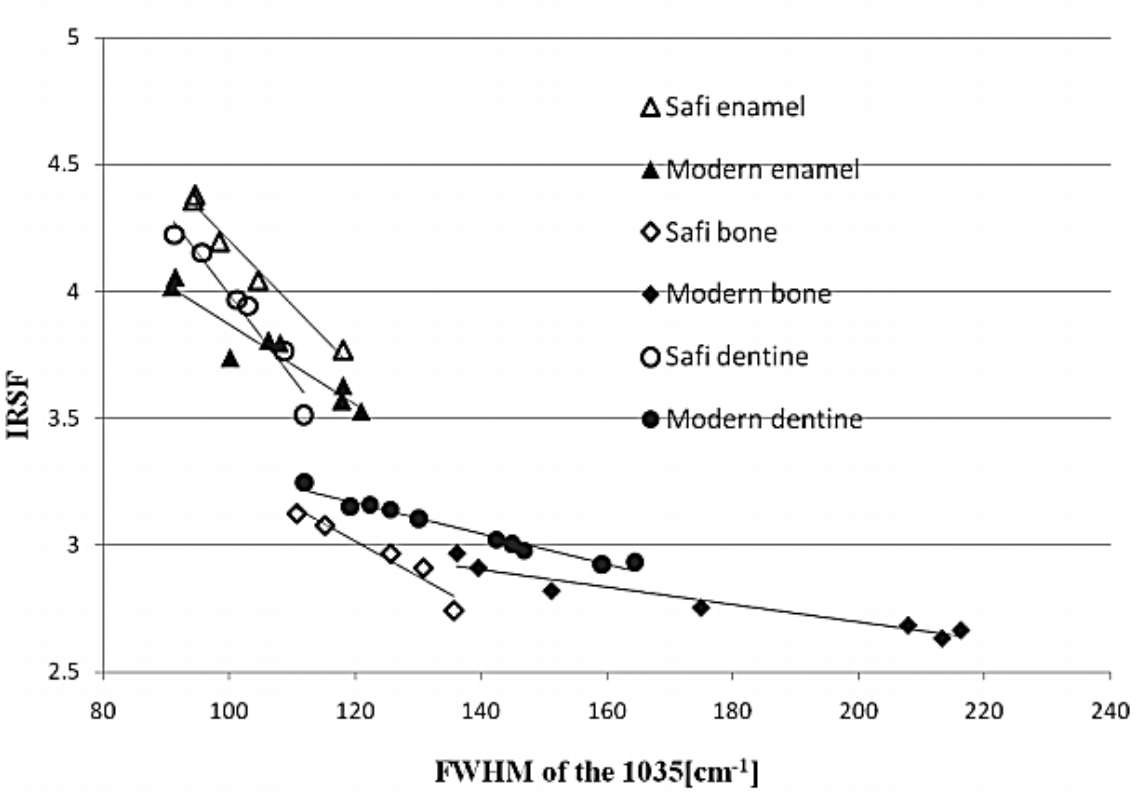

Figure 3.18. *Grinding curve* – Diferrent crystal disorder between modern and archaeological bovine enamel, dentine and bone samples (Asscher et al. 2011).

While this trendline method partly shows the importance of particle size (still uncontrolled) on the mid-IR spectrum, it requires regrinding and measuring the same sample repeatedly for several times. Furthermore, the powders were analysed in KBr pellets, requiring significant amounts of material mixed with KBr. Excessive grinding can also lead to a contamination of bone powder or even damage surviving biomolecules in samples that could be also used for DNA (e.g. Adler et al. 2011) or protein analysis (e.g. Collins and Galley 1998), making FTIR KBr and grinding

curves a destructive method and wasting precious material, in lieu of additional information on crystalline order.

Fluorine is also very important as its presence may affect the IRSF values (Lebon et al. 2010; Pleshko, Boskey and Mendelsohn 1991). Archaeological and fossil bones displaying increased crystallinity (i.e. larger crystal size), usually exhibit higher F content than modern bones due to diagenesis (Keenan et al. 2015; Trueman et al. 2008). Incorporation of F^- into the crystal is consistent with the formation of authigenic apatite, and it is assumed to increase its size and stability of the mineral phase, while it shifts dissolution towards more acidic conditions (Berna, Matthews and Weiner 2004; Pleshko, Boskey and Mendelsohn 1991; Wright and Schwarcz 1996). F^- is assumed to substitute OH^- in bioapatite crystals. The OH^- ions in BAp are characterized by a stretching mode at 3600 cm^{-1} and a libration band at 630 cm^{-1} (Antonakos, Liarokapis and Leventouri 2007). When there is fluorine uptake, a discrete peak at around 1092 cm^{-1} appears and this might also be related with the unit cell volume and α-axis length (Stathopoulou et al. 2008). The ratio of the peaks at c. 605 cm^{-1} to c. 565 cm^{-1} have been used for the assessment of the presence of F in bone bioapatite, as the F-containing apatites display modified intensities at c. 605 and c. 565 cm^{-1} (Lebon et al. 2010; Trueman, Privat and Field 2008). Apatites containing F^- (e.g. francolites) display more intense vibrations at c. 605 cm^{-1}, whilst F-deficient apatites exhibit more intense vibrations at 565 cm^{-1} (Trueman, Privat and Field 2008). Hence, the latter has relatively lower ratio values. Nonetheless, the relationship between IRSF and F^- is complex as samples with the same F^- content may exhibit very different IRSF values (Lebon et al. 2010).

A few other indices have been proposed for measuring crystallinity of the mineral component of bone in an effort to acquire as accurate as possible IR data. Specifically, based on previous observations by Pleshko et al. (1991) that the peak at 1060 cm^{-1} decreases when there is an increase in the c-axis length of the apatite crystal and the c. 1020 cm^{-1} component increases with increasing crystal size, Lebon et al. (2010) proposed the use of the 1030/1020 cm^{-1} and the 1060/1075 cm^{-1} ratios. Both indices have been found to correlate with the IRSF values, although the 1060/1075 cm^{-1} ratio is in better agreement with IRSF values (Lebon et al. 2011). Thus, it is possible to use these ratios to assess bone crystallinity (Lebon et al. 2010). Pleshko et al. (1991) and Lebon et al. (2010) also argue that the use of the ν_1 PO_4^{3-} area at c. 960 cm^{-1} can be used to assess the crystal size and perfection (i.e, maturation) as the ν_1 absorbance decreases with increasing crystallinity.

Acetic acid treatment has been used prior to isotopic investigations to remove most of the exogenous contaminants from bioapatite crystals (Garvie-Lok, Varney and Katzenberg 2004). However, treatment-induced recrystallization and excessive sample loss has been observed by Garvie-Lok, Varney and Katzenberg (2004). Treatment with acetic acid has been reported to

affect IRSF values as the PO_4^{3-} peak splitting at 605-565 cm^{-1} appears greater probably due to the dissolution of smaller crystals (Wright and Schwarcz 1996; Nielsen-Marsh and Hedges 2000b). In longer treatments and/or more concentrated solutions there is an incorporation of exogenous minerals into the crystal lattice (e.g. formation of brushite) and crystal characteristics (e.g. maturity) may also play a significant role in that phenomena (Garvie-Lok, Varney and Katzenberg 2004). More dilute solutions (e.g. 0.1 M acetic acid) and lower solution acidity are considered more appropriate for the removal of the exogenous sources and avoid recrystallization (Shin and Hedges 2012). Acetic acid may also significantly raise the IRSF values of modern bone as well as those of archaeological bone with poor histological preservation, while longer treatments with acetic acid can lead to complete recrystallization to brushite (Lee-Thorp and van der Merwe 1991; Nielsen-Marsh and Hedges 2000b; Shin and Hedges 2012; Wright and Schwarcz 1996).

X-RAY DIFFRACTION (XRD) AND TRANSMISSION ELECTRON MICROSCOPY (TEM)

Many studies have also examined bone mineral crystallinity using other techniques (King, Tayles and Gordon 2011; Person et al. 1995; Reiche, Vignaud and Menu 2002; Stathopoulou et al. 2008). Person et al. (1995) applied XRD to search if crystallinity index (CI) can be used as a semi-quantitative way to assess archaeological and fossil bone preservation. Their results indicated that the 211, 112, 300 and 202 reflections are related with high crystallinity and they defined crystallinity as CI= [h(202) + h(300) + h(112)/ h(211) (**Figure 3.19**). It was observed that the intensity of each of these peaks decreases in the same order, and when crystallinity increases there is usually a decrease in the organic matter and CO_3^{2-} (Person et al. 1995). Such a negative correlation between crystallinity and organic content, though not strong, was also observed by Götherström et al. (2002). As a result, XRD can be used to estimate crystallinity (i.e. size and homogeneity) and assess bone preservation (Person et al. 1995; Quattropani et al. 1999). Bartsiokas and Middleton (1992) who used a different crystallinity index [CI=10(a/b)] argue that the progressive increase of crystallinity in archaeological and fossil bone can be possibly used as a dating tool, although some of the youngest samples examined in this study displayed similar crystallinity with others 10 ky-120 ky older. No correlation between CI and chronological age has been observed by Person et al. (1995).

TEM can provide important information on crystallinity of archaeological bone as demonstrated in a study that successfully identified three distinct BAp crystal morphologies in archaeological bone that differ from modern bone (**Figure 3.20**; Reiche, Vignaud and Menu 2002). Type I BAp crystals are thin irregular platelets and they are the most common crystals observed in archaeological bone (Reiche, Vignaud and Menu 2002). Their shape is similar to the bioapatite crystals in modern bone; however, they are 2-5 times larger than the former (Reiche, Vignaud and Menu 2002). Type II crystals are needle-shaped (or acicular crystals) with a length of up to 200 nm (Reiche, Vignaud and Menu 2002). Type III crystals are large hexagonal single platelets of

80-150 nm diameter (Reiche, Vignaud and Menu 2002). The first two crystal types often coexist within a sample, whereas the third crystal type is mainly observed in heated bone (Reiche, Vignaud and Menu 2002).

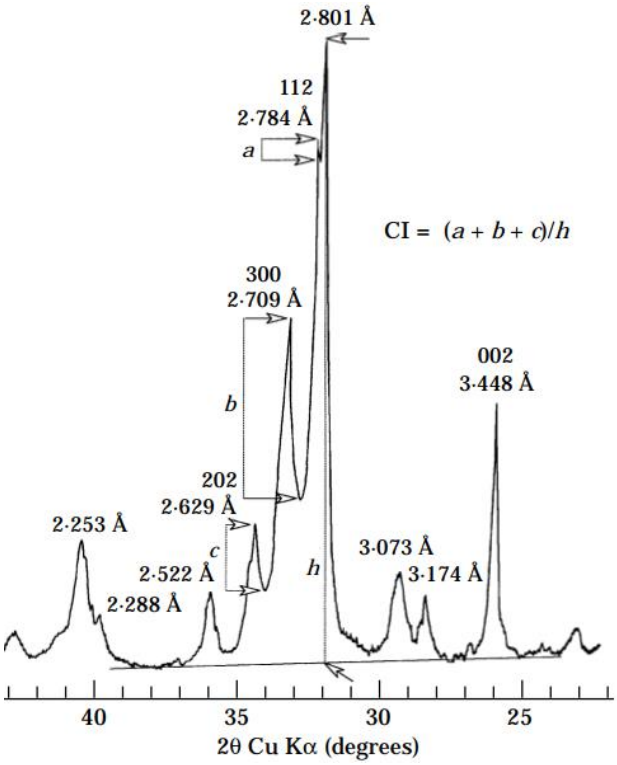

Figure 3.19. *XRD spectra* – Crystallinity between 24 and 38 2θ of bioapatite (Person et al. 1995).

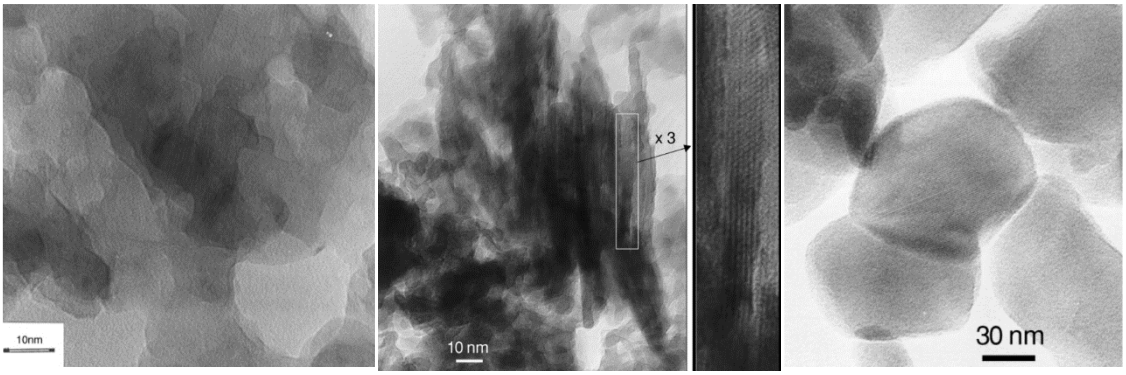

Figure 3.20. *Types of bioapatite crystals* – Type I (left), type II (centre), and type III (right) (adapted from Reiche, Vignaud and Menu 2002).

3.2.2. CARBONATE CONTENT

Post-mortem exchange of CO_3^{2-} changes BAp composition and preservation potential (Wright and Schwarcz 1996). Changes in the carbonate environment of bioapatite may occur via different processes that make it challenging to distinguish how the exogenous carbonate has been incorporated into the crystal lattice (Nielsen-Marsh and Hedges 2000b). Carbonate uptake may take place either via absorption in the mineral surface, substitution in the mineral lattice, and

exchange with the original carbonate content and/or crystallization of the calcite into the pore spaces (Nielsen-Marsh and Hedges 2000b). Ionic exchanges can alter the atomic-level bond spacings and orientations (Keenan et al. 2015). Shifts in Ca–O bonds following Ca^{2+} substitution, for example, and substitution and occupancy at one PO_4^{3-} position within the lattice can cause bond shortening in another PO_4^{3-} position (Keenan et al. 2015).

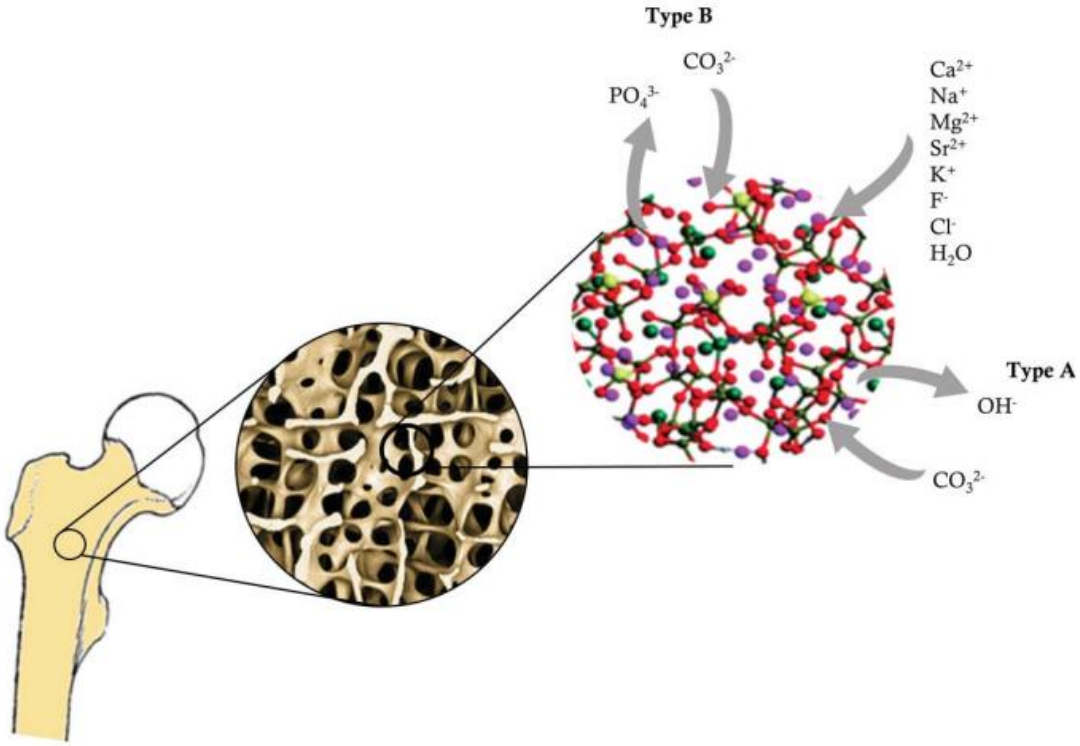

Figure 3.21. *Carbonate substitutions* – Type A and type B types in BAp crystals (Mamede et al. 2018).

Indices based on the carbonate stretching bands account for the structural CO_3^{2-} content in apatite and its distribution among the A- (carbonate ions replace hydroxide) and B-sites (carbonate ions replace phosphate ions) (**Figure 3.21**). The carbonate-to-phosphate (C/P) ratio expressed as 1415/1035 cm^{-1} using FTIR that is commonly applied as a measure to assess the changes in the carbonate environment of the bioapatite crystals is such an example (Wright and Schwarcz 1996). Absorption band at c. 1415 cm^{-1} is typical of v_3 CO_3^{2-} asymmetric stretching vibrations of type B apatite (Figueiredo, Gamelas and Martins 2012; Gourion-Arsiquaud, West and Boskey 2008), as diagenetically altered bone primarily exhibits carbonate type-B substitutions (Keenan et al. 2015; Stathopoulou et al. 2008; Wright and Schwarcz 1996). The A-type substitutions are not common in archaeological studies as conditions of high temperatures (i.e. 1000° C; LeGeros 1965) are not expected in common environmental conditions (Stathopoulou et al. 2008).

Wright and Schwarcz (1996) have reported a negative correlation between C/P and IRSF values in samples from the ancient Mayan site of Dos Pilas, Guatemala. In view of that, they argue that the amount of CO_3^{2-} present in bioapatite affects its crystallinity as higher C/P (i.e. B-type

substitutions) result in smaller crystals (Wright and Schwarcz 1996). However, even if a strong inverse relationship between C/P and IRSF has been reported in several other studies and many researchers employ this technique to assess bone preservation, it is still debated if these indices accurately reflect diagenetic modifications in bone (Beasley et al. 2014; Dal Sasso et al. 2016; Nielsen-Marsh and Hedges 2000a; Trueman et al. 2004; 2008; Weiner and Bar-Yosef 1990; Wright and Schwarcz 1996).

Assessment of the carbonate content might be difficult sometimes due to overprinting of ν_3 carbonate bands by unknown bands (e.g. C-H) (Trueman, Privat and Field 2008), while changes in the IR absorption bands may be related with the anatomical position, age, and/or disease (Gourion-Arsiquaud, West and Boskey 2008). Variations in C/P may also mirror the different taphonomic histories (e.g. microbially attacked vs microbially undamaged bones) of the specimens (Garvie-Lok, Varney and Katzenberg 2004; Nielsen-Marsh and Hedges 2000a). Carbonate content distribution has been found heterogeneous in archaeological bone with areas around the osteons exhibiting higher CO_3^{2-} content, while in interstitial lamellae the amounts of CO_3^{2-} were low (Lebon et al. 2011).

Stiner et al. (1995) have used an alternative ratio (i.e. 870/565 cm^{-1}) as the 1415 cm^{-1} absorbance peak is affected by the presence of organic content in relatively well-preserved bones. However, the major disadvantage of using the ν_2 CO_3^{2-} vibrations is that it reflects three different carbonate sites that appear at c. 878 cm^{-1} for type A1 ("stuffed"), c. 871 cm^{-1} for type B, and c. 866 cm^{-1} for type A2 ("labile"-surface) carbonate (Fleet 2009; Fleet and Liu 2004; Paschalis et al. 1996). Among these components, the c. 871 cm^{-1} type B carbonate is the more prominent, though the most important observation is the absence of the 866 cm^{-1} component from archaeological specimens (Kontopoulos et al. 2018). This observation justifies its characterization as "labile"-surface carbonate and shows that a possible removal of ions (e.g. carbonate) from the crystal surface during grinding of bone and its effect on Stiner et al. (1995) C/P ratio cannot be overlooked. Additionally, the peak at c. 870 cm^{-1} band can reflect CO_3^{2-} which might be incorporated into the apatite crystal structures (Pleshko, Boskey and Mendelsohn 1991) as it may contain non-apatitic carbonate signal from soil contaminants (Figueiredo, Gamelas and Martins 2012; Wright and Schwarcz 1996).

Indices reflecting the amount of type B carbonate-to-phosphate (BPI, 1415/605 cm^{-1}), the amount of type A carbonate-to-phosphate (API, 1540/605 cm^{-1}), and the relative amount of B- to A-site carbonate (BAI, 1415/1540 cm^{-1}) have been proposed by Sponheimer and Lee-Thorp (1999). Variations in type A carbonate contents have also been identified between modern and archaeological bone, with IRSF and API exhibiting a reciprocal relationship for specimens containing more than 10 wt. % organic content (Trueman, Privat and Field 2008). Samples from Cuddie Springs exhibited decreasing proportions of type A carbonate content with increasing

IRSF and decreasing organic content (Trueman, Privat and Field 2008). This redistribution of carbonate ions with a reduction in type A carbonate in the early diagenetic stages (i.e. 10 years post-mortem) has been considered as indicative of an exchange with F^- ions (Trueman, Privat and Field 2008). Thus, a decrease in type A carbonate might indicate an exchange with F^- ions as fluorapatites exhibit lower solubility and greater stability in soils (Trueman, Privat and Field 2008).

On the other hand, assessing carbonate content of modern, historical and fossil bones from Cuddie Springs by BPI values indicated that this can be problematic due to an overlap or contribution to the 1415 cm^{-1} band (Trueman, Privat and Field 2008). Although a strong inverse relationship (R^2=0.72) between BPI and IRSF was reported by Kontopoulos et al. (2018), this was significantly lower than this between C/P and IRSF (R^2=0.90) which is probably an indication that using the triply degenerate v_4 PO_4^{3-} band results to a less accurate picture.

Variations in unit cell volumes can be attributed to the presence of carbonates and the substitution in OH^- (A-type, large volume) and PO_4^{3-} (B-type, low volume) sites (Stathopoulou et al. 2008). Analysis of the carbonate absorbance band by curve-fitting may reveal if there is type A or type B substitution in the apatite crystals (Gourion-Arsiquaud, West and Boskey 2008; Trueman, Privat and Field 2008). Authigenic mineral apatites such as calcite, barite, dahllite, crandallite, sepiolite and trona are usually identified in diagenetically altered bone by FTIR analysis (Stathopoulou et al. 2008; Trueman et al. 2004). Calcite, for example, can be found in limestone, chalk, marble, travertine, even in wind-borne (loess) and cemented sediments (Regev et al. 2010). It has three characteristic absorption bands: a) v_3 at c. 1420 cm^{-1}; b) v_4 at c. 712 cm^{-1}; and c) a weaker v_2 at 874 cm^{-1} (Regev et al. 2010).

Anomalously high absorbance at c. 1415 cm^{-1} or the presence of a weak absorbance peak at c. 710 cm^{-1} can be indicative of $CaCO_3$ within the pore spaces (Nielsen-Marsh and Hedges 2000a; Trueman et al. 2004; 2008). A detection limit of 2.5-3 wt. % has been reported by Dal Sasso et al. (2016) and Nielsen-Marsh and Hedges (2000a), and this $CaCO_3$ wt. % has been found to correlate with the Cal/PO_4 (calcite to phosphate) ratio as calculated by dividing c. 710 cm^{-1} by the c. 1035 cm^{-1} (Dal Sasso et al. 2016). This carbonate absorption peak at c. 710 cm^{-1} is, thus, characteristic of $CaCO_3$ and can be used to detect absorbed $CaCO_3$ contaminants (Thompson, Gauthier and Islam 2009). The presence of calcite in sediments, however, stabilizes pH at around 8.0, hence minimizes mineral dissolution (Stiner et al. 2001).

Treatment of diagenetically altered samples with acetic acid to remove exogenous (i.e. labile) carbonates in bone has been used to obtain biogenic signals and spectra (Garvie-Lok, Varney and Katzenberg 2004; Lee-Thorp and van der Merwe 1991; Nielsen-Marsh and Hedges 2000b; Pate, Hutton and Norrish 1989; Wright and Schwarcz 1996). This acid treatment usually leads to a decrease of the height of the CO_3^{2-} peak at 1415 cm^{-1} resulting in a lower C/P ratio close to their

pristine values (Lee-Thorp and van der Merwe 1991; Nielsen-Marsh and Hedges 2000b). It also sharpens the shoulder at 1096 cm^{-1} on the 1035 cm^{-1} PO_4^{3-} peak (Lee-Thorp and van der Merwe 1991; Wright and Schwarcz 1996). The former is probably indicative of a loss of secondary carbonates as there is no loss of phosphate, while the latter might be fluoride substitutions in hydroxyl sites (Lee-Thorp and van der Merwe 1991; Wright and Schwarcz 1996). Furthermore, calcite peak at around 710 cm^{-1}, if present, often disappears after acetic acid treatments (Garvie-Lok, Varney and Katzenberg 2004; Lee-Thorp and van der Merwe 1991).

Preservation of ancient proteins is of great interest to the archaeologist and archaeological scientist as they can provide valuable information on the chronological age (^{14}C dating, amino acid racemization, e.g. Deviese et al. 2018; Penkman et al. 2011), past lifeways/palaeodietary reconstruction (e.g. Van Klinken, Richards and Hedges 2002), and taxonomic identification (e.g. Asara et al. 2007; Buckley, Collins and Thomas-Oates 2008; 2009). Although collagen type I, which is the most abundant protein in bone, is considered the longest-lived protein in the archaeological record (Buckley et al. 2009; Demarchi et al. 2016; Tuross 2002; Wadsworth and Buckley 2014), an extensive loss of the organic content may even lead to the complete destruction of bone. Understanding how collagen degrades in bone through the different pathways, i.e. a) microbial attack of the composite, b) chemical hydrolysis of collagen; and/or c) dissolution/recrystallization of BAp crystals (Collins et al. 2002) is thus of major importance.

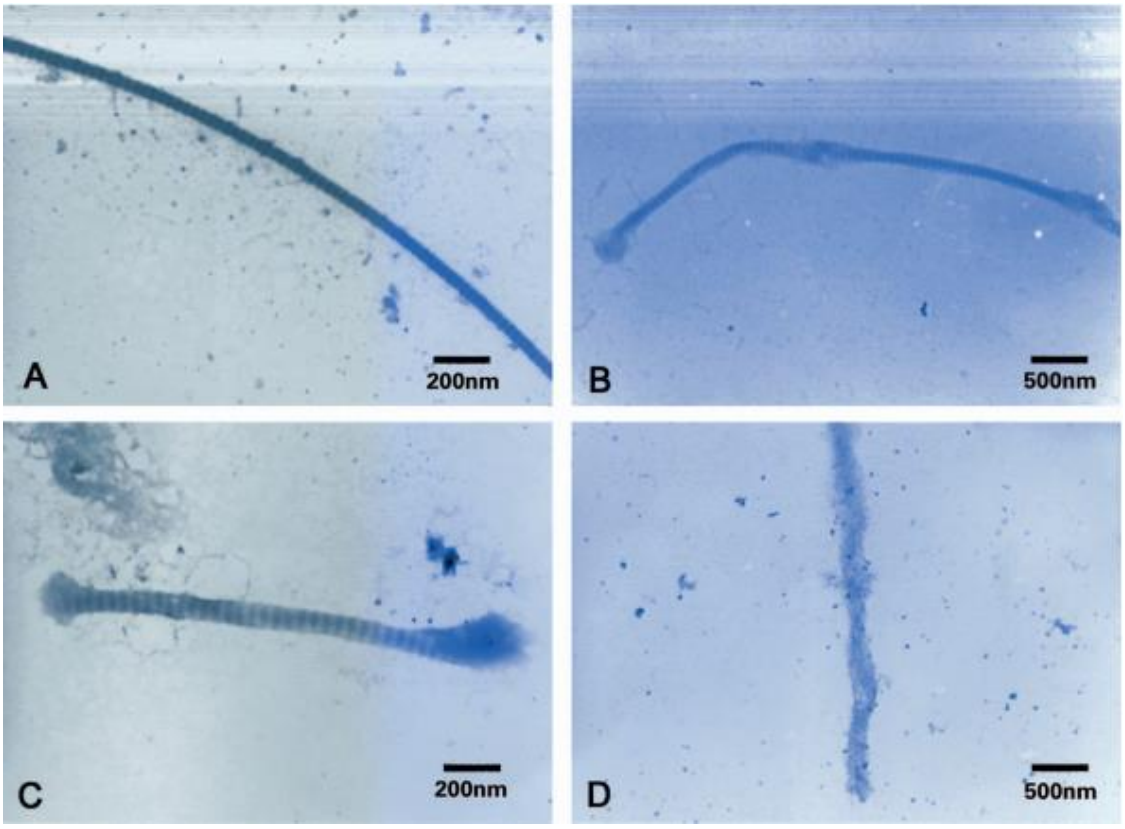

Figure 3.22. *Types of alteration to collagen fibrils* – (A) 'Unaltered' collagen fibril with fibrils of equal diameter throughout. (B) 'Beaded' collagen fibril with one or more localised areas of melting both along the fibril and at the end. (C) 'Dumbbell collagen fibril (typically <3 μm) with bulbous areas of melting at both ends (i.e. more advanced state of degradation). (D) 'Amorphous material', fully denatured collagen fibrils (Koon, Nicholson and Collins 2003).

Post-mortem modifications in BAp crystals are closely related to the decomposition of collagen (Susini, Baud and Lacotte 1988; Trueman et al. 2004), hence clearly affecting its post-mortem preservation potential (**Figure 3.22**). Collagen may suffer from microbial attack, which means it can be enzymatically degraded by collagenases (i.e. enzymolysis) produced primarily by bacteria

but also by other soil microorganisms (Balzer et al. 1997; Grupe, Balzer and Turban-Just 2002). Microorganisms use extracellular proteolytic enzymes to break the collagen molecule into smaller peptides that can be assimilated by bacteria and fungi (Turner-Walker 2008). BAp crystals can delay such fragmentation of the polypeptide chains from microbial collagenolytic enzymes (Brandt, Wiechmann and Grupe 2002; Grupe 1995; Nielsen-Marsh et al. 2000a, 2000b), however, post-mortem dissolution and/or recrystallisation of BAp crystals can expose collagen fibrils to collagenases (**Figure 3.23**; Collins et al. 1995). On the other hand, a slow loss of the organic matter through hydrolysis can lead to fossilization by leaving behind only the mineral component and secondary minerals to fill the pores (Collins et al. 2002). Collagen fills about the 1/3 of the volume of bone matrix *in vivo* and in a fully recrystallized bone this can be replaced by calcium phosphate that is entirely exogenous or secondary minerals until all inter-crystallite porosity has been filled (Trueman et al. 2008).

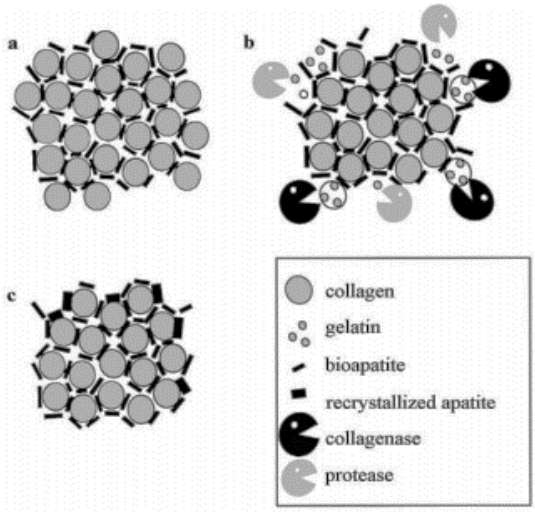

Figure 3.23. *Collagen degradation* – (a) Bioapatite crystals protect collagen from enzymolysis by physical exclusion of enzymes. (b) Collagenases attack any collagen exposed, followed by less specific proteases. No insoluble collagen remains in the exposed fraction. (c) Any insoluble collagen in the bone that survives microbial attack is assumed to remain intact and only degrades by slow and predictable chemical decomposition (Nielsen-Marsh et al. 2000b).

Collagen hydrolysis is heavily dependent on temperature, pH, hydrology and time (Collins et al. 2002; Koon, Nicholson and Collins 2003; 2010; Pestle and Colvard 2012; Grupe, Balzer and Turban-Just 2002). Peptide bond hydrolysis and gelatinization activation energies are very temperature-sensitive (Collins and Galley 1998) with collagen loss increasing with increasing temperature (**Figure 3.24**; Kendall et al. 2018). As a result, collagen degrades at higher rates in tropical/sub-tropical comparing to temperate environments (Pestle and Colvard 2012), and even more rapidly in arid environments (Van Klinken 1999; Weiner and Bar-Yosef 1990).

Collins et al. (1995) developed a temperature-sensitive simulation for non-mineralized type I collagen degradation to provide a theoretical framework for the better understanding of collagen chemical hydrolysis due to the presence of excess water. It was observed that chemical hydrolysis

leads to a depolymerisation of the peptide bonds and dissolution of the fragments and at the same time reduces the tensile strength of archaeological bone (Collins et al. 1995). The inter-chain hydrogen bonds were found to play a key role in collagen degradation rates as once fragments melt free, they cannot form hydrogen bonds again (Collins et al. 1995). The differences between mineralized and non-mineralized collagen, however, suggest a more complex process for the former due to its much higher gelatinizing temperature (Collins et al. 1995).

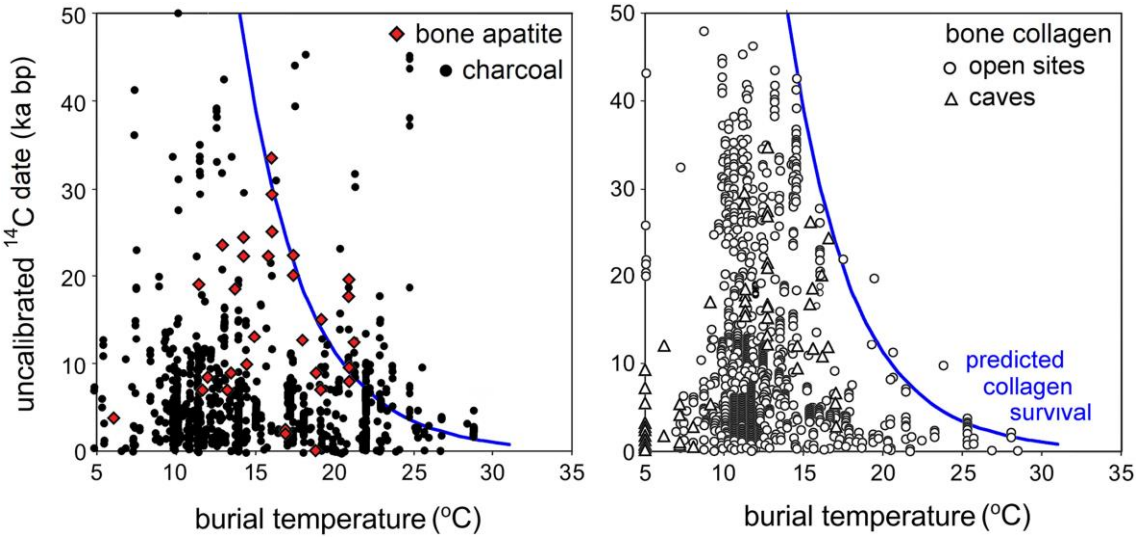

Figure 3.24. *Thermal age* - Radiocarbon dates of charcoal and bone apatite (left), and bone collagen (right) against temperature of burial environment. The blue line (thermal age) indicates the theoretical limit for collagen survival (Kendall et al. 2018).

Protein hydrolysis in acidic or alkaline aqueous environments can also cause fragmentation to collagen and may allow the more soluble components to be leached out as activation energies are also pH-dependent (Ajie, Hauschka and Kaplan 1991; Collins and Galley 1998; Turner-Walker 2008). Deamidation of asparagine (Asp) and glutamine (Gln) residues is known to occur in proteins by hydrolytic cleavage of the amide side chain, particularly at low pH and high temperatures, although deamidation of Gln occurs at much slower rates than that of asparagine (Van Doorn et al. 2012). Deamidation of Asp and Gln to aspartic and glutamic acid, respectively, cause structurally and biologically important alterations in peptide and protein structures (Robinson and Robinson 2001).

Local hydrology can also play a significant role in the survival of collagen (i.e. soluble fraction) as samples with higher thermal age (see **Figure 3.24**) may have better preserved organic content than samples of similar chronological age and lower thermal age, coming from areas with more active hydrology (Van Doorn et al. 2012). Water movement from topsoil to subsurface layers and evaporation from the subsoil to the soil surface the chances of collagen to survive are minimal (Grupe 1995). Grupe (1995) confirmed this relationship when she studied the preservation of collagen in archaeological human bones from Egypt buried in sandy soil. Collagen was poorly preserved in these samples as the sandy soil was not capable of absorbing and retaining water

(Grupe 1995). Evaporation caused a water flux from the deeper soil layers to the surface which led to a recrystallization of the soil ions within bone (Grupe 1995). This process commonly results in fissures in bone that are responsible for accelerating the loss of collagen (brittleness) in such arid areas (Grupe 1995). In such samples, direct side-chain hydrolysis will be the dominant mechanism for deamidation (Van Doorn et al. 2012).

3.3.1. QUALITATIVE ASSESSMENT

COLLAGEN YIELD, COLLAGEN C/N RATIO, NITROGEN OF WHOLE BONE

Efforts have been made to understand and characterize the preservation of the original collagen biological signal to avoid misinterpretations due to diagenetic signals (Collins et al. 1995, 2002; Dobberstein et al. 2009; Grupe 1995; Harbeck and Grupe 2009; Van Doorn et al. 2012; Van Klinken 1999). Collagen yield (wt.%) is the most widely used quality indicator to distinguish well-preserved from poorly-preserved collagen. Ambrose (1990) suggested a 3.5% threshold for problematic samples, DeNiro and Weiner (1988) proposed a 2% cut-off, while van Klinken (1999) suggested a 1%. Currently, 1 wt.% is considered a suitable threshold below which samples should not be used for isotopic and/or radiocarbon dating studies (Brock, Higham and Ramsey 2010; 2012; Dobberstein et al. 2009; Van Klinken 1999) and the exact reason is that when collagen content drops below 1% it is difficult to remove contamination (Van Klinken 1999).

A distinction between 'good' and 'bad' collagen based on the collagen wt. %, however, may result in an inclusion of 'bad' collagen samples in the 'good' ones, and vice versa (DeNiro and Weiner 1988). For that reason, collagen C/N ratio is used to improve screening practices. C/N values similar to modern bone (i.e. 2.9 to 3.6) are considered representative of good quality collagen, whereas much higher C/N ratios are linked to diagenesis (Ambrose 1990; DeNiro 1985; DeNiro and Weiner 1988). This range has been selected as samples exhibiting values outside this range may have either lost a considerable amount of nitrogen or gained exogenous carbon (Tuross 2002). The alterations of the carbon and nitrogen contents post-mortem involve more than one mechanism that proceed simultaneously, and they are responsible for the gradual loss of collagen and the differential loss of amino acids (Turner-Walker 2008; Tuross 2002). For instance, specific bacterial species may metabolize specific amino acids to utilize carbon as a source of energy (Turban-Just and Schramm 1998; Grupe, Balzer and Turban-Just 2002). This means that the larger amino acids such as histidine and phenylalanine are preferred as they contain more carbon atoms to satisfy bacterial demand (Balzer et al. 1997; Grupe 1995; Harbeck and Grupe 2009; Turban-Just and Schramm 1998; Grupe, Balzer and Turban-Just 2002). The smaller amino acids such as glycine and alanine which have fewer carbon atoms are less attractive for heterotrophic decomposers as they would have to metabolize larger amounts of small amino acids (Balzer et al. 1997; Grupe 1995; Turban-Just and Schramm 1998; Grupe, Balzer and Turban-Just 2002).

Microbial attack is usually followed by hydrolysis by other proteases which can give access to nitrogen (Balzer et al. 1997; Grupe, Balzer and Turban-Just 2002). Chemical hydrolysis of mineralized collagen requires the removal of the mineral and it usually leads to a further change to amino acid composition (Balzer et al. 1997; Masters 1987; Turner-Walker 2008; Tuross 2002; Grupe, Balzer and Turban-Just 2002). A loss of proline, for example, can be the result of collagen cleaving during autolysis, followed by non-specific protease activity which is capable of further destroying the collagen molecule after collagenase attack (Grupe 1995). Therefore, due to the different C/N ratios of the individual amino acids, a preferential loss of the hydrophobic amino acids (hydrolysis) and/or those with a higher number of carbons (microbial attack) would affect the C/N ratio (Harbeck and Grupe 2009; Masters 1987).

There are researchers, however, who claim that C/N ratio is an inadequate collagen quality indicator as good quality collagen can display higher than 3.6 C/N ratio (Ambrose 1990; Harbeck and Grupe 2009). Further to this argument, many archaeological bone samples that display an acceptable C/N ratio can have shifted stable isotope ratios due to poor collagen preservation (Harbeck and Grupe 2009). Thus, it is apparent that the simultaneous or successive degradation of collagen by microbial attack (decreased C/N ratio) and chemical degradation or contamination (increased C/N ratio) may result to an acceptable C/N ratio (Harbeck and Grupe 2009), and in such occasions C/N ratio can be a less reliable indicator for assessing collagen preservation (Ambrose 1990). Possible solutions that have been proposed include the widening of the C/N ratio range from 2.8 to 4.0 (Harbeck and Grupe 2009), or the use of C/N ratio of whole bone powder as an alternative solution, but currently they have not gained ground (Brock et al. 2012; Lebon et al. 2016).

The use of the % N of whole bone is assumed to significantly increase the successful screening of collagen (Brock, Higham and Ramsey 2010; 2012; Harbeck and Grupe 2009; Nielsen-Marsh et al. 2000b). It is c. 3.5-5.5 wt. % in modern bone (Baker, Butterworth and Langley 1946; Eastoe and Eastoe 1954) and gradually decreases in archaeological specimens. Bocherens et al. (2005) claim that % N can be effectively used to discriminate between well- and poorly-preserved samples, with a % N over 0.4 proposed as a threshold for samples to be further examined for stable isotopes and/or radiocarbon dating. Brock et al. (2012) similarly argue that a cut-off point of 0.7 % has a successful prediction rate about 73 % or over. Nonetheless, when samples contain >0.7 % N and give collagen yields <1 wt. %, the nitrogen may have been present as short-chain/degraded collagen or polypeptides, NCPs, soil contaminants, or conservation treatments (Brock et al. 2012; Lebon et al. 2016). Unfortunately, the % N content of whole bone powder cannot differentiate between nitrogen from collagen, NCPs and soil (Brock, Higham and Ramsey 2010; 2012), therefore collagen assessment of highly contaminated and/or degraded bones can be problematic (Brock et al. 2012).

Racemization involves the formation of one enantiomer (non-superimposable mirror images) from the other (L- to D- form) due to the thermodynamically unstable configuration of amino acids post-mortem (Johnson and Miller 1997). It stops when the solution is racemic, thus when D- and L-enantiomers reach an equilibrium value near 1 and this D-to-L ratio in a sample enables one to estimate how long ago the specimen died (**Figure 3.25**; Johnson and Miller 1997).

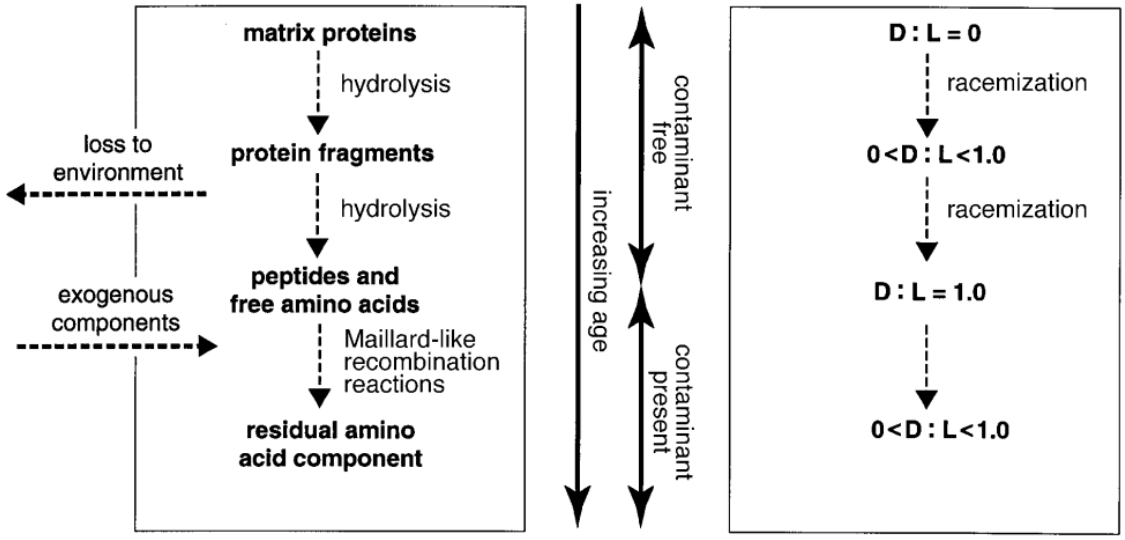

Figure 3.25. *Collagen degradation and racemization* – Peptide bond hydrolysis leading to a release of amino acids which are lost to the environment. Exogenous components may enter the bone tissue and may affect the racemization rates of the various amino acids (Bada, Wang and Hamilton 1999).

The application of amino acid racemization for the study of archaeological bone is controversial and its success is widely affected by the preservation state of the sample (Johnson and Miller 1997). The racemization rates increase with increasing temperatures and time, while they vary depending on the position of the amino acids in the peptide chain (Johnson and Miller 1997). Collagen might not be hydrolyzed, thus it might not be displayed in the amino acid profiles (Harbeck and Grupe 2009) making amino acid racemization relatively unhelpful as a quality indicator because it is applicable only to the hydrolysable fraction of the collagen (**Figure 3.25**; Van Klinken 1999). Although it can be used for the assessment of contamination to verify the absence of other proteinaceous substances, erroneous assessment of collagen preservation due to condensation reactions, diagenesis and the insensitivity of the method to other molecular species (e.g. humic acids) may occur (Van Klinken 1999). The extent of racemization can be a measure of overall collagen preservation as the relative rates of racemization of the various amino acids should follow a predictable sequence but only if no contaminants have been introduced into the bone matrix (Bada, Wang and Hamilton 1999). Consequently, amino acid analysis seems not to accurately depict the preservation state of collagen, as no gradual alterations are usually observed in amino acid compositions (Van Klinken 1999).

A good example is the use of aspartic acid (Asx) racemization as an indicator of collagen integrity (Collins et al. 1999, 2009; Tuross 2002). Specimens with poor collagen preservation should have higher D/L Asx values and samples with good collagen preservation should have low D/L Asx values (Ambrose 1990; Harbeck and Grupe 2009). However, Collins et al. (1999) support that Asx racemization is not likely to occur in triple helical collagen below its denaturation temperature (i.e. T_m=150^o C for mineralized collagen). Therefore, an increase in D-Asx in archaeological bones is probably caused by the racemization of the soluble non-collagenous proteins (NCPs) and the complete racemization of Asp in the telopeptides (Collins et al. 1999). Over archaeological timescales, the D:L ratio will increase due to the decreasing proportion of triple helical collagen and will reflect the rate of loss of helix (dependent on time and temperature) and leaching of soluble peptides (dependent on burial environment) (Collins et al. 1999). Thus, the atypical kinetics of Asx racemization in bone are complex and potentially unpredictable (Collins et al. 1999; Tuross 2002).

AMIDE-TO-PHOSPHATE RATIO (A_M/P)

Fourier transform infrared (FTIR) spectroscopy can be potentially used for the assessment of collagen preservation for the distinction between well- and poorly-preserved collagen (DeNiro and Weiner 1988). Amide I at c. 1640 cm^{-1} and amide II bands at c. 1540 cm^{-1} are considered characteristic of proteins and peptides (**Figure 3.26**; Chalmers 2010; Figueiredo, Gamelas and Martins 2012; Gourion-Arsiquaud, West and Boskey 2008). The former is attributed mainly to C=O stretching, whilst the latter involves N-H bending and C-N stretching vibrations (Chalmers 2010). 'Good' collagen displays a strong peak at c. 1640 cm^{-1} (amide I) and c. 1450 cm^{-1} (amide II/proline), whereas 'bad' collagen is characterized by a low absorbance in these spectral regions (DeNiro and Weiner 1988).

The 1640 cm^{-1}/1035 cm^{-1} ratio of the ν_1 amide and ν_1 PO_4^{3-} vibrational modes, respectively, has been used for the assessment of collagen in bone (e.g. Trueman et al. 2004; Lebon et al. 2016). Lebon et al. (2016) has also proposed an equation using the amide-to-phosphate ratio (Am/P) for the estimation of the remaining collagen wt. % in archaeological bone (i.e. collagen wt.% = 113.13 x Am/P + 1.69) with a standard error of estimation ± 1.21 wt%. However, the presence of overtones (e.g. O-H stretch at 1640-1660 cm^{-1} related with structural water) and N contamination can lead to an overestimation of the collagen content (Lebon et al. 2016). Lebon et al. (2016) observed such N contamination in several samples from catacombs due to exogenous organics (humic and/or fulvic acids) and/or minerals (ammonium and/or nitrates) possibly due to the accumulation of bodies in the mass burials which can promote the activity of microorganisms and the release of fluids that can contaminate bones (Lebon et al. 2016). The presence of humic (or fulvic) acids can also be observed at 1700-1500 cm^{-1} and 1100-1000 cm^{-1} absorption bands with the peaks at c. 1715 cm^{-1} and c. 1602 cm^{-1} assigned to humic acids that contain nitrogen (Lebon et al. 2016). Nonetheless, there is a limitation in distinguishing between humic acids, amide I and

phosphate domains as they all overlap (Lebon et al. 2016). Treatment of bone with NaOH may also result in increased Am/P ratios due to the absorption of water by bioapatite crystals (Lebon et al. 2016).

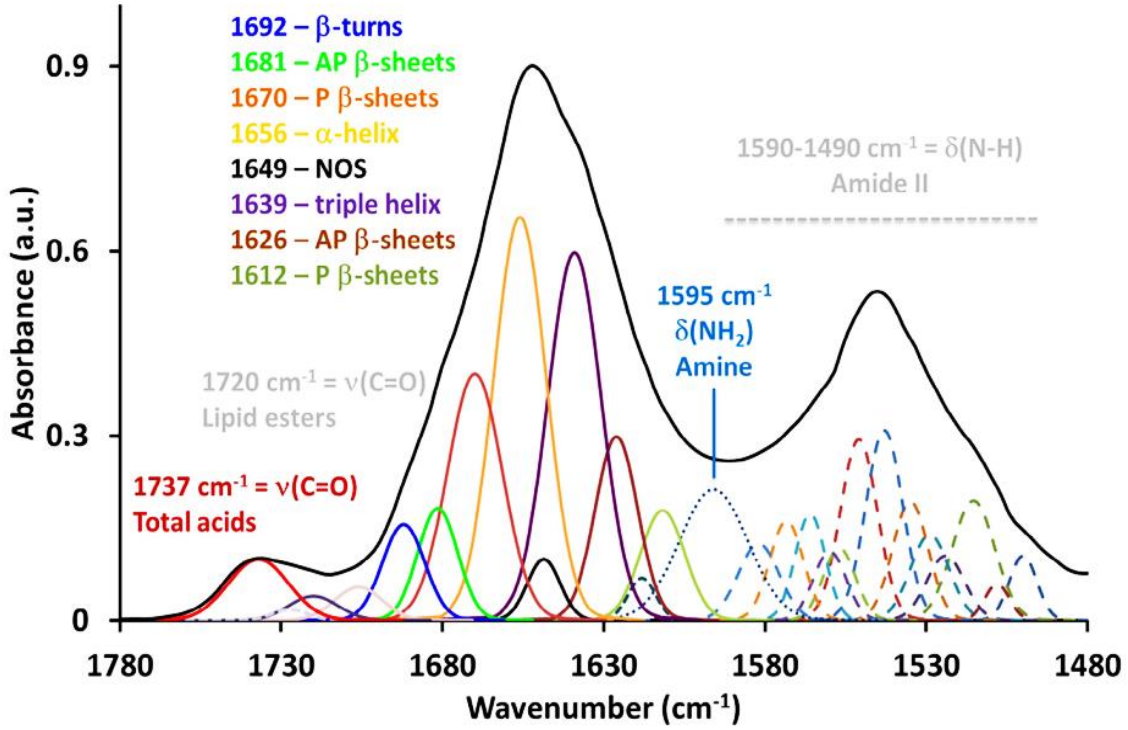

Figure 3.26. *Collagen type I mid-IR spectra* – Curve-fitted spectrum of the 1480-1780 cm^{-1} spectral region displaying the absorption bands and their sub-components (Bobroff et al. 2016).

Chadefaux et al. (2009) have also applied FTIR microspectroscopy to examine the diagenetic effects on the secondary structure of collagen preserved in the archaeological bone. Decomposition and reconstruction of the amide I band, and the position of the amide II band component were combined with curve-fitting to quantitatively estimate the relative proportion of each component representing a type of secondary structure (**Figure 3.26**; Chadefaux et al. 2009). The general feature of amide I components profile (the relative area of the α-helix and that of the random coils) seems to reflect a disorganisation in the collagen secondary structure; thus, the shape of the amide I band is representative of the collagen secondary structure (Chadefaux et al. 2009).

In archaeological samples, when the α-helix remains the major component it is an indication that the collagen secondary structure is still quite well preserved (Chadefaux et al. 2009). However, its relative area often decreases, while there is an increase in the fraction of the random coils (i.e. unordered structures) (Chadefaux et al. 2009). The decrease of the α-helix and the increase of the unordered structures are probably indicative of post-mortem modification in bone's structure (Chadefaux et al. 2009). The amide II absorption peak appears at around 1548 cm^{-1} in the archaeological bone, a shift that seems to be related with an alteration in the collagen structure

(Chadefaux et al. 2009). Therefore, FTIR-ATR mapping can be potentially used for the selection of the best-preserved parts of archaeological bone.

CHEMICAL PRE-TREATMENT EFFECTS

Collagen yields, C/N ratios, N% and C% vary greatly depending on the extraction method used (e.g. sample preparation, acid or EDTA demineralization processes, NaOH treatment) (Ambrose 1990; Jørkov, Heinemeier and Lynnerup 2007; Semal and Orban 1995; Van Klinken 1999). Some extraction protocols can lead to a more extensive degradation of large collagen peptide chains resulting to smaller fragments (Semal and Orban 1995). Thus, when assessing collagen preservation researchers should be aware that different extraction procedures affect collagen yields (Jørkov, Heinemeier and Lynnerup 2007).

Treatment of bone with a strong acid, for instance, can cause catalysis of amino acid residues (e.g. asparagine, glutamine) (Collins and Galley 1998). Grinding may also dramatically affect collagen extraction, especially in well-preserved samples where collagen fibres are long (Collins and Galley 1998). Although it seems that pulverization affects less the archaeological bone, especially, the poorly-preserved samples because collagen is already damaged, and it is less prone to chain scission, grinding samples should be avoided in the acid treatment method (Collins and Galley 1998). On the contrary, in the EDTA treatment where the surface area exposed to EDTA needs to be increased, grinding could improve demineralization (Collins and Galley 1998).

Collagen easily reacts with charged contaminant molecules but the interaction with the contaminants remains unclear (Van Klinken and Hedges 1995). Humic substances, for instance, may penetrate archaeological bone either from the soil and/or by *in situ* humification of collagen through Maillard reactions and irreversibly bound to the collagen molecules (Van Klinken and Hedges 1995). Uptake of humic acids by collagen has been found to be almost instantaneous as it initiates only few hours after first contact and the saturation levels have been found to reach even c. 25 wt. % (Van Klinken and Hedges 1995). Although NaOH treatment and gelatinization indicate that humic-collagen linkages are mainly in the form of hydrogen bonds, it is unknown what types of linkages might be involved (e.g. ionic, covalent, Van der Waals) and the effects of different reactions on those linkages (Van Klinken and Hedges 1995).

As a considerable amount of collagen can be broken down into products of lower molecular weight and sample clean-up chemistries usually do not remove all the humic acids present, ultrafiltration of samples is used to separate high molecular weight (i.e. >30 kDa) fractions of the gelatinized collagen from low molecular weight components (i.e. <30 kDa) (Higham, Jacobi and Ramsey 2006; Sealy et al. 2014; Van Klinken and Hedges 1995). Ultrafiltration is considered advantageous for the removal of environmental contaminants and it improves the quality of the extracted collagen as large molecular weight proteins retained are more likely to originate from the original bone collagen (Ramsey et al. 2004). Ultrafiltering samples that have low collagen

yields allows purification by removing the degraded collagen fragments, contaminated carbon from bones, soil-derived amino acids, salts, etc. (Higham, Jacobi and Ramsey 2006). It has been evidenced that this process improves the C/N ratios and other parameters which is an indication that it provides more reliable data by recovering collagen of sufficient quality (Higham, Jacobi and Ramsey 2006; Sealy et al. 2014).

One important limitation of ultrafiltration, however, is that it results in lower collagen yields to an unknown extent (Brock et al. 2012; Ramsey et al. 2004; Higham, Jacobi and Ramsey 2006; Sealy et al. 2014). Moreover, ultrafiltration cannot remove contaminants of higher molecular weights such as cross-linked humic substances (Higham, Jacobi and Ramsey 2006; Sealy et al. 2014). This makes ultrafiltration not very useful for assessing bone collagen preservation and it might have implications for the study of recent material with low collagen yields, especially for radiocarbon dating (Ramsey et al. 2004; Higham, Jacobi and Ramsey 2006; Sealy et al. 2014). Accordingly, well-preserved archaeological bone is not necessary to follow more stringent protocols that include the ultrafiltration step (Sealy et al. 2014).

3.3.2. PRESERVATION OF NON-COLLAGENOUS PROTEINS (NCPs)

The major diagenetic alterations that often result to poorly-preserved collagen in archaeological bones has led researchers on the quest for other non-collagenous proteins preserved in archaeological and fossil specimens (Ajie, Hauschka and Kaplan 1991; Ajie et al. 1992; Buckley et al. 2008; Masters 1987; Nielsen-Marsh et al. 2002). Several studies have explored the chances of NCPs being better preserved than collagen, as a potential recovery of NCPs may provide valuable information on palaeopathology, species identification, distribution patterns of some NCPs (i.e. polymorphism) in past populations (Brandt, Wiechmann and Grupe 2002; Collins et al. 2000; Grupe 1995; Masters 1987; Smith et al. 2005). Some researchers have even supported that some NCPs (i.e. osteocalcin) are superior to collagen for palaeodietary studies and radiocarbon dating, especially for poorly-preserved or fossilized specimens (Ajie, Hauschka and Kaplan 1991; Ajie et al. 1990; 1992).

Osteocalcin (i.e. gamma-glutamic acid or Gla protein) is the second most abundant protein in bone after collagen (Ajie et al. 1990). It controls calcium deposition and removal that regulate mineralization and crystal growth; therefore, the more mineralized the bone, the higher the osteocalcin content would be (Ajie et al. 1992). Its significant role for the stabilization of the mineral component of bone may protect osteocalcin from the biological and physicochemical processes that denature collagen (Ajie et al. 1990; Collins et al. 2002). Ajie et al. (1990) who first reported a set of data on osteocalcin from a series of modern and archaeological bones argue that when bound tightly to bioapatite, osteocalcin is well-protected from biochemical degradation as bioapatite acts as a buffer (Ajie et al. 1992).

However, quite often assumptions for the long-term survival of osteocalcin are contradictory as not much is known about its preservation (Collins et al. 2000; Buckley et al. 2008; Smith et al. 2005). The amount of osteocalcin that remains intact in archaeological samples depends on diagenesis (Ajie, Hauschka and Kaplan 1991). Thus, osteocalcin is not likely to survive in bones that display microbial attack, collagen hydrolysis, and/or mineral recrystallization (Smith et al. 2005). It is logically argued that the amount of osteocalcin decreases with increasing crystallinity of the bioapatite crystals, decreasing histological preservation and increasing collagen degradation (Smith et al. 2005).

Regarding crystallinity, it is believed that it affects the survival of osteocalcin as it limits the sites available for adsorption, hence it leads to its desorption (Smith et al. 2005). Although osteocalcin seems to decrease with increasing bone crystallinity, the exact relationship between mineral recrystallization and osteocalcin survival requires further investigation to better understand the relationship between the natural "packaging" and the effects of diagenesis (Collins et al. 2000). Osteocalcin also seems not to be preserved in bones with OHI values < 3 (Smith et al. 2005). The *in vivo* association between osteocalcin and collagen is also assumed to be strong, and osteocalcin would be expected to follow similar diagenetic pathways with collagen as they are both proteins (Smith et al. 2005). Although samples containing low amounts of collagen usually contain low amounts of osteocalcin, the amounts of osteocalcin in samples with well-preserved collagen are variable (Smith et al. 2005). With respect to radiocarbon dating of bones of similar age, osteocalcin may provide dates that are much older than those of collagen as a result of diagenesis (Ajie et al. 1990).

Using a kinetic approach for the study of the individual decomposition rates of the Gla-rich mid-region, N-terminus and C-terminus of osteocalcin, Collins et al. (2000) demonstrated that the Gla-rich mid-region is more stable, and the N-terminus is the least stable epitope. A loss of the mid-region with increasing temperatures also showed how temperature-sensitive is this region of osteocalcin (Collins et al. 2000). As a result, although residual amounts of osteocalcin or certain epitopes may be preserved in diagenetically altered bone, they might be insufficient for isotopic or radiocarbon studies (Smith et al. 2005). While this observation could mean that trace amounts of osteocalcin survive in archaeological bone, the situation is far more complex and their application to archaeology remains dubious (Brandt, Wiechmann and Grupe 2002; Smith et al. 2005).

Wadsworth and Buckley (2014) used proteomics techniques (i.e. liquid chromatography/tandem mass spectrometry-LC/MS/MS) to explore the complex protein mixtures in archaeological and fossil bones to determine an approximate temporal limit for the survival of NCPs in comparison to collagen and also to understand if NCPs are more useful for constructing phylogenies and species identification of ancient organisms than collagen (Wadsworth and Buckley 2014). In the

aggregate, 44 NCPs were identified in total, whilst 6 type I collagen chains were present in every sample (Wadsworth and Buckley 2014). Most of the NCPs were blood/serum proteins, with extracellular matrix, intracellular and bone-specific proteins following in numbers (Wadsworth and Buckley 2014). Among these, the most common were serum albumin, A2HSG, biglycan, chondroadherin, pigment epithelium-derived factor, lumican and prothrombin, while it was also found that, under favourable conditions, specific NCPs (e.g. albumin) can be recovered even from Early Pleistocene bone (Wadsworth and Buckley 2014).

Immunological methods have been used for the examination of polymorphic serum proteins in archaeological bones, but only the acidic groups of the NCPs were frequently preserved probably due to binding to calcium sites of the bioapatite crystals (Brandt, Wiechmann and Grupe 2002). A loss of specific side chains, thus, makes the identification of the epitopes during immunological assays problematic (Brandt, Wiechmann and Grupe 2002). ELISA may permit the identification and quantification of some NCPs; however, it is not clear if the information is false positive due to considerable charge alterations of the identified proteins due to diagenesis (Brandt, Wiechmann and Grupe 2002). Microbial attack can also introduce exogenous substances which may contribute to non-specific immunological reactions (Brandt, Wiechmann and Grupe 2002).

Collagen can also mask the presence of NCPs, hence the selection of an appropriate extraction method (e.g. enzymatic digestion of collagen) seems to be vital for the identification of the low-abundance NCPs (Brandt, Wiechmann and Grupe 2002; Wadsworth and Buckley 2014). Currently, it seems difficult to remove collagen via conventional means due to its diverse range in biochemical properties when hydrolysed (Wadsworth and Buckley 2014). Overall, it can be assumed that only well-preserved archaeological bone may retain osteocalcin and other NCPs in significant amounts that can be used for radiocarbon, isotopic investigations or other purposes (Brandt, Wiechmann and Grupe 2002; Smith et al. 2005; Wadsworth and Buckley 2014).

3.4. PRESERVATION OF DNA

Obtaining DNA from skeletal remains has revolutionized the way we understand our past as DNA can provide unique information on human evolution, migration events, sex, kinship, pathology, phylogenetics, and domestication of plants and animals (Gupta et al. 2015; Pääbo et al. 2004). aDNA is a relatively new field of research, and as such, there are several problems mainly related to its contamination and preservation (Gilbert et al. 2005; Lindahl 1993; Linderholm 2016; Mitchell, Willerslev and Hansen 2005; Pruvost et al. 2008). Publication of non-authentic results (e.g. exogenous DNA of microbial or human contaminants) has been a major problem despite the successful recovery of endogenous aDNA in a remarkable number of studies (Gilbert et al. 2005; Lindahl 1993; Mitchell, Willerslev and Hansen 2005; Willerslev and Cooper 2005). Thus, understanding its degradation post-mortem is an imperative necessity in aDNA research.

3.4.1. POST-MORTEM DECAY

DNA is a relatively unstable biomolecule as it undergoes progressive fragmentation post-mortem due to a wide range of biological and environmental factors (Adler et al. 2011; Lindahl 1993; Parsons and Weedn 2006). DNA degradation commences with the autolysis which takes place only few hours after the death of an organism (Burger et al. 1999; Parsons and Weedn 2006; Pruvost et al. 2007). It is rapidly degraded by endonucleases such as lysosomes that cut DNA strands at internal sites, while bacteria and other external microorganisms also proliferate and digest DNA with exonucleases from the ends (Hofreiter et al. 2001; Pääbo et al. 2004; Parsons and Weedn 2006; Pruvost et al. 2007).

Hydrolytic breakage of the polynucleotide strands (**Figure 3.27a**) is considered the main long-term reaction in aDNA degradation followed by chain breakage into shorter fragments usually between 100-500 bp in length (Bada, Wang and Hamilton 1999; Brown and Brown 2011; Hofreiter et al. 2001; Lindahl 1993; Pääbo et al. 2004; Parsons and Weedn 2006). The DNA molecule is particularly prone to this, as water attacks the β-*N*-glycosidic bonds and/or the phosphodiester bonds (Brown and Brown 2011; Lindahl 1993; Parsons and Weedn 2006). The attack on the phosphodiester bond leads to single-stranded nicks, whilst the attack on the glycosidic bond releases the nucleotides (Pääbo et al. 2004).

Hydrolysis predominantly releases the purines (i.e. depurination; **Figure 3.28**) as the purines are more susceptible to hydrolysis than pyrimidines (Brown and Brown 2011; Lindahl 1993). This release generates apurinic sites in the DNA strand (Bada, Wang and Hamilton 1999; Brown and Brown 2011). At these abasic sites, the free aldehyde form of the 2' deoxyribose group is involved in a β-elimination reaction which rapidly breaks the DNA backbone at the 3'-phosphodiester bond of the apurinic sugar (Bada, Wang and Hamilton 1999). A release of a base, however, does not automatically leads to a cleavage of the strand, as this requires the removal of several bases at

adjacent positions (Brown and Brown 2011). When that happens, hydrolysis results in gradual fragmentation of polynucleotide strands (Brown and Brown 2011; Lindahl 1993).

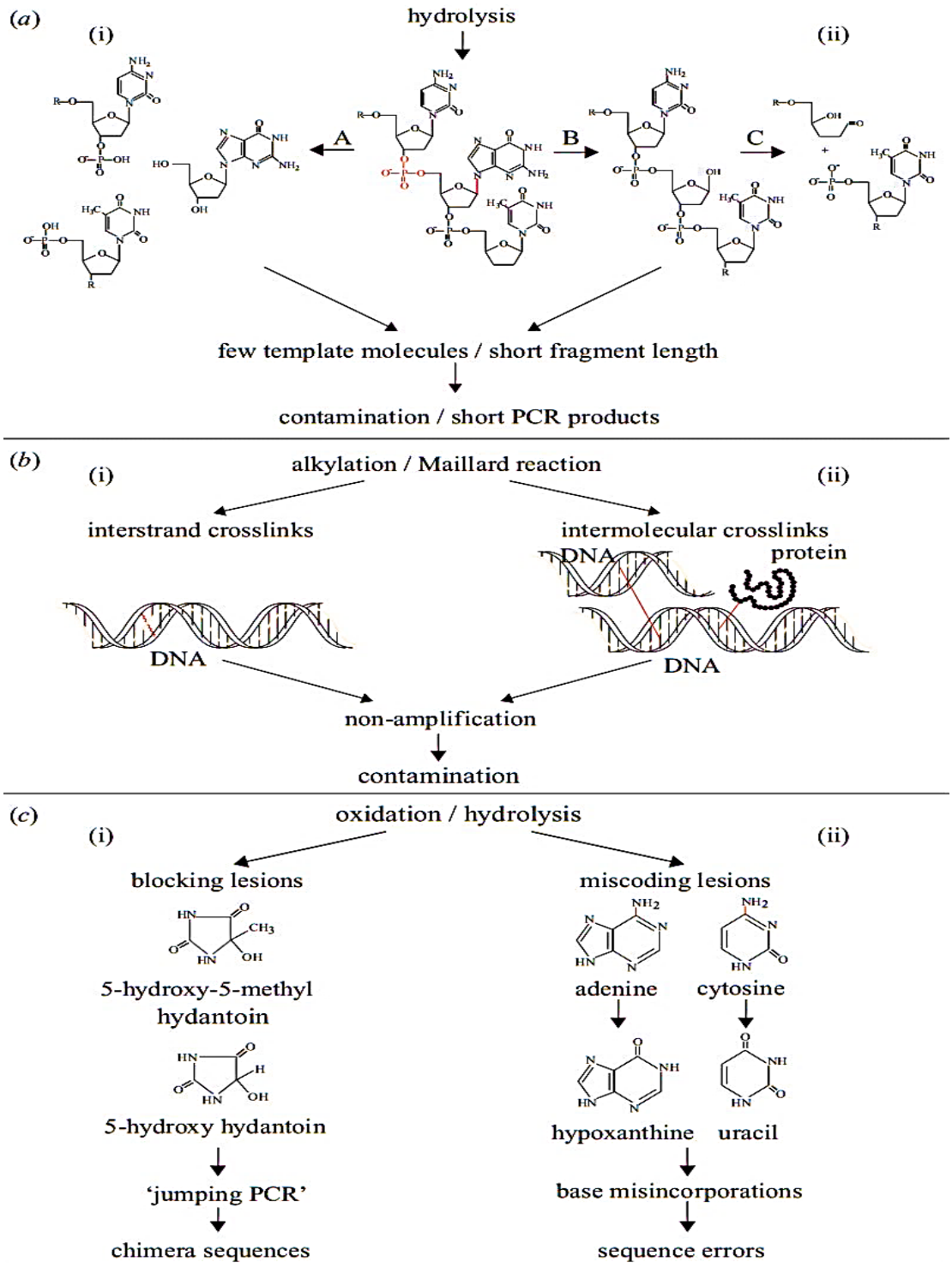

Figure 3.27. *Post-mortem DNA degradation* – Damaged patterns in red. (a) Hydrolytic damage that leads in the formation of strand breaks (single-stranded nicks) with (i) the cleavage of the phosphodiester bond (A) followed by (ii) depurination (abasic site - B) and breakage of the sugar backbone (C). (b) Cross-linking formation: (i) inter-strand crosslink by alkylation and (ii) intermolecular crosslinks by Maillard reaction. (c) Oxidation/hydrolysis of bases that results to (i) blocking lesions or (ii) miscoding lesions (Willerslev and Cooper 2005).

Hydrolysis can also cause the loss of the amino ($-NH_2$) group (i.e. deamination; **Figure 3.28**) with pyrimidines being more susceptible to such damage (Brown and Brown 2011; Lindahl 1993; Pääbo 1989). The deamination of cytosine to thymine is very common in aDNA and it generates a C→T sequence error (i.e. miscoding lesions; **Figure 3.27c**), as uracil (deaminated cytosine) binds to adenine (Brown and Brown 2011; Pääbo et al. 2004). The methyl ($-CH_3$) group attached to carbon 5', giving 5'-methyl cytosine in many cytosine bases (10-30% in nuclear DNA and much less in mtDNA) makes them more susceptible to deamination (Brown and Brown 2011; Hansen et al. 2001). G→A sequence errors should be also anticipated; however, different rates should be expected for each distinct miscoding lesion (Hansen et al. 2001).

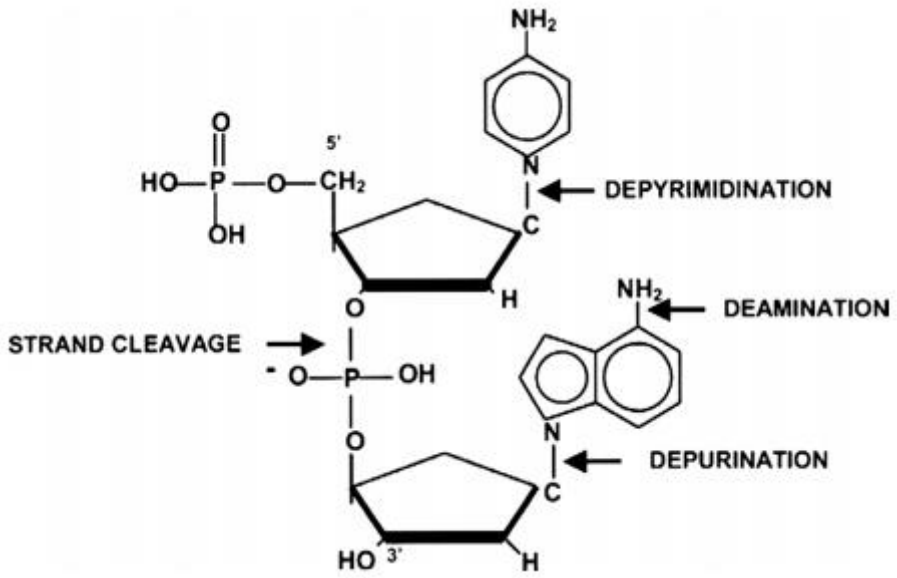

Figure 3.28. *DNA degradation* – Sites of chemical alteration in DNA (Schweitzer 2004).

Apart from thymine that cannot be deaminated (no amino group), adenine and guanine also undergo deamination, although their effects are not very significant (Brown and Brown 2011). An example would be the deamination of adenine to hypoxanthine (**Figure 3.27c**) that binds to cytosine rather than thymine, leading to A→G miscoding lesions (Brown and Brown 2011). The rate of this deamination is probably 2-3% that of cytosine (Brown and Brown 2011). Deamination of guanine to xanthine, however, does not lead to any miscoding as this base still binds to cytosine (Brown and Brown 2011). Miscoding lesions in mtDNA are concentrated in 'hot spots' such as the hypervariable region 1 possibly due to both *in vivo* mutations and post-mortem damage (Gilbert et al. 2003; Willerslev and Cooper 2005). Thus, the presence of miscoding lesions in aDNA complicates its correct determination (Brown and Brown 2011; Pääbo et al. 2004).

A different type of lesions called blocking lesions (**Figure 3.27c**) also prevent DNA polymerase to replicate the DNA (Brown and Brown 2011). The most important blocking lesions are those caused by oxidation of the bases and include hydrogen peroxide, super-oxide, and free hydroxyl radicals mainly from ionizing radiation (i.e. cosmic rays and geological radiation) (Brown and

Brown 2011; Parsons and Weedn 2006). Oxidative damage occurs through the strand scission and ring fragmentation of the 3–4′ carbon bond of the deoxyribose (Poinar 2003). The main site where oxidative attack is observed is the 5–6′ C=C double bonds of both pyrimidines, and the imidazole ring in purines, which lead to a ring fragmentation (Pääbo et al. 2004; Poinar 2003). The oxidation of the purines and/or pyrimidines, therefore, leads to a replacement of one or more double bonds with single bonds which can lead to the breakage of their rings (Brown and Brown 2011).

Another blocking lesion that can be caused by ultraviolet radiation via oxidation is the dimerization of purines on opposite strands (Brown and Brown 2011). Peptides attached to DNA strands can also be observed and may act as blocking lesions (Brown and Brown 2011). DNA fragmentation may also be the effect of denaturation when DNA molecules of several kilobases in length contain nicks in both strands (Brown and Brown 2011). Denaturation of DNA (i.e. separation of the double helix) is affected by low pH and high temperature (Parsons and Weedn 2006), as low temperature inhibits these processes, and if DNA withstands degradation in the early post-mortem phases, it may survive for long time-periods (Parsons and Weedn 2006).

Therefore, environmental conditions play a key role in the preservation of endogenous DNA (Poinar 2003). DNA decay is very temperature-dependent (Allentoft et al. 2012; Lindahl 1993; Lindahl and Nyberg 1972). Low temperatures have an advantageous effect on the survival of DNA, whereas high temperatures result in a significant loss of DNA (Burger et al. 1999; Poinar 2003). DNA yields are much higher in permafrost areas than in moderate temperate environments, while the latter better preserve DNA comparing to warmer areas such as the Mediterranean (Pruvost et al. 2008). A north-south decline in endogenous DNA yields has been reported by Bollongino et al. (2008), with a 67% success rate for the former compared to only a 7% for the Near Eastern open-air sites. Caves also undisputedly better preserve DNA as they have stable low temperatures all year-round and the soil environment usually protects bioapatite (Bollongino, Tresset and Vigne 2008).

BAp crystals are assumed to protect DNA from further degradation as it adsorbs onto the crystal surface (Götherström et al. 2002; Lindahl 1993; Parsons and Weedn 2006). Its preservation has been linked to the survival of DNA in bone, while its dissolution and recrystallization are related with considerable loss of DNA archaeological specimens (Allentoft et al. 2012; Götherström et al. 2002). The adsorption of DNA is controlled by environmental conditions (e.g. temperature, pH) according to data from an experimental study using biomimetic apatite (Grunenwald et al. 2014). More specifically, in lower temperatures (i.e. 4 °C) the amount of DNA adsorbed onto BAp crystals is significantly lower than in higher temperatures (i.e. 22 or 37 °C), with adsorption increasing in acidic environments and decreasing in alkaline contrary to what was previously believed (Götherström et al. 2002; Grunenwald et al. 2014; Lindahl 1993; Parsons and Weedn

2006). It was revealed that there is a loss of DNA when phosphate is added in the solution probably due to a competition for the available sites between DNA phosphate and inorganic phosphate (Grunenwald et al. 2014). Except for the evidence of the relationship between bioapatite and DNA, these studies also support that DNA cannot be located in osteocyte lacunae as it would be exposed to microbiological attack and the relationship crystallinity would be weaker (Götherström et al. 2002).

Regarding collagen, it is generally assumed to play an important role in DNA degradation as its survival is considered crucial for the survival of DNA. However, recent studies on thermally treated specimens have demonstrated that this is not true (Götherström et al. 2002; Ottoni et al. 2009). In fact, there is no relationship between collagen and DNA preservation as the survival of the latter appears variable (Ottoni et al. 2009; Poinar and Stankiewicz 1999).

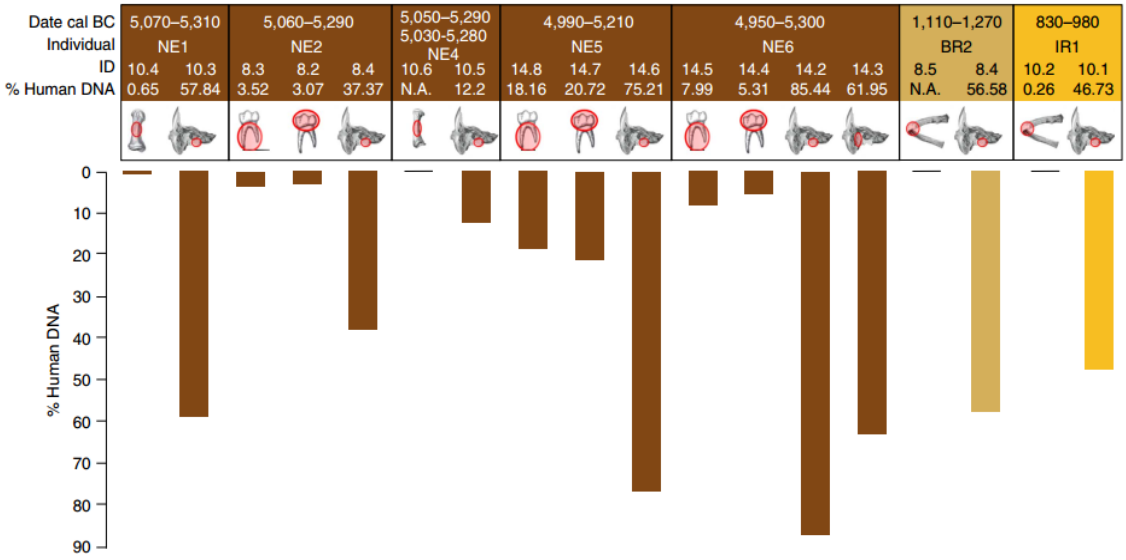

Figure 3.29. *Endogenous DNA in petrous vs other skeletal elements* – Percentage of non-clonal endogenous DNA recovered after shotgun sequencing. The sampled area is marked with red (Gamba et al. 2014).

A correlation between porosity and DNA preservation which has been linked to microbial activity has been observed by Gilbert et al. (2005). Archaeological bones with high diagenetic micro-porosity because of microbial reworking of bone apatite, would be expected to preserve much lower biomolecular information than bones with no diagenetic porosity (Turner-Walker et al. 2002). Staining of samples, especially dark colouration, has also been linked to loss of endogenous DNA (Hollund et al. 2016). This observation can have an impact on the selection of samples for aDNA studies as these often come from organic-rich, low oxygen environments that are considered good for DNA preservation (Hollund et al. 2016). Hollund et al. (2016) argue that the more diagenetically altered samples display IRSF, C/P and Am/P values indicative of these modifications. Hence, these diagenetic parameters can be used for the discrimination between

well- and poorly-preserved areas within the same specimens as they can be linked both to bioapatite and collagen degradation (Hollund et al. 2016).

Intra-individual and within bone variations have also been reported (Gamba et al. 2014; Pinhasi et al. 2015; Pruvost et al. 2008). A higher endogenous content in skeletal elements surrounded by more muscle mass has been observed by Pruvost et al. (2008). Particularly, DNA in limb bones, pelvis, ribs and scapula was better preserved than in skull, vertebrae, metatarsals and phalanges (Pruvost et al. 2008). Endogenous DNA yields from the petrous pyramid of the temporal bone (**Figure 3.29**) also exceed those from teeth by 4- to 16-fold and up to 183-fold those from other bones (Gamba et al. 2014; Hansen et al. 2017). Although yields of endogenous DNA from the petrous bone are exceptionally and consistently high, variation in endogenous DNA yields have also been observed with higher yields mainly obtained from the inner part of this skeletal element (**Figure 3.30**; (Pinhasi et al. 2015).

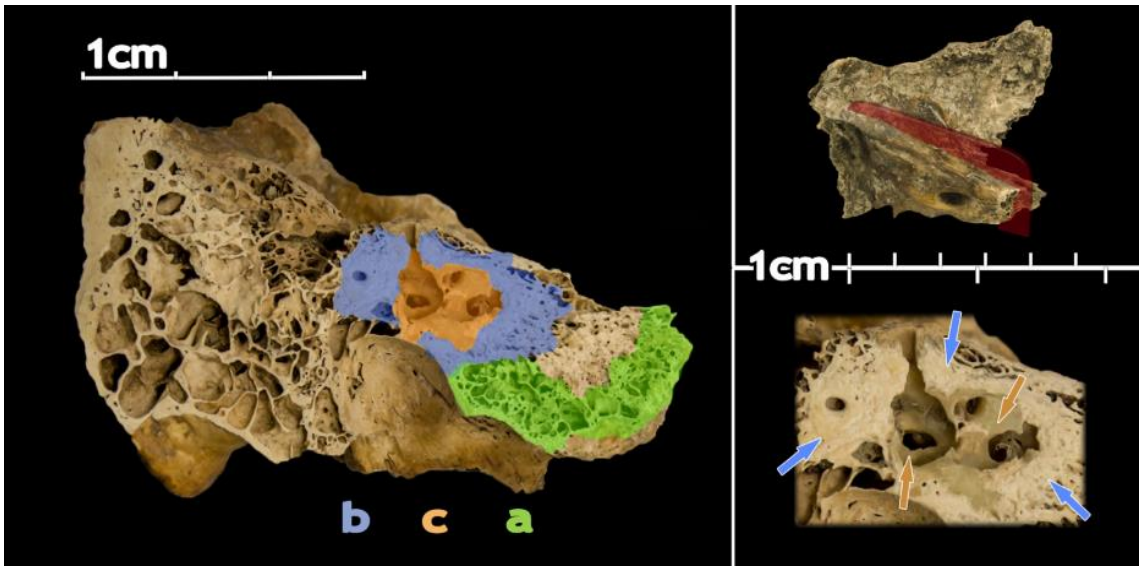

Figure 3.30. *Petrous bone* – Variations in endogenous DNA yields from parts a, b and c. The inner-ear bone (part c) usually preserves DNA in higher amounts than the other two areas (Pinhasi et al. 2015).

High-throughput sequencing data can also be potentially used to estimate DNA decay rates as the amount of amplifiable template should decline exponentially with increasing fragment size (Allentoft et al. 2012). Hence, all these data generated may provide an excellent source for the study of DNA decay (Allentoft et al. 2012). However, it is extremely difficult to predict the survival of DNA based on the time since deposition of a specimen (i.e. decay rate) as physical, chemical and biological factors affecting its preservation vary considerably (Allentoft et al. 2012). Allentoft et al., (2012) argue that endogenous bone DNA fragments may resist decay for more than 1 Myr after deposition in deep-frozen environments but it is highly unlikely to survive deeper in time. At present, no relationship between the chronological age of the specimens and DNA decay has been recognized (Poinar 2003). Therefore, careful consideration of the samples needs to be taken as the rate of fragmentation varies (Allentoft et al. 2012).

3.4.2. POST-EXCAVATION DECAY

Post-excavation treatment of samples affects DNA preservation and may further damage it (Hofreiter et al. 2001; Pruvost et al. 2007, 2008). After the removal of the skeletal remains from the soil, specimens are mainly stored in conditions that allow DNA decay to continue (Burger et al. 1999). Maintaining similar micro-environmental conditions for the specimens destined for DNA analysis is considered vital (e.g. no washing or brushing, preserving the sediment, placing them into plastic bags in the freezer) to increase chances for a successful extraction of endogenous DNA (Pruvost et al. 2008; Yang and Watt 2005).

Contamination of samples with modern DNA has been noted in several studies, with samples probably be more susceptible to contamination just after excavation, when they are still damp from the burial environment (Gilbert et al. 2006; Yang and Watt 2005; Yang, Eng and Saunders 2003). Contaminant DNA, which is identical or similar to the target aDNA, can be introduced into bone from the individuals who excavate, study and handle the skeletal remains, and this cannot be discriminately amplified by PCR (Pruvost et al. 2008; Yang and Watt 2005; Yang, Eng and Saunders 2003). Strict precautions and measures including isolated aDNA working areas, negative PCR control extractions and amplifications, assessment of biochemical preservation, cloning of products, and reproducibility, are necessary to ensure the quality of ancient DNA data (Gilbert et al. 2005; Poinar 2003; Pääbo et al. 2004). Additionally, pulverization or drilling of bone at low speed (c. 100 rpm) can limit the further damage of preserved DNA molecules as drilling skeletal tissues at high speed (c. 1000 rpm) results in a decrease in the quality and quantity of DNA (Adler et al. 2011).

CHAPTER 4: MATERIALS AND METHODS

Chapter 4 provides some general information on the samples and their origins, a detailed description of the techniques and methodological approaches used in this study, and a practical guide to petrous bone sampling. The analytical techniques employed include commonly used methods (histology, collagen analysis, elemental analysis, endogenous DNA content), new method developments (a newly developed protocol for FTIR-ATR analysis of bone powder, i.e. Kontopoulos et al. 2018), and novel approaches to bone diagenesis which can potentially provide useful additional data (2nd derivative analysis of mid-IR spectra, nano-indentation, and synchrotron micro-CT).

4.1. MATERIALS

Two hundred and seventy-two bones, including one-hundred and eight petrous bones, were used in this study (**Table A1-Appendix A**). Samples came from 18 archaeological sites (see **Table 1**) of which one in Germany (c. 10000 BC), one in Jordan (7500-5500 B.C.), six in Greece (8300-800 B.C.), one in Kazakhstan (2100-1800 B.C.), seven in Britain (3200 B.C.-1100 A.D.), one in Belgium (900-1800 A.D.), and one in Denmark (1650-1850 A.D.), with an aim to study both human and animal skeletal remains of different chronological age that originate from different geographic locations and burial environments. Samples from all British sites were provided in powder form, while samples from the remaining sites were chunks of bone from known skeletal elements and species (**Table A1-Appendix A**). Petrous bones are representative of the b and/or c areas (see section 3.4.1) as presented in Pinhasi et al. (2015). When sampling for aDNA analysis preceded sampling for histological, FTIR-ATR, collagen and elemental analyses, the samples did not derive exactly from the same anatomical location.

Statistical analysis was carried out using IBM SPSS v.25 and the significance level was set at p=0.05. An independent sample t-test is applied to assess whether the means of two unrelated groups show significant differences from each other on the same continuous, dependent variable. The values of the dependent variable of the two populations compared should be normally distributed (Shapiro-Wilk test for normality) and they should also display homogeneity of variances (Levene's test). When one of these two assumptions, or both, are violated, or when the sample size is relatively small (type II error), then a Mann-Whitney U test is carried out to determine if there are any differences in the medians between those two groups. When the population of either group is not normally distributed then the mean ranks are compared rather than the medians to determine whether the distribution (mean ranks) of the dependent values between the two independent groups is significantly different. Similarly, for the comparison of three or more independent groups of samples, the use of the one-way ANOVA test is applied, and

when there is a violation of any assumptions, then the equivalent non-parametric Kruskal–Wallis H test is used. The Holms-Bonferroni method is applied when performing multiple tests to reduce the possibility of getting a statistically significant result (i.e. a Type I error).

Coefficient of determination (R^2) of 0-0.19 is regarded as very weak, 0.2-0.39 as weak, 0.40-0.59 as moderate, 0.6-0.79 as strong and 0.8-1 as very strong correlation, but these are rather arbitrary limits and should be considered in the context of the results. In boxplots, the bold line across the box indicates the median. The bottom of the box indicates the Q1 quartile (25^{th} percentile) and the top of the box indicates the Q3 quartile (75^{th} percentile). The upper and lower whiskers extend to the highest and lowest values, respectively, which are no greater than 1.5 times the interquartile (IQ) range. Any values outside the ends of the whiskers represent the outliers (i.e. cases with values 1.5 to 3 times the IQ range) and any asterisks represent the extreme outliers (cases with values more than 3 times the IQ range).

Table 1. List of archaeological sites, dates and the number of samples studied from each site.

Site	Country	Date	No. of samples
Bedburg-Königshoven	Germany	12000 BP	5
Maroulas, Kythnos	Greece	8300-7600 BC	16
Ain Ghazal	Jordan	7500-5500 BC	6
Sarakenos Cave, Boeotia	Greece	6400-4000 BC	24
Promachon, Serres	Greece	5400-5000 BC	4
Tharrounia, Euboea	Greece	5300-3300 BC	11
Ness of Brodgar, Orkney	Britain	3200-2200 BC	7
Bornais, South Uist	Britain	3200-2200 BC	1
Silgenach, South Uist	Britain	3200-2200 BC	1
Manika, Euboea	Greece	2900-2300 BC	31
N/A	Kazakhstan	2100-1800 BC	6
Cladh Hallan, South Uit	Britain	2200-800 BC	6
Kastrouli, Delphi	Greece	1200-900 BC	24
Potterne, Wiltshire	Britain	1000-700 BC	7
Danebury, Hampshire	Britain	500-100 BC	3
York, Yorkshire	Britain	200-1100 AD	6
St. Rombout, Mechelen	Belgium	1100-1800 AD	101
Holmens Kirke, Copenhagen	Denmark	1650-1850 AD	9
Blackburn	Britain	1850 AD	4
		Total	**272**

4.2.1. HISTOLOGICAL ANALYSIS

One hundred and twenty-two transverse and thirty-three longitudinal thin sections of c. 200 μm from 147 samples (**Table A2-Appendix A**) were prepared using an Exact 300 CL diamond band saw. Sampling of petrous bone (n=36) was carried out by sectioning the element either longitudinally, or both longitudinally and transversely. Initially, specimens were cut longitudinally on the imaginary line drawn from the subarcuate fossa to the eminence between the jugular fossa and the cochlear canaliculus (**Figure 4.1**). This anatomical site allows the examination of both b and c areas of the inner ear (Pinhasi et al. 2015) as it intersects the inner ear into a medial part (that contains the cochlea) and a lateral part (that contains the semi-circular canals and other orifices for nerve supply and vascularisation) (see **Figure 4.2** for petrous bone morphology). With reference to the transverse sections, these were cut on a line drawn from the half of the internal auditory meatus to the middle of the vestibular aqueduct (**Figure 4.3**). These were used to complement histological assessment for the identification of micromorphological characteristics and post-mortem modifications. Material from the petrous bones used for the spectroscopic, elemental and molecular analyses was extracted from both medial and lateral parts as well as b and c areas of petrous bone, always following thin sectioning. When sampling for aDNA analysis preceded sampling for histological analysis, samples were still from the b and/or c areas of petrous bone but did not derive exactly from the same anatomical location.

Undecalcified thin sections were mounted onto glass microscope slides using Entellan New (Merck chemicals) for microscopy mounting medium (Wiggins and Drummond 2007) and covered by a glass coverslip, both cleaned with xylene before use. Thin sections were assessed under a Leica DM750 optical microscope using plane-polarized (PPL) and cross-polarized (XPL) transmitted light with total magnification ranging from 40x to 400x. Digital images were captured by a Leica ICC50 HD camera for microscopy imaging with a capture resolution of 2048 x 1536 pixel. The general histological index (GHI) introduced by Hollund et al. (2012) was used as it is analogous to the Oxford histological index (OHI) as described by Millard (2001), but includes generalized destruction, cracking, and staining. A GHI value of 5 represents excellent microstructural preservation similar to modern bone (>95% intact microstructure), whereas a GHI value of 0 indicates poor microstructural preservation (<5% intact microstructure) with almost no original histological features observed.

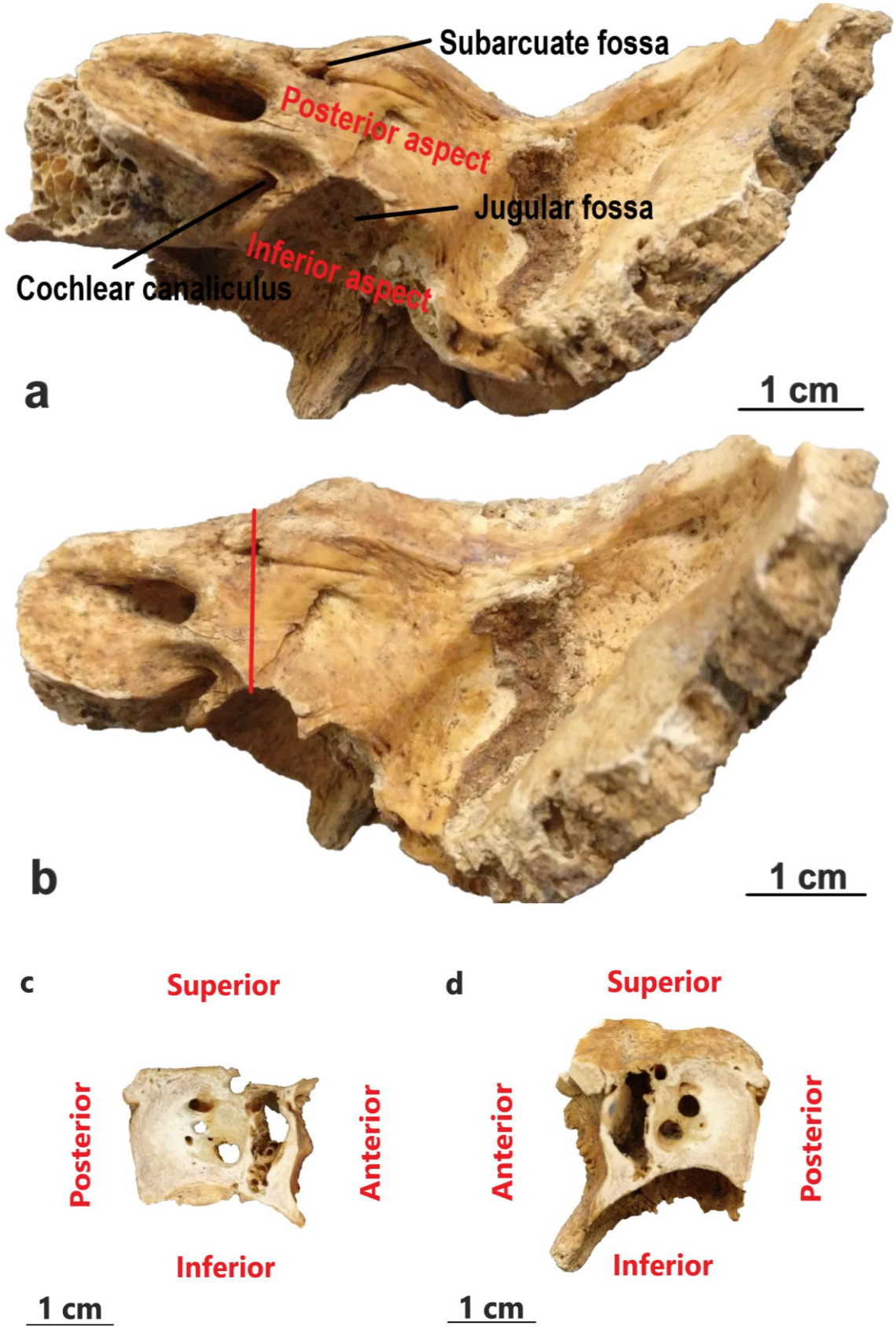

Figure 4.1. *Longitudinal sectioning of right human petrous bone* – (a) Section cut from the subarcuate fossa to the eminence between the jugular fossa and the cochlear canaliculus, in a posterior-anterior direction as seen in b. (c) The medial piece contains the cochlea which can be seen in the medial aspect of the section in Figure 4.2. (d) The lateral piece contains canals and other orifices for the vascular and nervous supply of the inner and middle ear.

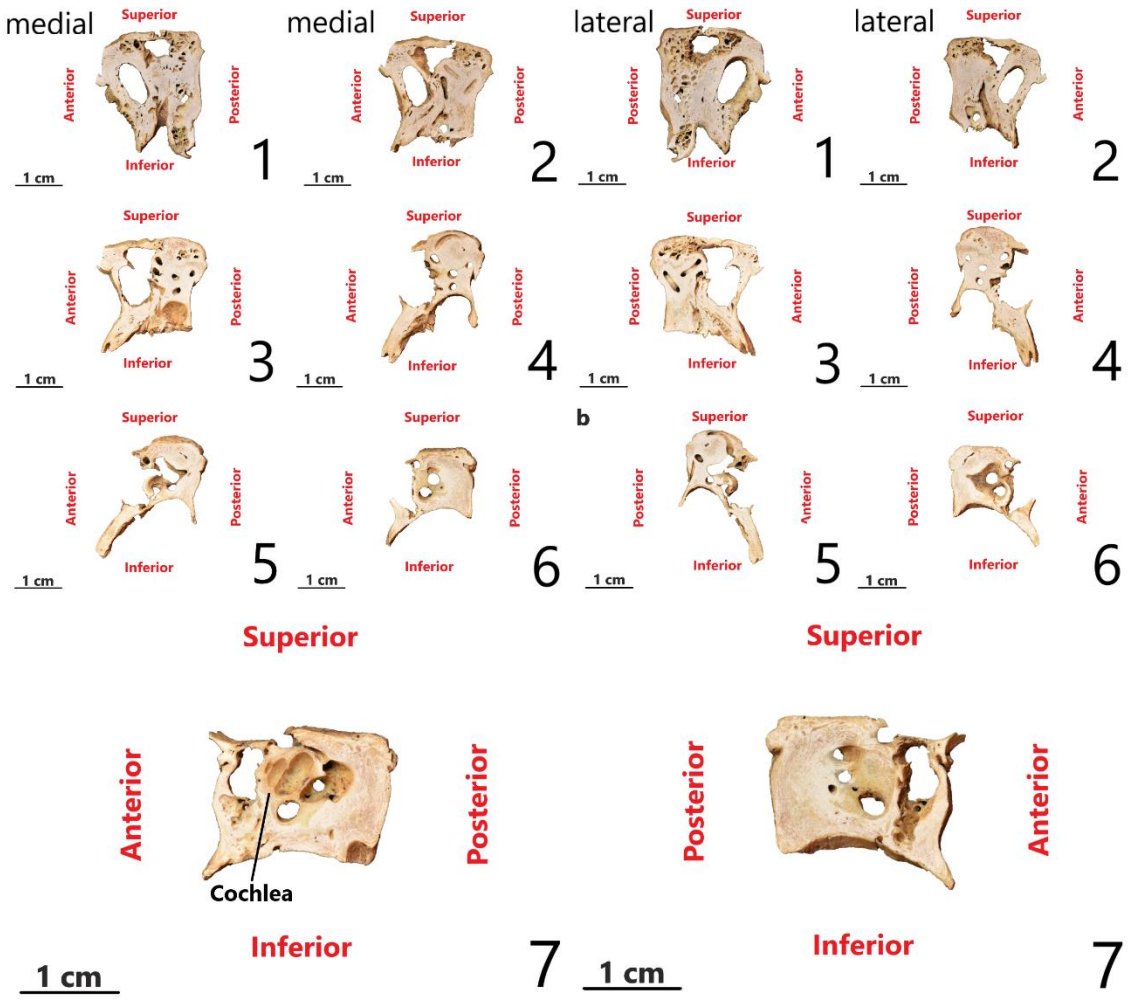

Figure 4.2. *Human petrous bone morphology*. Sections showing the differences in gross morphology of petrous bone every c. 2 mm at the longitudinal axis. The medial columns represent the medial aspects of the sections, while the lateral columns the lateral aspects of the same sections. Section 1 represents the most posterolateral part of the petrous bone mainly characterized by the large opening of the internal auditory meatus in the anterior aspect and some air cells mainly located posterosuperiorly. Section 7 represents the most anteromedial part of the petrous bone which includes the cochlea that is located at the center of the section (medial aspect). The cochlea can be identified by its characteristic 2.5 turns that resemble a snail shell. Adjacent to the cochlea there are two orifices for the vascular and nervous supply of inner and middle ear. In sections 2-4, the three semi-circular canals can be seen. Note the different colouration of the the tissues surrounding the cochlea and some canals, possibly related to the differences in their histomorphological and biomechanical characteristics.

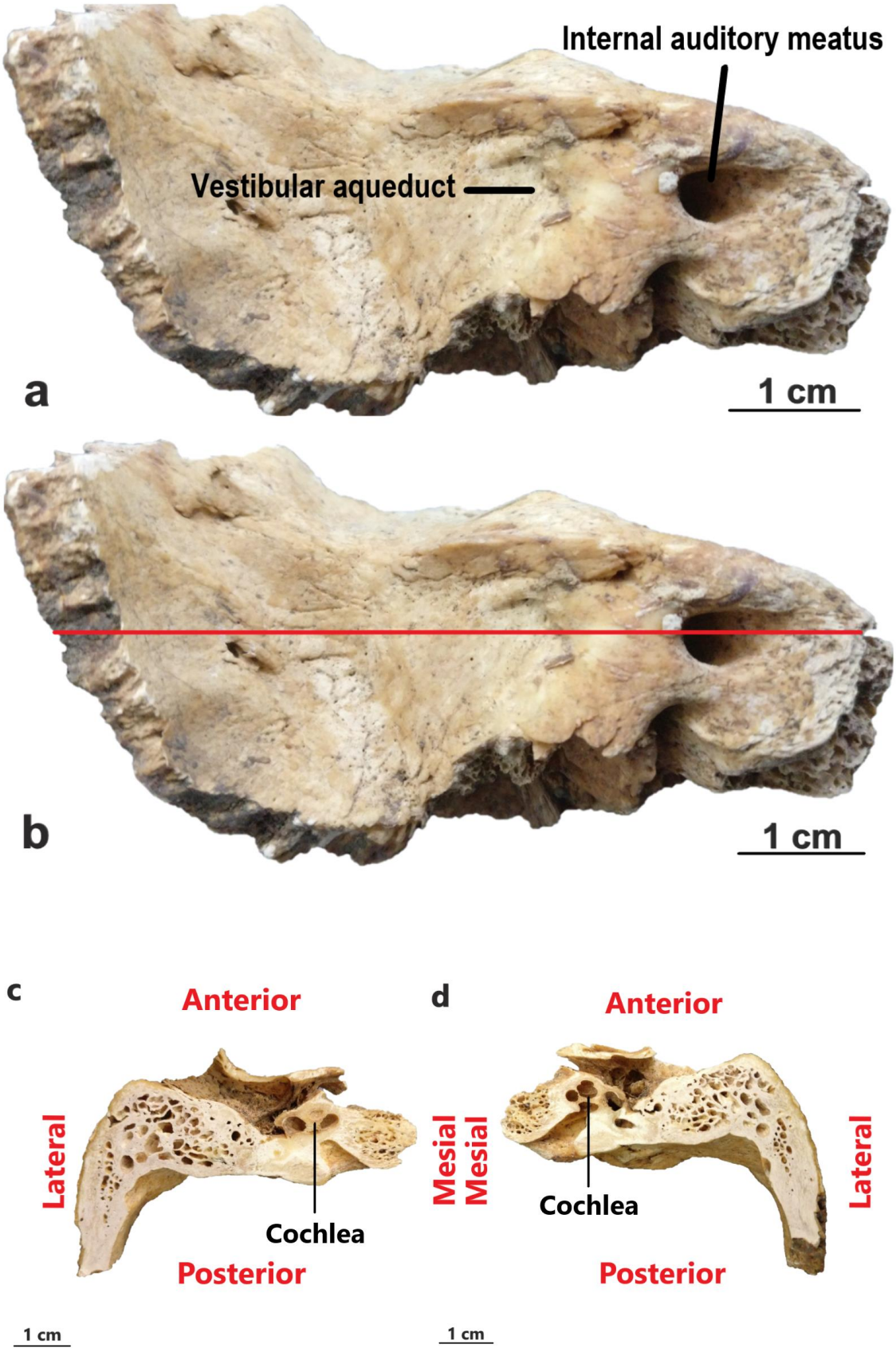

Figure 4.3. *Transverse sectioning of left human petrous bone* – (a) Section cut from the middle of the internal acoustic meatus to the centre of the vestibular aqueduct (posterior aspect of petrous bone), in a medial-lateral direction as seen in b. (c) The inferior and (d) the superior parts with the cochlea positioned in the anterior aspect.

4.2.2. SYNCHROTRON MICRO-CT

Synchrotron radiation micro-CT scanning was conducted at the Diamond Light Source labs (Didcot, Britain) on beamline I13. The five petrous bones analysed (**Table A1-Appendix A**) were prepared using an Exact 300 CL diamond band saw. The petrous bones were initially cut longitudinally in an antero-posterior direction as seen in **Figure 4.1**. Sections of 1 mm x 1 mm x Z (varying heights) were cut in a supero-inferior or antero-posterior direction.

Each sample was scanned with a pink X-ray beam with energies between 15 keV and 35 keV and a weighted mean spectral energy of 27 keV. A platinum coated mirror was used as a high energy filter and a combination of 1.35 mm pyrolytic graphite and 3.2 mm aluminium filters were used as low energy filters. A $CdWO_4$ single crystal scintillator (thickness = 500 μm) was used to convert the X-ray photons to visible light of 475 nm wavelength. An Olympus infinity corrected microscope system with M=4 and an additional M=2 tube lens was used to create the images on a pco.Edge 5.5 sCMOS detector. The effective pixel size of this setup is 0.82 μm.

The samples were mounted on an air-bearing Aerotech ABRT-260 rotation stage for the tomographic acquisition. A total of 2400 projections was acquired over 180° angular range. Projections were corrected for camera dark current and normalized with flat-images. The field of view was 2.1 mm x 1.8 mm (h x v) and a number of tomography scans were performed to cover the full height of the sample. An overlap of 0.3 mm was chosen to allow stitching of the individual scans and have a single volume for each sample.

For an initial 3D reconstruction, a single sub-volume of one of the petrous bone samples (SAR8) was selected. The collected data were processed in ImageJ using the BoneJ plugin. First the data converted to 8 bits and noise reduced by application of a 3D median filter with s=1. The data were thresholded to select the void spaces (blood vessels and lacunae) using the *triangles* algorithm as implemented in ImageJ. The void spaces were then analyzed using the particle analyzer plug in following the Birkedal methodology as in Bach-Gansmo et al. (2016a, 2016b) and Wittig et al. (2016), where only void spaces above 30 μm^3 volume were considered putative lacunae. The selected subvolume had a volume of 0.047 mm^3.

4.2.3. FTIR-ATR ANALYSIS

FTIR-ATR measurements were performed on two hundred sixty-eight archaeological bones, two modern human femora and one modern bovine femur (**Table A2-Appendix A**) using a Bruker Alpha Platinum spectrometer [range: 4000-400 cm^{-1}; no. of scans: 144; zero filling factor: 4; resolution: 4 cm^{-1}; mode: absorbance]. Sample preparation and analysis was carried out using Kontopoulos et al. (2018)'s protocol which was developed as part of this research study and improves data accuracy, precision, comparability and reproducibility. Specifically, Kontopoulos

et al. (2018) reported the effects of particle size and sample selection (i.e. periosteal, mesosteal, trabecular bone) on the mid-IR spectrum of bone powder measured by FTIR-ATR. It was demonstrated that IRSF increases with decreasing particle sizes from >500 μm to 20-63 μm both in unheated and heated archaeological bone and modern specimens (**Figure 4.4**). This is possibly an example of the Surovell and Stiner (2001) "separation hypothesis" down to the 20-63 μm particle size, giving way to the "destruction hypothesis" when bone powder is consisted of particles of c. 1 μm, as there was a large decrease in IRSF values at this point.

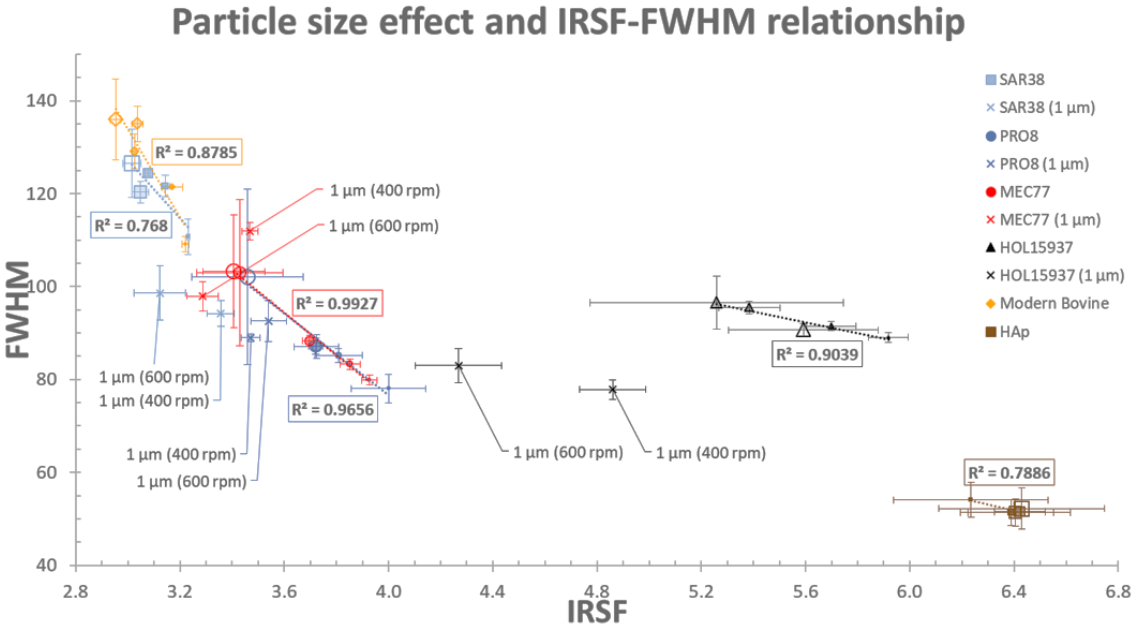

Figure 4.4. *Particle size effect on IRSF and FWHM at 1010 cm^{-1}* - IRSF-C/P relationship with the samples' particle size in modern and archaeological bone. Datapoint markers' sizes gradually decrease with decreasing particle size (i.e. **>500 μm**: size 10, 100% transparent; **250-500 μm**: size 8, 80% transparent; **125-250 μm**: size 6, 60% transparent; **63-125 μm**: size 4, 40% transparent; **20-63 μm**: size 2, 20% transparent). Error bars represent estimated standard deviations (Kontopoulos et al. 2018).

The FWHM at c. 1010 cm^{-1} showed a very strong inverse relationship with IRSF and a very strong linear relationship with particle size, decreasing with decreasing particle size from >500 μm to 20-63 μm (Figure 4.4). When bone powder consisted of particles of c. 1 μm, the FWHM at c. 1010 cm^{-1} did not show any characteristic pattern and relationship with crystallinity, confirming that the boundaries between order and disorder in BAp crystals are still unclear. Overall, these patterns were strongly related to the changes that occur at the short- and long-range order of the BAp crystals during grinding.

Absorbance of the IR radiation was also strongly affected by the particle size, with higher absorbances for smaller bone powder particles. This observation indicated that for smaller particle sizes, there was a better contact between the sample and the prism, as well as a higher exposure of the bone powder's components to the IR light. Further, removal of the periosteal, endosteal and trabecular tissues prior to pulverization of mesosteal (mid-cortical) bone was proved

necessary to eliminate uncertainties introduced by variations between IR data of the different bone areas.

Therefore, bone samples were ground using an agate pestle and mortar following the mechanical cleaning of the outer and inner bone surfaces. About 2-3 mg of bone powder of 20-50 μm particle size were used for each measurement, and after each measurement the crystal plate and the anvil of the pressure applicator were thoroughly cleaned using isopropyl alcohol. Samples were run in triplicate; spectra were analysed using OPUS 7.5 software, and the calculations of the FTIR indices were conducted after baseline correction as seen in **Box 1**. The average values of two modern human femora (IRSF=3.357±0.007, C/P=0.24±0.003, Am/P=0.182±0.001, BPI=0.482±0.000) and one modern bovine femur (IRSF=3.221±0.012, C/P=0.248±0.006, Am/P=0.216±0.007, BPI=0.469±0.018) were used as reference throughout.

Box 1. The mid-IR spectra of 20-63 μm particle size archaeological human mesosteal bone powder (MEC77). The spectral bands used for IRSF (a), C/P (b, c), and Am/P (b, d) are highlighted. Blue lines represent the peak positions for IRSF, C/P and Am/P indices and the red lines are the baselines.

Box 1. Indices and baseline correction

1. Infrared splitting factor (IRSF) was assessed using the equation introduced by Weiner and Bar-Yosef (1990, p. 191) that measures the heights at c. 600 cm^{-1} + c. 560 cm^{-1}, divided by the trough between them at c. 590 cm^{-1}, using a baseline correction from the c. 400-420 cm^{-1} to the c. 630-670 cm^{-1} troughs (a). The two peaks are characteristic of the v_4 antisymmetric bending mode of orthophosphate ion.

$$\mathrm{IRSF} = \frac{600\ \mathrm{cm^{-1}} + 560\ \mathrm{cm^{-1}}}{590\ \mathrm{cm^{-1}}}$$

2. Carbonate-to-phosphate (C/P) ratio was estimated as in Wright and Schwarcz (Wright and Schwarcz, 1996, p. 936) by dividing the main v_3 carbonate peak height at c. 1410 cm^{-1} with the main v_3 phosphate vibrational band at c. 1010 cm^{-1}. The baseline correction was drawn from c. 1590 cm^{-1} to c. 1290 cm^{-1} and from c. 1150-1180 cm^{-1} to c. 880-900 cm^{-1}, respectively (b and c).

$$\mathrm{C/P} = \frac{1410\ \mathrm{cm^{-1}}}{1010\ \mathrm{cm^{-1}}}$$

3. Amide-to-phosphate (Am/P) was assessed by the v_1 amide at c. 1640 cm^{-1} divided by the main v_3 phosphate peak at c. 1010 cm^{-1} (Trueman et al., 2004, p. 726). Baseline correction was from c. 1720 cm^{-1} to c. 1590 cm^{-1} and c. 1150 cm^{-1} to c. 890 cm^{-1}, respectively (b and d).

$$\mathrm{Am/P} = \frac{1640\ \mathrm{cm^{-1}}}{1010\ \mathrm{cm^{-1}}}$$

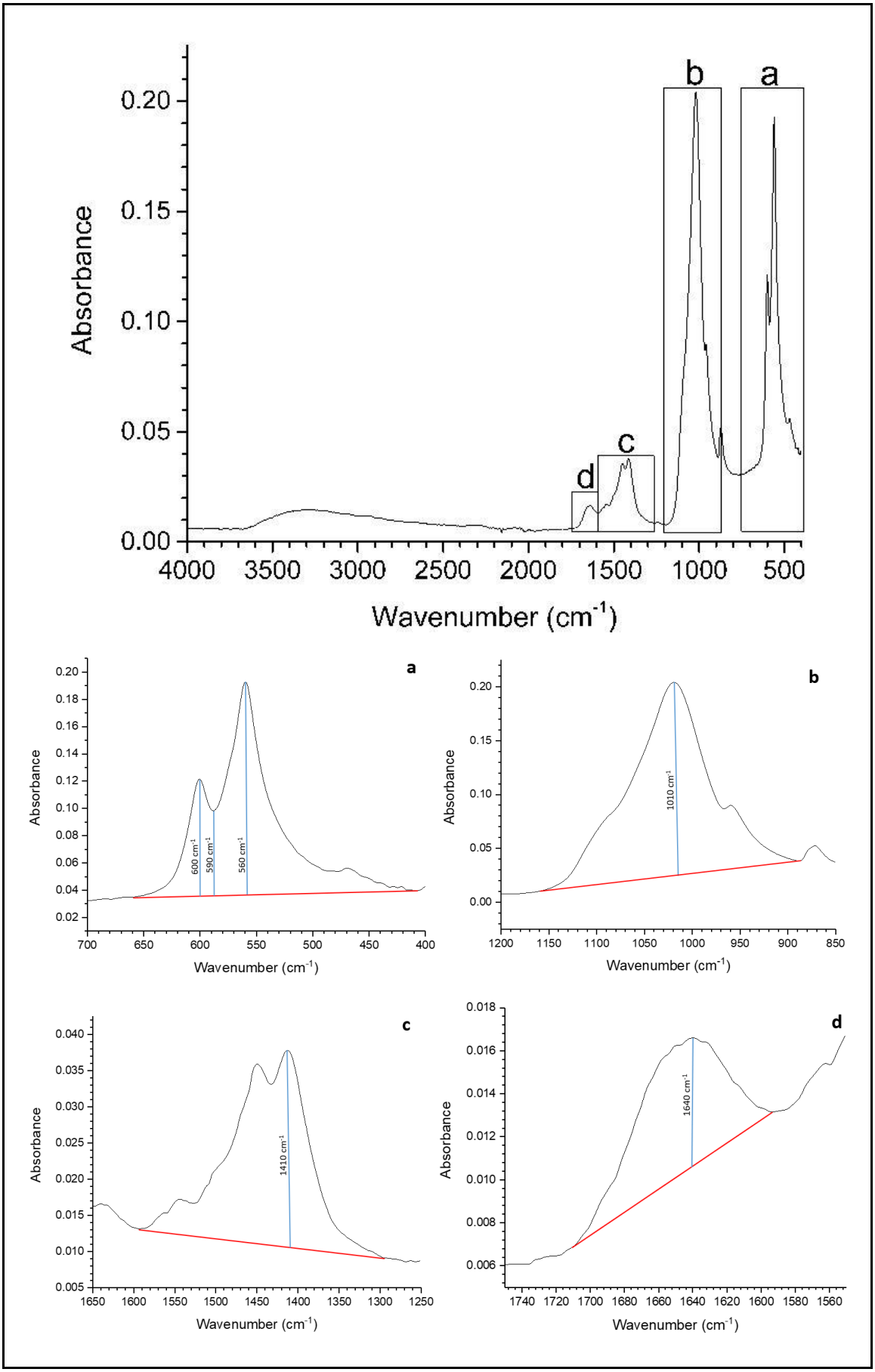

For the identification of overlapping/hidden components that cannot be distinguished in the zeroth order (basic) spectra, derivatization of the spectral curves was carried out (Talsky 1994; Kus,

Marczenko and Obarski 1996; Mark and Workman 2003). The distinction of the overlapping components of the broader amide I band, the v_2 and the v_3 CO_3^{2-} bands through 2nd derivative analysis was conducted using the OriginPro 2017 software. The Savitzky-Golay filter was applied to decrease the noise, and a polynomial order of 4 with 13 smoothing points were used for the analysis of the amide I bands and the v_2 CO_3^{2-} bands (Gander and von Matt 1993; Schafer 2011). As the method is sensitive to noise, a further increase in the number of the smoothing points to 25 was applied to the v_3 CO_3^{2-} band to reduce noise (Kus, Marczenko and Obarski 1996). Although smoothing reduces the noise, it requires careful consideration as it can also distort the spectral features (Kus, Marczenko and Obarski 1996).

4.2.4. COLLAGEN ANALYSIS

Collagen was extracted from 226 samples (**Table A3-Appendix A**) using a modified Longin (1971) method. The exterior surfaces of bone samples were mechanically cleaned using a scalpel. Bone chunks of 300-500 mg were demineralized in 8 mL 0.6 M HCl at 4∘ C. Samples were agitated twice daily, and acid solution was changed every two days. When demineralisation was completed, the supernatant was drained off and samples were rinsed three times with distilled water. Gelatinization was carried out by adding 8 ml pH 3 HCl and samples were placed in hot blocks at 80° C for 48 h. The supernatant liquor which contains the collagen was filtered off by using Eezee filters and was freeze dried for 2 days in pre-weighed plastic tubes.

Extracted collagen was analyzed in duplicate. Tin capsules containing 0.9-1.1 mg of collagen were dropped into an oxygen rich combustion tube held at 1000° C. The tin capsules were ignited and burnt exothermally at 1800°C causing the sample to oxidise. The samples were carried through a layer of chromium oxide and copper oxide which ensure complete oxidation, followed by a layer of silver wool to remove unwanted sulphur and halides. The samples' gases pass into a second furnace containing copper held at 600°C where excess oxygen was removed, and nitrogen oxides were reduced to elemental nitrogen. Any water was removed using a magnesium perchlorate trap. The samples then passed into a gas chromatography (GC) column held at 70° C which separates CO_2 and N_2 from each other. The resultant gases were then introduced into the Sercon 20-22 mass spectrometer where the samples were ionised, and the various masses separated in a magnetic field, focused into Faraday collector arrays and analyzed.

4.2.5. ELEMENTAL ANALYSIS

Whole bone elemental analysis (% C, % N) was performed on 2-3 mg of bone powder from 69 specimens (**Table A3-Appendix A**). Samples were run in duplicate on an Exeter Analytical CE-440 elemental analyser, used in conjunction with a Sartorius SE2 analytical balance automated carbon and nitrogen elemental analyser. Samples were weighed into smooth-walled tin capsules,

sealed and combusted in O_2 at 975 ºC. Combustion products were then analysed by thermal conductivity detectors, against a blank of helium.

4.2.6. DNA ANALYSIS

The endogenous DNA content of 90 samples (**Table A3-Appendix A**) was provided by three different labs in Europe. Laboratory work was performed according to strict aDNA standards in dedicated clean laboratory facilities at Trinity College Dublin (Dan Bradley), the University of Mainz (Joachim Burger), and the University of Copenhagen (Morten Allentoft). The exterior surfaces of bones were mechanically removed using a drill or by sandblasting, and UV-irradiated for 30 minutes per side before pulverization. DNA extraction, library preparation, sequencing, bioinformatics and DNA authenticity were conducted as described in Daly et al. (2018), Hofmanová et al. (2016), and Hansen et al. (2017) for Trinity College, Mainz and Copenhagen lab, respectively.

4.2.7. NANOINDENTATION

Nanoindentation was carried out on 3 mm transverse thick sections (longitudinal sections from the lateral part for petrous bones) from 19 samples (**Table A4-Appendix A**). The sections were first embedded in epoxy resin, ground with silicon carbide paper, polished using alumina suspension and dried naturally at room temperature. A CSM Nano-Hardness Tester was used with a loading rate=20 mN/min, unloading rate=20 mn/min, max depth=1000 nm, Poisson ratio=0.3, and delta slope contact=40%. Thirty indentations (600 in total) were performed on each sample (10 on each different tissue region, i.e. periosteal, mesosteal, endosteal, as well as tissue surrounding cochlea in petrous specimens) and each indentation was lasting for 120 s (30 s loading, 60 s pause, 30 s unloading).

CHAPTER 5: RESULTS AND DISCUSSION

This chapter presents the microstructural, bioapatite, collagen, biomechanical and DNA data in an attempt to answer the objectives set in Chapter 1. It builds on the work developed in this study and published in the following papers (Appendices D-F):

- Kontopoulos I., Presslee S., Penkman K., and Collins M.J. (2018). Preparation of bone powder for FTIR-ATR analysis: The particle size effect. *Vibrational spectroscopy*, 99, pp.167–177. [Online]. Available at: doi:10.1016/j.vibspec.2018.09.004.
- Kontopoulos, I., Penkman, K., McAllister, G. D., Lynnerup, N., Damgaard, P. B., Hansen, H. B., Allentoft, M. E., and Collins, M. J. (2019). Petrous bone diagenesis: A multi-analytical approach. *Palaeogeography, palaeoclimatology, palaeoecology*. Special issue: Advances in the study of diagenesis of fossil and subfossil bones and teeth.
- Kontopoulos, I., Penkman, K., Liritzis, I., and Collins M. J. (under review). Bone diagenesis in a Mycenaean secondary burial (Kastrouli, Greece). *Archaeological and Anthropological Sciences*.

It provides a synthesis of seven datasets gathered from the different analytical techniques to enable a deeper exploration of the diagenetic patterns of petrous bone. Chapter 5 is divided into four aspects (microstructural, bioapatite, collagen and DNA preservation) that are split into subsections which examine the preservation of the petrous versus other bones (sections 5.1.1, 5.2.1, 5.3.1, and 5.4.1), inter-site (sections 5.1.2, 5.2.2, 5.3.2), intra-site (sections 5.1.2, 5.2.2, 5.3.2), intra-individual (sections 5.1.3, 5.2.3, 5.3.3), and intra-bone (sections 5.1.3, 5.2.3, 5.3.3) variability and put the new information into context. The crystallinity-to-carbonate association (section 5.2.4) and the bioapatite-to-collagen relation (section 5.3.4) are further explored. New screening methods for collagen and DNA are also proposed at the end of the relevant sections (sections 5.3.5 and 5.4.2).

5.1.1. PETROUS VERSUS OTHER BONES

Histological examination of 36 petrous bones has allowed the identification of some unique features in petrous bone histomorphology compared to other skeletal elements. Interestingly, adult human petrous bones consist of highly osteocytic woven and lamellar-like tissues (**Figure 5.1a-b**), a combination that is not found in any other normal adult human bone. Woven tissue can be seen throughout petrous bone (**Figure 5.1a-d**) and its presence may indicate a lack of bone remodelling in large areas of the inner ear. Sorensen et al. (1992) have reported a persistence of woven bone to remodeling in rabbit otic capsule. Specifically, formation of woven bone as a response to trauma was not followed by a replacement with lamellar tissue contrary to long bones (Sørensen, Bretlau and Josrgensen 1992), which is probably linked to the high-density of viable osteocytes (i.e. anti-resorptive action) in the inner ear (Bloch and Sørensen 2010; Bloch, Kristensen and Sørensen 2012).

Here, lamellar-like tissue is observed primarily in the outer 100-200 μm of the outer periosteal tissue of the petrous bone, but also in limited areas of inner periosteal or endosteal tissues (**Figure 5.1a-b**). Many osteons can be observed in the posterior part throughout the medial-lateral axis of the petrous pyramid, but sparse osteons can also be found in tissue surrounding the cochlea, semi-circular or other canals (**Figure 5.1a-b**). This may indicate that bone remodelling can take place in some areas of the inner ear (Doden and Halves 1984; Frisch et al. 2000; Jeffery and Spoor 2004; Jørkov, Heinemeier and Lynnerup 2009), as continual, age-dependent and variable changes in the size and organization of the pneumatized spaces have been observed within the petrous pyramid (Hill 2011). A centrifugal distribution of secondary osteons of decreasing size towards the inner areas of the otic capsule has also been observed by Sørensen et al. (1990, 1992) and Sørensen (1994), suggesting a progressive lack of bone remodelling towards the inner areas of the bony labyrinth.

Here, osteons can be observed both in the longitudinal and transverse direction (**Figure 5.1c-f**) of petrous bone, which is another unique micromorphological characteristic of this skeletal element. The appearance of osteons in both directions can be explained by the fact that the vascular network of the otic capsule is a termination area for the internal auditory artery (IAA) and a communication area between the IAA and several other arteries (Mazzoni 1972). Thus, the osteons and other vascular canals need to accommodate the various arteries, nerves and their branches which travel in various directions.

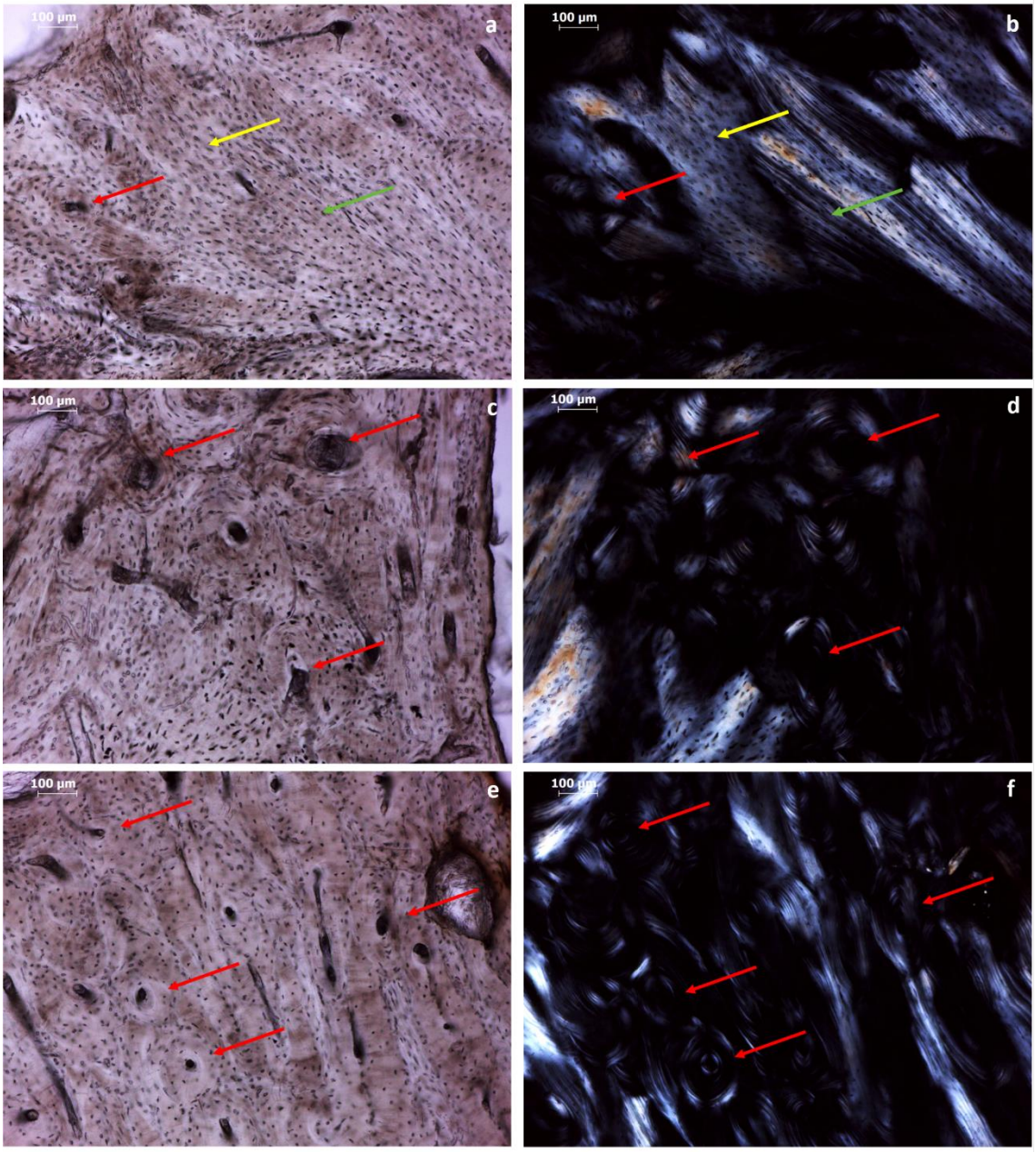

Figure 5.1. *The three bone tissue types coexisting in adult human petrous bone.* **DEN6 Longitudinal (a) PPL and (b) XPL - 100x**: Thin section showing an osteon (red arrow), woven tissue (yellow arrow), and lamellar-like tissue (green arrow) within a well-preserved area between semi-circular canals.
DEN3 Transverse (c) PPL and (d) XPL - 100x: Image showing the presence of osteons (red arrows) in the outer and inner periosteal tissue. **DEN6 Longitudinal (e) PPL and (f) XPL - 100x**: Another image showing the presence of osteons (red arrows) in the outer and inner periosteal tissue, this time in longitudinal section.

The preliminary 3D reconstructions of the synchrotron micro-CT images (**Figure 5.2**) confirm the 2D histological observations (**Figure 5.1**), as the selected petrous bone sub-volume contains a wealth of void spaces with a clear separation between small volumes (possibly lacunae cut in half, partially captured pieces of the canalicular network and noise) and what is assigned to lacunar volumes at 100 µm^3. The lacunar volume in the present case seems to be bimodal (**Figure 5.2C**), with a population centered around 230 µm^3 and another large volume distribution above 500 µm^3. This differs significantly from the behaviour seen by others (Bach-Gansmo et al. 2016b

and references therein), who found unimodal volume distributions in other bones. For instance, in the iliac crest biopsies, Bach-Gansmo et al. (2016b) found median lacunar volumes of c. 530 μm^3, while in the human femora Dong et al. (2014) reported an average lacunar volume of c. 410 μm^3. However, the two different lacunar volumes may be linked to the co-existence of woven and lamellar-like tissues, as it has been previously reported that woven bone osteocyte lacunae are larger than these in lamellar bone (Hernandez, Majeska and Schaffler 2004) and can vary in size (Buckwalter et al. 1995).

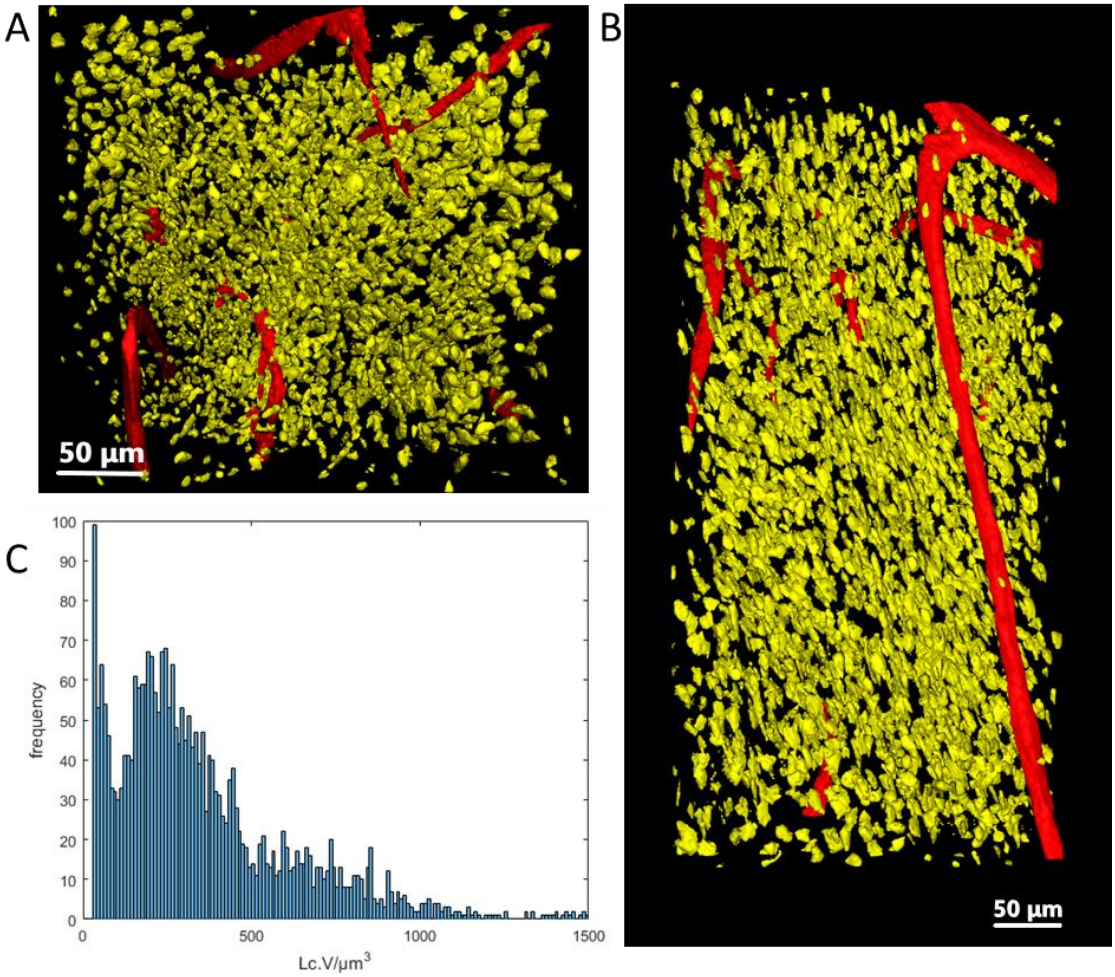

Figure 5.2. Preliminary results of synchrotron µCT for a single selected sub-volume of SAR8. (A) 3D rendering of void spaces in a section of petrous bone. Spaces in red are canals while the yellow shapes are putative osteocyte lacunae. (B) same as in (A), but rotated to offer a different view of the void space. (C) Histograms of apparent lacunar volumes.

The lacunar density is estimated to 4.96 x 10^4 lacunae/mm^3 which is very high compared to the values of 1.5 x 10^4 lacunae/mm^3 obtained for human iliac crest biopsies by Bach-Gansmo et al. (2016b), or the 2 x 10^4 lacunae/mm^3 in human femoral mid-diaphysis (Dong et al. 2014). This observation indicates that there are regions of very high lacunar densities in petrous bones which are only comparable to rat (*Rattus norvegicus*) and Lesser Galago (*Galago senegalensis*) lamellar tissue (Bromage et al. 2009). An increased number of osteocyte lacunae in the labyrinthine bone of the petrous has been reported by Bloch and Sørensen (2010) and Bloch, Kristensen and Sørensen (2012) and can be related to the bone formation rate (a higher number of bone cells

would lay down the bone matrix quicker; Bromage et al. 2009; Skedros, Grunander and Hamrick 2005), and the persistence of woven bone (Buckwalter et al. 1995). This would be a logical explanation for the petrous bone formation, as it is considered to form primarily *in utero* (Jeffery and Spoor 2004; Nemzek et al. 1996; Richard et al. 2010). However, how the functions (e.g. mineral homeostasis, bone remodelling) of osteocytes are influenced by the lacunar density remains unknown (Cullinane 2002; Goggin et al. 2016; Skedros, Grunander and Hamrick 2005; Teti and Zallone 2009).

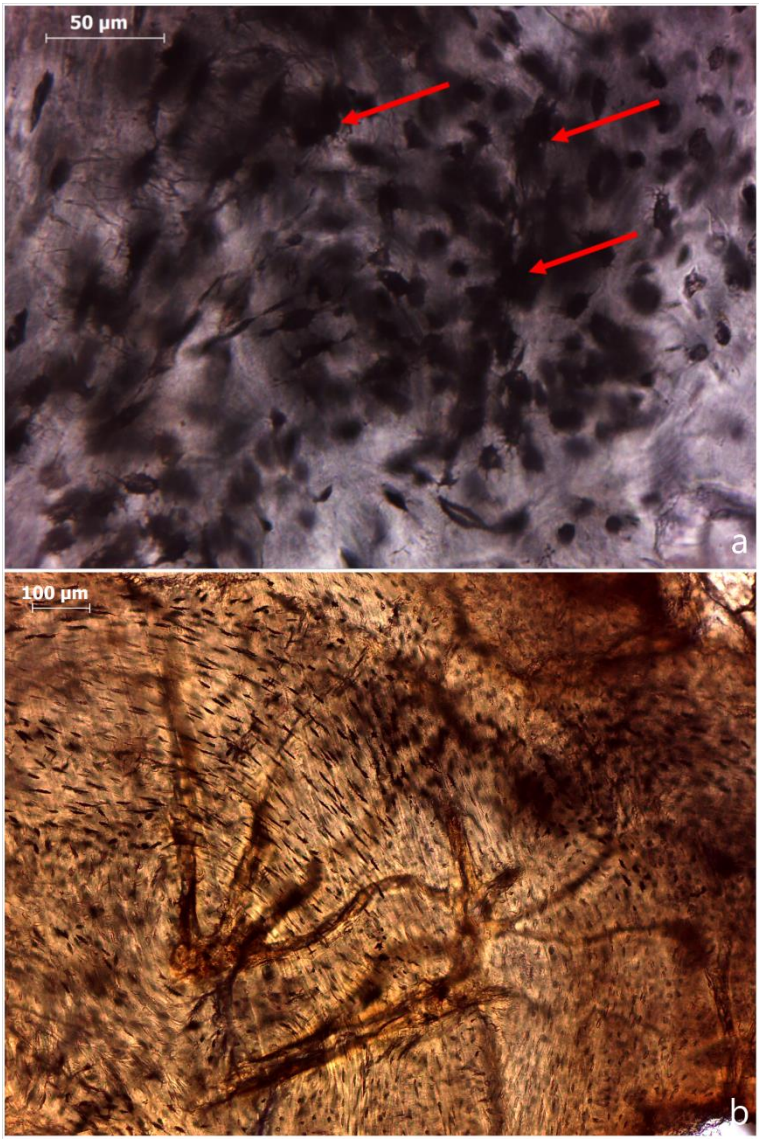

Figure 5.3. *MFD in human petrous bone*. (a) **DEN2 Transverse PPL 400x**: possible microbial activity that appears as merged osteocyte lacunae (opaque/black holes indicated by red arrows). (b) **KAZ1 Transverse PPL 100x**: tunnels with branched appearance resembling Wedl-type modifications in bone microstructure which have been linked to the presence of fungi.

In terms of histological preservation (**Table A2-Appendix A**), the petrous bones exhibit a generally moderate preservation state (average GHI=2) characterized by a resistance to the total loss of histological integrity (only two samples with GHI=0). This is likely to be due to its protected location, possible differences in its biomechanical properties and its *sui generis*

histomorphological characteristics (**Figure 5.3**). One should consider, however, the difficulties in estimating the degree of alterations on a spatial scale larger than the microscopic field of view (here at 40x total magnification the field of view is c. 5 mm) and the subjective nature of such evaluation.

Non-Wedl microscopic focal destruction (MFD) was not observed in the petrous bones in this study. Possible microbial activity is observed only in small areas of two of the petrous bone thin sections (DEN1 and DEN2). These few alterations identified as possible microbial activity (**Figure 5.3a**) show similarities to the early diagenetic stage characteristics (i.e. merging of osteocyte lacunae White and Booth 2014; Kontopoulos, Nystrom and White 2016). Although unlikely, microbially attacked specimens may have been unidentifiable in some cases due to prior sampling for aDNA analysis. A rather unexpected observation in one Central Asian specimen is a motif resembling Wedl-type tunnelling (**Figure 5.3b**). These branched, almost empty canals have an ill-defined outline with no cuffing under plane polarized light (Bell 1990; Hackett 1981; Wedl 1864) and they have been connected to fungal activity (Marchiafava, Bonucci and Ascenzi 1974).

More than half of the petrous bones (n=21, i.e. 60 %) exhibit microcracks, which has often lead to generalized destruction seen as amorphous, disintegrated, dark areas of bone (**Figure 5.4**). A key factor for the histological preservation of archaeological bone is also the presence of water within and around the skeletal remains. The three main hydrological scenarios (i.e. diffusive, recharge, and flow regimes) that have been outlined by Hedges and Millard (1995) can dramatically change the fate of bone regarding long-term survival. In diffusive regimes there is limited movement of water (or change in the amount of water) in the burial environment, whereas in recharge regimes there is fluctuation of water due to wetting and drying cycles (Hedges and Millard 1995). With regard to flow regimes, usually rainwater flows through the soil and then into bone (Hedges and Millard 1995; Nielsen-Marsh et al. 2000a). Thus, the prevailing hydrological conditions in the burial environment have a considerable impact on bone preservation.

Microcracks play an important role in bone diagenesis as they create new paths in the bone matrix that allow groundwater to accelerate collagen degradation, as well as promote the incorporation of exogenous ions into the bioapatite crystals (Pfretzschner 2004). This interaction with groundwater sometimes results in brown/orange staining (**Figure B2-Appendix B**) by the infiltration of iron oxides (Bodzioch and Kowal-Linka 2012; Hollund et al. 2012; Pesquero et al. 2015) or other exogenous substances that replace the osseous material (Garland 1989). However,

it seems that the petrous bone can moderate the expansion of microcracks and survive through time.

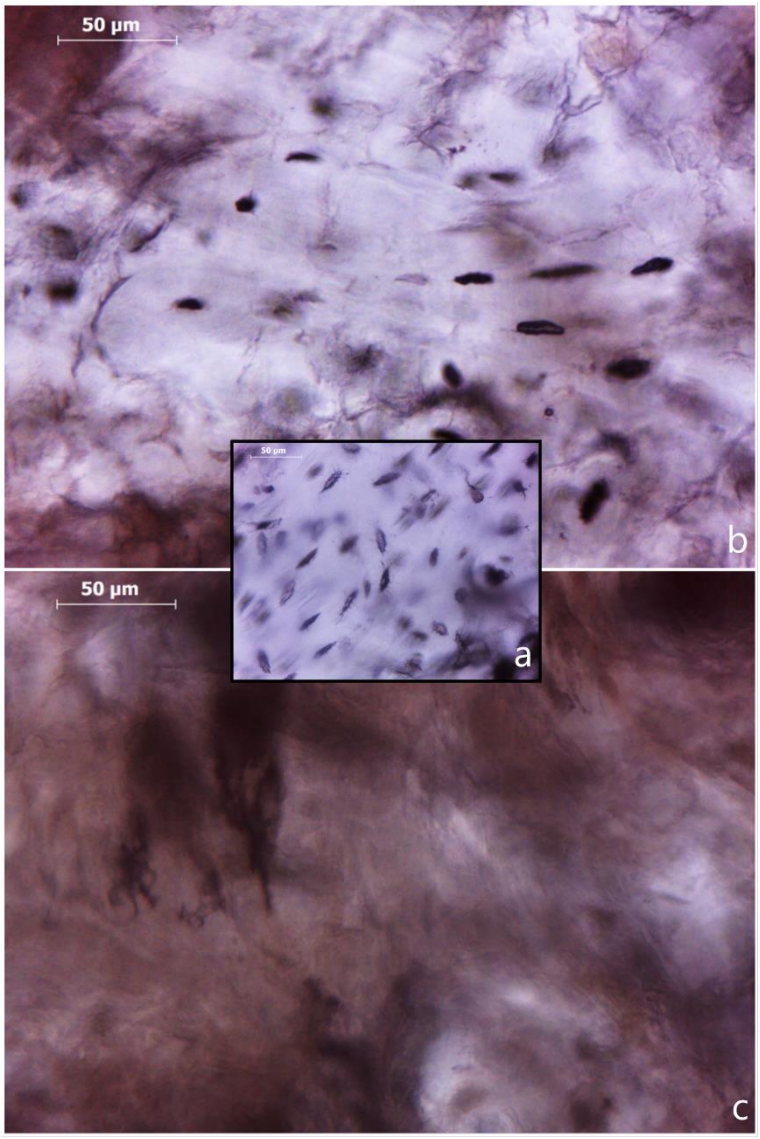

Figure 5.4. *Microcracking in petrous bones* (see also **Figure B1-Appendix B**). **DEN4 Transverse PPL 400x:** (a) well-preserved area versus (b) degraded areas due to microcracking that eventually leads to (c) generalized destruction characterized by loss of histological integrity (amorphous appearance) in adjacent areas within the same section.

Regarding histological preservation of the other skeletal elements compared to petrous bones, GHI values indicate moderate to poor histological preservation of most specimens (**Table A2-Appendix A**), which is poorer compared to the petrous bones from the same sites (**Figure 5.5**; U=1561, p=0.07). Except for the nine Kastrouli femora, MFD are not present in any of the other 102 skeletal elements. Therefore, a lack of MFD in petrous bones cannot yet be definitively linked to the higher endogenous DNA yields reported in palaeogenetic studies (e.g. Gamba et al. 2014; Hansen et al. 2017), as modifications that have been commonly associated with microbial activity are only present in 8 % of the non-petrous bones studied here.

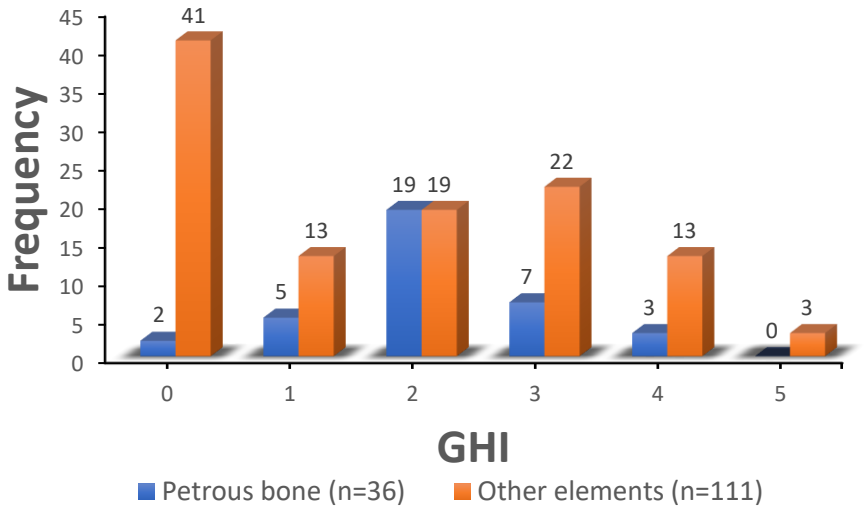

Figure 5.5. Differences in histological preservation (GHI: General histological index) between petrous and other bones.

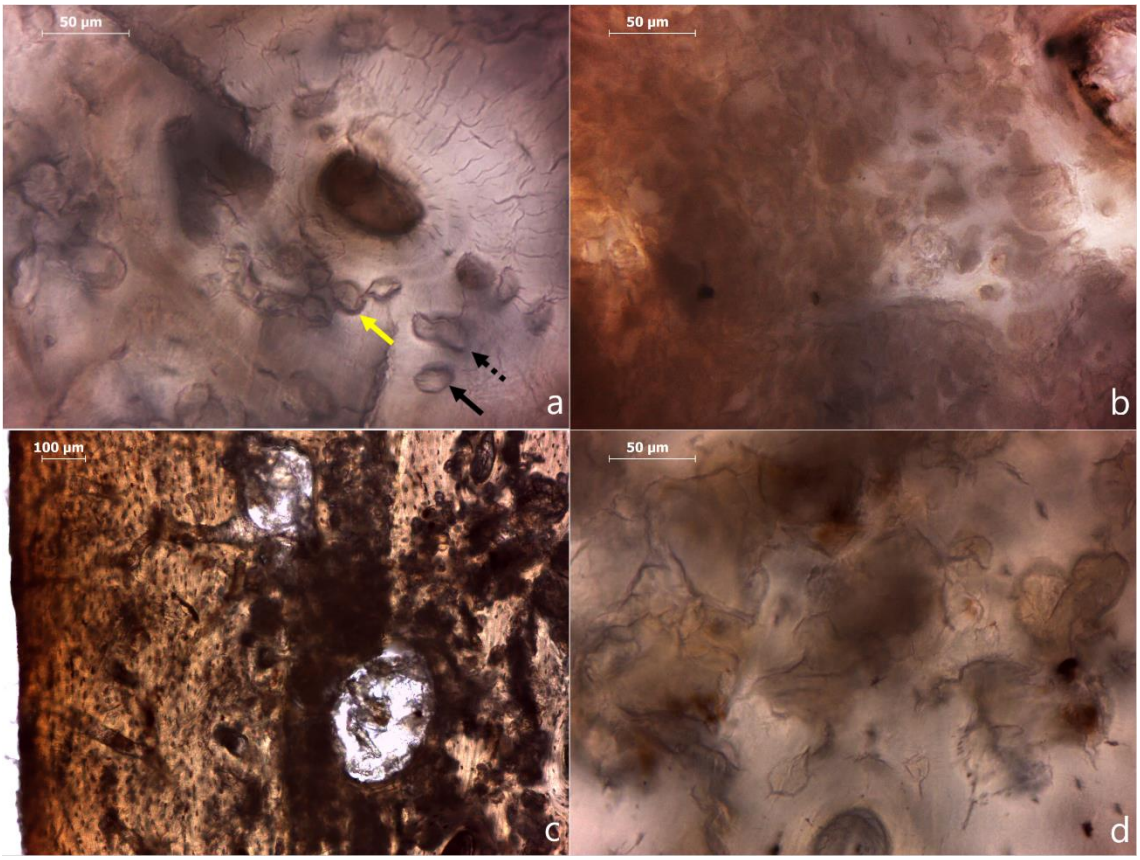

Figure 5.6. *MFD in Kastrouli human femora* (see **Figure B3-Appendix B** for additional examples). **(a) KAS9 Transverse PPL 400x - Human femur**: MFD in the form of linear-longitudinal (black arrow) and budded (dotted black arrow) tunnels surrounded by hypermineralized tissue (yellow arrow). **(b) KAS13 Transverse PPL 400x - Human femur**: The characteristic 'mosaic pattern' attributed to extensive bacterial activity. **MEC12 Transverse PPL (c) 100x and (d) 400x - Human femur**: modifications corresponding to MFD in low magnification (c) which are artifacts from microcracks and staining (d).

MFD in the Kastrouli human femora appear as non-Wedl linear-longitudinal (oval-shaped) or budded features in the bone matrix separated by hypermineralized tissue, as seen in transverse

sections under plane polarized light (**Figure 5.6a**). The hypermineralized tissue displays a dark coloration (brown/black) and it is assumed to be denser than the unaffected areas (Hackett 1981; Piepenbrink 1989; Bell 1990). This hypermineralized tissue is only few μm thick and surrounds the smaller non-Wedl MFD, while it seems to inhibit further expansion of the MFD, as has been noted in previous studies (e.g. Hackett 1981; Piepenbrink 1986). It is believed that the hypermineralized tissue forms by mineral redeposition and incorporation of waste products when microbes remove the inorganic matrix to attack collagen (Hackett 1981; Jackes et al. 2001; Hedges 2002; Fernandez-Jalvo et al. 2010), which agrees with the higher concentrations of Ca and P observed by Pesquero et al. (2015) compared to the unaffected bone tissue. The 'mosaic pattern' observed in **Figure 5.6b** is also considered to be associated with bacterial attack, representing the final stage where almost all microstructural features have been removed (Hackett 1981; Piepenbrink 1986; Turner-Walker and Jans 2008). Particular care, however, should be taken for the correct identification of MFD, as often in low magnification images features resembling MFD can be caused by microcracking (**Figure 5.6c-d**).

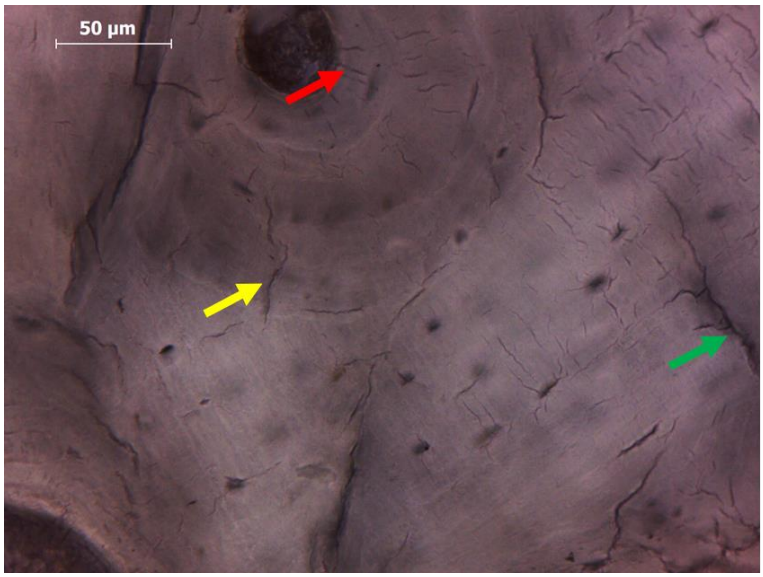

Figure 5.7. *Microcracking in long bones* (see also **Figure B4-Appendix B**). **SAR7 Transverse PPL 400x - Human Tibia (Distal Diaphysis)**: Different types of microcracking, i.e. central (red arrow), peripheral (yellow arrow) and interstitial (green arrow) micro-cracks.

Periodic contact of long bones with groundwater is manifested by microcracking in 93 samples, i.e. 84 % (**Figure 5.7**), with further degradation of microstructure by dissolving the BAp crystals and hydrolyzing collagen to varying degrees (Bell 1990; Hedges and Millard 1995; Pfretzschner and Tütken 2011). Kastrouli human femora microcracking, for instance, likely reflects interactions with water during cold and humid winters resulting in bone swelling, followed by drying and shrinking of bone during hot and dry summers (see Moustris and Petrou 2018 for weather data in the region). Desiccation is evidenced by micro-cracks observed centrally (**Figure 5.7**; spread from the Haversian canal outwards), peripherally (**Figure 5.7**; spread from the cement line inwards), circumferentially and interstitially (**Figure 5.7**; run across circumferential and

interstitial lamellae). However, it should be noted that sometimes microcracks may appear due to physical stresses during sample preparation (Turner-Walker 2012; Dal Sasso et al. 2014; Lander, Brits and Hosie 2014).

The wet and dry (oxygen-rich conditions) cycles in Kastrouli may have also favoured the survival and activity of microorganisms responsible for the previously mentioned MFD in femora (Reiche et al. 2003; Turner-Walker and Jans 2008; Hackett 1981). Moderate soil moisture with periodical, seasonal variation of water and temperature, e.g. warm summers, are favourable for tunnelling by the soil bacteria which are evidently aerobic in their metabolic pathways (Kendall et al. 2018). Fluctuating environments are the most detrimental for bone preservation (Fernandez-Jalvo et al. 2010; Hedges and Millard 1995; Nielsen-Marsh and Hedges 2000a; Reiche et al. 2003; Salesse et al. 2014; Smith et al. 2002; Trueman et al. 2004), as cyclical wetting and drying conditions result in cracking, flaking, and spalling of the bones (Fernandez-Jalvo et al. 2010; Pfretzschner and Tütken 2011; Pokines et al. 2016). The rate at which water travels through archaeological bone, combined with the speed of both the wetting and drying, control to a great extent the preservation or destruction of mineralized tissues in the archaeological record.

5.1.2. INTER- AND INTRA-SITE VARIATIONS

Despite similarities regarding the lack of microbial activity (MFD) and the widespread, but variable, interaction with water (microcracking), there are also considerable inter- and intra-site variations within the petrous bone samples. Except for local hydrology, differences in soil geochemistry, temperature and oxygen availability in the burial environment can have variable effects on the histological integrity of archaeological bone (Bell, Skinner and Jones 1996; Fernandez-Jalvo et al. 2010; Jans et al. 2002; Nielsen-Marsh and Hedges 2000a; Turner-Walker 1999). **Figure 5.8** illustrates the effect of the site-specific conditions on the preservation of petrous bones when there is limited or no microcracking, and when samples have similar chronological age (DEN6: 17^{th}-19^{th} cen. AD; MEC54: 14^{th}-17^{th} cen. AD). The Danish petrous bone exhibits excellent preservation of its micromorphological characteristics that can be observed both in plane-polarized and cross-polarized images (**Figure 5.8a-b**). Conversely, the petrous bone from Belgium is characterized by a complete loss of histological integrity accompanied by a loss of birefringence (**Figure 5.8c-d**).

Likewise, exceptional preservation of microstructure that resembles fossilization (i.e. excellent preservation of microstructure accompanied by a complete loss of the organic matter) can be observed in long bones from Maroulas (**Figure 5.9a**; 8300-7600 BC, Greece) and Manika (2900-2300 BC, Greece), while all Tharrounia bones demonstrate generalized destruction with no histological features surviving (**Figure 5.9b**; 5300-3300 BC, Greece). Moderate to excellent histological preservation can be observed in specimens from the Sarakenos cave (5700-4000 BC,

Greece) which is sometimes similar to modern bone (**Figure 5.9c-d**). In St. Rombout (12^{th}-18^{th} cen. AD, Belgium) a usual pattern can be seen in many bones, characterized by a moderate preservation with generalized destruction in periosteal and endosteal areas, and good preservation of mesosteal tissue (**Figure 5.9e-f**). Further, histological preservation shows no correlation with chronological age of samples.

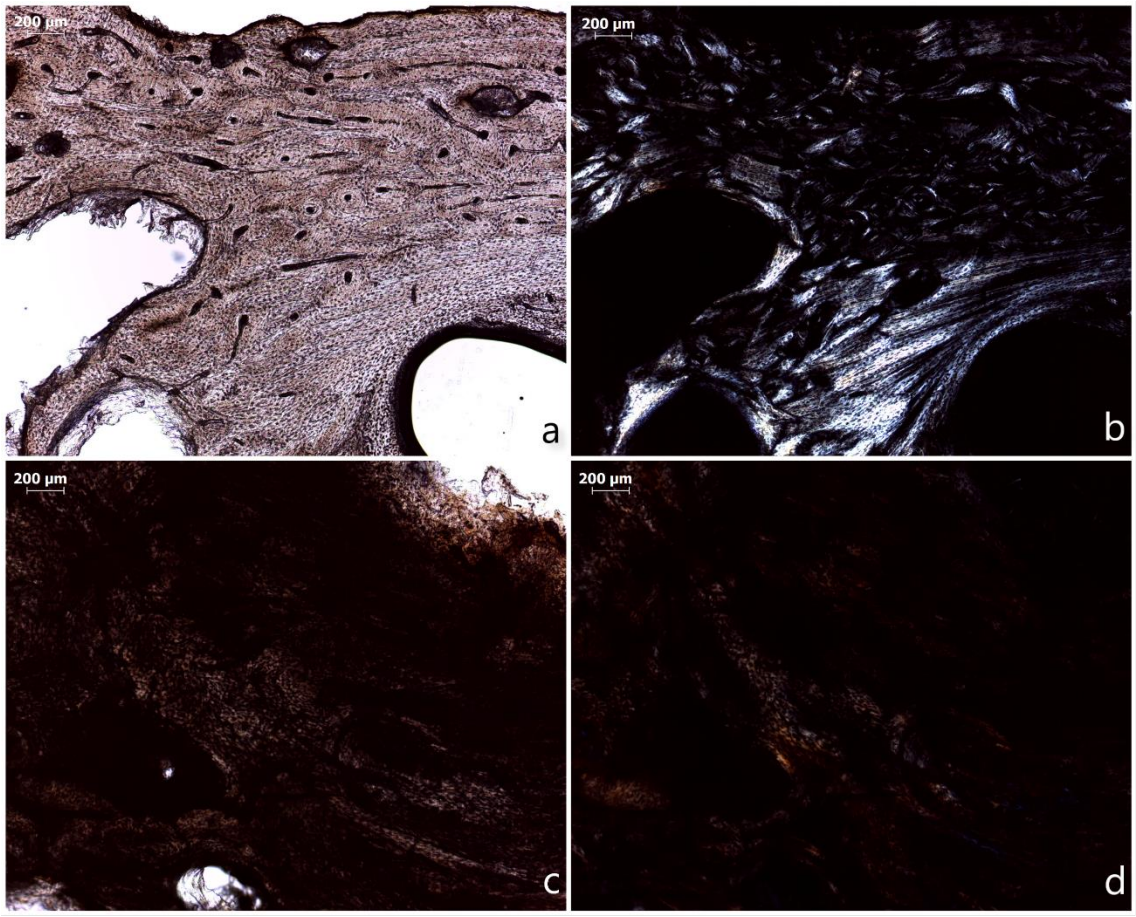

Figure 5.8. *Inter-site variations in petrous bone histological preservation* (see **Figure B5-Appendix B** for additional images). **DEN6 Longitudinal (a) PPL and (b) XPL - 40x**: very well-preserved microstructure with woven tissue surrounding canal areas, small lamellar-like areas and a large osteonic area seen both in PPL and XPL. **MEC54 Longitudinal (c) PPL and (d) XPL - 40x**: Generalized destruction across the entire section resulting in a dark, amorphous appearance and complete loss of collagen birefringence.

Consequently, soil geochemistry and the stability mechanisms in the burial environment (Karkanas 2010) play a fundamental role on the preservation of archaeological bone. Proximity to the surface also contributes as oxygen availability, the interaction with pore water and rainwater in open-air sites (or even dripping water in caves), and the effects of temperature are more prominent when bones are in shallow depths (Hedges and Millard 1995; Karkanas et al. 2000; Trueman et al. 2004).

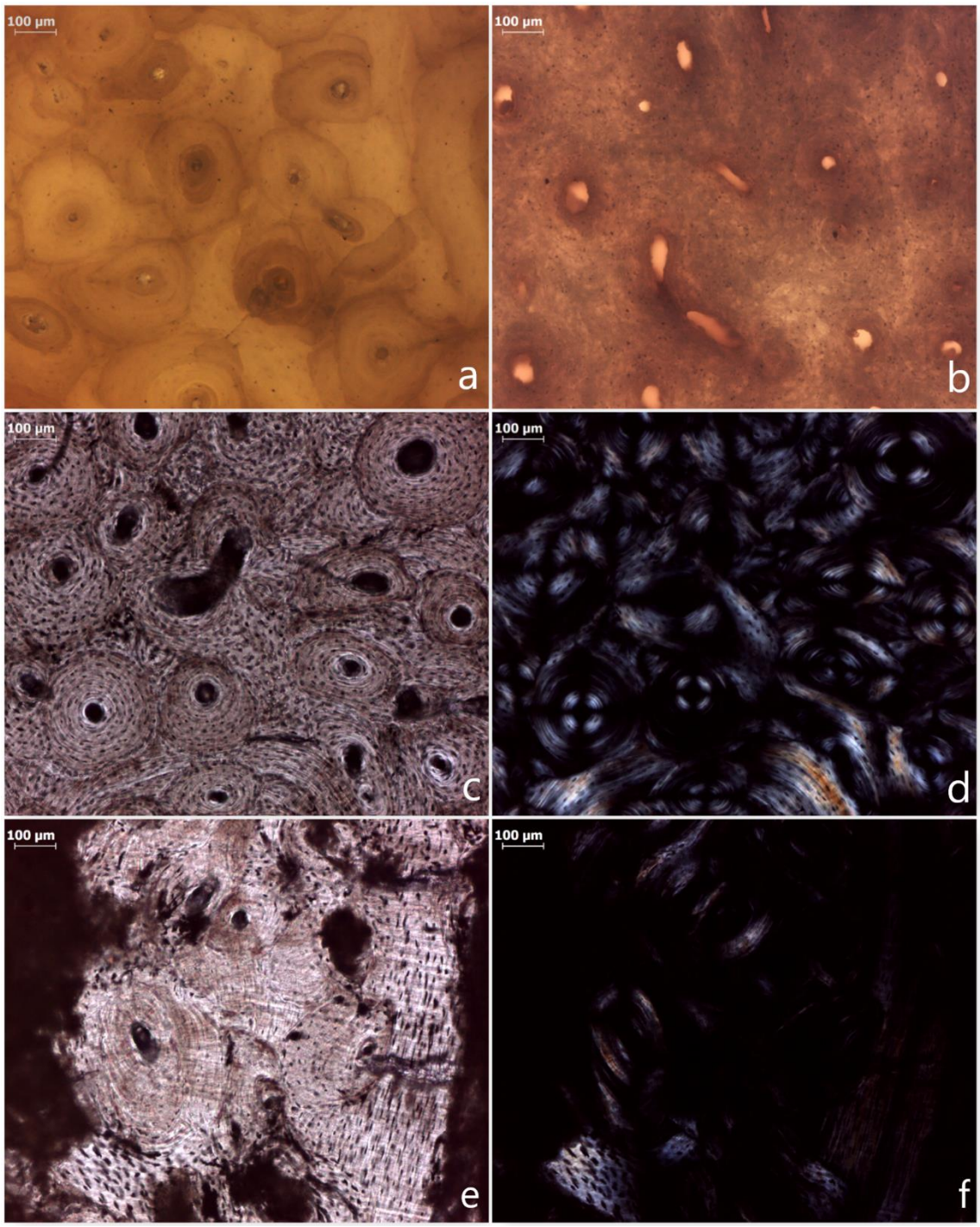

Figure 5.9. *Inter-site variations in long bone histological preservation*. **(a) MAR5 Transverse PPL 100x – Human humerus**: excellent preservation characteristic of all Maroulas specimens resembling fossilization with brown straining throughout. **(b) THA6 Transverse PPL 100x – Human femur**: very poor preservation with complete loss of histological features. **SAR10 Transverse (c) PPL 100x and (d) XPL 100x – Human femur**: (c) excellent preservation similar to modern bone, and (d) good preservation of collagen birefringence. **MEC16 Transverse (e) PPL 100x and (f) XPL 100x – Human humerus**: well-preserved mesosteal tissue sandwiched between degraded periosteal/sub-periosteal and endosteal/sub-endosteal tissue. Note the absence of birefringence in degraded areas in (f).

Figure 5.10. The three different diagenetic paths identified in Kastrouli.

Intra-site differences (see also **Figure B6Figure B9 - Appendix B** for further examples) are anticipated, and a very interesting case that illustrates the complexity of histological alterations is Kastrouli, where bones have been recovered from a secondary commingled Mycenaean burial (1350-1150 BC, Greece). While histological preservation in Kastrouli is very poor, three distinct paths can be identified based on the presence/absence of MFD, micro-cracking and orange/brown staining (**Figure 5.10**). Although within-site differences may be related to different micro-environment conditions (e.g. groundwater, contact with limestone), all bones were found within 30 cm of sediment, which makes this scenario highly unlikely. A logical explanation for this high variation is therefore that these bones have experienced different early taphonomic histories. In secondary burials, the skeletal remains of a body (either exposed on the ground surface, interred in a coffin or buried directly into the soil) are retrieved and relocated once the soft tissue has

decayed to some degree or excarnated. Therefore, histotaphonomy may help understand the sequence of these alterations and shed light on past funerary practices, i.e. primary and secondary treatment.

Table 2. Information on St. Rombout's burials.

Individual no.	Date AD	Burial type	Coffin	Wrapping
1 (MEC1-4)	17th cen.	Single	Yes	No
2 (MEC5-9)	16th cen.	Single	No	Possible
3 (MEC10-14)	17th cen.	Single	Yes	No
4 (MEC15-19)	12th cen.	Single	Yes	No
5 (MEC20-24)	18th cen.	Single	Yes	No
6 (MEC25-29)	18th cen.	Single	Yes	No
7 (MEC30-34)	16th cen.	Collective	?	No
8 (MEC35-39)	12-14th cen.	Single	No	No
9 (MEC40-43)	14-17th cen.	Multiple	No	No
10 (MEC44-48)	17th cen.	Single	No	No
11 (MEC49-53)	18th cen.	Single	Yes	No
12 (MEC54-58)	14-17th cen.	Single	No	Possible
13 (MEC59-63)	12-18th cen.	Single	Yes	No
14 (MEC64-68)	17-18th cen.	Multiple	No	No
15 (MEC69-73)	13-14th cen.	Single	Yes	No
16 (MEC74-78)	14-17th cen.	Multiple	No	No
17 (MEC79-83)	15-16th cen.	Single	No	Possible
18 (MEC84-87)	12th cen.	Single	Yes	No
19 (MEC88-92)	12th cen.	Single	Yes	No
20 (MEC93-97)	12th cen.	Single	Yes	No
21 (98-101)	12th-14th cen.	Single	Yes	No

The death history and the effects of various factors (e.g. season of death, clothing, type of burial) on bone degradation are often overlooked in archaeology due to lack of relevant information. Clothing, wrapping or burials in coffins have been found to prolong the soft tissue decay by changing the micro-environment conditions and delaying insect colonization (Forbes, Stuart and Dent 2005; Lee Goff 1992; Prats-Muñoz et al. 2013; Voss, Cook and Dadour 2011). An attempt to understand these phenomena has been made in a limited number of archaeological studies (Booth 2016; Booth and Madgwick 2016; Booth, Chamberlain and Parker Pearson 2015; Hollund, Blank and Sjögren 2018), as ritual processing can also have profound effects on bone histology. However, researchers either hyperbolize and misinterpret evidence (i.e. mummification in British prehistory due to lack of bioerosion, assuming an internal origin of bacterial attack; (Parker Pearson et al. 2005; Booth, Chamberlain and Parker Pearson 2015) or cannot connect the

histological modifications to specific funerary rituals (Booth 2016; Booth and Madgwick 2016; Hollund, Blank and Sjögren 2018), similar to the Kastrouli bones reported here.

The characteristic patterns in bone histology of samples from St. Rombout cemetery (Mechelen, Belgium) exemplify what can be realistically achieved through histotaphonomic investigations in terms of unravelling the funerary practices-to-bone histology relationship. St. Rombout's inhumations vary from single burials in coffins, single and multiple plain burials without coffins, and a few burials with indications of wrapping (**Table 2**; Van de Vijver, Kinnaer and Depuydt 2018). Inhumations within a wooden coffin can change the conditions of the burial environment, as the wooden coffin initially creates a partially closed system, enclosing putrefying soft tissues that gradually become more and more exposed until the coffin has completely decayed. Bones of corpses wrapped or clothed with textiles can experience different modifications in their histology, as degradation of textiles (e.g. wool, cotton) by bacterial and/or fungal action should be expected to be accomplished a few months following burial, except in frozen, waterlogged, or very dry conditions (Janaway 2002, 2008). Concerning multiple burials, the exact position (center or edges of burial) of the corpses and their relation to each other (e.g. superimposed bodies, in contact with each other, laid in rows parallel to each other), the number of individuals, in combination with the burial environment, can significantly change the rates of soft tissue decay (Haglund 2002) with unknown effects on bone micro-architecture.

Single burials in coffins display a characteristic preservation pattern, with generalized destruction across periosteal and endosteal tissue that expands towards the mesosteal (mid-cortical) area of long bones, and a sandwiched zone of well-preserved mid-cortical tissue between them (**Figure 5.11a-d**). These modifications are similar to the histological changes in bones of pig cadavers wrapped in nylon carpets reported by Kontopoulos et al. (2016). This probably happens as nylon, polyester or acrylic fibers degrade at slower rates compared to biodegradable fabrics (Janaway 2008), thus creating a micro-environment equivalent to the wooden coffins. The dark/black colouration seen in almost all specimens under plane polarized light might be related to manganese infiltrations entering bone through microcracks, as similar staining has been attributed to manganese compounds by Hollund et al. (2018).

Regarding petrous bones, these demonstrate a slightly different picture with more variation, no distinct pattern and better preservation (**Figure 5.12**). Thus, the anatomical location of this skeletal element (located inside the skull) may often moderate the changes in the micro-environment that other bones experience due to differences in burial practices. However, when the combination of the burial environment conditions and the funerary rituals is such that it leads to a complete loss of histological integrity in long bones, the petrous bone is likely to have the same fate, as seen in MEC30 from individual 8 in St. Rombout (**Table A2-Appendix A**).

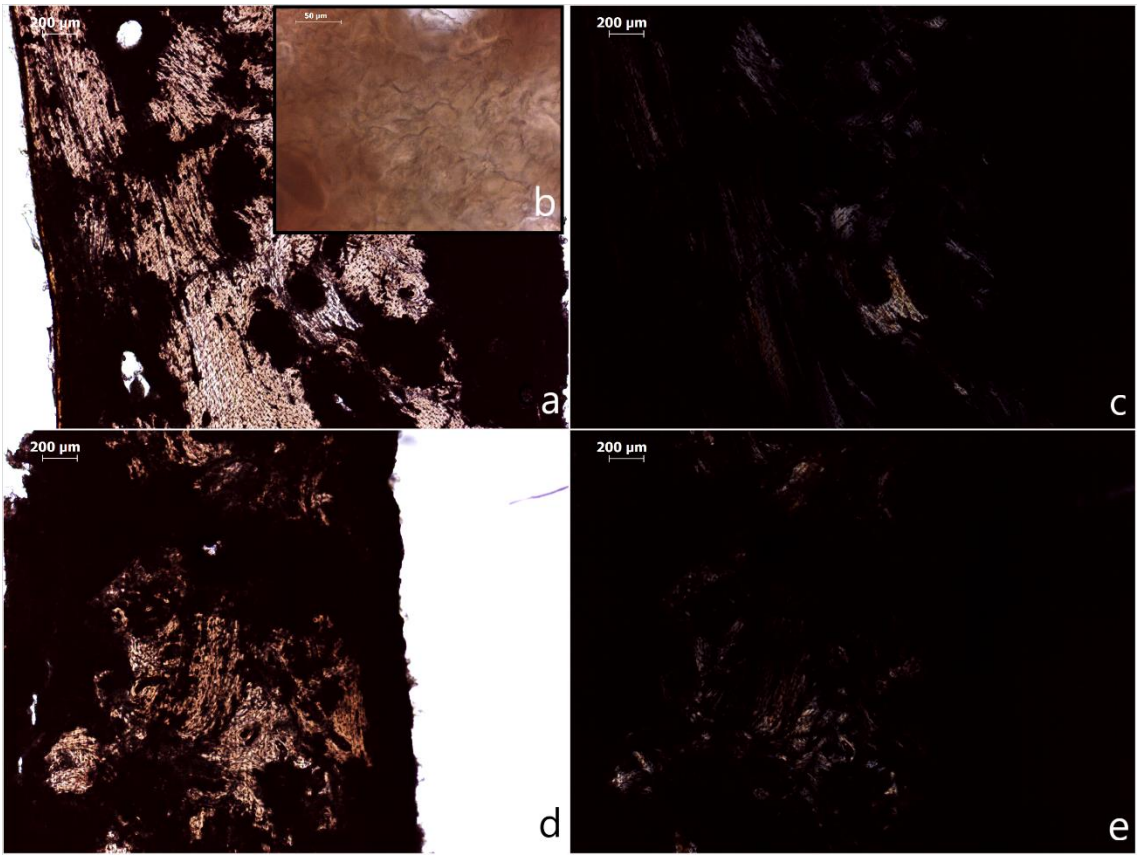

Figure 5.11. *Histological modifications in long bones from single burials in coffins at St. Rombout*. **MEC13 Transverse (a) PPL 40x, (b) PPL 400x of a degraded area, and (c) XPL 40x – Human tibia**: the characteristic pattern observed in bones from single burials in coffins. Here, a large area of mesosteal tissue survives in (a). In degraded areas, there is (b) extensive microcracking and (c) loss of collagen birefringence. **MEC11 Transverse (d) PPL 40x and (e) XPL 40x – Human femur**: same as MEC13 but with more degraded mesosteal tissue and almost complete loss of collagen birefringence.

Single burials with indications of wrapping but not coffined display a slightly modified pattern compared to coffin burials (**Figure 5.13**). Bones exhibit generalized destruction in sub-periosteal tissue that expands towards the mesosteal area, possibly depending on the micro-environment conditions and other specific characteristics (e.g. textile composition, burial depth, season of death). However, the periosteal tissue appears well-preserved (**Figure 5.13**). This observation confirms experimental data that show the effects of textiles (and their composition) on bone degradation in early diagenetic stages (i.e. 6 years post-mortem) in cadavers placed on the ground surface (Kontopoulos, Nystrom and White 2016) and contradicts Booth, Redfern and Gowland (2016) claim that wrapping the bodies has no effect on bone degradation. Additionally, it challenges the argument by Parker Pearson et al. (2005) and Booth, Chamberlain and Parker Pearson (2015) for intentional mummification in early prehistoric Britain. The samples from Cladh Hallan and Bradley Fen (see **Figure 3.14** for comparison) assumed to be intentionally mummified, show similar degradation patterns with MEC9 (**Figure 5.13c**), a wrapped individual from a 16th century AD single inhumation at the Christian cemetery of St. Rombout in Mechelen, Belgium (see also **Figure B10-Appendix B** for an additional example, this time of a single burial in coffin).

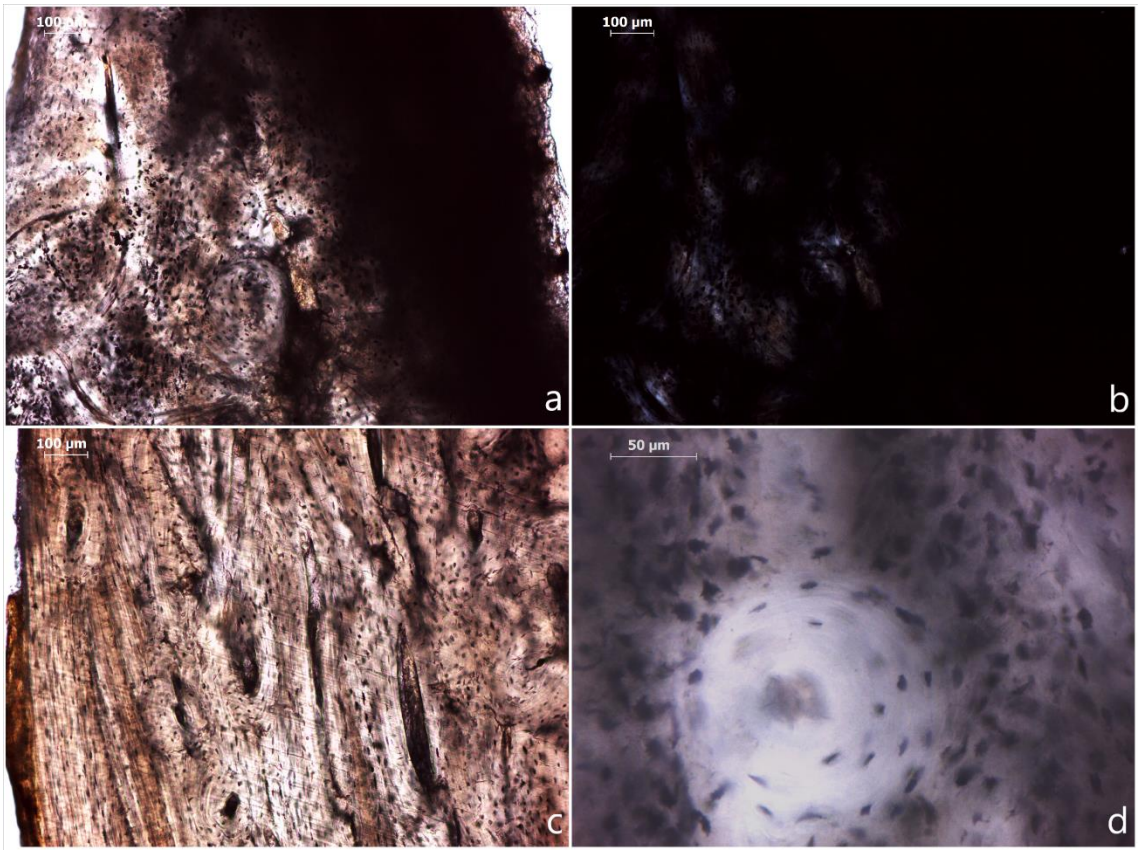

Figure 5.12. *Histological modifications in petrous bones from single burials in coffins at St. Rombout*. **MEC10 Longitudinal (a) PPL 100x and (b) XPL 100x – Human petrous bone**: degradation pattern similar to long bones with generalized destruction in the outer tissue areas and well-preserved mid-cortical areas. **MEC20 Longitudinal (c) PPL 100x and (d) PPL 400x – Human petrous bone**: excellent histological preservation across the entire section.

The preservation of all bones from the multiple burials show a significant variation, with no specific pattern identified (**Figure 5.14**). Sometimes a degradation pattern identical to coffin burials can be observed (**Figure 5.14a**), while on other occasions samples display an antithetical pattern with the mesosteal tissue completely degraded and the periosteal/endosteal tissues well-preserved (**Figure 5.14b**). Further, samples may display good histological preservation with orange/brown staining throughout (**Figure 5.14c**), or a total loss of histological integrity as seen in **Figure 5.14d**. This lack of a specific pattern in bones deriving from multiple burials possibly reflects the fact that multiple burials in St. Rombout were of varying types, with no uniform or common practice, and they were found in many different layers (Van de Vijver, Kinnaer and Depuydt 2018).

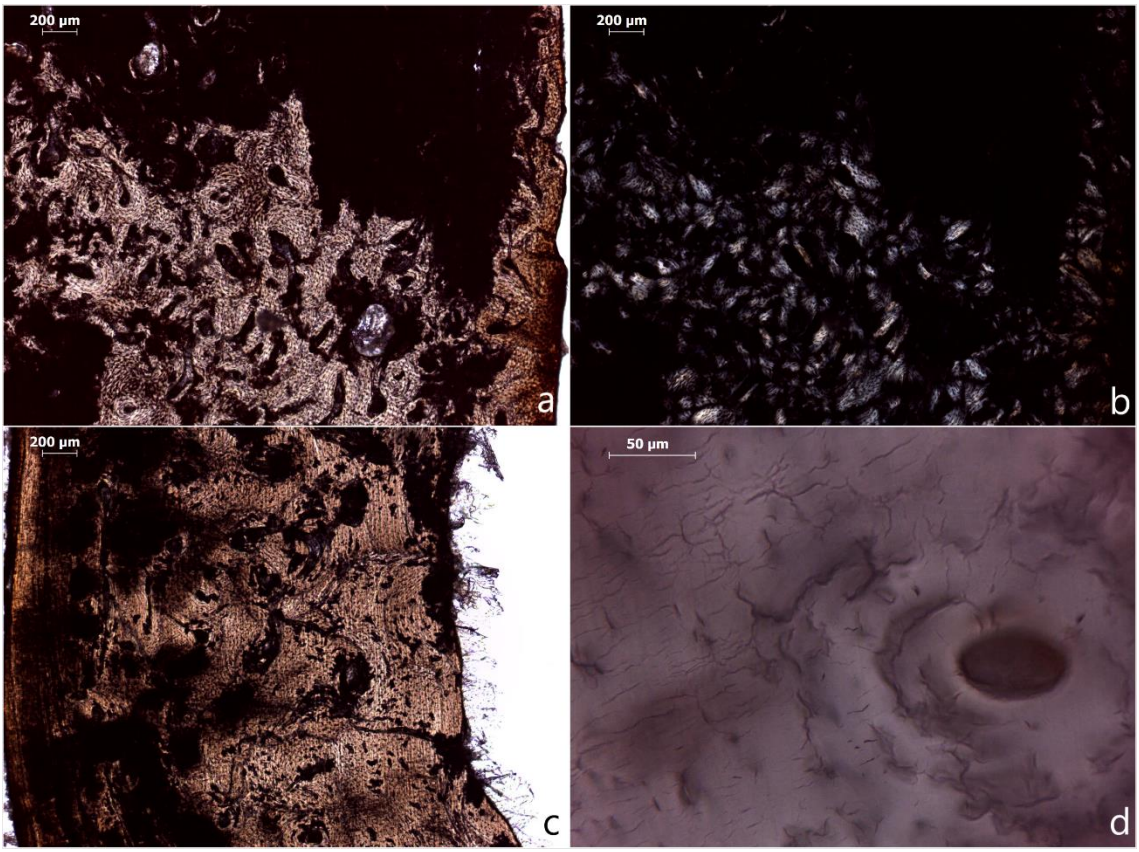

Figure 5.13. *Histological modifications in long bones from wrapped single burials.* **MEC55 Transverse (a) PPL 40x and (b) XPL 40x – Human femur**: preservation of mainly mesosteal tissue is accompanied by a relatively good condition of the periosteal tissue with orange staining. Sub-periosteal area shows generalized destruction that spans to mesosteal area but to variable extent. Endosteal tissue is also completely degraded. All dark sites display a complete loss of collagen birefringence contrary to well-preserved areas. **(c) MEC9 Transverse PPL 40x – Human radius (distal diaphysis)**: same pattern but with better-preserved mesosteal zone compared to MEC55. **(d) MEC8 Transverse PPL 400x – Human radius (proximal diaphysis)**: image from the same bone as in (c) revealing the extensive microcracking in degraded areas.

The St. Rombout case study, therefore, clearly brings us a step forward (compared to the Kastrouli example or other previous investigations (Booth 2016; Booth and Madgwick 2016; Hollund, Blank and Sjögren 2018) in terms of understanding the effects of burial practices on the microstructure of bone. However, the combination of several unknown parameters with others that are not yet well understood hinder further interpretations. Variations in the preservation state of specimens deriving from skeletons that have experienced similar funerary treatments can easily lead to erroneous assumptions. Hitherto, there has been a lack of relevant information, as no experimental projects have explored in detail the effects of different funerary practices on bone histology and the characteristics of the burial environment. Consequently, until targeted taphonomic experiments unravel the ambiguous relationship between funerary treatment of the corpse and microstructural preservation of bone, it is not possible to make any safe assumptions.

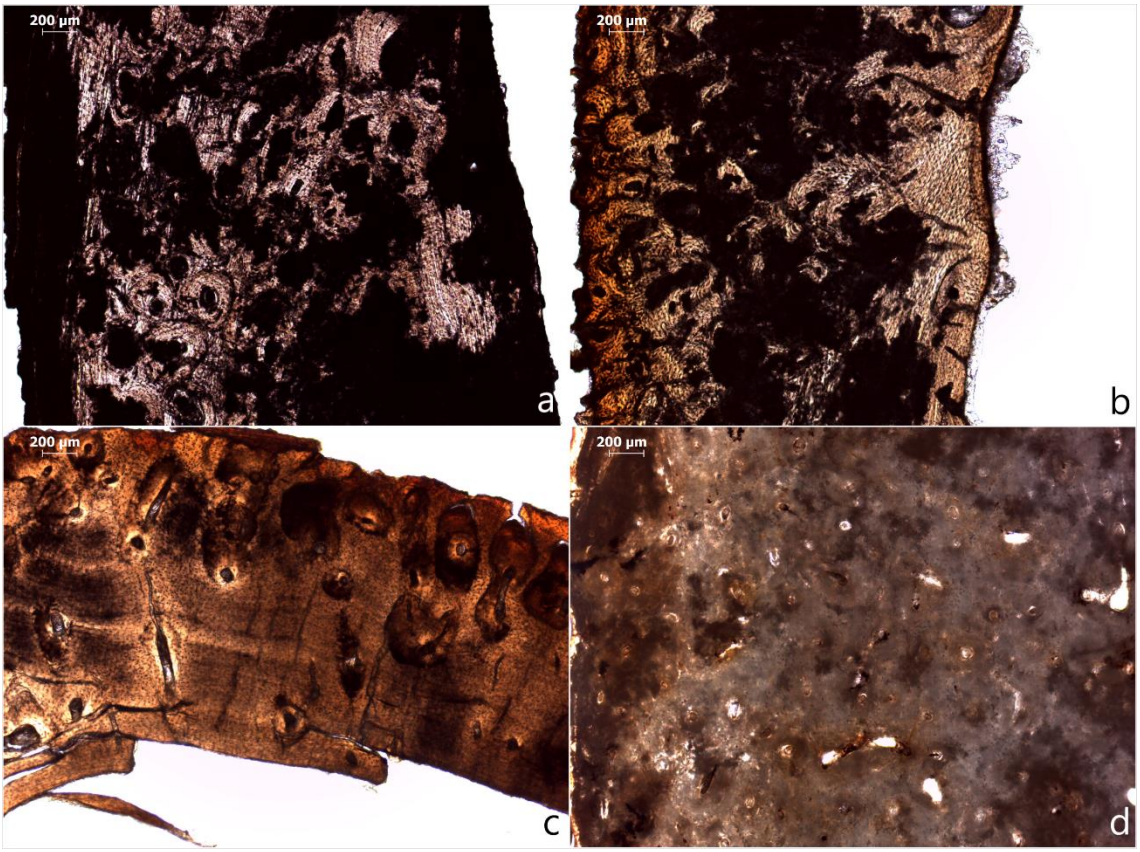

Figure 5.14. *Histological modifications in long bones from multiple burials*. **(a) MEC41 Transverse PPL 40x – Human humerus**: histological alterations analogous to coffined single burials. **(b) MEC65 Transverse PPL 40x – Human humerus**: histological modifications display a pattern opposite to coffined single burials with the mesosteal tissue suffering from generalized destruction and extensive microcracking, whereas the periosteal/sub-periosteal and endosteal/sub-endosteal areas showing good preservation of their microarchitecture. Note the staining at the outer 200-300 µm of the periosteal zone. **(c) MEC43 Transverse PPL 40x – Human radius**: orange/brown staining can be observed due to infiltration of exogenous elements that have coloured bone tissue. Histology is well-preserved although cracks and microcracks are present and cover a significant part of the section. **(d) MEC75 Transverse PPL 40x – Human femur**: generalized destruction throughout the cross-section. The pattern is similar to MEC41 in (a) but degradation has now expanded to mesosteal tissue that will eventually lose its original histological features due to the interaction with water and the incorporation of exogenous sources through microcracks.

5.1.3. INTRA-INDIVIDUAL AND INTRA-BONE VARIATIONS

Regarding intra-individual and intra-bone variations, although the skeletal elements are often expected to degrade at different rates due to the differences in biomechanical, chemical and physical characteristics of each bone (Hanson and Buikstra 1987), neither intra-individual patterns [St. Rombout $x^2(5)=2.409$, p=0.790; **Figure 5.15**] related to the proximity of the skeletal element to the abdominal area (internal gut bacteria) or a better preservation of the petrous bone compared to other bones, nor significant intra-bone differences in GHI values of proximal and distal diaphyses of long bones can be observed (**Figure 5.16**; humerus U=66.500, p=0.755; radius U=17.500, p=0.383; femur U=29.000, p=0.798; tibia U=7.000, p=0.937). A lack of intra-individual variability is thus not supportive of an internal origin of microbial communities in bone, strengthening the voices of researchers who contend that soil microbes are responsible for MFD (Fernandez-Jalvo et al. 2010; Hedges 2002; Nielsen-Marsh and Hedges 2000a; Turner-Walker 2008).

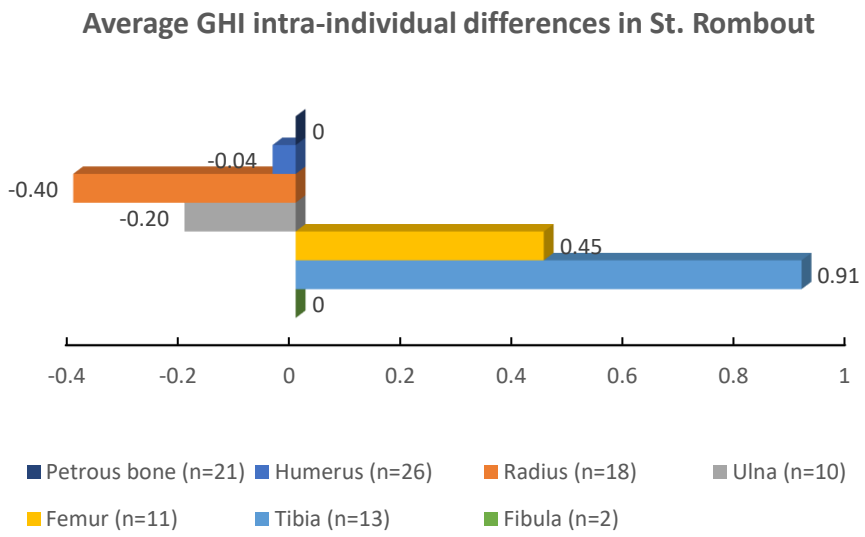

Figure 5.15. Intra-individual variations in histological preservation (GHI: general histological index) relative to petrous bone in St. Rombout, Belgium. Bars represent the average difference between the petrous bone and the other skeletal elements intra-individually (i.e. a positive value indicates a lower average value of this skeletal element compared to petrous bone, and vice versa).

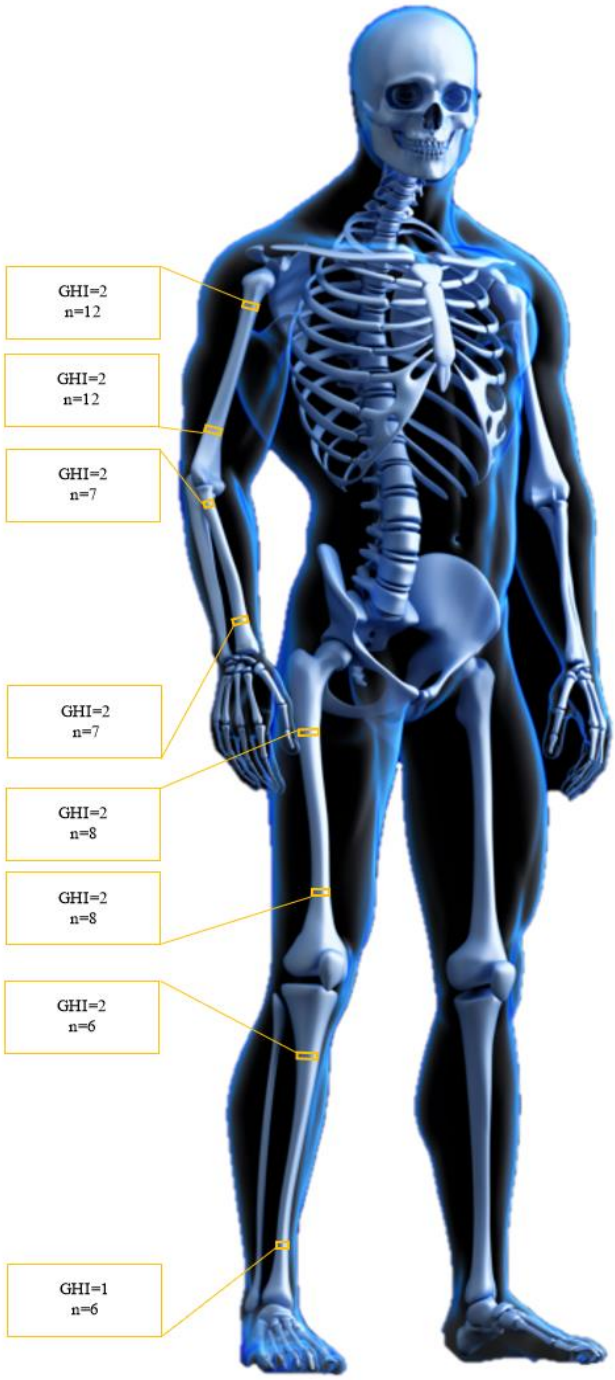

Figure 5.16. Histological preservation (GHI: general histological index) in proximal and distal diaphyses of long bones (see **Figure B11-Appendix B** for examples).

5.2.1. PETROUS VERSUS OTHER BONES

Archaeological bone displays increased crystallinity compared to modern bone (**Figure 5.17**), suggesting an increase in average BAp crystal length and short-range order due to Ostwald ripening (larger crystals absorb the smaller crystals), loss of the smaller crystals, or a combination of the two processes (Nielsen-Marsh et al. 2000b; Nielsen-Marsh and Hedges 2000a; Reiche, Vignaud and Menu 2002; Stiner et al. 1995; Trueman 2013; Weiner and Bar-Yosef 1990; Wright and Schwarcz 1996). Crystallinity shows statistically significant differences [t(266)=-5.011, p=0.000] in petrous bones (n=104) compared to the other skeletal elements (n=164), with the IRSF values ranging from 3.09 to 5.71 (average=3.64±0.5) in petrous bones, and from 3.13 to 5.91 (average=3.99±0.61) in other bones (**Table A2-Appendix A**).

In five sites which have a sufficient number of petrous bones as well as other skeletal elements for direct comparison, only the petrous bones (n=9) in Manika show lower IRSF values (4.33±0.93) compared to other bones (n=22) that have IRSF=5.11±0.62 (U=46.500, p=0.02; not statistically significant following Holms-Bonferroni correction). In Sarakenos cave (U=31.000, p=0.137) the average petrous bone (n=6) IRSF=3.35±0.09 is close to the average IRSF=3.44±0.16 in other bones (n=18), while in St. Rombout (U=808.000, p=0.789) the average petrous bone (n=21) IRSF=3.82±0.27 is similar to the average IRSF=3.85±0.23 in other bones (n=80). Tharrounia petrous bones (n=3) have an average IRSF=3.93±0.23, whereas the other bones (n=8) have an average IRSF=3.57±0.06 (U=0.000, p=0.012; not statistically significant following Holms-Bonferroni correction). Similarly, in Maroulas, petrous bone (n=4) display an average IRSF=4.25±0.78, whereas the other bones (n=12) have an average IRSF=3.73±0.08 (U=18.500, p=0.521).

Carbonate content varies in these archaeological bones and appears statistically significantly different [t(266)=2.792, p=0.006] in petrous bone versus other skeletal elements. The C/P values range from 0.07 to 0.34 (average=0.20±0.06) in petrous bones and from 0.06 to 0.32 (average=0.17±0.06) in other bones (**Table A2-Appendix A**). The former display an average loss of about 20 % of the initial carbonate, while the latter a loss of 30-40 % of their initial CO_3^{2-}. In terms of within-site variations, petrous bones (n=9) in Manika show higher C/P values (0.16±0.06) compared to the other bones (n=22) that have C/P=0.10±0.03 (U=47.500, p=0.023; not statistically significant following Holms-Bonferroni correction). In Sarakenos cave (U=36.000, p=0.251) the average petrous bone (n=6) C/P=0.29±0.03 is slightly higher than the average C/P=0.26±0.04 in other bones (n=18), both higher than modern bone C/P (**Figure 5.17**). In St. Rombout [t(99)=-1.250, p=0.214] the average petrous bone (n=21) C/P which is 0.15±0.05 approximates the average C/P=0.16±0.03 in other bones (n=80). Tharrounia petrous bones (n=3) have an average C/P=0.18±0.02, whereas the other bones (n=8) have an average C/P=0.24±0.01

(U=0.000, p=0.012; not statistically significant following Holms-Bonferroni correction). Likewise, Maroulas petrous bone (n=4) display an average C/P=0.20±0.11, whereas the other bones (n=12) have an average C/P=0.25±0.03 (U=17.500, p=0.446). Therefore, the overall lower crystallinity and higher carbonate content seen in petrous bones compared to the other skeletal elements may be misleading, as the low crystallinity and high carbonate content in most animal petrous bones from Britain, Germany and Jordan have masked the within-site patterns.

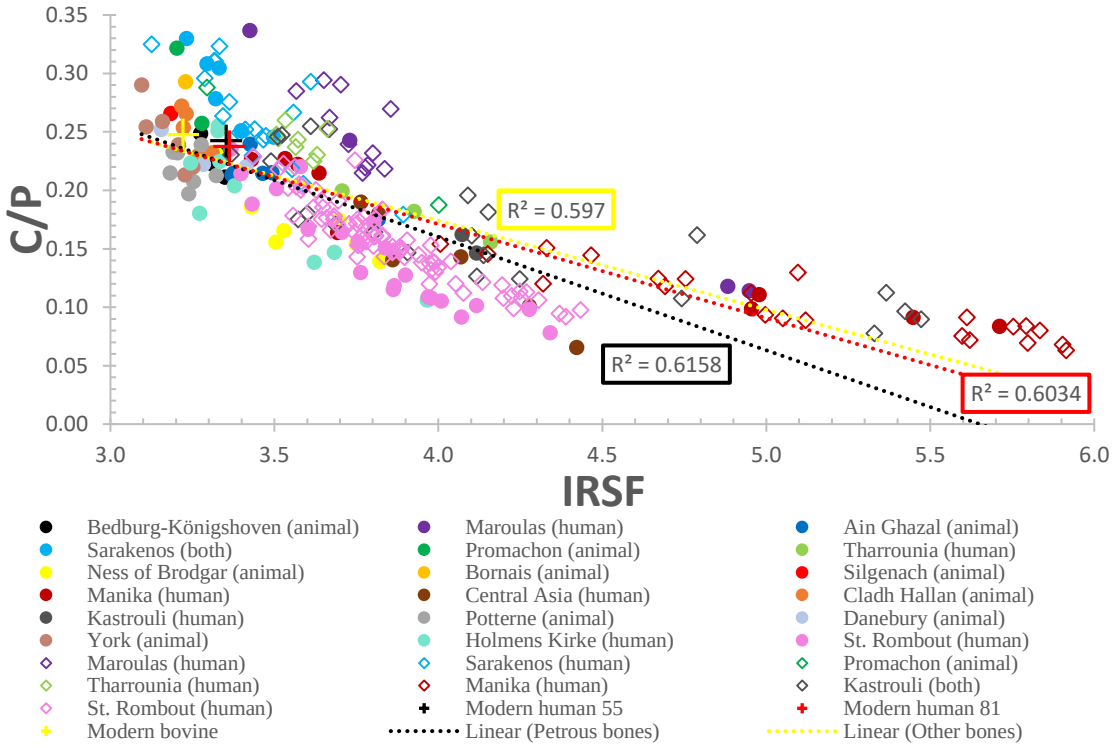

Figure 5.17. The strong relationship between crystallinity and carbonate content that illustrates the importance of CO_3^{2-} in BAp crystals short-range order. Circles represent petrous bones and diamonds represent other skeletal elements.

A strong inverse relationship between IRSF and C/P can be observed both in petrous bones (R^2=0.62) and the other bones (R^2=0.60) (**Figure 5.17**), with the overall correlation increasing from R^2=0.60 to R^2=0.69 when samples with calcite uptake are excluded. The crystallinity-carbonate relationship varies between sites (**Table 3**). In Manika, for instance, IRSF-C/P R^2=0.92 in petrous and R^2=0.86 in other bones, while in Cladh Hallan petrous bones R^2= 0.68 and in Tharrounia bones R^2=0.14. Therefore, although crystallinity and carbonate concentrations (C/P) are interrelated (Wopenka and Pasteris 2005), interaction of BAp crystals with the burial environment can significantly change that relationship.

Table 3. IRSF-C/P inverse correlation (R^2) in sites with samples n≥5 in each group. Overall values include samples from all sites.

Site	IRSF-C/P	
	Petrous	**Other**
Bedburg-Königshoven, Germany	0.70	N/A
Maroulas, Greece	N/A	0.40
Ain Ghazal, Jordan	0.69	N/A
Sarakenos, Greece	0.84	0.60
Tharrounia, Greece	N/A	0.14
Ness of Brodgar, Scotland	0.65	N/A
Manika, Greece	0.92	0.86
Cladh Hallan, Scotland	0.68	N/A
Kastrouli, Greece	N/A	0.70
Potterne, England	0.03	N/A
York, England	0.82	N/A
Holmens Kirke, Denmark	0.74	N/A
St. Rombout, Belgium	0.86	0.84

5.2.2. INTER- AND INTRA-SITE VARIATIONS

Inter-site variations in crystallinity and carbonate content are considerable and demonstrate the effects of the burial environment on the preservation of bioapatite crystals (**Figure 5.18**). The highest crystallinity values are observed in Manika (IRSF=4.88±0.8), whereas Sarakenos cave (IRSF=3.42±0.15), Manika (IRSF=3.44±0.37), and the petrous bones from Holmens Kirke (IRSF=3.46±0.24) display similar BAp preservation states. However the Mesolithic Maroulas bones that show characteristics of fossilization under the microscope (**Figure 5.9a**) show a moderate increase in crystallinity (IRSF=3.86±0.42; **Figure 5.18a**). The transformation of bioapatite in fossil bones occurs when the ionic substitutions change the structural and compositional characteristics of BAp crystals, increasing its size and order (Keenan et al. 2015; Piga et al. 2011, 2016).

The changes in bone mineralogy, however, can considerably vary depending on the conditions of the burial environment (e.g. Keenan et al. 2015). Dissolution/recrystallization of BAp crystals due to interaction with water was indicated by the microcracks and loss of histological integrity in many samples (section 5.1.). Following soft tissue decomposition, soil water can damage bone matrix by accessing bone through the lacuno–canalicular network. Thus, a recharge environment that is generated by wet and dry cycles (Hedges and Millard 1995; Nielsen-Marsh et al. 2000a) and/or the seasonal/sporadic flow of unsaturated rainwater (flow regime) through the bones situated near the ground surface has led to changes in bioapatite crystals at increased rates (Grupe 1995; Hedges and Millard 1995; Nielsen-Marsh et al. 2000a). As the porosity increases, the potential of the specimens for survival is reduced, because when water (and associated ions and microorganisms) flows freely through the bone, it can completely dissolve bone (Kendall et al. 2018). On the contrary, more stable environments (e.g. caves) that do not expose bone to such a variable interaction with soil water can allow BAp crystals to reach an equilibrium with their

surroundings and slow down dissolution/recrystallization (Pate, Hutton and Norrish 1989; Wilson and Pollard 2002). Sarakenos cave appears to be such an environment, where bones show limited recrystallization, indicated by the low IRSF values.

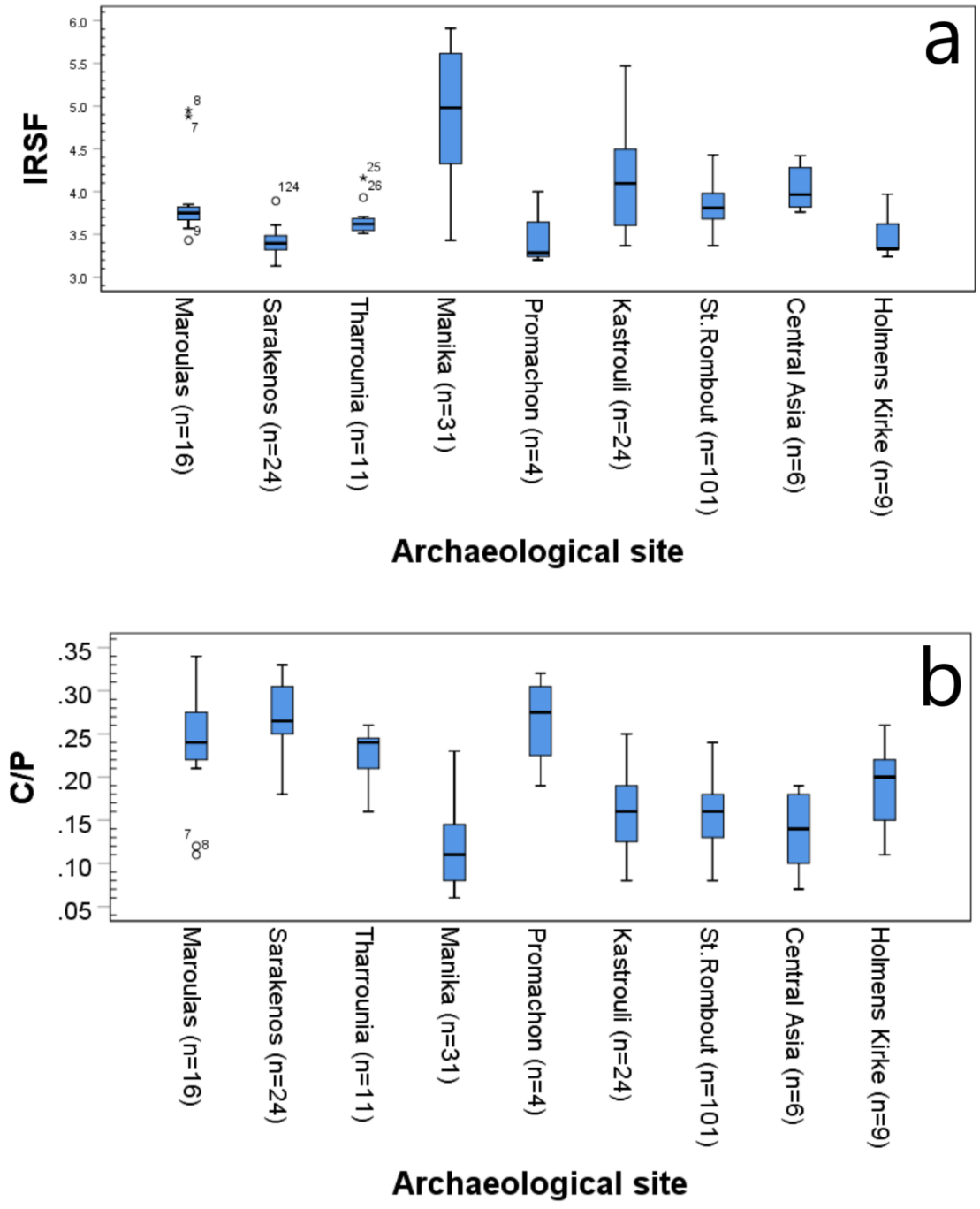

Figure 5.18. Inter-site variations in crystallinity and carbonate content.

Soil geochemistry is also a key factor that can lead to the inter-site variations in carbonate content (**Figure 5.18b**), as an acidic environment can lower CO_3^{2-} content (Chadefaux et al. 2009), whereas a slightly alkaline pH in areas close to the samples can favour the uptake of carbonates through interaction with soil water (Chadefaux et al. 2009; Hedges and Millard 1995; Lebon et

al. 2011). An absorption of exogenous carbonate in Maroulas, Sarakenos and Promachon bones, for example, may have occurred via different mechanisms such as the decay of C_3 flora in the form of bicarbonate (HCO_3^-) and/or from weathered bedrock $CaCO_3$ (Wright and Schwarcz 1996). Thus, the general pattern observed in archaeological bone (characterized by a loss of CO_3^{2-} content and an increase in crystallinity through phosphate uptake during dissolution/recrystallization) can alter when there is an ionic exchange between BAp and the burial environment (**Figure 5.17**).

Variable intra-site modifications in bioapatite can also be observed, especially in carbonate content (**Figure 5.18b**), which highlights the importance of the micro-environment conditions to the long-term survival of bone. Crystallinity shows more homogeneity and only bones in Manika and Kastrouli exhibit high intra-site variations (**Figure 5.18a**; **Table 3**). The Sarakenos cave bones, although recovered from different areas of the cave and different depths (which might be linked to variable preservation of bone (e.g. Karkanas et al. 2000; Stiner et al. 2001), show a lack of correlation with both area (no significant differences between trench E vs trench F samples; U=30.500, p=0.479 and U=32.500, p=0.596 for IRSF and C/P, respectively) and depth (trench E samples' IRSF-depth R^2=0.00 and R^2=0.15 for C/P-depth; trench F IRSF-depth R^2=0.35 and C/P-depth R^2=0.26). Similarly no correlation can be observed between type of burial and crystallinity [$x^2(3)$=0.532, p=0.912] or carbonate content [$x^2(3)$=1.281, p=0.734] in St. Rombout.

5.2.3. INTRA-INDIVIDUAL AND INTRA-BONE VARIATIONS

No significant intra-individual variations are observed in twenty-one individuals from St. Rombout and one from Maroulas, either for IRSF [$x^2(6)$=2.263, p=0.894; **Figure 5.19a**] or for C/P [$x^2(6)$=10.442, p=0.107; **Figure 5.19b**]. Regarding the petrous bone, it displays a slightly higher average IRSF value compared to these of the femora and tibiae, and lower than the humeri, radii, and ulnae (**Figure 5.19a**). The C/P intra-individual differences show a smaller variability, as only the femora and the tibiae show a higher C/P content compared to the petrous bone, with all other skeletal elements having average values similar to the petrous bone (**Figure 5.19b**).

Intra-bone variations (i.e. proximal-to-distal diaphyses) are not detected in long bones from Maroulas, Sarakenos cave, Tharrounia, Manika, and St. Rombout, both for IRSF (**Figure 5.20**; humerus U=100.500, p=0.624; radius U=37.500, p=0.796; ulna U=8.000, p=0.421; femur U=43.500, p=0.631; tibia U=16.500, p=0.818) and C/P (**Figure 5.20**; humerus U=103.000, p=0.713; radius U=34.000, p=0.605; ulna U=12.000, p=1.000; femur U=49.000, p=0.971; tibia U=16.500, p=0.818). Therefore, the burial environment can vary intra-site, leading to variations

in BAp composition and structure, but the conditions of the burial micro-environment appear more homogeneous.

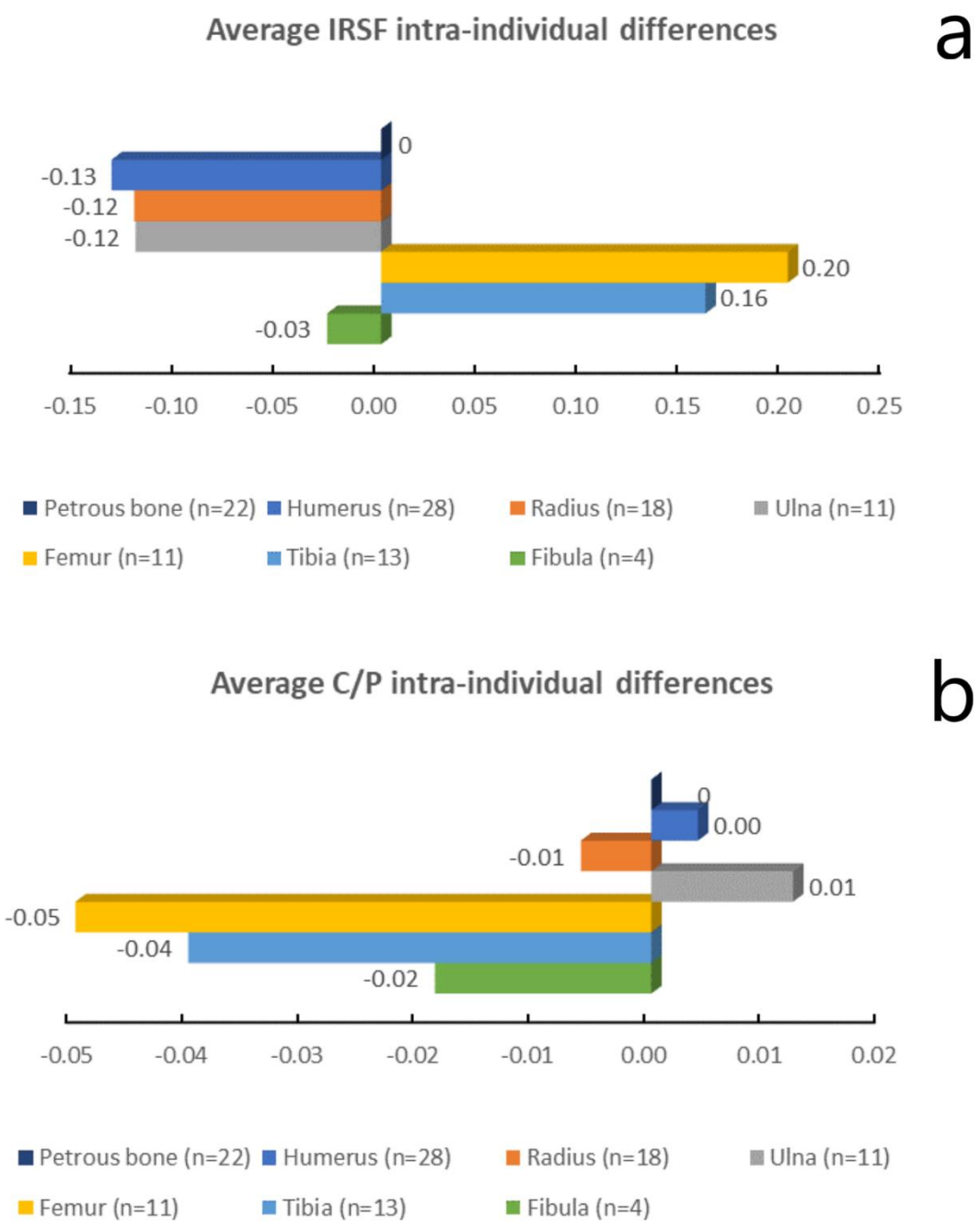

Figure 5.19. Intra-individual variations in crystallinity (a) and carbonate content (b) in twenty-one individuals from St. Rombout and one from Maroulas. Bars represent the average difference between the petrous bone and the other skeletal elements (i.e. a positive value indicates a lower average value of this skeletal element compared to petrous bone, and vice versa).

Within-sample variations can be observed in crystallinity and carbonate content of the different bone tissue areas (**Figure 5.21**). Although there is no statistically significant difference between periosteal, mesosteal and trabecular bone tissue either for IRSF (x^2=1.680, p= 0.432) or for C/P (x^2=0.306, p= 0.858). IRSF values in the periosteal tissue appear lower compared to the mesosteal

and trabecular tissues (**Figure 5.21a**), whereas carbonate content displays no observable pattern (**Figure 5.21b**). In modern human bone, a gradient from the osteon outwards (tissue specific, age-related variations) has been previously reported by Paschalis et al. (1996), with the areas farther from the Haversian canal displaying increased crystallinity, higher type B carbonate and lower type A carbonate content. Additionally, a small variation in carbonate content within trabecular bone tissue (i.e. center to edge gradient) has also been reported by Ou-Yang et al. (2001).

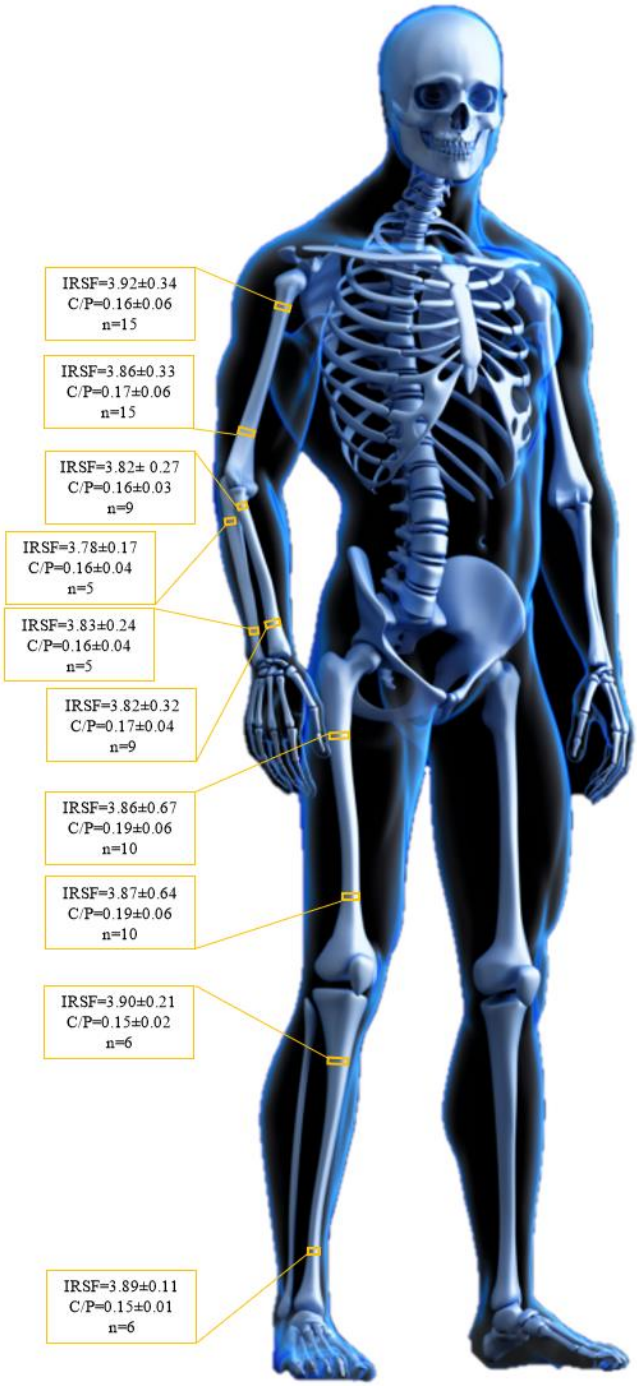

Figure 5.20. Crystallinity and carbonate content in proximal and distal diaphyses of long bones.

Apropos of that behaviour, Stiner et al. (1995) observed that the outer surfaces of modern bone which had been exposed for 2 and 9 years post-mortem in Israel and New Mexico (USA), respectively, displayed higher crystallinity than the inner cortical areas. In a similar attempt to record mineralogical and compositional changes in bones of large mammals exposed on the ground surface in Amboseli National Park (Kenya) for up to 26 years, Trueman et al. (2004) also observed that the crystallinity in the periosteal surfaces was higher than in the other bone tissue areas (inner cortical) as early as 2 years post-mortem. The higher periosteal IRSF values were accompanied by higher concentrations of rare earth elements (e.g. Ba and La) which also showed a gradual decrease towards the inner cortex (Trueman et al. 2004). When the cortical bone was compared with trabecular bone in the Middle Palaeolithic Hayonim cave (Israel), the IRSF values for spongy tissues were found to be slightly higher (Stiner et al. 2001).

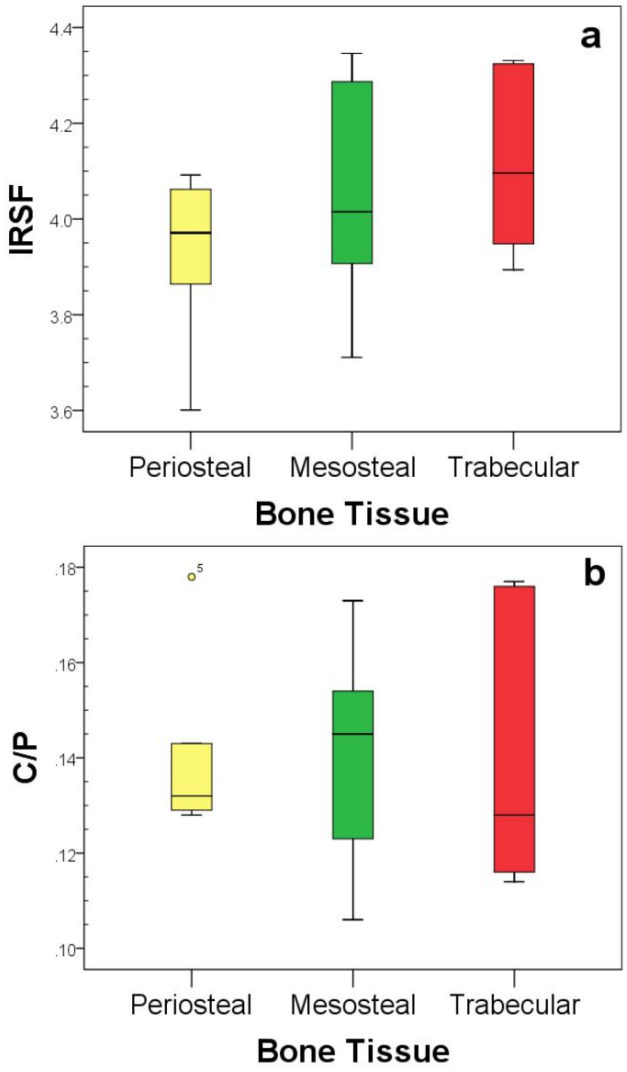

Figure 5.21. Box plots showing the IRSF (a) and C/P (b) values in the periosteal, mid cortical (mesosteal) and trabecular tissues. Notice the lower IRSF (a) and C/P (b) values in the periosteal tissue.

Consequently, the tissue-specific differences (i.e. periosteal, mesosteal, endosteal) in crystallinity and carbonate content can vary within and between sites (Stiner et al. 2001; Trueman, Privat and Field 2008; 2008), while other factors such as the size of the bone itself can also affect its post-mortem behaviour and interaction with its depositional environment (Surovell and Stiner 2001). Although there is no universal pattern for tissue-specific variations found in archaeological and fossil bone, the necessity of homogenization of samples prior to analysis through the mechanical removal of the periosteal, trabecular and endosteal bone tissues and use of the mesosteal (mid-cortical) tissue is indisputable for the improvement of accuracy, precision, reproducibility and comparability of data.

5.2.4. CRYSTALLINITY, CARBONATE CONTENT AND CRYSTAL ORDER

With reference to the ionic exchanges in BAp which cause the inter-site, intra-site and intra-sample variations, a deeper understanding of the carbonate environment is critical, as it is linked to the short-range order and dimensions of the crystals. Carbonate can either be exchanged with OH^- in the A-sites or it can be swapped with PO_4^{3-} ions in the B-sites (LeGeros 1965; Wopenka and Pasteris 2005). A CO_3^{2-} to PO_4^{3-} exchange generates a contraction of the unit cell of the BAp crystal as carbonate is smaller than phosphate, whereas a CO_3^{2-} to OH^- exchange results to an expansion of the unit cell, as CO_3^{2-} is larger than OH^- (LeGeros et al. 1969). In type A substitutions high temperature (900-1000˚ C) is required, hence the exclusion of water, while type B substitutions occur at c. 25-100˚ C, with water playing an important role to the ionic exchanges (LeGeros 1965). However, the incorporation of exogenous carbonate into BAp crystals often has no noticeable effect on IRSF, possibly due to small variations between bone structural carbonate and environmental carbonates (Rey et al. 1989).

Although quantification of these ionic exchanges is currently difficult, a qualitative assessment of the carbonate environment can be accomplished using the mid-IR spectra. Changes in the ν_2 carbon-oxygen out-of-plane bending vibrations identified through the 872 cm^{-1} absorbance height, and its correlation to the ν_3 carbon-oxygen asymmetric stretching at 1410 cm^{-1}, can provide useful qualitative information on the carbonate environment of BAp (Baxter, Biltz and Pellegrino 1966; Elliott 1964; LeGeros et al. 1969; White 1974). The very strong linear relationship (R^2=0.92; **Figure 5.22**) between the 1410 cm^{-1} and the 872 cm^{-1} peaks (both assigned to type B carbonate (Elliott 1964; LeGeros et al. 1969; Rey et al. 1989) proves the high proportion of type B carbonate environment in bioapatite and its role in crystallinity changes. Post-mortem substitution of CO_3^{2-} by exogenous PO_4^{3-} from biological sources (e.g. organic refuse), decomposition by-products of fresh wood ash, or limestone weathering (Stiner et al. 2001) during

recrystallization would increase the unit cell dimensions of BAp crystals due to the longer O-O distances in phosphate compared to carbonate (LeGeros et al. 1969).

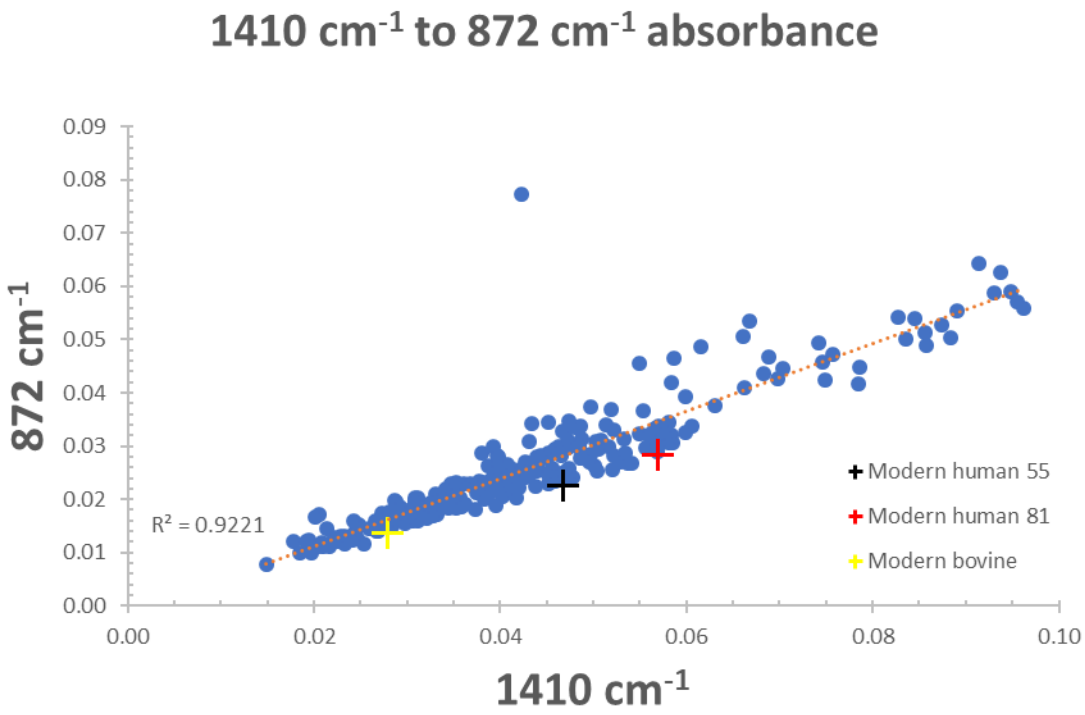

Figure 5.22. The very strong linear relationship between the main type-B carbonate peaks of bone apatite (outlier MEC7 excluded).

The ν_2 carbonate band at c. 850-900 cm^{-1} (which is considered free of organic constituents (Termine et al. 1973) and generally free of HPO_4^{2-} artifacts (Rey et al. 1989) can also offer useful information through 2nd derivative analysis. The two main carbonate bands in modern bone at 879 cm^{-1} and 871 cm^{-1} are frequently assigned to type A1 (stuffed) and type B (sloping faces) carbonates, respectively (**Figure 5.23**; Fleet 2009; Fleet and Liu 2004; Fleet, Liu and King 2004; LeGeros 1965; LeGeros et al. 1967). A third component which is assigned to type A2 (labile) CO_3^{2-} can be observed at 866 cm^{-1} (Rey et al. 1989), but this is mainly detected in coarse powder of modern bone (Kontopoulos et al. 2018). Regarding the relative proportion of the A1 and B components, it differs in modern human bone compared to modern bovine bone (**Figure 5.23**). This explains the differences between human and bovine bioapatite characteristics observed in **Figure 5.17** which are related to crystal order and size, as variations in the carbonate environment affect the α- and c-axis crystal dimensions (e.g. LeGeros et al. 1969).

The 2nd derivative spectra of archaeological bone (**Figure 5.24**) confirm that only the A1 and B types are present (Kontopoulos et al. 2018). The analysis of specimens that display a gradual increase in crystallinity and a gradual loss of carbonate indicate that A-sites decrease in all samples, although not in a predictable manner (**Figure 5.24**). Even in SAR3 (which displays a low crystallinity and a high C/P, indicative of an uptake of exogenous carbonate from the

surrounding environment), the 879 cm^{-1} component has almost vanished (**Figure 5.24b**), an indication of dissolution followed by incorporation of exogenous carbonate (C/P higher than in modern bone) during recrystallization. This loss of the type A1 component is often accompanied by an increase of the type B component at 872 cm^{-1}, as seen from the absorbance height (**Figure 5.24a-b**). In other bones such as MAR10 (**Figure 5.24c**), which is characterized by a high crystallinity and loss of half of its carbonate, the 2nd derivative spectra display a pattern similar to modern bovine bone (**Figure 5.23b**) with a small increase in B carbonate and a small decrease in A1 carbonate. Therefore, the carbonate environment of archaeological bone can be transformed post-mortem, but in a complex way that is not easily quantifiable.

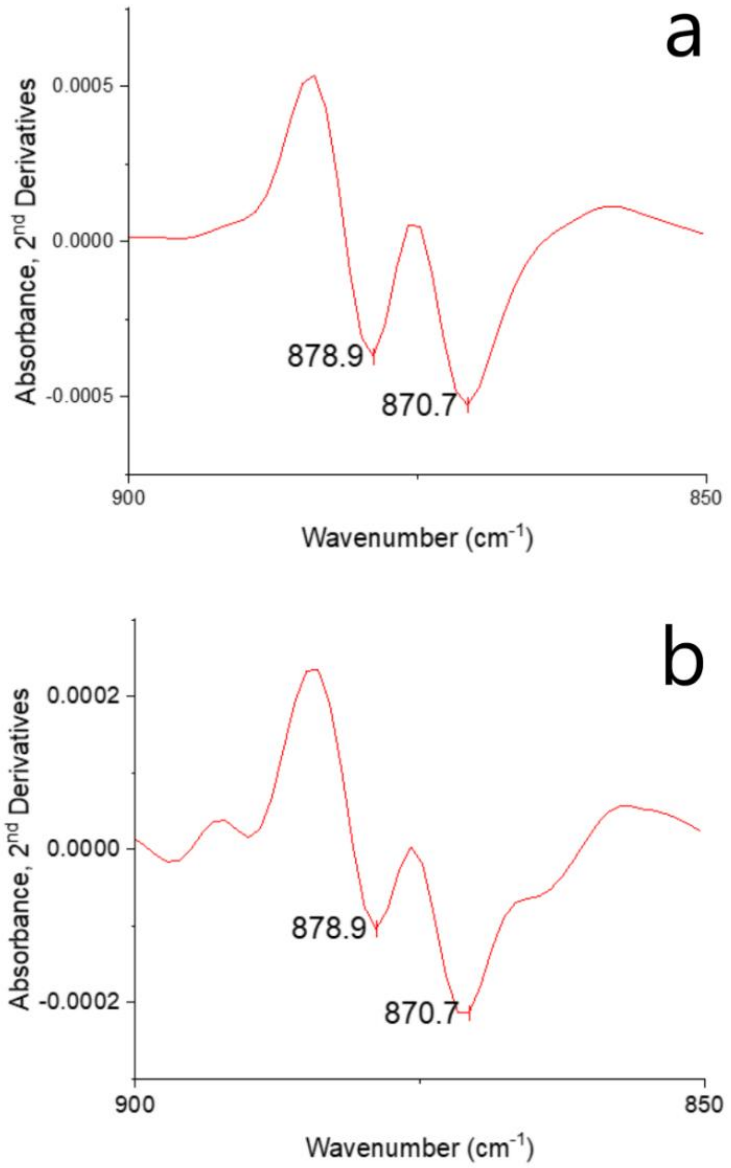

Figure 5.23. 2nd derivative spectra of the ν_2 carbonate band of (a) modern human bone (55 years old male) and (b) modern bovine bone.

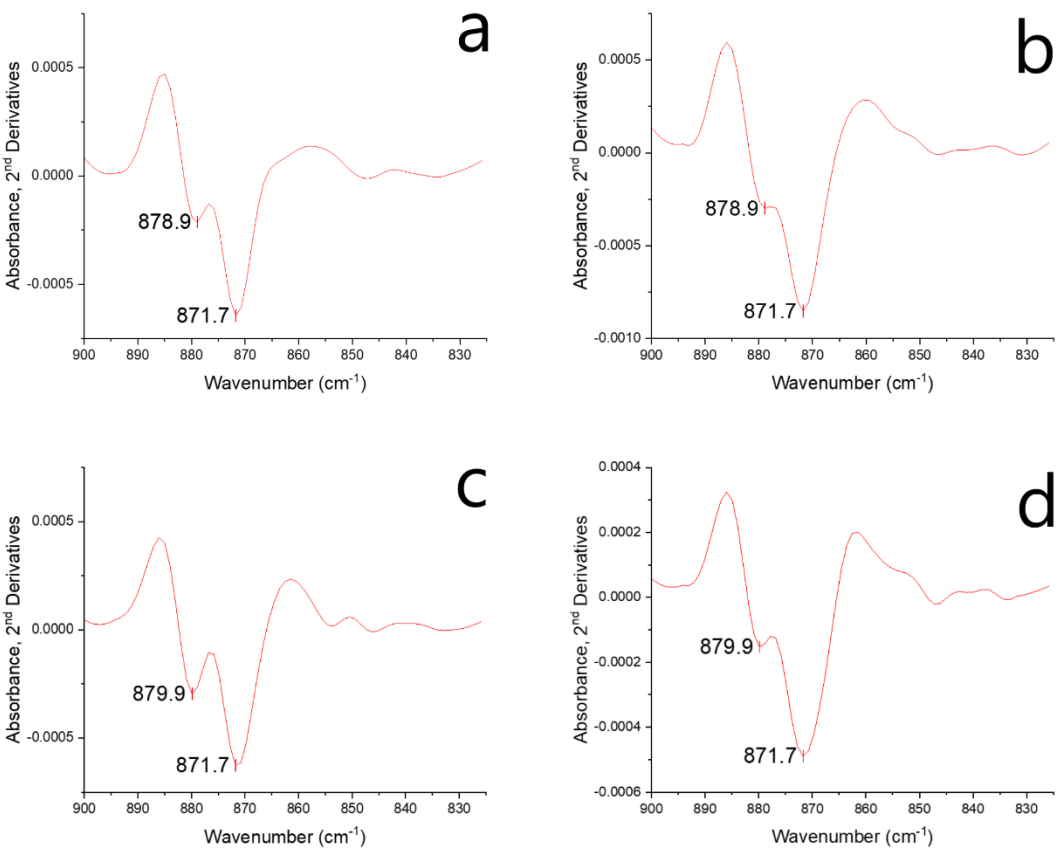

Figure 5.24. *2nd derivative spectra of the v_2 carbonate band*. (a) SAR3 (IRSF=3.56, C/P=0.27), (b) KAS5 (IRSF=4.15, C/P=0.18), (c) MAR10 (IRSF=4.95, C/P=0.12), and (d) MAN13 (IRSF=5.80, C/P=0.07).

Calcite is identified in 54 samples by the absorbance height of the v_4 carbon-oxygen in-plane bending at 712 cm^{-1} (**Table A2-Appendix A**). This peak is considered more sensitive to the changes in the Ca-O distance during vibration (Baxter, Biltz and Pellegrino 1966; Gueta et al. 2007; Hunt, Wisherd and Bonham 1950) than the v_3 at c. 1410 cm^{-1} and v_2 at 872 cm^{-1} vibrations (Regev et al. 2010). The weak correlation between the 1410-712 cm^{-1} (R^2=0.2) and the moderate relationship between the 872-712 cm^{-1} (R^2=0.36) absorbance heights confirms the lower sensitivity of these bands to calcite uptake. This is explained by the small differences in the asymmetric stretching and out-of-plane bending vibration between bone carbonate and calcite, as the C-H vibrations of the organic content of bone that superimpose on the CO_3^{2-} absorbance peak at 1410 cm^{-1} can mask modifications in bone carbonate (Trueman et al. 2004; 2008).

Calcite can be found in limestone, chalk, marble, travertine, even in wind-borne (loess) and cemented sediments, thus a distinction between a rather amorphous bone calcium carbonate (lower order with greater Ca-O and O_1-O_2 distances) and exogenous calcite (higher order with smaller distances) (Gueta et al. 2007) is of significance, especially for isotopic studies. A direct comparison of bones with and without calcite that exhibit similar IRSF and C/P values can potentially provide further information on the location of the exogenous ions incorporated into

BAp. A significant increase of the 872 cm^{-1} component is observed in bones that display calcite uptake (**Figure 5.25**). This increase in B-sites is often accompanied by a reduction of the 879 cm^{-1} A1 component (**Figure 5.25a-c**). Except for MAN31 (**Figure 5.25d**), where the carbonate environment appears similar to modern human bone (**Figure 5.25a**), in all other samples that show calcite uptake the 872 cm^{-1} peak is about x2 the height in modern human bone (**Figure 5.25a-c**). As a result, an uptake of calcite possibly occurs at the sloping faces of BAp crystals in B-sites, as demonstrated by the v_2 carbonate 2nd derivative analysis.

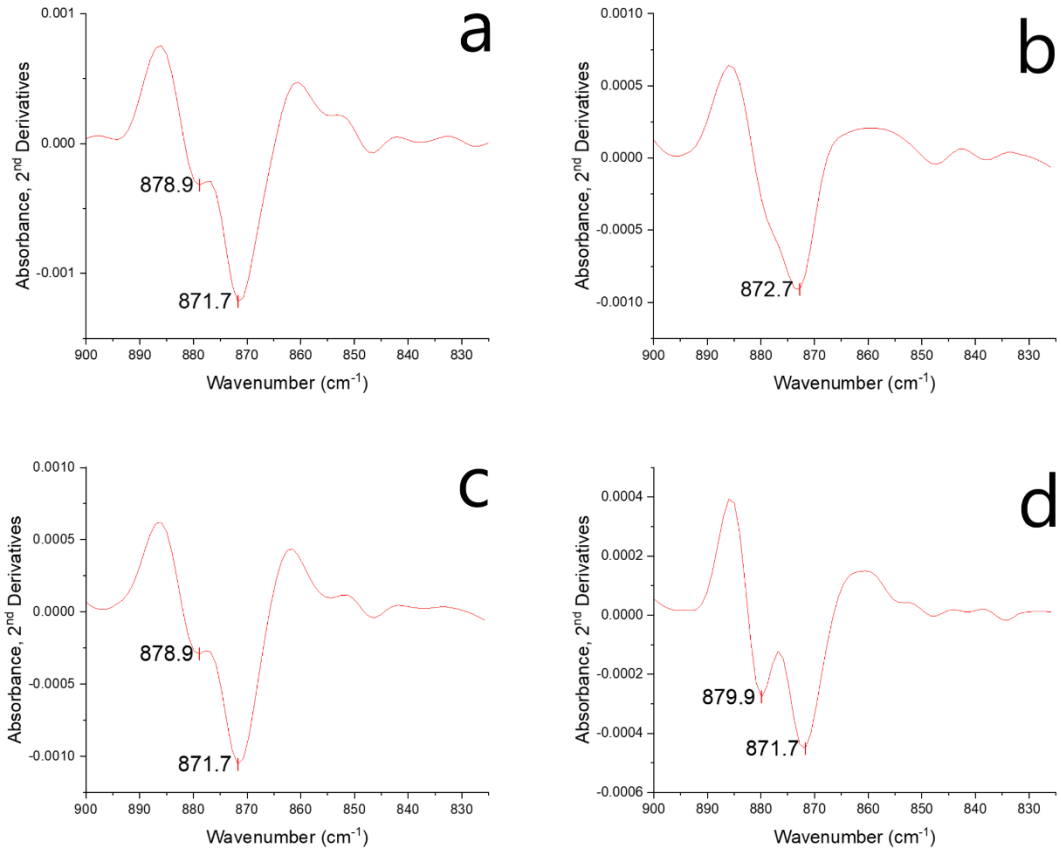

Figure 5.25. *2nd derivative spectra of the v_2 carbonate band (calcite uptake)*. (a) MAR12 (IRSF=3.70, C/P=0.29), (b) KAS12 (IRSF=4.09, C/P=0.20), (c) MAR9 (IRSF=4.88, C/P=0.12), and (d) MAN31 (IRSF=5.83, C/P=0.08). Absorbance height at 712 cm^{-1}: MAR12=0.00854, KAS12=0.00462, MAR9=0.00707, and MAN31=0.00600. IRSF and C/P are similar to these of samples in **Figure 5.24**.

The 2nd derivative analysis of the complex v_3 mode (c. 1400-1500 cm^{-1}) shows that the c. 1415 cm^{-1}, c. 1450 cm^{-1} site B CO_3^{2-} components, and the c. 1468 cm^{-1} and c. 1535 site A CO_3^{2-} components (Brangule and Gross 2015; Madupalli, Pavan and Tecklenburg 2017; Rey et al. 1989) are more prominent in modern bone (**Figure 5.26**) and decrease in archaeological bone (**Figure 5.27**). A decrease in the 1468 cm^{-1} and 1535 cm^{-1} peaks can be possibly related to loss of type A CO_3^{2-} (Rey et al. 1989; Madupalli, Pavan and Tecklenburg 2017), while a decrease in the 1415 cm^{-1} peak in the archaeological bone without calcite uptake can be linked to a loss of type B structural carbonate (Rey et al. 1989; Fleet and Liu 2004). On the other hand, this decrease in the

1415 cm^{-1} peak is not observed in samples with calcite uptake (**Figure 5.28**), as these demonstrate an increase in the 1415 cm^{-1} peak which possibly indicates the position that calcite predominantly occupies in BAp crystals (i.e. type B).

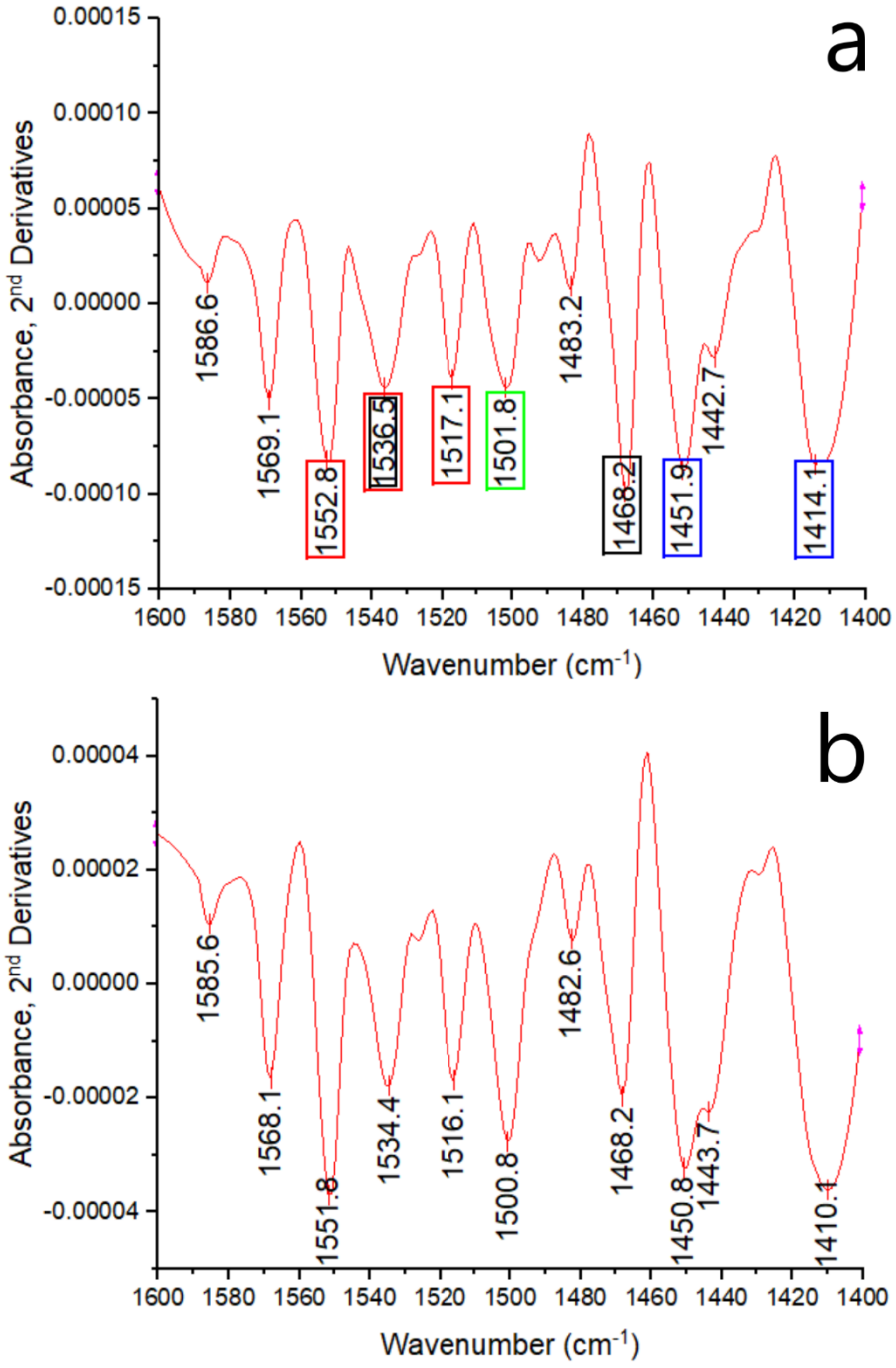

Figure 5.26. 2nd derivative spectra of the ν_3 carbonate band of (a) modern human bone (55 years old male) and (b) modern bovine bone. **Black boxes** highlight the possible type A carbonate components; **blue boxes** highlight the possible type B carbonate components; green box highlights a possible non-apatitic (labile) carbonate component; **red boxes** highlight the possible organic (amide II) components (Termine et al. 1973; Rey et al. 1989; Fleet and Liu 2004; Brangule and Gross 2015; Madupalli et al. 2017).

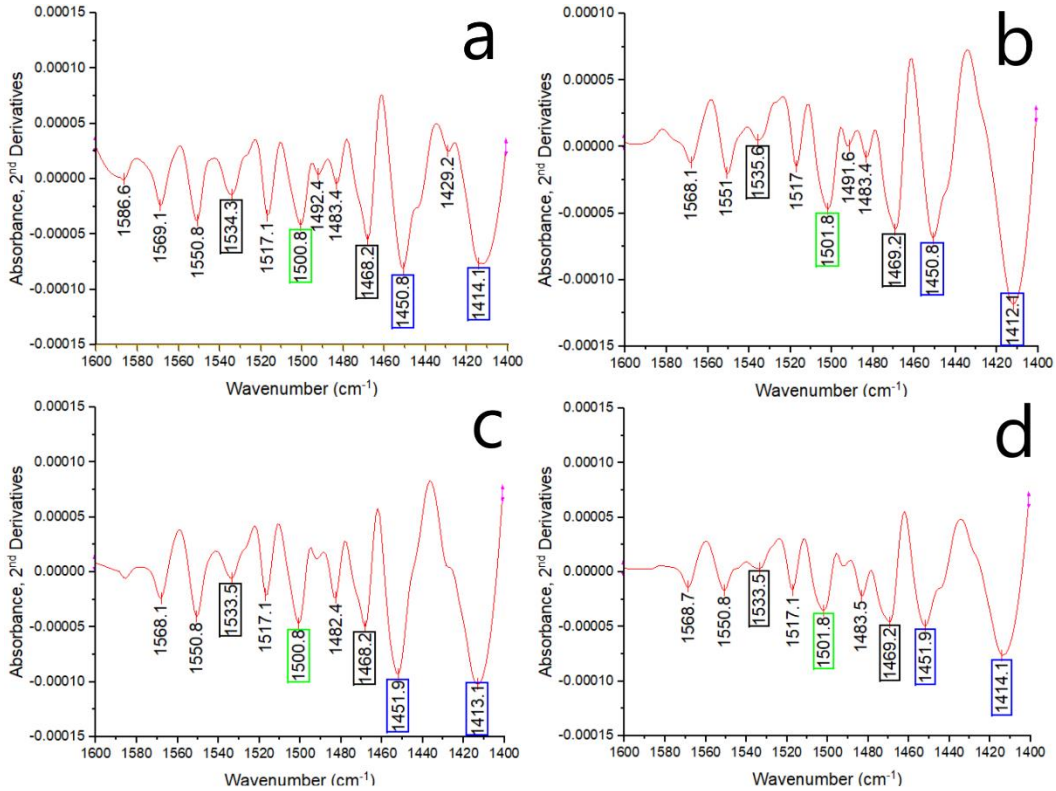

Figure 5.27. 2nd derivative spectra of the v_3 carbonate band. (a) SAR3 (IRSF=3.56, C/P=0.27), (b) KAS5 (IRSF=4.15, C/P=0.18), (c) MAR10 (IRSF=4.95, C/P=0.12), and (d) MAN13 (IRSF=5.80, C/P=0.07). **Black boxes** highlight the possible type A carbonate components; **blue boxes** highlight the possible type B carbonate components; green box highlights a possible non-apatitic (labile) carbonate component (Termine et al. 1973; Rey et al. 1989; Fleet and Liu 2004; Brangule and Gross 2015; Madupalli et al. 2017).

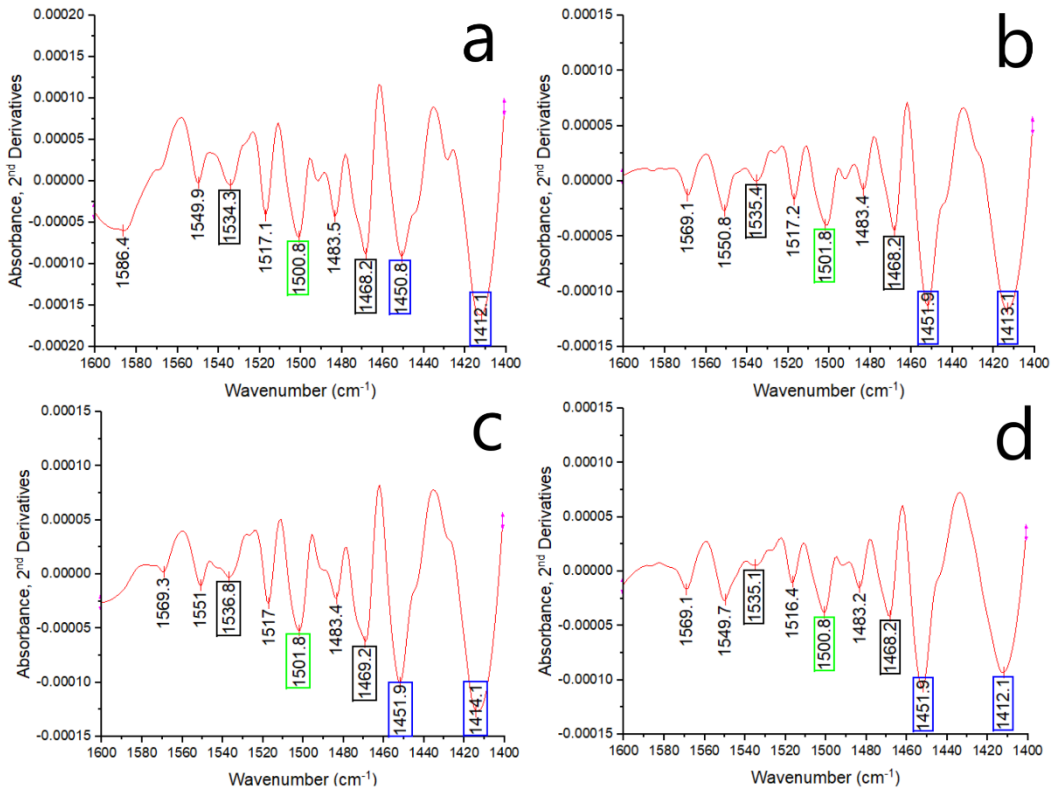

Figure 5.28. 2nd derivative spectra of the v_3 carbonate band (calcite uptake). (a) MAR12 (IRSF=3.70, C/P=0.29), (b) KAS12 (IRSF=4.09, C/P=0.20), (c) MAR9 (IRSF=4.88, C/P=0.12), and (d) MAN31 (IRSF=5.83, C/P=0.08). Absorbance height at 712 cm^{-1}: MAR12=0.00854, KAS12=0.00462,

MAR9=0.00707, and MAN31=0.00600. **Black boxes** highlight the possible type A carbonate components; **blue boxes** highlight the possible type B carbonate components; green box highlights a possible non-apatitic (labile) carbonate component (Termine et al. 1973; Rey et al. 1989; Fleet and Liu 2004; Brangule and Gross 2015; Madupalli et al. 2017).

Differences in most cases, however, are not unequivocal, which reflects the complexity of the ionic exchanges between bioapatite and its surrounding environment. Overall, an A-site carbonation in the apatitic c-axis channel that would require much higher energy than B-site carbonation of phosphate sites (Madupalli, Pavan and Tecklenburg 2017) seems unlikely through the 2nd derivative component analysis. Thus, exogenous carbonate is probably positioned at the sloping faces of BAp crystals, replacing type B CO_3^{2-} (Maurer et al. 2014; Wright and Schwarcz 1996) and any changes observed in the 2nd derivative components can also be caused by the changes in carbonate orientation (Madupalli, Pavan and Tecklenburg 2017). Calcite seems to follow the same pathway, i.e. adsorbing onto the BAp crystal surfaces. The alternative scenario in which calcite could partly be incorporated into the A sites during severe dissolution and recrystallization of BAp seems unlikely.

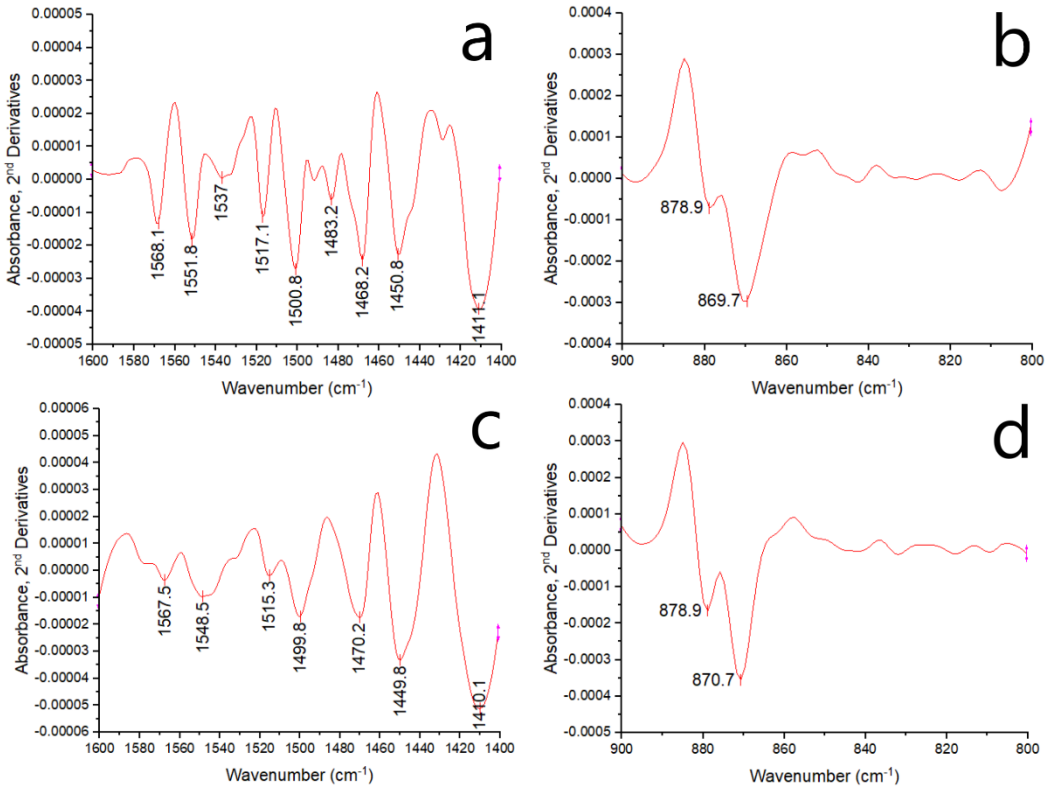

Figure 5.29. 2nd derivative spectra of the ν_3 (a and c) and the ν_2 carbonate bands (b and d) of SAR38 (bovine petrous bone) and DEN8 (human petrous bone). SAR38 (a and b) and DEN8 (c and d) display similar IRSF (3.23 and 3.27, respectively) but different C/P (0.33 and 0.18, respectively). Here, the carbonate bands are characterized by different proportions of type A and B carbonate.

Nevertheless, it is difficult to make any safe assumptions on the location of exogenous CO_3^{2-} in the BAp crystal lattice. The peaks and shoulders displayed in these regions are still not unambiguously assigned to a specific CO_3^{2-} site (Elliott 1964; Fleet and Liu 2004; LeGeros et al. 1969; Rey et al. 1989), and some domains also include absorption from other bands (e.g. CH, CN,

COO^-, NH) that overlap with CO_3^{2-} (Elliott 1964; Termine et al. 1973) and hinder further interpretation. It is also possible that the hypothesis of two carbonate environments, each of which has its own characteristic absorption spectrum, might be an oversimplification (Elliott 1964; Elliott, Holcomb and Young 1985).

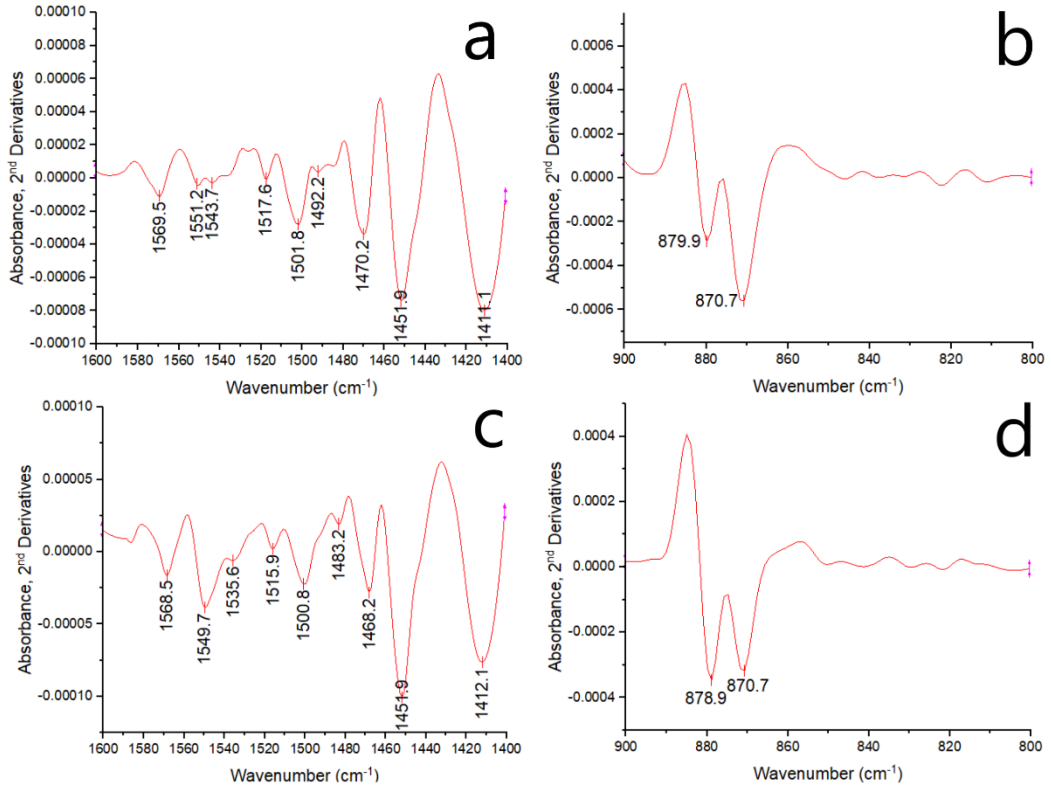

Figure 5.30. 2nd derivative spectra of the v_3 (a and c) and the v_2 carbonate bands (b and d) of PRO8 (bovine metacarpal) and MEC30 (human petrous bone). PRO8 (a and b) and MEC30 (c and d) display similar IRSF (4.00 and 4.07, respectively) but different C/P (0.19 and 0.09, respectively). Note the reduction in B-sites of MEC30 (c and d).

A comparison of the 2nd derivative spectra of the v_2 and v_3 carbonate bands of human and animal bones of similar crystallinity but different carbonate content also tells an interesting story for IRSF (**Figure 5.29** and **Figure 5.30**). One would expect that if the crystallinity is similar (hence the short-range order and average crystal size) the carbonate environment should exhibit similar characteristics, as this defines the shape and size of the crystal by changing the lattice's α- and c-axes (LeGeros 1965, 1981; LeGeros et al. 1967, 1969). However, **Figure 5.29** and **Figure 5.30** show that even if there are significant differences in the carbonate environments of the BAp crystals, samples can still display similar crystallinity. Therefore, this observation could possibly indicate that a loss of structural carbonate and its replacement by other non-carbonate ions from the burial environment (e.g. Fe, Mn, or REE; Keenan et al. 2015) may not cause changes in crystallinity, or that the C/P cannot accurately reflect the changes in the carbonate environment.

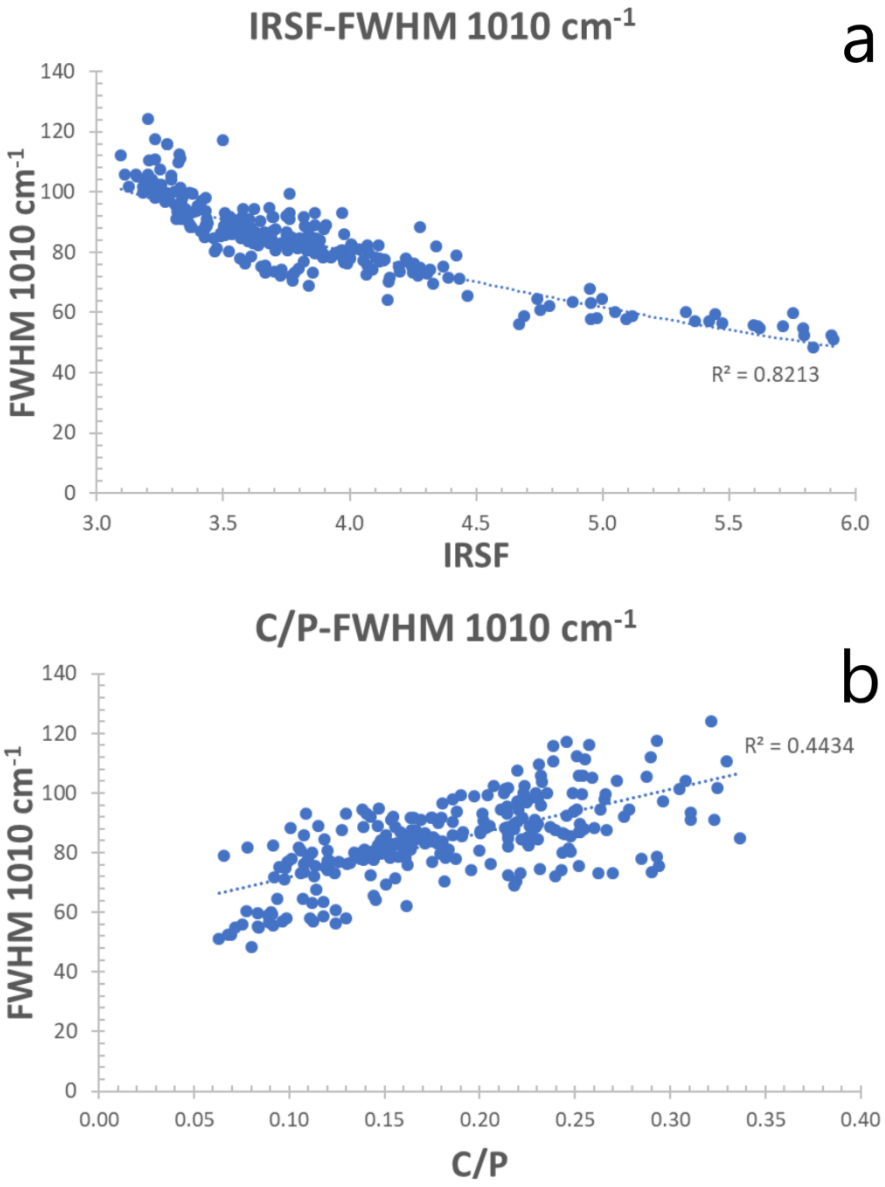

Figure 5.31. The relationship of the long-range crystal order with (a) crystallinity and (b) carbonate content.

Building further on the carbonate-crystal order/disorder relationship, the carbonate substitutions are also assumed to affect the long-range order of the crystals. The FWHM at 1010 cm^{-1} reflects the long-range order of BAp, hence the homogeneity between the different clusters of atoms arranged in a predictable pattern (Asscher et al. 2011; Asscher, Weiner and Boaretto 2011; Wopenka and Pasteris 2005). Higher FWHM values indicate higher long-range disorder, thus theoretically, when crystallinity increases and carbonate content decreases, the clusters' homogeneity improves. The very strong inverse relationship (R^2=0.82; **Figure 5.31a**) between IRSF and FWHM at 1010 cm^{-1} confirms that relationship; hence, increasing crystallinity leads to increased long-range order. However, when C/P is plotted against FWHM at 1010 cm^{-1} the moderate correlation (R^2=0.44; **Figure 5.31b**) between the carbonate content and cluster homogeneity in bone apatite indicates that CO_3^{2-} does not have such a significant effect on the

long-range order. The weak correlations between 872 cm^{-1} (R^2=0.37) and 1410 cm^{-1} (R^2=0.24) peak absorbances with the FWHM at 1010 cm^{-1} further highlights this lack of correlation between carbonate content and long-range order. Thus, phosphate content is primarily responsible for any observable changes in the observed homogeneity at both the short- and long-range.

5.3.1. PETROUS VERSUS OTHER BONES

Collagen preservation in petrous bones (n=62) does not display any statistically significant differences (U=4519.500, p=0.198) when compared to other skeletal elements (n=164). A high variability is observed, with collagen yields (wt. %) ranging from 0.00 to 17.84 (average=9.5±5.13) in petrous bones and from 0.00 to 22.55 wt. % (average col. wt. %=8.9 ± 6.56) in other bones (**Figure 5.32**; **Table A3-Appendix A**). Collagen yields are commonly used to distinguish well-preserved from poorly-preserved collagen and currently c. 1 wt. % is considered a suitable threshold below which samples should not be used for isotopic and/or radiocarbon dating studies (Brock, Higham and Ramsey 2010; Dobberstein et al. 2009; Van Klinken 1999). Here, 37 samples (of which 9 (15 %) were petrous bones), all from Greek prehistoric open-air sites display collagen yields below the 1 wt. % threshold. Consequently, from this sample set it does not seem that collagen has increased survival rates in petrous bones compared to other skeletal elements.

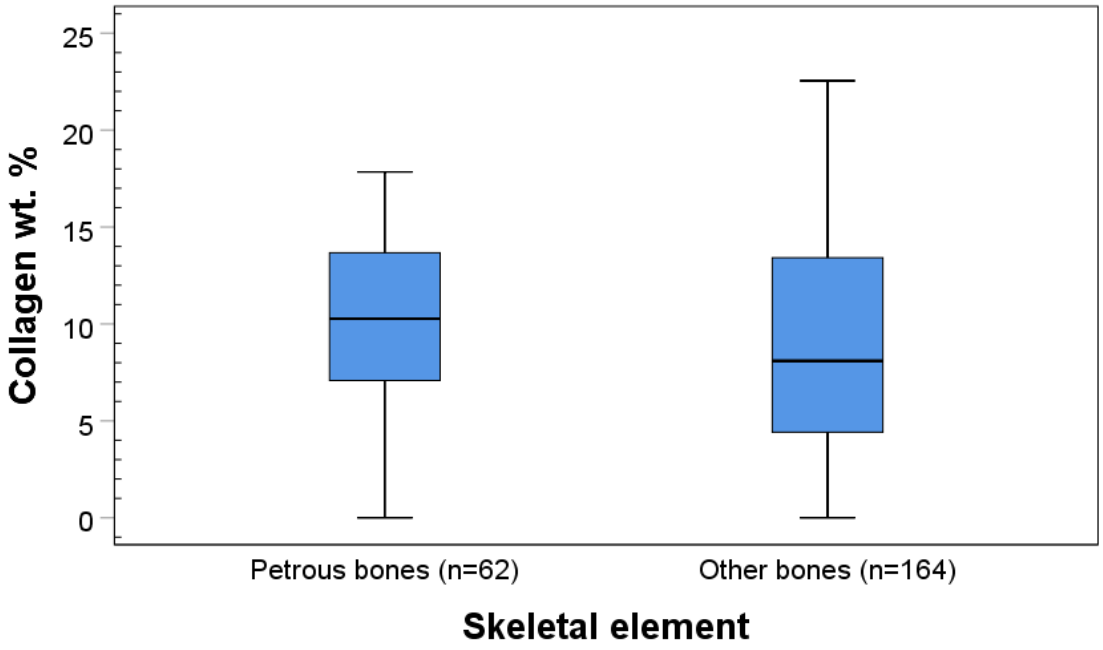

Figure 5.32. Box plot showing the distribution of collagen yields in petrous and other bones.

5.3.2. INTER- AND INTRA-SITE VARIATIONS

Statistically significant inter-site variations with no correlation to chronological age can be observed (U=118.713, p=0.000), with the poorest collagen preservation seen in the Mesolithic coastal site of Maroulas (collagen yields=0.42±0.27) followed by the late Bronze Age coastal site of Manika, with average collagen wt. % = 2.03±2.92 (**Figure 5.32**). The extremely poor collagen preservation in those two coastal sites is accompanied by well-preserved histology that shows no

micro-cracking or generalized destruction as seen in **Figure 5.9a**, but increased crystallinity (**Figure 5.33**; **Table A2-Appendix A**). This combination indicates a gradual, slow loss of the organic content through chemical hydrolysis, the rates of which were primarily controlled by temperature and soil pH (no microcracking, hence limited involvement of groundwater), which has eventually led to the almost complete fossilization of bones (Collins et al. 2002).

On the other hand, the best collagen preservation can be observed in the Bronze Age Central Asian petrous bones (n=6) and the Neolithic deposits of the Sarakenos cave (n=24), with collagen wt. % averaging 14.67±2.69 and 13.64±5.75, respectively. Preservation of the organic matter in Sarakenos cave confirms the assumption that better collagen preservation should be expected in caves compared to open-air sites due to the more stable conditions (only small fluctuations in temperature and groundwater). However, a few studies have demonstrated that collagen preservation can show considerable variation in caves (e.g. Bocherens et al. 1999; McClure et al. 2011). This is caused by horizontal and vertical diagenetic changes in cave sediments (Karkanas et al. 1999), which means that bones may be well-preserved in some areas of a cave but completely dissolve in others (e.g. Bocherens et al. 2008; Karkanas et al. 1999; Stiner et al. 2001).

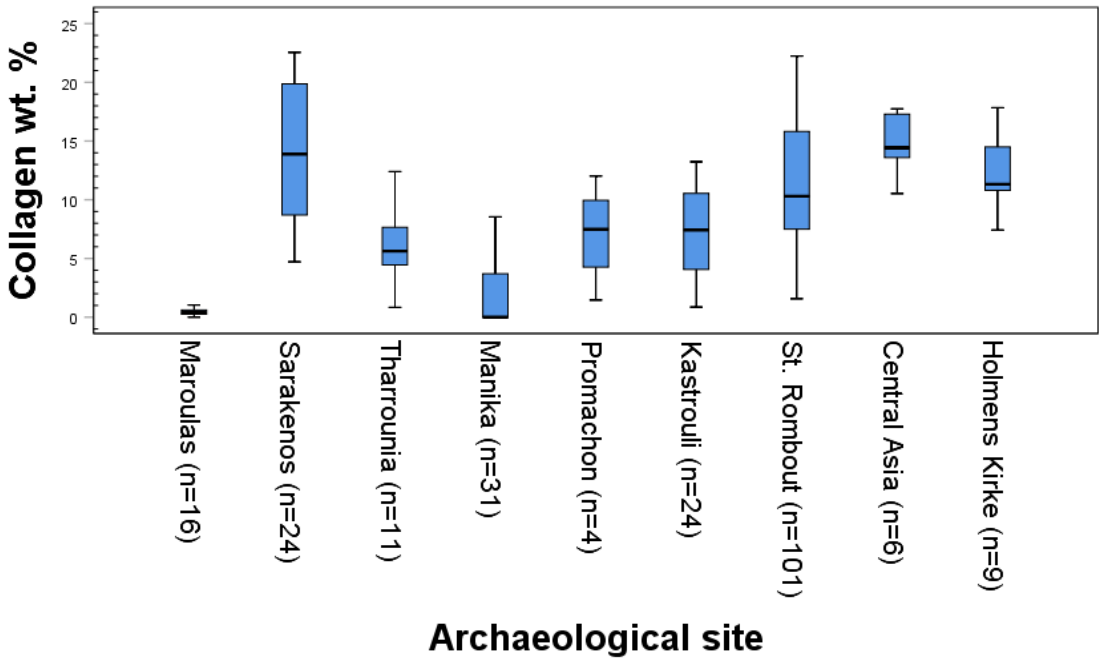

Figure 5.33. Inter-site variation in collagen preservation.

This also gives us information about intra-site variations, with Sarakenos cave displaying the highest variability among the 9 archaeological sites (**Figure 5.33**). Differences between two areas of Sarakenos cave, trenches E and F, can be clearly identified (**Figure 5.34a**). In particular, samples from trench E have higher collagen yields (17.15±4.63; n=11) than bones from trench F (9.50±4.04; n=7), a statistically significant difference (U=10.000, p=0.008). Nevertheless, no correlation with depth (trench E R^2=0.00 and trench F R^2=0.17) is apparent, contrary to previous

studies that have argued for increased diagenetic alterations in bones close to the surface (Karkanas et al. 2000).

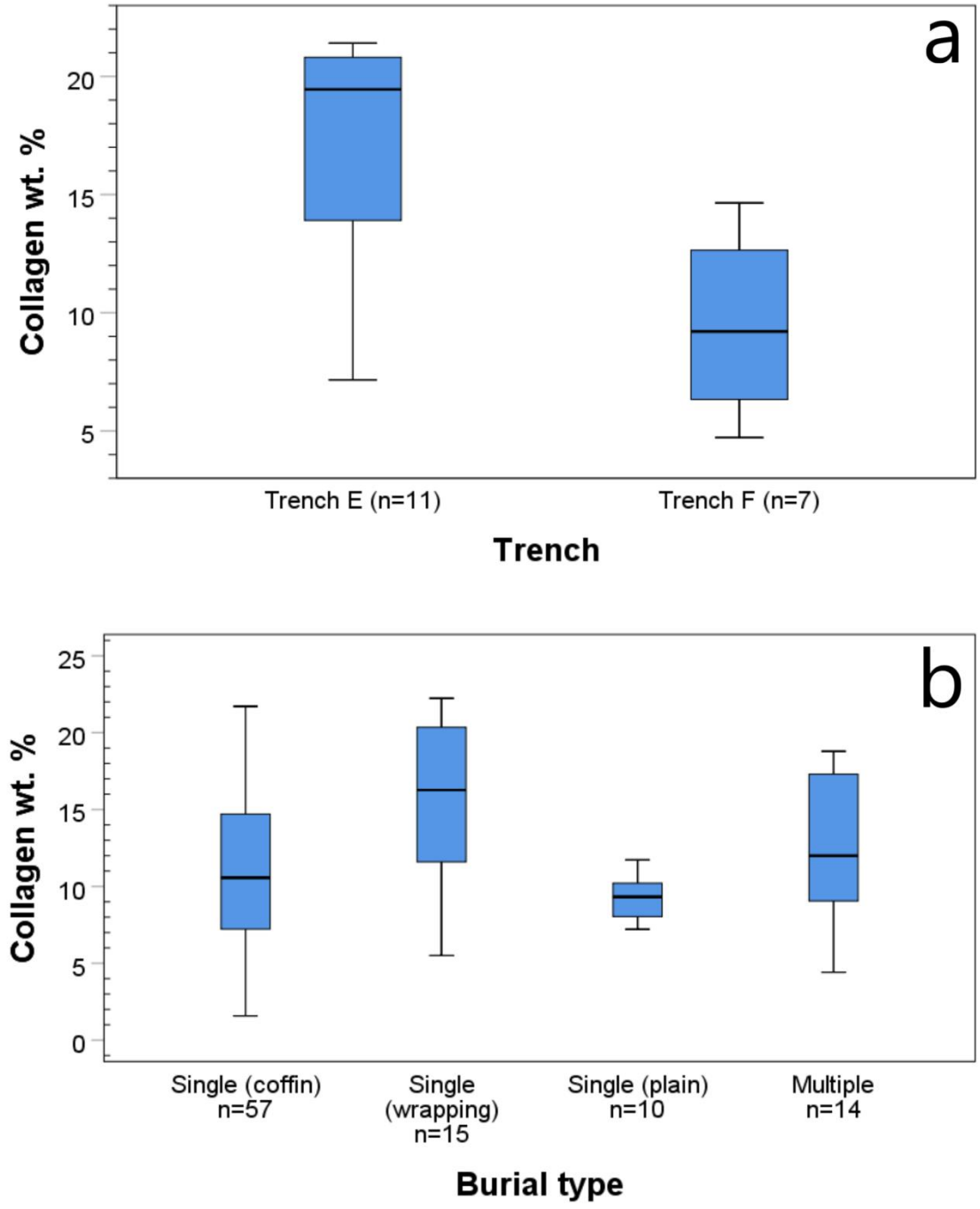

Figure 5.34. Intra-site variations in collagen preservation in Sarakenos cave (a) and St. Rombout (b).

An additional example of large within-site variations is Kastrouli, as the three different diagenetic paths identified (section 5.1.2) also display statistically significant collagen yields [$x^2(2)=7.623$, p=0.022]. *Diagenetic path 1* samples display very poor collagen preservation (collagen wt. %=1.8±1.06); the *diagenetic path 2* average collagen yield is 7.56±3.69, while *diagenetic path 3* samples display slightly higher collagen yields (8.32±3.08). These variations in Kastrouli

collagen can therefore be related to the funerary practices, a scenario confirmed in St. Rombout specimens. Specifically, collagen preservation shows a strong association with burial practices in St. Rombout, with single burials of wrapped corpses characterized by increased collagen survival rates, whereas single plain burials in soil have much lower collagen yields (**Figure 5.34b**; $x^2(3)=8.639$, p=0.034). Multiple burials and burials in coffins show intermediate values with similar collagen yields, although single coffined burials show more variability (**Figure 5.34b**).

5.3.3. INTRA-INDIVIDUAL AND INTRA-BONE VARIATIONS

Intra-individual variations are not statistically significant (**Figure 5.35**; $x^2(5)=2.340$, p=0.800). The differences between the petrous bone and the other skeletal elements is small, although the upper limb bones show slightly higher average values and the lower limb bones display slightly lower average collagen yields (**Figure 5.35**). Intra-bone variability (i.e. proximal-to-distal diaphyses) is also not observed in long bones from Maroulas, Sarakenos cave, Tharrounia, Manika, and St. Rombout (**Figure 5.36**; humerus U=110.500, p=0.935; radius U=28.000, p=0.297; ulna U=8.000, p=0.421; femur U=48.000, p=0.912; tibia U=17.000, p=0.937). A lack of intra-skeletal and intra-bone variability was expected as there was no indication of histological or bioapatite variability. Therefore, the micro-environmental conditions seem to have a similar impact on the preservation of bone collagen within the same individual and the same skeletal element.

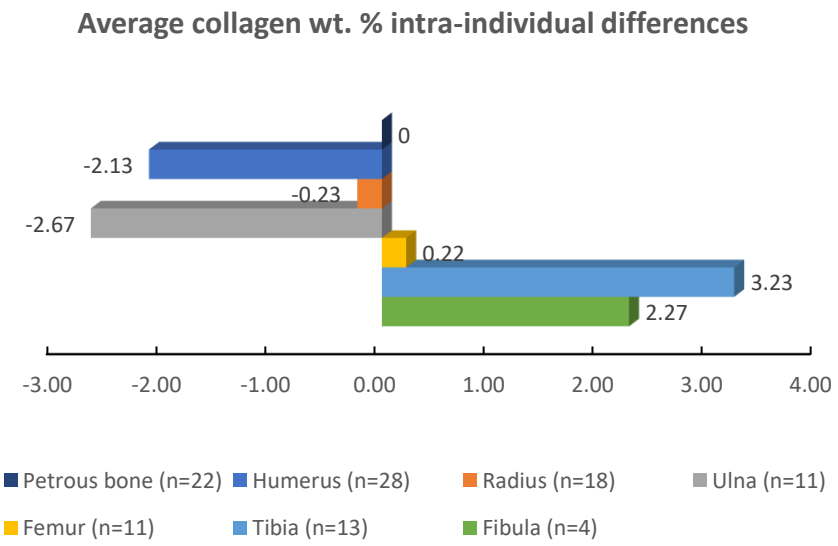

Figure 5.35. Intra-individual variations in collagen preservation in twenty-one individuals from St. Rombout and one from Maroulas. Bars represent the average difference between the petrous bone and the other skeletal elements (i.e. a positive value indicates a lower average value of this skeletal element compared to petrous bone, and vice versa).

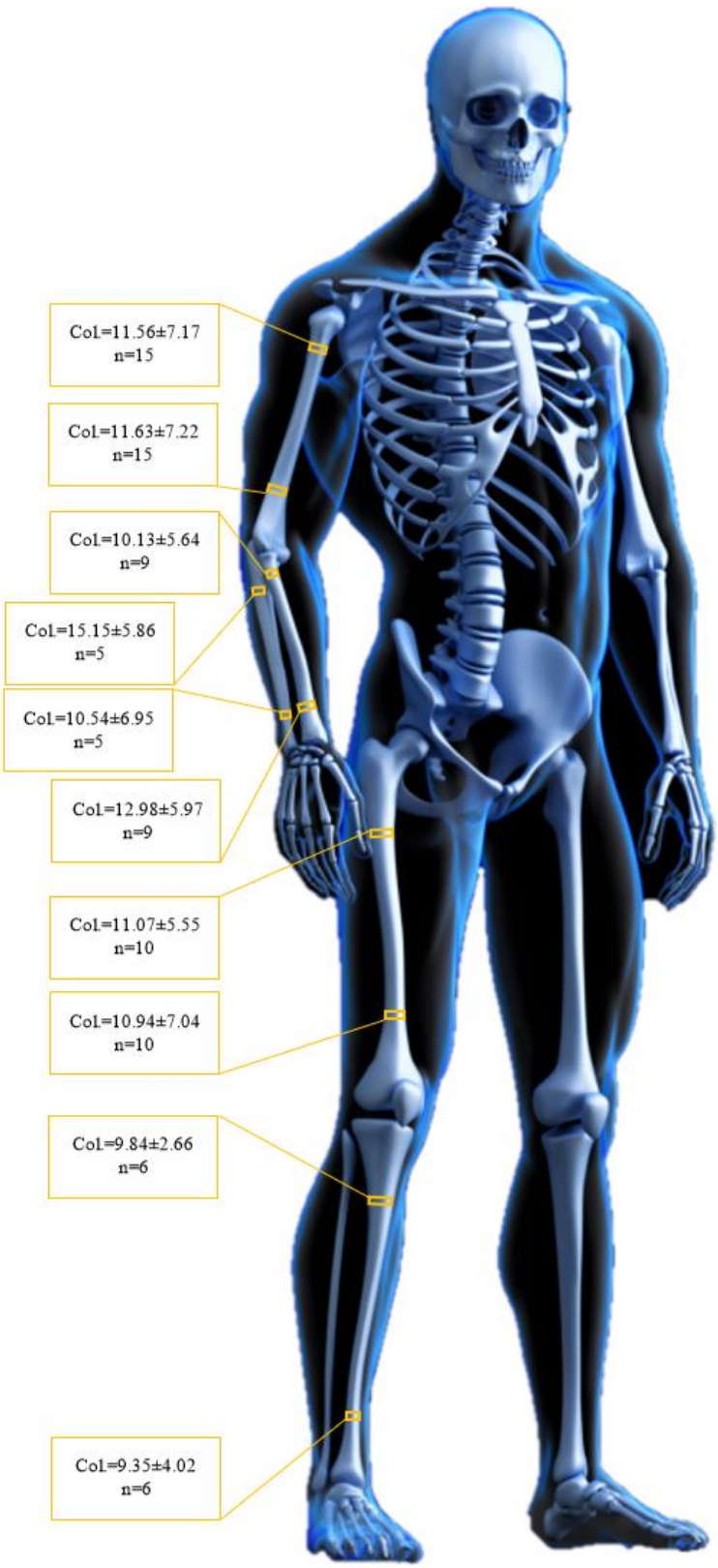

Figure 5.36. Collagen content in in proximal and distal diaphyses of long bones.

5.3.4. COLLAGEN-BIOAPATITE RELATIONSHIP

The orientation and size of BAp crystals are controlled *in vivo* by the collagen fibril structure and organization as the former are situated between (inter-fibrillar spaces) or on the surfaces (intra-fibrillar spaces) of collagen fibrils (Weiner and Traub 1986; Weiner and Price 1986; Boskey 2003). Hence the interaction between the mineral and organic fractions of bone during diagenesis is assumed to be strong (e.g. Bocherens et al. 2008; Götherström et al. 2002; Person et al. 1995, 1996), and only if this intimate association breaks can collagen decay. The volume that is left empty after collagen loss is assumed to be replaced by BAp crystals of increased size until inter-crystallite porosity has been filled (Susini, Baud and Lacotte 1988; Trueman et al. 2008).

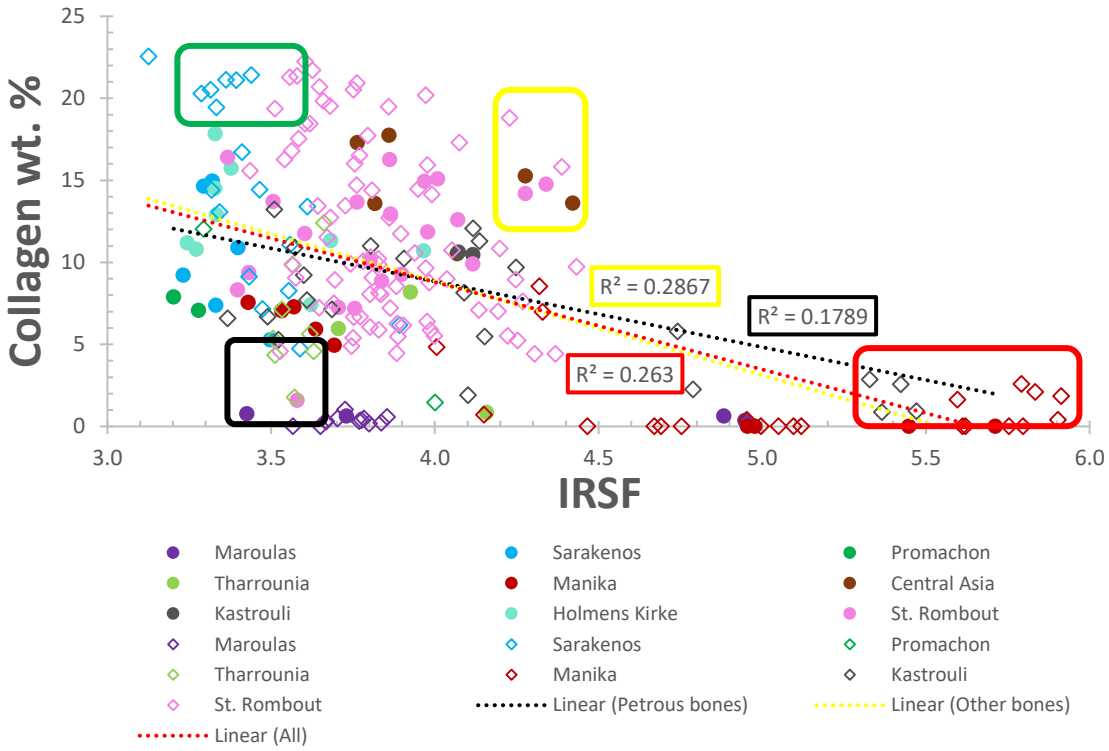

Figure 5.37. The lack of correlation between collagen wt. % and crystallinity. Four groups, one with low crystallinity and high collagen yields (green box), a second with low crystallinity and low collagen yields (black box), a third with high crystallinity and high collagen yields (yellow box), and a fourth that shows high crystallinity and low collagen yields (red circle), indicative of the different combination of diagenetic pathways followed by these specimens. Note the variable crystallinity (c. 3.4 to c. 6 IRSF) of samples displaying a complete loss of collagen.

However, a weak correlation between crystallinity (IRSF) and collagen content (R^2=0.26) is observed (**Figure 5.37**; **Table 4**), something that has also been reported in past studies (Lebon et al. 2010; Weiner and Bar-Yosef 1990; Hedges, Millard and Pike 1995). Thus, it seems that bioapatite recrystallization is possible even in the presence of reasonable amounts of collagen in bone (**Figure 5.37**), also described by Reiche et al. (2003). At the same time, in other bones the volume of the matrix that is filled with collagen *in vivo* can be replaced by BAp crystals of increased size (**Figure 5.37**; Trueman et al. 2008; Susini, Baud and Lacotte 1988; Pfretzschner 2004). There is no good explanation of this difference, which would benefit from a larger study

which might explore, for example, the selective leaching of proteins such as osteocalcin and osteonectin, which may play a role in limiting the extent of recrystallisation.

Table 4. Collagen-IRSF relationship (R^2) in sites with samples n≥5 in each group.

Site	Collagen-IRSF	
	Petrous	**Other**
Maroulas, Greece	N/A	0.13
Sarakenos, Greece	0.26	0.53
Tharrounia, Greece	N/A	0.16
Manika, Greece	0.92	0.15
Central Asia	0.16	N/A
Holmens Kirke, Denmark	0.19	N/A
St. Rombout, Belgium	0.10	0.15
Overall	0.62	0.60

5.3.5. SCREENING METHODS

With reference to screening of archaeological bone for collagen preservation, it has been previously shown that % N of whole bone, which is c. 3.5 - 5.5 wt. % in modern bone (Baker, Butterworth and Langley 1946; Eastoe and Eastoe 1954), is a reliable index (Bocherens et al. 2005; Brock, Higham and Ramsey 2010). Two different but similar thresholds have been proposed for bones in order to be further examined for stable isotopes and/or radiocarbon dating. Bocherens et al. (2005) support that 0.4 % N threshold is adequate, while Brock et al. (2010) propose a cut-off point of 0.7 %. However, it is possible that samples containing > 0.7 % N and give collagen yields < 1 wt. %, may contain nitrogen as short-chain/degraded collagen or polypeptides, non-collagenous proteins, soil contaminants, or conservation treatments (Brock et al. 2012).

In this study, % N of whole bone varies from 0.00 to 3.42 (**Table A3-Appendix A**) and all samples with % N >0.7 exhibit collagen C/N ratio between 3.2 to 3.51 (**Table A3-Appendix A**). Values similar to modern bone (i.e. 2.9 to 3.6) are considered representative of good quality collagen, whereas much higher C/N ratios are linked to diagenesis (Ambrose 1990; DeNiro 1985; DeNiro and Weiner 1988; Tuross 2002). Thus, all samples with total nitrogen over 0.7 % have collagen C/N within the acceptable limits. Unfortunately, the two samples that have lost all of their nitrogen (i.e. KAS26 and PRO8) did not yield enough collagen to allow the assessment of their collagen C/N.

The % N of whole bone also demonstrates a strong linear relationship with collagen wt. % (R^2=0.63; **Figure 5.38a**) which underlines the potential use of the former as collagen content predictor. However, a safe assumption on the quantitative potential of % N of whole bone would require several hundreds of samples, and in this study it was applied only to a limited number of samples (n=30 for collagen-% N whole bone relationship). It is also noteworthy that the Holmens Kirke bones have a higher average % N=2.51±0.71 compared to % N=2.04±0.8 in the Central Asian samples, and at the same time have lower average collagen yields (12.49±3.12) than the Central Asian bones (14.67±2.69), which could be possibly due to the presence of non-collagenous proteins in the former.

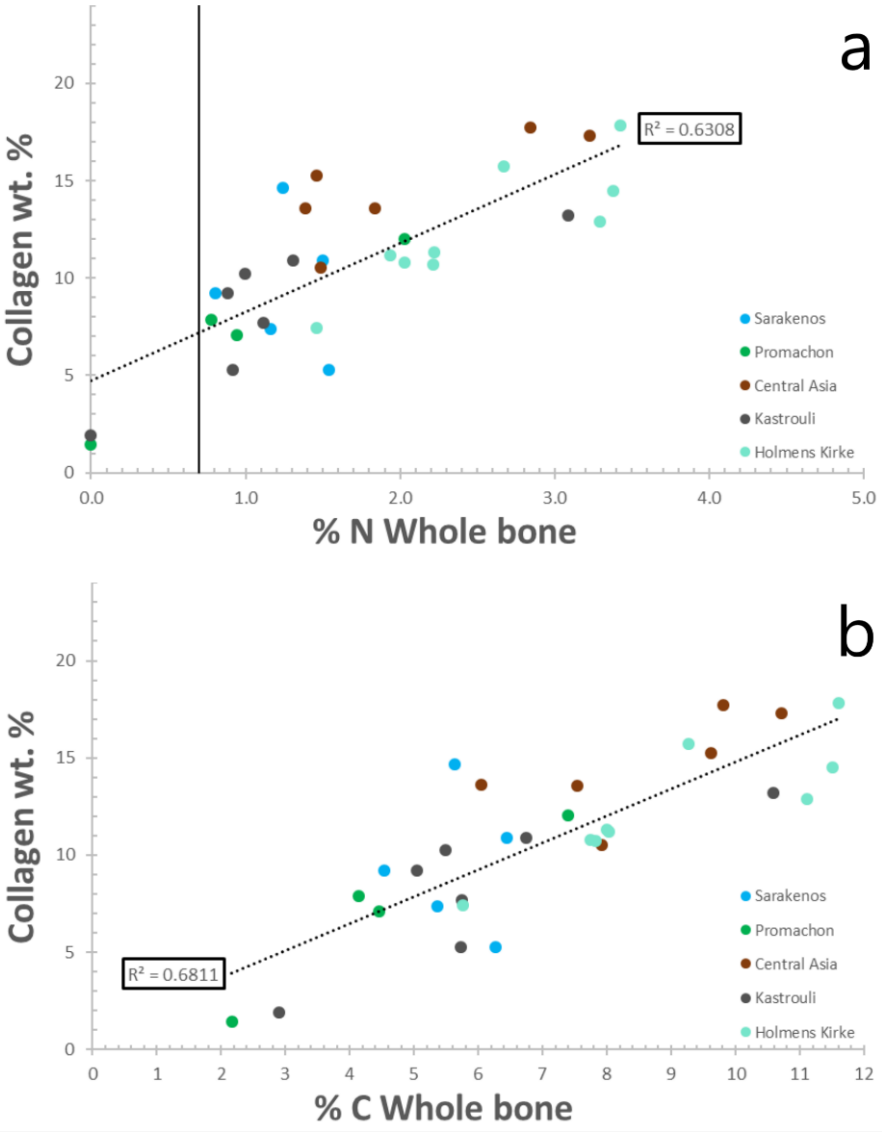

Figure 5.38. Data showing the reliability of (a) nitrogen and (b) carbon content of whole bone as indicators of collagen preservation. Threshold line in (a) according to Brock et al. (2010).

Overall, % N of whole bone data are in agreement with past studies (e.g. Brock et al. 2012; Lebon et al. 2016) which support that it can be a relatively good indicator of collagen preservation. However, assessment of highly contaminated and/or degraded bones can be problematic, as seen

in the two bones from Kastrouli (KAS26) and Promachon (PRO8) with no nitrogen content that may still retain small amounts of collagen in their structure (**Table A3-Appendix A**).

Archaeological bone usually displays a significant decrease in carbon content compared to modern animal bone that has c. 15 wt. % C (Ambrose 1990; Sillen and Parkington 1996; Van Klinken 1999). Here, the total amount of carbon ranges from 2.17 to 11.60% (**Table A3-Appendix A**). and shows a strong correlation (R^2=0.68) with collagen content (wt. %) (**Figure 5.38b**). This relationship indicates that % C of whole bone can be an equally strong predictor of collagen content to % N of whole bone. Although the C/N ratios of whole bone powder could provide an additional approach, the relationship with collagen wt. % (R^2=0.04) does not seem to be sensitive enough to discriminate well- from poorly-preserved samples. Such a poor correlation between C/N of whole bone and collagen yields has also been reported by Brock et al. (2012) and Lebon et al. (2016). Consequently, a combined use of % N and % C of whole bone, and collagen C/N ratio can significantly improve screening practices of archaeological bone for collagen preservation (Brock, Higham and Ramsey 2010; 2012; Harbeck and Grupe 2009).

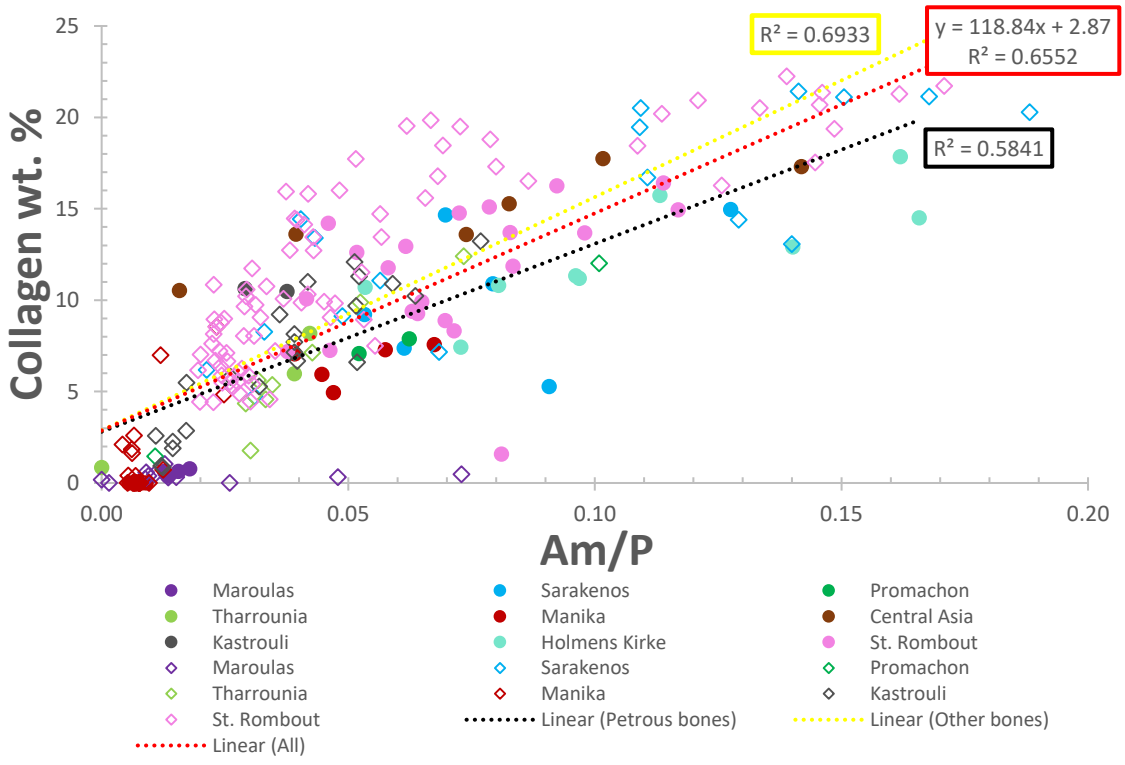

Figure 5.39. The reliability of Am/P for predicting collagen content in archaeological bone. A lower intercept of the more recent (Danish) bones suggests that the phosphate for carbonate exchange (relative phosphate content), and vice versa, can affect the reliability of Am/P as a collagen predictor.

The Am/P ratio derived from FTIR can also potentially provide valuable information on the relative amount of organic content in bone (Lebon et al. 2016; Trueman, Privat and Field 2008; Trueman et al. 2004). A strong correlation (R^2=0.66) between Am/P and collagen wt. % can be

seen in this dataset, highlighting the potential of Am/P as collagen predictor for rapid screening (**Figure 5.39**; **Table 5**). The application of the Am/P ratio as a quantitative approach to estimate collagen yields using the Lebon et al. (2016) equation (i.e. collagen wt. % = 113.13 Am/P + 1.69) also shows some potential, but an average offset of -1.70 ± 3.67 % is observed. Although the new equation provided in **Figure 5.39** gives an offset of -0.20 ± 3.67 % which is better than Lebon's et al. (2016) equation, in 98 samples (i.e. 36.5 %) the offset is higher than ±3 % (**Table A5-Appendix A**). While in a previous study by Trueman et al. (2004) it was argued that the Am/P index does not accurately reflect collagen preservation in samples with less than 10% collagen surviving, this was not observed in this dataset, with samples containing > 10 % collagen often displaying the largest offsets (**Table A5-Appendix A**).

The relative phosphate content (exogenous phosphate uptake) can lead to poor agreement of collagen estimates with collagen yields (**Figure 5.39**), thus to improve the accuracy decoupling the amide I peak from phosphate is necessary. Overtones related to O-H stretching vibrations at 1640-1660 cm^{-1} (water) can also interfere with the collagen signal and lead to increased estimates (Trueman, Privat and Field 2008; Chadefaux et al. 2009; Lebon et al. 2016). Moreover, any differences in collagen (e.g. Sealy et al. 2014) and FTIR protocols (e.g. Kontopoulos et al. 2018) can also have significant effects on the collagen content estimates. As a result, further research is required until the amide I peak can be safely used to assess collagen preservation and provide accurate collagen content estimates.

Table 5. Collagen-Am/P relationship (R^2) in sites with samples n≥5 in each group.

Site	Collagen-Am/P	
	Petrous	**Other**
Maroulas, Greece	0.48	0.01
Sarakenos, Greece	0.16	0.70
Tharrounia, Greece	N/A	0.88
Manika, Greece	0.92	0.55
Central Asia	0.83	N/A
Kastrouli, Greece	N/A	0.83
Holmens Kirke, Denmark	0.63	N/A
St. Rombout, Belgium	0.20	0.67
Overall	0.58	0.69

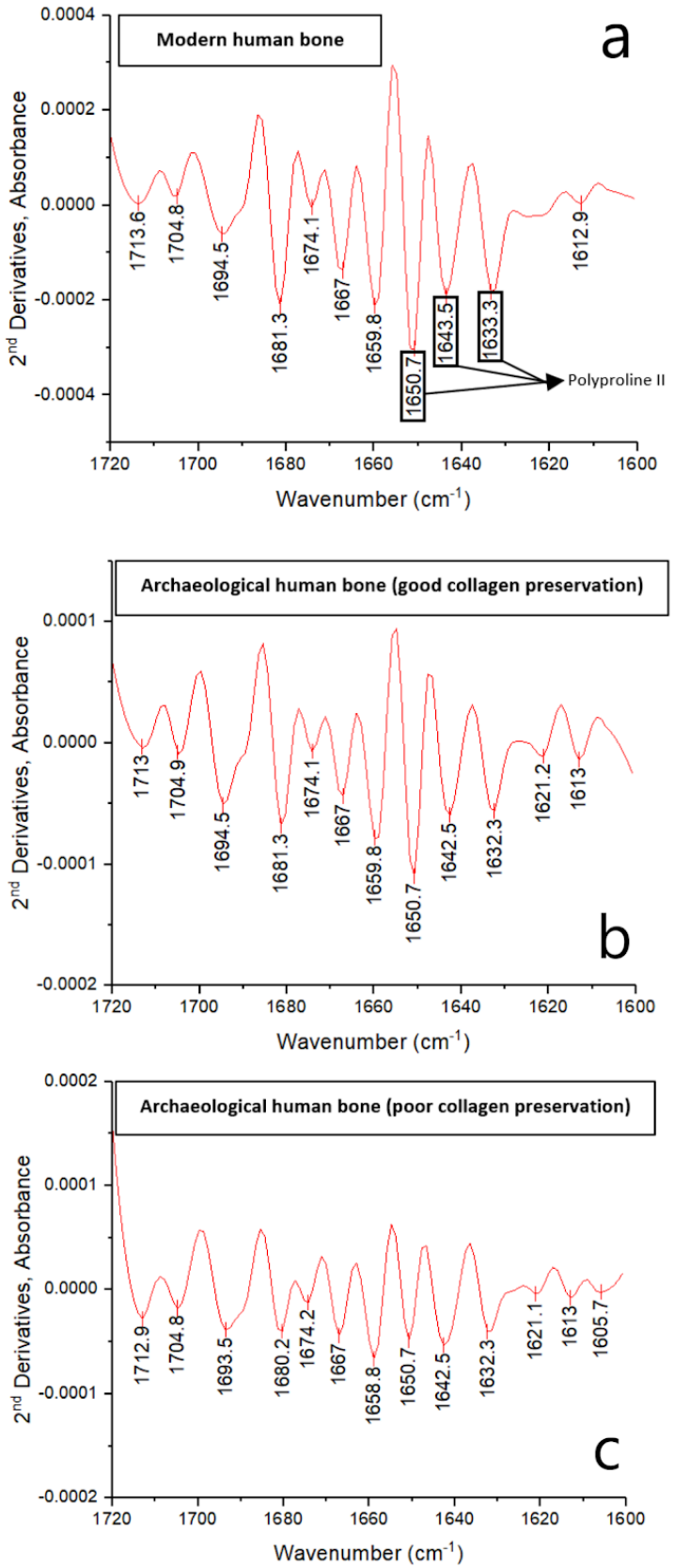

Figure 5.40. 2nd derivative spectra of the amide I band (c. 1600-1700 cm^{-1}) showing the disappearance of amide I components (black boxes) that accompany loss of collagen in archaeological bone (KAS8: b; KAS7: c).

Additional qualitative evidence can be obtained through the 2nd derivative analysis of the amide I band, which shows a gradual decrease of the 1632, 1640, and 1650 cm^{-1} components assigned to the polyproline II helix (Lazarev, Grishkovsky and Khromova 1985) with decreasing collagen yields in archaeological bone (**Figure 5.40**). Cleavage of collagen cross-linking (as seen from a decrease of the 1660 cm^{-1} and 1695 cm^{-1} components (**Figure 5.40**; Paschalis et al. 2001) has led to a loss of the three-dimensional structure and breaking of the polypeptides into smaller peptides during hydrolysis (Collins et al. 1995, 2002; Shoulders and Raines 2009; Adzhubei, Sternberg and Makarov 2013).

5.4.1. PETROUS VERSUS OTHER BONES

Preservation of endogenous DNA in petrous bones (n=82) ranges from 0.00 to 71.12 % with an average of 24.14±21.5, whereas in other skeletal elements (n=8) it varies from 0.06 to 4.10 % with an average of 0.70±1.39 (**Figure 5.41**; **Table A3-Appendix A**). An overall better performance of the petrous than other skeletal hard tissues was first reported by Gamba et al. (2014), while similar observations have been made by Hansen et al. (2017), this time compared to tooth cementum. The higher survival rates of endogenous DNA within the petrous bone have been attributed to its higher density protecting DNA from decay (Gamba et al. 2014; Pinhasi et al. 2015). However, only one study, which had explored intra-individual bone mineral density in equid, bovid and cervid species using computed tomography, has reported that the petrous bone is c. 10 % denser than the middle shaft portions of long bones (Lam, Chen and Pearson 1999).

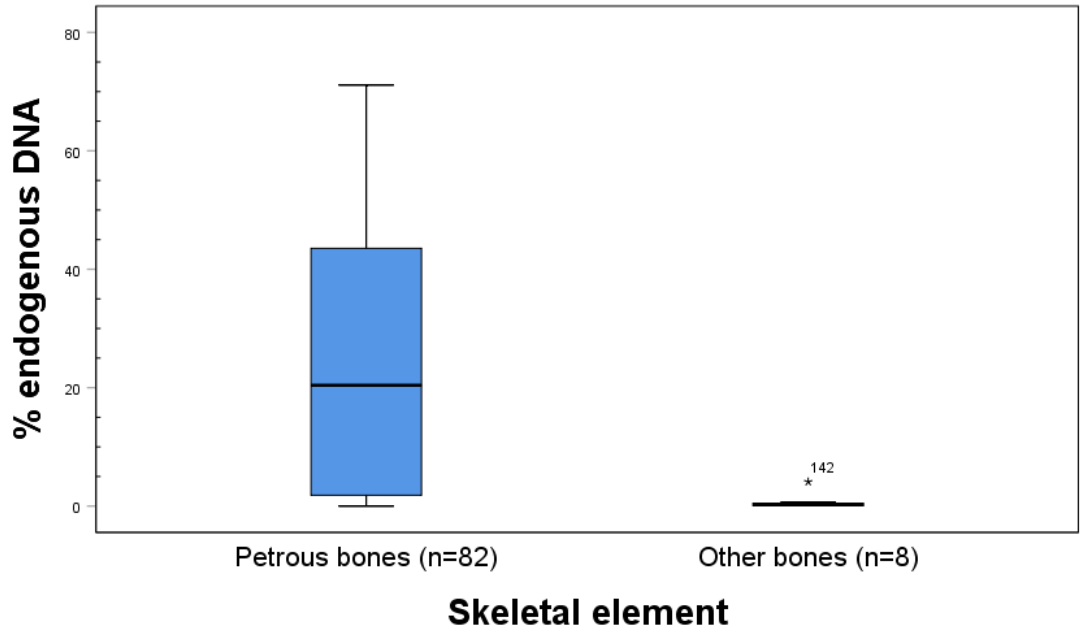

Figure 5.41. The high endogenous DNA yields in petrous compared to other skeletal elements.

No study has ever investigated the biomechanical properties of the petrous pyramid (e.g. Frisch et al. 1998) using sophisticated technology such as micro- or nanoindentation (e.g. Dall'Ara et al. 2015; Rho et al. 2001) and linked this to DNA preservation. Nanoindentation testing estimates the elastic (Young's) modulus and hardness (Vicker's) of bone with a resolution of c. 1 μm (Rho et al. 1999). The elastic modulus measures the stiffness of bone, hence how bone as a composite material withstands changes during stress and strain, i.e. how much it stretches and deforms (Zysset et al. 1999). Stiffer materials (e.g. steel, copper) have a high elastic modulus (low strain), whereas ductile materials (e.g. rubber, plastic) have a low elastic modulus (high strain). Hardness

(HV), on the other hand, shows the resistance of bone (i.e. depth of the indentation) to permanent compression deformation (Zysset et al. 1999).

The biomechanical properties of bone vary considerably between species (**Table 6**) with the very brittle *Mesoplodon rostrum* representing the most extreme biological example of highly mineralized (i.e. c. 96 %) bone (Zioupos et al. 1997). In modern human femora the elastic modulus ranges between c. 21 and c. 26 GPa in interstitial lamellae, and between c. 17 and c. 23 GPa in osteonal lamellae, while the inner osteonic lamellae also demonstrate increased modulus compared to the outermost osteonal lamellae (Rho et al. 1999, 2002). Hardness ranges from c. 40 to c. 80 HV in cortical bone and demonstrates a similar distribution to modulus (Rho et al. 1999; Zysset et al. 1999). Therefore, hardness and elastic modulus may vary in different anatomical sites of the same skeletal element (e.g. the neck of the femur displays average elastic moduli of c. 17 GPa in interstitial and c. 16 GPa in osteonal lamellae (Zysset et al. 1999)).

Table 6. Average stiffness, hardness and mineral content in different dry bone tissues (adapted from Rogers and Zioupos 1999).

	Elastic modulus (GPa)	**Hardness (HV)**	**Mineral content (%)**
Human femur	16-18	40-60	c. 55
Bovine femur	18-22	50-70	c. 65
Whale tympanic *bulla*	32-26	150-170	c. 83
Mesoplodon rostrum	40-42	200-220	c. 96

Regarding archaeological petrous bone, a total of 88 indentations on 3 samples provided some interesting data on its biomechanical properties. Its elastic modulus ranges between 12.62 and 27.31 GPa (20.12±3.14 GPa) and its hardness from 27.90 to 104.71 HV (61.59±15.15 HV) (**Table A4-Appendix A**). Within-petrous variability is also observed, with the outer periosteal tissue displaying statistically significant differences compared to the inner periosteal and endosteal tissues (**Figure 5.42**), both for the elastic modulus [$F(2,85)=114.826$, $p=0.000$] and hardness [$F(2,85)=2556.434$, $p=0.000$]. The inner periosteal and endosteal tissues, however, exhibit similar biomechanical properties ($p=0.644$).

The elastic modulus in the outer periosteal tissue (i.e. areas close to exterior surface) averages 17.41±2.52 GPa (12.62 to 21.47 GPa), whereas in the inner periosteal tissue (i.e. mesosteal tissue, including tissue between canals) the average elastic modulus is 20.97±3.16 GPa (13.55 to 25.25 GPa), and in the endosteal areas (i.e. tissue surrounding the canals) is 21.15±2.52 (16.59 to 27.31 GPa) (**Table A4-Appendix A**). Practically, a difference of 3-4 GPa in elastic modulus, when all other characteristics are the same, would result from a difference of about 10-20 % in mineralisation (Peter Zioupos, personal communication). Hardness in the outer periosteal tissue has an average of 48.95±10.28 HV (27.90 to 72.19 HV), the inner periosteal tissue hardness is 64.20±13.38 HV (39.18 to 91.97 HV), and in the endosteal areas average hardness is 67.22±14.53

(44.44 to 104.71 HV) (**Table A4-Appendix A**). Similar values can be seen in the elastic modulus of archaeological long bones, which varies from 3.86 to 62.86 GPa (17.91±9.56 GPa), while the hardness is between 5.25 and 186.72 HV (46.46±34.14 HV) (**Table A4-Appendix A**).

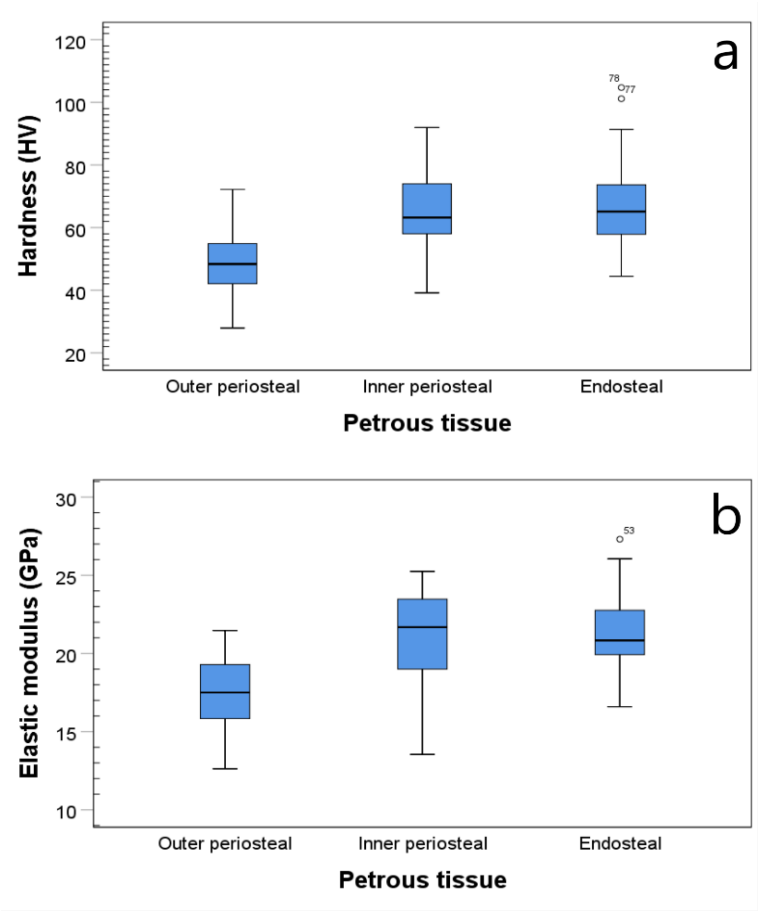

Figure 5.42. The differences in the biomechanical properties between the three petrous bone tissue areas.

Pinhasi et al. (2015) had described those two areas of the petrous as 1) a dense whitish bone that mostly surrounds the inner ear and areas between the semi-circular canals, the outer ear, and the mastoid process (i.e. part b); and 2) a dense yellowish bone that is found in the cochlea, vestibule and semi-circular canals (i.e. part c). Therefore, part b constitutes the inner periosteal tissue and part c the endosteal tissue, characterized by similar biomechanical characteristics that differ from the more osteonal, as seen in histological sections, outer periosteal zone (section 5.1.1).

Differences between those tissues, however, may be attributed to the osteocyte lacunar density that may vary in different regions of the petrous bone, affecting their biomechanical properties. Osteocytes are increasingly considered as key regulators (osteocytic osteolysis, mineral homeostasis) of bone remodelling of the perilacunar tissue, but their exact role is still in debate (Goldring 2015; Guo and Bonewald 2009; Komori 2013). Besides this, as the three petrous bones examined in this study date to c. 1850 AD, this does not allow any further interpretations, as the effects of diagenesis on hardness and elastic modulus are unknown.

Interestingly, while it is apparent that in some specimens the biomechanical properties of archaeological bone have been significantly modified (e.g. PRO8 to the high end, Manika and Kastrouli to the low end), hardness and elastic modulus retain their strong *in vivo* relationship (R^2=0.78; **Figure 5.43**). A similar claim has been made by Olesiak et al. (2010) in the only study on the nano-mechanical properties of fossil bone, which showed that fossilized tissue maintains the main anisotropic characteristics of modern bone despite the significant modifications in BAp crystals and the loss of collagen.

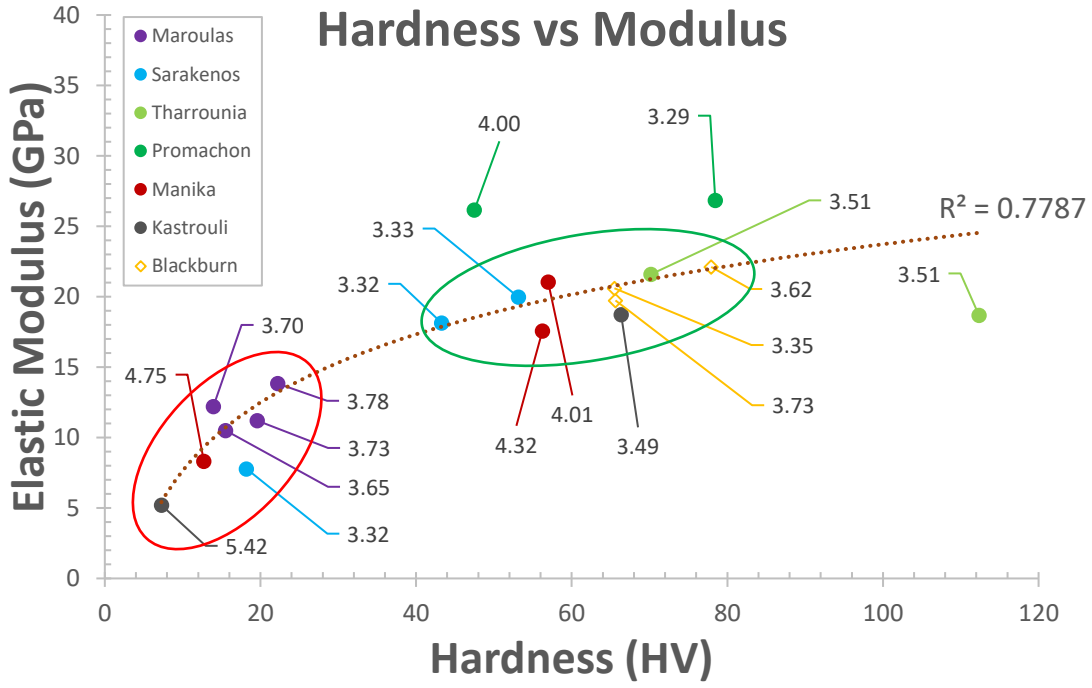

Figure 5.43. The logarithmic relationship between Vicker's hardness and Young's modulus (labels indicate crystallinity values). Stiffer and harder bones exhibit lower crystallinity values (green circle), whereas brittle and softer bones generally display higher crystallinity (red circle).

The nano-mechanical properties of bone tissue are partly determined by the changes in bioapatite crystals and the loss of collagen post-mortem as illustrated in **Figure 5.43** and **Figure 5.44**. Although the relationship of IRSF and collagen with either hardness (R^2=0.16 and R^2=0.10, respectively) or elastic modulus (R^2=0.23 and R^2=0.10, respectively) is weak (only mesosteal tissues compared), the two groups identified show statistically significant differences (hardness: U=0.000, p=0.000; elastic modulus: U=0.000, p=0.000; IRSF: U=10.500, p=0.05; collagen wt. %: U=0.000, p=0.002; n.b. the Sarakenos mandible has been excluded from the red group's statistics as an outlier). The green circle group is characterized by an average IRSF of 3.63±0.34, whereas the red group is 4.17±0.74. Similarly, collagen content (wt. %) has an average of 10.73±7.33 in the former, and 0.61±0.64 in the latter. The average hardness (61.69±10.31 HV) and elastic modulus (19.94±1.56 GPa) of the green group, which includes the 3 petrous bones, are comparable to modern human and bovine femora (**Table 6**), whereas these of the red group (15.21±5.28 HV and 10.21±3.06 GPa, respectively) are very similar to previously reported

trabecular bone mechanical properties (e.g. Zysset et al. 1999) and close to the elastic modulus values of dentin and tooth cementum (Ho et al. 2009; Zhang et al. 2014).

The example of the two bovine femora from Promachon (**Figure 5.43** and **Figure 5.44**) effectively demonstrates the complexity of the organic-inorganic-bone biomechanics interaction/relationship, as the different crystallinity values (3.29 versus 4.00) which are accompanied by a loss of collagen (collagen wt. % =12.02 and 1.46, respectively) have an effect only on hardness, but not on the elastic modulus which remains comparable to modern bovine bone (**Table 6**). This indicates that it is not purely the bioapatite crystal size and order, or the amount of collagen that defines the biomechanical characteristics of the different skeletal hard tissues, but their packing, orientation, and other nano-structural characteristics. However, there seems to be a point whereby when a certain amount of collagen is lost, archaeological bone becomes soft and brittle. Therefore, there is a strong, but complex inter-dependence of hardness and stiffness of archaeological bone on bioapatite recrystallization/dissolution and collagen hydrolysis.

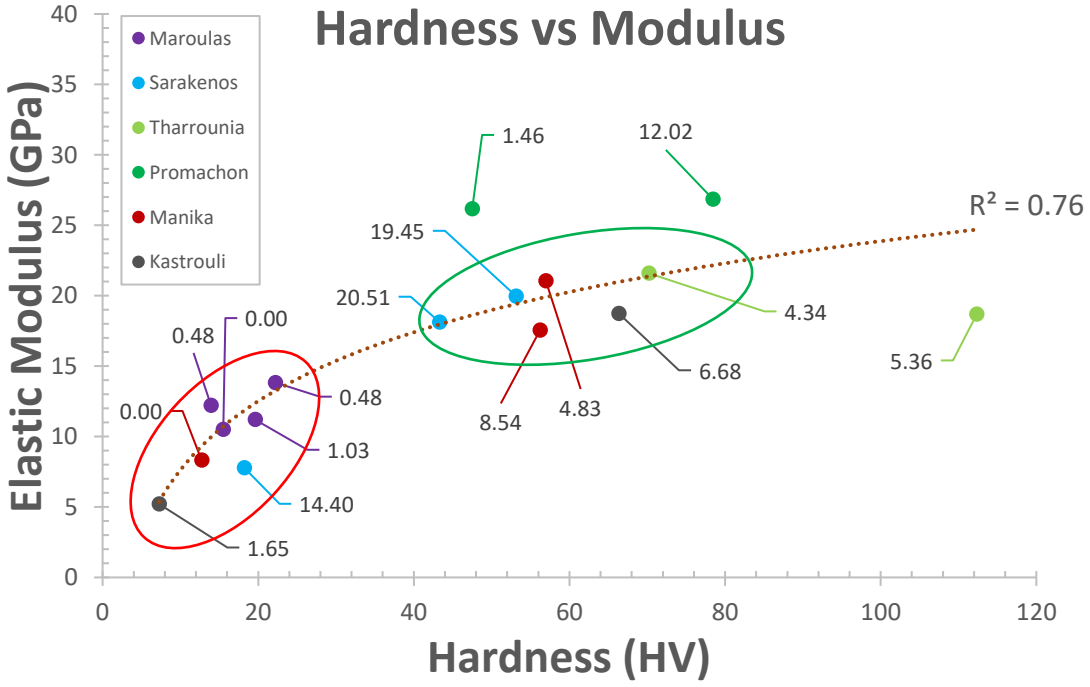

Figure 5.44. The logarithmic relationship between hardness and Young's modulus (labels indicate collagen yields). Stiffer and harder bones contain higher amounts of collagen (red circle), whereas brittle and softer bones generally display low collagen yields (green circle).

To sum up, the biomechanical properties of archaeological bone are evidently dependent on the skeletal element and anatomical site of bone, the collagen fibre orientation and content, the bioapatite crystal characteristics, and the collagen-BAp packing characteristics. Bone is not a uniform material and any measurements in archaeological bone should evaluate the initial heterogeneity of the tissues (e.g. Rho et al. 2002; Rogers and Zioupos 1999; Zioupos, Currey and Casinos 2000; e.g. Zysset et al. 1999) that can be maintained post-mortem, plus the complex

effects of the diagenetic changes on its biomechanical properties which add up to this heterogeneity.

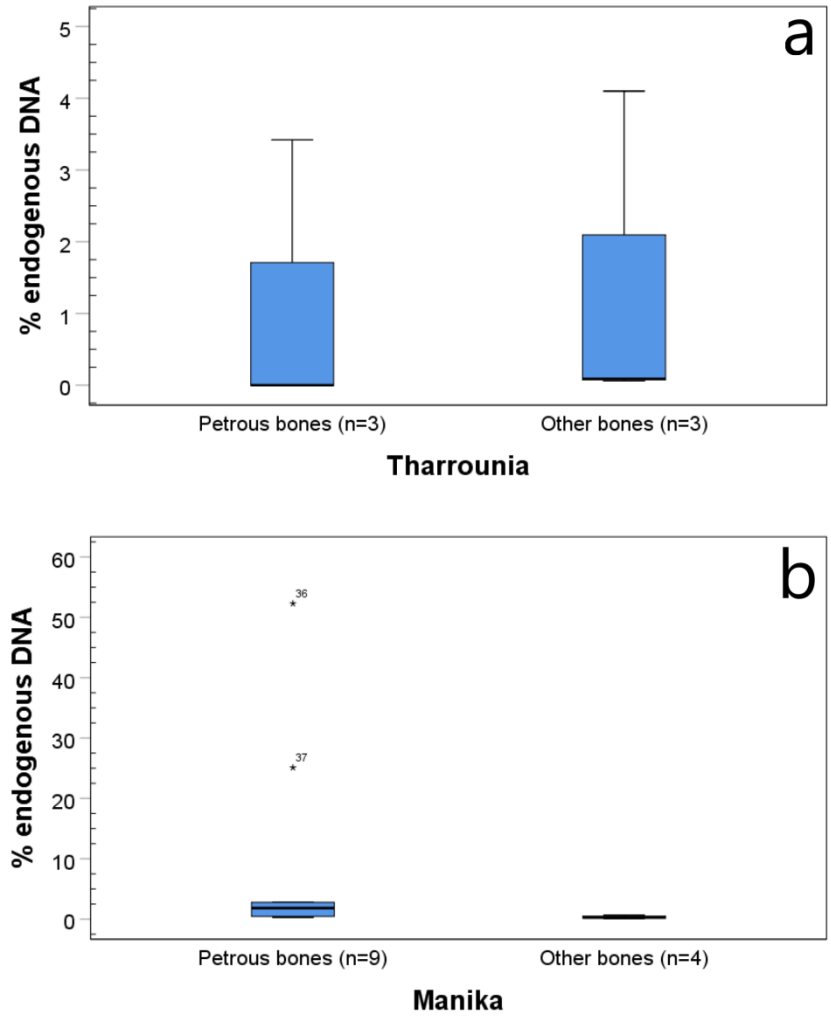

Figure 5.45. Endogenous DNA preservation in poorly preserved petrous and long bones from prehistoric open-air sites in Greece.

The variability observed in archaeological petrous bone is not generally different from that observed in long bones. If aDNA preservation in petrous bone is better predominantly due to its different biomechanical characteristics, how can the equal or even better sometimes preservation of aDNA in tooth cementum with > 10% endogenous content compared to petrous bones from the same individual be explained (Hansen et al. 2017)? An additional example that supports the complexity of bone diagenesis is the lack of intra-site variability in endogenous DNA content between petrous and long bones from two Prehistoric sites in Greece (**Figure 5.45**). Thus, this observation supports Hansen et al.'s (2017) claim that when the endogenous DNA preservation in the petrous bones is below 10 %, they do not outperform other skeletal elements (e.g. tooth cementum), which is the same story as in Tharrounia and Manika (**Figure 5.45**).

Therefore, it is concluded that since hardness and elastic modulus can vary from site to site even within the same tissue area (every indentation can yield different measurements depending also on degradation characteristics, e.g. micro-cracking, microbial activity, etc.), it is necessary to target specific areas of the petrous to identify the microniches that may possibly retain DNA in high quantities due to a combination of different factors (e.g. tissue type and characteristics, biomechanical properties, diagenetic alterations). Additionally, the unique histomorphological characteristics of this bone make the detailed exploration of the biomechanical properties (in both longitudinal and transverse directions to assess its anisotropy) mandatory.

5.4.2. SCREENING METHODS

Despite the falling costs in palaeogenetic studies, the technical difficulties associated with the recovery and analysis of aDNA from bone, the partial destruction of valuable or rare specimens, and the still high sequencing costs make any reliable screening method a valuable tool for aDNA labs. Previous studies have explored with varying degrees of success the association of endogenous DNA yields with several parameters including gross morphology and bone size (e.g. Haynes et al. 2002), histology (e.g. Guarino et al. 2000; Haynes et al. 2002; Hollund et al. 2016), or amino acid racemization (e.g. Collins et al. 2009; Poinar et al. 1996). As the survival of DNA in archaeological bone has been linked to mineral preservation (Lindahl 1993; Götherström et al. 2002; Allentoft et al. 2012; Parsons and Weedn 2006), BAp characteristics may be potentially connected to loss of DNA.

This dataset demonstrates that IRSF and C/P FTIR indices can be considered reliable predictors of DNA preservation despite the weak correlation (R^2=0.24) with crystallinity (IRSF; **Figure 5.46a**) and the very weak relationship (R^2=0.13) with carbonate content (C/P; **Figure 5.47a**) that demonstrate the complex interactions during diagenesis (e.g. local hydrology, pH, temperature). The categorization of samples into three groups based on their endogenous DNA yields (i.e. > 10%, 1-10 %, and < 1 %) allows some very interesting observations to be made. In the case of well-preserved specimens with endogenous DNA > 10 %, 90 % of the samples display IRSF values < 3.7, while only 6 % (n=3) have 3.7 ≤ IRSF ≤ 4, and 4 % exhibit IRSF > 4 (**Figure 5.46b**). When endogenous DNA yields drop between 1-10 %, 71 % of bones have an IRSF < 3.7, whereas 22 % have 3.7 ≤ IRSF ≤ 4, and only 7 % have IRSF > 4 (**Figure 5.46b**). Bones that yield endogenous DNA below 1 % predominantly display IRSF values over 3.7 (65 %), with a small number (i.e. 35 %) is characterized by crystallinity below the 3.7 threshold (**Figure 5.46b**). Overall, 70 % of all samples with IRSF < 3.7 contain endogenous DNA > 10 %, and a total of 86 % contain endogenous DNA over 1 %. Thus, IRSF can successfully distinguish bones likely to be suitable for aDNA analysis from those with poor DNA preservation.

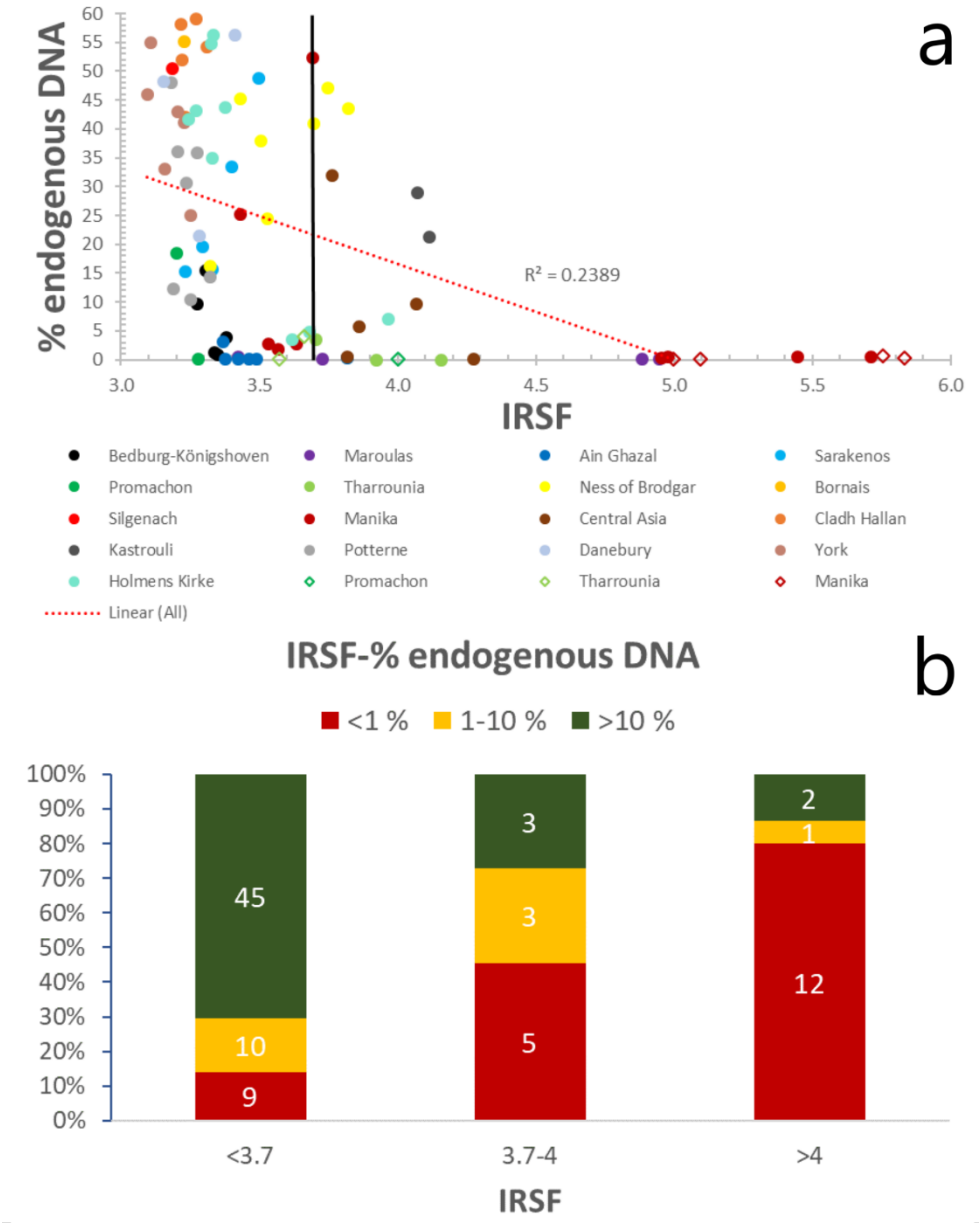

Figure 5.46. *Endogenous DNA-crystallinity relationship*. (a) Correlation of crystallinity with endogenous DNA yields. Line at 3.7 IRSF represents the proposed threshold. (b) Distribution of samples with well- (>10%), moderately- (1-10%), and poorly-preserved (<1%) endogenous DNA in categories based on crystallinity.

In tandem, carbonate content can be used as endogenous DNA indicator, as 66 % of the samples with C/P ratios > 0.20 contain endogenous DNA > 10 %, while 16 % display DNA yields between 1 and 10 %, and 18 % yield endogenous DNA below 1 % (**Figure 5.47b**). When C/P decreases to the 0.15-0.20 levels, still 67 % of bones yield more than 10 % endogenous DNA, with 6 % of bones yielding between 1-10 % endogenous DNA, and 27 % of samples have endogenous DNA yields below 1 % (**Figure 5.47b**). In levels below 0.15 C/P ratio, samples with endogenous DNA yields < 1 % prevail (i.e. 69 %), and only 6 % of samples show high amounts of aDNA (**Figure 5.47b**). Thus, in bones with C/P > 0.15, 66 % of bones contains over 10 % endogenous DNA, 14

% of samples have endogenous DNA yields between 1 and 10 %, and 20 % of samples exhibit below 1 % endogenous DNA.

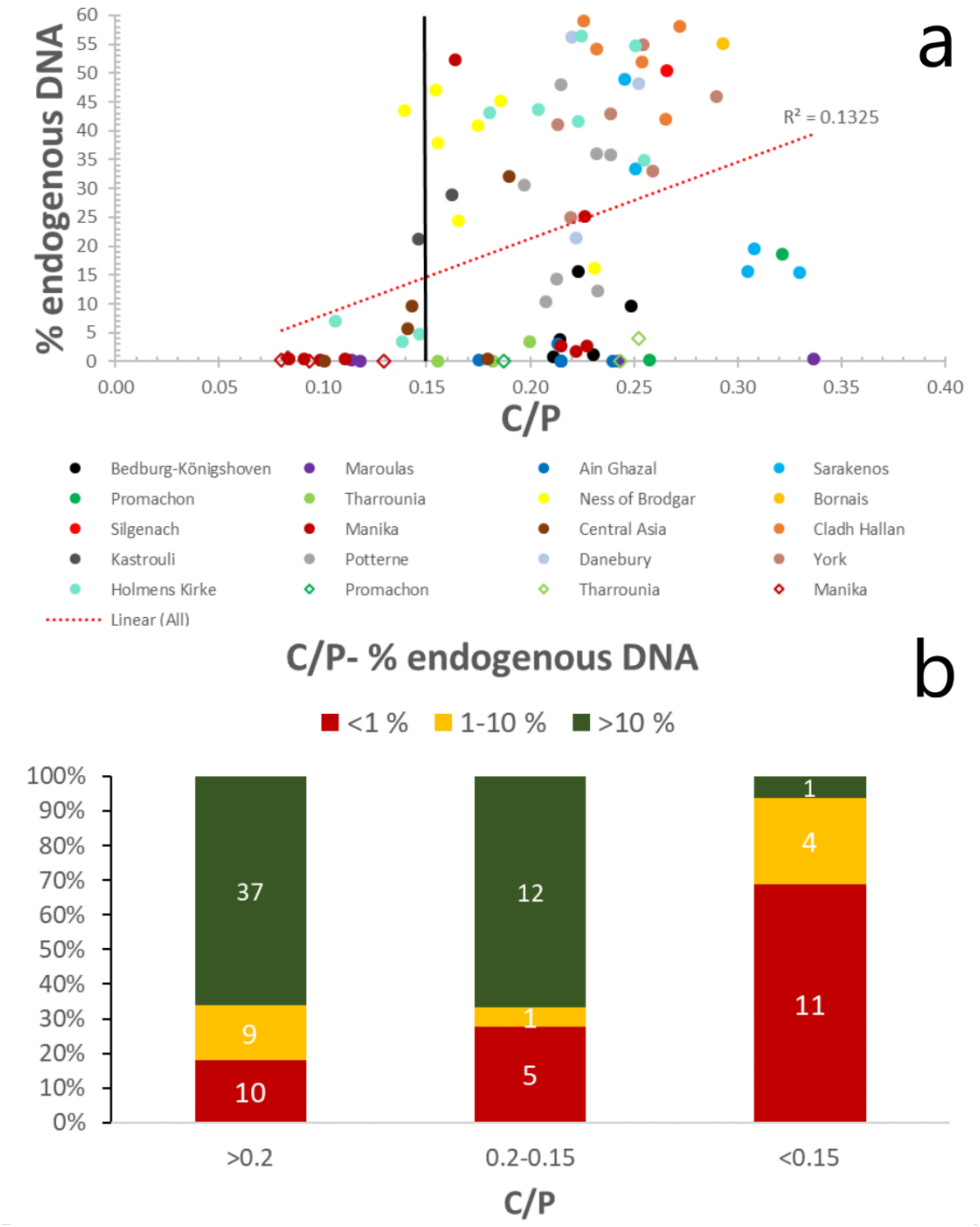

Figure 5.47. *Endogenous DNA-carbonate content relationship*. (a) Correlation of the relative carbonate content with endogenous DNA yields. Line represents the proposed C/P=0.15 cut-off point. (b) Distribution of samples with well- (>10%), moderately- (1-10%), and poorly-preserved (<1%) endogenous DNA in categories based on carbonate content.

Consequently, the combined use of IRSF and C/P as endogenous DNA predictors has a success rate of 92 % in bones containing endogenous DNA >10 %, 71 % successful identification of samples in which endogenous DNA ranges between 1 and 10 %, accompanied by an elimination of the 69 % of the poorly-preserved specimens with endogenous DNA yields below 1 %. Therefore, FTIR-ATR can be a very effective, minimally destructive, and rapid tool for DNA screening of archaeological bone with very high success rates.

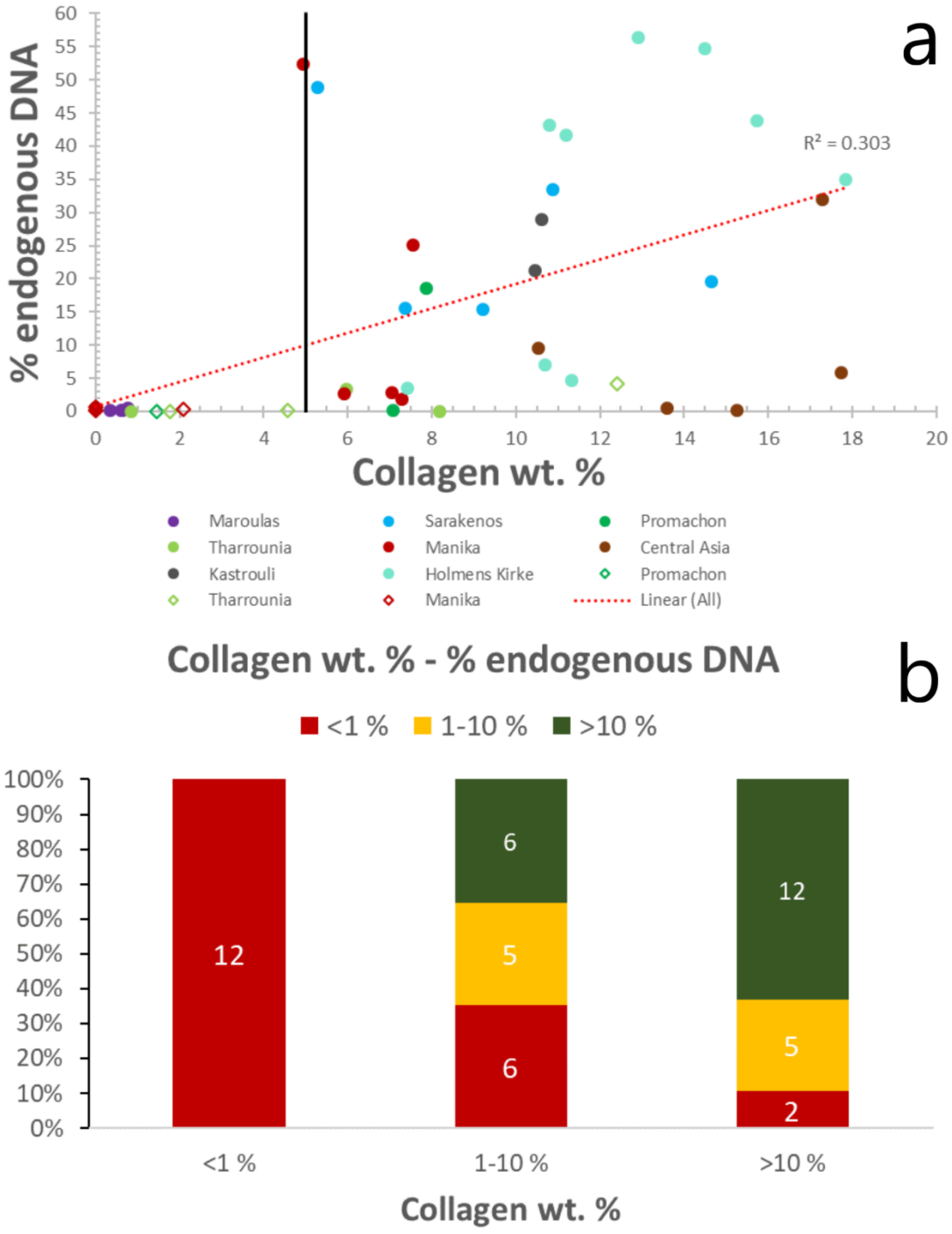

Figure 5.48. *Endogenous DNA-collagen content relationship*. (a) Endogenous DNA preservation indicates that collagen wt. % is not a reliable indicator for successful aDNA recovery. The vertical line represents a possible cut-off point. (b) Distribution of samples with well- (>10%), moderately- (1-10%), and poorly-preserved (<1%) endogenous DNA in categories based on collagen yield.

With reference to the collagen-DNA relationship and its potential use as DNA predictor, **Figure 5.48** demonstrates a weak correlation (R^2=0.30) between collagen wt. % and endogenous DNA yields, as samples that exhibit good collagen preservation may not yield endogenous DNA, and vice versa. A lack of correlation has also been reported in previous studies (e.g. Gravlund et al. 2012), however, there seems to be a cut-off point (here it seems to be the 5 % collagen wt.) and

when collagen drops below that point the chances for aDNA survival seems to diminish (**Figure 5.48**).

A handful of studies have previously reported a decisive role for collagen in DNA degradation (e.g. Campos et al. 2012; Götherström et al. 2002; Poinar and Stankiewicz 1999; Sosa et al. 2013). DNA molecules have the ability to bound to the collagen fibrils and create a DNA-collagen complex (Kitamura et al. 1997) that can have different structure and mechanical properties depending on the type of DNA adsorbed (Kaya et al. 2005). Thus, the variable correlation between collagen and DNA observed in archaeological bone (i.e. different decay rates) might be produced by a preferential loss or breaking of some collagen–DNA complexes and an intricate combination of other mechanisms (e.g. pH, temperature, groundwater). Indeed, even if DNA decay accelerates with increasing collagen hydrolysis, practically, screening archaeological bone using collagen analysis would require significant amounts of sample which would be an issue for rare or valuable specimens, while it would also be time-consuming and labour-intensive. Therefore, collagen analysis seems not to be the most effective method to predict endogenous DNA content.

GHI may potentially be a reliable predictor of DNA preservation, as it shows a moderate overall correlation with endogenous DNA yields (Spearman's r_s (15) = 0.47, p = 0.076) in the petrous specimens. Bone histology can offer some important qualitative information on DNA preservation, although the risk of contamination and the destructive nature of the method make it a less attractive option. Specifically, the histological assessment of the Danish petrous bones suggests that three of the samples (DEN4, DEN5, DEN9) which exhibit <10 % endogenous DNA also display poor histological preservation, with large areas suffering from generalized destruction. The DNA molecule is particularly prone to the interaction with water, which is also related to generalized destruction and ionic exchange in BAp crystals. Hydrolysis leads to breakage of the polynucleotide strands followed by chain breakage into shorter fragments (Bada, Wang and Hamilton 1999; Hofreiter et al. 2001; Lindahl 1993; Pääbo 1989) and any variations in long-term DNA fragmentation are assumed to be caused by differences in temperature, pH and local hydrology (Allentoft et al. 2012; Burger et al. 1999; Lindahl 1993; Lindahl and Nyberg 1972).

Hydrolysis can cause deamination (i.e. loss of the amino -NH_2 group) and/or depurination (i.e. release the purines) with purines being more susceptible to hydrolysis than pyrimidines (Lindahl 1993; Lindahl and Nyberg 1972; Pääbo 1989). Deamination of cytosine to uracil (C→T miscoding lesion) is the most common pathway and generates a C→T sequence error as the deaminated cytosine (now uracil) binds to adenine (Lindahl 1993; Pääbo et al. 2004). Here, the increased C→T damage rates (Hansen et al. 2017) confirms such a scenario (0.27±0.04 average C→T mismatch for Denmark and 0.39±0.09 for Central Asia). However, correlation of C→T mismatch with the diagenetic parameters was weak (% DNA-C→T= 0.22; % Collagen-C→T=

0.14; IRSF-C→T= 0.18; C/P-C→T= 0.03; % N-C→T= 0.14; 0.02; % C-C→T= 0.00). While the methyl (-CH_3) group attached to cytosine can make it more susceptible to deamination (Brown and Brown 2011; Hansen et al. 2001), increased methylation levels were not observed in our samples (see Hansen et al. 2017 for more information).

CHAPTER 6: CONCLUSION

This final chapter summarizes the key findings of this research project with a focus on petrous bone (**objectives 1 and 2**), the diagenetic variability (**objective 3**), and the screening practices for collagen and DNA (**objective 4**). Any challenges faced as well as the limitations of this study are highlighted, and potential routes for future research are proposed (**objective 5**).

6.1. SUMMARY, SYNTHESIS AND SIGNIFICANCE

The idea for this research was triggered by the recent palaeogenetic study published in *Nature Communications* by Gamba et al. (2014), who named the petrous bone as the richest aDNA repository of the human skeleton. As a result, the aim of this study was two-fold: to a) understand the factors underpinning the survival of petrous bone and its possible resistance to diagenesis compared to other bones, and b) to provide new data for the successful screening of archaeological bone prior to collagen and DNA analyses.

This research study therefore aimed to uncover the secrets of petrous bone structure which are responsible for the often unusually high aDNA survival rates in its tissues (**objective 1**). The histological analysis revealed some extraordinary characteristics of the adult human petrous bone. Its microstructure consists of highly osteocytic woven and lamellar-like tissues (section 5.1.1) which is a stunning micromorphological characteristic that has never been observed to my knowledge in any other normal adult human bone. The occurrence of osteons in at least two directions (i.e. transverse and longitudinal) is another astonishing discovery, while the presence of woven tissue in large areas of the petrous bone (that implies a lack of bone remodelling in a considerable part of its structure) is unparalleled. Regarding the latter, there is no other logical explanation for woven bone as it forms rapidly *in utero* and should have been gradually replaced in petrous bone by lamellar tissue as it has been continually shown in other normal bones (Currey 2002; White, Black and Folkens 2012).

The 3D reconstruction of the synchrotron micro-CT images allowed an accurate measurement of the osteocyte lacunae, as it does not artificially increase the number of lacunae like 2D methods (Bromage et al. 2016; Dong et al. 2014). Thus, the staggering number of c. 50.000 osteocyte lacunae/mm^3 detected in the 3D images of petrous bones (section 5.1.1) is probably linked to its largely woven appearance (Buckwalter et al. 1995; Hernandez, Majeska and Schaffler 2004) and its rapid formation *in utero*, as a higher number of osteocytes would be required to complete the ossification so quickly (e.g. Bromage et al. 2016; Skedros, Grunander and Hamrick 2005). The very high osteocyte lacunar density (which is about 3x that of human femur, e.g. Dong et al. 2014) or pelvis (i.e. iliac crest, Bach-Gansmo et al. 2016b), in combination with the presence of woven tissue (hence lack of remodelling) also indicates that the osteocytes may not play a pivotal role in

bone remodelling, or that their involvement is limited to the perilacunar tissue and mechanosensing (Cullinane 2002; Goggin et al. 2016; Skedros, Grunander and Hamrick 2005; Teti and Zallone 2009). The bimodal lacunar volume (i.e. c. 230 μm^3 and over 500 μm^3) in petrous bones, although unique in normal bone, it seems to be related with the co-existence of woven and lamellar-like tissue (Buckwalter et al. 1995).

The hardness and elastic modulus of well-preserved archaeological petrous bone did not differ radically from those reported for modern human and cattle femora, therefore not justifying a connection between DNA preservation and petrous bone density. Similar variations have been observed in long bones, while the increased elastic modulus and hardness of the inner periosteal and endosteal tissues compared to the outer periosteal tissue could be diagenesis-related. However, in the case that the measurements predominantly reflect the original biomechanical properties of those petrous tissues, this could be indeed linked to the differences in endogenous DNA yields from the different parts of the petrous pyramid reported by Pinhasi et al. (2015). The random collagen fibre orientation and irregular mineralization in woven bone compared to lamellar tissue could result to some variability, with some more flexible and soft areas than others (e.g. Buckwalter et al. 1995); hence specific areas may favour DNA preservation.

When it comes to diagenesis (**objectives 2 and 3**), no microscopic focal destruction was observed in petrous bones. Only one specimen displayed some modifications similar to Wedl-type tunnels, and two others few merged osteocyte lacunae that could possibly represent some limited bacterially-induced modifications during early diagenetic stages (section 5.1.1). However, destruction foci were also not found in the vast majority of long bones. Therefore, this stresses that the lack of microbial tunneling in petrous bones does not necessarily indicate good DNA preservation. Further, when petrous bone histological preservation was compared to other skeletal elements intra-individually, no distinct variations could be observed (section 5.1.3), something that was also observed for bioapatite and collagen preservation (sections 5.2.3 and 5.3.3).

Water flowing through petrous bones had clearly the most significant effect on petrous bone long-term preservation potential, with the most vulnerable areas histologically being those surrounding the cochlea and the various canals, as well as the outer periosteal tissue because of the direct contact with groundwater (section 5.1.1). Manifestations of this interaction include the microcracks and loss of microstructural characteristics in areas of varying sizes in more than half of the petrous bones, while these alterations were identified in almost all other bones.

Except for the effects on bone histology, groundwater also leached out and/or recrystallized bioapatite, whereas collagen preservation was also heavily dependent on temperature; for example, the bones from the Mediterranean had generally low collagen yields (e.g. Kendall et al. 2018 Fig. 7; Van Doorn et al. 2012). The changes in bone mineralogy considerably varied inter-site due to the critical role of pH and the preservation mechanisms (sediment diagenesis) in the

burial environment (e.g. Berna, Matthews and Weiner 2004; Karkanas 2010). Soil geochemistry also contributed to inter-site variations in collagen preservation, as protein hydrolysis activation energies are also pH-dependent (e.g. Ajie, Hauschka and Kaplan 1991; Collins and Galley 1998).

Bioapatite dissolution/recrystallization was associated with a significant loss of DNA (section 5.4.2), although there were cases where DNA molecules were trapped in bones with high crystallinity and survived over archaeological timescales, possibly by adsorbing onto the surfaces of the crystals. Temperature, pH, and local hydrology control the DNA-mineral bonding (e.g. Grunenwald et al. 2014) and the different conditions in the burial environments were responsible for the inter-site variations seen in the relationships between endogenous DNA content and crystallinity. However, as evidenced in cases of extreme crystallinity increase, DNA has no chance of survival when the structure and composition of BAp crystals were constantly altered for prolonged periods of time until an equilibrium with the burial environment was reached (section 5.4.2). Contrariwise, BAp-collagen relationship rarely followed the expected pattern that would be argued from the strong *in vivo* link between the organic and inorganic components of bone. Consequently, the weak relationship between crystallinity and collagen content indicated that bioapatite recrystallization is possible even in the presence of fair amounts of collagen in bone (e.g. Reiche et al. 2003).

The distinction between single burials in coffins and single burials with wrapped bodies was well-attested by the characteristic histological modifications identified in bones from the medieval/post-medieval cemetery at St. Rombout, Belgium (section 5.1.2). Similarly, collagen preservation, but not bioapatite, was strongly related to burial types (sections 5.3.2 and 5.2.2, respectively). This is the first study that has reported such a clear association between specific funerary practices and bone preservation. Not only did different types of burials leave their marks on bone, but also that they influence the microenvironment in such a way to even affect collagen degradation. This research thus demonstrated how the histological information can be realistically used in the efforts to puzzle out the relationship between funerary practices and bone diagenesis.

Lastly, neither intra-individual patterns related to the proximity of the skeletal element to the abdominal area (internal gut bacteria) nor significant differences in the preservation state of proximal and distal diaphyses of long bones were observed in any of the diagenetic parameters applied in this study (sections 5.1.3, 5.2.3, 5.3.3). While generalizing from these examples alone would be unwise, it seems that the argument which favours the soil origin of microbial attack in bone is more defensible (e.g. Fernandez-Jalvo et al. 2010; Hedges 2002; Nielsen-Marsh and Hedges 2000a; Turner-Walker 2008). If the MFD were caused purely or predominantly by the internal gut bacteria, tunneling should be always apparent in almost all bones. Additionally, collagen content should show some pattern related to the proximity to the abdominal area due to

collagen enzymolysis by the omnipresent endogenous bacteria, and this clearly has never been reported.

With regard to screening methods (**objective 4**), the most significant achievement of this study was the establishment of thresholds for IRSF (< 3.7) and C/P (> 0.15) indices when using FTIR-ATR to discriminate bones containing fair amounts of endogenous DNA (>1 %) from those containing no or very small amounts (< 1 %) of aDNA (section 5.4.2). The success rate of the combined use of IRSF and C/P cut-off points is very high, i.e. c. 85 % for the identification of 'good' samples, accompanied by a c. 70 % successful elimination of 'bad' samples. FTIR-ATR is cost-efficient, rapid and minimally destructive, while the bone powder can be extracted for biomolecules after analysis with no loss of material. Although the technological advancements in next-generation sequencing, in combination with the falling costs, have made large-scale studies of aDNA more realistic, the extraction of DNA is a very labour-intensive process, the analysis is still costly and destructive, and the targets are usually rare or valuable specimens. Therefore, the systematic screening of archaeological bone for endogenous DNA preservation using this rapid, non-destructive and very effective screening method can significantly minimize damage to rare or valuable target samples, as well as save labour-time and money.

To achieve this, however, issues related to the technical limitations of FTIR-ATR had to be overcome. The particle size variability and the inconsistent application of baseline correction during analysis were leading to systematic but variable changes in FTIR-ATR data, while the mixture of periosteal, mesosteal and endosteal bone was blending biogenic and exogenous signals (section 4.2.3). The development of the Kontopoulos et al. (2018) preparation strategy for the FTIR-ATR analysis of bone powder managed to eliminate these effects introduced by erroneous sampling, sample preparation, and analysis of the mid-IR spectra. This attainment was fundamental in this endeavour to improve accuracy, consistency, reliability, reproducibility and comparability of the FTIR-ATR data for the systematic evaluation of bone.

Rapid assessment of bone for collagen preservation can be achieved through nitrogen and carbon analysis of whole bone. The % N and % C content of whole bone were found reliable indicators of collagen content, as demonstrated by the strong linear relationships with collagen wt. % (section 5.3.5). The observation for nitrogen was in agreement with previous studies (e.g. Brock et al. 2012; Lebon et al. 2016) which claim that % N of whole bone can be a relatively good indicator of collagen preservation, whereas this research found that the % C of whole bone can be as equally strong as % N of whole bone predictor of collagen content.

Finally, the 2nd derivative analysis of the ν_2 (c. 850-900 cm^{-1}) and ν_3 (c. 1400-1500 cm^{-1}) carbonate bands, and of the amide I band (c. 1600-1700 cm^{-1}) of bone mid-IR spectra provided useful information on the carbonate environment and the organic components lost (e.g. polyproline II, cross-links) during collagen degradation (sections 5.2.4 and 5.3.5). This data treatment has

considerable potential for the assessment of the organic and inorganic components prior to isotopic investigations.

6.2. CHALLENGES, LIMITATIONS AND FUTURE RESEARCH

Multi-analytical approaches can provide deeper information on particular diagenetic mechanisms. However, the most important challenge for this study was its multi-analytical nature, as each petrous bone had to be analysed by several methods while trying to be as minimally destructive as possible. The preparation of thin sections from poorly-preserved, unembedded petrous bones for histological examination was often difficult, as samples frequently fell apart or were washed away by water during sectioning due to their morphological characteristics (i.e. many canals and fossae) and preservation state. Additionally, even when thin sections were complete and cut exactly at the same anatomical sites, due to slight variations in the inner ear morphology between individuals (e.g. Osipov et al. 2013; Ponce de León et al. 2018), the sections were not always identical, limiting the direct comparison of exactly the same layers of bone. Future research should, therefore, further explore the important histomorphological findings of this study by examining a series of transverse and longitudinal (and perhaps oblique) thin and thick sections to record changes across the entire petrous bone.

With regard to petrous bone density, since the assessment of its biomechanical properties in this study did not include any modern specimens, the necessary information which would allow its direct comparison with long bones was unavailable. Sourcing modern human petrous bones for archaeological research was deemed impossible, as a destruction of the skull of the deceased would be required in order to conduct further destructive analysis on the petrous bone, with implications for ethical approval. Therefore, while this dataset approach had some limitations, gaining approvals to conduct research on modern petrous bone mechanical properties was not possible within the scope of this study. As a result, future nano-indentation investigations on petrous bone should either be carried out on recent archaeological specimens with bioapatite characteristics and collagen preservation similar to modern bone, or through collaborations with biomedical and forensic centres, which would share any relevant data that could be used to answer archaeological questions. Furthermore, scanning electron microscopy (SEM) with energy dispersive X-ray analysis (EDX) would allow the comparison of the biomechanical properties of each area in petrous bone with the P and Ca concentrations (e.g. Henmi et al. 2016 Fig.3).

The development and operation of the FTIR-ATR protocol allowed the successful analysis of BAp crystallinity and carbonate environment, and the effective screening of archaeological bone for DNA preservation. Nonetheless, the potential of the amide components for the quantification of bone collagen content was limited by the relative phosphate concentrations, which led to poor agreement of collagen estimates with collagen yields. What is thus required is the decoupling of

the amide peak from the phosphate peak. Therefore, the conception of a new ratio that does not include the phosphate peak should be one of the main aims of future studies using FTIR for the examination of archaeological bone collagen. To further improve the reliability and accuracy of the amide I band for the quantitative assessment of bone collagen, the contribution of water-related overtones (O-H stretching vibrations at 1640-1660 cm^{-1}; Trueman, Privat and Field 2008; Chadefaux et al. 2009; Lebon et al. 2016) need to be quantified through experimental projects and removed during analysis.

A significant limitation on the effort to confidently link the effects of burial practices (e.g. coffin, wrapping) to bone histology (and therefore better understand their role in bone diagenesis) was the lack of relevant detailed information from experimental taphonomic projects. Similarities in diagenetic alterations in specimens deriving from skeletons that have experienced different funerary treatments (or the variability in those that had experienced similar funerary treatments) can easily lead to misinterpretation of the data. No experimental project has heretofore thoroughly and systematically investigated the effects of burial practices on bone preservation and the burial micro-environment. Consequently, future experimental analyses may help understand the sequence of these alterations and shed light on past burial practices.

6.3. CONCLUDING REMARKS

Bone diagenesis is incredibly complex, and many of its processes are still uncertain. Although each bone has a story to tell, the narrative can be unclear, as it is often difficult to understand how the different parts of each episode relate to each other, in what order they occurred, and how they progressed. Consequently, it is difficult to arrive at any safe conclusions regarding the characteristics responsible for the often exceptional preservation of endogenous DNA in petrous bone. Consideration of the previously-mentioned data and hypotheses can lead to some conclusions, but also leaves some open questions about the specific role of its *sui generis* structural characteristics.

First, the rapid development of petrous bone *in utero*, the presence of highly osteocytic woven tissue in large areas, and most importantly the possible lack of remodelling, unambiguously play a crucial role when high amounts of endogenous DNA are recovered from archaeological petrous bones. Their exact role is still unclear, but further studies may unravel these relationships.

Another compelling question is whether it is the density that predominantly controls the fate of DNA. This is a very difficult question to address, as it appears possible for petrous bone to have small, sparse areas which can act as microniches that allow DNA survival due to increased hardness and elasticity. Although sceptical about the significance and extent of this characteristic, only the detailed mapping of modern petrous bone hardness and elastic modulus can provide irrefutable data on that matter. Combined with a recovery of aDNA from targeted areas through

microsampling of archaeological petrous bone, it will enable the connection between density and DNA survival. Ultimately, petrous bone is also one of the most protected bones of the mammalian skeletons. As such, it is protected from a strong interaction with groundwater when long bones are fully exposed, while its anatomical location may often moderate the changes in the micro-environment that other bones experience. Therefore it is likely that it is the interplay between those three components that make this mystical part of the skeleton to look supernormal. The work described in this thesis is just the start:

'Now this is not the end. It is not even the beginning of the end. But it is, perhaps, the end of the beginning.'

Sir Winston Churchill (10 November 1942)

APPENDIX A – TABLES

Table A1. *List of samples*. Skeletal elements, species, origin, archaeological periods and chronological age of each sample. When more than one samples derive from one individual, the number next to the species denotes the individual they derive from in each site. When the sex and/or the age of the individual is known, it is reported in parenthesis under the species column. The data on the sex of the human individuals from St. Rombout derives from the macroscopic analysis of their skeletal remains, whereas the data on the sex of the animals derives from the aDNA analysis of their skeletal remains. The asterisk (*) indicates the petrous bones used for synchrotron micro-CT.
L=left; R=right; P=proximal diaphysis; M=mid diaphysis; D=distal diaphysis; F=female; M=male; Y/O=years old. Grey shaded samples derive from the same skeletal element.

Sample	Skeletal element	Species	Country	Site	Period	Date
BED1	Petrous	Aurochs	Germany	Bedburg-Königshoven	Early Mesolithic	10000 BC
BED2	Petrous	Aurochs				
BED3	Petrous	Aurochs				
BED4	Petrous	Aurochs				
BED9	Petrous	Aurochs				
MAR1	R. Petrous	Human 1	Greece	Maroulas, Kythnos	Mesolithic	8300-7600 BC
MAR2	Rib					
MAR3	R. Clavicle					
MAR4	R. Humerus (D)					
MAR5	L. Humerus (D)					
MAR6	L. Ulna (D)					
MAR7	R. Fibula (P)					
MAR8	R. Fibula (D)					
MAR9	R. Petrous	Human				
MAR10	L. Petrous	Human				
MAR11	R. Tibia (M)	Human				
MAR12	L. Tibia (M)	Human				
MAR13	Tibia	Human				
MAR14	Femur	Human				
MAR15	Humerus	Human				
MAR16	Petrous	Human				
VEM139	Petrous	Cattle	Jordan	Ain Ghazal	Neolithic	7500-5500 BC
VEM140	Petrous	Goat				
VEM141	Petrous	Sheep				
VEM143	Petrous	Sheep				

Sample	Skeletal element	Species	Country	Site	Period	Date
VEM144	Petrous	Sheep				
VEM145	Petrous	Goat				
SAR1	Mandible (L. I2)	Human	Greece	Sarakenos Cave, Boeotia	Middle Neolithic	5750-5600 BC
SAR2	Mandible (L. M2)	Human			Late Neolithic Ia	5000-4800 BC
SAR3	Mandible (L. M1)	Human				
SAR4	R. Femur (D)	Human				
SAR5	R. Humerus (P)	Human				
SAR6	R. Humerus (D)	Human				
SAR7	R. Tibia (D)	Human				
SAR8*	R. Petrous	Human			Late Neolithic Ib	4800-4500 BC
SAR9	Mandible (R. M3)	Human				
SAR10	L. Femur (M)	Human			Late Neolithic II	4300-4000 BC
SAR11	L. Ulna (M)	Human				
SAR12	Metatarsal (fragment)	Human				
SAR13	L. Femur (P)	Human				
SAR14	L. Femur (D)	Human				
SAR15	L. Tibia (D)	Human				
SAR16	R. Femur (P)	Human				
SAR17	R. Femur (D)	Human				
SAR18	Mandible (mental spine)	Human			LN?	N/A
SAR19	R. Humerus (M)	Human			N/A	N/A
SAR24	R. Petrous	Sheep (F)			Early Neolithic	6400-6000 BC
SAR28	L. Petrous	Sheep (F)				
SAR35	R. Petrous	Sheep (F)			Middle Neolithic	5750-5600 BC
SAR38*	R. Petrous	Cattle (M)				
SAR40	R. Petrous	Sheep (M)			Late Neolithic Ia	5300-5000 BC
PRO1	L. Petrous	Cattle (F)	Greece	Promachon, Serres	Late Neolithic I	5400-5000 BC
PRO2	R. Petrous	Cattle				
PRO8	Metacarpal	Cattle				
PRO9	Femur	Sheep/goat				
THA1	L. Petrous	Human	Greece	Tharrounia, Euboea	Neolithic	5300-3300 BC
THA2	L. Petrous	Human				

Sample	Skeletal element	Species	Country	Site	Period	Date
THA3	R. Petrous	Human				
THA4	L. Femur (P)	Human				
THA5	L. Femur (D)	Human				
THA6	L. Femur (P)	Human				
THA7	L. Femur (D)	Human				
THA8	Unknown element	Human				
THA9	Tibia	Human				
THA10	Femur	Human				
THA11	Femur	Human				
VEM202	Petrous	Cattle (F)				
VEM203	Petrous	Cattle (F)				
VEM204	Petrous	Cattle (F)				
VEM205	Petrous	Cattle (F)	Britain	Ness of Brodgar, Orkney	Neolithic	3200-2200 BC
VEM206	Petrous	Cattle (F)				
VEM207	Petrous	Sheep (M)				
VEM208	Petrous	Sheep (M)				
VEM209	Petrous	Sheep (F)	Britain	Bornais, South Uist	Neolithic	3200-2200 BC
VEM210	Petrous	Sheep (F)	Britain	Silgenach, South Uist	Neolithic	3200-2200 BC
MAN1	R. Petrous	Human				
MAN2	Rib (fragment)	Human				
MAN3	Femur (M)	Human				
MAN4	R. Petrous	Human				
MAN5	L. Petrous	Human				
MAN6	R. Petrous	Human				
MAN7	L. Petrous	Human				
MAN8	R. Humerus (P)	Human	Greece	Manika, Euboea	Early Bronze Age	2900-2300 BC
MAN9	R. Humerus (D)	Human				
MAN10	R. Ulna (P)	Human				
MAN11	R. Ulna (M)	Human				
MAN12	R. Clavicle (medial end)	Human				
MAN13	L. Tibia (M)	Human				
MAN14	R. Fibula (D)	Human				

Sample	Skeletal element	Species	Country	Site	Period	Date
MAN15	L. Petrous	Human				
MAN16	R. Humerus (D)	Human				
MAN17	Tibia (M)	Human				
MAN18	R. Humerus (D)	Human				
MAN19	R. Femur (M)	Human				
MAN20	R. Tibia (D)	Human				
MAN21	L. Petrous	Human				
MAN22	L. Petrous	Human				
MAN23	R. Femur (P)	Human				
MAN24	R. Femur (D)	Human				
MAN25	R. Petrous	Human				
MAN26	R. Radius (P)	Human				
MAN27	L. Radius (P)	Human				
MAN28	Long bone	Human				
MAN29	Long bone	Human				
MAN30	R. Radius	Human				
MAN31	Long bone	Human				
KAZ1	Petrous	Human	Central Asia	N/A	Bronze Age	2100-1800 BC
KAZ2	Petrous	Human				
KAZ3	Petrous	Human				
KAZ4	Petrous	Human				
KAZ5	Petrous	Human				
KAZ6	Petrous	Human				
VEM146	Petrous	Cattle (F)	Britain	Cladh Hallan, South Uit	Bronze Age	2200-800 BC
VEM147	Petrous	Sheep				
VEM148	Petrous	Cattle (F)				
VEM149	Petrous	Cattle (M)				
VEM178	Petrous	Cattle (F)				
VEM179	Petrous	Cattle (F)				
KAS1	R. Femur (P)	Human	Greece	Kastrouli, Delphi	Late Bronze Age	1200-800 BC
KAS2	R. Femur (P)	Human				
KAS3	R. Femur (P)	Human				

Sample	Skeletal element	Species	Country	Site	Period	Date
KAS4	R. Femur (P)	Human				
KAS5	R. Femur (P)	Human				
KAS6	R. Femur (P)	Human				
KAS7	R. Femur (P)	Human				
KAS8	R. Femur (P)	Human				
KAS9	R. Femur (P)	Human				
KAS10	R. Femur (P)	Human				
KAS11	R. Femur (P)	Human				
KAS12	R. Femur (P)	Human				
KAS13	R. Femur (P)	Human				
KAS14	R. Femur (P)	Human				
KAS15	R. Femur (P)	Human				
KAS16	L. Petrous	Human				
KAS17	R. Petrous	Human				
KAS18	R. Carpometacarpus	Chicken				
KAS19	R. Carpometacarpus (D)	Chicken				
KAS22	Phalanx	Cattle				
KAS23	L. Humerus (D)	Pig				
KAS26	R. Calcaneus	Cattle				
KAS28	Phalanx	Sheep/goat				
KAS29	Long Bone	Sheep/goat				
VEM193	Petrous	Cattle (F)				
VEM194	Petrous	Cattle (F)				
VEM195	Petrous	Cattle (M)				
VEM196	Petrous	Cattle (F)	Britain	Potterne, Wiltshire	Late Bronze Age	1000-700 BC
VEM197	Petrous	Cattle (F)				
VEM198	Petrous	Cattle (M)				
VEM201	Petrous	Sheep (F)				
VEM180	Petrous	Cattle (F)				
VEM181	Petrous	Cattle (F)	Britain	Danebury, Hampshire	Iron Age	500-100 BC
VEM182	Petrous	Cattle (F)				
VEM100	Petrous	Cattle (F)	Britain	York	Roman	100-200 AD

Sample	Skeletal element	Species	Country	Site	Period	Date
VEM101	Petrous	Cattle (M)	Britain	York	Viking	700-1100 AD
VEM102	Petrous	Cattle (M)			Viking	700-1100 AD
VEM103	Petrous	Cattle (M)			Viking	700-1100 AD
VEM108	Petrous	Cattle (F)			Viking	700-1100 AD
VEM111	Petrous	Cattle (F)			Viking	700-1100 AD
MEC1	L. Petrous	Human 1 (M, 26-50 y/o)	Belgium	St. Rombout, Mechelen	Middle Ages	900-1800 AD
MEC2	R. Femur (D)					
MEC3	R. Tibia (P)					
MEC4	R. Tibia (D)					
MEC5	R. Petrous	Human 2 (12-17 y/o)				
MEC6	L. Humerus (P)					
MEC7	L. Humerus (D)					
MEC8	L. Radius (P)					
MEC9	L. Radius (D)					
MEC10	R. Petrous	Human 3 (12-17 y/o)				
MEC11	L. Femur (D)					
MEC12	L. Femur (P)					
MEC13	L. Tibia (P)					
MEC14	L. Tibia (D)					
MEC15	L. Petrous	Human 4 (F, 26-50y/o)				
MEC16	L. Humerus (P)					
MEC17	L. Humerus (D)					
MEC18	L. Radius (P)					
MEC19	L. Radius (D)					
MEC20	L. Petrous	Human 5 (F, 26-50y/o)				
MEC21	L. Humerus (P)					
MEC22	L. Humerus (D)					
MEC23	L. Radius (P)					
MEC24	L. Radius (D)					
MEC25	R. Petrous	Human 6 (12-17 y/o)				
MEC26	L. Femur (P)					
MEC27	L. Femur (D)					

Sample	Skeletal element	Species	Country	Site	Period	Date
MEC28	L. Tibia (P)					
MEC29	L. Tibia (D)					
MEC30	L. Petrous	Human 7 (M, 18-25 y/o)				
MEC31	L. Humerus (P)					
MEC32	L. Humerus (D)					
MEC33	L. Radius (P)					
MEC34	L. Radius (D)					
MEC35	R. Petrous	Human 8 (F, 26-50 y/o)				
MEC36	R. Humerus (P)					
MEC37	R. Humerus (D)					
MEC38	R. Radius (P)					
MEC39	R. Radius (D)					
MEC40	L. Petrous	Human 9 (M, 26-50 y/o)				
MEC41	L. Humerus (D)					
MEC42	L. Radius (P)					
MEC43	L. Radius (D)					
MEC44	R. Petrous	Human 10 (6-11 y/o)	Belgium	St. Rombout, Mechelen	Middle Ages	900-1800 AD
MEC45	R. Humerus (P)					
MEC46	R. Humerus (D)					
MEC47	R. Radius (P)					
MEC48	R. Radius (D)					
MEC49	L. Tibia (P)	Human 11 (M, 26-50 y/o)				
MEC50	L. Tibia (D)					
MEC51	L. Femur (D)					
MEC52	L. Femur (P)					
MEC53	L. Petrous					
MEC54	R. Petrous	Human 12 (M, 18-25 y/o)				
MEC55	R. Femur (P)					
MEC56	R. Femur (D)					
MEC57	R. Tibia (P)					
MEC58	R. Tibia (D)					
MEC59	R. Petrous	Human 13				

Sample	Skeletal element	Species	Country	Site	Period	Date
MEC60	R. Humerus (P)	(M, >50 y/o)				
MEC61	R. Humerus (D)					
MEC62	R. Radius (P)					
MEC63	R. Radius (D)					
MEC64	R. Petrous	Human 14 (12-17 y/o)				
MEC65	R. Humerus (P)					
MEC66	R. Humerus (D)					
MEC67	R. Radius (P)					
MEC68	R. Radius (D)					
MEC69	R. Petrous	Human 15 (F, 26-50 y/o)				
MEC70	R. Humerus (P)					
MEC71	R. Humerus (D)					
MEC72	R. UIna (P)					
MEC73	R. Ulna (D)					
MEC74	L. Petrous	Human 16 (M, 18-25 y/o)	Belgium	St. Rombout, Mechelen	Middle Ages	900-1800 AD
MEC75	L. Femur (P)					
MEC76	L. Femur (D)					
MEC77	L. Tibia (P)					
MEC78	L. Tibia (D)					
MEC79	R. Petrous	Human 17 (12-17 y/o)				
MEC80	L. Humerus (P)					
MEC81	L. Humerus (D)					
MEC82	L. Ulna (P)					
MEC83	L. Ulna (D)					
MEC84	R. Petrous	Human 18 (1-5 y/o)				
MEC85	R. Fibula (P)					
MEC86	R. Fibula (D)					
MEC87	R. Tibia (D)					
MEC88	R. Petrous	Human 19 (F, 18-25 y/o)				
MEC89	L. Humerus (P)					
MEC90	L. Humerus (D)					
MEC91	L. Ulna (D)					

Sample	Skeletal element	Species	Country	Site	Period	Date
MEC92	L. Ulna (P)					
MEC93	R. Petrous	Human 20 (F, 26-50 y/o)				
MEC94	R. Humerus (P)					
MEC95	R. Humerus (D)					
MEC96	R. UIna (P)					
MEC97	R. Ulna (D)					
MEC98	L. Petrous	Human 21 (F, >50 y/o)				
MEC99	L. Humerus (P)					
MEC100	L. Ulna (P)					
MEC101	L. Ulna (D)					
DEN 1	Petrous	Human	Denmark	Holmens Kirke	Historical Period	1650-1850 AD
DEN 2	Petrous	Human				
DEN 3	Petrous	Human				
DEN 4	Petrous	Human				
DEN 5	Petrous	Human				
DEN 6	Petrous	Human				
DEN 7	Petrous	Human				
DEN 8	Petrous	Human				
DEN 9	Petrous	Human				
BLA2*	Petrous	Human	Britain	Blackburn	Victorian period	1850 AD
BLA5*	Petrous	Human				
BLA6*	Petrous	Human				
BLA7	Petrous	Human				

Table A2. *Histological and FTIR data*. General Histological Index (GHI), Infrared Splitting Factor (IRSF), Carbonate-to-Phosphate (C/P), Amide-to-Phosphate (Am/P), type B Carbonate-to-Phosphate (BPI), Full width at half maximum (FWHM) at 1010 cm^{-1}. Columns 1410 cm^{-1}, 872 cm^{-1} and 712 cm^{-1}absorbance heights. The symbols next to the GHI values indicate: * samples with transverse thin sections; ** samples with longitudinal thin sections; *** samples with both transverse and longitudinal thin sections. The + symbol next to samples' names indicate samples that sampling for DNA analysis preceded.

Sample	GHI	IRSF	C/P	Am/P	BPI	FWHM 1010 cm^{-1}	1410 cm^{-1}	872 cm^{-1}	712 cm^{-1}
BED1+	N/A	3.38 ± 0.07	0.21 ± 0.01	0.06 ± 0.00	0.37 ± 0.01	93.20 ± 3.09	0.04097 ± 0.007	0.02149 ± 0.00358	0.00000
BED2+	N/A	3.35 ± 0.04	0.21 ± 0.01	0.05 ± 0.00	0.37 ± 0.01	94.53 ± 2.64	0.04114 ± 0.008	0.02122 ± 0.00405	0.00000
BED3+	N/A	3.27 ± 0.07	0.25 ± 0.02	0.06 ± 0.01	0.40 ± 0.02	99.85 ± 2.58	0.03320 ± 0.006	0.01714 ± 0.00289	0.00000
BED4+	N/A	3.31 ± 0.01	0.22 ± 0.00	0.05 ± 0.00	0.35 ± 0.01	100.05 ± 1.48	0.02473 ± 0.005	0.01266 ± 0.00227	0.00000
BED9+	N/A	3.34 ± 0.03	0.23 ± 0.00	0.05 ± 0.00	0.38 ± 0.02	98.20 ± 2.81	0.03213 ± 0.010	0.01638 ± 0.00507	0.00000
MAR1+	N/A	3.73 ± 0.14	0.24 ± 0.03	0.01 ± 0.00	0.56 ± 0.03	74.30 ± 4.67	0.08901 ± 0.012	0.05534 ± 0.00823	0.00279 ± 0.00052
MAR2	N/A	3.77 ± 0.11	0.21 ± 0.02	0.02 ± 0.00	0.53 ± 0.01	72.28 ± 3.42	0.09484 ± 0.008	0.05908 ± 0.00512	0.00177 ± 0.00036
MAR3	N/A	3.78 ± 0.09	0.22 ± 0.02	0.01 ± 0.00	0.53 ± 0.02	70.49 ± 3.43	0.08563 ± 0.012	0.05125 ± 0.00726	0.00230 ± 0.00008
MAR4	4*	3.73 ± 0.08	0.24 ± 0.02	0.01 ± 0.00	0.57 ± 0.02	72.13 ± 2.99	0.09624 ± 0.010	0.05588 ± 0.00666	0.00196 ± 0.00022
MAR5	4*	3.78 ± 0.07	0.22 ± 0.01	0.01 ± 0.00	0.51 ± 0.02	73.23 ± 2.69	0.08842 ± 0.006	0.05046 ± 0.00319	0.00120 ± 0.00013
MAR6	N/A	3.84 ± 0.10	0.22 ± 0.02	0.01 ± 0.00	0.53 ± 0.04	68.91 ± 3.69	0.09556 ± 0.025	0.05717 ± 0.01574	0.00277 ± 0.00091
MAR7	N/A	3.85 ± 0.16	0.27 ± 0.03	0.01 ± 0.00	0.63 ± 0.04	73.12 ± 4.90	0.09378 ± 0.012	0.06250 ± 0.00776	0.00671 ± 0.00071
MAR8	N/A	3.80 ± 0.05	0.23 ± 0.01	0.00 ± 0.00	0.54 ± 0.02	74.66 ± 1.75	0.07459 ± 0.003	0.04586 ± 0.00238	0.00265 ± 0.00006
MAR9+	N/A	4.88 ± 0.26	0.12 ± 0.09	0.02 ± 0.00	0.38 ± 0.03	63.61 ± 5.21	0.06603 ± 0.003	0.05057 ± 0.00175	0.00707 ± 0.00066
MAR10+	N/A	4.95 ± 0.19	0.11 ± 0.01	0.01 ± 0.00	0.25 ± 0.01	67.76 ± 3.70	0.04304 ± 0.004	0.03085 ± 0.00288	0.00294 ± 0.00038
MAR11	4*	3.65 ± 0.04	0.29 ± 0.01	0.00 ± 0.00	0.68 ± 0.01	75.39 ± 2.87	0.08274 ± 0.015	0.05422 ± 0.00995	0.00586 ± 0.00060
MAR12	4*	3.70 ± 0.06	0.29 ± 0.01	0.07 ± 0.00	0.68 ± 0.03	73.56 ± 0.51	0.09141 ± 0.010	0.06442 ± 0.00762	0.00854 ± 0.00077
MAR13	N/A	3.67 ± 0.06	0.26 ± 0.01	0.01 ± 0.00	0.62 ± 0.02	73.12 ± 3.11	0.09309 ± 0.022	0.05882 ± 0.01364	0.00461 ± 0.00057
MAR14	N/A	3.67 ± 0.14	0.25 ± 0.03	0.05 ± 0.01	0.57 ± 0.04	75.66 ± 3.58	0.07040 ± 0.008	0.04464 ± 0.00511	0.00264 ± 0.00023
MAR15	N/A	3.57 ± 0.10	0.28 ± 0.03	0.03 ± 0.00	0.63 ± 0.03	77.81 ± 4.26	0.07575 ± 0.015	0.04718 ± 0.00901	0.00341 ± 0.00075
MAR16+	N/A	3.43 ± 0.10	0.34 ± 0.03	0.02 ± 0.00	0.66 ± 0.03	84.88 ± 4.92	0.06831 ± 0.012	0.04356 ± 0.00706	0.00363 ± 0.00085
VEM139+	N/A	3.43 ± 0.05	0.24 ± 0.00	0.01 ± 0.00	0.46 ± 0.02	87.64 ± 2.37	0.05496 ± 0.010	0.03236 ± 0.00628	0.00000
VEM140+	N/A	3.37 ± 0.05	0.21 ± 0.01	0.01 ± 0.00	0.39 ± 0.01	88.20 ± 2.23	0.04272 ± 0.004	0.02576 ± 0.00221	0.00000
VEM141+	N/A	3.49 ± 0.08	0.22 ± 0.01	0.01 ± 0.00	0.45 ± 0.03	86.23 ± 5.83	0.05076 ± 0.022	0.03119 ± 0.01316	0.00000
VEM143+	N/A	3.46 ± 0.12	0.21 ± 0.02	0.01 ± 0.00	0.43 ± 0.03	84.71 ± 6.41	0.05584 ± 0.016	0.03202 ± 0.00866	0.00000
VEM144+	N/A	3.38 ± 0.04	0.21 ± 0.01	0.01 ± 0.00	0.41 ± 0.04	88.48 ± 1.92	0.05656 ± 0.016	0.03318 ± 0.00916	0.00000
VEM145+	N/A	3.82 ± 0.10	0.18 ± 0.01	0.01 ± 0.00	0.37 ± 0.02	76.95 ± 4.44	0.05161 ± 0.014	0.02999 ± 0.00791	0.00000
SAR1	4***	3.32 ± 0.06	0.31 ± 0.01	0.13 ± 0.01	0.60 ± 0.02	93.28 ± 2.04	0.05683 ± 0.011	0.02887 ± 0.00554	0.00053 ± 0.00055
SAR2	N/A	3.43 ± 0.08	0.23 ± 0.02	0.05 ± 0.00	0.45 ± 0.01	88.58 ± 3.97	0.05836 ± 0.015	0.03210 ± 0.00871	0.00000
SAR3	N/A	3.56 ± 0.07	0.27 ± 0.02	0.06 ± 0.00	0.52 ± 0.02	87.50 ± 5.60	0.05810 ± 0.016	0.03455 ± 0.00941	0.00150 ± 0.00025
SAR4	N/A	3.59 ± 0.07	0.21 ± 0.01	0.03 ± 0.00	0.47 ± 0.03	76.36 ± 3.39	0.07487 ± 0.020	0.04247 ± 0.01160	0.00000
SAR5	2*	3.33 ± 0.05	0.32 ± 0.01	0.11 ± 0.00	0.63 ± 0.02	91.13 ± 0.43	0.05337 ± 0.006	0.02863 ± 0.00314	0.00157 ± 0.00006
SAR6	3*	3.32 ± 0.06	0.31 ± 0.02	0.11 ± 0.01	0.62 ± 0.03	91.18 ± 1.24	0.05012 ± 0.003	0.02638 ± 0.00162	0.00105 ± 0.00014
SAR7	4*	3.29 ± 0.08	0.30 ± 0.02	0.19 ± 0.02	0.57 ± 0.05	97.16 ± 2.42	0.04178 ± 0.004	0.02021 ± 0.00164	0.00000
SAR8+	2**	3.32 ± 0.01	0.28 ± 0.01	0.13 ± 0.01	0.54 ± 0.03	94.60 ± 0.54	0.05210 ± 0.005	0.02557 ± 0.00273	0.00000

Sample	GHI	IRSF	C/P	Am/P	BPI	FWHM 1010 cm^{-1}	1410 cm^{-1}	872 cm^{-1}	712 cm^{-1}
SAR9	N/A	3.89 ± 0.09	0.18 ± 0.01	0.02 ± 0.00	0.38 ± 0.02	79.66 ± 3.52	0.05697 ± 0.009	0.03369 ± 0.00555	0.00000
SAR10	4*	3.13 ± 0.04	0.32 ± 0.02	0.21 ± 0.01	0.62 ± 0.04	101.65 ± 3.05	0.03953 ± 0.005	0.01888 ± 0.00229	0.00000
SAR11	5*	3.34 ± 0.02	0.26 ± 0.01	0.14 ± 0.00	0.50 ± 0.01	94.38 ± 1.93	0.04521 ± 0.006	0.02282 ± 0.00299	0.00000
SAR12	N/A	3.61 ± 0.08	0.29 ± 0.03	0.04 ± 0.01	0.64 ± 0.04	78.54 ± 3.67	0.08458 ± 0.011	0.05393 ± 0.00679	0.00743 ± 0.00081
SAR13	3*	3.41 ± 0.03	0.25 ± 0.01	0.11 ± 0.00	0.51 ± 0.01	86.98 ± 0.85	0.05281 ± 0.003	0.02703 ± 0.00173	0.00000
SAR14	5*	3.36 ± 0.02	0.28 ± 0.00	0.17 ± 0.00	0.54 ± 0.01	92.22 ± 1.38	0.05411 ± 0.008	0.02676 ± 0.00406	0.00000
SAR15	4*	3.44 ± 0.02	0.25 ± 0.00	0.14 ± 0.00	0.50 ± 0.00	89.60 ± 0.93	0.05371 ± 0.006	0.02673 ± 0.00315	0.00000
SAR16	3*	3.47 ± 0.12	0.24 ± 0.03	0.04 ± 0.01	0.55 ± 0.04	80.18 ± 4.14	0.08579 ± 0.007	0.04893 ± 0.00371	0.00000
SAR17	2*	3.47 ± 0.05	0.25 ± 0.01	0.07 ± 0.01	0.55 ± 0.03	81.39 ± 1.54	0.07845 ± 0.003	0.04158 ± 0.00195	0.00000
SAR18	N/A	3.39 ± 0.01	0.25 ± 0.00	0.15 ± 0.00	0.50 ± 0.02	93.83 ± 1.04	0.05042 ± 0.008	0.02523 ± 0.00380	0.00000
SAR19	0*	3.55 ± 0.07	0.22 ± 0.02	0.03 ± 0.00	0.42 ± 0.02	87.97 ± 3.58	0.05676 ± 0.009	0.03329 ± 0.00519	0.00000
SAR24+	N/A	3.29 ± 0.00	0.31 ± 0.01	0.07 ± 0.00	0.54 ± 0.02	104.12 ± 1.20	0.03442 ± 0.003	0.01838 ± 0.00152	0.00000
SAR28+	N/A	3.33 ± 0.01	0.30 ± 0.00	0.06 ± 0.00	0.53 ± 0.01	101.39 ± 2.57	0.03137 ± 0.002	0.01777 ± 0.00138	0.00082 ± 0.00015
SAR35+	N/A	3.40 ± 0.06	0.25 ± 0.01	0.08 ± 0.01	0.45 ± 0.01	94.42 ± 2.97	0.04738 ± 0.007	0.02582 ± 0.004	0.00000
SAR38+	2***	3.23 ± 0.01	0.33 ± 0.01	0.05 ± 0.00	0.53 ± 0.02	110.67 ± 4.02	0.03040 ± 0.003	0.01760 ± 0.00152	0.00071 ± 0.00006
SAR40+	2**	3.50 ± 0.02	0.25 ± 0.01	0.09 ± 0.01	0.39 ± 0.02	117.16 ± 0.82	0.02160 ± 0.002	0.01108 ± 0.00120	0.00023 ± 0.00024
PRO1+	N/A	3.20 ± 0.02	0.32 ± 0.01	0.06 ± 0.00	0.49 ± 0.00	124.07 ± 2.48	0.03061 ± 0.004	0.01597 ± 0.00163	0.00000
PRO2+	N/A	3.28 ± 0.01	0.26 ± 0.00	0.05 ± 0.01	0.43 ± 0.01	115.97 ± 1.47	0.02441 ± 0.002	0.01370 ± 0.00102	0.00011 ± 0.00010
PRO8+	N/A	4.00 ± 0.14	0.19 ± 0.01	0.01 ± 0.00	0.39 ± 0.00	77.99 ± 3.03	0.04765 ± 0.011	0.03028 ± 0.00662	0.00121 ± 0.00038
PRO9	N/A	3.29 ± 0.05	0.29 ± 0.01	0.10 ± 0.01	0.51 ± 0.02	105.43 ± 6.28	0.04373 ± 0.006	0.02244 ± 0.003	0.00000
THA1+	N/A	3.71 ± 0.03	0.20 ± 0.00	0.04 ± 0.00	0.40 ± 0.02	80.73 ± 1.72	0.05791 ± 0.009	0.03092 ± 0.00433	0.00000
THA2+	N/A	4.16 ± 0.13	0.16 ± 0.02	0.00 ± 0.00	0.35 ± 0.02	71.57 ± 4.61	0.05335 ± 0.011	0.03147 ± 0.00654	0.00093 ± 0.00029
THA3+	N/A	3.93 ± 0.15	0.18 ± 0.02	0.04 ± 0.01	0.37 ± 0.03	78.18 ± 4.38	0.04653 ± 0.002	0.02494 ± 0.00103	0.00000
THA4	0*	3.51 ± 0.10	0.25 ± 0.02	0.03 ± 0.00	0.48 ± 0.01	85.68 ± 4.70	0.06056 ± 0.014	0.03370 ± 0.00834	0.00023 ± 0.00020
THA5	1*	3.56 ± 0.17	0.24 ± 0.04	0.05 ± 0.01	0.44 ± 0.07	88.73 ± 6.60	0.04184 ± 0.006	0.02268 ± 0.00367	0.00000
THA6	0*	3.51 ± 0.04	0.24 ± 0.02	0.03 ± 0.00	0.46 ± 0.03	86.23 ± 1.07	0.05716 ± 0.007	0.03133 ± 0.00401	0.00030 ± 0.00032
THA7	N/A	3.53 ± 0.09	0.26 ± 0.02	0.04 ± 0.01	0.50 ± 0.03	88.14 ± 3.53	0.05214 ± 0.005	0.02814 ± 0.00254	0.00009 ± 0.00016
THA8+	N/A	3.57 ± 0.06	0.24 ± 0.02	0.03 ± 0.00	0.46 ± 0.04	86.50 ± 1.93	0.05769 ± 0.005	0.03284 ± 0.00284	0.00000
THA9+	N/A	3.66 ± 0.05	0.25 ± 0.01	0.07 ± 0.00	0.49 ± 0.02	86.76 ± 1.57	0.04859 ± 0.012	0.02786 ± 0.00679	0.00232 ± 0.00040
THA10	N/A	3.62 ± 0.08	0.22 ± 0.02	0.03 ± 0.00	0.44 ± 0.03	83.13 ± 2.58	0.05982 ± 0.005	0.03252 ± 0.00283	0.00000
THA11+	N/A	3.63 ± 0.06	0.23 ± 0.01	0.03 ± 0.00	0.45 ± 0.02	84.60 ± 1.83	0.04955 ± 0.005	0.02692 ± 0.00267	0.00020 ± 0.00017
VEM202+	N/A	3.50 ± 0.07	0.16 ± 0.01	0.05 ± 0.00	0.30 ± 0.01	88.53 ± 3.26	0.04512 ± 0.005	0.02825 ± 0.00299	0.00000
VEM203+	N/A	3.43 ± 0.07	0.19 ± 0.02	0.06 ± 0.01	0.31 ± 0.03	97.94 ± 1.83	0.02659 ± 0.004	0.01585 ± 0.00214	0.00000
VEM204+	N/A	3.32 ± 0.03	0.23 ± 0.01	0.07 ± 0.00	0.37 ± 0.01	109.65 ± 6.67	0.02586 ± 0.003	0.01451 ± 0.00179	0.00000
VEM205+	N/A	3.53 ± 0.04	0.17 ± 0.01	0.04 ± 0.00	0.30 ± 0.01	91.62 ± 0.85	0.03041 ± 0.003	0.01820 ± 0.00208	0.00000
VEM206+	N/A	3.70 ± 0.06	0.17 ± 0.01	0.04 ± 0.00	0.32 ± 0.02	91.54 ± 0.92	0.02282 ± 0.003	0.01303 ± 0.00167	0.00000
VEM207+	N/A	3.75 ± 0.09	0.15 ± 0.02	0.05 ± 0.01	0.30 ± 0.04	91.90 ± 2.17	0.02271 ± 0.003	0.01242 ± 0.00168	0.00000
VEM208+	N/A	3.82 ± 0.09	0.14 ± 0.01	0.04 ± 0.00	0.25 ± 0.01	88.73 ± 0.83	0.02796 ± 0.003	0.01619 ± 0.00196	0.00000
VEM209+	N/A	3.23 ± 0.04	0.29 ± 0.01	0.10 ± 0.00	0.48 ± 0.02	117.37 ± 0.98	0.02324 ± 0.004	0.01165 ± 0.00166	0.00000
VEM210+	N/A	3.18 ± 0.06	0.27 ± 0.03	0.08 ± 0.01	0.44 ± 0.04	99.66 ± 3.59	0.03107 ± 0.001	0.01601 ± 0.00059	0.00000

Sample	GHI	IRSF	C/P	Am/P	BPI	FWHM 1010 cm^{-1}	1410 cm^{-1}	872 cm^{-1}	712 cm^{-1}
MAN1+	N/A	3.69 ± 0.09	0.16 ± 0.02	0.05 ± 0.01	0.30 ± 0.03	91.55 ± 3.49	0.03225 ± 0.002	0.01867 ± 0.00111	0.00000
MAN2	N/A	4.01 ± 0.07	0.15 ± 0.01	0.02 ± 0.00	0.30 ± 0.01	82.65 ± 2.21	0.03441 ± 0.002	0.02185 ± 0.00099	0.00000
MAN3	1*	4.32 ± 0.08	0.12 ± 0.01	0.02 ± 0.00	0.26 ± 0.01	74.22 ± 1.91	0.04307 ± 0.006	0.02637 ± 0.00420	0.00000
MAN4+	N/A	3.43 ± 0.01	0.23 ± 0.00	0.07 ± 0.00	0.44 ± 0.01	89.03 ± 0.58	0.04704 ± 0.004	0.02534 ± 0.00219	0.00000
MAN5+	N/A	3.53 ± 0.10	0.23 ± 0.02	0.04 ± 0.01	0.44 ± 0.03	85.87 ± 4.23	0.05556 ± 0.012	0.02978 ± 0.00619	0.00000
MAN6+	N/A	3.57 ± 0.05	0.22 ± 0.01	0.06 ± 0.00	0.44 ± 0.03	84.52 ± 2.13	0.05848 ± 0.009	0.03069 ± 0.00474	0.00000
MAN7+	N/A	3.64 ± 0.03	0.21 ± 0.01	0.04 ± 0.00	0.44 ± 0.03	82.17 ± 0.95	0.05807 ± 0.009	0.03067 ± 0.00458	0.00000
MAN8	4*	4.75 ± 0.14	0.12 ± 0.01	0.01 ± 0.00	0.31 ± 0.01	60.90 ± 2.47	0.06299 ± 0.003	0.03756 ± 0.00220	0.00000
MAN9	N/A	4.69 ± 0.13	0.12 ± 0.01	0.01 ± 0.00	0.31 ± 0.01	58.85 ± 3.06	0.06977 ± 0.005	0.04266 ± 0.00360	0.00000
MAN10	N/A	4.47 ± 0.24	0.14 ± 0.02	0.01 ± 0.00	0.29 ± 0.09	65.51 ± 6.24	0.05186 ± 0.020	0.03680 ± 0.00561	0.00000
MAN11	N/A	4.67 ± 0.07	0.12 ± 0.01	0.01 ± 0.00	0.35 ± 0.00	56.24 ± 1.86	0.08746 ± 0.004	0.05274 ± 0.00255	0.00097 ± 0.00005
MAN12	N/A	4.15 ± 0.08	0.15 ± 0.01	0.01 ± 0.00	0.38 ± 0.01	64.04 ± 1.64	0.08352 ± 0.004	0.05023 ± 0.00216	0.00000
MAN13	N/A	5.80 ± 0.11	0.07 ± 0.00	0.01 ± 0.00	0.18 ± 0.00	52.38 ± 2.82	0.03801 ± 0.006	0.02866 ± 0.00468	0.00232 ± 0.00069
MAN14	N/A	5.12 ± 0.12	0.09 ± 0.01	0.01 ± 0.00	0.21 ± 0.01	58.94 ± 2.02	0.04743 ± 0.002	0.03343 ± 0.00247	0.00080 ± 0.00072
MAN15+	N/A	4.98 ± 0.13	0.11 ± 0.01	0.01 ± 0.00	0.27 ± 0.01	57.99 ± 2.86	0.05842 ± 0.008	0.04196 ± 0.00653	0.00302 ± 0.00036
MAN16	N/A	5.05 ± 0.16	0.09 ± 0.01	0.01 ± 0.00	0.22 ± 0.01	60.06 ± 3.04	0.04727 ± 0.007	0.03108 ± 0.00542	0.00093 ± 0.00027
MAN17	0*	4.33 ± 0.16	0.15 ± 0.01	0.01 ± 0.00	0.35 ± 0.01	69.47 ± 3.45	0.06623 ± 0.006	0.04107 ± 0.00385	0.00000
MAN18	N/A	5.79 ± 0.28	0.08 ± 0.01	0.01 ± 0.00	0.22 ± 0.01	54.88 ± 3.52	0.04803 ± 0.001	0.03357 ± 0.00084	0.00207 ± 0.00026
MAN19	N/A	5.91 ± 0.14	0.06 ± 0.00	0.01 ± 0.00	0.17 ± 0.01	51.21 ± 1.01	0.04665 ± 0.006	0.03272 ± 0.00432	0.00000
MAN20	N/A	5.90 ± 0.18	0.07 ± 0.01	0.01 ± 0.00	0.18 ± 0.00	52.43 ± 3.52	0.03925 ± 0.007	0.02996 ± 0.00604	0.00210 ± 0.00049
MAN21+	N/A	4.95 ± 0.06	0.10 ± 0.00	0.01 ± 0.00	0.25 ± 0.01	57.85 ± 1.05	0.05986 ± 0.002	0.03937 ± 0.00167	0.00000
MAN22+	N/A	5.71 ± 0.06	0.08 ± 0.00	0.01 ± 0.00	0.21 ± 0.01	55.31 ± 1.87	0.04336 ± 0.004	0.03429 ± 0.00288	0.00258 ± 0.00011
MAN23	N/A	5.60 ± 0.34	0.08 ± 0.01	0.01 ± 0.00	0.18 ± 0.01	55.79 ± 5.87	0.03980 ± 0.006	0.02795 ± 0.00449	0.00000
MAN24	N/A	5.61 ± 0.14	0.09 ± 0.01	0.01 ± 0.00	0.23 ± 0.00	55.42 ± 3.38	0.04742 ± 0.009	0.03475 ± 0.00794	0.00235 ± 0.00080
MAN25+	N/A	5.45 ± 0.12	0.09 ± 0.00	0.01 ± 0.00	0.22 ± 0.01	59.37 ± 1.93	0.04857 ± 0.007	0.03383 ± 0.00557	0.00205 ± 0.00023
MAN26	N/A	5.62 ± 0.14	0.07 ± 0.01	0.01 ± 0.00	0.19 ± 0.00	54.75 ± 3.10	0.04623 ± 0.003	0.03001 ± 0.00221	0.00000
MAN27	N/A	4.95 ± 0.12	0.11 ± 0.01	0.01 ± 0.00	0.27 ± 0.00	63.29 ± 2.76	0.05535 ± 0.009	0.03665 ± 0.00618	0.00000
MAN28+	N/A	5.10 ± 0.14	0.13 ± 0.01	0.01 ± 0.00	0.33 ± 0.02	57.97 ± 4.48	0.06159 ± 0.020	0.04861 ± 0.01704	0.00773 ± 0.00245
MAN29+	N/A	5.75 ± 0.27	0.08 ± 0.01	0.01 ± 0.00	0.20 ± 0.00	59.81 ± 7.31	0.03969 ± 0.012	0.02819 ± 0.00903	0.00000
MAN30+	N/A	5.00 ± 0.37	0.09 ± 0.02	0.01 ± 0.00	0.21 ± 0.02	64.66 ± 7.57	0.03474 ± 0.007	0.02299 ± 0.00433	0.00000
MAN31+	N/A	5.83 ± 0.07	0.08 ± 0.00	0.00 ± 0.00	0.21 ± 0.00	48.31 ± 1.46	0.05872 ± 0.003	0.04658 ± 0.00223	0.00600 ± 0.00023
KAZ1+	2***	4.28 ± 0.08	0.10 ± 0.00	0.08 ± 0.00	0.20 ± 0.00	88.28 ± 1.44	0.01486 ± 0.002	0.00776 ± 0.00107	0.00000
KAZ2+	4***	3.86 ± 0.02	0.14 ± 0.01	0.10 ± 0.00	0.25 ± 0.01	93.10 ± 0.79	0.01845 ± 0.001	0.00996 ± 0.00049	0.00000
KAZ3+	N/A	3.76 ± 0.02	0.19 ± 0.01	0.14 ± 0.01	0.32 ± 0.02	99.44 ± 1.28	0.01971 ± 0.003	0.00996 ± 0.00141	0.00000
KAZ4+	N/A	4.07 ± 0.12	0.14 ± 0.02	0.02 ± 0.00	0.31 ± 0.02	72.55 ± 3.75	0.03984 ± 0.006	0.02254 ± 0.00345	0.00000
KAZ5+	N/A	4.42 ± 0.15	0.07 ± 0.01	0.04 ± 0.00	0.13 ± 0.01	78.90 ± 4.69	0.01775 ± 0.002	0.01199 ± 0.00128	0.00000
KAZ6+	N/A	3.82 ± 0.06	0.18 ± 0.01	0.07 ± 0.01	0.31 ± 0.02	91.58 ± 2.19	0.02711 ± 0.003	0.01508 ± 0.00146	0.00000
VEM146+	N/A	3.27 ± 0.02	0.23 ± 0.00	0.06 ± 0.00	0.38 ± 0.01	98.07 ± 0.16	0.03047 ± 0.002	0.01681 ± 0.00129	0.00000
VEM147+	N/A	3.23 ± 0.03	0.27 ± 0.02	0.07 ± 0.00	0.37 ± 0.11	97.95 ± 1.88	0.03526 ± 0.004	0.01838 ± 0.00235	0.00000
VEM148+	N/A	3.27 ± 0.01	0.23 ± 0.00	0.05 ± 0.00	0.37 ± 0.00	99.88 ± 1.26	0.02833 ± 0.003	0.01642 ± 0.00150	0.00000

Sample	GHI	IRSF	C/P	Am/P	BPI	FWHM 1010 cm^{-1}	1410 cm^{-1}	872 cm^{-1}	712 cm^{-1}
VEM149+	N/A	3.22 ± 0.02	0.25 ± 0.00	0.06 ± 0.00	0.41 ± 0.00	99.60 ± 0.69	0.03195 ± 0.002	0.01706 ± 0.00094	0.00000
VEM178+	N/A	3.22 ± 0.04	0.27 ± 0.01	0.07 ± 0.01	0.43 ± 0.03	104.15 ± 1.04	0.02669 ± 0.003	0.01421 ± 0.00147	0.00000
VEM179+	N/A	3.31 ± 0.01	0.23 ± 0.00	0.06 ± 0.00	0.39 ± 0.00	95.80 ± 0.30	0.02845 ± 0.003	0.01500 ± 0.00166	0.00000
KAS1	1*	5.42 ± 0.05	0.10 ± 0.00	0.01 ± 0.00	0.24 ± 0.00	57.03 ± 0.90	0.04964 ± 0.002	0.03741 ± 0.00173	0.00393 ± 0.00014
KAS2	0*	3.49 ± 0.02	0.22 ± 0.01	0.04 ± 0.00	0.45 ± 0.01	85.32 ± 1.40	0.05661 ± 0.006	0.02972 ± 0.00293	0.00000
KAS3	0*	4.79 ± 0.11	0.16 ± 0.01	0.01 ± 0.00	0.38 ± 0.01	62.19 ± 1.80	0.06674 ± 0.007	0.05356 ± 0.00629	0.00949 ± 0.00110
KAS4	0*	3.69 ± 0.02	0.17 ± 0.00	0.04 ± 0.00	0.34 ± 0.00	84.42 ± 0.85	0.04966 ± 0.003	0.02843 ± 0.00170	0.00000
KAS5	0*	4.15 ± 0.13	0.18 ± 0.01	0.02 ± 0.00	0.41 ± 0.01	70.28 ± 3.68	0.06880 ± 0.006	0.04684 ± 0.00409	0.00394 ± 0.00036
KAS6	0*	4.74 ± 0.09	0.11 ± 0.01	0.03 ± 0.00	0.25 ± 0.01	64.55 ± 2.39	0.05220 ± 0.006	0.03308 ± 0.00466	0.00000
KAS7	0*	5.47 ± 0.09	0.09 ± 0.00	0.01 ± 0.00	0.22 ± 0.01	56.62 ± 1.79	0.04516 ± 0.010	0.03455 ± 0.00873	0.00296 ± 0.00060
KAS8	1*	4.14 ± 0.17	0.14 ± 0.02	0.05 ± 0.01	0.29 ± 0.02	77.76 ± 4.86	0.03744 ± 0.003	0.02125 ± 0.00206	0.00000
KAS9	0*	4.12 ± 0.11	0.13 ± 0.01	0.05 ± 0.01	0.25 ± 0.03	76.79 ± 2.57	0.03868 ± 0.005	0.02309 ± 0.00303	0.00000
KAS10	0*	4.25 ± 0.06	0.12 ± 0.01	0.05 ± 0.00	0.25 ± 0.01	73.22 ± 1.69	0.03836 ± 0.003	0.02203 ± 0.00193	0.00000
KAS11	0*	5.33 ± 0.01	0.08 ± 0.00	0.02 ± 0.00	0.18 ± 0.00	60.24 ± 1.27	0.03864 ± 0.004	0.02635 ± 0.00367	0.00000
KAS12	0*	4.09 ± 0.08	0.20 ± 0.01	0.04 ± 0.00	0.42 ± 0.01	74.24 ± 2.86	0.07427 ± 0.008	0.04938 ± 0.00550	0.00462 ± 0.00036
KAS13	0*	3.80 ± 0.16	0.16 ± 0.03	0.04 ± 0.01	0.32 ± 0.03	83.42 ± 5.46	0.04269 ± 0.007	0.02420 ± 0.00481	0.00000
KAS14	0*	3.37 ± 0.12	0.23 ± 0.03	0.05 ± 0.01	0.45 ± 0.04	89.51 ± 5.74	0.05694 ± 0.009	0.03007 ± 0.00556	0.00000
KAS15	0*	5.37 ± 0.35	0.11 ± 0.02	0.01 ± 0.00	0.27 ± 0.01	57.06 ± 5.42	0.05489 ± 0.010	0.04564 ± 0.00909	0.00623 ± 0.00166
KAS16+	2**	4.12 ± 0.12	0.15 ± 0.01	0.04 ± 0.00	0.28 ± 0.02	82.34 ± 3.12	0.03308 ± 0.003	0.01955 ± 0.00192	0.00000
KAS17+	2**	4.07 ± 0.08	0.16 ± 0.01	0.03 ± 0.00	0.34 ± 0.01	75.74 ± 3.34	0.05021 ± 0.008	0.03085 ± 0.00489	0.00129 ± 0.00016
KAS18	0*	3.57 ± 0.01	0.18 ± 0.00	0.06 ± 0.00	0.35 ± 0.01	91.84 ± 0.37	0.03058 ± 0.007	0.01695 ± 0.00398	0.00012 ± 0.00021
KAS19	N/A	3.60 ± 0.04	0.18 ± 0.01	0.04 ± 0.00	0.38 ± 0.01	83.65 ± 2.86	0.04553 ± 0.009	0.02577 ± 0.00518	0.00000
KAS22	0*	3.52 ± 0.06	0.25 ± 0.01	0.03 ± 0.00	0.54 ± 0.01	80.26 ± 2.51	0.07865 ± 0.008	0.04486 ± 0.00474	0.00192 ± 0.00020
KAS23	0*	3.61 ± 0.04	0.25 ± 0.01	0.04 ± 0.00	0.48 ± 0.01	88.08 ± 1.96	0.04947 ± 0.009	0.02833 ± 0.00503	0.00200 ± 0.00057
KAS26	0*	4.10 ± 0.24	0.16 ± 0.03	0.01 ± 0.00	0.33 ± 0.04	78.17 ± 8.00	0.04262 ± 0.007	0.02628 ± 0.00451	0.00000
KAS28	0*	3.51 ± 0.06	0.25 ± 0.02	0.08 ± 0.01	0.48 ± 0.04	92.47 ± 2.21	0.03735 ± 0.003	0.01820 ± 0.00152	0.00000
KAS29	0*	3.91 ± 0.05	0.15 ± 0.01	0.06 ± 0.01	0.28 ± 0.01	88.95 ± 1.88	0.02336 ± 0.002	0.01295 ± 0.00157	0.00000
VEM193+	N/A	3.20 ± 0.01	0.23 ± 0.01	0.09 ± 0.00	0.38 ± 0.00	105.71 ± 1.29	0.02095 ± 0.002	0.01116 ± 0.00082	0.00000
VEM194+	N/A	3.24 ± 0.06	0.20 ± 0.02	0.05 ± 0.01	0.34 ± 0.02	99.04 ± 3.96	0.03010 ± 0.008	0.01782 ± 0.00477	0.00000
VEM195+	N/A	3.19 ± 0.08	0.23 ± 0.03	0.07 ± 0.01	0.39 ± 0.03	103.86 ± 4.43	0.03106 ± 0.004	0.01743 ± 0.00285	0.00000
VEM196+	N/A	3.18 ± 0.04	0.21 ± 0.02	0.06 ± 0.01	0.37 ± 0.03	101.65 ± 2.72	0.03365 ± 0.002	0.01914 ± 0.00135	0.00000
VEM197+	N/A	3.32 ± 0.03	0.21 ± 0.01	0.08 ± 0.01	0.38 ± 0.02	100.08 ± 2.49	0.03387 ± 0.003	0.01868 ± 0.00223	0.00000
VEM198+	N/A	3.25 ± 0.00	0.21 ± 0.00	0.05 ± 0.00	0.35 ± 0.02	102.53 ± 1.27	0.02947 ± 0.005	0.01661 ± 0.00294	0.00000
VEM201+	N/A	3.28 ± 0.01	0.24 ± 0.00	0.10 ± 0.00	0.41 ± 0.01	115.92 ± 0.68	0.02417 ± 0.003	0.01264 ± 0.00179	0.00000
VEM180+	N/A	3.15 ± 0.04	0.25 ± 0.02	0.06 ± 0.01	0.40 ± 0.02	105.91 ± 2.77	0.02422 ± 0.002	0.01328 ± 0.00111	0.00000
VEM181+	N/A	3.28 ± 0.03	0.22 ± 0.00	0.05 ± 0.00	0.38 ± 0.02	97.38 ± 2.33	0.03115 ± 0.009	0.01724 ± 0.00492	0.00000
VEM182+	N/A	3.41 ± 0.02	0.22 ± 0.01	0.04 ± 0.00	0.37 ± 0.02	97.08 ± 0.87	0.03034 ± 0.002	0.01733 ± 0.00147	0.00000
VEM100+	N/A	3.11 ± 0.02	0.25 ± 0.01	0.07 ± 0.00	0.41 ± 0.01	105.88 ± 1.78	0.02348 ± 0.001	0.01245 ± 0.00083	0.00000
VEM101+	N/A	3.16 ± 0.03	0.26 ± 0.01	0.07 ± 0.00	0.43 ± 0.01	104.98 ± 2.84	0.03074 ± 0.006	0.01676 ± 0.00322	0.00000
VEM102+	N/A	3.23 ± 0.04	0.21 ± 0.01	0.05 ± 0.00	0.35 ± 0.00	101.18 ± 2.75	0.02960 ± 0.003	0.01717 ± 0.00205	0.00000

Sample	GHI	IRSF	C/P	Am/P	BPI	FWHM 1010 cm^{-1}	1410 cm^{-1}	872 cm^{-1}	712 cm^{-1}
VEM103+	N/A	3.25 ± 0.05	0.22 ± 0.02	0.06 ± 0.01	0.34 ± 0.03	107.55 ± 2.64	0.02082 ± 0.001	0.01176 ± 0.00032	0.00000
VEM108+	N/A	3.21 ± 0.07	0.24 ± 0.01	0.07 ± 0.00	0.38 ± 0.02	110.51 ± 3.83	0.02149 ± 0.003	0.01165 ± 0.00198	0.00000
VEM111+	N/A	3.09 ± 0.04	0.29 ± 0.02	0.07 ± 0.01	0.43 ± 0.01	112.18 ± 4.51	0.02041 ± 0.004	0.01105 ± 0.00216	0.00000
MEC1	3**	4.34 ± 0.07	0.08 ± 0.01	0.07 ± 0.00	0.16 ± 0.01	81.79 ± 0.85	0.02049 ± 0.002	0.01711 ± 0.00178	0.00000
MEC2	2*	4.27 ± 0.10	0.11 ± 0.01	0.02 ± 0.00	0.26 ± 0.01	72.23 ± 2.84	0.03973 ± 0.004	0.02564 ± 0.00289	0.00000
MEC3	2*	4.19 ± 0.10	0.12 ± 0.01	0.02 ± 0.00	0.27 ± 0.01	75.27 ± 4.30	0.04079 ± 0.007	0.02660 ± 0.00508	0.00000
MEC4	1*	3.88 ± 0.08	0.15 ± 0.01	0.03 ± 0.00	0.29 ± 0.01	84.06 ± 2.43	0.02809 ± 0.003	0.01770 ± 0.00207	0.00000
MEC5	0**	3.75 ± 0.02	0.16 ± 0.00	0.04 ± 0.00	0.33 ± 0.00	83.03 ± 0.58	0.04850 ± 0.002	0.02966 ± 0.00106	0.00000
MEC6	3*	3.66 ± 0.06	0.18 ± 0.01	0.07 ± 0.01	0.36 ± 0.02	84.58 ± 1.13	0.04876 ± 0.007	0.02769 ± 0.00432	0.00000
MEC7	3*	3.68 ± 0.08	0.18 ± 0.01	0.06 ± 0.00	0.36 ± 0.01	85.19 ± 2.64	0.04230 ± 0.007	0.07739 ± 0.08456	0.00000
MEC8	3*	3.54 ± 0.13	0.20 ± 0.03	0.13 ± 0.02	0.39 ± 0.05	90.74 ± 4.24	0.04194 ± 0.008	0.02216 ± 0.00456	0.00000
MEC9	3*	3.65 ± 0.05	0.19 ± 0.01	0.15 ± 0.01	0.36 ± 0.02	90.49 ± 1.74	0.03580 ± 0.001	0.01862 ± 0.00029	0.00000
MEC10	1**	3.87 ± 0.04	0.12 ± 0.00	0.06 ± 0.00	0.23 ± 0.01	84.62 ± 2.37	0.03086 ± 0.006	0.01954 ± 0.00396	0.00000
MEC11	2*	3.77 ± 0.14	0.16 ± 0.03	0.09 ± 0.02	0.32 ± 0.04	84.89 ± 5.49	0.03573 ± 0.005	0.02024 ± 0.00350	0.00000
MEC12	2*	3.86 ± 0.06	0.15 ± 0.01	0.07 ± 0.00	0.29 ± 0.01	82.60 ± 1.48	0.03728 ± 0.001	0.02241 ± 0.00051	0.00000
MEC13	3*	3.99 ± 0.06	0.13 ± 0.01	0.04 ± 0.00	0.29 ± 0.01	76.27 ± 2.23	0.04364 ± 0.005	0.02604 ± 0.00285	0.00000
MEC14	2*	3.98 ± 0.14	0.13 ± 0.02	0.04 ± 0.00	0.29 ± 0.02	76.59 ± 4.84	0.04019 ± 0.006	0.02401 ± 0.00339	0.00000
MEC15	2**	3.40 ± 0.06	0.21 ± 0.02	0.07 ± 0.01	0.40 ± 0.03	95.37 ± 2.99	0.03865 ± 0.003	0.02125 ± 0.00181	0.00000
MEC16	3*	3.68 ± 0.17	0.18 ± 0.03	0.04 ± 0.01	0.38 ± 0.03	82.98 ± 6.75	0.05049 ± 0.011	0.02939 ± 0.00648	0.00000
MEC17	3*	3.57 ± 0.07	0.20 ± 0.01	0.05 ± 0.01	0.41 ± 0.03	88.26 ± 1.57	0.04408 ± 0.004	0.02579 ± 0.00195	0.00000
MEC18	3*	3.65 ± 0.12	0.19 ± 0.02	0.02 ± 0.00	0.39 ± 0.03	85.49 ± 4.42	0.04649 ± 0.007	0.02815 ± 0.00446	0.00000
MEC19	N/A	3.44 ± 0.04	0.23 ± 0.01	0.07 ± 0.00	0.47 ± 0.01	91.06 ± 1.19	0.04511 ± 0.004	0.02467 ± 0.00230	0.00000
MEC20	3**	3.86 ± 0.05	0.12 ± 0.01	0.09 ± 0.01	0.21 ± 0.01	88.93 ± 2.52	0.02486 ± 0.005	0.01527 ± 0.00323	0.00000
MEC21	4*	3.63 ± 0.04	0.20 ± 0.01	0.17 ± 0.01	0.39 ± 0.01	86.54 ± 1.30	0.04782 ± 0.004	0.02403 ± 0.00232	0.00000
MEC22	4*	3.58 ± 0.04	0.20 ± 0.01	0.15 ± 0.01	0.39 ± 0.02	87.21 ± 3.02	0.04586 ± 0.006	0.02335 ± 0.00316	0.00000
MEC23	4*	3.60 ± 0.12	0.16 ± 0.02	0.11 ± 0.01	0.30 ± 0.03	86.89 ± 2.94	0.03616 ± 0.001	0.01904 ± 0.00042	0.00000
MEC24	5*	3.56 ± 0.01	0.18 ± 0.01	0.16 ± 0.01	0.34 ± 0.02	89.91 ± 0.20	0.03833 ± 0.007	0.02012 ± 0.00350	0.00000
MEC25	3**	3.98 ± 0.04	0.11 ± 0.01	0.08 ± 0.01	0.20 ± 0.01	86.00 ± 1.27	0.02727 ± 0.002	0.01732 ± 0.00118	0.00000
MEC26	2*	3.73 ± 0.09	0.17 ± 0.01	0.04 ± 0.00	0.36 ± 0.01	82.95 ± 2.88	0.04336 ± 0.003	0.02605 ± 0.00208	0.00000
MEC27	2*	3.81 ± 0.02	0.16 ± 0.00	0.04 ± 0.00	0.33 ± 0.01	83.38 ± 0.44	0.03742 ± 0.004	0.02259 ± 0.00248	0.00000
MEC28	1*	3.83 ± 0.10	0.16 ± 0.02	0.04 ± 0.01	0.34 ± 0.03	82.21 ± 2.57	0.03746 ± 0.005	0.02223 ± 0.00298	0.00000
MEC29	1*	3.97 ± 0.18	0.14 ± 0.02	0.03 ± 0.01	0.30 ± 0.03	77.90 ± 4.80	0.03768 ± 0.003	0.02341 ± 0.00233	0.00000
MEC30	0**	4.07 ± 0.09	0.09 ± 0.01	0.05 ± 0.01	0.18 ± 0.02	82.34 ± 1.99	0.02141 ± 0.004	0.01462 ± 0.00268	0.00000
MEC31	0*	3.88 ± 0.03	0.15 ± 0.00	0.02 ± 0.00	0.33 ± 0.01	79.66 ± 1.14	0.04717 ± 0.002	0.02965 ± 0.00116	0.00000
MEC32	0*	3.83 ± 0.18	0.16 ± 0.02	0.02 ± 0.00	0.34 ± 0.02	80.69 ± 5.56	0.04670 ± 0.007	0.02891 ± 0.00446	0.00000
MEC33	0*	3.75 ± 0.14	0.18 ± 0.02	0.03 ± 0.00	0.36 ± 0.03	83.96 ± 3.59	0.03994 ± 0.001	0.02456 ± 0.00061	0.00000
MEC34	1*	3.90 ± 0.08	0.16 ± 0.01	0.02 ± 0.00	0.34 ± 0.03	78.68 ± 2.27	0.04523 ± 0.003	0.02867 ± 0.00180	0.00000
MEC35	1**	3.43 ± 0.07	0.19 ± 0.01	0.06 ± 0.00	0.35 ± 0.02	93.73 ± 1.81	0.03984 ± 0.005	0.02257 ± 0.00295	0.00000
MEC36	0*	3.83 ± 0.04	0.14 ± 0.00	0.03 ± 0.00	0.31 ± 0.01	80.47 ± 1.17	0.03743 ± 0.004	0.02232 ± 0.00252	0.00000
MEC37	0*	3.81 ± 0.14	0.16 ± 0.02	0.03 ± 0.00	0.33 ± 0.03	84.45 ± 5.29	0.03905 ± 0.001	0.02399 ± 0.00043	0.00000

Sample	GHI	IRSF	C/P	Am/P	BPI	FWHM 1010 cm^{-1}	1410 cm^{-1}	872 cm^{-1}	712 cm^{-1}
MEC38	0*	3.80 ± 0.13	0.17 ± 0.02	0.03 ± 0.01	0.35 ± 0.04	84.40 ± 4.78	0.03607 ± 0.003	0.02300 ± 0.00150	0.00000
MEC39	0*	3.83 ± 0.12	0.18 ± 0.02	0.03 ± 0.00	0.40 ± 0.02	80.89 ± 4.27	0.04587 ± 0.004	0.02933 ± 0.00316	0.00000
MEC40	3**	3.37 ± 0.06	0.24 ± 0.02	0.11 ± 0.01	0.41 ± 0.03	99.84 ± 3.15	0.03040 ± 0.004	0.01609 ± 0.00247	0.00000
MEC41	3*	3.56 ± 0.23	0.22 ± 0.06	0.07 ± 0.03	0.42 ± 0.08	90.26 ± 10.84	0.03468 ± 0.011	0.01937 ± 0.00684	0.00000
MEC42	3*	3.79 ± 0.22	0.16 ± 0.03	0.05 ± 0.01	0.35 ± 0.05	81.19 ± 6.42	0.04197 ± 0.002	0.02397 ± 0.00109	0.00000
MEC43	4*	3.58 ± 0.09	0.20 ± 0.02	0.14 ± 0.01	0.40 ± 0.02	88.91 ± 3.38	0.04021 ± 0.005	0.02041 ± 0.00258	0.00000
MEC44	2**	3.90 ± 0.10	0.13 ± 0.01	0.06 ± 0.01	0.24 ± 0.02	87.74 ± 3.69	0.02425 ± 0.003	0.01596 ± 0.00240	0.00000
MEC45	N/A	4.20 ± 0.12	0.11 ± 0.01	0.02 ± 0.00	0.25 ± 0.02	73.41 ± 3.89	0.03522 ± 0.006	0.02319 ± 0.00462	0.00000
MEC46	2*	3.90 ± 0.17	0.14 ± 0.02	0.03 ± 0.00	0.32 ± 0.02	78.22 ± 6.32	0.04637 ± 0.009	0.02923 ± 0.00575	0.00000
MEC47	N/A	3.86 ± 0.19	0.15 ± 0.03	0.04 ± 0.01	0.32 ± 0.03	79.68 ± 7.81	0.04141 ± 0.005	0.02552 ± 0.00389	0.00000
MEC48	N/A	3.78 ± 0.14	0.16 ± 0.02	0.04 ± 0.01	0.33 ± 0.02	82.63 ± 5.33	0.03681 ± 0.008	0.02287 ± 0.00547	0.00000
MEC49	3*	3.67 ± 0.08	0.17 ± 0.02	0.05 ± 0.01	0.34 ± 0.04	84.35 ± 1.89	0.03859 ± 0.010	0.02265 ± 0.00589	0.00000
MEC50	3*	3.74 ± 0.10	0.16 ± 0.02	0.05 ± 0.01	0.34 ± 0.02	83.26 ± 4.08	0.04095 ± 0.006	0.02472 ± 0.00349	0.00000
MEC51	3*	3.64 ± 0.01	0.18 ± 0.00	0.06 ± 0.00	0.37 ± 0.01	83.81 ± 1.70	0.04886 ± 0.010	0.02843 ± 0.00633	0.00000
MEC52	3*	3.62 ± 0.09	0.19 ± 0.02	0.07 ± 0.01	0.38 ± 0.02	85.98 ± 4.00	0.04308 ± 0.009	0.02463 ± 0.00550	0.00000
MEC53	1**	3.97 ± 0.07	0.11 ± 0.01	0.12 ± 0.01	0.20 ± 0.01	93.05 ± 1.62	0.02012 ± 0.001	0.01666 ± 0.00153	0.00000
MEC54	2**	4.28 ± 0.11	0.10 ± 0.01	0.05 ± 0.00	0.21 ± 0.01	74.98 ± 3.86	0.02819 ± 0.005	0.01745 ± 0.00299	0.00000
MEC55	2*	4.39 ± 0.22	0.09 ± 0.01	0.04 ± 0.01	0.21 ± 0.02	71.70 ± 4.82	0.03299 ± 0.004	0.02106 ± 0.00249	0.00000
MEC56	0*	4.00 ± 0.10	0.13 ± 0.01	0.03 ± 0.00	0.27 ± 0.03	79.89 ± 1.28	0.03092 ± 0.008	0.02018 ± 0.00516	0.00000
MEC57	0*	4.04 ± 0.20	0.14 ± 0.02	0.02 ± 0.01	0.29 ± 0.03	81.00 ± 6.95	0.03106 ± 0.005	0.01997 ± 0.00358	0.00000
MEC58	1*	3.99 ± 0.09	0.14 ± 0.01	0.03 ± 0.00	0.30 ± 0.02	77.97 ± 3.29	0.04273 ± 0.009	0.02700 ± 0.00618	0.00000
MEC59	2**	3.84 ± 0.13	0.15 ± 0.02	0.07 ± 0.01	0.28 ± 0.02	86.03 ± 4.48	0.03244 ± 0.005	0.01935 ± 0.00328	0.00000
MEC60	0*	4.25 ± 0.15	0.11 ± 0.02	0.02 ± 0.00	0.25 ± 0.02	75.40 ± 4.38	0.03097 ± 0.003	0.01988 ± 0.00194	0.00000
MEC61	1*	4.37 ± 0.10	0.09 ± 0.01	0.02 ± 0.00	0.20 ± 0.01	75.23 ± 2.69	0.02871 ± 0.003	0.01980 ± 0.00234	0.00000
MEC62	1*	4.25 ± 0.07	0.11 ± 0.01	0.03 ± 0.00	0.23 ± 0.01	76.13 ± 1.89	0.03117 ± 0.000	0.02019 ± 0.00008	0.00000
MEC63	1*	4.22 ± 0.23	0.11 ± 0.02	0.03 ± 0.01	0.23 ± 0.02	78.08 ± 7.04	0.02877 ± 0.006	0.01967 ± 0.00451	0.00000
MEC64	2**	3.76 ± 0.12	0.13 ± 0.03	0.10 ± 0.02	0.22 ± 0.04	92.92 ± 4.71	0.01921 ± 0.002	0.01215 ± 0.00152	0.00000
MEC65	2*	4.23 ± 0.05	0.10 ± 0.00	0.08 ± 0.00	0.21 ± 0.01	76.79 ± 2.46	0.02943 ± 0.007	0.01754 ± 0.00469	0.00000
MEC66	2*	4.08 ± 0.18	0.11 ± 0.02	0.08 ± 0.01	0.23 ± 0.02	80.11 ± 5.13	0.02783 ± 0.002	0.01669 ± 0.00123	0.00000
MEC67	0*	4.30 ± 0.12	0.11 ± 0.01	0.02 ± 0.00	0.24 ± 0.01	73.04 ± 2.82	0.03115 ± 0.001	0.01980 ± 0.00042	0.00000
MEC68	2*	4.43 ± 0.23	0.10 ± 0.02	0.03 ± 0.01	0.22 ± 0.02	71.06 ± 6.90	0.03378 ± 0.006	0.02093 ± 0.00446	0.00000
MEC69	2**	3.71 ± 0.05	0.16 ± 0.01	0.05 ± 0.00	0.32 ± 0.01	87.64 ± 3.39	0.03747 ± 0.008	0.02257 ± 0.00535	0.00000
MEC70	2*	3.94 ± 0.18	0.14 ± 0.02	0.03 ± 0.00	0.31 ± 0.02	79.41 ± 5.63	0.04394 ± 0.006	0.02806 ± 0.00385	0.00000
MEC71	2*	3.86 ± 0.09	0.15 ± 0.01	0.04 ± 0.00	0.32 ± 0.02	80.41 ± 2.01	0.04500 ± 0.005	0.02769 ± 0.00347	0.00000
MEC72	2*	3.76 ± 0.09	0.16 ± 0.02	0.06 ± 0.01	0.32 ± 0.02	84.23 ± 2.83	0.04050 ± 0.002	0.02456 ± 0.00109	0.00000
MEC73	N/A	3.98 ± 0.12	0.14 ± 0.01	0.02 ± 0.00	0.31 ± 0.01	77.44 ± 4.40	0.04435 ± 0.006	0.02812 ± 0.00359	0.00000
MEC74	2**	4.12 ± 0.05	0.10 ± 0.01	0.06 ± 0.00	0.21 ± 0.01	78.06 ± 1.74	0.03085 ± 0.001	0.01971 ± 0.00097	0.00000
MEC75	0*	3.58 ± 0.12	0.21 ± 0.03	0.05 ± 0.01	0.40 ± 0.03	88.99 ± 5.05	0.04295 ± 0.006	0.02546 ± 0.00403	0.00000
MEC76	0*	3.88 ± 0.11	0.15 ± 0.01	0.03 ± 0.00	0.32 ± 0.02	80.87 ± 2.67	0.03530 ± 0.004	0.02103 ± 0.00226	0.00000
MEC77	0*	3.69 ± 0.10	0.17 ± 0.02	0.06 ± 0.01	0.35 ± 0.03	84.49 ± 3.23	0.04328 ± 0.004	0.02526 ± 0.00243	0.00000

Sample	GHI	IRSF	C/P	Am/P	BPI	FWHM 1010 cm^{-1}	1410 cm^{-1}	872 cm^{-1}	712 cm^{-1}
MEC78	0*	3.80 ± 0.13	0.16 ± 0.02	0.04 ± 0.00	0.34 ± 0.03	81.50 ± 3.60	0.04290 ± 0.002	0.02523 ± 0.00135	0.00000
MEC79	2**	4.01 ± 0.05	0.11 ± 0.01	0.08 ± 0.01	0.21 ± 0.01	81.85 ± 1.39	0.02916 ± 0.003	0.01869 ± 0.00203	0.00000
MEC80	3*	3.76 ± 0.07	0.15 ± 0.02	0.12 ± 0.01	0.32 ± 0.03	90.98 ± 3.83	0.03028 ± 0.004	0.01642 ± 0.00281	0.00000
MEC81	3*	3.75 ± 0.01	0.14 ± 0.00	0.13 ± 0.01	0.28 ± 0.01	91.97 ± 2.84	0.02245 ± 0.002	0.01204 ± 0.00106	0.00000
MEC82	3*	3.97 ± 0.10	0.12 ± 0.01	0.11 ± 0.01	0.25 ± 0.02	80.77 ± 2.30	0.02851 ± 0.005	0.01608 ± 0.00291	0.00000
MEC83	3*	3.60 ± 0.07	0.17 ± 0.02	0.14 ± 0.01	0.34 ± 0.03	90.94 ± 3.12	0.02980 ± 0.001	0.01545 ± 0.00094	0.00000
MEC84	1**	3.80 ± 0.09	0.17 ± 0.02	0.04 ± 0.01	0.34 ± 0.02	84.50 ± 4.08	0.04234 ± 0.002	0.02564 ± 0.00172	0.00000
MEC85	N/A	3.75 ± 0.15	0.23 ± 0.03	0.03 ± 0.01	0.47 ± 0.03	82.57 ± 8.31	0.05142 ± 0.009	0.03400 ± 0.00610	0.00000
MEC86	N/A	3.77 ± 0.15	0.18 ± 0.02	0.02 ± 0.00	0.37 ± 0.03	83.81 ± 5.00	0.03808 ± 0.007	0.02325 ± 0.00422	0.00000
MEC87	2*	3.83 ± 0.13	0.18 ± 0.02	0.02 ± 0.00	0.39 ± 0.03	81.11 ± 4.59	0.04881 ± 0.006	0.03129 ± 0.00394	0.00000
MEC88	2**	3.58 ± 0.09	0.22 ± 0.02	0.08 ± 0.01	0.41 ± 0.03	94.42 ± 3.42	0.03716 ± 0.003	0.02248 ± 0.00168	0.00000
MEC89	1*	4.13 ± 0.16	0.12 ± 0.02	0.03 ± 0.00	0.26 ± 0.02	77.30 ± 5.41	0.03422 ± 0.004	0.02195 ± 0.00237	0.00000
MEC90	1*	3.95 ± 0.04	0.14 ± 0.01	0.04 ± 0.00	0.29 ± 0.01	79.90 ± 1.58	0.04065 ± 0.005	0.02489 ± 0.00343	0.00000
MEC91	N/A	3.75 ± 0.14	0.15 ± 0.02	0.05 ± 0.01	0.33 ± 0.03	80.48 ± 5.21	0.04387 ± 0.005	0.02529 ± 0.00308	0.00000
MEC92	N/A	4.05 ± 0.09	0.12 ± 0.01	0.03 ± 0.00	0.26 ± 0.02	77.25 ± 2.57	0.03319 ± 0.001	0.02055 ± 0.00096	0.00000
MEC93	2**	3.60 ± 0.04	0.17 ± 0.01	0.06 ± 0.00	0.33 ± 0.00	87.50 ± 2.11	0.04141 ± 0.008	0.02458 ± 0.00457	0.00000
MEC94	0*	3.75 ± 0.10	0.17 ± 0.02	0.03 ± 0.00	0.34 ± 0.03	86.64 ± 4.49	0.03319 ± 0.001	0.02010 ± 0.00069	0.00000
MEC95	0*	3.80 ± 0.08	0.15 ± 0.01	0.03 ± 0.00	0.32 ± 0.01	83.08 ± 3.36	0.04120 ± 0.003	0.02498 ± 0.00214	0.00000
MEC96	N/A	3.89 ± 0.10	0.15 ± 0.01	0.02 ± 0.00	0.32 ± 0.02	80.77 ± 3.23	0.03983 ± 0.003	0.02404 ± 0.00168	0.00000
MEC97	N/A	3.53 ± 0.12	0.22 ± 0.03	0.03 ± 0.01	0.43 ± 0.04	91.71 ± 5.67	0.03369 ± 0.006	0.02032 ± 0.00374	0.00000
MEC98	2**	3.51 ± 0.05	0.20 ± 0.01	0.08 ± 0.00	0.37 ± 0.01	92.95 ± 1.19	0.03882 ± 0.006	0.02123 ± 0.00322	0.00000
MEC99	N/A	3.69 ± 0.17	0.19 ± 0.03	0.05 ± 0.01	0.38 ± 0.04	86.83 ± 6.07	0.04061 ± 0.005	0.02317 ± 0.00301	0.00000
MEC100	3*	3.51 ± 0.07	0.22 ± 0.02	0.15 ± 0.02	0.42 ± 0.04	89.81 ± 2.53	0.04732 ± 0.008	0.02419 ± 0.00432	0.00000
MEC101	0*	3.98 ± 0.16	0.15 ± 0.02	0.02 ± 0.00	0.33 ± 0.03	78.27 ± 5.58	0.04845 ± 0.005	0.03027 ± 0.00353	0.00000
DEN1+	4***	3.33 ± 0.04	0.25 ± 0.01	0.17 ± 0.00	0.44 ± 0.01	112.48 ± 1.61	0.02414 ± 0.001	0.01234 ± 0.00074	0.00000
DEN2+	3***	3.24 ± 0.02	0.22 ± 0.00	0.10 ± 0.00	0.39 ± 0.01	102.45 ± 1.49	0.02668 ± 0.004	0.01405 ± 0.00223	0.00000
DEN3+	3*	3.33 ± 0.01	0.26 ± 0.00	0.16 ± 0.00	0.44 ± 0.01	111.29 ± 2.58	0.02690 ± 0.005	0.01398 ± 0.00229	0.00000
DEN4+	2*	3.97 ± 0.11	0.11 ± 0.01	0.05 ± 0.01	0.22 ± 0.02	80.74 ± 4.13	0.02530 ± 0.002	0.01170 ± 0.01016	0.00000
DEN5+	2*	3.68 ± 0.02	0.15 ± 0.00	0.10 ± 0.00	0.25 ± 0.01	94.66 ± 1.87	0.02215 ± 0.005	0.01280 ± 0.00265	0.00000
DEN6+	4***	3.33 ± 0.02	0.22 ± 0.01	0.14 ± 0.01	0.41 ± 0.02	96.80 ± 1.14	0.03281 ± 0.006	0.01686 ± 0.00327	0.00000
DEN7+	3***	3.38 ± 0.03	0.20 ± 0.01	0.11 ± 0.01	0.35 ± 0.02	99.30 ± 1.26	0.02781 ± 0.003	0.01498 ± 0.00151	0.00000
DEN8+	N/A	3.27 ± 0.02	0.18 ± 0.00	0.08 ± 0.00	0.32 ± 0.00	96.65 ± 0.48	0.03130 ± 0.002	0.01790 ± 0.00103	0.00000
DEN9+	1*	3.62 ± 0.10	0.14 ± 0.02	0.07 ± 0.01	0.24 ± 0.02	94.53 ± 3.41	0.01943 ± 0.002	0.01225 ± 0.00102	0.00000

Table A3. Collagen, DNA and CN whole of bone data. [1]Collagen content estimates calculated using the equation *collagen wt. % = 113.13 Am/P + 1.69* presented in Lebon et al. (2016). The + symbol next to samples' names indicate samples that sampling for DNA analysis preceded. The letter next to endogenous DNA yields denotes the ancient DNA lab the data originate, i.e. C=Copenhagen, D=Dublin and M=Mainz.

Sample	Collagen wt. %	Collagen C wt. %	Collagen N wt. %	Collagen C/N	Whole bone C wt. %	Whole bone N wt. %	Whole bone C/N	Endogenous DNA %
BED1+	N/A	N/A	N/A	N/A	6.63	1.31	5.05	3.85M
BED2+	N/A	N/A	N/A	N/A	6.09	1.13	5.38	0.88M
BED3+	N/A	N/A	N/A	N/A	5.80	1.11	5.24	9.71M
BED4+	N/A	N/A	N/A	N/A	5.71	1.03	5.57	15.53M
BED9+	N/A	N/A	N/A	N/A	5.52	0.98	5.64	1.15M
MAR1+	0.63	N/A	N/A	N/A	N/A	N/A	N/A	0.15M
MAR2	0.31	N/A	N/A	N/A	N/A	N/A	N/A	N/A
MAR3	0.38	N/A	N/A	N/A	N/A	N/A	N/A	N/A
MAR4	1.03	10.21	0.11	109.18	N/A	N/A	N/A	N/A
MAR5	0.48	1.85	0.15	14.80	N/A	N/A	N/A	N/A
MAR6	0.23	N/A	N/A	N/A	N/A	N/A	N/A	N/A
MAR7	0.58	N/A	N/A	N/A	N/A	N/A	N/A	N/A
MAR8	0.17	N/A	N/A	N/A	N/A	N/A	N/A	N/A
MAR9+	0.63	3.03	0.16	21.54	N/A	N/A	N/A	0.12M
MAR10+	0.36	N/A	N/A	N/A	N/A	N/A	N/A	0.18M
MAR11	0.00	N/A	N/A	N/A	N/A	N/A	N/A	N/A
MAR12	0.48	N/A	N/A	N/A	N/A	N/A	N/A	N/A
MAR13	0.29	N/A	N/A	N/A	N/A	N/A	N/A	N/A
MAR14	0.32	N/A	N/A	N/A	N/A	N/A	N/A	N/A
MAR15	0.00	N/A	N/A	N/A	N/A	N/A	N/A	N/A
MAR16+	0.78	1.41	0.16	10.45	N/A	N/A	N/A	0.41M
VEM139+	N/A	N/A	N/A	N/A	2.10	0.00	0.00	0.07D
VEM140+	N/A	N/A	N/A	N/A	2.35	0.00	0.00	3.10D
VEM141+	N/A	N/A	N/A	N/A	2.72	0.00	0.00	0.06D
VEM143+	N/A	N/A	N/A	N/A	2.81	0.00	0.00	0.08D
VEM144+	N/A	N/A	N/A	N/A	2.16	0.00	0.00	0.07D
VEM145+	N/A	N/A	N/A	N/A	2.50	0.00	0.00	0.30D
SAR1	14.40	36.74	13.46	3.18	N/A	N/A	N/A	N/A
SAR2	9.13	35.69	13.02	3.20	N/A	N/A	N/A	N/A
SAR3	11.07	34.35	12.51	3.20	N/A	N/A	N/A	N/A
SAR4	4.72	20.19	7.70	3.06	N/A	N/A	N/A	N/A
SAR5	19.45	37.00	13.63	3.17	N/A	N/A	N/A	N/A
SAR6	20.51	39.26	14.41	3.18	N/A	N/A	N/A	N/A
SAR7	20.29	39.10	14.39	3.17	N/A	N/A	N/A	N/A
SAR8+	14.95	40.81	14.74	3.23	N/A	N/A	N/A	60.60M

Sample	Collagen wt. %	Collagen C wt. %	Collagen N wt. %	Collagen C/N	Whole bone C wt. %	Whole bone N wt. %	Whole bone C/N	Endogenous DNA %
SAR9	6.18	35.98	13.01	3.23	N/A	N/A	N/A	N/A
SAR10	22.55	42.38	15.50	3.19	N/A	N/A	N/A	N/A
SAR11	13.06	41.59	15.23	3.19	N/A	N/A	N/A	N/A
SAR12	13.39	39.77	14.63	3.17	N/A	N/A	N/A	N/A
SAR13	16.71	40.82	15.01	3.17	N/A	N/A	N/A	N/A
SAR14	21.13	41.22	15.13	3.18	N/A	N/A	N/A	N/A
SAR15	21.41	41.87	15.42	3.17	N/A	N/A	N/A	N/A
SAR16	14.42	41.09	15.08	3.18	N/A	N/A	N/A	N/A
SAR17	7.16	42.84	15.60	3.20	N/A	N/A	N/A	N/A
SAR18	21.11	39.85	14.51	3.20	N/A	N/A	N/A	N/A
SAR19	8.26	29.51	10.74	3.21	N/A	N/A	N/A	N/A
SAR24+	14.65	37.26	13.51	3.22	5.63	1.24	4.55	19.62D
SAR28+	7.38	30.30	10.61	3.33	5.36	1.16	4.63	15.55D
SAR35+	10.89	32.95	11.72	3.28	6.44	1.50	4.30	33.44D
SAR38+	9.21	30.34	10.42	3.40	4.53	0.81	5.63	15.35D
SAR40+	5.28	37.12	12.35	3.51	6.26	1.54	4.08	48.85D
PRO1+	7.88	36.66	12.51	3.42	4.15	0.78	5.35	18.53D
PRO2+	7.08	31.82	10.89	3.41	4.46	0.95	4.72	0.18D
PRO8+	1.46	N/A	N/A	N/A	2.17	0.00	0.00	0.06D
PRO9	12.02	38.23	13.79	3.23	7.39	2.03	3.65	N/A
THA1+	5.97	38.99	13.90	3.27	N/A	N/A	N/A	3.42D
THA2+	0.84	38.28	13.28	3.36	N/A	N/A	N/A	0M
THA3+	8.18	41.71	15.07	3.23	N/A	N/A	N/A	0M
THA4	5.36	40.60	14.55	3.25	N/A	N/A	N/A	N/A
THA5	9.87	41.55	15.05	3.22	N/A	N/A	N/A	N/A
THA6	4.34	36.47	13.07	3.26	N/A	N/A	N/A	N/A
THA7	7.13	41.31	14.67	3.29	N/A	N/A	N/A	N/A
THA8+	1.77	41.68	14.67	3.32	N/A	N/A	N/A	0.06M
THA9+	12.40	42.83	15.65	3.19	N/A	N/A	N/A	4.1M
THA10	5.62	39.76	14.21	3.27	N/A	N/A	N/A	N/A
THA11+	4.57	40.46	14.39	3.28	N/A	N/A	N/A	0.09M
VEM202+	N/A	N/A	N/A	N/A	5.36	0.98	5.47	37.86D
VEM203+	N/A	N/A	N/A	N/A	4.53	0.93	4.86	45.13D
VEM204+	N/A	N/A	N/A	N/A	4.66	0.93	4.99	16.19D
VEM205+	N/A	N/A	N/A	N/A	4.81	0.77	6.23	24.46D
VEM206+	N/A	N/A	N/A	N/A	N/A	N/A	N/A	40.84D
VEM207+	N/A	N/A	N/A	N/A	5.78	1.18	4.89	47.11D
VEM208+	N/A	N/A	N/A	N/A	5.40	1.05	5.13	43.54D
VEM209+	N/A	N/A	N/A	N/A	N/A	N/A	N/A	55.04D
VEM210+	N/A	N/A	N/A	N/A	N/A	N/A	N/A	50.46D

Sample	Collagen wt. %	Collagen C wt. %	Collagen N wt. %	Collagen C/N	Whole bone C wt. %	Whole bone N wt. %	Whole bone C/N	Endogenous DNA %
MAN1+	4.95	39.08	13.76	3.31	N/A	N/A	N/A	52.29D
MAN2	4.83	32.37	11.46	3.30	N/A	N/A	N/A	N/A
MAN3	8.54	29.55	10.62	3.24	N/A	N/A	N/A	N/A
MAN4+	7.57	40.28	14.47	3.25	N/A	N/A	N/A	25.10M
MAN5+	7.06	41.52	14.98	3.23	N/A	N/A	N/A	2.77M
MAN6+	7.28	40.08	14.39	3.25	N/A	N/A	N/A	1.83M
MAN7+	5.93	41.63	14.90	3.26	N/A	N/A	N/A	2.65M
MAN8	0.00	N/A	N/A	N/A	N/A	N/A	N/A	N/A
MAN9	0.00	N/A	N/A	N/A	N/A	N/A	N/A	N/A
MAN10	0.00	N/A	N/A	N/A	N/A	N/A	N/A	N/A
MAN11	0.00	N/A	N/A	N/A	N/A	N/A	N/A	N/A
MAN12	0.72	N/A	N/A	N/A	N/A	N/A	N/A	N/A
MAN13	0.00	N/A	N/A	N/A	N/A	N/A	N/A	N/A
MAN14	0.00	N/A	N/A	N/A	N/A	N/A	N/A	N/A
MAN15+	0.00	N/A	N/A	N/A	N/A	N/A	N/A	0.41M
MAN16	0.00	N/A	N/A	N/A	N/A	N/A	N/A	N/A
MAN17	6.98	13.84	4.92	3.28	N/A	N/A	N/A	N/A
MAN18	2.58	0.45	0.10	5.28	N/A	N/A	N/A	N/A
MAN19	1.84	0.70	0.25	4.02	N/A	N/A	N/A	N/A
MAN20	0.40	0.78	0.25	4.27	N/A	N/A	N/A	N/A
MAN21+	0.00	N/A	N/A	N/A	N/A	N/A	N/A	0.3M
MAN22+	0.00	N/A	N/A	N/A	N/A	N/A	N/A	0.45M
MAN23	1.63	N/A	N/A	N/A	N/A	N/A	N/A	N/A
MAN24	0.00	N/A	N/A	N/A	N/A	N/A	N/A	N/A
MAN25+	0.00	N/A	N/A	N/A	N/A	N/A	N/A	0.5M
MAN26	0.00	N/A	N/A	N/A	N/A	N/A	N/A	N/A
MAN27	0.39	N/A	N/A	N/A	N/A	N/A	N/A	N/A
MAN28+	0.00	N/A	N/A	N/A	N/A	N/A	N/A	0.13M
MAN29+	0.00	N/A	N/A	N/A	N/A	N/A	N/A	0.64M
MAN30+	0.00	N/A	N/A	N/A	N/A	N/A	N/A	0.17M
MAN31+	2.10	0.61	0.21	4.09	N/A	N/A	N/A	0.36M
KAZ1+	15.26	43.40	12.89	3.25	9.62	1.46	6.59	0.12C
KAZ2+	17.74	44.36	11.08	3.25	9.80	2.85	3.45	5.77C
KAZ3+	17.29	43.83	10.98	3.26	10.72	3.23	3.32	32.01C
KAZ4+	10.53	43.73	11.50	3.31	7.92	1.49	5.32	9.58C
KAZ5+	13.60	42.57	12.89	3.26	6.04	1.39	4.35	N/A
KAZ6+	13.59	42.72	11.20	3.24	7.53	1.84	4.10	0.46D
VEM146+	N/A	N/A	N/A	N/A	6.49	1.60	4.06	59.13D
VEM147+	N/A	N/A	N/A	N/A	7.25	1.85	3.91	42.03D
VEM148+	N/A	N/A	N/A	N/A	5.34	1.35	3.96	71.12D

Sample	Collagen wt. %	Collagen C wt. %	Collagen N wt. %	Collagen C/N	Whole bone C wt. %	Whole bone N wt. %	Whole bone C/N	Endogenous DNA %
VEM149+	N/A	N/A	N/A	N/A	5.88	1.16	5.08	51.99D
VEM178+	N/A	N/A	N/A	N/A	6.07	1.13	5.38	58.16D
VEM179+	N/A	N/A	N/A	N/A	6.25	1.36	4.59	54.26D
KAS1	2.57	4.95	1.56	3.70	N/A	N/A	N/A	N/A
KAS2	6.68	42.97	9.13	3.24	N/A	N/A	N/A	N/A
KAS3	2.26	41.44	8.16	3.27	N/A	N/A	N/A	N/A
KAS4	7.14	40.03	8.15	3.19	N/A	N/A	N/A	N/A
KAS5	5.48	33.72	9.39	3.23	N/A	N/A	N/A	N/A
KAS6	5.79	40.30	9.75	3.29	N/A	N/A	N/A	N/A
KAS7	0.92	34.15	9.99	3.99	N/A	N/A	N/A	N/A
KAS8	11.29	39.45	14.36	3.21	N/A	N/A	N/A	N/A
KAS9	12.07	46.13	16.78	3.21	N/A	N/A	N/A	N/A
KAS10	9.68	37.71	13.70	3.21	N/A	N/A	N/A	N/A
KAS11	2.86	30.06	10.44	3.36	N/A	N/A	N/A	N/A
KAS12	8.14	39.89	14.49	3.21	N/A	N/A	N/A	N/A
KAS13	11.00	42.57	15.46	3.21	N/A	N/A	N/A	N/A
KAS14	6.59	37.76	13.63	3.23	N/A	N/A	N/A	N/A
KAS15	0.86	40.30	12.95	3.63	N/A	N/A	N/A	N/A
KAS16+	10.47	31.49	11.13	3.30	N/A	N/A	N/A	21.22M
KAS17+	10.62	42.67	15.07	3.30	N/A	N/A	N/A	28.93M
KAS18	10.89	41.34	5.56	3.26	6.75	1.31	5.17	N/A
KAS19	9.21	29.55	5.95	3.22	5.05	0.89	5.70	N/A
KAS22	5.28	41.54	6.15	3.27	5.73	0.92	6.26	N/A
KAS23	7.70	37.75	6.67	3.23	5.74	1.12	5.14	N/A
KAS26	1.90	N/A	N/A	N/A	2.90	0.00	0.00	N/A
KAS28	13.23	34.44	3.98	3.25	10.59	3.08	3.43	N/A
KAS29	10.23	28.91	6.62	3.26	5.49	1.00	5.51	N/A
VEM193+	N/A	N/A	N/A	N/A	7.46	1.77	4.22	35.95D
VEM194+	N/A	N/A	N/A	N/A	5.36	0.96	5.61	30.67D
VEM195+	N/A	N/A	N/A	N/A	5.92	1.29	4.60	12.33D
VEM196+	N/A	N/A	N/A	N/A	5.95	1.25	4.77	48.01D
VEM197+	N/A	N/A	N/A	N/A	N/A	N/A	N/A	14.37D
VEM198+	N/A	N/A	N/A	N/A	4.86	0.99	4.92	10.32D
VEM201+	N/A	N/A	N/A	N/A	7.44	1.84	4.06	35.83D
VEM180+	N/A	N/A	N/A	N/A	5.71	1.19	4.78	48.20D
VEM181+	N/A	N/A	N/A	N/A	6.25	1.32	4.74	21.40D
VEM182+	N/A	N/A	N/A	N/A	4.87	0.90	5.43	56.20D
VEM100+	N/A	N/A	N/A	N/A	5.68	1.20	4.72	55.00D
VEM101+	N/A	N/A	N/A	N/A	6.34	1.44	4.40	33.00D
VEM102+	N/A	N/A	N/A	N/A	5.28	1.06	5.00	41.00D

Sample	Collagen wt. %	Collagen C wt. %	Collagen N wt. %	Collagen C/N	Whole bone C wt. %	Whole bone N wt. %	Whole bone C/N	Endogenous DNA %
VEM103+	N/A	N/A	N/A	N/A	4.68	1.15	4.08	25.00D
VEM108+	N/A	N/A	N/A	N/A	5.45	1.15	4.75	43.00D
VEM111+	N/A	N/A	N/A	N/A	5.35	1.19	4.50	46.00D
MEC1	14.76	37.43	13.67	3.19	N/A	N/A	N/A	N/A
MEC2	7.62	42.71	15.39	3.24	N/A	N/A	N/A	N/A
MEC3	7.01	35.53	12.72	3.26	N/A	N/A	N/A	N/A
MEC4	4.45	40.75	14.51	3.28	N/A	N/A	N/A	N/A
MEC5	7.18	43.12	14.65	3.43	N/A	N/A	N/A	N/A
MEC6	19.84	62.32	28.70	2.74	N/A	N/A	N/A	N/A
MEC7	19.52	38.51	14.10	3.19	N/A	N/A	N/A	N/A
MEC8	16.27	42.92	15.73	3.18	N/A	N/A	N/A	N/A
MEC9	20.69	44.53	16.35	3.18	N/A	N/A	N/A	N/A
MEC10	12.94	37.16	13.14	3.30	N/A	N/A	N/A	N/A
MEC11	16.52	42.10	15.43	3.18	N/A	N/A	N/A	N/A
MEC12	19.48	37.07	13.61	3.18	N/A	N/A	N/A	N/A
MEC13	14.13	43.16	15.76	3.20	N/A	N/A	N/A	N/A
MEC14	15.93	37.26	13.66	3.18	N/A	N/A	N/A	N/A
MEC15	8.32	43.54	15.22	3.34	N/A	N/A	N/A	N/A
MEC16	12.74	40.63	14.78	3.21	N/A	N/A	N/A	N/A
MEC17	9.83	39.16	14.15	3.23	N/A	N/A	N/A	N/A
MEC18	7.22	41.53	14.90	3.25	N/A	N/A	N/A	N/A
MEC19	15.59	44.35	16.24	3.19	N/A	N/A	N/A	N/A
MEC20	16.25	44.69	16.10	3.24	N/A	N/A	N/A	N/A
MEC21	21.71	21.24	7.78	1.61	N/A	N/A	N/A	N/A
MEC22	21.35	47.84	18.02	2.11	N/A	N/A	N/A	N/A
MEC23	18.44	43.58	15.93	3.19	N/A	N/A	N/A	N/A
MEC24	21.28	43.15	15.79	3.19	N/A	N/A	N/A	N/A
MEC25	11.85	65.20	23.57	3.25	N/A	N/A	N/A	N/A
MEC26	13.46	40.63	14.78	3.21	N/A	N/A	N/A	N/A
MEC27	14.40	42.00	15.30	3.20	N/A	N/A	N/A	N/A
MEC28	9.87	35.85	12.93	3.24	N/A	N/A	N/A	N/A
MEC29	9.64	37.30	13.47	3.23	N/A	N/A	N/A	N/A
MEC30	12.60	42.05	14.98	3.28	N/A	N/A	N/A	N/A
MEC31	8.54	15.01	5.39	3.25	N/A	N/A	N/A	N/A
MEC32	5.89	30.77	10.99	3.26	N/A	N/A	N/A	N/A
MEC33	6.65	30.60	10.98	3.25	N/A	N/A	N/A	N/A
MEC34	6.16	35.15	12.49	3.28	N/A	N/A	N/A	N/A
MEC35	9.38	38.18	13.40	3.32	N/A	N/A	N/A	N/A
MEC36	8.04	33.70	12.08	3.25	N/A	N/A	N/A	N/A
MEC37	9.06	21.09	7.68	3.20	N/A	N/A	N/A	N/A

Sample	Collagen wt. %	Collagen C wt. %	Collagen N wt. %	Collagen C/N	Whole bone C wt. %	Whole bone N wt. %	Whole bone C/N	Endogenous DNA %
MEC38	8.04	19.74	7.16	3.22	N/A	N/A	N/A	N/A
MEC39	10.21	21.25	7.75	3.20	N/A	N/A	N/A	N/A
MEC40	16.41	44.05	15.41	3.34	N/A	N/A	N/A	N/A
MEC41	16.78	43.61	15.95	3.19	N/A	N/A	N/A	N/A
MEC42	17.72	44.97	16.45	3.19	N/A	N/A	N/A	N/A
MEC43	17.53	44.50	16.23	3.20	N/A	N/A	N/A	N/A
MEC44	9.27	45.07	15.69	3.35	N/A	N/A	N/A	N/A
MEC45	10.85	21.76	7.82	3.25	N/A	N/A	N/A	N/A
MEC46	11.73	32.89	12.00	3.20	N/A	N/A	N/A	N/A
MEC47	7.21	36.98	13.26	3.25	N/A	N/A	N/A	N/A
MEC48	10.07	36.76	13.05	3.28	N/A	N/A	N/A	N/A
MEC49	11.53	46.77	16.99	3.21	N/A	N/A	N/A	N/A
MEC50	9.91	45.51	16.51	3.22	N/A	N/A	N/A	N/A
MEC51	13.44	45.83	16.79	3.18	N/A	N/A	N/A	N/A
MEC52	18.45	45.48	16.66	3.18	N/A	N/A	N/A	N/A
MEC53	14.93	42.94	15.25	3.28	N/A	N/A	N/A	N/A
MEC54	14.20	42.06	15.13	3.24	N/A	N/A	N/A	N/A
MEC55	15.81	42.20	15.47	3.18	N/A	N/A	N/A	N/A
MEC56	5.51	42.15	15.43	3.19	N/A	N/A	N/A	N/A
MEC57	8.99	43.22	15.71	3.21	N/A	N/A	N/A	N/A
MEC58	5.87	42.68	15.57	3.20	N/A	N/A	N/A	N/A
MEC59	8.87	43.06	15.07	3.33	N/A	N/A	N/A	N/A
MEC60	8.95	44.58	16.11	3.23	N/A	N/A	N/A	N/A
MEC61	4.42	41.89	14.97	3.26	N/A	N/A	N/A	N/A
MEC62	5.23	39.99	14.59	3.20	N/A	N/A	N/A	N/A
MEC63	5.52	44.62	16.10	3.23	N/A	N/A	N/A	N/A
MEC64	13.67	44.58	16.23	3.21	N/A	N/A	N/A	N/A
MEC65	18.79	42.67	15.73	3.17	N/A	N/A	N/A	N/A
MEC66	17.30	44.01	16.17	3.18	N/A	N/A	N/A	N/A
MEC67	4.41	41.74	15.14	3.22	N/A	N/A	N/A	N/A
MEC68	9.73	43.48	16.07	3.16	N/A	N/A	N/A	N/A
MEC69	7.24	42.29	14.90	3.31	N/A	N/A	N/A	N/A
MEC70	10.57	43.58	15.94	3.19	N/A	N/A	N/A	N/A
MEC71	12.72	44.24	16.16	3.19	N/A	N/A	N/A	N/A
MEC72	14.71	44.61	16.33	3.19	N/A	N/A	N/A	N/A
MEC73	8.77	44.22	16.03	3.22	N/A	N/A	N/A	N/A
MEC74	9.91	45.56	16.30	3.26	N/A	N/A	N/A	N/A
MEC75	9.05	45.71	16.73	3.19	N/A	N/A	N/A	N/A
MEC76	6.25	45.41	16.52	3.21	N/A	N/A	N/A	N/A
MEC77	7.50	45.81	16.74	3.19	N/A	N/A	N/A	N/A

Sample	Collagen wt. %	Collagen C wt. %	Collagen N wt. %	Collagen C/N	Whole bone C wt. %	Whole bone N wt. %	Whole bone C/N	Endogenous DNA %
MEC78	10.31	44.27	16.24	3.18	N/A	N/A	N/A	N/A
MEC79	15.09	43.37	15.62	3.24	N/A	N/A	N/A	N/A
MEC80	20.93	44.06	16.27	3.16	N/A	N/A	N/A	N/A
MEC81	20.51	42.85	15.72	3.18	N/A	N/A	N/A	N/A
MEC82	20.19	42.78	15.61	3.20	N/A	N/A	N/A	N/A
MEC83	22.24	41.50	15.34	3.16	N/A	N/A	N/A	N/A
MEC84	10.07	37.64	12.98	3.38	N/A	N/A	N/A	N/A
MEC85	4.88	39.82	14.50	3.20	N/A	N/A	N/A	N/A
MEC86	6.69	41.76	15.03	3.24	N/A	N/A	N/A	N/A
MEC87	8.14	41.09	14.93	3.21	N/A	N/A	N/A	N/A
MEC88	1.58	40.50	14.64	3.23	N/A	N/A	N/A	N/A
MEC89	7.10	40.83	14.87	3.20	N/A	N/A	N/A	N/A
MEC90	14.47	35.32	12.87	3.20	N/A	N/A	N/A	N/A
MEC91	16.01	40.92	14.99	3.18	N/A	N/A	N/A	N/A
MEC92	10.75	39.47	14.36	3.21	N/A	N/A	N/A	N/A
MEC93	11.76	40.47	14.37	3.29	N/A	N/A	N/A	N/A
MEC94	5.39	39.97	14.38	3.24	N/A	N/A	N/A	N/A
MEC95	6.06	41.01	14.88	3.22	N/A	N/A	N/A	N/A
MEC96	5.48	40.03	14.47	3.23	N/A	N/A	N/A	N/A
MEC97	4.57	40.96	14.86	3.22	N/A	N/A	N/A	N/A
MEC98	13.70	40.14	14.50	3.23	N/A	N/A	N/A	N/A
MEC99	8.93	39.27	14.35	3.19	N/A	N/A	N/A	N/A
MEC100	19.36	44.43	16.32	3.18	N/A	N/A	N/A	N/A
MEC101	6.38	40.51	14.74	3.20	N/A	N/A	N/A	N/A
DEN1+	14.50	42.98	15.54	3.23	11.52	3.38	3.41	54.79C
DEN2+	11.19	44.43	16.02	3.24	8.03	1.94	4.14	41.62C
DEN3+	17.84	43.22	15.73	3.20	11.60	3.42	3.39	34.90C
DEN4+	10.71	44.08	15.95	3.22	7.83	2.22	3.54	6.97C
DEN5+	11.33	44.16	15.17	3.40	8.00	2.22	3.60	4.74C
DEN6+	12.91	44.65	15.91	3.27	11.11	3.29	3.37	56.34C
DEN7+	15.73	44.12	15.68	3.28	9.27	2.67	3.47	43.77C
DEN8+	10.80	45.20	16.06	3.28	7.75	2.03	3.82	43.22C
DEN9+	7.42	44.07	15.96	3.22	5.76	1.46	3.95	3.54C

Table A4. The biomechanical properties of archaeological bone. Measurements conducted at the transverse axis except for the petrous bone which were analysed at the longitudinal axis. Abbreviations - HVIT: hardness, EIT: elastic modulus, Er: elastic modulus without Poisson's ratio taken into account, CIT: visco-elasticity, nIT: elasticity-plasticity, P: proximal diaphysis, M: mid diaphysis, D: distal diaphysis.

Sample	Element	Tissue	HVIT	EIT	Er	CIT	nIT
MAR4	Humerus (D)	Periosteal	17.31 ± 2.06	12.44 ± 1.50	13.51 ± 1.61	3.23 ± 0.29	11.89 ± 1.60
		Mesosteal	19.61 ± 4.89	11.20 ± 1.41	12.18 ± 1.52	1.91 ± 1.14	14.68 ± 2.39
		Endosteal	18.46 ± 3.14	10.66 ± 1.50	11.59 ± 1.61	3.01 ± 1.08	13.61 ± 1.08
		Average	18.46 ± 3.36	11.43 ± 1.47	12.42 ± 1.58	2.72 ± 0.84	13.39 ± 1.69
MAR5	Humerus (D)	Periosteal	21.25 ± 4.75	12.45 ± 1.59	13.52 ± 1.71	1.97 ± 0.80	13.91 ± 1.97
		Mesosteal	22.21 ± 3.99	13.83 ± 2.14	15.00 ± 2.29	3.64 ± 1.24	12.99 ± 1.24
		Endosteal	21.51 ± 2.73	13.03 ± 1.82	14.14 ± 1.95	3.01 ± 0.88	13.32 ± 0.87
		Average	21.65 ± 3.82	13.10 ± 1.85	14.22 ± 1.98	2.87 ± 0.97	13.41 ± 1.36
MAR11	Tibia (M)	Periosteal	18.24 ± 2.63	14.76 ± 3.20	15.99 ± 3.42	6.59 ± 0.62	9.80 ± 0.57
		Mesosteal	15.51 ± 2.39	10.51 ± 1.39	11.43 ± 1.50	4.74 ± 0.72	11.20 ± 1.33
		Endosteal	16.45 ± 2.46	10.12 ± 1.10	11.01 ± 1.19	3.59 ± 0.84	12.69 ± 1.01
		Average	16.73 ± 2.49	11.80 ± 1.90	12.81 ± 2.03	4.97 ± 0.73	11.23 ± 0.97
MAR12	Tibia (M)	Periosteal	13.89 ± 1.77	11.61 ± 0.38	12.61 ± 0.41	8.25 ± 2.24	9.09 ± 0.87
		Mesosteal	13.95 ± 2.56	12.20 ± 1.79	13.25 ± 1.92	9.02 ± 1.48	8.29 ± 1.01
		Endosteal	12.53 ± 1.42	10.45 ± 1.73	11.37 ± 1.86	10.39 ± 0.95	8.69 ± 0.80
		Average	13.45 ± 1.91	11.42 ± 1.30	12.41 ± 1.40	9.22 ± 1.55	8.69 ± 0.89
SAR1	Mandible	Periosteal	56.39 ± 4.90	10.69 ± 0.34	11.62 ± 0.37	4.10 ± 1.07	38.37 ± 3.25
		Mesosteal	18.21 ± 1.59	7.78 ± 0.28	8.49 ± 0.30	4.01 ± 1.74	17.00 ± 1.66
		Average	37.30 ± 3.25	9.24 ± 0.31	10.06 ± 0.34	4.05 ± 1.40	27.69 ± 2.46
SAR5	Humerus (P)	Periosteal	58.39 ± 3.70	20.79 ± 1.52	22.40 ± 1.60	4.17 ± 0.72	23.79 ± 1.61
		Mesosteal	53.15 ± 12.45	19.97 ± 1.80	21.53 ± 1.91	4.94 ± 1.32	22.49 ± 2.72
		Endosteal	48.82 ± 6.88	19.53 ± 1.66	21.06 ± 1.76	5.33 ± 1.07	20.62 ± 2.15

Sample	Element	Tissue	HVIT	EIT	Er	CIT	nIT
		Average	53.45 ± 7.67	20.10 ± 1.66	21.66 ± 1.76	4.81 ± 1.04	22.30 ± 2.16
SAR6	Humerus (D)	Periosteal	44.84 ± 3.91	24.05 ± 2.69	25.83 ± 2.83	9.21 ± 1.00	17.35 ± 1.42
		Mesosteal	43.30 ± 4.74	18.13 ± 1.50	19.58 ± 1.59	4.99 ± 0.88	20.19 ± 1.76
		Endosteal	44.38 ± 3.51	16.93 ± 1.50	18.30 ± 1.60	5.42 ± 1.21	19.75 ± 1.65
		Average	44.17 ± 4.05	19.70 ± 1.89	21.24 ± 2.00	6.54 ± 1.03	19.09 ± 1.61
THA4	Femur (P)	Periosteal	51.48 ± 0.00	11.67 ± 0.00	12.69 ± 0.00	2.05 ± 0.00	32.36 ± 0.00
		Mesosteal	112.34 ± 0.00	18.68 ± 0.00	20.16 ± 0.00	2.65 ± 0.00	34.83 ± 0.00
		Endosteal	58.62 ± 20.73	12.63 ± 3.40	13.71 ± 3.64	2.21 ± 1.74	33.97 ± 0.18
		Average	74.14 ± 6.91	14.33 ± 1.13	15.52 ± 1.21	0.94 ± 0.58	33.72 ± 0.06
THA6	Femur (P)	Periosteal	86.11 ± 8.00	16.85 ± 2.09	18.22 ± 2.22	1.13 ± 0.54	37.37 ± 2.25
		Mesosteal	70.19 ± 19.02	21.59 ± 4.09	23.23 ± 4.32	4.55 ± 1.15	23.02 ± 1.25
		Endosteal	96.17 ± 40.07	18.16 ± 3.87	19.60 ± 4.11	1.75 ± 1.11	35.03 ± 5.72
		Average	84.15 ± 22.37	18.87 ± 3.35	20.35 ± 3.55	2.47 ± 0.94	31.81 ± 3.07
MAN2	Rib	Periosteal	44.16 ± 10.79	16.00 ± 3.98	17.31 ± 4.25	4.60 ± 2.92	23.61 ± 4.42
		Mesosteal	56.97 ± 10.28	21.05 ± 1.47	22.67 ± 1.56	5.18 ± 1.12	22.02 ± 3.57
		Endosteal	54.48 ± 6.19	16.99 ± 1.89	18.37 ± 2.01	4.76 ± 0.91	26.89 ± 4.74
		Average	51.87 ± 9.09	18.01 ± 2.45	19.45 ± 2.60	4.85 ± 1.65	24.17 ± 4.24
MAN3	Femur (M)	Periosteal	57.95 ± 16.69	17.78 ± 3.18	19.21 ± 3.38	1.85 ± 1.15	29.15 ± 7.07
		Mesosteal	56.23 ± 5.75	17.56 ± 1.71	18.98 ± 1.81	2.94 ± 0.80	26.89 ± 1.48
		Endosteal	40.23 ± 6.01	15.53 ± 1.62	16.82 ± 1.72	5.27 ± 1.39	21.79 ± 3.72
		Average	51.47 ± 9.48	16.96 ± 2.17	18.33 ± 2.30	3.35 ± 1.11	25.94 ± 4.09
MAN8	Humerus (P)	Periosteal	11.25 ± 1.57	7.82 ± 1.19	8.53 ± 1.29	4.16 ± 1.38	11.79 ± 0.69
		Mesosteal	12.73 ± 0.63	8.32 ± 0.93	9.07 ± 1.00	4.34 ± 0.68	11.46 ± 2.09
		Endosteal	13.49 ± 0.53	8.75 ± 0.83	9.53 ± 0.90	4.23 ± 1.49	11.55 ± 0.96
		Average	12.49 ± 0.91	8.30 ± 0.98	9.04 ± 1.06	4.24 ± 1.18	11.60 ± 1.25

Sample	Element	Tissue	HVIT	EIT	Er	CIT	nIT
KAS1	Femur	Periosteal	8.77 ± 0.84	5.54 ± 1.32	6.05 ± 1.44	5.92 ± 1.61	12.40 ± 0.91
		Mesosteal	7.27 ± 2.46	5.21 ± 1.48	5.69 ± 1.61	9.37 ± 8.12	10.50 ± 1.45
		Endosteal	10.08 ± 4.23	6.38 ± 2.42	6.97 ± 2.63	6.27 ± 0.70	13.15 ± 0.67
		Average	8.71 ± 2.51	5.71 ± 1.74	6.24 ± 1.89	7.19 ± 3.48	12.02 ± 1.01
KAS2	Femur	Periosteal	65.93 ± 17.93	14.64 ± 1.95	15.86 ± 2.09	2.14 ± 1.13	32.64 ± 2.27
		Mesosteal	66.35 ± 13.23	18.74 ± 2.25	20.22 ± 2.38	3.28 ± 0.64	27.93 ± 4.02
		Endosteal	62.72 ± 0.00	16.39 ± 0.00	17.73 ± 0.00	1.44 ± 0.00	26.48 ± 0.00
		Average	65.00 ± 10.39	16.59 ± 1.40	17.94 ± 1.49	2.29 ± 0.59	29.01 ± 2.09
BLA2	Petrous	Periosteal	60.18 ± 10.26	18.77 ± 2.08	20.26 ± 2.20	3.57 ± 1.82	28.74 ± 6.07
		Canal	61.88 ± 11.64	22.70 ± 2.96	24.41 ± 3.11	5.53 ± 0.92	24.12 ± 2.62
		Perio to canal	57.37 ± 11.07	20.88 ± 2.61	22.48 ± 2.75	5.22 ± 0.90	25.08 ± 4.01
		Between canal	74.91 ± 16.63	16.83 ± 1.62	18.20 ± 1.72	3.57 ± 1.91	36.82 ± 4.15
		Canal	65.39 ± 10.34	19.73 ± 1.31	21.28 ± 1.39	3.74 ± 0.88	31.07 ± 3.30
		Between canals	67.91 ± 7.92	22.87 ± 1.83	24.59 ± 1.92	4.46 ± 0.56	25.49 ± 2.13
		Periosteal	52.24 ± 8.43	13.94 ± 1.29	15.12 ± 1.38	1.53 ± 0.36	32.44 ± 3.39
		Average	62.84 ± 10.90	19.39 ± 1.95	20.91 ± 2.07	3.95 ± 1.05	29.11 ± 3.67
BLA6	Petrous	Periosteal	52.07 ± 3.54	17.48 ± 1.32	18.89 ± 1.40	3.72 ± 1.21	25.63 ± 3.03
		Canal	61.04 ± 9.73	20.40 ± 1.78	21.98 ± 1.88	5.40 ± 0.90	25.06 ± 2.65
		Canal	94.81 ± 7.62	23.84 ± 0.99	25.61 ± 1.04	2.86 ± 0.78	31.39 ± 3.33
		Average	69.31 ± 6.96	20.57 ± 1.36	22.16 ± 1.44	3.99 ± 0.96	27.36 ± 3.00
BLA7	Petrous	Periosteal	38.95 ± 5.91	18.84 ± 1.99	20.34 ± 2.11	7.09 ± 1.62	19.65 ± 3.29
		Mesosteal	65.16 ± 24.50	19.75 ± 5.41	21.28 ± 5.74	4.62 ± 1.16	29.29 ± 3.54
		Canal	66.09 ± 10.61	19.72 ± 2.13	21.27 ± 2.26	3.65 ± 1.13	30.12 ± 2.74
		Average	56.73 ± 13.68	19.44 ± 3.18	20.96 ± 3.37	5.12 ± 1.30	26.35 ± 3.19
PRO8	Metacarpal (Bos)	Periosteal	155.04 ± 21.15	53.67 ± 5.58	56.06 ± 5.56	3.37 ± 0.34	25.39 ± 1.97

Sample	Element	Tissue	HVIT	EIT	Er	CIT	nIT
		Mesosteal	47.50 ± 6.34	26.17 ± 2.27	28.05 ± 2.38	5.37 ± 0.66	14.70 ± 1.67
		Endosteal	36.78 ± 2.14	20.03 ± 2.11	21.60 ± 2.22	4.91 ± 0.61	14.95 ± 0.70
		Average	79.77 ± 9.88	33.29 ± 3.32	35.23 ± 3.39	4.55 ± 0.54	18.34 ± 1.45
PRO9	Femur (Ovicaprid)	Periosteal	97.67 ± 8.00	29.50 ± 1.63	31.53 ± 1.70	3.61 ± 0.90	27.44 ± 2.98
		Mesosteal	78.45 ± 7.46	26.85 ± 2.81	28.76 ± 2.94	4.46 ± 0.39	25.46 ± 3.06
		Endosteal	59.44 ± 9.47	22.01 ± 1.31	23.69 ± 1.38	3.28 ± 0.56	21.99 ± 1.72
		Average	78.52 ± 8.31	26.12 ± 1.92	27.99 ± 2.01	3.78 ± 0.62	24.96 ± 2.59

Table A5. Collagen content estimates using the Lebon et al. (2016) equation and a new equation produced by this dataset that utilize the Am/P FTIR index. Offsets from actual collagen yields, average offsets and standard deviations are provided.

Sample	Am/P	Collagen wt. %	Lebon et al. (2016) equation	Offset	New equation	Offset
MAR1	0.01	0.63	3.12	2.50	4.38	3.75
MAR2	0.02	0.31	3.40	3.09	4.72	4.41
MAR3	0.01	0.38	2.76	2.38	4.46	4.08
MAR4	0.01	1.03	3.14	2.10	4.99	3.96
MAR5	0.01	0.48	2.91	2.43	11.15	10.67
MAR6	0.01	0.23	2.68	2.45	10.15	9.92
MAR7	0.01	0.58	2.71	2.12	12.29	11.71
MAR8	0.00	0.17	1.69	1.52	9.20	9.03
MAR9	0.02	0.63	3.45	2.82	13.65	13.02
MAR10	0.01	0.36	3.21	2.85	18.03	17.67
MAR11	0.00	0.00	1.86	1.86	10.28	10.28
MAR12	0.07	0.48	9.94	9.46	9.07	8.59
MAR13	0.01	0.29	3.21	2.92	7.51	7.22
MAR14	0.05	0.32	7.10	6.78	2.87	2.55
MAR15	0.03	0.00	4.62	4.62	7.88	7.88
MAR16	0.02	0.78	3.70	2.93	8.45	7.67
SAR1	0.13	14.40	16.30	1.90	10.88	-3.52
SAR2	0.05	9.13	7.21	-1.92	7.52	-1.61
SAR3	0.06	11.07	8.07	-2.99	9.70	-1.37
SAR4	0.03	4.72	5.20	0.47	8.17	3.45
SAR5	0.11	19.45	14.03	-5.42	3.83	-15.62
SAR6	0.11	20.51	14.05	-6.46	3.94	-16.57

Sample	Am/P	Collagen wt. %	Lebon et al. (2016) equation	Offset	New equation	Offset
SAR7	0.19	20.29	22.98	2.69	3.52	-16.77
SAR8	0.13	14.95	16.12	1.17	3.72	-11.23
SAR9	0.02	6.18	4.09	-2.09	12.68	6.5
SAR10	0.21	22.55	25.25	2.70	14.95	-7.6
SAR11	0.14	13.06	17.51	4.46	19.73	6.67
SAR12	0.04	13.39	6.58	-6.81	4.74	-8.65
SAR13	0.11	16.71	14.21	-2.50	7.55	-9.16
SAR14	0.17	21.13	20.67	-0.46	11.65	-9.48
SAR15	0.14	21.41	17.67	-3.74	7.33	-14.08
SAR16	0.04	14.42	6.25	-8.17	6.32	-8.1
SAR17	0.07	7.16	9.43	2.27	22.56	15.4
SAR18	0.15	21.11	18.71	-2.40	14.37	-6.74
SAR19	0.03	8.26	5.41	-2.85	22.11	13.85
SAR24	0.07	14.65	9.57	-5.08	9.21	-5.44
SAR28	0.06	7.38	8.62	1.25	14.29	6.91
SAR35	0.08	10.89	10.66	-0.23	19.52	8.63
SAR38	0.05	9.21	7.71	-1.50	16.32	7.11
SAR40	0.09	5.28	11.95	6.68	12.43	7.15
PRO1	0.06	7.88	8.74	0.86	11.52	3.64
PRO2	0.05	7.08	7.59	0.51	11.48	4.4
PRO8	0.01	1.46	2.91	1.45	7.35	5.89
PRO9	0.10	12.02	13.09	1.07	10.19	-1.83
THA1	0.04	5.97	6.11	0.14	11.36	5.39
THA2	0.00	0.84	1.69	0.85	13.83	12.99
THA3	0.04	8.18	6.46	-1.72	12.77	4.59

Sample	Am/P	Collagen wt. %	Lebon et al. (2016) equation	Offset	New equation	Offset
THA4	0.03	5.36	5.60	0.24	9.02	3.66
THA5	0.05	9.87	7.62	-2.25	10.35	0.48
THA6	0.03	4.34	4.99	0.66	16.40	12.06
THA7	0.04	7.13	6.52	-0.61	10.48	3.35
THA8	0.03	1.77	5.10	3.34	16.76	14.99
THA9	0.07	12.40	9.99	-2.41	8.33	-4.07
THA10	0.03	5.62	5.27	-0.35	11.14	5.52
THA11	0.03	4.57	5.45	0.87	14.50	9.93
MAN1	0.05	4.95	7.00	2.06	8.37	3.42
MAN2	0.02	4.83	4.49	-0.34	10.58	5.75
MAN3	0.02	8.54	4.33	-4.21	12.21	3.67
MAN4	0.07	7.57	9.31	1.75	7.81	0.24
MAN5	0.04	7.06	6.11	-0.94	12.50	5.44
MAN6	0.06	7.28	8.19	0.91	9.77	2.49
MAN7	0.04	5.93	6.74	0.81	12.71	6.78
MAN8	0.01	0.00	2.48	2.48	4.67	4.67
MAN9	0.01	0.00	2.57	2.57	3.99	3.99
MAN10	0.01	0.00	2.77	2.77	4.39	4.39
MAN11	0.01	0.00	2.53	2.53	4.15	4.15
MAN12	0.01	0.72	3.10	2.38	3.91	3.19
MAN13	0.01	0.00	2.42	2.42	3.94	3.94
MAN14	0.01	0.00	2.54	2.54	2.87	2.87
MAN15	0.01	0.00	2.61	2.61	3.05	3.05
MAN16	0.01	0.00	2.54	2.54	11.54	11.54
MAN17	0.01	6.98	3.03	-3.95	4.47	-2.51

Sample	Am/P	Collagen wt. %	Lebon et al. (2016) equation	Offset	New equation	Offset
MAN18	0.01	2.58	2.43	-0.15	8.56	5.98
MAN19	0.01	1.84	2.38	0.54	5.95	4.11
MAN20	0.01	0.40	2.30	1.90	18.22	17.82
MAN21	0.01	0.00	2.71	2.71	8.67	8.67
MAN22	0.01	0.00	2.31	2.31	9.58	9.58
MAN23	0.01	1.63	2.38	0.75	6.55	4.92
MAN24	0.01	0.00	2.56	2.56	15.83	15.83
MAN25	0.01	0.00	2.50	2.50	15.86	15.86
MAN26	0.01	0.00	2.28	2.28	25.23	25.23
MAN27	0.01	0.39	2.47	2.08	5.39	5.00
MAN28	0.01	0.00	2.40	2.40	27.62	27.62
MAN29	0.01	0.00	2.45	2.45	19.49	19.49
MAN30	0.01	0.00	2.44	2.44	8.01	8.01
MAN31	0.00	2.101	2.16	0.06	16.02	13.92
CA1	0.08	15.26	11.03	-4.23	22.81	7.55
CA2	0.10	17.74	13.19	-4.55	19.66	1.92
CA3	0.14	17.29	17.74	0.45	7.67	-9.62
CA4	0.02	10.53	3.47	-7.06	11.00	0.47
CA5	0.04	13.60	6.14	-7.46	20.75	7.15
CA6	0.07	13.59	10.05	-3.54	6.78	-6.81
KAS1	0.01	2.57	2.93	0.36	4.15	1.58
KAS2	0.04	6.68	6.17	-0.50	14.85	8.17
KAS3	0.01	2.26	3.32	1.06	6.98	4.72
KAS4	0.04	7.14	6.11	-1.03	9.10	1.96
KAS5	0.02	5.48	3.64	-1.84	6.34	0.86

Sample	Am/P	Collagen wt. %	Lebon et al. (2016) equation	Offset	New equation	Offset
KAS6	0.03	5.79	4.64	-1.15	7.94	2.15
KAS7	0.01	0.92	3.05	2.13	6.45	5.53
KAS8	0.05	11.29	7.59	-3.69	11.59	0.3
KAS9	0.05	12.07	7.49	-4.59	6.63	-5.44
KAS10	0.05	9.68	7.53	-2.15	6.82	-2.86
KAS11	0.02	2.86	3.62	0.77	5.81	2.95
KAS12	0.04	8.14	6.11	-2.03	5.64	-2.5
KAS13	0.04	11.00	6.41	-4.59	3.70	-7.3
KAS14	0.05	6.59	7.54	0.95	3.79	-2.8
KAS15	0.01	0.86	3.09	2.23	4.00	3.14
KAS16	0.04	10.47	5.94	-4.53	3.75	-6.72
KAS17	0.03	10.62	4.98	-5.64	4.35	-6.27
KAS18	0.06	10.89	8.36	-2.52	3.64	-7.25
KAS19	0.04	9.21	5.77	-3.44	3.76	-5.45
KAS22	0.03	5.28	5.30	0.02	3.77	-1.51
KAS23	0.04	7.70	6.11	-1.59	4.28	-3.42
KAS26	0.01	1.90	3.32	1.42	3.65	1.75
KAS28	0.08	13.23	10.38	-2.84	3.59	-9.64
KAS29	0.06	10.23	8.88	-1.35	3.51	-6.72
DEN1	0.17	14.50	20.44	5.94	3.60	-10.9
DEN2	0.10	11.19	12.64	1.46	3.79	-7.4
DEN3	0.16	17.84	20.01	2.17	3.49	-14.35
DEN4	0.05	10.71	7.73	-2.98	3.69	-7.02
DEN5	0.10	11.33	12.56	1.24	3.61	-7.72
DEN6	0.14	12.91	17.54	4.64	3.67	-9.24

Sample	Am/P	Collagen wt. %	Lebon et al. (2016) equation	Offset	New equation	Offset
DEN7	0.11	15.73	14.49	-1.24	3.65	-12.08
DEN8	0.08	10.80	10.79	-0.01	3.37	-7.43
DEN9	0.07	7.42	9.92	2.50	4.17	-3.25
MEC1	0.07	14.76	9.89	-4.87	7.58	-7.18
MEC2	0.02	7.62	4.22	-3.40	4.58	-3.04
MEC3	0.02	7.01	3.96	-3.06	7.51	0.5
MEC4	0.03	4.45	5.10	0.65	4.91	0.46
MEC5	0.04	7.18	5.95	-1.23	5.97	-1.21
MEC6	0.07	19.84	9.24	-10.60	4.30	-15.54
MEC7	0.06	19.52	8.68	-10.83	9.07	-10.45
MEC8	0.13	16.27	15.91	-0.36	8.96	-7.31
MEC9	0.15	20.69	18.15	-2.53	9.00	-11.69
MEC10	0.06	12.94	8.66	-4.28	4.90	-8.04
MEC11	0.09	16.52	11.47	-5.05	7.51	-9.01
MEC12	0.07	19.48	9.91	-9.57	7.83	-11.65
MEC13	0.04	14.13	6.33	-7.80	9.02	-5.11
MEC14	0.04	15.93	5.92	-10.02	4.34	-11.59
MEC15	0.07	8.32	9.77	1.46	9.88	1.56
MEC16	0.04	12.74	6.01	-6.73	7.16	-5.58
MEC17	0.05	9.83	7.04	-2.79	6.66	-3.17
MEC18	0.02	7.22	4.39	-2.83	7.51	0.29
MEC19	0.07	15.59	9.11	-6.48	4.58	-11.01
MEC20	0.09	16.25	12.13	-4.13	12.00	-4.25
MEC21	0.17	21.71	21.01	-0.69	10.42	-11.29
MEC22	0.15	21.35	18.22	-3.13	5.53	-15.82

Sample	Am/P	Collagen wt. %	Lebon et al. (2016) equation	Offset	New equation	Offset
MEC23	0.11	18.44	13.98	-4.46	5.25	-13.19
MEC24	0.16	21.28	19.99	-1.29	6.45	-14.83
MEC25	0.08	11.85	11.12	-0.73	10.80	-1.05
MEC26	0.04	13.46	6.54	-6.92	10.22	-3.24
MEC27	0.04	14.40	6.16	-8.23	17.81	3.41
MEC28	0.04	9.87	6.27	-3.59	20.17	10.3
MEC29	0.03	9.64	4.96	-4.68	13.15	3.51
MEC30	0.05	12.60	7.54	-5.06	11.50	-1.1
MEC31	0.02	8.54	4.32	-4.22	7.75	-0.79
MEC32	0.02	5.89	4.44	-1.45	7.31	1.42
MEC33	0.03	6.65	4.58	-2.08	7.40	0.75
MEC34	0.02	6.16	3.90	-2.26	8.49	2.33
MEC35	0.06	9.38	8.81	-0.57	5.70	-3.68
MEC36	0.03	8.04	5.18	-2.86	10.66	2.62
MEC37	0.03	9.06	5.33	-3.73	23.17	14.11
MEC38	0.03	8.04	4.95	-3.09	20.23	12.19
MEC39	0.03	10.21	5.00	-5.21	15.78	5.57
MEC40	0.11	16.41	14.57	-1.83	22.09	5.68
MEC41	0.07	16.78	9.40	-7.38	7.96	-8.82
MEC42	0.05	17.72	7.52	-10.20	7.57	-10.15
MEC43	0.14	17.53	18.05	0.53	7.68	-9.85
MEC44	0.06	9.27	8.93	-0.34	6.31	-2.96
MEC45	0.02	10.85	4.25	-6.59	5.63	-5.22
MEC46	0.03	11.73	5.14	-6.59	5.76	-5.97
MEC47	0.04	7.21	5.66	-1.55	5.90	-1.31

Sample	Am/P	Collagen wt. %	Lebon et al. (2016) equation	Offset	New equation	Offset
MEC48	0.04	10.07	5.86	-4.21	5.19	-4.88
MEC49	0.05	11.53	7.65	-3.88	6.54	-4.99
MEC50	0.05	9.91	6.79	-3.12	6.69	-3.22
MEC51	0.06	13.44	8.11	-5.33	6.29	-7.15
MEC52	0.07	18.45	9.51	-8.94	6.35	-12.1
MEC53	0.12	14.93	14.91	-0.02	10.97	-3.96
MEC54	0.05	14.20	6.89	-7.31	8.99	-5.21
MEC55	0.04	15.81	6.42	-9.39	20.06	4.25
MEC56	0.03	5.51	4.80	-0.71	5.56	0.05
MEC57	0.02	8.99	4.50	-4.49	6.49	-2.5
MEC58	0.03	5.87	5.06	-0.81	7.05	1.18
MEC59	0.07	8.87	9.56	0.69	7.25	-1.62
MEC60	0.02	8.95	4.27	-4.68	9.13	0.18
MEC61	0.02	4.42	3.94	-0.48	8.23	3.81
MEC62	0.03	5.23	4.69	-0.54	9.61	4.38
MEC63	0.03	5.52	4.63	-0.89	11.09	5.57
MEC64	0.10	13.67	12.77	-0.90	7.84	-5.83
MEC65	0.08	18.79	10.60	-8.19	6.14	-12.65
MEC66	0.08	17.30	10.73	-6.57	5.82	-11.48
MEC67	0.02	4.41	4.25	-0.16	6.41	2
MEC68	0.03	9.73	5.22	-4.51	5.58	-4.15
MEC69	0.05	7.24	6.92	-0.32	5.23	-2.01
MEC70	0.03	10.57	5.02	-5.55	6.02	-4.55
MEC71	0.04	12.72	6.54	-6.18	5.95	-6.77
MEC72	0.06	14.71	8.08	-6.63	12.23	-2.48

Sample	Am/P	Collagen wt. %	Lebon et al. (2016) equation	Offset	New equation	Offset
MEC73	0.02	8.77	4.42	-4.35	12.37	3.6
MEC74	0.06	9.91	9.03	-0.88	5.56	-4.35
MEC75	0.05	9.05	6.94	-2.11	6.57	-2.48
MEC76	0.03	6.25	4.90	-1.35	6.36	0.11
MEC77	0.06	7.50	7.96	0.46	7.97	0.47
MEC78	0.04	10.31	6.41	-3.90	9.58	-0.73
MEC79	0.08	15.09	10.58	-4.51	5.74	-9.35
MEC80	0.12	20.93	15.37	-5.56	8.38	-12.55
MEC81	0.13	20.51	16.78	-3.73	6.24	-14.27
MEC82	0.11	20.19	14.54	-5.65	9.45	-10.74
MEC83	0.14	22.24	17.40	-4.84	7.83	-14.41
MEC84	0.04	10.07	6.39	-3.68	17.24	7.17
MEC85	0.03	4.88	4.84	-0.04	18.73	13.85
MEC86	0.02	6.69	4.30	-2.39	16.36	9.67
MEC87	0.02	8.14	4.26	-3.88	19.38	11.24
MEC88	0.08	1.58	10.86	9.28	6.18	4.6
MEC89	0.03	7.10	4.55	-2.55	5.61	-1.49
MEC90	0.04	14.47	6.12	-8.35	5.57	-8.9
MEC91	0.05	16.01	7.15	-8.86	5.88	-10.13
MEC92	0.03	10.75	5.47	-5.28	7.52	-3.23
MEC93	0.06	11.76	8.26	-3.50	8.60	-3.16
MEC94	0.03	5.39	5.14	-0.25	6.84	1.45
MEC95	0.03	6.06	4.82	-1.24	6.50	0.44
MEC96	0.02	5.48	4.46	-1.02	6.16	0.68
MEC97	0.03	4.57	5.54	0.97	5.78	1.21

Sample	Am/P	Collagen wt. %	Lebon et al. (2016) equation	Offset	New equation	Offset
MEC98	0.08	13.70	11.06	-2.64	6.91	-6.79
MEC99	0.05	8.93	7.70	-1.23	9.19	0.26
MEC100	0.15	19.36	18.49	-0.87	20.52	1.16
MEC101	0.02	6.38	4.41	-1.97	5.73	-0.65
			Average:	-1.70		-0.014
			St. Deviation:	3.67		8.15

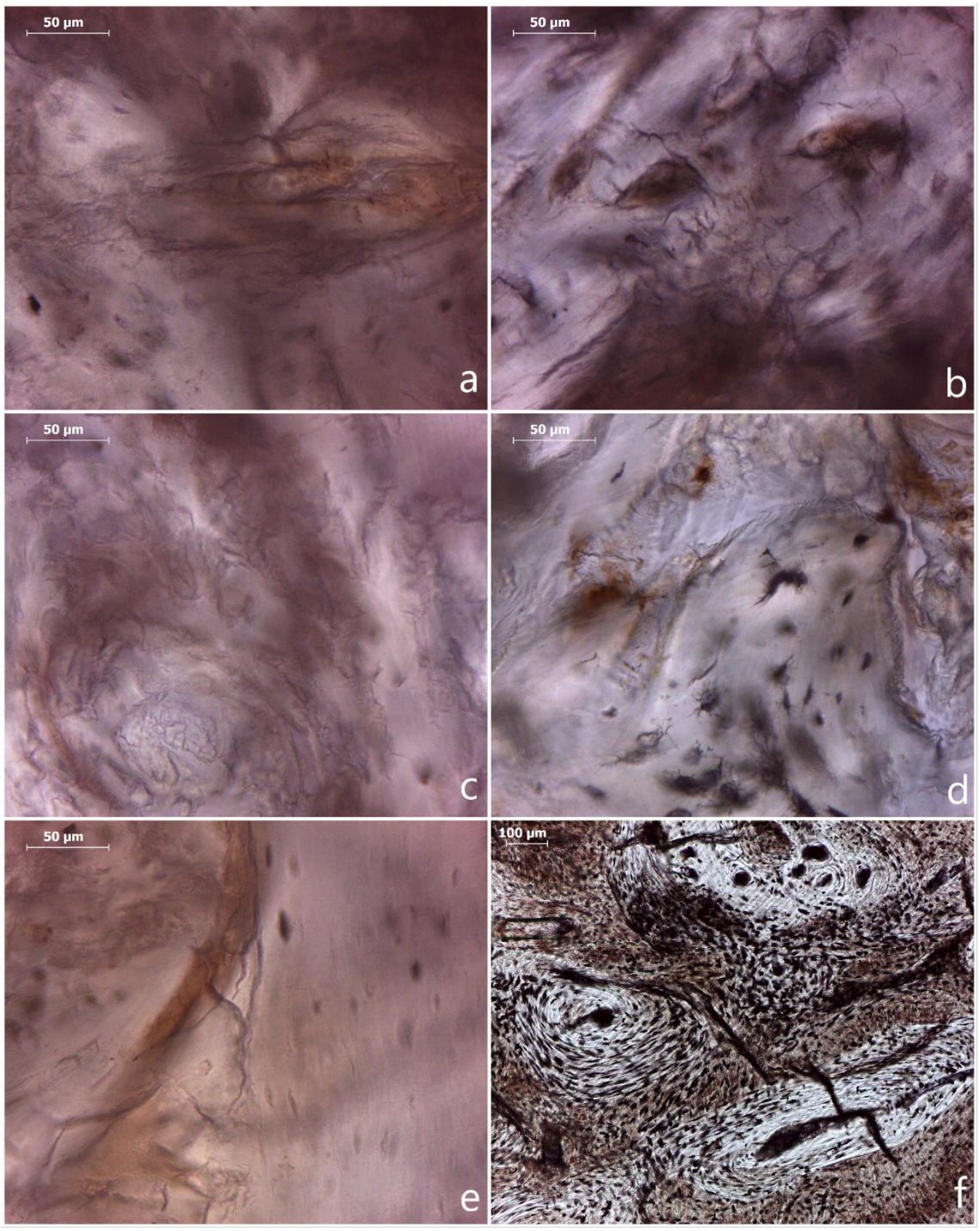

Figure B1. *Microcracking in petrous bone*. **(a) MEC44 Longitudinal PPL 400x – single burial, no coffin. (b) MEC79 Longitudinal PPL 400x - single burial, no coffin. (c) MEC59 Longitudinal PPL 400x - single burial, coffin (d) MEC25 Longitudinal PPL 400x - single burial, coffin. (e) MEC64 Longitudinal PPL 400x – multiple burial, no coffin (f) DEN1 Longitudinal PPL 100x**.

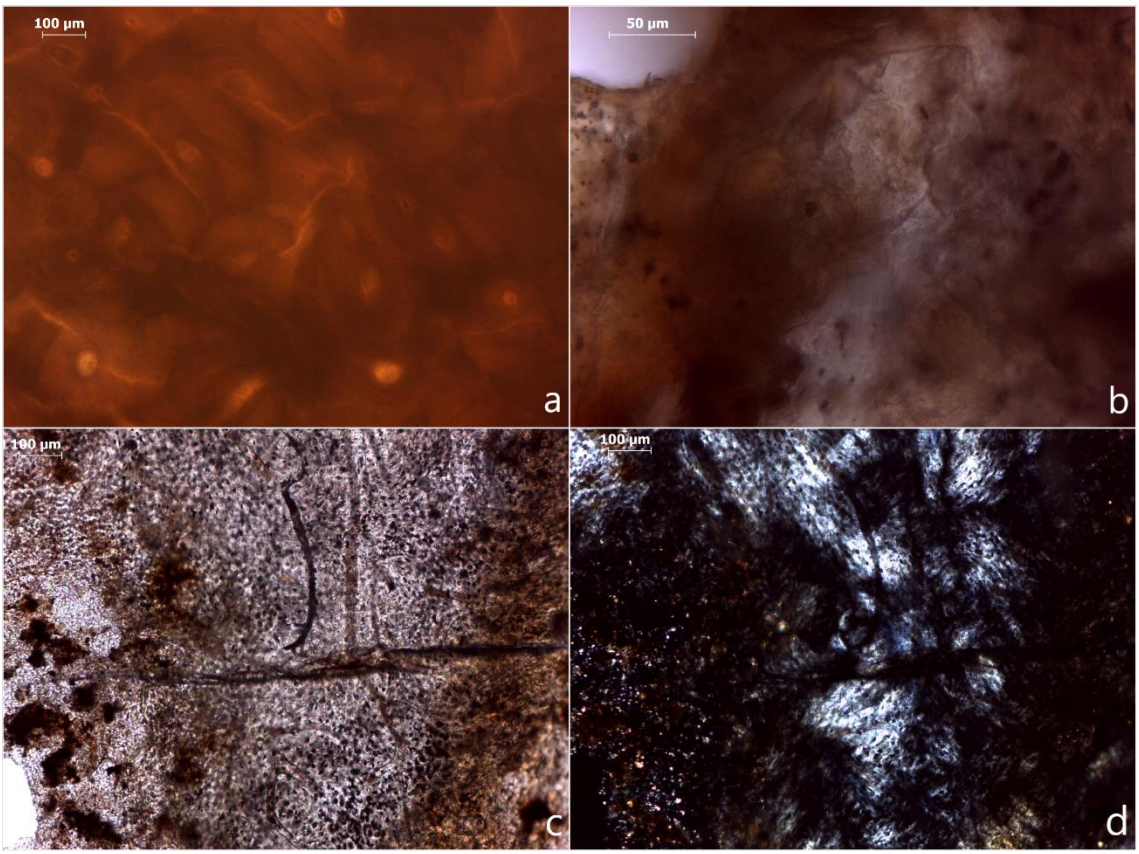

Figure B2. *Petrous bone staining and inclusions due to interaction with groundwater*. **(a) MAR1 PPL 100x, (b) MEC15 Longitudinal PPL 400x, (c) DEN2 Longitudinal PPL and (d) XPL – 100x.**

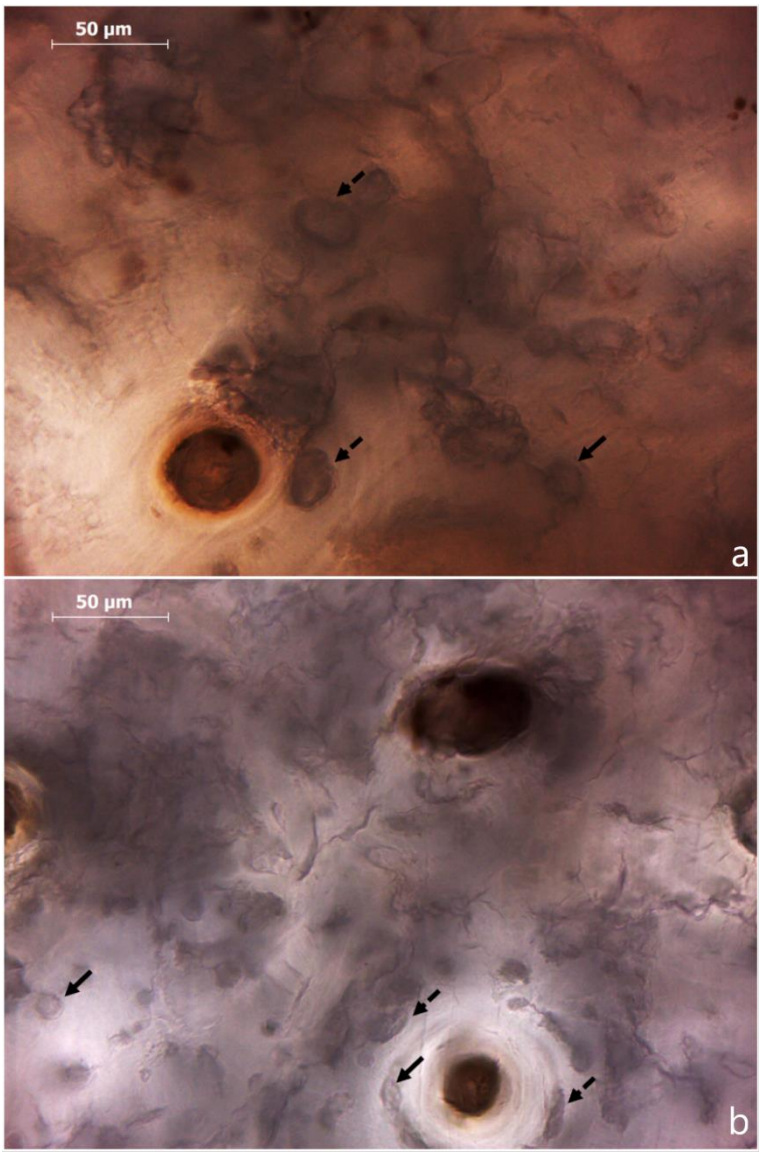

Figure B3. *MFD in Kastrouli human femora*. **(a) KAS3 Transverse PPL 400x; (b) KAS4 Transverse PPL 400x** (black arrows: linear-longitudinal MFD; dashed black arrows: budded MFD).

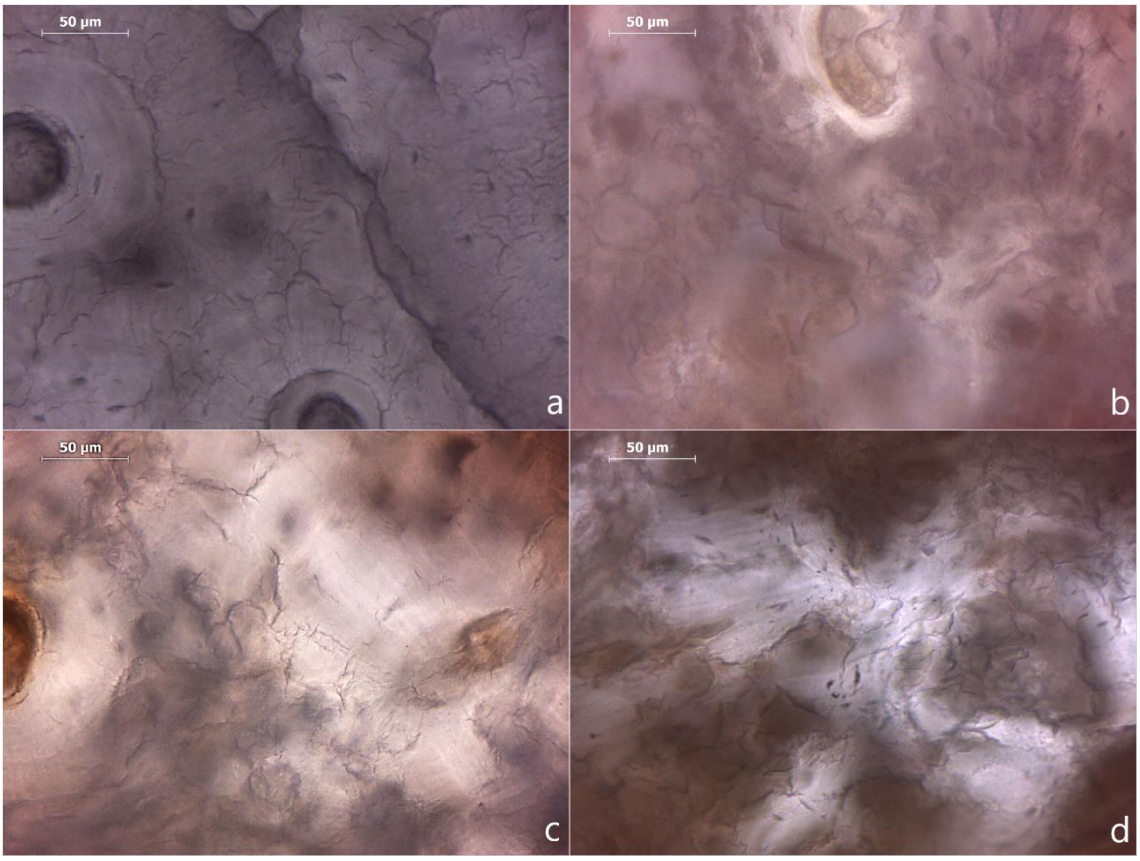

Figure B4. *Microcracking in human femora*. **(a) SAR13, (b) MAN3, (c) KAS12, and (d) MEC2 Transverse PPL 400x**.

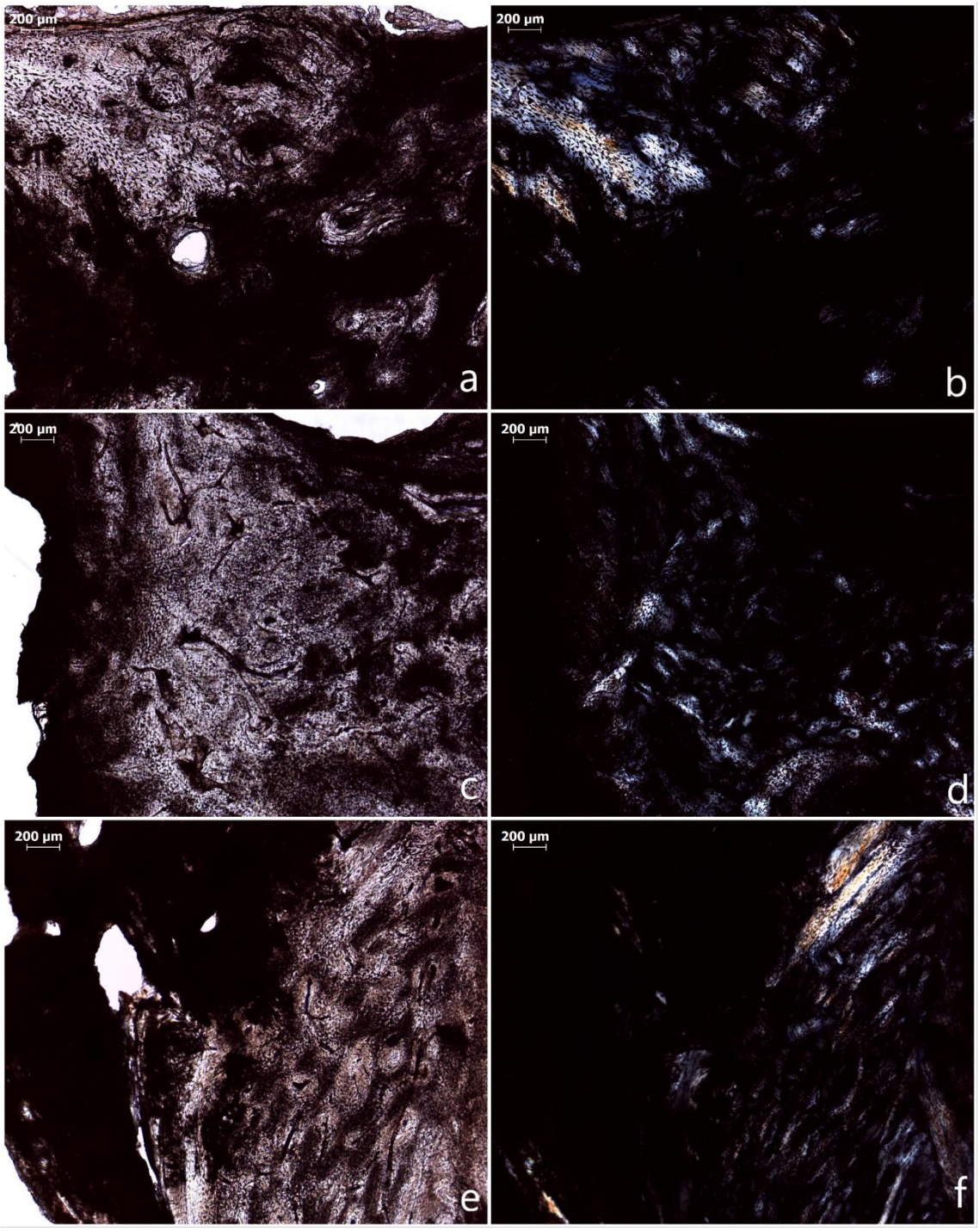

Figure B5. *Inter-site variations in petrous bone histological preservation*. **DEN4 Transverse (a) PPL 40x and (b) XPL 40x**: generalized destruction across a wide area of endosteal and inner periosteal tissue and well-preserved outer periosteal tissue that can in areas extend towards the mid-cortical area. Except for the well-preserved tissue, small islands of mid-cortical tissue retain their microarchitectural characteristics and collagen birefringence. **KAS16 Longitudinal (a) PPL 40x and (b) XPL 40x**: degraded outer periosteal and endosteal bone matrix with well-preserved mid-cortical bone. Collagen birefringence can be seen only in mid-cortical region. **MEC93 Longitudinal (a) PPL 40x and (b) XPL 40x**: generalized destruction observed only in the outer periosteal tissue, while the inner periosteal and endosteal regions exhibit good histological preservation.

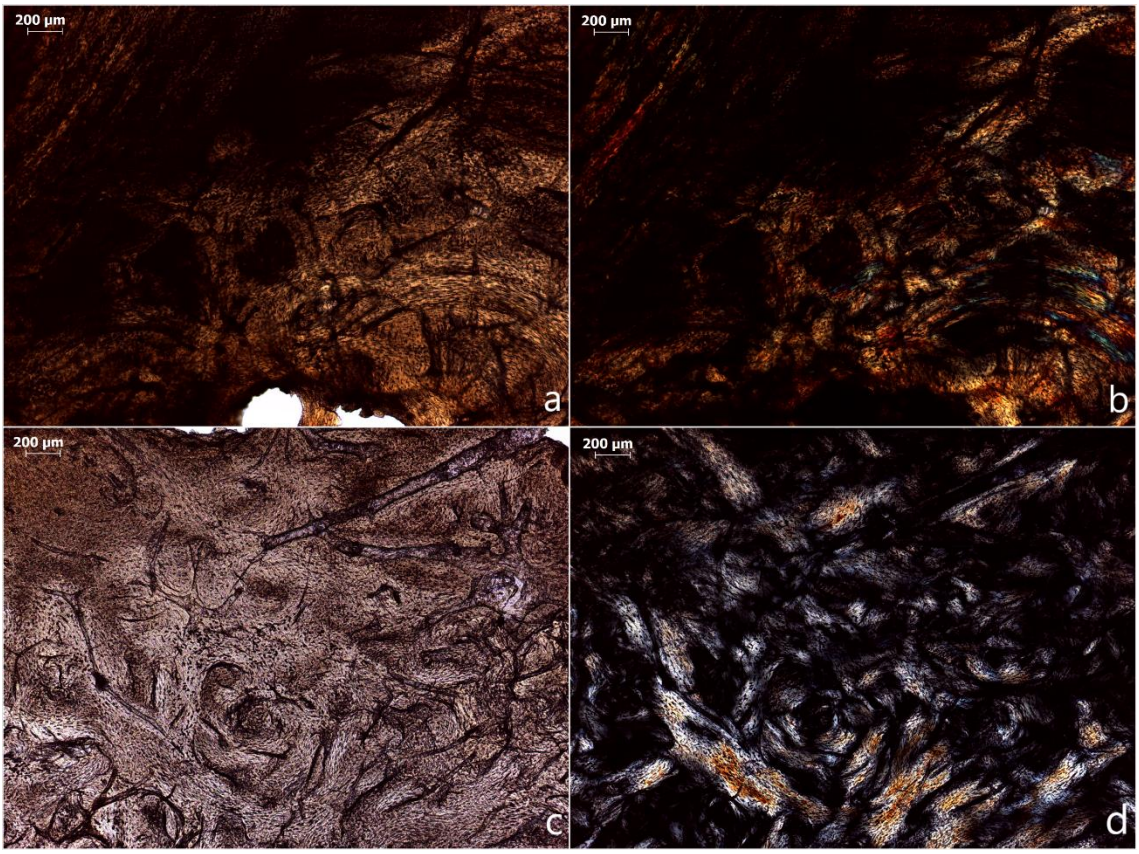

Figure B6. *Intra-site variations in petrous bone histological preservation.* **KAZ1 Transverse (a) PPL 40x and (b) XPL 40x**: poor preservation with only a small endosteal/inner periosteal area surviving. Note the absence of birefringence and the inclusions in XPL. **KAZ2 Transverse (a) PPL 40x and (b) XPL 40x**: well-preserved micro-architecture and collagen birefringence with no signs of generalized destruction.

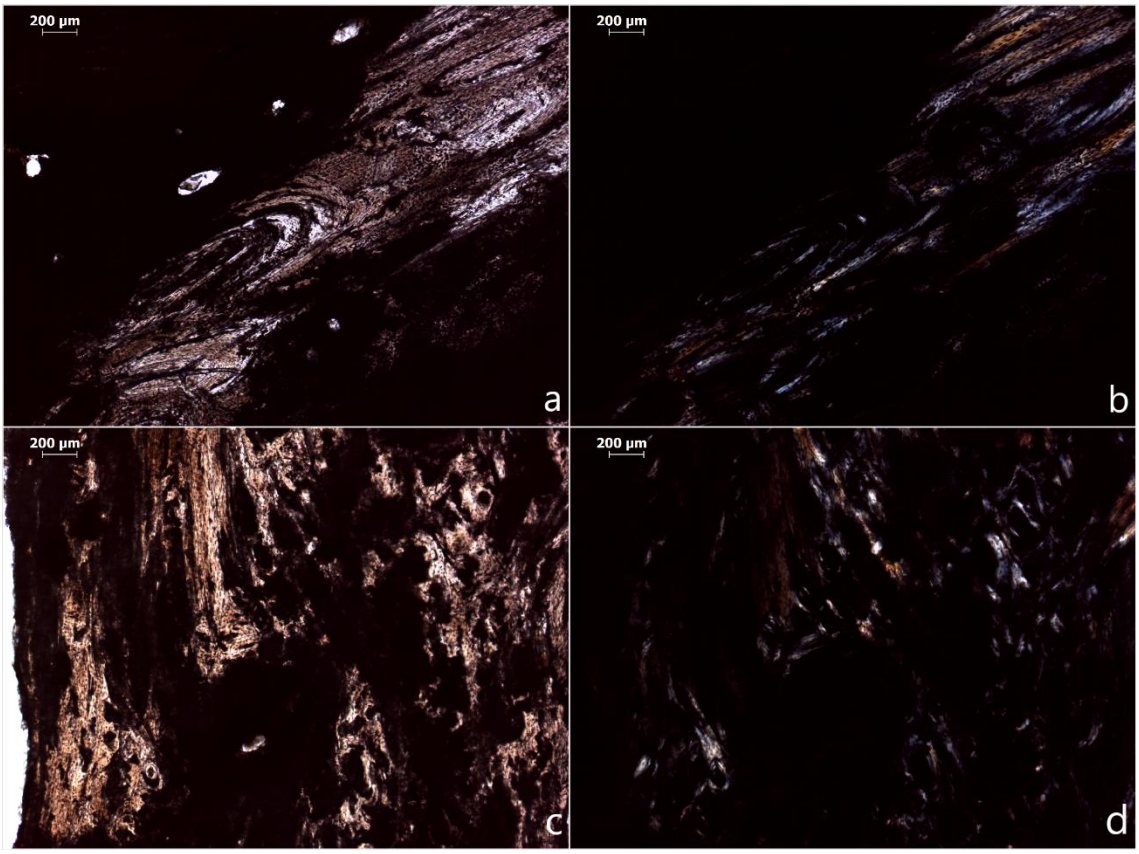

Figure B7. *Intra-site variations in petrous bone histological preservation.* **MEC69 Transverse (a) PPL 40x and (b) XPL 40x**: generalized destruction across the entire section with a mid-cortical zone retaining its histological integrity and collagen birefringence. **MEC74 Longitudinal (c) PPL 40x and (d) XPL 40x**: interchanging areas of well-preserved and degraded bone tissue. The degraded areas are characterized by loss of birefringence.

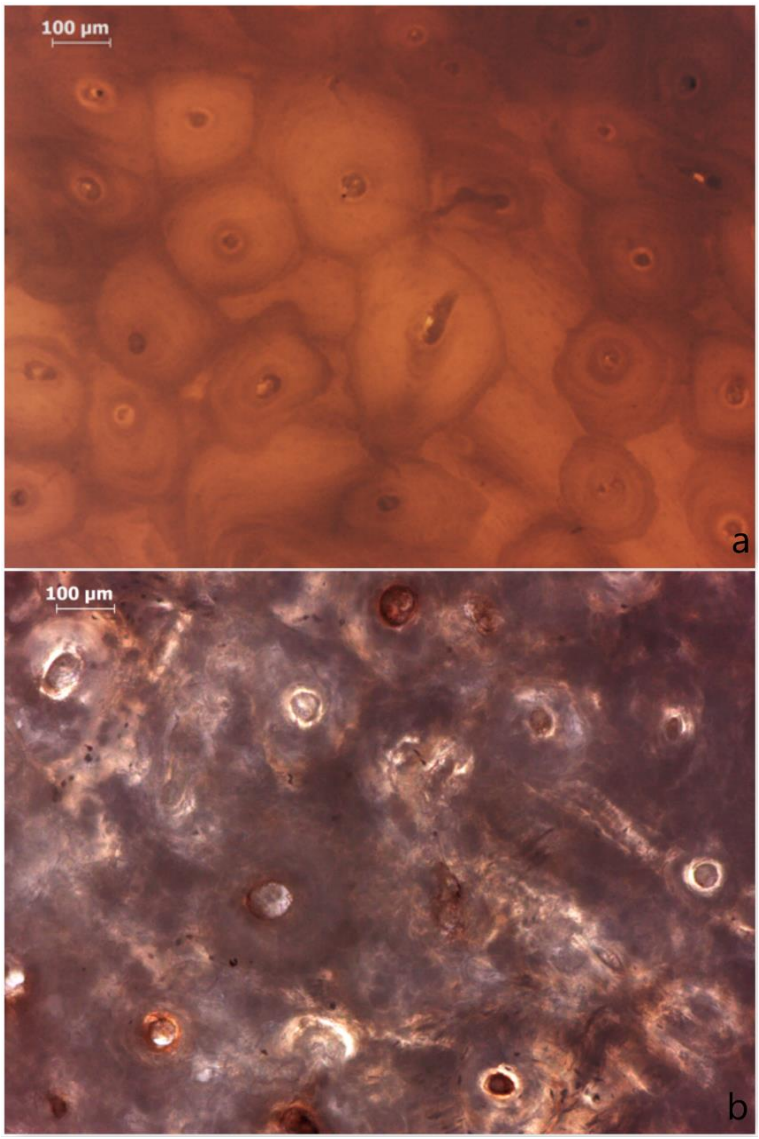

Figure B8. *Intra-site variations in histological preservation of Mamika long bones*. **(a) MAN8 Transverse PPL 100x – Humam humerus (proximal diaphysis)**: excellet microscopic preservation with signs of fossilization. **(b) MAN3 Transverse PPL 100x – Humam femur (mid diaphysis)**: poor preservation characterized by an almost complete loss of its histological features.

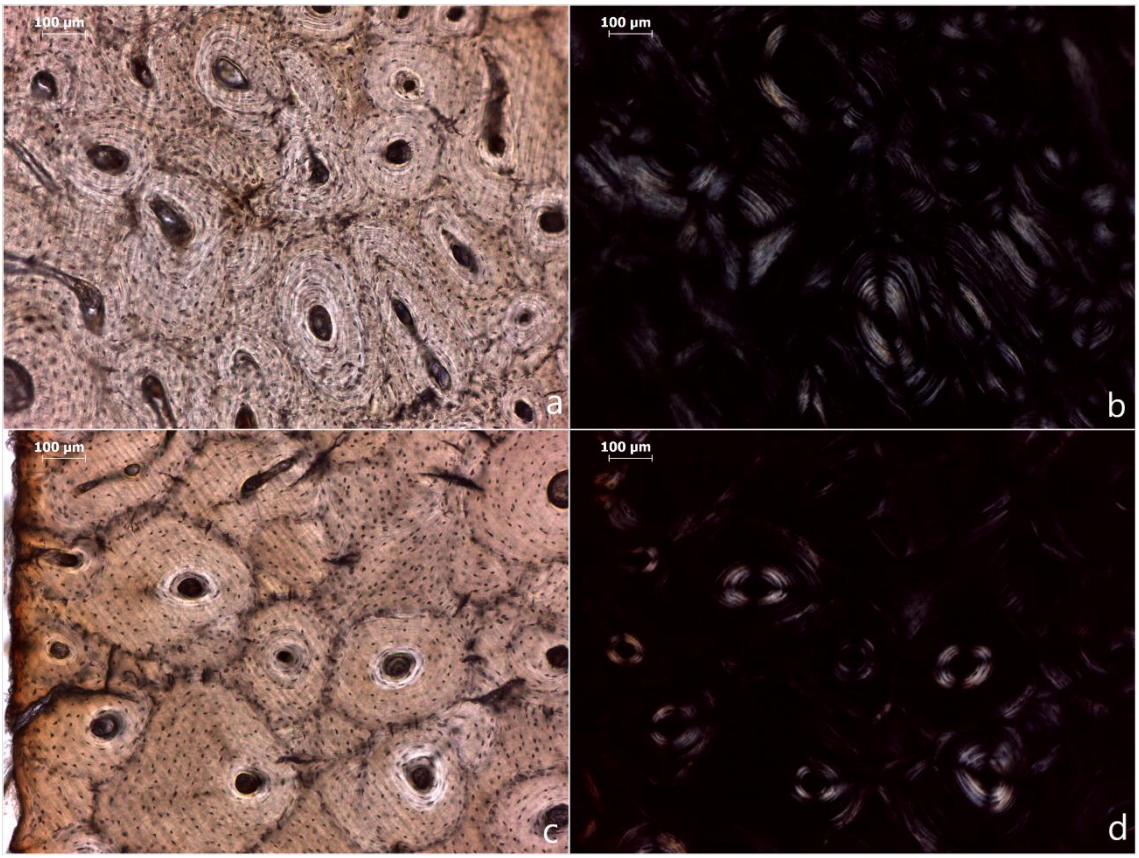

Figure B9. *Excellent histological preservation of individual no.5 from St. Rombout*. **MEC22 Transverse (a) PPL 100x and (b) XPL 100x – Human humerus and MEC24 Transverse (c) PPL 100x and (d) XPL 100x – Human radius**: the only individual from a single coffined burial in this assemblage that displays excellent histological preservation.

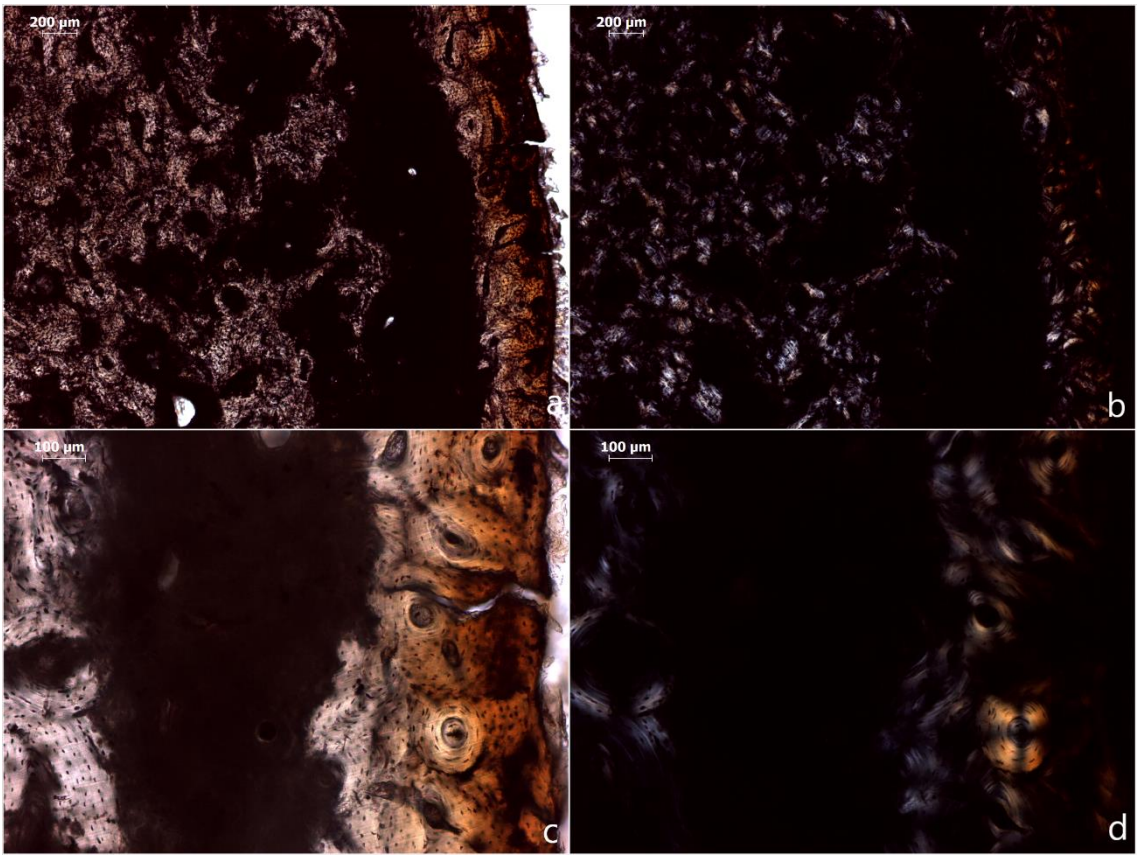

Figure B10. *Degradation pattern similar to Cladh Hallan and Bradley Fen 'mummified' human femora*. **MEC52 Transverse (a) PPL 40x, (b) XPL 40x, (c) PPL 100x, (d) XPL 100x**.

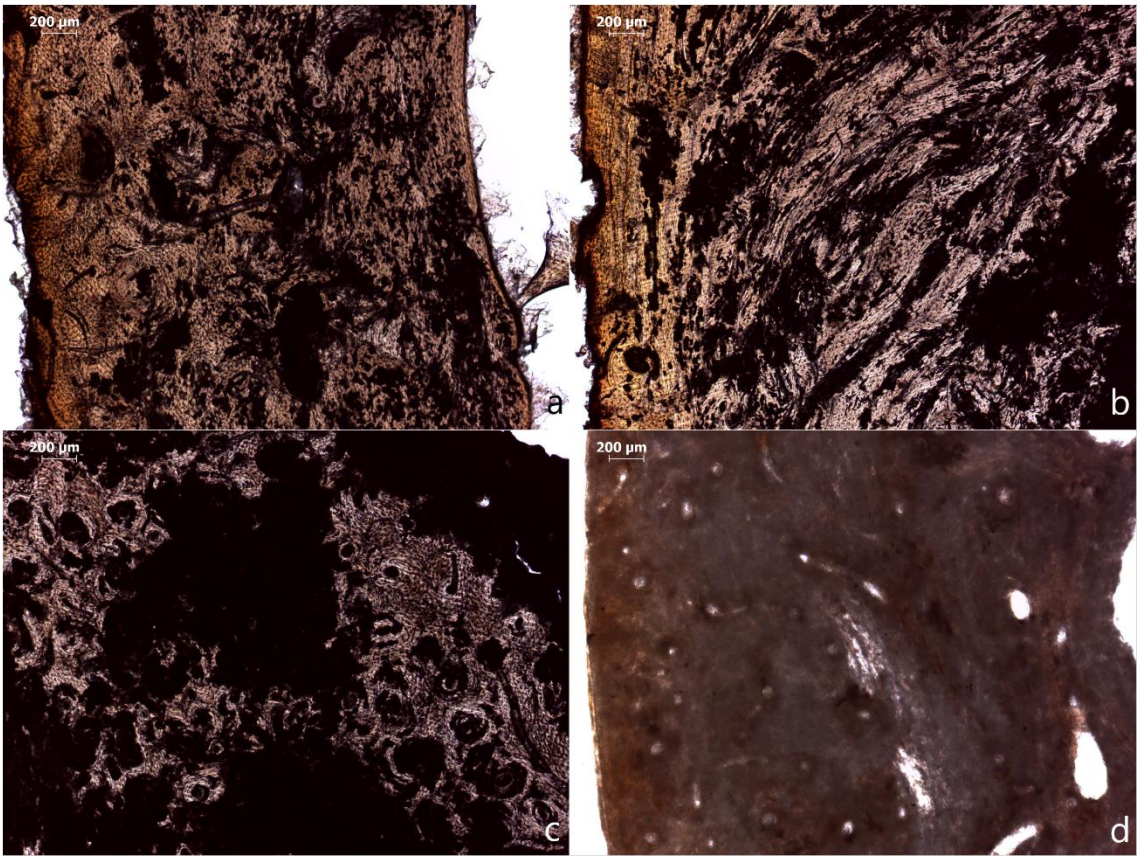

Figure B11. *Intra-bone variations in histological preservation of long bones*. **(a) MEC6 Transverse PPL 40x – Human humerus (proximal diaphysis) and (b) MEC7 Transverse PPL 40x – Human humerus (distal diaphysis):** samples display similar histological preservation. **(c) MEC55 Transverse PPL 40x – Human femur (proximal diaphysis) and (b) MEC56 Transverse PPL 40x – Human femur (distal diaphysis)** samples show distinct differences in histological preservation.

1. KENDALL, C., ERIKSEN, A. M., KONTOPOULOS, I., COLLINS, M. J., AND TURNER-WALKER, G. (2018). DIAGENESIS OF ARCHAEOLOGICAL BONE AND TOOTH. *PALAEOGEOGRAPHY, PALAEOCLIMATOLOGY, PALAEOECOLOGY, 491, 21-37*

Abstract

An understanding of the structural complexity of mineralised tissues is fundamental for exploration into the field of diagenesis. Here we review aspects of current and past research on bone and tooth diagenesis using the most comprehensive collection of literature on diagenesis to date. Environmental factors such as soil pH, soil hydrology and ambient temperature, which influence the preservation of skeletal tissues are assessed, while the different diagenetic pathways such as microbial degradation, loss of organics, mineral changes, and DNA degradation are surveyed. Fluctuating water levels in and around the bone are the most harmful for preservation and lead to rapid skeletal destruction. Diagenetic mechanisms are found to work in conjunction with each other, altering the biogenic composition of skeletal material. This illustrates that researchers must examine multiple diagenetic pathways to fully understand the post-mortem interactions of archaeological skeletal material and the burial environment.

Keywords: Bone diagenesis, environment, bioerosion, collagen, hydroxyapatite, ancient DNA

1. Introduction

The survival of biomolecules in archaeological and fossil bone has attracted the attention of a great number of researchers over the past few decades. The post-mortem preservation of bone, however, depends upon a number of complex processes. Thus, some bones survive well, whilst others degrade rapidly. Here we attempt to survey the major ways in which skeletal tissues, specifically those made of mineralised collagen (bone and dentine), become transformed following deposition in the archaeological or geological record, a process known as diagenesis.

2. Chemistry and structure of bone and tooth dentine

2.1. Skeletal tissues

Bone is a composite material made up of both organic and inorganic components, and water. The fibrous protein, collagen, makes up the vast majority of the organic fraction, and carbonated hydroxyapatite (or HAp) comprises the inorganic, or mineral, fraction (Currey, 2011; White et al., 2012). Bone is only one of several vertebrate collagenous tissues that are strengthened and hardened in vivo by the precipitation of poorly-soluble inorganic minerals - a process that in technical terms is called biomineralisation. In mammals the other mineralised tissues include antler, dentine and cementum which all share a common chemistry – collagen, HAp and water in various proportions – but they have different microarchitectures and modes of growth. Consequently they share similar diagenetic histories. Tooth enamel, which differs from the other

mineralised tissues in its mode of formation - protein scaffolding is removed and replaced with mineral - has an extremely low porosity and low organic content. It is typically, therefore, much more resistant to diagenesis and does not form part of this review.

The percentage of organic and water by weight of the various mineralized tissues differs depending upon species and skeletal element (Fig. 1). Oven-dried human bone has approximately 26 wt. % organic matter, with 9-10 wt. % water and 64 wt. % mineral, which can be compared to bovine bone, as an example, which has a makeup of 24 wt. %, 8 wt. % and 68 wt. %, respectively (Zioupos et al., 2000). In terms of volume percent, the relative proportions of collagen/water and mineral roughly proportional due to the higher density of hydroxyapatite (bulk density 2.8, He et al., 2010) than either dry collagen (bulk density 1.4, Podrazký and Sedmerová, 1966) or water (bulk density 1). Reptiles and marine mammals are typically less heavily mineralised than terrestrial mammal bone (Rogers and Zioupos, 1999; Zioupos et al., 2000). Although sperm whales and sea lions have a higher mineral content than humans, fin whales have less well mineralised bones and fish considerably less so, with as little as half the mineral content as land mammals (Tont et al., 1977).

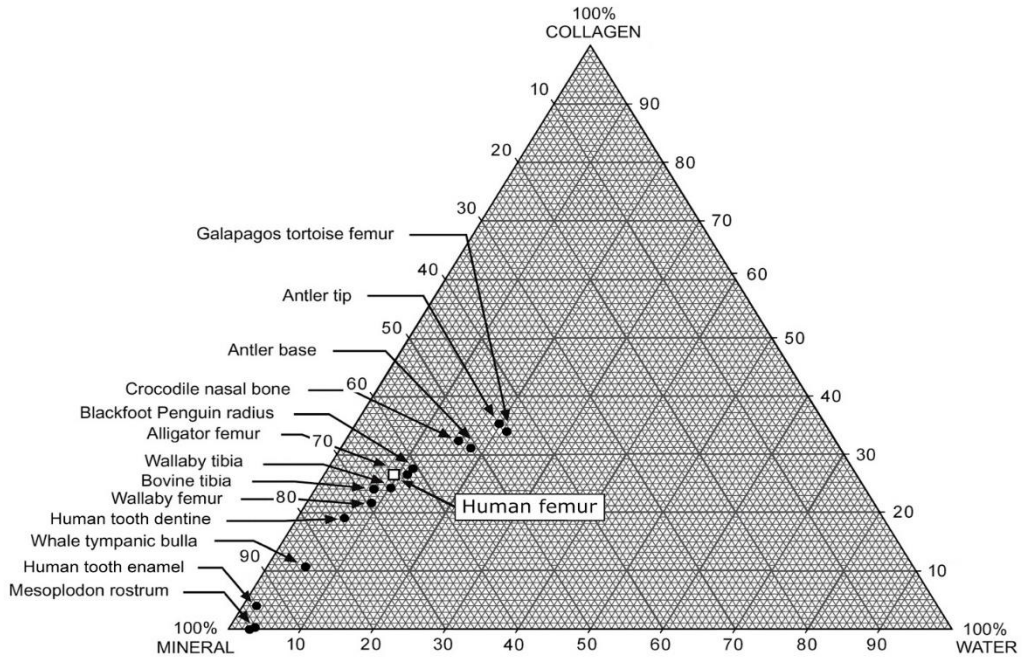

Figure 1. Relative proportions (as weight %) of collagen, mineral and water for a range of species and tissues. (Diagram adapted from Zioupos et al. 2000).

Amongst land mammals, the collagen content ranges from approximately 35% for deer antler to only around 21% for wallaby femur. Some highly specialized bony elements such as the bulla tympanum and rostrum of whales are almost totally mineralized with only 11 %, and <1% collagen, respectively (Zioupos et al., 2000). Bird bones are stronger and have higher densities

(Dumont, 2010) but it is unclear whether this truly reflects a higher proportion of mineral or simply a lower porosity (Schuhmann et al., 2014). Amongst humans, the highly mineralised petrous portion of the temporal bone is attracting attention due to the often high levels of protein and endogenous DNA that can survive in archaeological specimens compared to non-petrous skeletal elements (Gamba et al., 2014; Jørkov et al., 2009). Different species and different skeletal elements not only have differing mineral contents but exhibit a variety of microarchitectures as revealed by histological examination. These reflect the speed and pattern of growth but also the mechanical loads placed upon the various tissues. These are discussed in greater detail below.

2.1.1 Collagen

The organic portion of bone is composed largely of Type I collagen, which accounts for approximately 90% of the organic fraction of bone, the remainder being composed of non-collagenous proteins – including bone sialoproteins (Termine, 1988) and osteocalcin (Lian et al., 1978; Price et al., 1976) – various lipoproteins, and mucopolysaccharides (Morgan et al., 2013; Ortner and Turner-Walker, 2003; Tuross, 2003). Collagen is a fibrous protein and the dominant structural protein in most eukaryotes, although (a similar Gly-Xaa-Yaa motif is found in prokaryotes, Yu et al., 2014). The glycine-triad polypeptide chain found in the procollagen molecule, typically depicted as Gly-Xaa-Yaa, is a repetitious sequence in which every third position is glycine (Gly), while the Xaa and Yaa positions are typically found to be the amino acids proline or lysine (Whitford, 2013), which reflect the structural constraints of the polyproline motif. The constituent amino acids confer a structural twist to the peptide bonds, and thus, to the final procollagen molecule. Because each side chain is offset 120° from the preceding residue, every third residue has to be Gly, since the side chain of larger amino acids cannot be accommodated when the side chain is facing in towards the centre of the helix.

Two different polypeptides make up the Type I collagen triple helix, known as tropocollagen. Two of the chains are denoted as α1 (I) the third is the α2 (I) chain (Garnero, 2015; Orgel et al., 2006). A high percentage of the Yaa position prolines are hydroxylated but only a handful of those in the Xaa position (Eyre et al., 2011). These hydroxylation reactions are catalyzed by two different enzymes: prolyl-4-hydroxylase and lysyl-hydroxylase. Although the structural advantage of this hydroxylation is still unclear (Shoulders and Raines, 2009), hydroxylation in the Xaa position does show evidence of stabilization and maintenance of the triple-helix structure (Jenkins et al., 2003; Vitagliano et al., 2001). Furthermore, if the amino acid sequence is changed, for example by a mutation in the relevant gene, or hydroxylation is incomplete as a result of absence of catalytic enzymes or cofactors, then the resulting disruption and destabilisation of the collagen fibrils gives rise to diseases such as osteogenesis imperfecta and scurvy (Bentley and Jackson, 1965).

Collagen also forms cross-links with adjacent collagen molecules. Cross-links are the byproduct of collagenic lysine and hydroxylysine ε-amino group conversion into aldehydes, which through

a reaction with lysyl oxidase, form a connection with adjacent collagen molecules (i.e. a cross-link) that are easily reducible (Tanzer, 1973). However, these reducible cross-links diminish and make way for pyridinoline cross-links in matured bone (Eyre et al., 1988; Uchiyama et al., 1981). Pyridinoline cross-links are characterized through a stabilization process brought about after the intermolecular bonds of younger collagen fibrils and cross-links become reduced (Robins et al., 1973). There are two types of pyridinoline cross-links, hydroxylysyl-pyridinoline and lysyl-pyridinoline, where the hydroxyl form is found predominantly in internal connective tissues, and the latter form is typically seen in bone and dentin (Hanson and Eyre, 1996). Most lysyl-pyridinolines are concentrated at the N-telopeptide site of collagen, while only 33% are seen at the C-telopeptide sites (Hanson and Eyre, 1996).

Cross-links not only stabilise the collagen matrix in vivo. Post mortem cross-linking of collagenous tissues, either intentionally during the tanning of leather or incidentally as in the formation of bog bodies in sphagnum bogs, increases the shrinkage temperature of the collagen but also renders it less susceptible to fungal and bacterial degradation (Painter, 1991, 1983). This has obvious implications for diagenesis and collagen-humic interactions will be discussed further below.

Tropocollagen molecules, each around 300 nm in length and 1.5 nm in diameter, spontaneously self aggregate extra-cellularly into fibrils with mean diameters of around 50 nm (Tzaphlidou and Berillis, 2005). The intermolecular bonds are such that there is an offset in the alignment between adjacent molecules with the result that there are gaps between the head of one molecule and the tail of the previous one. This permits the creation of fibrils that are much longer than individual tropocollagen molecules. The molecules interdigitate in such a way that there are gap zones (where there is high density of gaps) and overlap zones where the molecules are well aligned and more closely packed. The 40 nm gap zone together and the 27 nm overlap zone give rise to the 67 nm banded appearance of collagen fibrils seen in TEM images, experimentally mineralization of reassemble fibrils is initiated in this gap region (Nudelman et al., 2013/8)

2.1.2 Apatite

The inorganic portion of living bone is a non-stoichiometric, carbonate-substituted form of geologic hydroxyapatite containing traces of F, Na, Mg, Zn and Sr, hereafter referred to as bioapatite or simply HAp (Mathew and Takagi, 2001; Ortner and Turner-Walker, 2003). Bioapatite has different crystal size, composition and atomic disorder than geologic apatites that form hydrothermally (Boskey, 2007, 2003). If basic calcium phosphate is precipitated from a solution containing carbonate or hydrogen carbonate, at room temperature the product is an apatite that invariably contains carbonate up to a few percent and these apatites are of a similar small size to bone mineral. In fact, strictly carbonate-free solutions and a thorough purging of the laboratory apparatus with nitrogen are required if pure hydroxyapatite is to be precipitated (Posner, 1985). Even in mature bone, the crystallites of bone mineral are exceedingly small, with

estimated lengths of 16-50 nm, widths of 8-20 nm and thickness c. 2 nm (Eppell et al., 2001; Glimcher, 2006). However, there remains active debate regarding the shape and organization of crystallites in bone (e.g. Georgiadis et al., 2016; Reznikov et al., 2015; Schwarcz, 2015). Their vanishingly small size, combined with the various substitutions and surface adsorbed ions that occur in the non-apatitic hydrated layer, which covers the core of apatite, are responsible for the poor ordering and crystallinity of bioapatite (Figueiredo et al., 2012) and their consequent higher solubility than geologic apatites (Sillen and LeGeros, 1991).

Size, shape and composition of the bioapatite crystals are affected by several intrinsic and extrinsic factors including collagen properties and the distribution of non-collagenous proteins, which are involved in the nucleation and growth of crystals, diet, disease, cell viability and bone turnover (Boskey, 2007, 2003). With reference to crystals' size and orientation in normal living bone, these are controlled by the structure and organization of the collagen fibrils, while size and shape are also regulated by non-collagenous proteins such as phosphorylated proteins, glycoproteins, and proteoglycans (Boskey, 2007, 2003; Duer and Veis, 2013). Changes in crystal size and homogeneity also affect bone mechanical properties, with an increase being either related with an incorporation of ions into the smaller crystals, merging of existing crystals, or secondary nucleation/mineralization (Boskey, 2003).

Early study of crystallite change *in vivo* show that in rat bone aged two weeks to one year, older bone had an increase in the crystal size and disorder of the crystal lattice (Matsushima and Hikichi, 1989). In mammals, mature bone is both more heavily mineralised and the mineral is more crystalline compared to recently deposited tissues due to carbonate substitutions and a reduction of the hydrated layer that result in a more stoichiometric structure (Figueiredo et al., 2012). Carbonate ions (3-8 wt.%) may either replace OH^- (type A apatite) or PO_4^{3-} (type B apatite) ions in the crystal lattice (Figueiredo et al., 2012; Lee-Thorp and van der Merwe, 1991; Stathopoulou et al., 2008). These ionic substitutions are responsible for the crystal disorder as the replacing ions and molecules may differ in size, configuration, and charge compared to the ions and molecules they are substituting (Yotam Asscher et al., 2011).

Primary sites of mineral deposition are in the gap zones and that subsequent mineralisation takes place between tropocollagen molecules (in the overlap zone) and in intra-fibrillar spaces (Fratzl et al., 1991; Nudelman et al., 2013/8). Full mineralization is accomplished by the replacement of water within and between collagen fibrils by HAp, with small crystallites developing both within and on the surfaces of the collagen, with the bulk of the mineral load being deposited between fibrils and fibre bundles. Thus, as the volume of the mineral in bone tissue increases, the volume of water decreases correspondingly. Collectively, in dry, mature bone, collagen and bioapatite each account for 46% of the volume of bone, while water makes up the remaining 8% (Todoh et al., 2009). Water plays an important role in stabilising the collagen molecule and it has long been known that the mechanical properties of bone are strongly dependent on its hydration state (Duer

and Veis, 2013; Nyman et al., 2006). Furthermore, mineralised tissues swell and shrink with the adsorption and desorption of water into their structure, predominantly as a result of water entering the collagen fibrils. Although the bulk of the volumetric changes occur at right angles to the long axis of the collagen molecules there is evidence that the lengths of fibrils change slightly as the gap zone is filled or emptied (Habelitz et al., 2002).

2.2 Bone tissue organization

As stated previously, the mineralised collagen in vertebrates is found with a variety of tissue types and microstructural organisation. The three-dimensional architecture of these different tissue types reflects the growth, function, vascularity and especially speed of growth of the bone. These variations have been discussed at length by two giants of the study of comparative histopathology, Donald Endelow and Armand de Ricqlès (de Ricqlès, 2011, 2007). There are even instances of bone in certain fishes that is completely acellular, lacking the osteocytes found in the bone of all living tetrapods (Shahar and Dean, 2013).

The two most commonly found types of bone tissue in adult mammals are cortical (compact) and cancellous (spongy) bone (Ortner and Turner-Walker, 2003; Weiner et al., 1999; White et al., 2012). Cancellous bone is much more porous and it is typically found at the jointed ends of long bones, as flat plates in the cranium, sternum, and ilium, and underlying tendon attachments (Weiner et al., 1999; White et al., 2012). Cortical bone is primarily found along the diaphysis of long bones, the petrous pyramid and the mandible, and as a thin outer sheath at the ends of long and flat bones (Ortner and Turner-Walker, 2003; White et al., 2012).

Bone undergoes several stages of development over an organism's lifespan. Initial, rapidly-growing bone, which is typically found in foetal development through early childhood, but also found in healing fractures and in certain bone tumours, takes the form of woven or fibrous bone and it is characterized by being less dense with greater histological disorder compared to more mature tissues (Manilay et al., 2013). It is gradually resorbed and replaced by appositional growth of lamellar bone, where layers of new bone stack over one another with a microarchitecture analogous to plywood, or by Haversian bone where specialised teams of cells replace old bone tissues with new bone (Ortner and Turner-Walker, 2003). This remodelling of bone throughout life is controlled by a number of factors, including hormonal triggers that are themselves influenced by diet, reproductive status, exercise and mechanical loading (Kini and Nandeesh, 2012; Robling et al., 2006). Medical literature commonly states a bone remodelling rate of approximately 10% per year, often without reference (e.g. Lerner, 2016). Despite this medical truism, based upon markers of bone turnover measured in body fluids, is shown to be 4-10 times higher than the directly measured rate of turnover in cortical bone assessed measuring either the steady increase in levels of racemization (Ritz-Timme et al., 1999; Ritz-Timme and Collins, 2002) or the incorporation of bomb pulse 14C (Hedges et al., 2007). Similar slow levels of turnover

have also been reported for cartilage using direct bomb pulse 14C measurements (Heinemeier et al., 2016; Libby et al., 1964).

2.3 Dental tissues

Mammalian teeth contain four dental tissues. With the exception of pulp, three of these are mineralised (hard) tissues: enamel, dentine (dentin), and cementum (Hillson, 2005). Compared to enamel, tooth dentine is more similar to bone tissues in terms of organic to inorganic ratios (Hillson, 2005) and protein composition (Alves et al., 2011; Jágr et al., 2012; Park et al., 2009; Salmon et al., 2016). Whereas human enamel contains only 5.9 % organic matter and 2.0 % water, dentine contains 19.2 and 6.5 %, respectively (Teruel et al., 2015). Like bone, dentine contains trace amounts of non-collagenous organic matter (mucopolysaccharides, lipoproteins, etc.) collectively called ground substance (Hillson, 2005). Ivory is essentially the dentine of any large mammal including elephant, mammoth, sperm whale and walrus tusks from which objects can be carved, but also includes narwhal, hippo and wild pig teeth which are suitable only for smaller items. Cementum is the most variable portion of a tooth coating the entire tooth in some mammals, but in others, it may cover just the root (Hillson, 2005). Generally, the thickness of the cementum layer increases with age of the individual and, histologically, cementum has a structure very similar to bone (Elliott, 2002; Hillson, 2005) and has been shown, like the petrous portion, to be a good source of ancient DNA (Adler et al., 2011; Hansen et al., 2017). Enamel is the hardest, densest and least porous of the mineralised tissues, and consequently, it is the most durable of human tissues. In some environments, the enamel tooth crowns survive where all other traces of the skeleton have been destroyed by chemical or microbial attack (Kimbel and Delezene, 2009; Zanolli, 2013). Nevertheless, tooth enamel does undergo diagenesis over timescales relevant to the study of human origins and palaeontology, especially in the study of trace elements and stable isotope content (Gehler et al., 2011; Pellegrini et al., 2011; Tütken et al., 2008; Tütken and Vennemann, 2011).

3. Porosity of mineralised tissues

The porosity of mineralised tissues influences the speed and nature of post-mortem alterations to bones and teeth. The diameter and interconnectedness of the various pores determines the ease with which water, microorganisms, and dissolved ions enter and leave the tissue (Hedges and Millard, 1995). As the most common mineralised tissue in the archaeological record we should look at bone first. Bone is a living tissue containing blood vessels and nerves that enter the bone via one or more relatively large nutrient foramina where they branch into Haversian canals running the length of the bone and Volkmann's canals that allow centrifugal flow of blood from arteries in the marrow cavity to the periosteal veins (Brookes, 1974; Bryan, 1996; White et al., 2012).

Bone cells, which require connection to the blood system and a sensory apparatus to detect mechanical strain, are found in lacunae (i.e. depressions/cavities) that are connected by a fine network of canaliculi (i.e. channels) (Kollmannsberger et al., 2017; Ortner and Turner-Walker, 2003). The lacunae are shaped like flattened ellipsoids approximately 10 μm x 5 μm and each is connected to its neighbours by 50-70 canaliculi, which pass through the hard bone tissue. The cells are approximately 20 μm apart and the average diameter of the canaliculi is approximately 259 ± 129 nm or a quarter of a micron (You et al., 2004). This lacuno–canalicular system forms a syncytium of interconnected cells and the extracellular space within canaliculi is accessible to blood in peripheral vessels (Nango et al., 2016). Confocal laser scanning microscopy of modern human femur shows that compact bone contains approximately 10 million osteocytes per cubic centimetre, each with a volume of approximately 500 μm3 and implying a total length of the canaliculi in that volume of approximately five kilometres (Papageorgopoulou et al., 2010). In mammals, the larger the body, the lower the density of osteocyte lacunae, with osteocyte lacunar density being around 17,000/mm3 for hippopotamus, 20,000/mm3 for humans and 50,000–66,000/mm3 in mouse femora (Nango et al., 2016).

Porosity has been found to vary considerably between different species (Fig. 2). Dry, acellular human, bovine and porcine compact bone specimens have been measured with total porosities of 9.2%, 5.2% and 14.3 % respectively (Figueiredo et al., 2010). These porosities are made up of three different pore size ranges at the micro- and nano-level: a) vascular porosity (VP), with average pore diameters around 50 μm; b) lacunae-canaliculi porosity (LCP) corresponding to an average pore size of 0.1 μm; and c) collagen-apatite porosity (CAP) related to the voids between and within collagen molecules (Figure 3), and HAp crystallites with diameters of only a few nanometers (Figueiredo et al., 2010; Mansilla et al., 2014).

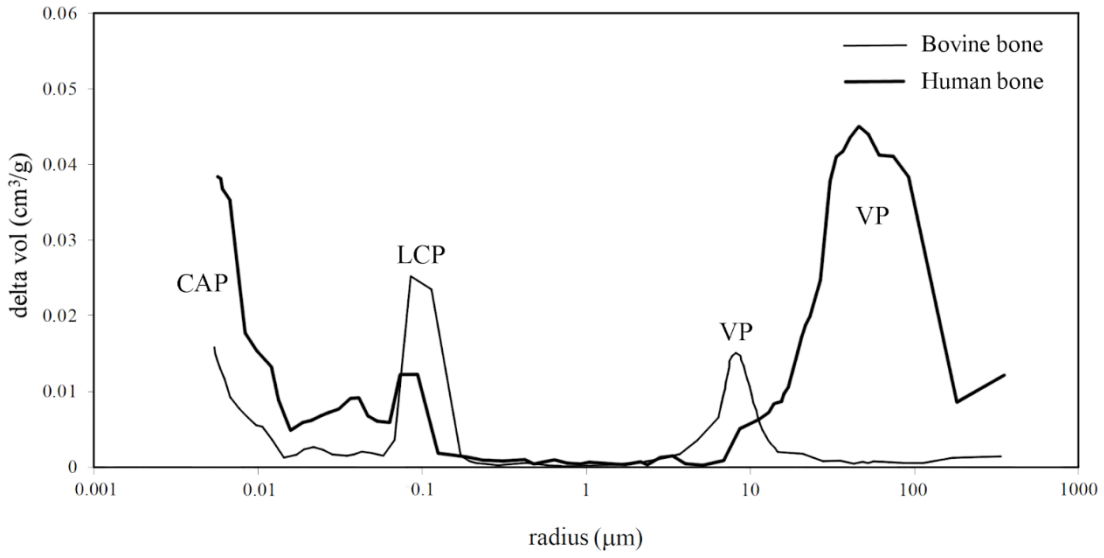

Figure 2. Differences in porosity of human and bovine compact bone measured by mercury intrusion porosimetry. CAP = collagen-apatite porosity; LCP = lacunae-canaliculi porosity; VP = vascular porosity. (Data adapted from Figueiredo et al., 2010)

A great deal of porosity in dead bone arises from the destruction of soft tissue in the blood vessels and bone cells which are housed in osteocyte lacunae. After loss of soft tissues, the lacuno–canalicular network allows soil water (and associated ions and microorganisms) to infiltrate the bone cortex irrespective of the direction of net flow of water within the sediment. The type and scale of diagenetic alteration influence the porosity of bones post-mortem in such a way that if the porosity decreases the survival prospects of the bone increase with permineralisation gradually leading to the fossilization of the specimen. Alternatively, if the porosity increases then the survival prospects of the specimen are severely diminished as water flows increasingly freely through the bone such that it may disappear completely from the archaeological or fossil record. Bones in a free-draining, acid soil, for instance, are particularly prone to this since they suffer both bioerosion and dissolution.

The volume of the pore network and its directionality in the other mineralised tissues differ from that of bone. As it might be expected, ivory and tooth dentine is known to survive well in the archaeological and fossil record. The directionality of porosity in different tissues has a very visible influence on patterns of microbial degradation as can be seen in Figure 4 below where, even after considerable bioerosion, the dentine in this tooth root is readily distinguishable from the surrounding cementum. The porosity in dentine has a smaller average diameter than found in bone and does not connect with the exterior of the skeletal element via large Haversian canals (Heckel et al., 2016). The dentinal tubules are not interconnected except via the pulp cavity, which itself is an enclosed volume accessible to soil water predominantly via the apical foramen. This local isolation from sediment pore water may well be reflected in the relatively better preservation of tooth dentine (and associated DNA) compared to bone (Hollund et al., 2014).

The mineralised tissues in antler are more porous, more chaotic in the orientation of blood vessels and have a lower mineral content than the bone found in the axial and appendicular skeleton. One might, therefore, expect it to be more susceptible to diagenesis than human or animal bone. Certainly, antler is less well represented in the archaeological record but this may reflect taphonomic rather than diagenetic factors. Antler is physically weaker and less dense than cortical bone and is more accessible to the predations of scavengers as is often the case with the spongy bone at the jointed ends of long bones that are exposed on the soil surface. By comparison with both antler and bone, ivory is both compact and, being composed of acellular dentine, has a low porosity. Mercury intrusion porosimetry of un-demineralised dentine gives a total pore volume of only 4-5% and a mean pore diameter of ~750 nm (Vennat et al., 2009).

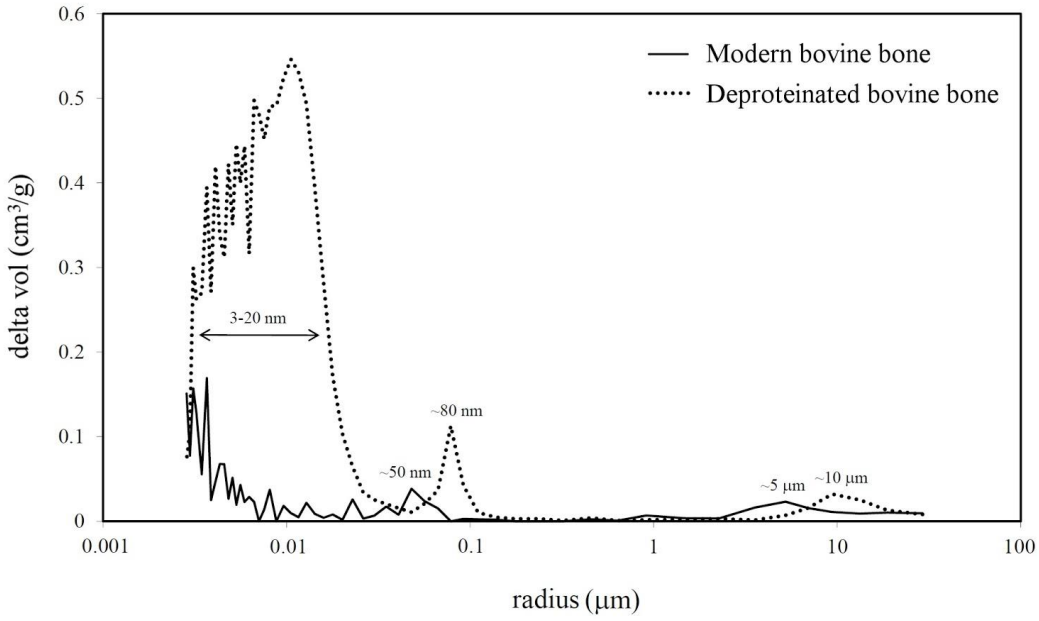

Figure 3. Changes in porosity of bovine compact bone before and after stripping out the collagen in a non-aqueous medium using hydrazine. Note the large increase in porosity with radii below ~25 nm arising from loss of collagen fibrils. Porosity below 10 nm must reflect pores spaces between HAp crystallites. Note the increase in pore radius and volume associated with the lacunae-canaliculi porosity and vascular porosity revealing a loss of un-mineralised osteoid from their internal surfaces.

4. Density of mineralised tissues

There is considerable confusion concerning the densities of different skeletal elements arising, in part, from the various different ways of expressing density. Here, a clear distinction should be made between the density values quoted in the osteoarchaeological literature, which is mainly concerned with the survivability and water transport characteristics of different skeletal elements (Boaz and Behrensmeyer, 1976; Lyman, 2014, 1984), and the densities quoted in a clinical context. In the former, density may be expressed as relative density in grams per cubic centimeter (g/cm-3) whereas in the latter, bone mineral densities are measured as grams of mineral per unit area in the projected X-ray shadow of a region of interest (Bonnick, 2000) – although they are more commonly presented in a clinical setting as a comparison with the peak bone mineral density of a healthy 30-year-old adult (T-score) or an age-matched cohort (Z-score).

In bone diagenesis studies, there are two ways to measure density, namely, bulk density in which the measured volume includes the pore space, and the real density (also called material density and/or skeletal density) in which the pore volume is subtracted from the volume used in the calculation (Turner-Walker, 2009; Zioupos et al., 2008). The real density of a skeletal element depends upon the ratios of organic, mineral and water, and as stated above, this may vary considerably from species to species and from one bone element to another (Figueiredo et al., 2010; Zioupos et al., 2000). Regarding faunal measurements of density, an extensive and

reasonably up-to-date list of various taxa with density data is available elsewhere (Lyman, 2014). Initially, it was discovered that between deer, sheep, and pronghorn antelope, little density variation was evident between subspecies and species, and larger but nonsignificant variation was seen between genera (Lyman, 1984). Additional studies found similar results and conclude that species of generally similar morphology will have similar bone density values (Lam et al., 1999). Terrestrial faunal bones with higher bulk density values are found to correlate more strongly with survivorship over time (Lyman, 1984), with similar findings in fish (Butler and Chatters, 1994) and aquatic birds (Broughton et al., 2007).

5. Depositional Environment

In vivo, the mineralized tissues experience an environment that is strictly controlled by the body's cellular and metabolic processes that remodel and repair the skeleton, maintain calcium homeostasis, and limit the action of microorganisms. After death, this protective envelope ceases to function and once skeletonisation has begun the skeleton is exposed to one or more of a wide range of environments that frequently represent an "open system" in terms of physical, chemical, and biological insults to the mineralised tissues. Depending upon the nature of the environment, a skeletal element will undergo a somewhat predictable diagenetic trajectory that may, or may not, result in its preservation in the archaeological or geological record. Of course, if the environment evolves over time, that diagenetic trajectory may change in speed and/or direction such that any excavated bone may exhibit chemical and physical deterioration corresponding to different environments. Nevertheless, it is sometimes possible to untangle these changes in depositional environment with clever use of chemical and histological techniques (Hollund et al., 2012; Pfretzschner and Tütken, 2011; Trueman and Benton, 1997; Turner-Walker and Jans, 2008). In the case of human inhumations, the local environment can change dramatically over short time periods if the decomposing corpse is enclosed within a wooden coffin or stone kist. In the case of a wooden coffin, the skeleton will experience an initially closed system enclosing putrefying soft tissues which becomes progressively more open and free draining once the coffin has begun to decay. The complex chemistry of a decomposing corpse are covered comprehensively in the forensic literature, (e.g. Dent et al., 2004 and references therein). The various factors influencing the survivability of a bone over time and its susceptibility to destructive, rather than preserving diagenetic factors are discussed in more detail below.

5.1 Soil pH and Eh

Because of the difficulties in fully reconstructing past soil burial conditions for archaeological bones, field experiments in which the soil pH, hydrologic regime, and temperatures are monitored have been extremely useful in understanding preserving as opposed to destructive environments. Collins et al. (1995, Figure 1) note the greater susceptibility of collagen to alkali rather than acid pH. However, a study of various mammal, bird and fish bones experimentally buried in a range of pH and hydrologic environments found that the acidic (pH 3.5-4.5) soils are more aggressive

than alkaline (7.5-8.0) soils (Nicholson, 1996). Similar results have been reported with human bones (Nielsen-Marsh et al., 2007), implying that it is the mineral and not the protein that controls early diagenesis. Increased availability of hydrogen ions leads bioapatite to readily dissolve (Nielsen-Marsh et al., 2000), because bioapatite is found to be most stable at pH 7.8 (Berna et al., 2004), and begins to dissolve in environments below pH 6.0 (White and Hannus, 1983). Decomposing bodies have been shown to change the pH of the localized burial environment, first by dropping pH levels (Gill-King, 1997), followed by more alkaline conditions (Gill-King, 1997; Janaway, 2008). Acidic environments can also arise from the presence of decomposing biomass producing humic and tannic acids, the leaching of base ions such as calcium and potassium, and the formation of carbonic acid by the dissolution of carbon dioxide (CO2) arising as a decomposition by-product (Pokines and Baker, 2014).

The colour of excavated bones provides clues to the evolution of the burial environment. The soil profile generally exhibits a succession of chemical regimes with oxygen reduction in the uppermost levels; underlain by successive levels of nitrate reduction; Mn4+ reduction, Fe3+ reduction; sulphate reduction and methane fermentation at the lowest levels. Bones from anoxic layers tend to be stained brown or black from manganese and iron oxides adsorbed onto the pore structure or fixed within the tissues since their solubilities, and hence availability to enter the pore structure of buried remains and interact with either the collagen or mineral, are dependent upon both pH and Eh (Mielki et al., 2016; Rengel, 2015). Redox and pH values also influence the availability of fulvic and humic acids which stain bone tissues anything from pale brown to dark brown or almost black such as the almost black bones of two women recovered from the Oseberg Ship burial in Norway (Holck, 2007, pers comm).

5.2 Soil hydrology

One of the most important factors for archaeological preservation and/or modification of mineralized tissues is water in and around the archaeological elements. Originally, three important hydrological scenarios had been outlined: a) diffusive; b) recharge; and c) flow regimes (Hedges and Millard, 1995). Diffusive regimes are found where there is little net movement of or change in the amount of water in an environment, recharge regimes are seen where fluctuations and subsequent wetting and drying cycles occur, and lastly, flow regimes occur when water flows through both the mineralized tissue and the soil, such as rainfall in unsaturated or free-draining sandy soils (Hedges and Millard, 1995; Nielsen-Marsh et al., 2000).

Fluctuating environments are the most damaging to mineralized tissues while diffusive environments tended to produce the smallest amount of diagenetic alteration (Fernández-Jalvo et al., 2010; Field et al., 2003; Hedges and Millard, 1995; Nielsen-Marsh et al., 2000; Nielsen-Marsh and Hedges, 2000b; Reiche et al., 2003; Salesse et al., 2014; Smith et al., 2002; Trueman et al., 2004). Cyclical wetting and drying as well as freezing and thawing regimes cause bones to swell and shrink setting up physical strains which result in radial cracking, flaking, and spalling of the

bones (Fernández-Jalvo et al., 2010; Pfretzschner and Tütken, 2011; Pokines et al., 2016). This is commonly observed both in bone weathering (i.e. destruction of bone by various physical and chemical processes) at the surface (Behrensmeyer, 1978; Fernández-Jalvo et al., 2010) and those buried in the soil (Fernández-Jalvo et al., 2010; Pfretzschner and Tütken, 2011).

Archaeological bone (i.e. more porous bone) has been shown to adsorb more water, and more quickly, than does fresh bone, and will in turn have a greater desorption rate (Turner-Walker, 1993). The rate at which water moves into and through archaeological material, combined with the speed of both the wetting and drying of the material factors into the preservation or destruction of mineralized tissues in the archaeological record. Water flowing through a bone will leach out mineral, the rate of removal being a function of pH and the volumes of water moving through the bone. Collagenases are too large to penetrate the intimate association of bone and mineral (the collagen-apatite porosity in Figure 2) but the removal of mineral is a prerequisite for collagen decay (Klont et al., 1991). A leaching regimen will expose demineralised collagen to potential microbial enzymolysis, leading to the eventual destruction of the tissue given enough time (Nielsen-Marsh and Hedges, 2000b; Reiche et al., 2003; Trueman et al., 2004; Von Endt and Ortner, 1984). Since well-drained soils also tend to be acidic and well-aerated, both chemical and microbial action can rapidly degrade a skeleton to a few fragments of compact bone (Johns, 2006) or reduce it to no more than a stain in the soil (Bethell and Carver, 1987). Water also substantially alters the element distribution in the bone, which combined with dissolution and recrystallisation, continues to shift the bone mineral composition closer to equilibrium with the burial environment (Lambert et al., 1985; Müller et al., 2011; Müller and Reiche, 2011; Ina Reiche et al., 2002; Reiche et al., 1999; Trueman et al., 2004; Tuross et al., 1989; Tütken et al., 2008).

5.3 Bone-humic interactions

The breakdown of vegetable matter in the soil is a complex process which lies outside the focus of this review paper. However, because the end results of these processes are often reactive organic molecules that can not only form permanent or semi-permanent cross-links in collagen but also sequester calcium from bone mineral, a short discussion is pertinent.

Humic substances are formed by the modification of plant matter, especially lignin, and the resulting molecules are very resistant to further biodegradation. Although they may derive from various sources, their general properties are very similar and the humic matter in soils may be very diverse. Humic substances may be divided into humic acids, fulvic acids and humins, distinguishable by their different solubilities in water at different pHs. Typically, humic substances are large polyphenolic molecules containing phenolic and carboxylic groups. The presence of these carboxylate and phenolate groups gives them the ability to form complexes with ions such as Mg^{2+}, Ca^{2+}, Fe^{2+} and Fe^{3+}. Many humic acids have two or more of these groups

arranged in such a way to enable the formation of chelate complexes with divalent and trivalent ions (Evangelou and Marsi, 2001). There is considerable evidence that these humic substances in the soil can form random, non-specific cross-links with bone collagen (van Klinken and Hedges, 1995).

In bones from wet soils (rather than waterlogged), the outer 1-2 mm where the bones tissues have been in direct contact with the soil are partly demineralised and stained a much darker brown than the underlying cortical bone (Turner-Walker, 2008, 1993). This phenomenon is also seen on the fracture edges of broken bones, and thus, does not reflect microstructural differences in the periosteal surface. An extreme example of this demineralisation is seen in the so-called mound people such as the Egtved Girl (Breuning-Madsen and Holst, 1998). These Bronze Age finds are inhumations in oaken log coffins in which the skin, hair, fingernails, and textiles are exceptionally well-preserved, but the skeleton has vanished completely, leaving only the enamel tooth crowns (Thomsen, 1929). It may be speculated that tannins derived from the oak coffin, combined with waterlogged, anoxic conditions are responsible for both the loss of bone mineral and the spectacular preservation of proteinaceous materials.

Another breakdown product of vegetation that has a bearing on bone diagenesis is found in sphagnum peat bogs and in peat derived from sphagnum. Research has identified a chemical breakdown product of sphagnum mosses, namely sphagnan, a polysaccharide which has powerful tanning and calcium chelating properties (Painter, 1991, 1983). This polysaccharide has been postulated as responsible for the spectacular preservation of the bog bodies found during peat cutting in northern Europe and Scandinavia. Typically, in these finds, the skin, intestines, clothing, and cordage are preserved in a semi-tanned state, whereas, once again, the skeleton has either been completely demineralised or has disappeared entirely. Bog bodies have been found in peat derived mainly or almost exclusively from sphagnum mosses. Field experiments over several years have demonstrated that bones buried in a sphagnum peat bog suffer much more rapid surface demineralisation than those buried in a fenland bog (Turner-Walker and Peacock, 2008).

6. Microbial degradation (bioerosion)

6.1 Patterns of microbial bioerosion

In the bone diagenesis literature, microbiological alterations of bone are generally divided into damage caused either by fungi (Marchiafava et al., 1974), bacteria (Hackett, 1981; Jackes et al., 2001), or in marine and freshwater environments by aquatic microorganisms (Bell et al., 1991; Davis, 1997; Pesquero et al., 2017, 2010; Turner-Walker, 2012). Studies on microbial post-mortem alterations of mineralised tissues have some antiquity. In the 19th century, Wedl was the first to describe microbial activity on human dentine (and later a piece of horse rib) that he had soaked in well water (Wedl, 1864). Wedl assumed the causal organism he saw to be a fungus (Bell, 1995). As such, Wedl was not only the first to report microbial degradation of mineralised

collagen but was one of very few researchers to replicate this in the laboratory. Wedl subsequently went on to look at ancient and fossil specimens in which he identified similar tunnelling. Towards the end of the 19th century Roux (1887) and Schaffer (1895) went on to examine fossil bones and teeth with similar results, and similarly concluded that the causal agent was a fungus which Roux named Mycelites ossifragus. Rather interestingly, this term has also been used to describe microborings in fossil fish teeth, dinosaur eggs and seashells (Taylor et al., 2014).

Investigations into the tunnelling of ancient skeletal remains resumed in the 1950s (e.g. Sognnaes, 1959, 1956) and have continued up to the present day (e.g. Turner-Walker and Jans, 2008). Hackett (1981) first characterised tunnelling presumably caused by fungi as Wedl microscopical focal destruction (MFD) and tunnels attributed to bacteria as non-Wedl MFD. He described three distinct types of non-Wedl MFD: linear longitudinal, budded, and lamellate (Hackett, 1981). Today, the characterisation of the microorganisms responsible for bone degradation is typically identified by the type of tunnelling present in the bone (Jans, 2008), because success in culturing and identifying the microorganisms has proved elusive.

Marchiafava et al. (1974) are frequently cited as having successfully created tunnels in bones using inoculation with Mucor sp. isolated from fresh cadaver vertebrae buried in garden soil. What is less frequently reported is that they autoclaved their bone specimens at 100-200 ºC before inoculating them with fungi. This is hardly a good model for bone degradation in human interments but may well be a good model for domestic bone waste. Furthermore, it is telling that although the fungi grew luxuriantly in the unsterilized soil/bone samples, it only grew sparsely on the sterilised bones – suggesting that the bones may not have been the major source of nutrition for the microorganism. It is also interesting to note that when Piepenbrink inoculated X-ray sterilised bone with a range of fungi he found no tunnelling but did describe rapid and uniform growth of fungi which penetrated the vascular channels (Piepenbrink, 1986). This suggests that heating the bone above the gelatinisation temperature of mineralised collagen can disrupt the protein-mineral bond and leave the bone tissues more susceptible to fungal degradation.

Bones exposed above the sediment (i.e. exposed to light) in a marine or freshwater environment are rapidly tunnelled by aquatic microorganisms which are able to penetrate to a depth of around 500-700 μm below the surface, leaving meandering tunnels 5-10 μm across (Turner-Walker, 2012). These tunnels are tightly-spaced, with typically less than one micron between tunnel walls, and appear not to respect the bone microarchitecture. They branch only occasionally, and some tunnels contain clusters of spherical grains of redeposited HAp. These grains vary in diameter from 1-2 μm (Pesquero et al., 2010) and are slightly enriched in manganese (Turner-Walker, 2012) suggesting that the organisms responsible may belong to the cyanobacteria family. It is interesting to note that in Wedl's original research on tunnelling found in teeth, his samples were immersed in "untreated well water" and that the tunnels that had formed after 10 days did not penetrate deeper into the tissues than 0.2-0.25 mm. After immersion for more than a month the

organisms responsible were unable to tunnel further. He also described some “few shining grains appearing in the interior” of the tunnels (Wedl, 1864). This raises the intriguing possibility that Wedl’s original tunnelling, so often now attributed to fungi (Hollund, 2013; Jans, 2008; Jans et al., 2004; Müller et al., 2011) may actually have been due to cyanobacteria after all.

Bones excavated from the majority of terrestrial archaeological contexts are unlikely to exhibit tunnelling by cyanobacteria. When Wedl-type bioerosion in exhumed bones is attributed to fungi it is most commonly, if not exclusively, along the periosteal margins of bones, whereas non-Wedl MFD commonly occurs around vascular (Haversian) canals (Lam et al., 2009). The dimensions of the tunnels described by Wedl were around 8 μm in diameter. Other researchers have described varying dimensions for different morphologies of MFDs ranging from 5 μm for Type I Wedl tunnels, 5-10 μm for linear longitudinal and anything up to 60 μm for budded and lamellate tunnelling (Jans, 2008).

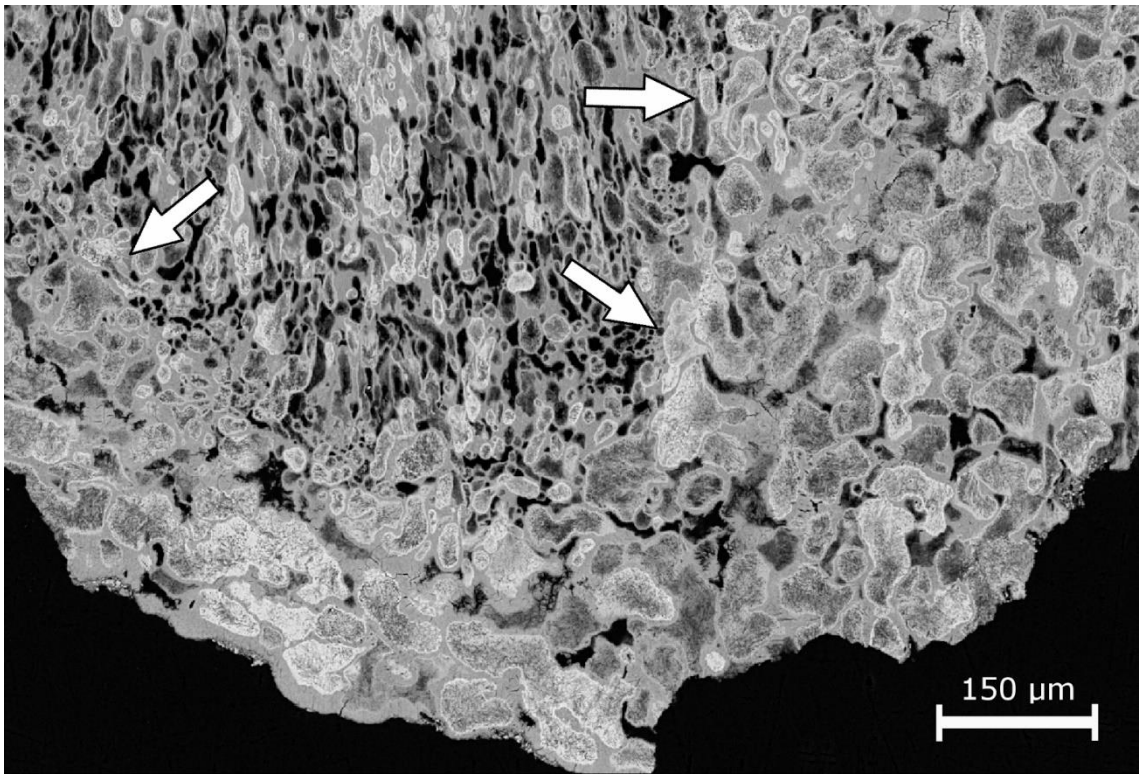

Figure 4. Differences in the pattern of bacterial degradation between tissue types in the root of a human incisor from the Medieval site of Wharram Percy, UK. Arrows indicate the border between dentine and cementum.

It is hazardous, and not supported by available evidence, to assign different causative organisms to these different sizes and morphologies of MFDs. Sognnaes (1955) found a similar range of sizes (2-10 microns; 15-25 microns and 50-100 microns) of focal destruction in ancient teeth from Europe and America. He thought that tunnels of different diameters did not mean that they were caused by different organisms but rather were caused by differences in the tissue type tunnelled. This explanation is supported by data coming from mercury intrusion porosimetry (Jans et al., 2004) which shows that all of the MFD types – linear longitudinal, budded, lamellate and even Wedl tunnels – have very similar porosities, exhibiting the double-peaked trace normally

attributed to bacterial tunnelling, which supports the interpretation of Sognnaes (1955). The influence of tissue microarchitecture is dramatically demonstrated by the change in the pattern of diagenetic alteration at the transition from cementum to dentine in Figure 4.

Bacterial tunnelling is associated with a dissolution and redistribution of HAp within the affected zones (Turner-Walker et al., 2002), as was noted by both (Hackett, 1981) and (Bell, 1995) in earlier studies. In fact, Hackett specifically noted the importance of seasonal variations in soil water content and their importance not only for the proliferation of the tunnelling bacteria but also the pattern of distribution (or loss) of the mineral (Hackett, 1981). The most parsimonious explanation for the different morphologies and sizes of MFDs is that one or more closely related species of bacteria are responsible for tunnelling into mineralised collagen and that perceived differences are due to a combination of tissue microarchitecture and local hydrologic flow within and surrounding the bone. Tunnelling that occurs close to the periosteum or in any surface in close contact with the surrounding soil is more likely to be empty because solubilised mineral has a greater likelihood of being swept out of the bone. This may account for some of the Wedl-type porosity attributed to soil fungi penetrating the periosteal surface in some specimens (see Fig. 5A). Bacterial degradation that occurs deeper inside the tissues is more likely to result in any dissolved mineral re-precipitating within the tunnelled space, leading to the observed pattern of often ragged demineralised spaces interspersed with hypermineralised cuffs or infillings which represent HAp re-precipitated within the tissues (Turner-Walker and Syversen, 2002).

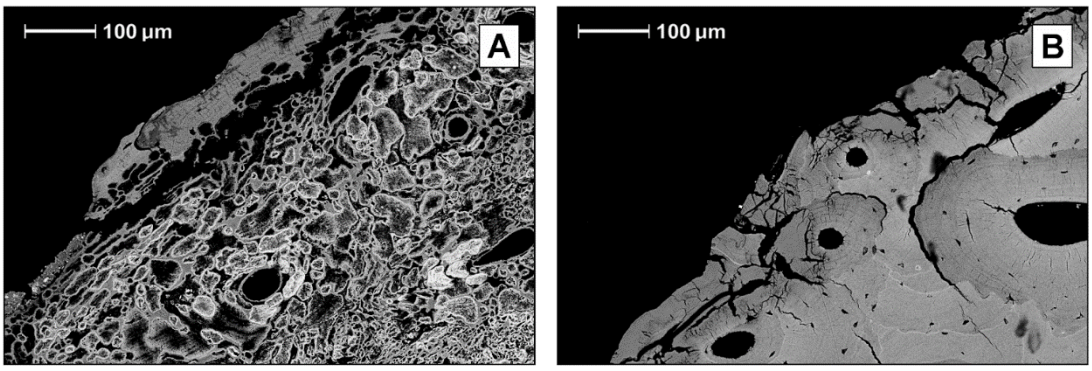

Figure 5. A: BSEM image of human bone from the Medieval monastery at Cleeve Abbey, UK. This specimen is from the free-draining part of the site and is extensively tunnelled by bacteria. Note that the periosteal bone is characterised by empty pores ~10 µm in diameter, whereas the outer 50 µm where it has been in contact with the soil is un-tunnelled. B: BSEM image of bone from the waterlogged part of the cemetery. Bacterial tunnelling is absent but there is considerable demineralisation and cracking of the periosteal bone. Demineralisation appears to respect the cement lines delineating secondary osteons.

As recognition of the far-seeing contribution of Hackett, it is worth quoting him with regard to how he saw future developments in the subject of post-mortem alteration of bone microstructure. “The application of more sophisticated techniques would contribute to the fuller understanding

of these changes and their causes" (Hackett, 1981). It is somewhat surprising, therefore, that so many researchers persist in applying low-power optical microscopy to the question of diagenetic alterations to bone tissues.

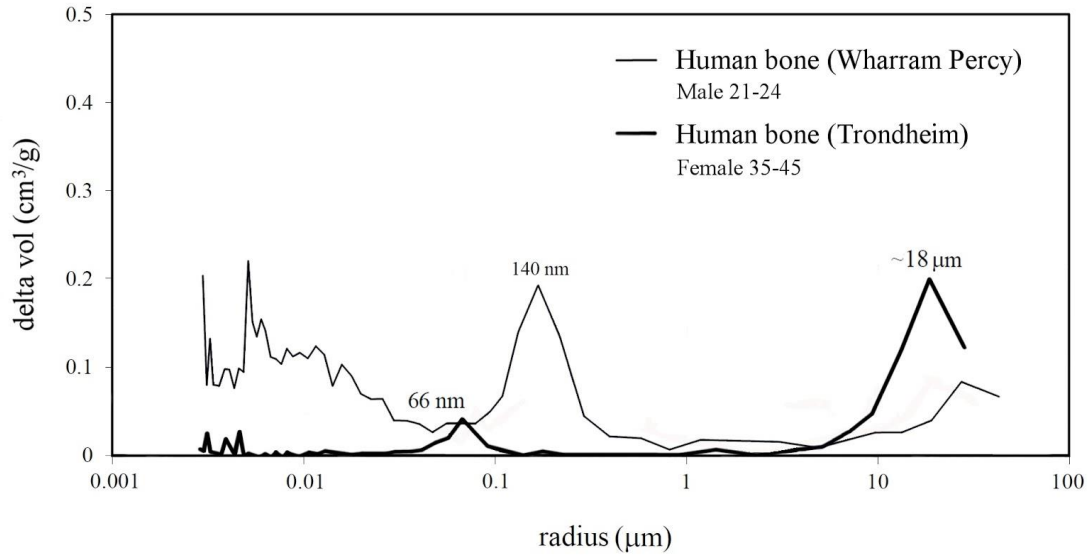

Figure 6. Differences in porosity for human femora from Mediaeval individuals excavated from two different inhumation environments – aerated soils (Wharram Percy, UK) and waterlogged, anoxic (Trondheim, Norway). Note the increased vascular porosity in the older, female specimen compared to the young male. (unpublished data MJC) as well as the increase in the collagen-apatite porosity in the bone from the warmer, aerated soil.

6.2 Environment and microbial bioerosion

The soil environment is without doubt the dominating factor in whether a buried bone will survive within the archaeological record or whether it degrades rapidly and is lost. Skeletonised remains in the tropics degrade much more rapidly than those in temperate zones, which in turn degrade more rapidly than those close to the arctic circle. Similarly, deeply buried remains tend to survive for longer than those in shallow burial environments. Part of this is because temperature is an obvious factor but so too is access to oxygen. Once again, (Hackett, 1981) was prescient in his understanding of the relationships between post-mortem changes to skeletons and burial environment - "tunnelling in bone does not appear to develop readily in wet, or waterlogged conditions. Moderate soil moisture with periodical, seasonal variation of water table and temperature, e.g. warm summers, are favourable for tunnelling." This conclusion is supported by evidence from the Medieval cemetery at Cleeve Abbey, UK. This cemetery has burials from both free-draining and waterlogged soils and the skeletons show a dramatic difference in microscopic preservation state (Fig. 5 A & B).

The soil bacteria responsible for tunnelling in buried bones are evidently aerobic in their metabolic pathways. Bones that are buried in wet soils with restricted access to oxygen tend to exhibit none of the characteristic diagenetic signatures seen in bones buried in oxygenated soils. Occasionally, bones exhibit limited bacterial tunnelling but show evidence for diagenetic pyrite

within the tunnelled tissues that is testament to a transition from an oxygenated to anoxic environment (Turner-Walker and Jans, 2008). Bones from deeply-buried, water-saturated sediments tend to have a higher collagen content and lower porosity (Fig. 6) than similar specimens from free-draining, aerated soils, although because of the deposition of iron sulphides within their pore structure they are prone to rapid deterioration if the environment changes to one with freely available oxygen (Turner-Walker, 2009).

6.3 The origin of the bacteria responsible for tunnelling in bone

It is argued that due to the low frequency of microbially altered bones in the fossil record, microbially degraded bones seldom survive into the geological record (Trueman and Martill, 2002). It is certainly true that archaeological bones and teeth tend to fall into a bimodal distribution on the Oxford histological index (OHI) scale - being either well preserved or poorly preserved (Hedges et al., 1995; Hollund et al., 2014). It has also been demonstrated that bacterial alteration in human bones is more than twice as common as in animal bone (Jans et al., 2004).

These findings have initiated a debate as to whether the way bones have entered the archaeological record (e.g. articulated- vs. disarticulated bodies) could have an influence on whether the bacteria responsible for non-Wedl tunnelling originate from the gut microbiome or from the burial soil post-skeletonisation (Bell, 1995; Damann and Jans, 2017; Jans et al., 2004; White and Booth, 2014). If a link between the bacterial alteration of bone and the presence of gut microbes exists, it can have great implications for the interpretation of the early post mortem period. In whole body decomposition, the bloat event, where the body cavity ruptures, is suggested to be a key point where a shift in the diversity of microbes from anaerobic to aerobic is observed (Bucheli and Lynne, 2016; Metcalf et al., 2013). A link between bone bioerosion and soft tissue decomposition would provide strong evidence that non-Wedl tunnels are produced by an organism's enteric gut microbiota and that these bacteria migrated from the intestines in the first few days after death, and go on to penetrate the bone microstructure (Booth and Madgwick, 2016; Jans, 2008; Kellerman et al., 1976).

Contrary evidence comes from an experimental burial of whole pig carcass which showed no specific histological attack patterns and no clear relationship between histological preservation and proximity to the abdominal area after 7 years (Kontopoulos et al., 2016). More pertinently, Bell et al. (1996) found no evidence of bacterial degradation of any kind in the skeletons (ribs) of three executed prisoners exhumed after 70-83 years from wooden coffin burials in Canada. These had been isolated from the soil and the coffins were dry when exhumed. We can infer a short interval between death and interment because execution and burial of condemned prisoners under the British Commonwealth followed strict protocols and bodies were buried promptly, without autopsy, soon after the individual was declared dead. Supporting evidence for tunnelling bacteria originating in the burial environment is provided by the identification of this characteristic tunnelling in archaeological ivory artefacts (Large et al., 2011).

Taphonomic setting undoubtedly influences the microstructural decay of bones. In forensic science, the use of genetic analysis to study the microbial diversity in the soil around a body has recently been investigated to estimate time since death (Metcalf et al., 2013; Pechal et al., 2014, 2013). A study by (Metcalf et al., 2015) found that 40% of the microbes responsible for the decomposition of the cadavers are already present in the soil before placement of the body and that other sources, such as insects, may provide a large proportion of the microbial decomposer community. The findings of Metcalf and colleagues are interesting as White and Booth (2014) found in their study of whole pig burials, that there was no bioerosion on the bones of stillborn pigs, which were considered not to have developed microbiota, and therefore concluded that exogenous soil bacteria do not contribute to microbial attack of bones over the first year of decomposition. However, they note that heavy rainfall during the first few months of the experiment could have created anoxic waterlogged conditions that slowed down degradation.

7. Protein degradation

7.1 Collagen

Collagen is linked with the strength of bone (Saito and Marumo, 2010; Schultz, 1997), and loss of collagen is responsible for the weakening of bone structure, potentially causing loss of the skeletal element entirely. Collagen loss happens due to both biological and chemical degradation. Biological loss of collagen, such as from microbial tunneling, assists in the destruction of mineralized collagen due to collagenase properties found on many microbes (Child, 1995a, 1995b; Marchiafava et al., 1974). Due to the size of the microbes and collagenases, which are both too large to fit into the collagen-apatite porosity, bone mineral would first have to be removed to expose the collagen triple helix (Child, 1995a, 1995b; Hedges, 2002; Marchiafava et al., 1974; Nielsen-Marsh et al., 2000; Turner-Walker, 1993) as it is during bone resorption. Microbial tunneling has been described earlier and is clearly a principal mechanism of collagen loss in environments and sites where bone degrading bacteria can flourish (Balzer et al., 1997; Child, 1995a, 1995b; Marchiafava et al., 1974; Nielsen-Marsh and Hedges, 2000b; Smith et al., 2002; Turban-Just and Schramm, 1998).

Chemical destruction of collagen, however, is influenced by many factors. Collagen is a protein held together by peptide bonds, and peptide bonds can be broken down by hydrolysis (Collins et al., 1995; Smith, 2002). Initial studies demonstrated that collagen degradation was a by product of both temperature and time, but increased collagen loss over shorter amounts of time corresponded with an increase in mean temperature (Ortner et al., 1972; Von Endt and Ortner, 1984). Similar results were also seen with cooked bone, where higher temperatures yielded more efficient collagen loss (Roberts et al., 2002; Solari et al., 2013). Figure 7 depicts collagen loss across a temperature gradient. Soil conditions, such as either extreme acidity or alkalinity can exacerbate the effects of hydrolysis, causing collagen to be lost much more effectively (Collins et al., 1995; Smith et al., 2002). Higher numbers of cross-links (i.e. stronger bone structure) retain

collagen better over time than does bone with little, or no cross-linkage (Collins et al., 1995). However, close examination of this model reveals that it is flawed as it demands too large a number of cross-links to explain the stability of chrome-tanned collagen. Subsequently, an alternative hypothesis, the link-lock model, shows it was physical constraint, rather than cross-links, which prevent collagen from melting (Covington et al., 2008).

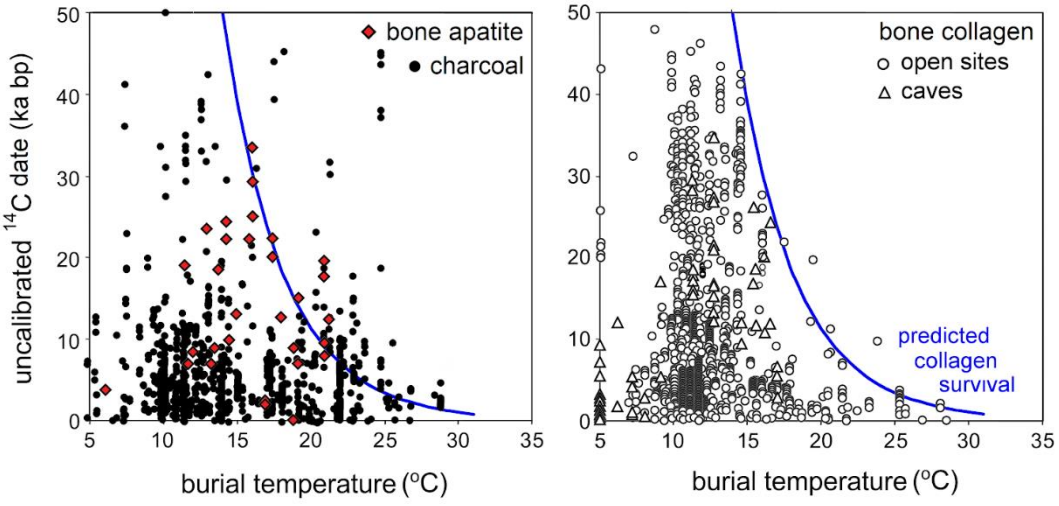

Figure 7. Plots of radiocarbon dates of charcoal and bone apatite (left), and bone collagen (right) against temperature of burial environment. The blue line indicates the theoretical limit for collagen survival. Drawing adapted from (Buckley et al., 2008b; Smith, 2002).

Therefore, an intricate collection of processes are necessary for the complete removal of the collagen content of an archaeological specimen in less than several thousand years. It has been shown that areas around cracked bone surfaces lose collagen much more rapidly than do non-cracked regions (Boaks et al., 2014; Trueman et al., 2004). These cracks may be due to either taphonomic conditions such as gnawing or weathering, or from density mediated attrition, where less dense bones are more likely to crack over time (Lyman, 2014). If they occur, cracks can then allow exogenous material into the bone, drastically altering the mineral structure (Smith et al., 2007), indicating that protein loss of bone in general is not an independent process, and proceeds in concert with other diagenetic changes such as microbial attack and deterioration of the inorganic content (Collins et al., 2002; Nielsen-Marsh and Hedges, 2000b; Trueman et al., 2004). Bone interaction with water can also increase the speed at which these processes work (Smith, 2002). Essentially, the process of collagen loss can be described as a rapid initial loss of collagen as a byproduct of increasing temperature, followed by a secondary, slower rate of decay of endogenous bone collagen due to chemical damage over extended periods of time (Turner-Walker, 2011).

Chemical degradation and loss of collagen can be identified as an increase in the smallest porosity in many archaeological bones (Turner-Walker et al., 2002). Comparing Figures 3 and 6 above it is clear that bone deposited in an aerated, free draining soil (Wharram Percy) exhibits an increase

in porosity at the collagen-apatite level compared to the bone from the waterlogged site (Trondheim). Figure 8A shows a high resolution BSEM image of bone that has not been bacterially tunnelled. Superficially, it appears that the smallest pore spaces (~30-50 nm) may represent lost collagen fibre bundles. However, a secondary electron image of an EDTA- treated sample of the same bone (Figure 8B) shows that these pores actually represent the inter fibrillar spaces that have suffered mineral loss. This supports the hypothesis that collagen and bone mineral are mutually protective, leading to the long-term survival of mineralised tissues in the burial environment, and that disruption of this intimate association will make bone tissue more susceptible to diagenesis (Koon, 2006; Turner-Walker, 2008).

7.2 Other Proteins

Skeletal material is made up of a series of proteins that are less abundant than collagen. Osteocalcin is one of many non-collagenous proteins found in skeletal material and comprises between 10-20% of the non-collagenous protein of bone (Ajie et al., 1992). Osteocalcin (Bone Gla Protein) is responsible for calcium binding and mineralization regulation (Lian et al., 1978; Price et al., 1976). Matrix Gla protein is similar in construction to osteocalcin, while proteoglycans and sialoprotein are phosphoproteins (Al-Qtaitat and Aldalaen, 2014). Phosphoproteins are likely responsible for calcium binding (Mundy, 1999). Lipids and proteolipids, along with alkaline phosphatase, are attributed to mineralization processes in bone and tooth (George and Veis, 2008). Other proteins in bone include a host of cell-attachment proteins and proteins responsible for regulating growth and cell activity (Al-Qtaitat and Aldalaen, 2014). For the purposes of this review, only osteocalcin diagenesis will be discussed, as a thorough literature search of diagenetic studies on these other proteins yielded no results.

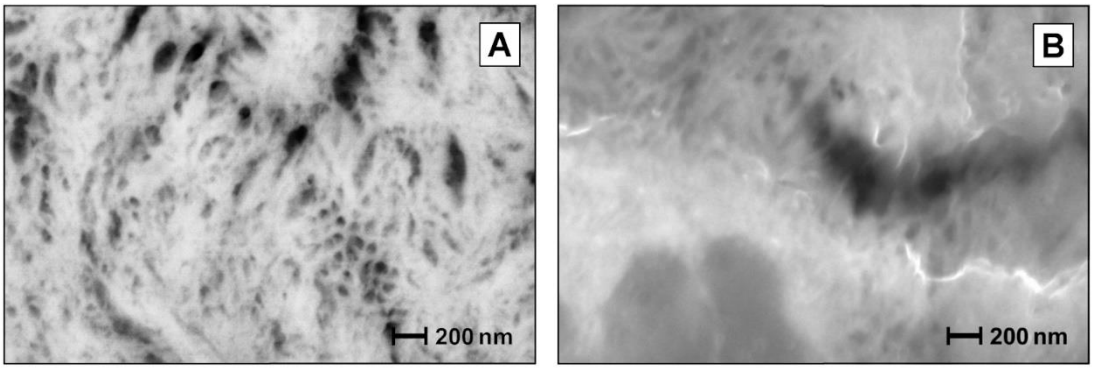

Figure 8. A: High resolution BSEM image of un-tunnelled cortical bone from Cleeve Abbey. The section was treated with NaOCl for 60 seconds. Larger pores (100-200 nm) are canaliculi. On initial inspection the smaller pores appear to be where collagen has been removed. However, if we look at a secondary electron image of a sample from the same bone treated with 0.1 Mol EDTA for 60 seconds (shown in Figure B) we see that bone mineral from between the fibre bundles has been removed, exposing partly demineralised collagen fibres. (Compare Figure 5D with (Habelitz et al., 2002): Fig. 1)

Osteocalcin is typically bound to bone bioapatite (Tuross, 1993) and due to this, similarly to collagen, osteocalcin loss is linked with increased bioapatite crystallinity (Collins et al., 2000; Smith et al., 2005), microbial destruction of bone (Smith et al., 2005), and temperature (Buckley et al., 2008). There is evidence from FTIR studies that 1-2 wt.% of the protein in fresh bone is resistant to hydrazinolysis. Either this may represent osteocalcin or collagen that is tightly bound to, or surrounded by, mineral. Collagen has been found to survive longer than both DNA and osteocalcin in ancient material (Buckley et al., 2008). Therefore, this indicates that at present collagen may be relatively easier to detect and analyze in older mineralised tissues.

8. Mineral changes

Crystallinity changes in archaeological bone were discovered when larger bioapatite crystals were noted in both museum specimens of eight ancient humans compared to modern, wild-killed Wildebeest (Tuross et al., 1989). In the modern samples, crystallite size was seen to increase over a period of 10 years, while the ancient samples showed significantly larger crystallite size in comparison to the modern samples (Tuross et al., 1989). As biogenic apatite is a relatively unstable and disordered form of geological mineral, its survival post-mortem depends on reorganization and growth through dissolution (loss of less stable components) and recrystallization (formation of more stable structure) (Nielsen-Marsh et al., 2000; Trueman, 2013). Although early bioapatite diagenetic changes are still unclear (Keenan and Engel, 2017; Tuross et al., 1989), post-mortem alterations of its biogenic chemical signals and composition have long been recognized (Lee–Thorp, 2002; Lee-Thorp and van der Merwe, 1991; Shin and Hedges, 2012; Stiner et al., 2001; Wright and Schwarcz, 1996).

Bone recrystallization increases crystallinity (i.e. crystal size and lattice perfection) and promotes the formation of a more stable, more authigenic mineral phase characterized by lower carbonate content as the initial more disordered crystals are less energetically stable (Asscher et al., 2011; Bartsiokas and Middleton, 1992; Götherström et al., 2002; Gourion-Arsiquaud et al., 2008; King et al., 2011; Nielsen-Marsh and Hedges, 2000b; Person et al., 1995; Reiche et al., 2002; Salesse et al., 2014; Stathopoulou et al., 2008; Surovell and Stiner, 2001; Termine and Posner, 1966; Trueman, 2013; Wright and Schwarcz, 1996). An increase in average and maximum crystal length post-mortem may be due to: i) particle coarsening, a process whereby the larger crystals increase at the expense of the smaller ones (i.e. Ostwald ripening); ii) dissolution of the smaller crystals; iii) or both (Nielsen-Marsh et al., 2000; I. Reiche et al., 2002; Stiner et al., 1995; Trueman, 2013; Trueman et al., 2008, 2004; Tuross et al., 1989; Weiner and Bar-Yosef, 1990; Wright and Schwarcz, 1996).

Increases in crystallinity have been used as one of the parameters to characterise the degree of diagenetic alteration of ancient degraded bones (Asscher et al., 2011; Dal Sasso et al., 2016; Salesse et al., 2014; Trueman et al., 2004; Tuross et al., 1989; Weiner and Bar-Yosef, 1990) and

as a possible screening method for DNA analyses (Grunenwald et al., 2014a). Nevertheless, despite its widespread use as a measure of diagenesis the splitting factor or crystallinity index measured from FTIR spectra is not always a predictor of other measured parameters (Trueman et al., 2008). The degree of recrystallization and change is usually higher in fossil bone comparing to archaeological bone (Berna et al., 2004; Keenan, 2016; Smith et al., 2002). Mineral changes require active hydrology (recharging with fresh water) or a reduction in pH (Hedges, 2002; Hedges and Millard, 1995; High et al., 2015; Nielsen-Marsh et al., 2000; Trueman, 2013). Berna et al. (2004) and Keenan and Engel, (2017) demonstrated that hydroxyapatite is more stable in pH around 7.5-8, displays low solubility (recrystallization) in slightly alkaline to near neutral environments and gives way to dissolution and recrystallization in pH environments below 6 or over 9. This indicates that bone apatite is more soluble than authigenic apatites that form naturally from solution in the soil, meaning that bones lying within this "recrystallisation window" begin to more closely reflect the composition of soluble ions in the burial environment (heteromorphic recrystallization) (Fernández-Jalvo et al., 2016).

Protein loss can also influence crystallinity (Nielsen-Marsh and Hedges, 2000b; Smith et al., 2007; Trueman et al., 2004) as the loss of organic matrix in mineralised tissues may expose some poorly crystalline mineral fractions to water flowing through the bone, allowing leaching and reprecipitation onto existing crystals and into the empty pore spaces. This interaction of the groundwater with the hydrated layer of the apatite crystals allows the incorporation of diverse labile and reactive ions (e.g. HPO_4^{2-}, PO_4^{3-}, CO_3^{2-}, Ca^{2+}, Mg^{2+}), which may in turn substitute other ions into the core domain (Figueiredo et al., 2012; Lee-Thorp and van der Merwe, 1991; Stathopoulou et al., 2008). This ionic exchange is controlled by the pH of the groundwater which can vary from 2.8 to 10 (Nielsen-Marsh et al., 2000; Turner-Walker, 2008). These episodes of dissolution and recrystallization result in a loss of tensile strength (i.e. bone becomes more susceptible to fracture) and mass (High et al., 2015; Turner-Walker, 2011). Changes in the composition of bone apatites also take place, even in neutral to alkaline soils.

Recrystallization can also lead to a distinct drop in microporosity accompanied by increasing macroporosity as seen at a variety of post-Ice Age, European, archaeological sites (Nielsen-Marsh and Hedges, 2000a, 2000b), in human, deer, goat, and sheep bones of between 1 and 55,000 years of age (Berna et al., 2004), fossilized remains of African animals (Trueman et al., 2004), and in assorted, experimentally altered bone (Hiller and Wess, 2006; Turner-Walker, 2011). Crystallite change and porosity alteration, however, is not always due to Ostwald ripening. Microbial tunnelling, in addition to mineral dissolution and recrystallization, also alters crystallinity (Turner-Walker et al., 2002). Recrystallization into authigenic apatite may be assisted by bacterially mediated mineral precipitation (Carpenter, 2005, 1999; Daniel and Chin, 2010). For microbes, this is in good agreement with research showing that microbes would first have to alter the mineral component of bone in order to get to the collagen (Nielsen-Marsh et al., 2000; Turner-

Walker, 1993). Microbial activity can, therefore, lead to mineral dissolution, followed by a redistribution of phosphate for the growth of adjacent hydroxyapatite crystals (Trueman et al., 2004).

9. Ancient DNA degradation

Deoxyribonucleic acid (DNA) is a macromolecule responsible for the construction of cellular proteins, which is passed to daughter cells during cell division. DNA is a polymer made up of four nucleotide bases - adenine and guanine, which are double-ringed purines, and cytosine and thymine that are single-ringed pyrimidines - all of which are attached to a deoxyribose sugar and a phosphate group, which make up the structural "sugar-phosphate backbone" of DNA (Jobling et al., 2013). Adenine and thymine pair in double-stranded DNA, as do guanine and cytosine (Jobling et al., 2013). Carbon atoms make up the deoxyribose molecule, where phosphate groups attach at the 3′ and 5′ (3 prime and 5 prime) carbon atoms, where the 3′ and 5′ each have an unattached hydroxyl (-OH) group on these respective carbon atoms (Jobling et al., 2013). A phosphodiester bond is then formed when a 3′ and 5′ carbon from differing sugar molecules conjoin through a covalent bond resulting in the formation of the double-stranded sister bond characteristic of DNA (Watson and Crick, 1953).

Ancient DNA (aDNA) analysis concerns itself with getting DNA out of "old" tissues (Sarkissian et al., 2015), that is, specimens that are typically older than 100 years of age. However, post-mortem, DNA is very susceptible to attack and degradation (Dabney et al., 2013) with quite limited calculated survivorship potential (Allentoft et al., 2012). DNA degradation commences with autolysis, taking place only a few hours after the death of an organism (Burger et al., 1999; Parsons and Walter Weedn, 2006; Pruvost et al., 2007). DNA is rapidly degraded by endonucleases such as lysosomes that cut DNA strands at internal sites (Hofreiter et al., 2001; Pääbo et al., 2004; Parsons and Walter Weedn, 2006). Bacteria and other external microorganisms also proliferate and digest DNA strands with exonucleases from the ends (Pääbo et al., 2004; Parsons and Walter Weedn, 2006; Pruvost et al., 2007).

Initial research believed that bacterial attack was a likely cause for the total loss of endogenous DNA in a sample (Rollo et al., 2002). However, this is unlikely, as many samples commonly produce exogenous bacterial fingerprints while still producing authentic, endogenous DNA (Zaremba-Niedźwiedzka and Andersson, 2013). Also endogenous bacterial attack affecting the cortical bone tissue may preserve endogenous DNA, while environmental conditions may also build reservoirs or niches where DNA is preserved (Geigl, 2002). Hydrolytic breakage of the polynucleotide strands is considered the main long-term reaction in aDNA degradation followed by chain breakage into shorter fragments usually between 100-500 bp in length (Bada et al., 1999; Brown and Brown, 2011; Hofreiter et al., 2001; Lindahl, 1993; Pääbo, 1989). The DNA molecule is particularly prone to this, as water attacks the β-N-glycosidic bonds and/or the phosphodiester

bonds (Brown and Brown, 2011; Lindahl, 1993; Parsons and Walter Weedn, 2006). The attack to the phosphodiester bond leads to single-stranded nicks, whilst the attack to the glycosidic bond releases the nucleotides (Pääbo et al., 2004).

Environmental conditions play a key role in the preservation of endogenous DNA (Poinar, 2003). DNA decay is highly temperature-dependent (Allentoft et al., 2012; Lindahl, 1993; Lindahl and Nyberg, 1972). Low temperatures have an advantageous effect on the survival of DNA, whereas high temperatures result in significant loss of DNA (Burger et al., 1999; Poinar, 2003). DNA yields are much higher in tissues from permafrost areas than from moderate temperate environments, while the latter better preserve DNA compared to warmer areas such as the Mediterranean (Pruvost et al., 2008). A north-south decline in endogenous DNA yields has been reported in the Northern Hemisphere (Bollongino et al., 2008), with a 67% success rate for central European open-air sites compared to only 7% for Near Eastern open-air sites (Bollongino et al., 2008). Caves also undisputedly preserve DNA more effectively as they have stable low temperatures all year-round and the alkaline sediment environment usually protects bone apatite from dissolution (Bollongino et al., 2008). Any variations in long-term DNA fragmentation is assumed to be caused by differences in pH and local hydrology (Allentoft et al., 2012; Burger et al., 1999; Lindahl, 1993; Lindahl and Nyberg, 1972).

Hydroxyapatite crystals are assumed to protect DNA from further degradation as it adsorbs onto the crystal surface (Götherström et al., 2002; Lindahl, 1993; Parsons and Walter Weedn, 2006). Mineral preservation has been linked to the survival of DNA in bone, while its dissolution and recrystallization are related with considerable loss of DNA in archaeological specimens (Allentoft et al., 2012; Götherström et al., 2002). Collagen loss is also assumed to play a crucial role in DNA degradation (Sosa et al., 2013). Experiments modelling the loss of DNA over time have shown that there is a drastic loss of DNA within the first year of burial, which causes a concomitant loss of DNA from the organic fraction of bone as collagen is removed (Campos et al., 2012). As a result, higher proportions of DNA are found more regularly in the bioapatite portion (Campos et al., 2012). This is also in agreement with later studies that found DNA was intimately linked with the maturation, and thus increase in size of bioapatite crystallinity, and the preservation of DNA in bones between 0 and 3,800 years of age (Grunenwald et al., 2014b). A possible explanation of this is that chemical processes, such as hydrolysis and collagenases, are removing proteins, and mineral is then filling in the gap spaces, while other processes are denaturing cells and releasing DNA from the collagen, so it then freely binds to the newly formed bioapatite surfaces. This explanation is lent additional support by the observation that in bone artificially aged in water at 60 ºC there are changes in both microporosity and tensile strength associated with dissolution and reprecipitation of mineral as collagen undergoes early degradation (Turner-Walker, 2011). However, the exact mechanisms of DNA preservation in ancient bones remains under debate (Götherström et al., 2002; Ottoni et al., 2009).

Some skeletal elements have been shown to yield larger amounts of DNA than others, meaning that it is easier to obtain authentic DNA from these samples (Gamba et al., 2014; Hansen et al., 2017; Pinhasi et al., 2015; Pruvost et al., 2008). For instance, the petrous bone, one of the inner ear portions of the temporal bone of the skull, has had remarkable success in providing large amounts of endogenous aDNA, which has been attributed to its density, believed to be protecting it from potential destructive attack (Gamba et al., 2014; Pinhasi et al., 2015). However, in other skeletal elements, the unique porosity of human compared to animal bone means contaminating DNA (exogenous DNA) may enter human bone much more easily in an archaeological setting (Gilbert et al., 2005). In teeth, it has been demonstrated that cementum is a much more rich source of aDNA than the typically used dentine, which may be explained by higher mineral content of cementum (Adler et al., 2011; Damgaard et al., 2015; Hansen et al., 2017). It should be noted that in mineralising collagen, the mineral grows at the expense of interstitial water, and if that water contains DNA fragments then increasing mineralisation will result in more DNA becoming bound up in the mineral phase.

10. Conclusions and suggestions for future research

We have outlined a thorough synthesis of all the ways in which mineralized tissues can be altered through the processes of diagenesis. This palimpsest of diagenesis has highlighted the key and influential research from the initial forays into this research field and connected it with more recent research and innovative techniques attempting to explain diagenetic phenomena. We have illustrated the ways in which diagenesis can work to preserve bone, and agree with other researchers that central to this preservation is the interplay between the organic and inorganic constituents and how the environment interacts with the skeletal tissues. We conclude with others that diagenesis works as a collective process, since bone and tooth are made up of intrinsically linked components. Finally, we have argued that while histological preservation is important for samples, this comes at a cost of lowered recoverability of the proteins and endogenous DNA.

Diagenetic processes are all interlinked. A loss of collagen causes the DNA to be lost from the organic fraction. Thus, this causes recoverable DNA to be extracted more readily from bioapatite as time goes on until total loss of DNA is observed (Campos et al., 2012). Some microbes are believed to be assistive in bone survivorship over time (Daniel and Chin, 2010; Smith et al., 2007; Trueman and Martill, 2002), whereas others (those responsible for tunnelling) actually hamper collagen preservation (Child, 1995a, 1995b; Marchiafava et al., 1974), assist in at least some loss of DNA (Rollo et al., 2002), and influence biogenic isotope values through selective feeding (Balzer et al., 1997; Grupe et al., 2002; Turban-Just and Schramm, 1998). Research into exactly how microbes work in the diagenetic framework is key, since they appear to be influential in all aspects of diagenesis of mineralised tissue. They have been shown to remove collagen, alter the inorganic portion of bone, and erode the structure of bone through tunnelling. Further, diverse microorganisms are found in all types of environments and have a hand in both the preservation

and destruction of mineralised tissue. Therefore, they are an influential aspect of diagenesis, yet their role remains the least understood.

Limited interaction with water is key for the preservation of the organic and inorganic contents, as well as DNA (Dabney et al., 2013; Smith, 2002). Environments where bone and water interaction remain static preserve bone better than do environments where cyclic wetting and drying occurs (Field et al., 2003; Hedges and Millard, 1995; Nielsen-Marsh et al., 2000; Nielsen-Marsh and Hedges, 2000b). Increased temperatures also affect collagen survival (Ortner et al., 1972; Turner-Walker, 2011; Von Endt and Ortner, 1984) and tend to accelerate loss of DNA (Shapiro, 2015) compared to cooler temperatures, while soil pH has been shown to influence the preservation of skeletal remains (Nielsen-Marsh et al., 2007; Turner-Walker and Peacock, 2008).

Future research could usefully investigate any possible influence of in vivo disease on post-mortem diagenetic degradation of bone tissues. One obvious area is the detection of ante- and peri-mortem infections in archaeological skeletons. Staphylococcus DNA has successfully been identified in bones exhibiting osteomyelitic infection in an historic osteological collection (Flux et al., 2017). It remains to be seen if this can be repeated on archaeological specimens. And whether the infectious lesions influence diagenesis. Non-infectious diseases have also been shown to result in microdamage to bone tissues. For example, non-enzymatic cross-linking, called advanced glycation end-products (AGEs), causes micro-damage to living bone tissue, leading to microcracks while simultaneously halting the repair process by stimulating osteoblast apoptosis (Alikhani et al., 2007; Tang and Vashishth, 2010). Microcracks are seen in the early stages of diagenesis (Hollund et al., 2012; Pfretzschner and Tütken, 2011) and may be expected that AGE compromised tissues may experience accelerate chemical degradation of bone tissue (compared to bone comprised of normal collagen) by increasing both porosity and surface area available to percolating pore waters. However, at the present time we are unaware of any way to explore this hypothesis apart from perhaps using artificially AGE-damaged bone and comparing its diagenetic change to unaltered samples.

Because of recent developments in which the presence, or absence, of bacterial tunneling in human remains has been attributed to specific cultural practices, it is of considerable importance that the question of the origin of the organisms responsible is resolved. Identification based on recovered bacterial DNA is a tantalising prospect but is likely to be definitive. Field and laboratory investigations, combined with histological analyses and DNA studies seem to offer a fruitful area of future research. The soil bacteria versus endogenous gut bacteria hypotheses may prove more difficult to disentangle than it seems, however, since many gut bacteria are commonly found in the soil. Nevertheless, the fact that archaeological ivory is also tunnelled in the same way as bones (Large et al., 2011) suggests that the diagenetic trajectory can be followed in isolation from a decaying corpse. Finally, much of the published research on bone diagenesis to date has focussed on European archaeological sites. Although that material covers terrestrial, freshwater

and marine environments from the sub-arctic to the Mediterranean, the range of environments and climates explored should be expanded. That being said, results of field experiments in tropical southeast asia and archaeological bones examined from the Chinese mainland would indicate that differences in diagenesis are one of degree rather than substance.

Acknowledgments

We would like to thank all of the pioneering researchers that have been cited in this paper. Without them, diagenesis would remain even more perplexing. We would also like to thank Dr. Meghan Burchell, Dr. Susan Pfeiffer and Dr. Henning Matthiesen for their editorial comments on the structure of this manuscript. IK would like to thank Onassis Foundation, Leventis Foundation and the Greek Archaeological Committee UK (GACUK). AME would like to thank the Danish Council for Independent Research grant no. DFF – 4090-00037. Matthew Collins acknowledges the support from the Danish National Research Foundation and the European Union's EU Framework Programme for Research and Innovation Horizon 2020 under Grant Agreement No 676154.

Personal communication

Holck, P., 2007. Personal visit to the Anatomisk Institutt, Universitetet i Oslo, Norway. January 2007.

References

Adler, C.J., Haak, W., Donlon, D., Cooper, A., 2011. Survival and recovery of DNA from ancient teeth and bones. J. Archaeol. Sci. 38, 956–964.

Ajie, H.O., Kaplan, I.R., Hauschka, P.V., Kirner, D., Slota, P.J., Jr, Taylor, R.E., 1992. Radiocarbon dating of bone osteocalcin: isolating and characterizing a non-collagen protein. Radiocarbon 34, 296–305.

Alikhani, M., Alikhani, Z., Boyd, C., MacLellan, C.M., Raptis, M., Liu, R., Pischon, N., Trackman, P.C., Gerstenfeld, L., Graves, D.T., 2007. Advanced glycation end products stimulate osteoblast apoptosis via the MAP kinase and cytosolic apoptotic pathways. Bone 40, 345–353.

Allentoft, M.E., Collins, M., Harker, D., Haile, J., Oskam, C.L., Hale, M.L., Campos, P.F., Samaniego, J.A., Gilbert, M.T.P., Willerslev, E., Zhang, G., Scofield, R.P., Holdaway, R.N., Bunce, M., 2012. The half-life of DNA in bone: measuring decay kinetics in 158 dated fossils. Proc. Biol. Sci. 279, 4724–4733.

Al-Qtaitat, A.I., Aldalaen, S.M., 2014. A Review of Non-Collagenous Proteins; their Role in Bone. American Journal of Life Sciences 2, 351–355.

Alves, R.D.A.M., Demmers, J.A.A., Bezstarosti, K., van der Eerden, B.C.J., Verhaar, J.A.N., Eijken, M., van Leeuwen, J.P.T.M., 2011. Unraveling the human bone microenvironment beyond the classical extracellular matrix proteins: a human bone protein library. J. Proteome Res. 10, 4725–4733.

Asscher, Y., Regev, L., Weiner, S., Boaretto, E., 2011. Atomic disorder in fossil tooth and bone mineral: an FTIR study using the grinding curve method. ArcheoSciences. Revue d'.

Asscher, Y., Weiner, S., Boaretto, E., 2011. Variations in Atomic Disorder in Biogenic Carbonate Hydroxyapatite Using the Infrared Spectrum Grinding Curve Method. Adv. Funct. Mater. 21, 3308–3313.

Bada, J.L., Wang, X.S., Hamilton, H., 1999. Preservation of key biomolecules in the fossil record: current knowledge and future challenges. Philos. Trans. R. Soc. Lond. B Biol. Sci. 354, 77–86; discussion 86–7.

Balzer, A., Gleixner, G., Grupe, G., Schmidt, H.-L., Schramm, S., Turban-Just, S., 1997. In vitro decomposition of bone collagen by soil bacteria: the implications for stable isotope analysis in archaeometry. Archaeometry 39, 415–429.

Bartsiokas, A., Middleton, A.P., 1992. Characterization and Dating of Recent and Fossil Bone by X-Ray Diffraction. Science 19, 63–12.

Behrensmeyer, A.K., 1978. Taphonomic and ecologic information from bone weathering. Paleobiology 4, 150–162.

Bell, L.S., 1995. Post mortem microstructural change to the skeleton (Doctoral). University of London.

Bell, L.S., Boyde, A., Jones, S.J., 1991. Diagenetic alteration to teeth in situ illustrated by backscattered electron imaging. Scanning 13, 173–183.

Bell, L.S., Skinner, M.F., Jones, S.J., 1996. The speed of post mortem change to the human skeleton and its taphonomic significance. Forensic Sci. Int. 82, 129–140.

Bentley, P.J., Jackson, D.S., 1965. Collagen synthesis and fibrogenesis in scurvy. Biochimica et Biophysica Acta (BBA) - General Subjects 107, 519–523.

Berna, F., Matthews, A., Weiner, S., 2004. Solubilities of bone mineral from archaeological sites: the recrystallization window. J. Archaeol. Sci. 31, 867–882.

Bethell, P.H., Carver, M.O.H., 1987. Detection and enhancement of decayed inhumations at Sutton Hoo, in: Boddington, A., Garland, N., Janaway, R.C. (Eds.), Death, Decay and Reconstruction. Manchester University Press, pp. 10–21.

Boaks, A., Siwek, D., Mortazavi, F., 2014. The temporal degradation of bone collagen: A histochemical approach. Forensic Sci. Int. 240, 104–110.

Boaz, N.T., Behrensmeyer, A.K., 1976. Hominid taphonomy: transport of human skeletal parts in an artificial fluviatile environment. Am. J. Phys. Anthropol. 45, 53–60.

Bollongino, R., Tresset, A., Vigne, J.-D., 2008. Environment and excavation: Pre-lab impacts on ancient DNA analyses. C. R. Palevol 7, 91–98.

Bonnick, S.L., 2000. The Osteoporosis Handbook. Taylor Trade Publishing.

Booth, T.J., Madgwick, 2016. New evidence for diverse secondary burial practices in Iron Age Britain: A histological case study. J. Archaeol. Sci. 67, 14–24.

Boskey, A.L., 2007. Mineralization of Bones and Teeth. Elements 3, 385–391.

Boskey, A.L., 2003. Bone mineral crystal size. Osteoporos. Int. 14 Suppl 5, S16–20; discussion S20–1.

Breuning-Madsen, H., Holst, M.K., 1998. Recent Studies on the Formation of Iron Pans around the Oaken Log Coffins of the Bronze Age Burial Mounds of Denmark. Journal of Archaeological Science 25, 1103–1110.

Brookes, M., 1974. Approaches to non-invasive blood flow measurement in bone. Biomed. Eng. 9, 342–347.

Broughton, J.M., Mullins, D., Ekker, T., 2007. Avian resource depression or intertaxonomic variation in bone density? A test with San Francisco Bay avifaunas. J. Archaeol. Sci. 34, 374–391.

Brown, T., Brown, K.A., 2011. Biomolecular archaeology, 1. publ. ed. Wiley-Blackwell, Oxford.

Bryan, G.J., 1996. Skeletal anatomy. Elsevier Health Sciences.

Bucheli, S.R., Lynne, A.M., 2016. The microbiome of human decomposition. Microbe Wash. DC 11, 165–171.

Buckley, M., Anderung, C., Penkman, K., Raney, B.J., Götherström, A., Thomas-Oates, J., Collins, M.J., 2008. Comparing the survival of osteocalcin and mtDNA in archaeological bone from four European sites. J. Archaeol. Sci. 35, 1756–1764.

Buckley, M., Walker, A., Ho, S.Y.W., Yang, Y., Smith, C., Ashton, P., Oates, J.T., Cappellini, E., Koon, H., Penkman, K., Elsworth, B., Ashford, D., Solazzo, C., Andrews, P., Strahler, J., Shapiro, B., Ostrom, P., Gandhi, H., Miller, W., Raney, B., Zylber, M.I., Gilbert, M.T.P., Prigodich, R.V., Ryan, M., Rijsdijk, K.F., Janoo, A., Collins, M.J., 2008b. Comment on "Protein sequences from mastodon and Tyrannosaurus rex revealed by mass spectrometry." Science 319, 33; author reply 33.

Burger, J., Hummel, S., Herrmann, B., Henke, W., 1999. DNA preservation: A microsatellite-DNA study on ancient skeletal remains. Electrophoresis 20, 1722–1728.

Butler, V.L., Chatters, J.C., 1994. The Role of Bone Density in Structuring Prehistoric Salmon Bone Assemblages. J. Archaeol. Sci. 21, 413–424.

Campos, P.F., Craig, O.E., Turner-Walker, G., Peacock, E., Willerslev, E., Gilbert, M.T.P., 2012. DNA in ancient bone - Where is it located and how should we extract it? Annals of Anatomy-Anatomischer Anzeiger 194, 7–16.

Carpenter, K., 2005. Experimental investigation of the role of bacteria in bone fossilization.(With 3 figures). Neues Jahrbuch fur Geologie und Palaontologie-Monatshefte 83–94.

Carpenter, K., 1999. Role of bacteria in the permineralization of bone: Experimental results, in: Journal of Vertebrate Paleontology Abstracts. p. 36.

Child, A.M., 1995a. Microbial taphonomy of archaeological bone. Stud. Conserv. 40, 19–30.

Child, A.M., 1995b. Towards and Understanding of the Microbial Decomposition of Archaeological Bone in the Burial Environment. J. Archaeol. Sci. 22, 165–174.

Collins, M.J., Gernaey, A.M., Nielsen-Marsh, C.M., Vermeer, C., Westbroek, P., 2000. Slow rates of degradation of osteocalcin: Green light for fossil bone protein? Geology 28, 1139–1142.

Collins, M.J., Nielsen–Marsh, C.M., Hiller, J., Smith, C.I., Roberts, J.P., Prigodich, R.V., Wess, T.J., Csapò, J., Millard, A.R., Turner–Walker, G., 2002. The survival of organic matter in bone: a review. Archaeometry 44, 383–394.

Collins, M.J., Riley, M.S., Child, A.M., Turner-Walker, G., 1995. A Basic Mathematical Simulation of the Chemical Degradation of Ancient Collagen. J. Archaeol. Sci. 22, 175–183.

Covington, A.D., Song, L., Suparno, O., Koon, H., Collins, M.J., 2008. Link-lock: an explanation of the chemical stabilisation of collagen. J. Soc. Leather Technol. Chem. 92, 1–7.

Currey, J.D., 2011. The structure and mechanics of bone. J. Mater. Sci. 47, 41–54.

Dabney, J., Meyer, M., Pääbo, S., 2013. Ancient DNA damage. Cold Spring Harb. Perspect. Biol. 5. doi:10.1101/cshperspect.a012567

Dal Sasso, G., Lebon, M., Angelini, I., Maritan, L., Usai, D., Artioli, G., 2016. Bone diagenesis variability among multiple burial phases at Al Khiday (Sudan) investigated by ATR-FTIR spectroscopy. Palaeogeogr. Palaeoclimatol. Palaeoecol. 463, 168–179.

Damann, F.E., Jans, M.M.E., 2017. Microbes, anthropology, and bones. Forensic Microbiology 312.

Damgaard, P.B., Margaryan, A., Schroeder, H., Orlando, L., Willerslev, E., Allentoft, M.E., 2015. Improving access to endogenous DNA in ancient bones and teeth. Nature 5, 1–12.

Daniel, J.C., Chin, K., 2010. The role of bacterially mediated precipitation in the permineralization of bone. Palaios 25, 507–516.

Davis, P.G., 1997. The bioerosion of bird bones. International Journal of Osteoarchaeology.

Dent, B.B., Forbes, S.L., Stuart, B.H., 2004. Review of human decomposition processes in soil. Environ. Geol. 45, 576–585.

de Ricqlès, A.J., 2011. Vertebrate palaeohistology: Past and future. C. R. Palevol 10, 509–515.

de Ricqlès, A.J., 2007. Fifty years after Enlow and Brown's Comparative histological study of fossil and recent bone tissues (1956–1958): A review of Professor Donald H. Enlow's contribution to palaeohistology and comparative histology of bone. Elsevier Oceanogr. Ser. 6, 591–601.

Duer, M., Veis, A., 2013. Bone mineralization: Water brings order. Nat. Mater. 12, 1081–1082.

Dumont, E.R., 2010. Bone density and the lightweight skeletons of birds. Proc. Biol. Sci. 277, 2193–2198.

Elliott, J.C., 2002. Calcium Phosphate Biominerals. Rev. Mineral. Geochem. 48, 427–453.

Eppell, S.J., Tong, W., Katz, J.L., Kuhn, L., Glimcher, M.J., 2001. Shape and size of isolated bone mineralites measured using atomic force microscopy. J. Orthop. Res. 19, 1027–1034.

Evangelou, V.P., Marsi, M., 2001. Composition and metal ion complexation behavour of humic fractions derived from corn tissue. Plant Soil 229, 13–24.

Eyre, D.R., Dickson, I.R., Van Ness, K., 1988. Collagen cross-linking in human bone and articular cartilage. Age-related changes in the content of mature hydroxypyridinium residues. Biochem. J 252, 495–500.

Eyre, D.R., Weis, M., Hudson, D.M., Wu, J.-J., Kim, L., 2011. A novel 3-hydroxyproline (3Hyp)-rich motif marks the triple-helical C terminus of tendon type I collagen. J. Biol. Chem. 286, 7732–7736.

Fernández-Jalvo, Y., Andrews, P., Pesquero, D., Smith, C., Marín-Monfort, D., Sánchez, B., Geigl, E.-M., Alonso, A., 2010. Early bone diagenesis in temperate environments: Part I: Surface features and histology. Palaeogeogr. Palaeoclimatol. Palaeoecol. 288, 62–81.

Fernández-Jalvo, Y., Pesquero, M.D., Tormo, L., 2016. Now a bone, then calcite. Palaeogeogr. Palaeoclimatol. Palaeoecol. 444, 60–70.

Field, N., Baker, J., Pearson, M.P., 2003. Fiskerton: An Iron Age Timber Causeway with Roman Votive Offerings: the 1981 Excavations. Oxbow books.

Figueiredo, M., Fernando, A., Martins, G., Freitas, J., Judas, F., Figueiredo, H., 2010. Effect of the calcination temperature on the composition and microstructure of hydroxyapatite derived from human and animal bone. Ceram. Int. 36, 2383–2393.

Figueiredo, M.M., Gamelas, J.A.F., Martins, A.G., 2012. Characterization of Bone and Bone-Based Graft Materials Using FTIR Spectroscopy, in: Infrared Spectroscopy - Life and Biomedical Sciences.

Flux, A.L., Mazanec, J., Strommenger, B., Hummel, S., 2017. Staphylococcus aureus Sequences from Osteomyelitic Specimens of a Pathological Bone Collection from Pre-Antibiotic Times. Diversity 9, 43.

Fratzl, P., Fratzl-Zelman, N., Klaushofer, K., Vogl, G., Koller, K., 1991. Nucleation and growth of mineral crystals in bone studied by small-angle X-ray scattering. Calcif. Tissue Int. 48, 407–413.

Gamba, C., Jones, E.R., Teasdale, M.D., McLaughlin, R.L., Gonzalez-Fortes, G., Mattiangeli, V., Domboróczki, L., Kővári, I., Pap, I., Anders, A., Whittle, A., Dani, J., Raczky, P., Higham,

T.F.G., Hofreiter, M., Bradley, D.G., Pinhasi, R., 2014. Genome flux and stasis in a five millennium transect of European prehistory. Nat. Commun. 5, 5257.

Garnero, P., 2015. The role of collagen organization on the properties of bone. Calcif. Tissue Int. 97, 229–240.

Gehler, A., Tütken, T., Pack, A., 2011. Triple oxygen isotope analysis of bioapatite as tracer for diagenetic alteration of bones and teeth. Palaeogeogr. Palaeoclimatol. Palaeoecol. 310, 84–91.

Geigl, E.M., 2002. On the circumstances surrounding the preservation and analysis of very old DNA. Archaeometry 44, 337–342.

George, A., Veis, A., 2008. Phosphorylated proteins and control over apatite nucleation, crystal growth, and inhibition. Chem. Rev. 108, 4670–4693.

Georgiadis, M., Müller, R., Schneider, P., 2016. Techniques to assess bone ultrastructure organization: orientation and arrangement of mineralized collagen fibrils. J. R. Soc. Interface 13. doi:10.1098/rsif.2016.0088

Gilbert, M.T.P., Rudbeck, L., Willerslev, E., Hansen, A.J., Smith, C., Penkman, K.E.H., Prangenberg, K., Nielsen-Marsh, C.M., Jans, M.E., Arthur, P., Lynnerup, N., Turner-Walker, G., Biddle, M., Kjølbye-Biddle, B., Collins, M.J., 2005. Biochemical and physical correlates of DNA contamination in archaeological human bones and teeth excavated at Matera, Italy. J. Archaeol. Sci. 32, 785–793.

Gill-King, H., 1997. Chemical and ultrastructural aspects of decomposition. Forensic taphonomy: the postmortem fate of human remains. CRC, Boca Raton, FL 93–108.

Glimcher, M.J., 2006. Bone: Nature of the Calcium Phosphate Crystals and Cellular, Structural, and Physical Chemical Mechanisms in Their Formation. Rev. Mineral. Geochem. 64, 223–282.

Götherström, A., Collins, M.J., Angerbjörn, A., Lidén, K., 2002. Bone preservation and DNA amplification. Archaeometry 44, 395–404.

Gourion-Arsiquaud, S., West, P.A., Boskey, A.L., 2008. Fourier transform-infrared microspectroscopy and microscopic imaging. Methods Mol. Biol. 455, 293–303.

Grunenwald, A., Keyser, C., Sautereau, A.M., Crubézy, E., Ludes, B., Drouet, C., 2014a. Novel contribution on the diagenetic physicochemical features of bone and teeth minerals, as substrates for ancient DNA typing. Anal. Bioanal. Chem. doi:10.1007/s00216-014-7863-z

Grunenwald, A., Keyser, C., Sautereau, A.M., Crubézy, E., Ludes, B., Drouet, C., 2014b. Adsorption of DNA on biomimetic apatites: Toward the understanding of the role of bone and tooth mineral on the preservation of ancient DNA. Appl. Surf. Sci. 292, 867–875.

Grupe, G., Balzer, A., Turban-Just, S., 2002. Modeling Protein Diagenesis in Ancient Bone: Towards a Validation of Stable Isotope Data, in: Biogeochemical Approaches to Paleodietary Analysis, Advances in Archaeological and Museum Science. Springer US, pp. 173–187.

Habelitz, S., Balooch, M., Marshall, S.J., Balooch, G., Marshall, G.W., Jr, 2002. In situ atomic force microscopy of partially demineralized human dentin collagen fibrils. J. Struct. Biol. 138, 227–236.

Hackett, C.J., 1981. Microscopical focal destruction (tunnels) in ex-humed human bones. Med. Sci. Law 21, 243–265.

Hansen, H.B., Damgaard, P.B., Margaryan, A., Stenderup, J., Lynnerup, N., Willerslev, E., Allentoft, M.E., 2017. Comparing Ancient DNA Preservation in Petrous Bone and Tooth Cementum. PLoS One 12, e0170940.

Hanson, D.A., Eyre, D.R., 1996. Molecular site specificity of pyridinoline and pyrrole cross-links in type I collagen of human bone. J. Biol. Chem. 271, 26508–26516.

He, B., Huang, S., Jing, J., Hao, Y., 2010. Measurement of hydroxyapatite density and Knoop hardness in sound human enamel and a correlational analysis between them. Arch. Oral Biol. 55, 134–141.

Heckel, C., Müller, K., White, R., Wolf, S., Conard, N.J., Normand, C., Floss, H., Reiche, I., 2016. F-content variation in mammoth ivory from Aurignacian contexts: Preservation, alteration, and implications for ivory-procurement strategies. Quat. Int. 403, 40–50.

Hedges, R.E.M., 2002. Bone diagenesis: an overview of processes. Archaeometry 44, 319–328.

Hedges, R.E.M., Clement, J.G., Thomas, C.D.L., O'connell, T.C., 2007. Collagen turnover in the adult femoral mid-shaft: modeled from anthropogenic radiocarbon tracer measurements. Am. J. Phys. Anthropol. 133, 808–816.

Hedges, R.E.M., Millard, A.R., 1995. Bones and Groundwater: Towards the Modelling of Diagenetic Processes. J. Archaeol. Sci. 22, 155–164.

Hedges, R.E.M., Millard, A.R., Pike, A.W.G., 1995. Measurements and Relationships of Diagenetic Alteration of Bone from Three Archaeological Sites. J. Archaeol. Sci. 22, 201–209.

Heinemeier, K.M., Schjerling, P., Heinemeier, J., Møller, M.B., Krogsgaard, M.R., Grum-Schwensen, T., Petersen, M.M., Kjaer, M., 2016. Radiocarbon dating reveals minimal collagen turnover in both healthy and osteoarthritic human cartilage. Sci. Transl. Med. 8, 346ra90.

High, K., Milner, N., Panter, I., Penkman, K.E.H., 2015. Apatite for destruction: investigating bone degradation due to high acidity at Star Carr. J. Archaeol. Sci. 59, 159–168.

Hiller, J.C., Wess, T.J., 2006. The use of small-angle X-ray scattering to study archaeological and experimentally altered bone. J. Archaeol. Sci. 33, 560–572.

Hillson, S., 2005. Teeth, Cambridge Manuals in Archaeology. Cambridge University Press.

Hofreiter, M., Serre, D., Poinar, H.N., Kuch, M., Pääbo, S., 2001. Ancient DNA. Nat. Rev. Genet. 2, 353–359.

Hollund, H.I., 2013. Diagenetic screening of bone samples; tools to aid taphonomic and archaeolmetric investigations. Geoarchaeological and Bioarchaeological Studies 15, 1–162.

Hollund, H.I., Jans, M.M.E., Collins, M., Kars, H., Joosten, I., Kars, S.M., 2012. What happened here? Bone histology as a tool in decoding the postmortem histories of archaeological bone from Castricum, the Netherlands. International Journal of Osteoarchaeology 22, 537–548.

Hollund, H.I., Jans, M.M.E., Kars, H., 2014. How are teeth better than bone? An investigation of dental tissue diagenesis and state of preservation at a histological scale. Internet Archaeology 36. doi:10.11141/ia.36.7

Jackes, M., Sherburne, R., Lubell, D., Barker, C., Wayman, M., 2001. Destruction of microstructrue in archaeological bone: a case study from Portugal. International Journal of Osteoarchaeology 11, 415–432.

Jágr, M., Eckhardt, A., Pataridis, S., Mikšík, I., 2012. Comprehensive proteomic analysis of human dentin. Eur. J. Oral Sci. 120, 259–268.

Janaway, R.C., 2008. The Decomposition of Materials Associated with Buried Cadavers, in: Tibbett, M., Carter, D.O. (Eds.), Soil Analysis in Forensic Taphonomy: Chemical and Biological Effects of Buried Human Remains. CRC Press, pp. 153–201.

Jans, M.M.E., 2008. Microbial bioerosion of bone - a review, in: Wisshak, M., Tapanila, L. (Eds.), Current Developments in Bioerosion. Springer-Verlag Berlin Heidelberg, Berlin, pp. 397–413.

Jans, M.M.E., Nielsen-Marsh, C.M., Smith, C.I., Collins, M.J., Kars, H., 2004. Characterisation of microbial attack on archaeological bone. J. Archaeol. Sci. 31, 87–95.

Jenkins, C.L., Bretscher, L.E., Guzei, I.A., Raines, R.T., 2003. Effect of 3-hydroxyproline residues on collagen stability. J. Am. Chem. Soc. 125, 6422–6427.

Jobling, M., Hurles, M., Tyler-Smith, C., 2013. Human Evolutionary Genetics: Origins, Peoples & Disease. Garland Science.

Johns, C., 2006. An Iron Age sword and mirror cist burial from Bryher, Isles of Scilly. Cornish archaeology 41, 1–80.

Jørkov, M.L.S., Heinemeier, J., Lynnerup, N., 2009. The petrous bone—A new sampling site for identifying early dietary patterns in stable isotopic studies. Am. J. Phys. Anthropol. 138, 199–209.

Keenan, S.W., 2016. From bone to fossil: A review of the diagenesis of bioapatite. Am. Mineral. 101, 1943–1951.

Keenan, S.W., Engel, A.S., 2017. Early diagenesis and recrystallization of bone. Geochim. Cosmochim. Acta 196, 209–223.

Kellerman, G.D., Waterman, N.G., Scharfenberger, L.F., 1976. Demonstration in vitro of post mortem bacterial migration. Am. J. Clin. Pathol. 66, 911–915.

Kimbel, W.H., Delezene, L.K., 2009. "Lucy" redux: a review of research on Australopithecus afarensis. Am. J. Phys. Anthropol. 140 Suppl 49, 2–48.

King, C.L., Tayles, N., Gordon, K.C., 2011. Re-examining the chemical evaluation of diagenesis in human bone apatite. J. Archaeol. Sci. 38, 2222–2230.

Kini, U., Nandeesh, B.N., 2012. Physiology of Bone Formation, Remodeling, and Metabolism, in: Fogelman, I., Gnanasegaran, G., van der Wall, H. (Eds.), Radionuclide and Hybrid Bone Imaging. Springer Berlin Heidelberg, pp. 29–57.

Klont, B., Damen, J.J., ten Cate, J.M., 1991. Degradation of bovine incisor root collagen in an in vitro caries model. Arch. Oral Biol. 36, 299–304.

Kollmannsberger, P., Kerschnitzki, M., Repp, F., Wagermaier, W., Weinkamer, R., Fratzl, P., 2017. The Small World of Osteocytes: Connectomics of the Lacuno-Canalicular Network in Bone. arXiv [physics.bio-ph].

Kontopoulos, I., Nystrom, P., White, L., 2016. Experimental taphonomy: post-mortem microstructural modifications in Sus scrofa domesticus bone. Forensic Sci. Int. 266, 320–328.

Koon, H.E.C., 2006. Detecting cooked bone in the archaeological record : a study of the thermal stability and deterioration of bone collagen (phd). University of York.

Lambert, J.B., Vlasak, S., Simpson, Szpunar, C.B., Buikstra, J.E., 1985. Bone diagenesis and dietary analysis. J. Hum. Evol. 14, 477–482.

Lam, B.V., Murray, R.H., Andres, B.W., Boyle-Mejia, O., Curry Rogers, K., 2009. Patterns of microbial bioerosion in bones from the Campanian Judith River Formation of Montana, in: 2009 Portland GSA Annual Meeting. gsa.confex.com.

Lam, Y.M., Chen, X., Pearson, O.M., 1999. Intertaxonomic Variability in Patterns of Bone Density and the Differential Representation of Bovid, Cervid, and Equid Elements in the Archaeological Record. Am. Antiq. 64, 343–362.

Large, D., Müller, K., Reiche, 2011. Approche analytique pour l'étude des ivoires archéologiques. Les défenses d'éléphant du site de Jinsha (1200-650 BC, Sichuan, Chine). ArchaeoSciences, Revue d'archéométrie. 35, 167–177.

Lee–Thorp, J., 2002. Two decades of progress towards understanding fossilization processes and isotopic signals in calcified tissue minerals. Archaeometry 44, 435–446.

Lee-Thorp, J.A., van der Merwe, N.J., 1991. Aspects of the chemistry of modern and fossil biological apatites. J. Archaeol. Sci. 18, 343–354.

Lerner, U.H., 2016. Bone remodeling in post-menopausal osteoporosis. J. Dent. Res.

Lian, J.B., Hauschka, P.V., Gallop, P.M., 1978. Properties and biosynthesis of a vitamin K-dependent calcium binding protein in bone. Fed. Proc. 37, 2615–2620.

Libby, W.F., Berger, R., Mead, J.F., Alexander, G.V., Ross, J.F., 1964. Replacement rates for human tissue from atmospheric radiocarbon. Science 146, 1170–1172.

Lindahl, T., 1993. Instability and decay of the primary structure of DNA. Nature 362, 709–715.

Lindahl, T., Nyberg, B., 1972. Rate of Depurination of Native Deoxyribonucleic Acid? Biochemistry 11.

Lyman, R.L., 2014. Bone Density and Bone Attrition, in: Manual of Forensic Taphonomy. pp. 51–72.

Lyman, R.L., 1984. Bone density and differential survivorship of fossil classes. Journal of Anthropological Archaeology 3, 259–299.

Manilay, Z., Novitskaya, E., Sadovnikov, E., McKittrick, J., 2013. A comparative study of young and mature bovine cortical bone. Acta Biomater. 9, 5280–5288.

Mansilla, J., Moreno-Castilla, C., Bosch, P., Aleman, I., Pijoan, C., Botella, M., 2014. On porosity of archaeological bones II. Textural characterization of Mesoamerican human bones. Palaeogeogr. Palaeoclimatol. Palaeoecol. 414, 493–499.

Marchiafava, V., Bonucci, E., Ascenzi, A., 1974. Fungal osteoclasia: a model of dead bone resorption. Calcif. Tissue Res. 14, 195–210.

Mathew, M., Takagi, S., 2001. Structures of Biological Minerals in Dental Research. J. Res. Natl. Inst. Stand. Technol. 106, 1035–1044.

Matsushima, N., Hikichi, K., 1989. Age changes in the crystallinity of bone mineral and in the disorder of its crystal. Biochim. Biophys. Acta 992, 155–159.

Metcalf, J.L., Parfrey, L.W., Gonzalez, A., Lauber, C.L., Knights, D., Ackermann, G., Humphrey, G.C., Gebert, M.J., Treuren, W.V., Berg-Lyons, D., Keepers, K., Guo, Y., Bullard, J., Fierer, N., Carter, D.O., Knight, R., 2013. A microbial clock provides an accurate estimate of the postmortem interval in a mouse model system. Elife 1–19.

Metcalf, J.L., Xu, Z.Z., Weiss, S., Lax, S., van Treuren, W., Hyde, E.R., Song, S.J., Amir, A., Larsen, P., Sangwan, N., Haarmann, D., Humphrey, G.C., Ackermann, G., Thompson, L.R., Gebert, M.J., Petrosino, J.F., Reed, S.C., Gilbert, J.A., Lynne, A.M., Bucheli, S.R., Carter, D.O., Knight, R., 2015. Microbial community assembly and metabolic function during mammalian corpse decomposition. ScienceExpress 1–8.

Mielki, G.F., Novais, R.F., Ker, J.C., Vergütz, L., Castro, G.F. de, 2016. Iron Availability in Tropical Soils and Iron Uptake by Plants. Rev. Bras. Cienc. Solo 40. doi:10.1590/18069657rbcs20150174

Morgan, E.F., Barnes, G.L., Einhorn, T.A., Marcus, R., 2013. The bone organ system: form and function. Academic Press, Cambridge, MA, USA.

Müller, K., Chadefaux, C., Thomas, N., Reiche, I., 2011. Microbial attack of archaeological bones versus high concentrations of heavy metals in the burial environment. A case study of animal bones from a mediaeval copper workshop in Paris. Palaeogeogr. Palaeoclimatol. Palaeoecol. 310, 39–51.

Müller, K., Reiche, I., 2011. Differentiation of archaeological ivory and bone materials by micro-PIXE/PIGE with emphasis on two Upper Palaeolithic key sites: Abri Pataud and Isturitz, France. J. Archaeol. Sci. 38, 3234–3243.

Mundy, G.R., 1999. Bone Remodelling and its Disorders. CRC Press.

Nango, N., Kubota, S., Hasegawa, T., Yashiro, W., Momose, A., Matsuo, K., 2016. Osteocyte-directed bone demineralization along canaliculi. Bone 84, 279–288.

Nicholson, R.A., 1996. Bone Degradation, Burial Medium and Species Representation: Debunking the Myths, an Experiment-based Approach. J. Archaeol. Sci. 23, 513–533.

Nielsen-Marsh, C., Gernaey, A., Turner-Walker, G., Hedges, R., Pike, A.W.G., Collins, M., 2000. The chemical degradation of bone, in: Cox, M., Mays, S. (Eds.), Human Osteology: In Archaeology and Forensic Science. Cambridge University Press, pp. 439–454.

Nielsen-Marsh, C.M., Hedges, R.E.M., 2000a. Patterns of Diagenesis in Bone I: The Effects of Site Environments. J. Archaeol. Sci. 27, 1139–1150.

Nielsen-Marsh, C.M., Hedges, R.E.M., 2000b. Patterns of Diagenesis in Bone II: Effects of Acetic Acid Treatment and the Removal of Diagenetic CO32−. J. Archaeol. Sci. 27, 1151–1159.

Nielsen-Marsh, C.M., Smith, C.I., Jans, M.M.E., Nord, A., Kars, H., Collins, M.J., 2007. Bone diagenesis in the European Holocene II: taphonomic and environmental considerations. J. Archaeol. Sci. 34, 1523–1531.

Nudelman, F., Lausch, A.J., Sommerdijk, N.A.J.M., Sone, E.D., 2013/8. In vitro models of collagen biomineralization. J. Struct. Biol. 183, 258–269.

Nyman, J.S., Roy, A., Shen, X., Acuna, R.L., Tyler, J.H., Wang, X., 2006. The influence of water removal on the strength and toughness of cortical bone. J. Biomech. 39, 931–938.

Orgel, J.P.R.O., Irving, T.C., Miller, A., Wess, T.J., 2006. Microfibrillar structure of type I collagen in situ. Proc. Natl. Acad. Sci. U. S. A. 103, 9001–9005.

Ortner, D.J., Turner-Walker, G., 2003. The Biology of Skeletal Tissues, in: Identification of Pathological Conditions in Human Skeletal Remains. Elsevier, pp. 11–35.

Ortner, D.J., von Endt, D.W., Robinson, M.S., 1972. The Effect of Temperature on Protein Decay in Bone: Its Significance in Nitrogen Dating of Archaeological Specimens. Am. Antiq. 37, 514–520.

Ottoni, C., Koon, H.E.C., Collins, M.J., Penkman, K.E.H., Rickards, O., Craig, O.E., 2009. Preservation of ancient DNA in thermally damaged archaeological bone. Naturwissenschaften 96, 267–278.

Pääbo, S., 1989. Ancient DNA: extraction, characterization, molecular cloning, and enzymatic amplification. Proc. Natl. Acad. Sci. U. S. A. 86, 1939–1943.

Pääbo, S., Poinar, H., Serre, D., Jaenicke-Despres, V., Hebler, J., Rohland, N., Kuch, M., Krause, J., Vigilant, L., Hofreiter, M., 2004. Genetic analyses from ancient DNA. Annu. Rev. Genet. 38, 645–679.

Painter, T.J., 1991. Lindow man, tollund man and other peat-bog bodies: The preservative and antimicrobial action of Sphagnan, a reactive glycuronoglycan with tanning and sequestering properties. Carbohydr. Polym. 15, 123–142.

Painter, T.J., 1983. Residues of d-lyxo-5-hexosulopyranuronic acid in Sphagnum holocellulose, and their role in cross-linking. Carbohydr. Res. 124, C18–C21.

Papageorgopoulou, C., Kuhn, G., Ziegler, U., Rühli, F.J., 2010. Diagnostic morphometric applicability of confocal laser scanning microscopy in Osteoarchaeology. Int. J. Osteoarchaeol. 20, 708–718.

Park, E.-S., Cho, H.-S., Kwon, T.-G., Jang, S.-N., Lee, S.-H., An, C.-H., Shin, H.-I., Kim, J.-Y., Cho, J.-Y., 2009. Proteomics analysis of human dentin reveals distinct protein expression profiles. J. Proteome Res. 8, 1338–1346.

Parsons, T.J., Walter Weedn, V., 2006. Preservation and recovery of DNA in postmortem specimens and trace samples, in: Forensic Taphonomy: The Postmortem Fate of Human Remains. CRC Press.

Pechal, J.L., Crippen, T.L., Benbow, M.E., Tarone, A.M., Dowd, S., Tomberlin, J.K., 2014. The potential use of bacterial community successtion in forensics as described by high throughput metagenomic sequencing. Int. J. Legal Med. 128, 193–205.

Pechal, J.L., Crippen, T.L., Tarone, A.M., Lewis, A.J., Tomberlin, J.K., Benbow, M.E., 2013. Microbial community functional change during vertebrate carrion decomposition. PlosOne 8, 1–11.

Pellegrini, M., Lee-Thorp, J.A., Donahue, R.E., 2011. Exploring the variation of the δ18Op and δ18Oc relationship in enamel increments. Palaeogeogr. Palaeoclimatol. Palaeoecol. 310, 71–83.

Person, A., Bocherens, H., Saliege, J.-F., Paris, F., Zeitoun, V., Gerard, M., 1995. Early Diagenetic Evolution of Bone Phosphate: An X-ray DiVractometry Analysis. J. Archaeol. Sci. 22, 211–221.

Pesquero, M.D., Ascaso, C., Alcala, L., Fernandez-Jalvo, Y., 2010. A new taphonomic bioerosion in a Miocene lakeshore environment. Palaeogeogr. Palaeoclimatol. Palaeoecol. 295, 192–198.

Pesquero, M.D., Bell, L.S., Fernández-Jalvo, Y., 2017. Skeletal modification by microorganisms and their environments. Hist. Biol. 1–12.

Pfretzschner, H.-U., Tütken, T., 2011. Rolling bones – Taphonomy of Jurassic dinosaur bones inferred from diagenetic microcracks and mineral infillings. Palaeogeogr. Palaeoclimatol. Palaeoecol. 310, 117–123.

Piepenbrink, H., 1986. Two examples of biogenous dead bone decomposition and their consequences for taphonomic interpretation. J. Archaeol. Sci. 13, 417–430.

Pinhasi, R., Fernandes, D., Sirak, K., Novak, M., Connell, S., Alpaslan-Roodenberg, S., Gerritsen, F., Moiseyev, V., Gromov, A., Raczky, P., Anders, A., Pietrusewsky, M., Rollefson, G., Jovanovic, M., Trinhhoang, H., Bar-Oz, G., Oxenham, M., Matsumura, H., Hofreiter, M., 2015. Optimal Ancient DNA Yields from the Inner Ear Part of the Human Petrous Bone. PLoS One 10, e0129102.

Podrazký, V., Sedmerová, V., 1966. Densities of collagen dehydrated by some organic solvents. Experientia 22, 792.

Poinar, H.N., 2003. The top 10 list: criteria of authenticity for DNA from ancient and forensic samples. Int. Congr. Ser. 1239, 575–579.

Pokines, J.T., Baker, J.E., 2014. Effects of Burial Enviroment on Osseous Remains, in: Pokines, J.T., Symes, S.A. (Eds.), Manual of Forensic Taphonomy. CRC Press, pp. 73–114.

Pokines, J.T., King, R.E., Graham, D.D., Costello, A.K., Adams, D.M., Pendray, J.M., Rao, K., Siwek, D., 2016. The effects of experimental freeze-thaw cycles to bone as a component of subaerial weathering. Journal of Archaeological Science: Reports 6, 594–602.

Posner, A.S., 1985. The Mineral of Bone. Clin. Orthop. Relat. Res. 200, 87–99.

Price, P.A., Otsuka, A.A., Poser, J.W., Kristaponis, J., Raman, N., 1976. Characterization of a gamma-carboxyglutamic acid-containing protein from bone. Proc. Natl. Acad. Sci. U. S. A. 73, 1447–1451.

Pruvost, M., Schwarz, R., Bessa Correia, V., Champlot, S., Grange, T., Geigl, E.-M., 2008. DNA diagenesis and palaeogenetic analysis: Critical assessment and methodological progress. Palaeogeogr. Palaeoclimatol. Palaeoecol. 266, 211–219.

Pruvost, M., Schwarz, R., Correia, V.B., Champlot, S., Braguier, S., Morel, N., Fernandez-Jalvo, Y., Grange, T., Geigl, E.-M., 2007. Freshly excavated fossil bones are best for amplification of ancient DNA. Proc. Natl. Acad. Sci. U. S. A. 104, 739–744.

Reiche, I., Favre-Quattropani, L., Calligaro, T., Salomon, J., Bocherens, H., Charlet, L., Menu, M., 1999. Trace element composition of archaeological bones and post-mortem alteration in the burial environment. Nucl. Instrum. Methods Phys. Res. B 150, 656–662.

Reiche, I., Favre-Quattropani, L., Vignaud, C., Bocherens, H., Charlet, L., Menu, M., 2003. A multi-analytical study of bone diagenesis: the Neolithic site of Bercy (Paris, France). Measurement Science and Technology 14, 1608.

Reiche, I., Vignaud, C., Favre-Quattropani, L., Menu, M., 2002. Fluorine analysis in biogenic and geological apatite by analytical transmission electron microscopy and nuclear reaction analysis. J. Trace Microprobe Tech. 20, 211–231.

Reiche, I., Vignaud, C., Menu, M., 2002. The crystallinity of ancient bone and dentine: new insights by transmission electron microscopy. Archaeometry 44, 447–459.

Rengel, Z., 2015. Availability of Mn, Zn and Fe in the rhizosphere. Journal of Soil Science and Plant nutrition.

Reznikov, N., Chase, H., Brumfeld, V., Shahar, R., Weiner, S., 2015. The 3D structure of the collagen fibril network in human trabecular bone: relation to trabecular organization. Bone 71, 189–195.

Ritz-Timme, S., Collins, M.J., 2002. Racemization of aspartic acid in human proteins. Ageing Res. Rev. 1, 43–59.

Ritz-Timme, S., Schütz, H.W., Collins, M.J., 1999. Evaluation of aspartic acid racemization ratios in the human femur for age estimation. J. Forensic Sci. 44, 874–876.

Roberts, S.J., Smith, C.I., Millard, A., Collins, M.J., 2002. The taphonomy of cooked bone: characterizing boiling and its physico–chemical effects. Archaeometry 44, 485–494.

Robins, S.P., Shimokomaki, M., Bailey, A.J., 1973. The chemistry of the collagen cross-links. Age-related changes in the reducible components of intact bovine collagen fibres. Biochem. J 131, 771–780.

Robling, A.G., Castillo, A.B., Turner, C.H., 2006. Biomechanical and molecular regulation of bone remodeling. Annu. Rev. Biomed. Eng. 8, 455–498.

Rogers, K.D., Zioupos, P., 1999. The bone tissue of the rostrum of a Mesoplodon Densirostris whale: a mammalian biomineral demonstrating extreme texture. J. Mater. Sci. Lett. 18, 651–654.

Rollo, F., Ubaldi, M., Marota, I., Luciani, S., Ermini, L., 2002. DNA Diagenesis: Effect of Environment and Time on Human Bone. Anc. Biomol. 4, 1–7.

Roux, W., 1887. Über eine im Knochen lebende Gruppe von Fadenpilzen (Mycelites ossifragus).

Saito, M., Marumo, K., 2010. Collagen cross-links as a determinant of bone quality: a possible explanation for bone fragility in aging, osteoporosis, and diabetes mellitus. Osteoporos. Int. 21, 195–214.

Salesse, K., Dufour, E., Lebon, M., Wurster, C., Castex, D., Bruzek, J., Zazzo, A., 2014. Variability of bone preservation in a confined environment: The case of the catacomb of Sts Peter and Marcellinus (Rome, Italy). Palaeogeogr. Palaeoclimatol. Palaeoecol. doi:10.1016/j.palaeo.2014.07.021

Salmon, C.R., Giorgetti, A.P.O., Paes Leme, A.F., Domingues, R.R., Sallum, E.A., Alves, M.C., Kolli, T.N., Foster, B.L., Nociti, F.H., Jr, 2016. Global proteome profiling of dental cementum under experimentally-induced apposition. J. Proteomics 141, 12–23.

Sarkissian, C.D., Allentoft, M.E., Avila-Arcos, M.C., Barnett, R., Campos, P.F., Cappellini, E., Ermini, L., Fernandez, R., Fonseca, R.D., Ginolhac, A., Hansen, A.J., Jonsson, H., Korneliussen, T., Margaryan, A., Martin, M.D., Moreno-Mayar, J.V., Raghavan, M., Rasmussen, M., Velasco, M.S., Schroeder, H., Schubert, M., Seguin-Orlando, A., Wales, N., Gilbert, M.T.P., Willerslev, E., Orlando, L., 2015. Ancient genomics. Philos. Trans. R. Soc. Lond. B Biol. Sci. 370.

Schaffer, J., 1895. Bemerkungen zur Geschichte der Bohrkanäle in Knochen und Zähnen.

Schuhmann, B., Brunnberg, L., Zentek, J., Müller, K., 2014. Bone composition and bone mineral density of long bones of free-living raptors. Veterinary Science Development 4. doi:10.4081/vsd.2014.5601

Schultz, M., 1997. Microscopic structure of bone. Forensic taphonomy: the postmortem fate of human remains. London: CRC Press, 1997a 187–199.

Schwarcz, H.P., 2015. The ultrastructure of bone as revealed in electron microscopy of ion-milled sections. Semin. Cell Dev. Biol. 46, 44–50.

Shahar, R., Dean, M.N., 2013. The enigmas of bone without osteocytes. Bonekey Rep 2, 343.

Shapiro, B., 2015. How to Clone a Mammoth: The Science of De-Extinction. Princeton University Press.

Shin, J.Y., Hedges, R.E.M., 2012. Diagenesis in bone and enamel apatite carbonate; the potential of density separation to assess the original composition. J. Archaeol. Sci. 39, 1123–1130.

Shoulders, M.D., Raines, R.T., 2009. Collagen structure and stability. Annu. Rev. Biochem. 78, 929–958.

Sillen, A., LeGeros, R., 1991. Solubility profiles of synthetic apatites and of modern and fossil bones. J. Archaeol. Sci. 18, 385–397.

Smith, C., 2002. Modelling Diagenesis in Archaeological Bone (PhD). University of Newcastle-Upon-Tyne.

Smith, C.I., Craig, O.E., Prigodich, R.V., Nielsen-Marsh, C.M., Jans, M.M.E., Vermeer, C., Collins, M.J., 2005. Diagenesis and survival of osteocalcin in archaeological bone. J. Archaeol. Sci. 32, 105–113.

Smith, C.I., Nielsen–Marsh, C.M., Jans, M.M.E., Arthur, P., Nord, A.G., Collins, M.J., 2002. The strange case of Apigliano: early “fossilization” of medieval bone in southern Italy. Archaeometry 44, 405–415.

Smith, C.I., Nielsen-Marsh, C.M., Jans, M.M.E., Collins, M.J., 2007. Bone diagenesis in the European Holocene I: patterns and mechanisms. J. Archaeol. Sci. 34, 1485–1493.

Sognnaes, R.F., 1959. Microradiographic observations on demineralization gradients in the pathogenesis of hard-tissue destruction. Arch. Oral Biol. 1, 106–121.

Sognnaes, R.F., 1956. Histologic evidence of developmental lesions in teeth originating from paleolithic, prehistoric, and ancient man. Am. J. Pathol. 32, 547–577.

Sognnaes, R.F., 1955. Postmortem microscopic defects in the teeth of ancient man: AMA Archives of Pathology, v. 59.

Solari, A., Olivera, D., Gordillo, I., Bosch, P., Fetter, G., Lara, V.H., Novelo, O., 2013. Cooked Bones? Method and Practice for Identifying Bones Treated at Low Temperature. International Journal of Osteoarchaeology. doi:10.1002/oa.2311

Sosa, C., Vispe, E., Nunez, C., Beata, M., Casalod, Y., Bolea, M., Hedges, R.E.M., Martinez-Jarreta, B., 2013. Association between ancient bone preservation and DNA yield: a multidisciplinary approach. Am. J. Phys. Anthropol. 151, 102–109.

Stathopoulou, E.T., Psycharis, V., Chryssikos, G.D., Gionis, V., Theodorou, G., 2008. Bone diagenesis: New data from infrared spectroscopy and X-ray diffraction. Palaeogeogr. Palaeoclimatol. Palaeoecol. 266, 168–174.

Stiner, M.C., Kuhn, S.L., Surovell, T.A., Goldberg, P., Meignen, L., Weiner, S., Bar-Yosef, O., 2001. Bone Preservation in Hayonim Cave (Israel): a Macroscopic and Mineralogical Study. J. Archaeol. Sci. 28, 643–659.

Stiner, M.C., Kuhn, S.L., Weiner, S., Bar-Yosef, O., 1995. Differential burning, recrystallization, and fragmentation of archaeological bone. J. Archaeol. Sci. 22, 223–237.

Surovell, T.A., Stiner, M.C., 2001. Standardizing Infra-red Measures of Bone Mineral Crystallinity: an Experimental Approach. J. Archaeol. Sci. 28, 633–642.

Tang, S.Y., Vashishth, D., 2010. Non-enzymatic glycation alters microdamage formation in human cancellous bone. Bone 46, 148–154.

Tanzer, M.L., 1973. Cross-linking of collagen. Science 180, 561–566.

Taylor, T.N., Krings, M., Taylor, E.L., 2014. Fossil fungi.

Termine, J.D., 1988. Non-collagen proteins in bone. Ciba Found. Symp. 136, 178–202.

Termine, J.D., Posner, A.S., 1966. Infrared analysis of rat bone: age dependency of amorphous and crystalline mineral fractions. Science 153, 1523–1525.

Teruel, J. de D., Alcolea, A., Hernández, A., Ruiz, A.J.O., 2015. Comparison of chemical composition of enamel and dentine in human, bovine, porcine and ovine teeth. Arch. Oral Biol. 60, 768–775.

Thomsen, T., 1929. Egekistefundet fra Egtved, fra den ældre Bronzealder. Nordiske Fortidsminder II, 165–201.

Todoh, M., Tadano, S., Giri, B., Nishimoto, M., 2009. Effect of gradual demineralization on the mineral fraction and mechanical properties of cortical bone. Journal of Biomechanical Science and Engineering 4, 230–238.

Tont, S.A., Pearcy, W.G., Arnold, J.S., 1977. Bone structure of some marine vertebrates. Mar. Biol. 39, 191–196.

Trueman, C.N., 2013. Chemical taphonomy of biomineralized tissues. Palaeontology 56, 475–486.

Trueman, C.N., Benton, M.J., 1997. A geochemical method to trace the taphonomic history of reworked bones in sedimentary settings. Geology 25, 263–266.

Trueman, C.N.G., Behrensmeyer, A.K., Tuross, N., Weiner, S., 2004. Mineralogical and compositional changes in bones exposed on soil surfaces in Amboseli National Park, Kenya: diagenetic mechanisms and the role of sediment pore fluids. J. Archaeol. Sci. 31, 721–739.

Trueman, C.N., Martill, D.M., 2002. The long–term survival of bone: the role of bioerosion. Archaeometry 44, 371–382.

Trueman, C.N., Privat, K., Field, J., 2008. Why do crystallinity values fail to predict the extent of diagenetic alteration of bone mineral? Palaeogeogr. Palaeoclimatol. Palaeoecol. 266, 160–167.

Turban-Just, S., Schramm, S., 1998. Stable carbon and nitrogen isotope ratios of individual amino acids give new insights into bone collagen degradation. Bull. Soc. Geol. Fr. 169, 109–114.

Turner-Walker, G., 2012. Early bioerosion in skeletal tissues: persistence through deep time. Neues Jahrbuck für Geologie und Paläontogie 265, 165–183.

Turner-Walker, G., 2011. The mechanical properties of artificially aged bone: Probing the nature of the collagen–mineral bond. Palaeogeogr. Palaeoclimatol. Palaeoecol. 310, 17–22.

Turner-Walker, G., 2009. Degradation pathways and conservation strategies for ancient bone from wet, anoxic sites, in: Proceedings of the 10th Triennial Meeting of the ICOM-CC Working Group for Wet Organic Archaeological Materials. pp. 659–675.

Turner-Walker, G., 2008. The chemical and microbial degradation of bones and teeth, in: Pinhasi, R., Mays, S. (Eds.), Advances in Human Palaeopathology. John Wiley & Sons, Chinchester, pp. 3–30.

Turner-Walker, G.H., 1993. The characterisation of fossil bone (Doctoral). Durham University.

Turner-Walker, G., Jans, M.M.E., 2008. Reconstructing taphonomic histories using histological analysis. Palaeogeogr. Palaeoclimatol. Palaeoecol. 266, 227–235.

Turner-Walker, G., Nielsen-Marsh, C.M., Syversen, U., Kars, H., Collins, M.J., 2002. Sub-micron spongiform porosity is the major ultra-structural alteration occurring in archaeological bone. International Journal of Osteoarchaeology 12, 407–414.

Turner-Walker, G., Peacock, E.E., 2008. Preliminary results of bone diagenesis in Scandinavian bogs. Palaeogeogr. Palaeoclimatol. Palaeoecol. 266, 151–159.

Turner-Walker, G., Syversen, U., 2002. Quantifying histological changes in archaeological bones using BSE-SEM image analysis. Archaeometry 44, 461–468.

Tuross, N., 2003. Recent advances in bone, dentin, and enamel biochemistry. Identification of pathological conditions in human skeletal remains. Ortner DJ, Editor. Academic Press: New York 65–72.

Tuross, N., 1993. The Other Molecules in Ancient Bone: Noncollagenous Proteins and DNA, in: Professor Dr Joseph, Grupe, P.D.G. (Eds.), Prehistoric Human Bone. Springer Berlin Heidelberg, pp. 275–292.

Tuross, N., Behrensmeyer, A.K., Eanes, E.D., 1989. Strontium increases and crystallinity changes in taphonomic and archaeological bone. J. Archaeol. Sci. 16, 661–672.

Tütken, T., Vennemann, T.W., 2011. Fossil bones and teeth: Preservation or alteration of biogenic compositions? Palaeogeography Palaeoclimatology Palaeoecology 310, 1–8.

Tütken, T., Vennemann, T.W., Pfretzschner, H.-U., 2008. Early diagenesis of bone and tooth apatite in fluvial and marine settings: Constraints from combined oxygen isotope, nitrogen and REE analysis. Palaeogeogr. Palaeoclimatol. Palaeoecol. 266, 254–268.

Tzaphlidou, M., Berillis, P., 2005. Collagen fibril diameter in relation to bone site. a quantitative ultrastructural study. Micron 36, 703–705.

Uchiyama, A., Inoue, T., Fujimoto, D., 1981. Synthesis of Pyridinoline during In Vitro Aging of Bone Collagen1. J. Biochem. 90, 1795–1798.

van Klinken, G.J., Hedges, R.E.M., 1995. Experiments on Collagen-Humic Interactions: Speed of Humic Uptake, and Effects of Diverse Chemical Treatments. J. Archaeol. Sci. 22, 263–270.

Vennat, E., Bogicevic, C., Fleureau, J.-M., Degrange, M., 2009. Demineralized dentin 3D porosity and pore size distribution using mercury porosimetry. Dent. Mater. 25, 729–735.

Vitagliano, L., Berisio, R., Mazzarella, L., Zagari, A., 2001. Structural bases of collagen stabilization induced by proline hydroxylation. Biopolymers 58, 459–464.

Von Endt, D.W., Ortner, D.J., 1984. Experimental effects of bone size and temperature on bone diagenesis. J. Archaeol. Sci. 11, 247–253.

Watson, J.D., Crick, F.H.C., 1953. A structure for deoxyribose nucleic acid. Nature 171, 737–738.

Wedl, C., 1864. Über einen im Zahnbein und Knochen keimenden Pilz. Akademie der Wissenschaften, mathematisch-naturwissenschaftliche Classe, Vienna 50, 171–193.

Weiner, S., Bar-Yosef, O., 1990. States of preservation of bones from prehistoric sites in the Near East: A survey. J. Archaeol. Sci. 17, 187–196.

Weiner, S., Traub, W., Wagner, H.D., 1999. Lamellar Bone: Structure–Function Relations. J. Struct. Biol. 126, 241–255.

White, E.M., Hannus, L.A., 1983. Chemical Weathering of Bone in Archaeological Soils. Am. Antiq. 48, 316–322.

White, L., Booth, T.J., 2014. The origin of bacteria responsible for bioerosion to the internal bone microstucture: results from experimentally-deposited pig carcasses. Forensic Sci. Int. 239, 92–102.

White, T.D., Black, M.T., Folkens, P.A., 2012. Human Osteology. Elsevier Science.

Whitford, D., 2013. Proteins: Structure and Function. John Wiley & Sons.

Wright, L.E., Schwarcz, H.P., 1996. Infrared and Isotopic Evidence for Diagenesis of Bone Apatite at Dos Pilas, Guatemala: Palaeodietary Implications. J. Archaeol. Sci. 23, 933–944.

You, L.-D., Weinbaum, S., Cowin, S.C., Schaffler, M.B., 2004. Ultrastructure of the osteocyte process and its pericellular matrix. Anat. Rec. A Discov. Mol. Cell. Evol. Biol. 278, 505–513.

Yu, Z., An, B., Ramshaw, J.A.M., Brodsky, B., 2014. Bacterial collagen-like proteins that form triple-helical structures. J. Struct. Biol. 186, 451–461.

Zanolli, C., 2013. Additional evidence for morpho-dimensional tooth crown variation in a New Indonesian H. erectus sample from the Sangiran Dome (Central Java). PLoS One 8.

Zaremba-Niedźwiedzka, K., Andersson, S.G.E., 2013. No ancient DNA damage in Actinobacteria from the Neanderthal bone. PLoS One 8, e62799.

Zioupos, P., Cook, R.B., Hutchinson, J.R., 2008. Some basic relationships between density values in cancellous and cortical bone. J. Biomech. 41, 1961–1968.

Zioupos, P., Currey, J.D., Casinos, A., 2000. Exploring the effects of hypermineralisation in bone tissue by using an extreme biological example. Connect. Tissue Res. 41, 229–248.

Abstract

Fourier transform infrared (FTIR) spectroscopy using attenuated total reflection (ATR) is commonly used for the examination of bone. During sample preparation bone is commonly ground, changing the particle size distribution. Although previous studies have examined changes in crystallinity caused by the intensity of grinding using FTIR, the effect of sample preparation (i.e. particle size and bone tissue type) on the FTIR data is still unknown.

This study reports on the bone powder particle size effects on mid-IR spectra and within sample variation (i.e. periosteal, mesosteal, trabecular) using FTIR-ATR. Twenty-four archaeological human and faunal bone samples (5 heated and 19 unheated) of different chronological age (Neolithic to post-Medieval) and origin (Belgium, Britain, Denmark, Greece) were ground using either (1) a ball-mill grinder, or (2) an agate pestle and mortar, and split into grain fractions (>500 μm, 250-500 μm, 125-250 μm, 63-125 μm, and 20-63 μm).

Bone powder particle size has a strong but predictable effect on the infrared splitting factor (IRSF), carbonate/phosphate (C/P) ratio, and amide/phosphate (Am/P) values. The absorbance and positions of the main peaks, the 2nd derivative components of the phosphate and carbonate bands, as well as the full width at half maximum (FWHM) of the 1010 cm^{-1} phosphate peak are particle size dependent. This is likely to be because of the impact of the particle size on the short- and long-range crystal order, as well as the contact between the sample and the prism, and hence the penetration depth of the IR light. Variations can be also observed between periosteal, cortical and trabecular areas of bone. We therefore propose a standard preparation method for bone powder for FTIR-ATR analysis that significantly improves accuracy, consistency, reliability, replicability and comparability of the data, enabling systematic evaluation of bone in archaeological, anthropological, paleontological, forensic and biomedical studies.

Keywords: Bone; FTIR-ATR; sample preparation; particle size; bioapatite; crystal order/disorder

1. Introduction

Bone is a complex inorganic/organic composite material with a hierarchical structural order that is reflected in its biomechanical properties [1–7]. Biological apatite (BAp) nanocrystals are carbonated calcium phosphate mineral compounds with species, age, or pathology related compositional/structural variation generally represented by the formula $(Ca^{2+}, Na^{+}, Mg^{2+}, [])_{10}$ $(PO_4^{3-}, HPO_4^{3-}, CO_3^{2-})_6$ $(OH^{-}, F^{-}, Cl^{-}, CO_3^{2-}, O, [])_2$ [4,8–14]. BAp dominates bone (i.e. 65-70 wt. %), with the organic content (primarily collagen type I) accounting for 20-25 wt. % and the remaining 5-10 wt. % being water [2].

The information that can be preserved within skeletal tissues has shaped the way we interpret the past [15,16]. However, in archaeological and fossil bone, diagenesis leads to its partial or complete destruction, with accompanying loss of vital biochemical information [17–21]. Over the past decades, Fourier transform infrared (FTIR) spectroscopy has been increasingly used to better understand bone diagenesis, as well as for screening of archaeological and fossil bone [22–34]. The correspondence between measurements taken with transmission FTIR, ATR (attenuated total reflection) and DRIFT (diffuse reflectance infrared Fourier transform) can be problematic [34–36]. Nevertheless, because FTIR is so minimally invasive/destructive and provides information on both the inorganic and organic structures present, it has been commonly used to assess the postmortem changes in BAp crystals (e.g. crystallinity, carbonate to phosphate content, fluorine and calcite content), and the organic preservation in heated, unheated and pathological bones [25,31,35,37–44].

The infrared splitting factor (IRSF, also termed crystallinity) is assumed to be related to the crystal order and size of bone mineral [2,25,45–47] which can change *in vivo* (ontogenetic bone growth/maturity) and post-mortem (diagenesis, heating) [e.g. 8,22,48,49]. Higher crystallinity is considered to be an indication of an increase in BAp crystals' size and atomic order due to either: a) a growth of the larger crystals at the expense of the smaller ones (i.e. Ostwald ripening); b) a loss of the smaller crystals; or c) both. Lower IRSF values reflect the smaller size and higher atomic disorder of the BAp crystals [2,22,25,26,29,46,47,50].

These changes in bioapatite characteristics are caused by several ionic substitutions that take place both in the hydrated layer and the apatite core, and strongly affect its dissolution/recrystallization behaviour [4,51]. Carbonate (CO_3^{2-}) content (c. 4-6 wt. %), which is considered to be related to crystallinity (and thus IRSF), is such an example of ionic substitution of carbonate for phosphate (type B), and vice versa, in the bioapatite structure [4,25,52–58]. Although type A substitution (CO_3^{2-} for OH^{-}) might be relatively limited in BAp, its role should not be neglected [4,25,31,56,57,59]. FTIR has also been used to assess organic preservation in archaeological and fossil bone using the Am/P (amide to phosphate) ratio [e.g. 29,60], while other minor ionic

concentrations of elements (such as Mg, Na, Sr, K, Zn and F) also play a special role in its structure and function [4,11,53–55,61,62].

Although the contribution of FTIR to the study of archaeological and fossil bone is indisputable, the usefulness of the indices (such as IRSF) as a measure of BAp preservation and change has been questioned [26,31,48,58,63,64]. The introduction of the relatively new FTIR-ATR technique offers rapid, cost efficient and minimally destructive analysis [30,34,49], but the issues of accuracy, precision, reproducibility and comparability of the data have not yet been resolved [36,48].

Past studies have tried to tackle these issues by investigating the effect of sample preparation methods on bone IRSF values, with a decrease in IRSF reported with more intensive pulverization [26]. Surovell & Stiner [26] argue that grinding may actually introduce variations in crystallinity that may mask the original signal due to structural changes caused to the BAp crystals. They propose two possibilities that could explain the phenomenon: a) changes are primarily caused by the particle separation of bone mineral of differing crystallinity (i.e. separation hypothesis), or b) grinding affects the bioapatite crystal structure (i.e. destruction hypothesis), and subsequently, the mid-IR spectra. Overall, it has been argued that there seems to be a destruction of BAp crystals during grinding, although when there is no control, or grinding is excessive, it is difficult to differentiate between the actual bone crystallinity from that introduced during sample preparation [26]. Hollund et al. [34] also observed significant preparation-based differences (i.e. drilling and grinding with and without sieving) between IRSF, C/P and Am/P values. The grinding effect was more evident in samples of higher crystallinity, so Hollund et al. [34] proposed drilling bone without sieving as an alternative to the Surovell and Stiner [26] preparation method.

Repeated grinding of calcite during preparation for FTIR measurements has been shown to affect the material's atomic order as revealed by changes in the mid-IR spectrum [65,66]. Asscher et al. [46,47] tried to explore the effects of grinding on bone and tooth, and decouple it from the atomic disorder effect to better assess the preservation state of archaeological/fossil bone. They compared the IRSF values of samples repeatedly ground for variable amounts of time and plotted them against the full width at half maximum (FWHM) of the main v_3 phosphate peak in mid-IR spectra (i.e. 1010 cm^{-1}). From the relationship observed, it was shown that grinding (i.e. particle size) affects both the short (IRSF) and long (FWHM at 1010 cm^{-1}) range order of bone. Thus, the use of the grinding curve approach can significantly increase the sensitivity of FTIR for monitoring diagenesis (slopes of the grinding curves increase with poorer preservation), as compared to the IRSF alone, and it can also allow the identification of differences in crystal size/atomic order of different animal species and hard tissues (bone, dentine and enamel mineral) [46].

While this trendline method partly shows the importance of particle size (still uncontrolled) on the mid-IR spectrum, it requires regrinding and measuring the same sample repeatedly for several

times. Furthermore, the powders were analysed in KBr pellets, requiring significant amounts of material mixed with KBr. Excessive grinding can also lead to a contamination of bone powder or even damage surviving biomolecules in samples that could be also used for DNA or protein analysis [e.g. 67,68], making FTIR KBr and grinding curves a destructive method and wasting precious material, in lieu of additional information on crystalline order.

Therefore, although previous studies have recommended optimal methods, the precise effects of particle size on FTIR data has never been thoroughly explored, and only in a limited number of studies particles have been homogeneous [25–27,36]. Excluding the variations due to sample preparation methods that are related with the atomic order/disorder, small but insignificant tissue specific variations have also been reported for both unheated [27] and heated bone [48].

The increased adoption of FTIR-ATR further changes the equation. The method is being increasingly commonly used because it is a cost efficient, rapid and minimally destructive method, and has the potential to act as screening method to determine which bones show optimal preservation. The powder can be extracted for biomolecules after analysis with no loss of material. This study presents the effects of sample selection (i.e. periosteal, mesosteal, trabecular bone) as well as particle size on the mid-IR spectrum of bone measured by FTIR-ATR. We propose a standard preparation procedure for the analysis of bone powder using FTIR-ATR to improve data accuracy, precision, comparability and reproducibility. The process focuses on the particle size effect and requires bone powder of even sized particles. This approach improves the contact between the sample and the prism, allows a deeper penetration depth of the IR radiation into individual BAp crystals, and avoids damage in the short- and long-range order of bioapatite crystals by using optimal bone powder particle sizes.

2. Materials and Methods

Twenty-four archaeological human and animal bone samples (5 heated and 19 unheated) of different chronological age (Neolithic to post-Medieval) and origin (Belgium, Britain, Denmark, Greece) were used in this study (Table S1 - supplementary material). Prior to analysis, the trabecular, periosteal/sub-periosteal and endosteal/sub-endosteal tissues were mechanically removed using a scalpel. For the examination of the particle size effect on mid-IR spectra, the mesosteal (mid-cortical) tissue of nineteen specimens was ground using either (1) a Retsch oscillating steel ball mill grinder at 20 Hz for 20-25 seconds x 3-5 times, or (2) an agate pestle and mortar.

Samples were sieved using Endecotts woven stainless steel mesh sieves with an aperture size of 500 μm, 250 μm, 125 μm, 63 μm, and 20 μm to produce 5 particle size classes (i.e. > 500 μm, 250-500 μm, 125-250 μm, 63-125 μm, 20-63 μm). Six of the archaeological samples (3 fauna, 2 heated and 1 unheated human) were also ground down to c. 1 μm using a Retsch PM100 ball mill

grinder. The container, lid and ball grinders were cooled using liquid nitrogen to reduce potential destruction of crystals due to heat produced during the grinding process. One subsample from each of the six samples was ground for 3 minutes at 400 rpm twice, the container being cooled in liquid nitrogen in between each run, while a second subsample was ground at 600 rpm for 5 minutes. Particle size of the subsamples was compared to other previously measured microground samples under the microscope and were shown to be of similar size, i.e. c. 1 μm. Samples were split into three different groups (i.e. fauna, unheated human and heated human specimens) to allow the observation of any differences that might be related to the pre-burial histories of bones (e.g. cooking, boiling), preservation state and animal species related BAp crystal order/disorder.

Bone powder of 20-63 μm particle size from the periosteal, mesosteal and trabecular tissues of 5 human samples was also analyzed by FTIR-ATR (Table S2 - supplementary material). Additionally, bone powder from two modern human mesosteal samples (particle size 20-63 μm), one modern bovine (particle size from >500 μm to 20-63 μm) and synthetic hydroxyapatite (HAp) (particle size from >500 μm to 20-63 μm) were used as references (see Table S3 - supplementary material).

FTIR measurements were performed in triplicate for each sample on each different particle size powder fraction using an Alpha Platinum FTIR-ATR spectrometer (range: 4000-400 cm^{-1}; no. of scans: 144; zero-filling factor: 4; resolution: 4 cm^{-1}; mode: absorbance). About 2-3 mg of bone powder were put on the optic window with a diamond crystal. For good contact with uniform pressure between the crystal and the sample, the pressure of the applicator was controlled using the pressure control spot. After each measurement, the crystal plate and the anvil of the pressure applicator were thoroughly cleaned using isopropyl alcohol. Spectra were analysed using OPUS 7.5 software.

Infrared splitting factor (IRSF) was assessed after Weiner and Bar-Yosef [22], carbonate-to-phosphate (C/P) ratio was calculated as in Wright and Schwarcz [25], type B carbonate substitutions relative to phosphate (BPI) was estimated as in Sponheimer and Lee-Thorp [38], and amide-to-phosphate (Am/P) was assessed according to Trueman et al. [29]. All indices were estimated after baseline correction (Figure 1; Box 1).

The full width at half maximum (FWHM) of the c. 1010 cm^{-1} peak was measured after baseline subtraction to assess the atomic order/disorder of the samples [9,46,47]. The 2nd derivatives were produced to explore the overlapping bands at the v_4, v_3, v_1 PO_4^{3-} and v_2 CO_3^{2-} bands using the OriginPro 2017 and the Savitzky-Golay filter with 9 smoothing points and a polynomial order of 4. Statistical analysis carried out using IBM SPSS v.24 and the significance level was set at $p = 0.05$.

Box 7. Indices - Baseline correction

4. Infrared splitting factor (IRSF) was assessed using the equation introduced by Weiner and Bar-Yosef [26] that measures the heights at c. 600 cm^{-1} + c. 560 cm^{-1}, divided by the trough between them at c. 590 cm^{-1}, using a baseline correction from the c. 400-420 cm^{-1} to the c. 630-670 cm^{-1} troughs (Figure 1a). The two peaks are characteristic of the v_4 antisymmetric bending mode of orthophosphate ion [49].

$$\mathrm{IRSF} = \frac{600\ \mathrm{cm^{-1}} + 560\ \mathrm{cm^{-1}}}{590\ \mathrm{cm^{-1}}}$$

5. Carbonate-to-phosphate (C/P) ratio was estimated as in Wright and Schwarcz [29] by dividing the main v_3 carbonate peak height at c. 1410 cm^{-1} with the main v_3 phosphate vibrational band at c. 1010 cm^{-1} [29]. The baseline correction was drawn from c. 1590 cm^{-1} to c. 1290 cm^{-1} and from c. 1150-1180 cm^{-1} to c. 880-900 cm^{-1}, respectively (Figure 1b and Figure 1c).

$$\mathrm{C/P} = \frac{1410\ \mathrm{cm^{-1}}}{1010\ \mathrm{cm^{-1}}}$$

6. The type B carbonate substitutions relative to phosphate (BPI) were calculated from the ratio of the peak heights at c. 1410 cm^{-1} and c. 600 cm^{-1} as in Sponheimer and Lee-Thorp [42] using the same baselines for both peaks as above (Figure 1a and Figure 1c).

$$\mathrm{BPI} = \frac{1410\ \mathrm{cm^{-1}}}{600\ \mathrm{cm^{-1}}}$$

7. Amide-to-phosphate (Am/P) was assessed by the v_1 amide at c. 1640 cm^{-1} divided by the main v_3 phosphate peak at c. 1010 cm^{-1} [33]. Baseline correction was from c. 1720 cm^{-1} to c. 1590 cm^{-1} and c. 1150 cm^{-1} to c. 890 cm^{-1}, respectively (Figure 1b and Figure 1d).

$$\mathrm{Am/P} = \frac{1640\ \mathrm{cm^{-1}}}{1010\ \mathrm{cm^{-1}}}$$

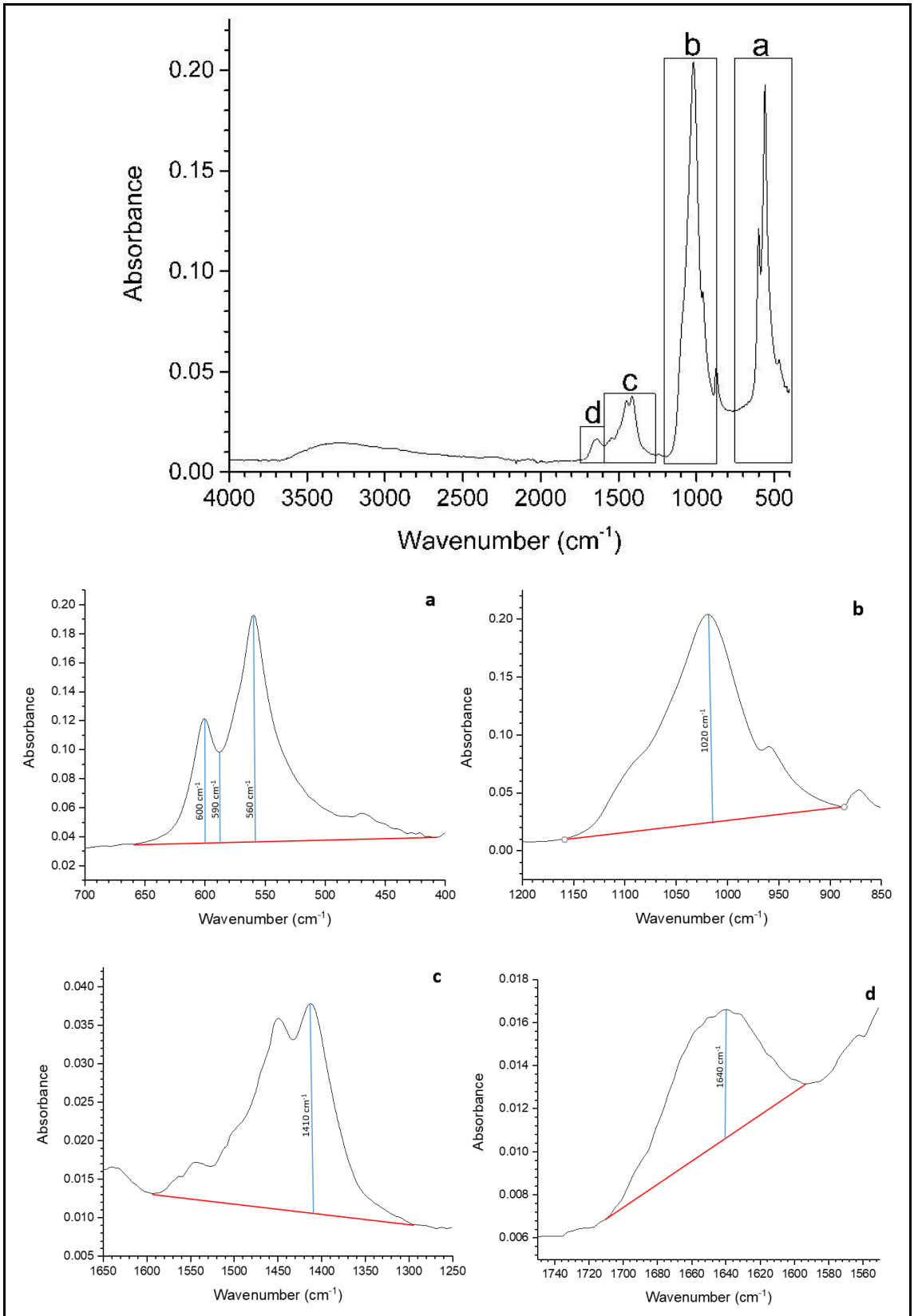

Figure 1. The mid-IR spectra of 20-63 μm particle size archaeological human mesosteal bone powder (MEC77). The spectral bands used for IRSF (a), C/P (b, c), and Am/P (b, d) are highlighted. Figures 1a-d display the peak positions (blue lines) for IRSF, C/P and Am/P indices as well as the baselines (red lines).

3. Results and Discussion

3.1. Tissue-specific variations

Within-sample variations can be observed in crystallinity, carbonate and organic content of the different bone tissue areas (Figure 2 and Table S4 - supplementary material), although there is no statistically significant difference between periosteal, mesosteal and trabecular bone tissue for either IRSF (x^2=1.680, p= 0.432), C/P (x^2=0.306, p= 0.858) or Am/P (x^2=3.847, p= 0.146). IRSF values in the periosteal tissue appear lower compared to the mesosteal and trabecular tissues (Figure 2a), carbonate content displays no observable pattern (Figure 2b), whereas Am/P values appear higher in the periosteal tissue (Figure 2c).

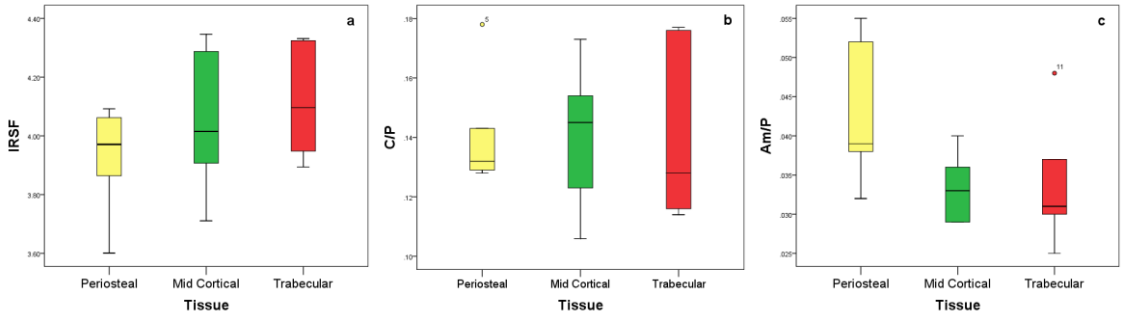

Figure 2. Box plots showing the IRSF (a), C/P (b) and Am/P (c) indices in the periosteal, mid cortical (mesosteal) and trabecular tissues. Notice the lower IRSF (a) and C/P (b) values in the periosteal tissue.

The organization of bone and the conditions of the depositional micro-environment (e.g. local hydrology, pH, depth) may strongly affect BAp structural characteristics, composition and their dissolution/recrystallization rate [5,6,8,60,69–71]. In modern human bone, a gradient from the osteon outwards (tissue specific, age-related variations) has been previously observed by Paschalis et al. [8], with the areas farther from the haversian canal displaying increased crystallinity, higher type B carbonate and lower type A carbonate content. A small variation in carbonate content within trabecular bone tissue (i.e. center to edges gradient) has also been reported by Ou-Yang et al. [72].

In archaeological and fossil bone, when an equilibrium between bone and its burial environment is reached and dissolution/recrystallization slows down, any change in the conditions would result in re-equilibration between the bone chemistry and its surroundings [51,71]. With respect to that behaviour, Stiner et al. [23] have observed that the outer surfaces of modern bone which had been exposed for 2 and 9 years post-mortem in Israel and New Mexico (USA), respectively, displayed higher crystallinity than the inner cortical areas. In a similar attempt to record mineralogical and compositional changes in bones of large mammals exposed on the ground surface in Amboseli National Park (Kenya) for up to 26 years, Trueman et al. [29] also observed that the crystallinity in the periosteal surfaces was higher than in the other bone tissue areas (inner cortical) as early as 2 years post-mortem. The higher periosteal IRSF values were accompanied by higher concentrations of rare earth elements (e.g. Ba and La) which also showed a gradual decrease

towards the inner cortex [29]. When the cortical bone was compared with trabecular bone in the Middle Palaeolithic Hayonim cave (Israel) the IRSF values for spongy tissues were found slightly higher [27].

Therefore, the tissue-specific differences in crystallinity, carbonate and organic content can vary within and between sites [27,31,60], while other factors such as the post-mortem interval or the size of the bone itself can also affect its post-mortem behaviour and interaction with its depositional environment [26]. Consequently, although there is no universal pattern for tissue-specific variations found in archaeological and fossil bone, the necessity for homogenization of samples prior to analysis using FTIR-ATR through the mechanical removal of the periosteal, trabecular and endosteal bone tissues and use of the mesosteal (mid-cortical) tissue is indisputable for the improvement of accuracy, precision, reproducibility and comparability of data.

3.2. Particle size effect

3.2.1. Effects on IR indices

Bone powder particle size predictably affects the IRSF, C/P and Am/P values in all samples (Tables S3 and S5 - supplementary material). Very strong inverse relationships are observed when IRSF is plotted against C/P (Figure 3). Carbonate content strongly affects crystallinity changes as it is inversely related to crystal growth (i.e. it acts as an inhibitor) [4,11], and the very strong inverse relationship of C/P with IRSF seen in our data supports an interaction between carbonate and phosphate in BAp crystals (e.g. [25]). A very strong correlation is also observed between these two indices and the samples' particle size (Figure 3).

Faunal bones (n=9) display a very strong relationship between particle size and mid-IR indices that reflect crystal composition (Figure 3; Fig.S1 - supplementary material). IRSF, C/P and Am/P demonstrate statistically significant differences for particle sizes ranging from >500 μm to 20-63 μm (IRSF: x^2= 20.809, p= 0.000; C/P: x^2= 13.910, p= 0.008; Am/P: x^2= 10.783, p= 0.029). IRSF gradually increases with decreasing particle size and drops at the 1 μm powder (Figure 3; Fig.S1a - supplementary material). On the contrary, C/P gradually decreases with decreasing particle size, except for the 1 μm at 600 rpm that increases to the 20-63 μm levels (Figure 3; Fig.S1b - supplementary material). Am/P gradually decreases with decreasing particle size and stabilises at the 1 μm particle size (Fig.S1c - supplementary material). Additionally, at the 1 μm size the samples' powder colour becomes dark grey/blackish.

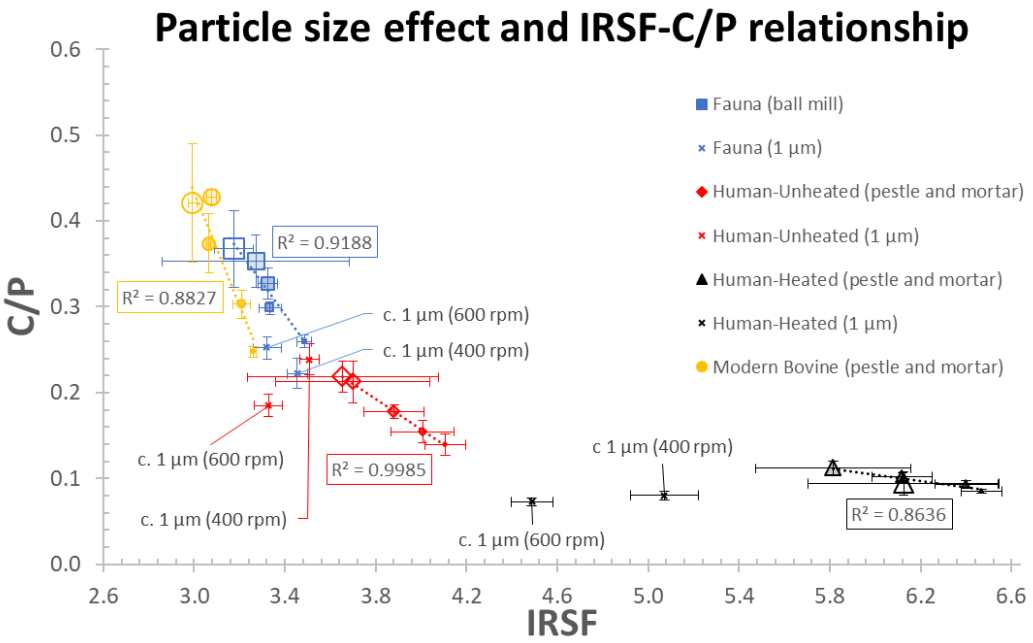

Figure 3. IRSF-C/P relationship with the samples' particle size in modern and archaeological bone. Datapoint markers' sizes gradually decrease with decreasing particle size (i.e. **>500 µm**: size 10, 100% transparent; **250-500 µm**: size 8, 80% transparent; **125-250 µm**: size 6, 60% transparent; **63-125 µm**: size 4, 40% transparent; **20-63 µm**: size 2, 20% transparent). Error bars represent estimated standard deviations.

The unheated human samples' (n=5) IRSF and C/P values also display statistically significant differences between the different particle sizes (x^2= 16.903, p= 0.002) and (x^2= 17.853, p= 0.001), respectively. Specifically, there is a gradual increase in IRSF and a gradual decrease in C/P with decreasing particle size (Figure 3; Fig.S2a and S2b - supplementary material). On the other hand, while Am/P shows almost no statistically significant differences (x^2= 9.343, p= 0.053), a similar general pattern can be observed, with a gradual decrease in Am/P values with decreasing particle size; the exception is the 250-500 µm that displays an increase in both C/P and Am/P (Fig.S2b and S2c - supplementary material). In particle sizes of c. 1 µm, IRSF significantly drops for both the 400 rpm and 600 rpm preparation methods (Fig.S2a - supplementary material). However, C/P and Am/P are increased at 400 rpm (similar values to the >500 µm powder) but decreased when prepared at 600 rpm (similar values to the 125-250 µm powder) (Fig.S2b and S2c - supplementary material). A similar discoloration (dark grey/blackish) of the samples' powder is also observed at the 1 µm level.

In contrast, in the heated human samples, there is no statistically significant difference between different particle sizes (>500 µm to 20-63 µm) and any of the indices [IRSF: (x^2=2.267, p=0.687); C/P: (x^2=3.244, p=0.518)]; Am/P: (x^2=2.722, p=0.605)]. Not surprisingly, however, a pattern can be observed for crystallinity, with an overall increase in IRSF that is accompanied by a decrease in C/P with decreasing particle size (Fig.S3a and S3b - supplementary material). For particle sizes of about 1 µm, there seems to be a rapid decrease in IRSF and a more gentle drop in C/P values (Fig.S3a and S3b - supplementary material). With regard to the reference samples, modern bovine bone shows similar relationships to the archaeological fauna and human unheated specimens,

while synthetic HAp displays a decrease in IRSF values with decreasing particle size (Figure 3; Fig.S4 and Table S5 - supplementary material).

The effect of particle size distribution and shape on IR spectra has been previously reported by Kristova et al. [73], and it is assumed to be primarily because of the better packing and higher surface area of the samples consisting of smaller particles [74]. In our samples, the smaller the particle size, the higher the crystallinity and the lower the carbonate content; this could be simply assumed to be because of the better contact between the sample and the prism, and the deeper penetration depth of the IR radiation into individual BAp crystals [74]. The exposure of a larger amount of BAp crystals to the IR radiation in samples consisting of smaller particle size powders also results in more accurate, precise and reproducible data. On the other hand, the coarser the sample, the poorer the contact between the sample and the prism due to increased void spaces (i.e. porosity) in the sample [74].

Breaking the crystal-crystal interaction (i.e. crystal fusion) may also contribute to the phenomenon observed in our data [11]. While it is still poorly understood as a process, the interaction between the crystals' hydrated layers (i.e. amorphous hydrophilic surface layers) in bone has been proposed as a possible explanation for the binding between the BAp crystals, pulled together by van der Waals forces [75,76]. As BAp crystals are often seen as aggregate clusters in transmission electron microscopy (TEM) (e.g. [29]), this supports a "separation hypothesis" up to the 20-63 μm level, as grinding could simply divide and expose some of the merged BAp crystals which have amalgamated to form larger crystals (i.e. Ostwald ripening).

It is, therefore, likely that the initial small size of the BAp crystals (i.e. about 30 nm long x 20 nm wide x 2-4 nm thick) [1,2] makes their destruction difficult during grinding when bone powder particle size remains over 20 μm [11], even when the BAp crystals further increase in size due to diagenesis (e.g. [31] estimated that for IRSF between 3.0-3.9, the average maximum BAp crystal length would be about 65 nm). Hence the Surovell and Stiner [26] "destruction hypothesis" (i.e. grinding damages the BAp crystal structure) seems rather unlikely for unheated modern and archaeological bone with over 20 μm bone powder particle size. However, the large drop in IRSF values observed at the 1 μm level is probably an indication that the BAp crystals are distorted by some breaking during grinding at a critical point between 1 μm and 20 μm, leading again to a more disordered (short-range) crystal state and a more variable particle size distribution that affects the penetration depth and accuracy of data [77].

3.2.2. Effects on IR absorbance

A very strong relationship between IR absorbance at 560 cm^{-1}, 600 cm^{-1}, 1010 cm^{-1} and 1410 cm^{-1} and particle size can be observed from the peak heights after baseline correction in all samples (Figure 4 and Figure 5). Absorbance is higher when the particle size decreases, except for C/P in heated samples (due to the loss of carbonate content during heating; Figure 5). Samples also

display a small average shift towards higher wavenumbers with decreasing particle size (Table S6 - supplementary material).

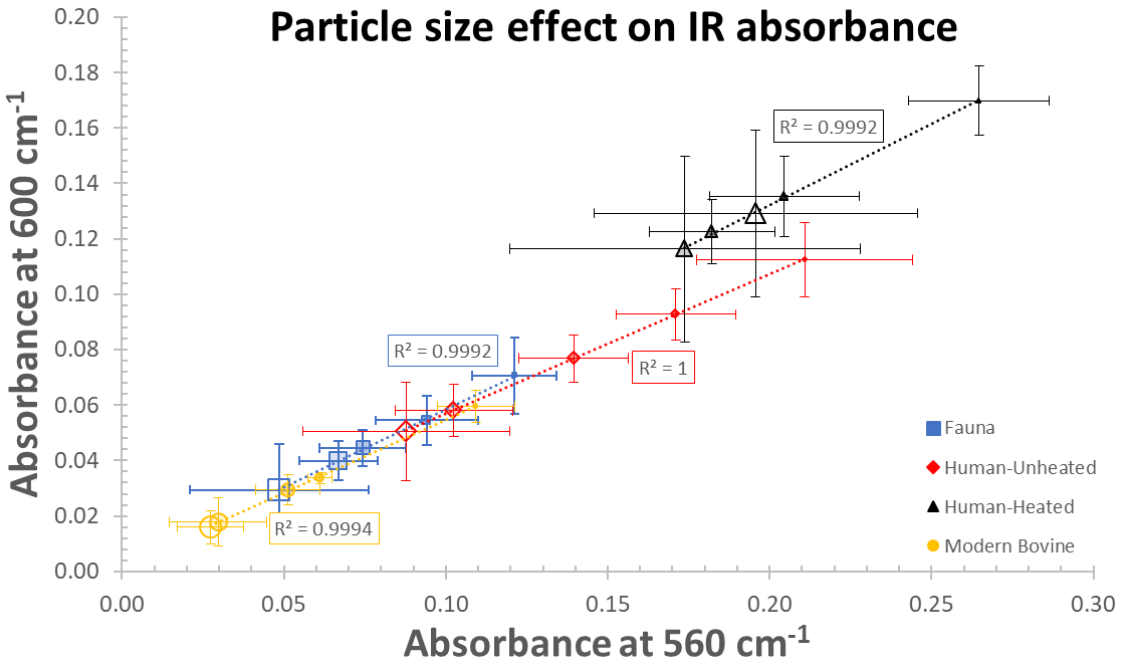

Figure 4. The particle size effect on the absorbance of IR of the main v_4 phosphate peaks at 560 cm^{-1} and 600 cm^{-1}. Markers and error bars as in **Figure 3**.

The absorbance of the IR radiation in our samples exhibited a very strong linear relationship with particle size, with the smaller the particle size, the higher the absorbance. This further supports the effectiveness of the 20-63 μm particle size powders compared to coarser samples. The only exception was the absorbance at the c. 1410 cm^{-1} peak for the heated human samples, due to the prior loss of most of their carbonate content during heating. Such an effect of particle size on the intensity and region of IR bands of minerals has been reported in past studies [e.g. 65,66,74], with the smaller the particle size, the higher the absorbance of IR and the narrower the bandwidth. Although the penetration depth of the IR light for diamond ATR crystals has been found to correlate with grinding [78], the IR penetration depths (i.e. full effective path length) and absorbance may sometimes vary due to scattering, interference and refractive index of the crystal (i.e. diamond vs Ge) [74].

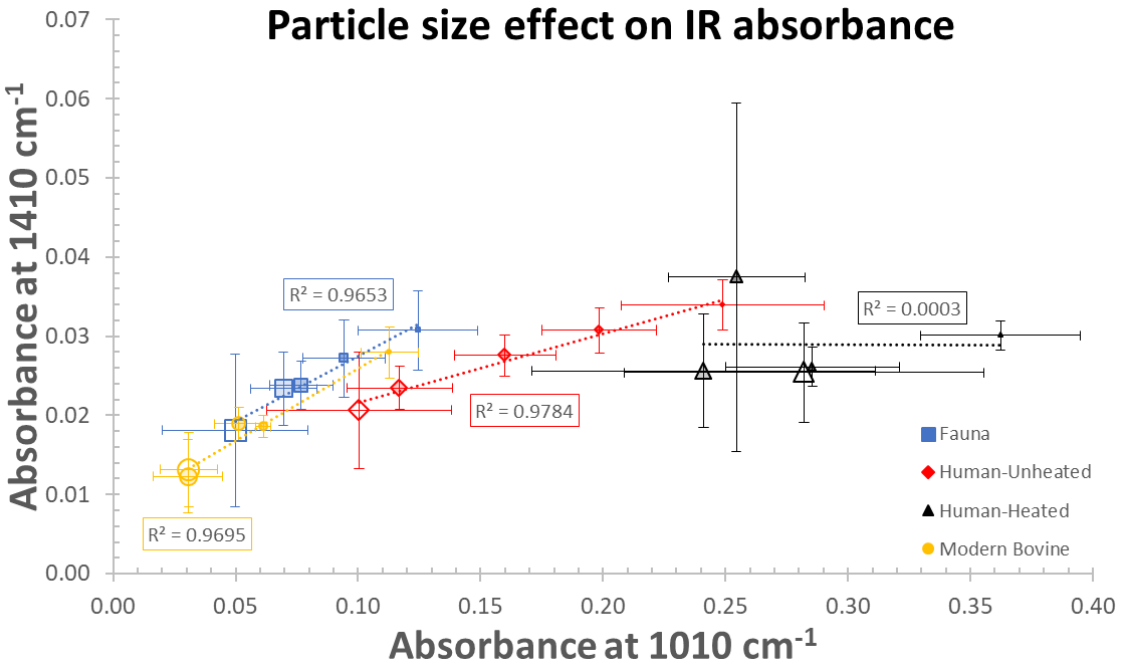

Figure 5. The particle size effect on the absorbance of IR of the main v_3 phosphate peak at 1010 cm^{-1} and the main v_3 carbonate peak at 1410 cm^{-1}. Markers and error bars as in **Figure 3**.

3.2.3. Effects on BAp order/disorder

The FWHM at 1010 cm^{-1} is considered to reflect the long-range order of a crystal (higher FWHM values indicate higher long-range disorder), hence the homogeneity between the different clusters of atoms arranged in a predictable pattern [4,50]. IRSF reflects the short-range order (higher IRSF values indicate higher short-range order) which is affected by the ionic substitutions in neighbouring atoms [38]. In this study, the FWHM of the 1010 cm^{-1} main phosphate peak is strongly related with crystallinity and particle size (>500 to 20-63 μm) with three main patterns being identified (Figure 6). The first is observed in modern bovine bone, exhibiting a rapid decrease in FWHM with decreasing particle size but a small increase in IRSF values, similar to the pattern seen in the well-preserved archaeological bovine specimen SAR38. The second pattern is that observed in the poorly preserved PRO8 (archaeological bovine) and MEC77 (archaeological human) samples, which demonstrate slightly different trendlines with the increase in crystallinity accompanying the decrease in FWHM being higher. Finally, the third pattern (i.e. heated archaeological human bone and synthetic HAp) is characterised by a much flatter trendline, resulting from a smaller decrease in FWHM and a stronger IRSF increase. When the particle size drops to c. 1 μm, IRSF and FWHM show no clear relationships (Figure 6).

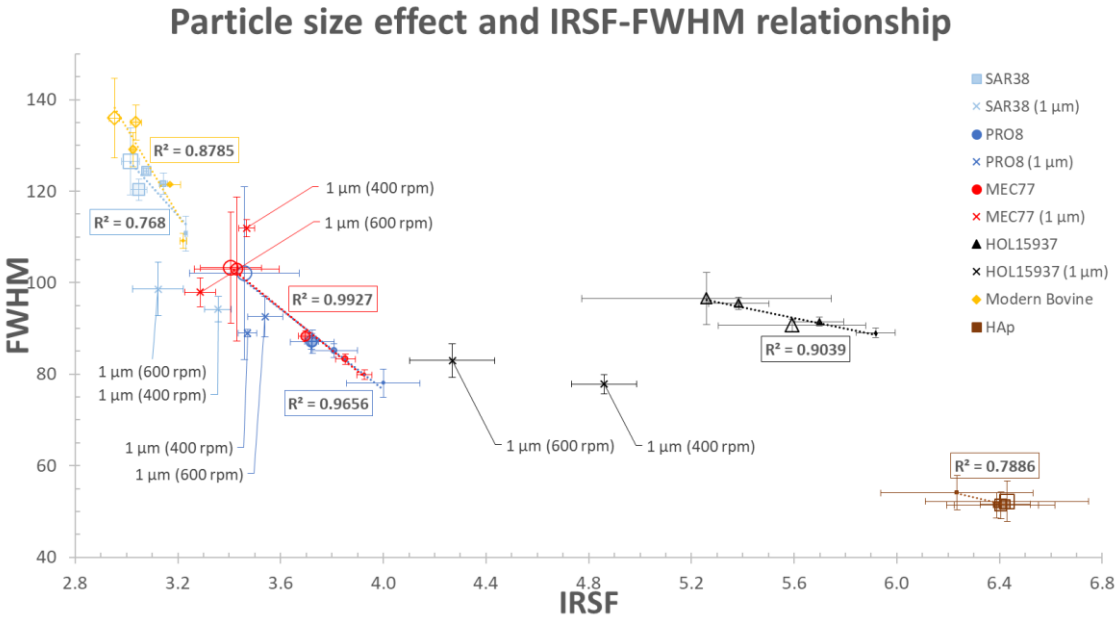

Figure 6. Graph displaying the particle size effect on the IRSF and the FWHM at 1010 cm^{-1}. Markers and error bars as in **Figure 3**.

Grinding and particle size can thus affect both IRSF and FWHM, with the different gradients of the curves reflecting the differences in BAp crystal size, and short- and long-range order of the samples associated with the particle size effect. On a similar note, synthetic HAp displays a decrease in IRSF with decreasing particle size and an almost unaltered FWHM, indicative of a fairly constant long-range order and a damage to the crystals' size and short-range order (Figure 6). Therefore, crystal distortion depends on the powder particle size and the size of the BAp crystals related to the preservation state or characteristics of each species.

The effect of particle size on the C/P to FWHM relationship is also marked in all samples for particle sizes varying from >500 µm to 20 µm (Figure 7). As with IRSF, the same three groups can be recognised: a) the modern bovine and SAR38 having similar trend lines characterized by a decrease in carbonate content as well as in FWHM with decreasing particle size; b) PRO8 and MEC77 showing a slightly smaller drop in C/P and FWHM values; and c) the HOL15937 heated archaeological human sample that displays a lesser degree of carbonate and FWHM change due to the loss of most carbonate during heating. In samples of c. 1 µm particle size, C/P also displays no specific patterns (Figure 7).

The atomic order/disorder, the morphology and the size of the BAp crystals are highly interrelated and dependent on carbonate concentrations [4]. The very strong linear relationship of CO_3^{2-} with FWHM (Figure 7) confirms the assumptions made by other researchers (e.g. [4,11,52,53]) that, except for the effects on the crystal dimensions, the higher the carbonate content in the crystal lattice the more disordered the crystal will be. An exchange of carbonate for phosphate has been found to correlate with a change in the *α*- and *c*-axis crystal dimensions that results in more disordered crystals [52,53]. This assumption is supported by the differences in the O-O distances

in PO_4^{3-} and CO_3^{2-}; thus a substitution of the smaller CO_3^{2-} by the larger PO_4^{3-} or a replacement of the larger CO_3^{2-} for the smaller OH^- would increase the unit cell dimensions [54].

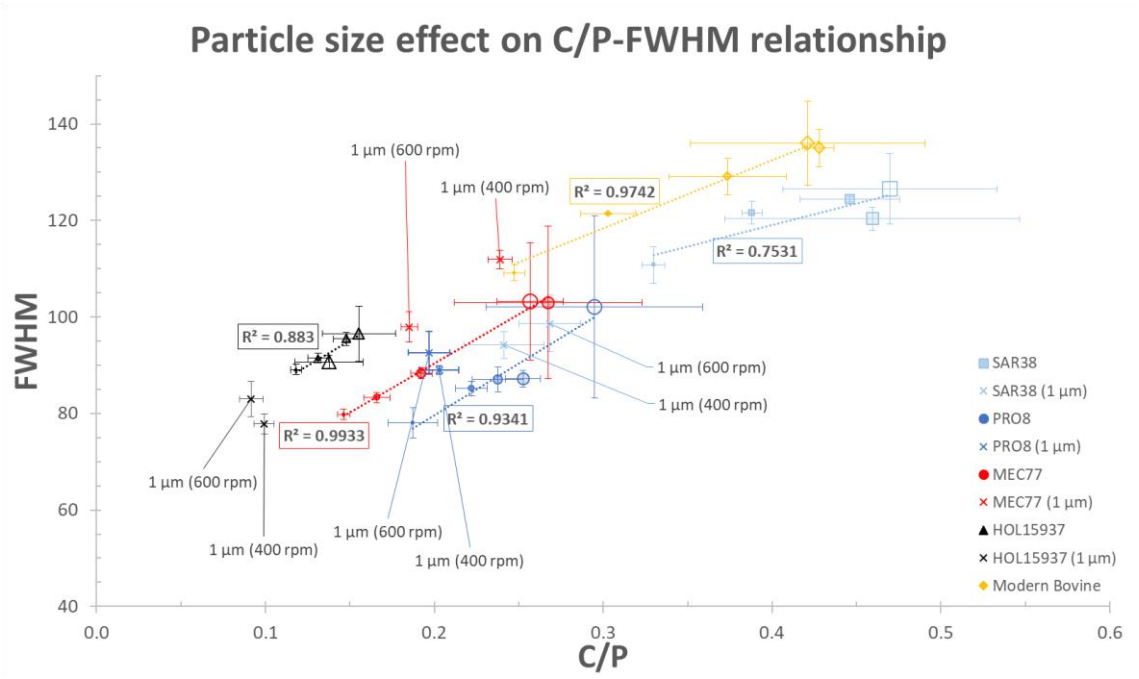

Figure 7. Graph displaying the particle size effect on the C/P and the FWHM at 1010 cm^{-1}. Markers and error bars as in **Figure 3**.

The peak height at c. 1410 cm^{-1} displays a very strong linear relationship (R^2=0.96) with this at c. 872 cm^{-1}. As both peaks reflect the type B carbonate environment in bioapatite crystals [57] it corroborates LeGeros [52] account of the bone carbonate exchange that primarily occurs at the phosphate sites of the crystal lattice (i.e. type B) [4]. Type A carbonate substitutions are considered to occur at high temperatures (e.g. 900-1000º C) with the exclusion of water, while type B CO_3^{2-} substitutions can take place at much lower temperatures (e.g. 25-100º C) [52]. Thus, as precipitation of carbonate for phosphate (and vice versa in archaeological and fossil bone) in bone occurs at the lower temperature range, type B CO_3^{2-}, which seems to be the predominant form of carbonate in skeletal tissues, is possibly adsorbed on the surfaces of the BAp crystals (i.e. the sloping faces of the substituted phosphate ions) and not incorporated into the crystal structure [52,53,59,79,80].

The characteristic v_2 carbonate vibrations that appear at c. 871 cm^{-1} for type B, c. 878 cm^{-1} for type A1 ("stuffed") and c. 866 cm^{-1} for type A2 ("labile"-surface) CO_3^{2-} [8,56,59,80] are also observed in the 2nd derivative components of our modern bovine data from >500 µm to 63-125 µm (Figure 8). Among these components, the c. 871 cm^{-1} type B carbonate appears to be more prominent than the other two (Figure 8). The most important observation, however, is the disappearance of the c. 866 cm^{-1} peak in the 2nd derivative spectra of the modern bovine bone at the 20-63 µm particle size and its absence from all the 2nd derivative spectra of all the archaeological specimens in all particle sizes (Fig. S5-S8 - supplementary material). This observation justifies its characterization

as “labile”-surface carbonate [8,56,80] and shows that a possible removal of ions (e.g. carbonate) from the crystal surface during grinding of modern bone cannot be overlooked [11]. The very strong correlation between C/P and type B CO_3^{2-} for the more degraded samples in this experiment could also be an indication of such a loss of the “labile” type A carbonate from the BAp crystal.

Regarding the number of the 2nd derivative components of the phosphate bands, they display a very small decrease with decreasing particle size, except at c. 1 μm particle size where a small increase is observed (Figure 8). Although the peak positions of the overlapping bands shift towards higher wavenumbers with decreasing particle size, this does not happen in a progressive manner or with a characteristic pattern. Additionally, the c. 630 cm^{-1} component, which is considered the vibration mode of OH, is observed in modern bone but shifts towards higher wavenumbers when crystallinity increases, due to diagenesis.

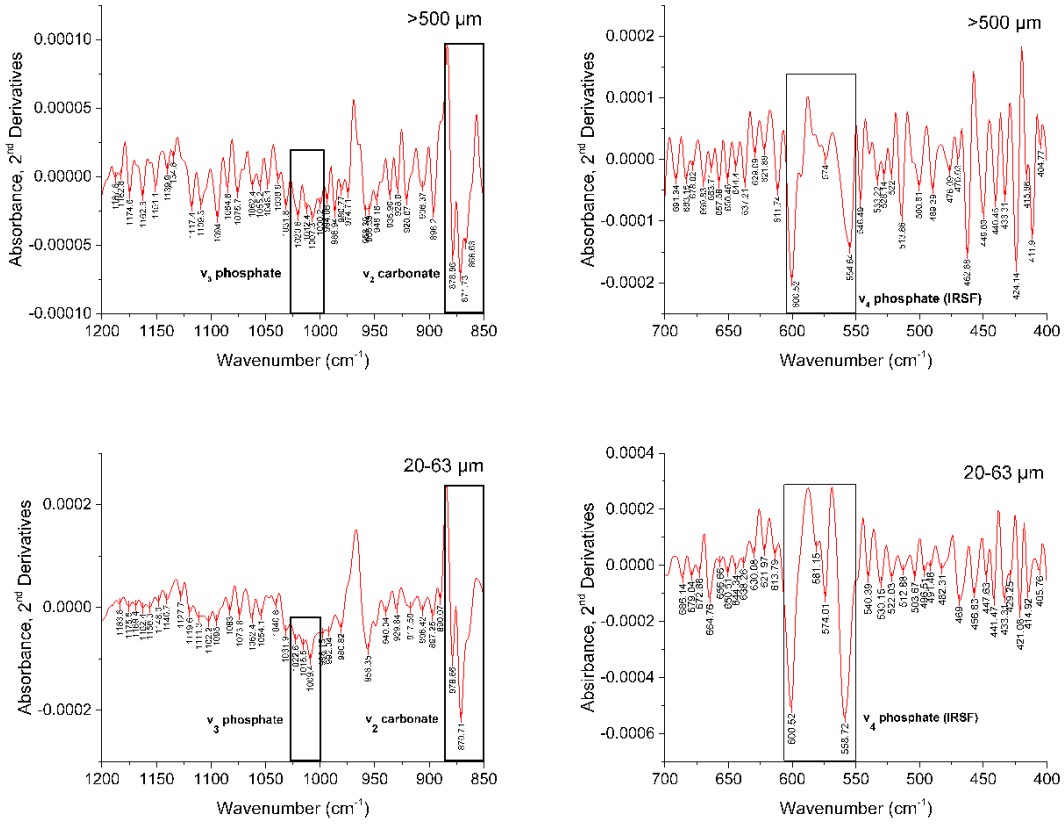

Figure 8. Example of 2nd derivative spectra of the v_4 PO_4^{3-} asymmetric bending vibrations in the region of 400-700 cm^{-1} (right column) and v_3 PO_4^{3-} asymmetric stretching modes at around 1010 cm^{-1} (left column) at different particle sizes for modern bovine mesosteal bone.

4. Conclusion

To summarize, we have shown in this study that particle size distribution leads to systematic changes in FTIR-ATR data as expressed by IRSF, C/P and Am/P indices. Specifically:

1. Removing the periosteal, endosteal and trabecular tissues prior to pulverization of mesosteal (mid-cortical) bone is necessary and eliminates uncertainties when using these semi-quantitative mid-IR indices for bone.
2. IRSF increases with decreasing particle sizes from >500 μm to 20-63 μm both in unheated and heated archaeological and modern bone samples. This is possibly an example of the Surovell and Stiner [26] "separation hypothesis" down to the 20-63 μm particle size, giving way to the "destruction hypothesis" when bone powder is consisted of particles of c. 1 μm, as there is a large decrease in IRSF values at this point.
3. The FWHM at c. 1010 cm^{-1} demonstrates a very strong inverse relationship with IRSF and a very strong linear relationship with particle size, decreasing with decreasing particle size from >500 μm to 20-63 μm. When bone powder consists of particles of c. 1 μm, the FWHM at c. 1010 cm^{-1} does not show any characteristic pattern and relationship with crystallinity, confirming that the boundaries between order and disorder in BAp crystals are still unclear. Overall, these patterns are strongly related to the changes that occur at the short- and long-range order of the BAp crystals during grinding.
4. C/P and Am/P follow an opposite relationship to IRSF, both decreasing from >500 μm to 20-63 μm particle size. When bone powder consists of particles of c. 1 μm, C/P and Am/P values vary with no characteristic patterns observed. The inverse relationship between IRSF and C/P also supports the effect of carbonate in the atomic order/disorder of BAp crystals.
5. The wavenumber of the main peaks and the 2nd derivative components of the bands in bone alter with decreasing particle size. The absence of the "labile" A_1 carbonate at 866 cm^{-1} in archaeological bone and its loss at lower particle sizes during grinding in modern bovine is noteworthy.
6. Absorbance of the IR radiation is strongly affected by the particle size, with higher absorbances for smaller bone powder particles. This observation indicates that for smaller particle sizes, there is a better contact between the sample and the prism, as well as a higher exposure of the bone powder's components to the IR light.

Therefore, we propose a standard preparation procedure for bone powder analysed using FTIR-ATR (Figure 9). This standard process should be followed to improve accuracy, consistency, reliability, reproducibility and comparability of the data for the systematic evaluation of bone in archaeological, anthropological, paleontological, forensic and biomedical studies:

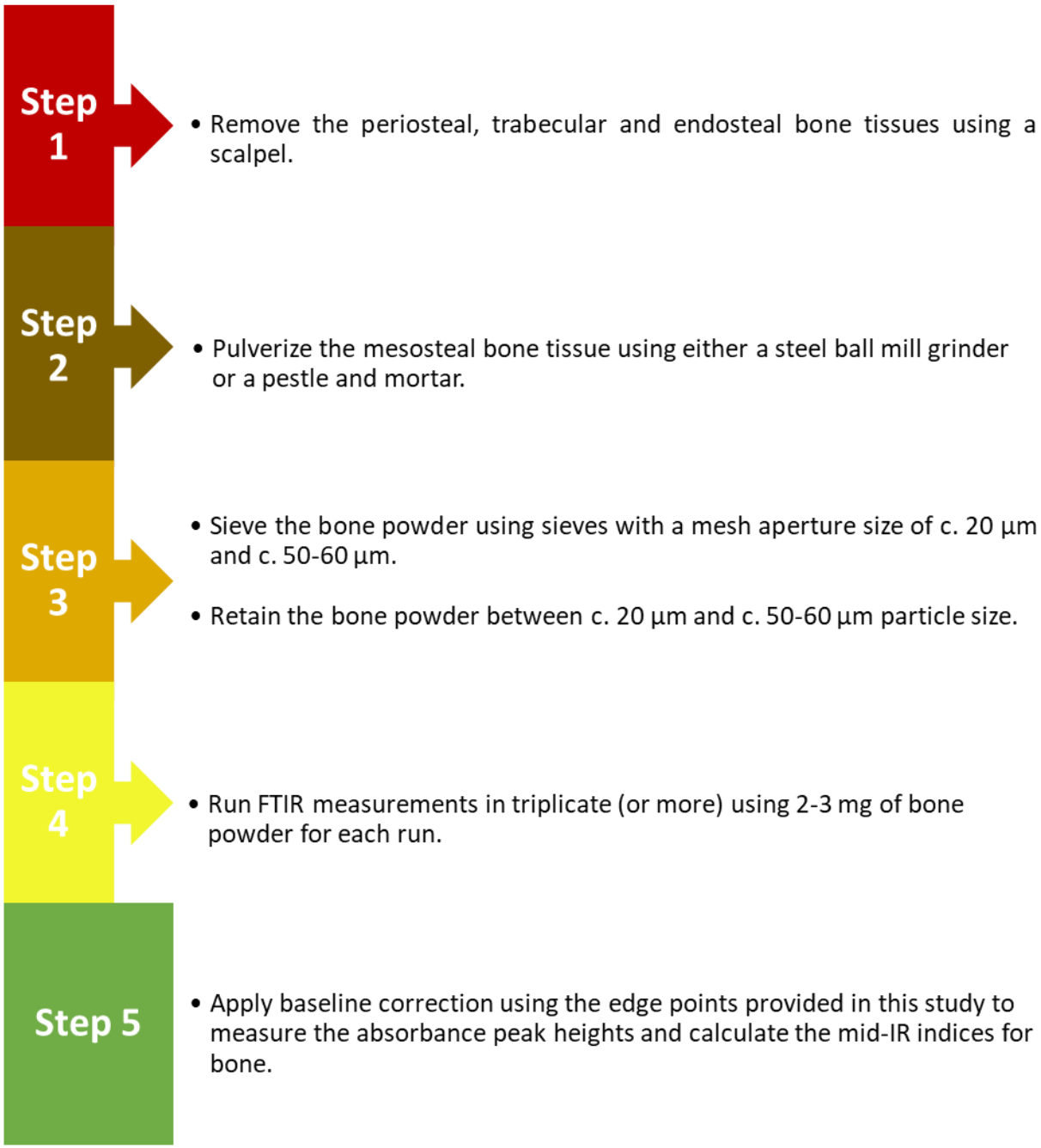

Figure 9. Sample preparation and analysis strategy for bone powder analysed using FTIR-ATR.

Acknowledgements

We are grateful to Dan Bradley, Adamantios Sampson, Morten Allentoft, Chaido Koukouli-Chrysanthaki, Ingrid Mainland, Jacqui Mulville, David Allen, Victoria Mullin, Georgios Kazantzis, Katrien Van de Vijver and Bart Robberechts, the Greek Ministry of Culture and Sports, the Ephorate of Palaeoanthropology and Speleology (Greece), the Ephorates of Antiquities in Boeotia and Serres (Greece), and the Archaeology department of the city council of Mechelen for giving us access to the material used in this study. We are also indebted to Peter Zioupos for the two modern human samples (NHS REC approval 10/H0107/14) which were used as references with the kind permission of the Department of Biology Ethics Committee (BEC) of the University of York.

IK would like to thank Onassis Foundation (Grant no. F ZL 047-1/2015-2016), Leventis Foundation and the Greek Archaeological Committee UK (GACUK). SP would like to thank Brian Chait and the Laboratory of Mass Spectrometry and Gaseous Ion Chemistry (Rockefeller University) for use of the Retsch PM100 ball mill and useful help and support. KP thanks the Leverhulme Trust (PLP-2012-116) and MJC thanks the DNRF for the award of a Niels Bohr Professorship.

References

[1] S. Weiner, W. Traub, Organization of hydroxyapatite crystals within collagen fibrils, FEBS Lett. 206 (1986) 262–266. https://www.ncbi.nlm.nih.gov/pubmed/3019771.

[2] S. Weiner, H.D. Wagner, The material bone: Structure-mechanical function relations, Annu. Rev. Mater. Sci. 28 (1998) 271–298.

[3] A.L. Boskey, Bone mineral crystal size, Osteoporos. Int. 14 Suppl 5 (2003) S16–20; discussion S20–1. doi:10.1007/s00198-003-1468-2.

[4] B. Wopenka, J.D. Pasteris, A mineralogical perspective on the apatite in bone, Materials Science and Engineering: C. 25 (2005) 131–143. doi:10.1016/j.msec.2005.01.008.

[5] P. Zioupos, J.D. Currey, A. Casinos, Exploring the effects of hypermineralisation in bone tissue by using an extreme biological example, Connect. Tissue Res. 41 (2000) 229–248. https://www.ncbi.nlm.nih.gov/pubmed/11264871.

[6] P. Zioupos, C. Kaffy, J.D. Currey, Tissue heterogeneity, composite architecture and fractal dimension effects in the fracture of ageing human bone, Int. J. Fract. 139 (2006) 407–424. doi:10.1007/s10704-006-6581-8.

[7] J.S. Yerramshetty, O. Akkus, The associations between mineral crystallinity and the mechanical properties of human cortical bone, Bone. 42 (2008) 476–482. doi:10.1016/j.bone.2007.12.001.

[8] E.P. Paschalis, E. DiCarlo, F. Betts, P. Sherman, R. Mendelsohn, A.L. Boskey, FTIR microspectroscopic analysis of human osteonal bone, Calcif. Tissue Int. 59 (1996) 480–487. http://www.ncbi.nlm.nih.gov/pubmed/8939775.

[9] J.D. Pasteris, B. Wopenka, J.J. Freeman, K. Rogers, E. Valsami-Jones, J.A.M. van der Houwen, M.J. Silva, Lack of OH in nanocrystalline apatite as a function of degree of atomic order: implications for bone and biomaterials, Biomaterials. 25 (2004) 229–238. doi:10.1016/S0142-9612(03)00487-3.

[10] T. Leventouri, Synthetic and biological hydroxyapatites: crystal structure questions, Biomaterials. 27 (2006) 3339–3342. doi:10.1016/j.biomaterials.2006.02.021.

[11] C. Rey, C. Combes, C. Drouet, H. Sfihi, A. Barroug, Physico-chemical properties of nanocrystalline apatites: Implications for biominerals and biomaterials, Materials Science and Engineering: C. 27 (2007) 198–205. doi:10.1016/j.msec.2006.05.015.

[12] S. Gourion-Arsiquaud, J.C. Burket, Spatial variation in osteonal bone properties relative to tissue and animal age, Journal of Bone and Mineral Research. (2009). http://onlinelibrary.wiley.com/doi/10.1359/jbmr.090201/full.

[13] T. Sakae, H. Nakada, J.P. LeGeros, Historical review of biological apatite crystallography, J. Hard Tissue Biol. 24 (2015) 111–122. doi:10.2485/jhtb.24.111.

[14] H.C.W. Skinner, Mineralogy of bones, in: O. Selinus (Ed.), Essentials of Medical Geology: Revised Edition, Springer Netherlands, Dordrecht, 2013: pp. 667–693. doi:10.1007/978-94-007-4375-5_30.

[15] D.R. Brothwell, A.M. Pollard, Handbook of archaeological sciences, anchecata.colmich.edu.mx, 2001. http://anchecata.colmich.edu.mx/janium/Tablas/tabla108546.pdf.

[16] T. Brown, K. Brown, Biomolecular archaeology An introduction, Wiley-blackwell, Sussex, 2011.

[17] C. Nielsen-Marsh, A. Gernaey, G. Turner-Walker, R. Hedges, A.W.G. Pike, M. Collins, The chemical degradation of bone, in: M. Cox, S. Mays (Eds.), Human Osteology: In Archaeology and Forensic Science, Cambridge University Press, 2000: pp. 439–454. http://eprints.soton.ac.uk/394456/ (accessed September 20, 2016).

[18] M.J. Collins, C.M. Nielsen-Marsh, J. Hiller, C.I. Smith, J.P. Roberts, R.V. Prigodich, T.J. Wess, J. Csapo, A.R. Millard, G. Turner-Walker, The survival of organic matter in bone: a review, Archaeometry. 44 (2002) 383–394.

[19] J. Lee–Thorp, Two decades of progress towards understanding fossilization processes and isotopic signals in calcified tissue minerals, Archaeometry. 44 (2002) 435–446. doi:10.1111/1475-4754.t01-1-00076.

[20] S.W. Keenan, From bone to fossil: A review of the diagenesis of bioapatite, Am. Mineral. 101 (2016) 1943–1951. doi:10.2138/am-2016-5737.

[21] C. Kendall, A.M.H. Eriksen, I. Kontopoulos, M.J. Collins, G. Turner-Walker, Diagenesis of archaeological bone and tooth, Palaeogeogr. Palaeoclimatol. Palaeoecol. 491 (2018) 21–37. doi:10.1016/j.palaeo.2017.11.041.

[22] S. Weiner, O. Bar-Yosef, States of preservation of bones from prehistoric sites in the Near East: A survey, J. Archaeol. Sci. 17 (1990) 187–196. doi:10.1016/0305-4403(90)90058-D.

[23] M.C. Stiner, S.L. Kuhn, S. Weiner, O. Bar-Yosef, Differential burning, recrystallization, and fragmentation of archaeological bone, J. Archaeol. Sci. 22 (1995) 223–237.

[24] A. Sillen, J. Parkington, Diagenesis of bones from Eland's bay cave, J. Archaeol. Sci. 23 (1996) 535–542. doi:10.1006/jasc.1996.0050.

[25] L.E. Wright, H.P. Schwarcz, Infrared and isotopic evidence for diagenesis of bone apatite at Dos Pilas, Guatemala: palaeodietary implications, J. Archaeol. Sci. 23 (1996) 933–944.

[26] T.A. Surovell, M.C. Stiner, Standardizing infra-red measures of bone mineral crystallinity: an experimental approach, J. Archaeol. Sci. 28 (2001) 633–642. doi:10.1006/jasc.2000.0633.

[27] M.C. Stiner, S.L. Kuhn, T.A. Surovell, P. Goldberg, L. Meignen, S. Weiner, O. Bar-Yosef, Bone Preservation in Hayonim Cave (Israel): a Macroscopic and Mineralogical Study, J. Archaeol. Sci. 28 (2001) 643–659. doi:10.1006/jasc.2000.0634.

[28] I. Reiche, C. Vignaud, M. Menu, The crystallinity of ancient bone and dentine: new insights by transmission electron microscopy, Archaeometry. 44 (2002) 447–459. doi:10.1111/1475-4754.00077.

[29] C.N.G. Trueman, A.K. Behrensmeyer, N. Tuross, S. Weiner, Mineralogical and compositional changes in bones exposed on soil surfaces in Amboseli National Park, Kenya: diagenetic mechanisms and the role of sediment pore fluids, J. Archaeol. Sci. 31 (2004) 721–739. doi:10.1016/j.jas.2003.11.003.

[30] E.T. Stathopoulou, V. Psycharis, G.D. Chryssikos, V. Gionis, G. Theodorou, Bone diagenesis: New data from infrared spectroscopy and X-ray diffraction, Palaeogeogr. Palaeoclimatol. Palaeoecol. 266 (2008) 168–174. doi:10.1016/j.palaeo.2008.03.022.

[31] C.N. Trueman, K. Privat, J. Field, Why do crystallinity values fail to predict the extent of diagenetic alteration of bone mineral?, Palaeogeogr. Palaeoclimatol. Palaeoecol. 266 (2008a) 160–167. doi:10.1016/j.palaeo.2008.03.038.

[32] F. Brock, T. Higham, C.B. Ramsey, Pre-screening techniques for identification of samples suitable for radiocarbon dating of poorly preserved bones, J. Archaeol. Sci. 37 (2010) 855–865. doi:10.1016/j.jas.2009.11.015.

[33] G. Piga, A. Santos-Cubedo, A. Brunetti, M. Piccinini, A. Malgosa, E. Napolitano, S. Enzo,

A multi-technique approach by XRD, XRF, FT-IR to characterize the diagenesis of dinosaur bones from Spain, Palaeogeogr. Palaeoclimatol. Palaeoecol. 310 (2011) 92–107. doi:10.1016/j.palaeo.2011.05.018.

[34] H.I. Hollund, F. Ariese, R. Fernandes, M.M.E. Jans, H. Kars, Testing an alternative high-throughput tool for investigating bone diagenesis: FTIR in attenuated total reflection (ATR) mode, Archaeometry. 55 (2013) 507–532. doi:10.1111/j.1475-4754.2012.00695.x.

[35] T.J.U. Thompson, M. Gauthier, M. Islam, The application of a new method of Fourier transform infrared spectroscopy to the analysis of burned bone, J. Archaeol. Sci. 36 (2009) 910–914. doi:10.1016/j.jas.2008.11.013.

[36] M.M. Beasley, E.J. Bartelink, L. Taylor, R.M. Miller, Comparison of transmission FTIR, ATR, and DRIFT spectra: implications for assessment of bone bioapatite diagenesis, J. Archaeol. Sci. 46 (2014) 16–22. doi:10.1016/j.jas.2014.03.008.

[37] J.A. Lee-Thorp, N.J. van der Merwe, Aspects of the chemistry of modern and fossil biological apatites, J. Archaeol. Sci. 18 (1991) 343–354. doi:10.1016/0305-4403(91)90070-6.

[38] M. Sponheimer, J.A. Lee-Thorp, Alteration of enamel carbonate environments during fossilization, J. Archaeol. Sci. 26 (1999) 143–150. doi:10.1006/jasc.1998.0293.

[39] G. Nagy, T. Lorand, Z. Patonai, G. Montsko, I. Bajnoczky, A. Marcsik, L. Mark, Analysis of pathological and non-pathological human skeletal remains by FT-IR spectroscopy, Forensic Sci. Int. 175 (2008) 55–60. doi:10.1016/j.forsciint.2007.05.008.

[40] C. Chadefaux, A.-S. Le Hô, L. Bellot-Gurlet, I. Reiche, Curve-fitting micro-ATR-FTIR studies of the amide I and II bands of type I collagen in archaeological bone materials, E-PS. 6 (2009) 129–137.

[41] K.E. Squires, T.J.U. Thompson, M. Islam, A. Chamberlain, The application of histomorphometry and Fourier transform infrared spectroscopy to the analysis of early Anglo-Saxon burned bone, J. Archaeol. Sci. 38 (2011) 2399–2409. doi:10.1016/j.jas.2011.04.025.

[42] J.D. Fredericks, P. Bennett, A. Williams, K.D. Rogers, FTIR spectroscopy: a new diagnostic tool to aid DNA analysis from heated bone, Forensic Sci. Int. Genet. 6 (2012) 375–380.

[43] G. Piga, D. Gonçalves, T.J.U. Thompson, A. Brunetti, A. Malgosa, S. Enzo, Understanding the crystallinity indices behavior of burned bones and teeth by ATR-IR and XRD in the presence of bioapatite mixed with other phosphate and carbonate phases, International Journal of Spectroscopy. 2016 (2016). doi:10.1155/2016/4810149.

[44] G. Dal Sasso, M. Lebon, I. Angelini, L. Maritan, D. Usai, G. Artioli, Bone diagenesis variability among multiple burial phases at Al Khiday (Sudan) investigated by ATR-FTIR spectroscopy, Palaeogeogr. Palaeoclimatol. Palaeoecol. 463 (2016) 168–179. doi:10.1016/j.palaeo.2016.10.005.

[45] J.D. Termine, A.S. Posner, Infra-red determination of the percentage of crystallinity in apatitic calcium phosphates, Nature. 211 (1966) 268–270. doi:10.1038/211268a0.

[46] Y. Asscher, L. Regev, S. Weiner, E. Boaretto, Atomic disorder in fossil tooth and bone mineral: An FTIR study using the grinding curve method, Archeosciences. (2011) 135–141. doi:10.4000/archeosciences.3062.

[47] Y. Asscher, S. Weiner, E. Boaretto, Variations in atomic disorder in biogenic carbonate hydroxyapatite using the infrared spectrum grinding curve method, Adv. Funct. Mater. 21 (2011) 3308–3313. doi:10.1002/adfm.201100266.

[48] T.J.U. Thompson, M. Islam, K. Piduru, A. Marcel, An investigation into the internal and external variables acting on crystallinity index using Fourier transform infrared spectroscopy on unaltered and burned bone, Palaeogeogr. Palaeoclimatol. Palaeoecol. 299

(2011) 168–174. doi:10.1016/j.palaeo.2010.10.044.

[49] C. Snoeck, J. Lee-Thorp, R.J. Schulting, From bone to ash: compositional and structural changes in burned modern and archaeological bone, Palaeogeogr. Palaeoclimatol. Palaeoecol. 416 (2014) 55–68.

[50] C.N. Trueman, Chemical taphonomy of biomineralized tissues, Palaeontology. 56 (2013) 475–486. doi:10.1111/pala.12041.

[51] F.D. Pate, J.T. Hutton, K. Norrish, Ionic exchange between soil solution and bone: toward a predictive model, Appl. Geochem. 4 (1989) 303–316.

[52] R.Z. LeGeros, Effect of carbonate on the lattice parameters of apatite, Nature. 206 (1965) 403. doi:10.1038/206403a0.

[53] R.Z. LeGeros, O.R. Trautz, J.P. LeGeros, E. Klein, W.P. Shirra, Apatite crystallites: effects of carbonate on morphology, Science. 155 (1967) 1409–1411. doi:10.1126/science.155.3768.1409.

[54] R.Z. LeGeros, O.R. Trautz, E. Klein, J.P. LeGeros, Two types of carbonate substitution in the apatite structure, Experientia. 25 (1969) 5–7. doi:10.1007/BF01903856.

[55] R.Z. LeGeros, Apatites in biological systems, Prog. Cryst. Growth Charact. Mater. 4 (1981) 1–45.

[56] J.C. Elliott, D.W. Holcomb, R.A. Young, Infrared determination of the degree of substitution of hydroxyl by carbonate ions in human dental enamel, Calcif. Tissue Int. 37 (1985) 372–375. https://www.ncbi.nlm.nih.gov/pubmed/3930033.

[57] C. Rey, B. Collins, T. Goehl, I.R. Dickson, M.J. Glimcher, The carbonate environment in bone mineral: a resolution-enhanced Fourier Transform Infrared Spectroscopy Study, Calcif. Tissue Int. 45 (1989) 157–164. https://www.ncbi.nlm.nih.gov/pubmed/2505907.

[58] E. Pucéat, B. Reynard, C. Lécuyer, Can crystallinity be used to determine the degree of chemical alteration of biogenic apatites?, Chem. Geol. 205 (2004) 83–97. doi:10.1016/j.chemgeo.2003.12.014.

[59] M.E. Fleet, X. Liu, Location of type B carbonate ion in type A–B carbonate apatite synthesized at high pressure, J. Solid State Chem. 177 (2004) 3174–3182. doi:10.1016/j.jssc.2004.04.002.

[60] C.N. Trueman, M.R. Palmer, J. Field, K. Privat, N. Ludgate, V. Chavagnac, D.A. Eberth, R. Cifelli, R.R. Rogers, Comparing rates of recrystallisation and the potential for preservation of biomolecules from the distribution of trace elements in fossil bones, C. R. Palevol. 7 (2008b) 145–158. doi:10.1016/j.crpv.2008.02.006.

[61] A. Antonakos, E. Liarokapis, T. Leventouri, Micro-Raman and FTIR studies of synthetic and natural apatites, Biomaterials. 28 (2007) 3043–3054. doi:10.1016/j.biomaterials.2007.02.028.

[62] M. Lebon, I. Reiche, J.-J. Bahain, C. Chadefaux, A.-M. Moigne, F. Fröhlich, F. Sémah, H.P. Schwarcz, C. Falguères, New parameters for the characterization of diagenetic alterations and heat-induced changes of fossil bone mineral using Fourier transform infrared spectrometry, J. Archaeol. Sci. 37 (2010) 2265–2276. doi:10.1016/j.jas.2010.03.024.

[63] C.L. King, N. Tayles, K.C. Gordon, Re-examining the chemical evaluation of diagenesis in human bone apatite, J. Archaeol. Sci. 38 (2011) 2222–2230. doi:10.1016/j.jas.2011.03.023.

[64] T.J.U. Thompson, M. Islam, M. Bonniere, A new statistical approach for determining the crystallinity of heat-altered bone mineral from FTIR spectra, J. Archaeol. Sci. 40 (2013) 416–422. doi:10.1016/j.jas.2012.07.008.

[65] L. Regev, K.M. Poduska, L. Addadi, S. Weiner, E. Boaretto, Distinguishing between calcites formed by different mechanisms using infrared spectrometry: archaeological

applications, J. Archaeol. Sci. 37 (2010) 3022–3029. doi:10.1016/j.jas.2010.06.027.

[66] K.M. Poduska, L. Regev, E. Boaretto, L. Addadi, S. Weiner, L. Kronik, S. Curtarolo, Decoupling local disorder and optical effects in infrared spectra: differentiating between calcites with different origins, Adv. Mater. 23 (2011) 550–554. doi:10.1002/adma.201003890.

[67] M.J. Collins, P. Galley, Towards an optimal method of archaeological collagen extraction: the influence of pH and grinding, Anc. Biomol. 2 (1998) 209–223.

[68] C.J. Adler, W. Haak, D. Donlon, A. Cooper, Survival and recovery of DNA from ancient teeth and bones, J. Archaeol. Sci. 38 (2011) 956–964. doi:10.1016/j.jas.2010.11.010.

[69] F.D. Pate, J.T. Hutton, The use of soil chemistry data to address post-mortem diagenesis in bone mineral, J. Archaeol. Sci. 15 (1988) 729–739.

[70] P. Karkanas, O. Bar-Yosef, P. Goldberg, S. Weiner, Diagenesis in Prehistoric Caves: The use of minerals that form in situ to assess the completeness of the archaeological record, J. Archaeol. Sci. 27 (2000) 915–929. doi:10.1006/jasc.1999.0506.

[71] L. Wilson, A.M. Pollard, Here today, gone tomorrow? integrated experimentation and geochemical modeling in studies of archaeological diagenetic change, Acc. Chem. Res. 35 (2002) 644–651. doi:10.1021/ar000203s.

[72] H. Ou-Yang, E.P. Paschalis, W.E. Mayo, A.L. Boskey, R. Mendelsohn, Infrared microscopic imaging of bone: Spatial distribution of CO_3^{2-}, J. Bone Miner. Res. 16 (2001) 893–900. doi:10.1359/jbmr.2001.16.5.893.

[73] P. Kristova, K.J. Rutt, L.J. Hopkinson, The effect of the particle size on the fundamental vibrations of the [CO32-] anion in calcite, J. Phys. Chem. A. 119 (2015) 4891–4897. doi:10.1021/acs.jpca.5b02942.

[74] B. Udvardi, I.J. Kovács, T. Fancsik, P. Kónya, M. Bátori, F. Stercel, G. Falus, Z. Szalai, Effects of particle size on the attenuated total reflection spectrum of minerals, Appl. Spectrosc. 71 (2017) 1157–1168. doi:10.1177/0003702816670914.

[75] C. Rey, C. Combes, What bridges mineral platelets of bone?, Bonekey Rep. 3 (2014) 586. doi:10.1038/bonekey.2014.81.

[76] Y. Wang, S. Von Euw, F.M. Fernandes, S. Cassaignon, M. Selmane, G. Laurent, G. Pehau-Arnaudet, C. Coelho, L. Bonhomme-Coury, M.-M. Giraud-Guille, F. Babonneau, T. Azaïs, N. Nassif, Water-mediated structuring of bone apatite, Nat. Mater. 12 (2013) 1144–1153. doi:10.1038/nmat3787.

[77] H. Tong, P. Tan, N. Xu, From crystals to disordered crystals: A hidden order-disorder transition, Sci. Rep. 5 (2015) 15378. doi:10.1038/srep15378.

[78] J. Aufort, L. Ségalen, C. Gervais, C. Brouder, E. Balan, Modeling the attenuated total reflectance infrared (ATR-FTIR) spectrum of apatite, Phys. Chem. Miner. 43 (2016) 615–626. doi:10.1007/s00269-016-0821-x.

[79] M.E. Fleet, X. Liu, P.L. King, Accommodation of the carbonate ion in apatite: An FTIR and X-ray structure study of crystals synthesized at 2–4 GPa, Am. Mineral. 89 (2004) 1422–1432. doi:10.2138/am-2004-1009.

[80] M.E. Fleet, Infrared spectra of carbonate apatites: v2-Region bands, Biomaterials. 30 (2009) 1473–1481. doi:10.1016/j.biomaterials.2008.12.007.

Abstract

The discovery of petrous bone as an excellent repository for ancient biomolecules has been a turning point in biomolecular archaeology, especially in aDNA research, but excessive and uncontrolled sampling could result in loss of this valuable resource for future research. This study reports on the histological (optical microscopy), physical (FTIR-ATR), elemental (CHN) and biochemical (collagen and DNA analysis) preservation of 15 human petrous bones spanning from the c. 2100 BC to 1850 AD. Through the combined application of a number of diagenetic parameters (general histological index; infrared splitting factor; carbonate/phosphate ratio; amide/phosphate ratio; collagen wt. %; % C, % N and C/N of whole bone and collagen; % endogenous DNA), we provide new insights into petrous bone micromorphological characteristics and diagenesis, and new evidence to enhance screening practices for aDNA and collagen analysis.

Keywords: petrous bone; diagenesis; microstructure; bioapatite; collagen; aDNA

1. Introduction

The extraction and analysis of ancient biomolecules preserved within archaeological bone tissue can provide valuable information for studying past populations (Bentley, 2006; Brown and Barnes, 2015; Buckley et al., 2009; Cappellini et al., 2018; Colonese et al., 2015; Hendy et al., 2018; Katzenberg, 2008; Lee-Thorp, 2008; Orlando and Cooper, 2014). However, bone diagenesis leads to the partial or complete loss of the biochemical information (Collins et al., 2002; Kendall et al., 2018; Nielsen-Marsh et al., 2000). The recent discovery that the petrous bone, a massive portion of the endocranial aspect of the temporal bone, is an excellent repository for long term DNA survival presumably due to its high density (Gamba et al., 2014; Hansen et al., 2017; Pinhasi et al., 2015) represents a major breakthrough in ancient DNA (aDNA) research as the expense of genome sequencing can often be prohibitive due to the the low abundance of the endogenous DNA from the target (e.g. Green et al., 2010). Collagen extracted from petrous bone has also been identified as a potential indicator of fetal and early years diet (Jørkov et al., 2009) as ossification of the petrous pyramid is mainly completed *in utero* and during early fetal years (Jeffery and Spoor, 2004; Sørensen, 1994; Sørensen et al., 1992). Similarly, petrous bone can potentially provide information on the geographic area in which individuals had spent their childhood through strontium isotope analysis (Harvig et al., 2014), providing an additional layer of information to the strontium analyses of teeth.

Petrous bone's *sui generis* nature is manifested by the three different tissue zones recognised by Doden and Halves (1984): a) an outer periosteal; b) an endosteal that surrounds the canals and

cochlear surfaces; and c) an inner periosteal that can replace both the outer periosteal and endosteal tissues. A lack of bone remodelling has also been noted in earlier studies (Doden and Halves, 1984; Frisch et al., 2000; Jeffery and Spoor, 2004) and the increased mineralization (i.e. hardness) in some areas of the petrous bone (Doden and Halves, 1984) compared to other skeletal elements (Currey, 1999; Zioupos et al., 2000) is another unique feature. The outer periosteal tissue is considered less mineralized *in vivo* and has its collagen fibres arranged parallel to the bone's surface (Doden and Halves, 1984). Contrariwise, the inner periosteal tissue has randomly oriented collagen fibres (Doden and Halves, 1984) and two different degrees of mineralization (Doden and Halves, 1984) linked to different concentrations of Ca, P, Sr and Mg (Katić et al., 1991).

Here some commonly and successfully applied diagenetic parameters, namely the general histological index (Hollund et al., 2012), infrared splitting factor (Weiner and Bar-Yosef, 1990), carbonate/phosphate ratio (Wright and Schwarcz, 1996), amide/phosphate ratio (Trueman et al., 2004), collagen weight % (van Klinken, 1999), % C, % N and C/N of whole bone and collagen (Brock et al., 2010), and % endogenous DNA (e.g. Hansen et al., 2017), are combined to provide new insights into petrous bone characteristics and diagenesis. This study therefore seeks to understand the factors underpinning the survival and possible resistance of petrous bone to diagenesis, but more importantly explore potential methods to enhance screening practices for aDNA and collagen preservation in petrous bone specimens irrespective of the conditions of the burial environment.

2. Materials and Methods

Fifteen archaeological human petrous bones were used in this study (Table 8) from two contrasting sites, 9 samples from the later historical period in Denmark (c. 1650–1850 AD) and 6 samples from the Bronze Age period in Central Asia (c. 2100–1800 BC). Samples are representative of the *b* and/or *c* areas of petrous bone as presented in Pinhasi et al. (2015). Sampling for aDNA analysis preceded sampling for histological, FTIR-ATR, collagen and elemental analyses, thus samples do not derive exactly from the same anatomical location. The genetic results presented here (endogenous DNA content) have been sourced in Hansen et al. (2017). Statistical analysis was carried out using IBM SPSS v.25 and the significance level was set at $p = 0.05$. Regression correlation (R^2) of 0-0.19 is regarded as very weak, 0.2-0.39 as weak, 0.40-0.59 as moderate, 0.6-0.79 as strong and 0.8-1 as very strong correlation, but these are rather arbitrary limits and should be considered in the context of the results.

2.1. Histology

Sixteen transverse and longitudinal thin sections of c. 200 μm from 10 samples were prepared using an Exact 300 CL diamond band saw. Undecalcified thin sections were mounted onto glass microscope slides using Entellan New (Merck chemicals) for microscopy mounting medium and covered by a glass coverslip, both cleaned with xylene before use. Thin sections were assessed

under a Leica DM750 optical microscope using plane-polarized (PPL) and cross-polarized (XPL) transmitted light with total magnification ranging from 40x to 400x. Digital images were captured by a Leica ICC50 HD camera for microscopy imaging with a capture resolution of 2048 x 1536 pixels. The general histological index (GHI) introduced by Hollund et al. (2012) was used as it is analogous to the Oxford histological index (OHI) as described by Millard (2001) but includes generalized destruction, cracking, and staining. A GHI value of 5 represents excellent microstructural preservation similar to modern bone (>95% intact microstructure), whereas a GHI value of 0 indicates poor microstructural preservation (<5% intact microstructure) with almost no original histological features observed.

2.2. FTIR

FTIR-ATR measurements were performed in triplicate on 15 human petrous bones and two modern human femora using a Bruker Alpha Platinum [range: 4000-400 cm^{-1}; no. of scans: 144; zero filling factor: 4; resolution: 4 cm^{-1}; mode: absorbance]. Sample preparation and analysis was carried out using Kontopoulos et al. (2018)'s protocol. Bone samples were ground using an agate pestle and mortar following the mechanical cleaning of the outer and inner bone surfaces. About 2-3 mg of bone powder of 20-50 μm particle size were used for each measurement, and after each measurement the crystal plate and the anvil of the pressure applicator were thoroughly cleaned using isopropyl alcohol. Spectra were analysed using OPUS 7.5 software.

The calculations of FTIR indices were conducted as follows: a) infrared splitting factor (IRSF) was assessed after Weiner and Bar-Yosef (1990, p. 191); b) carbonate-to-phosphate (C/P) ratio (Wright and Schwarcz, 1996, p. 936); c) type B carbonate substitutions relative to phosphate (BPI) (Sponheimer and Lee-Thorp, 1999, p. 145); and d) amide-to-phosphate (Am/P) (Trueman et al., 2004, p. 726). The average values of two modern human femora were used as reference throughout (IRSF=3.357±0.007, C/P=0.24±0.003, Am/P=0.182±0.001, BPI=0.482±0.000).

2.3. Collagen

Collagen was extracted using a modified Longin (1971) method. The exterior surfaces of bone samples were mechanically cleaned using a scalpel. Bone chunks of 300-500 mg were demineralized in 8 ml 0.6 M HCl at 4◦ C. Samples were agitated twice daily and acid solution was changed every two days. When demineralisation was completed, the supernatant was drained off and samples were rinsed three times with distilled water. Gelatinization was carried out by adding 8 ml pH3 HCl and samples were placed in hot blocks at 80◦ C for 48h. The supernatant liquor which contains the collagen was filtered off by using Ezee™ filters (Evergreen) and was freeze dried for 2 days in pre-weighed plastic tubes.

Extracted collagen was analyzed in duplicate. Tin capsules containing 0.9-1.1 mg of collagen were dropped into an oxygen rich combustion tube held at 1000° C. The tin capsules were ignited

and burnt exothermally at 1800°C causing the sample to oxidise. The samples were carried through a layer of chromium oxide and copper oxide which ensure complete oxidation, followed by a layer of silver wool to remove unwanted sulphur and halides. The samples' gases pass into a second furnace containing copper held at 600°C where excess oxygen was removed and nitrogen oxides were reduced to elemental nitrogen. Any water was removed using a magnesium perchlorate trap. The samples then passed into a gas chromatography (GC) column held at 70°C which separates CO_2 and N_2 from each other. The resultant gases were then introduced into the Sercon 20-22 mass spectrometer where the samples were ionised, and the various masses separated in a magnetic field, focused into Faraday collector arrays and analyzed.

2.4. Elemental analysis

Whole bone elemental analysis (% C, % N) was performed on 2-3 mg of bone powder. Samples were run in duplicate on an Exeter Analytical CE-440 elemental analyser, used in conjunction with a Sartorius SE2 analytical balance automated carbon and nitrogen elemental analyser. Samples were weighed into smooth-walled tin capsules, sealed and combusted in O_2 at 975 ºC. Combustion products were then analysed by thermal conductivity detectors, against a blank of helium.

3. Results and Discussion

3.1. Histological preservation

Histological analysis provides useful information on the microstructural characteristics of the human petrous bones. The thin sections of the Danish and Central Asian archaeological human petrous bones consist of woven and lamellar-like tissue (Figure 10a-b). Highly osteocytic woven tissue can be seen throughout petrous bone (Figure 10a-d) and its presence may indicate a lack of bone remodelling in specific areas. Osteonic tissue that appears both in the longitudinal and transverse direction (Figure 10c-f) of our specimens is a unique characteristic of the petrous bone, and to our knowledge this is the first report of the presence of osteons in both transverse and longitudinal directions of any skeletal element.

The presence of osteons suggests that bone remodelling can take place in some areas of the inner ear (Doden and Halves, 1984; Frisch et al., 2000; Jeffery and Spoor, 2004; Jørkov et al., 2009). This might be linked to the continual, age dependent and variable changes in the size and organization of the pneumatized spaces observed within the petrous pyramid by Hill (2011). Furthermore, the appearance of osteons in both directions can be explained by the fact that the vascular network of the otic capsule is a termination area for the internal auditory artery (IAA) and a communication area between the IAA and several other arteries (Mazzoni, 1972). Thus the osteons and other vascular canals need to accommodate the various arteries and their branches which travel in various directions.

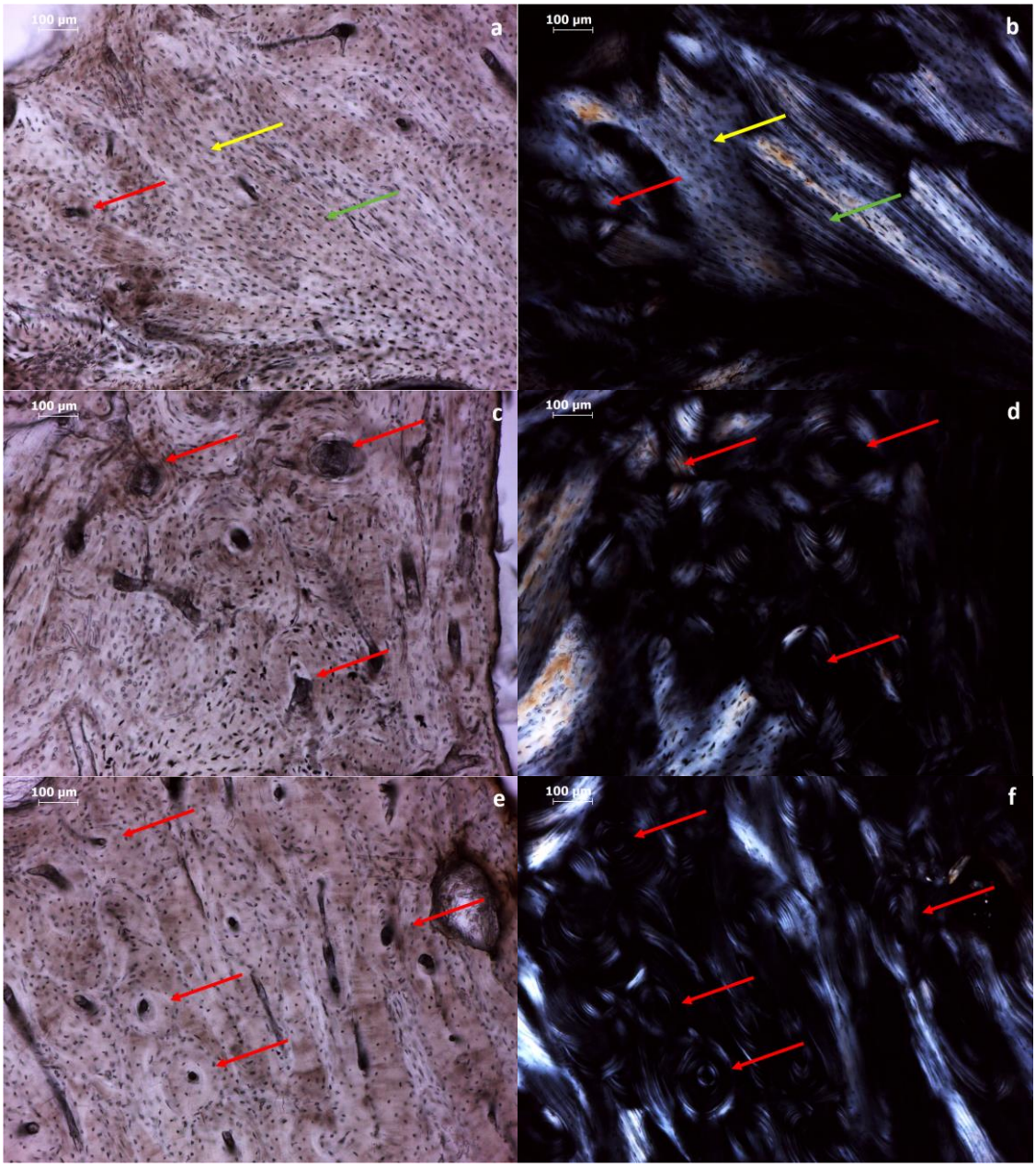

Figure 10. ***DEN6 Longitudinal PPL (a) and XPL (b) 100x - Petrous bone***: Thin section showing an osteon (red arrow), woven tissue (yellow arrow), and lamellar-like tissue (green arrow) in inner periosteal tissue between semi-circular canals.

DEN3 Transverse PPL (c) and XPL (d) 100x - Petrous bone: Image showing the presence of osteons (red arrows) in the outer and inner periosteal tissue.

DEN6 Longitudinal PPL (e) and XPL (f) 100x - Petrous bone: Another image showing the presence of osteons (red arrows) in the outer and inner periosteal tissue, this time in longitudinal section.

In terms of histological preservation, GHI values indicate moderate to good preservation of most specimens (Table 8). Our data also indicate a very strong correlation (Denmark R^2=0.81) between GHI and collagen yields (Figure 11a), with less altered bone having more collagen. However, it is difficult to estimate the degree of alterations on a spatial scale larger than the microscopic field of view (here at 40x total magnification the field of view is c. 5 mm). Inter-observer variations cannot be avoided, while section thickness and decalcification can also affect GHI (or OHI)

reliability for screening collagen preservation (Caruso et al., 2018). Inter-site variations (thermally older sites will have less collagen, e.g. Kendall et al., 2018 Fig.7) and preservation of microstructure without preservation of collagen content due to hydrolysis can further limit GHI's use as collagen indicator (Collins et al., 2002; Hedges et al., 1995).

Table 8. Summary of data (GHI: general histological index; IRSF: Infrared splitting factor; C/P: carbonate-to-phosphate; BPI: carbonate type B-to-phosphate index; Am/P: amide-to-phosphate). C/N collagen= % C/% N x atomic weight C/atomic weight N. The samples' names as presented in Hansen et al. (2017) are provided in parentheses as the genetic data (endogenous DNA content) derives directly from this study.

The symbols next to the GHI values indicate: * samples with transverse thin sections; ** samples with longitudinal thin sections; *** samples with both transverse and longitudinal thin sections.

[1]Collagen content estimates calculated using the equation *collagen wt. % = 113.13 Am/P + 1.69* presented in Lebon et al. (2016).

Sample	GHI	IRSF	C/P	BPI	Am/P	wt. % C whole	wt. % N whole	C/N whole	% C Collagen	% N Collagen	C/N Collagen	wt. % Collagen	wt. % Collagen Estimates[1]	% endogenous DNA
DEN1 (H1)	4***	3.328 ±0.036	0.251 ±0.009	0.441 ±0.010	0.166 ±0.004	11.52	3.38	3.41	42.98	15.54	3.23	14.50	20.44	54.79
DEN2 (H3)	2***	3.244 ±0.019	0.223 ±0.003	0.386 ±0.008	0.097 ±0.002	8.03	1.94	4.14	44.43	16.02	3.24	11.19	12.64	41.62
DEN3 (H4)	4*	3.329 ±0.007	0.255 ±0.003	0.441 ±0.008	0.162 ±0.002	11.60	3.42	3.39	43.22	15.73	3.20	17.84	20.00	34.90
DEN4 (H5)	2*	3.965 ±0.109	0.106 ±0.015	0.220 ±0.018	0.053 ±0.008	7.83	2.22	3.54	44.08	15.95	3.22	10.71	7.73	6.97
DEN5 (H6)	2*	3.682 ±0.024	0.147 ±0.002	0.250 ±0.005	0.096 ±0.002	8.00	2.22	3.60	44.16	15.17	3.40	11.33	12.56	4.74
DEN6 (H7)	4***	3.333 ±0.017	0.225 ±0.008	0.412 ±0.020	0.140 ±0.006	11.11	3.29	3.37	44.65	15.91	3.27	12.91	17.54	56.34
DEN7 (H8)	4***	3.378 ±0.028	0.204 ±0.008	0.355 ±0.018	0.113 ±0.007	9.27	2.67	3.47	44.12	15.68	3.28	15.73	14.49	43.77
DEN8 (H9)	N/A	3.271 ±0.019	0.180 ±0.001	0.323 ±0.003	0.080 ±0.000	7.75	2.03	3.82	45.20	16.06	3.28	10.80	10.79	43.22
DEN9 (H10)	1*	3.621 ±0.096	0.139 ±0.017	0.244 ±0.021	0.073 ±0.015	5.76	1.46	3.95	44.07	15.96	3.22	7.42	9.92	3.54
CA1 (BA3)	2***	4.277 ±0.085	0.101 ±0.003	0.204 ±0.003	0.083 ±0.004	9.62	1.46	6.59	43.40	12.89	3.25	15.26	11.03	0.12
CA2 (BA4)	3***	3.860 ±0.019	0.141 ±0.006	0.253 ±0.010	0.102 ±0.004	9.80	2.85	3.45	44.36	11.08	3.25	17.74	13.19	5.77
CA3 (BA2)	N/A	3.763 ±0.020	0.190 ±0.007	0.323 ±0.016	0.142 ±0.006	10.72	3.23	3.32	43.83	10.98	3.26	17.29	17.74	32.01
CA4 (BA5)	N/A	4.068 ±0.120	0.143 ±0.015	0.313 ±0.017	0.016 ±0.002	7.92	1.49	5.32	43.73	11.50	3.31	10.53	3.47	9.58
CA5 (N/A)	N/A	4.421 ±0.154	0.065 ±0.007	0.128 ±0.007	0.039 ±0.004	6.04	1.39	4.35	42.57	12.89	3.26	13.60	6.14	N/A
CA6 (BA1)	N/A	3.817 ±0.065	0.180 ±0.012	0.308 ±0.016	0.074 ±0.006	7.53	1.84	4.10	42.72	11.20	3.24	13.59	10.05	0.46

GHI may also be a reliable predictor of DNA preservation as it shows strong correlation in Danish samples with endogenous DNA yields (R^2=0.67) (Figure 11b). Changes in crystallinity (IRSF), however, show a weak relationship (R^2=0.27) with GHI, which indicates that the localized mineral redeposition during microbial attack (e.g. Hackett, 1981; Pesquero et al., 2015) and the loss of integrity during generalized destruction may not be reflected in average bioapatite (BAp) characteristics of comparatively large sampling areas (Figure 11c).

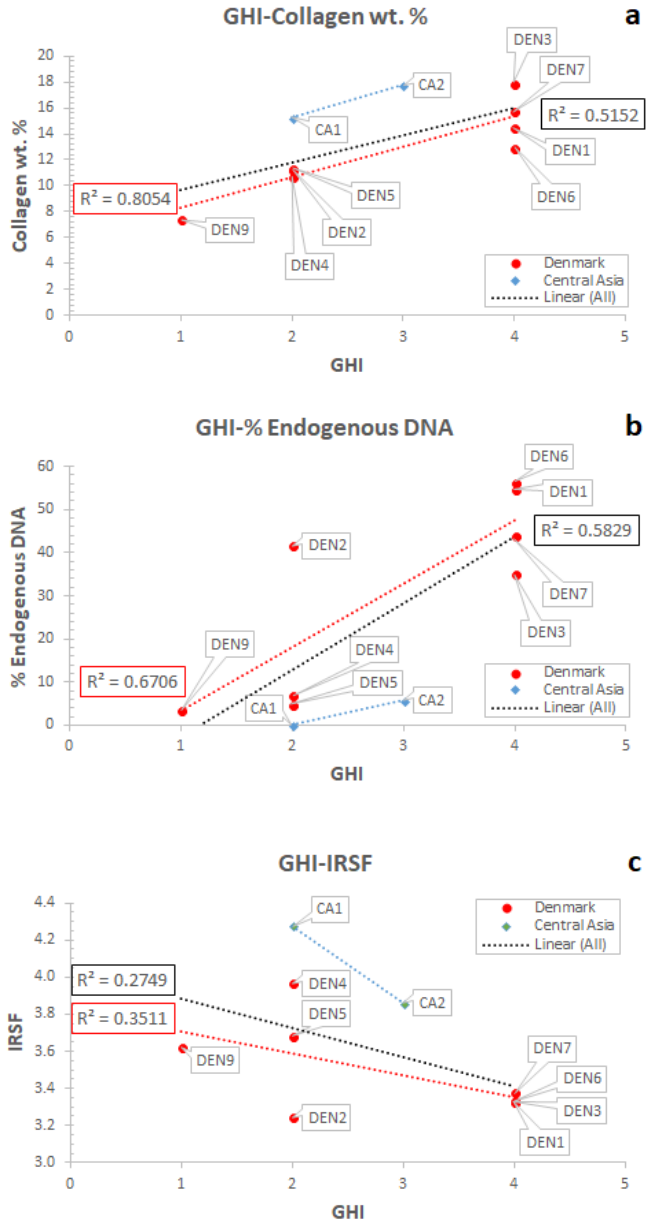

Figure 11. Correlation of GHI with collagen yield (a), endogenous DNA content (b), and BAp crystallinity (c).

Possible microbial activity is only observed in small areas of samples DEN1 and DEN2, although microbially attacked areas may have been missed due to prior sampling for aDNA analysis. The few alterations identified (Figure 12b) show similarities to the early diagenetic stages characteristics (Kontopoulos et al., 2016; i.e. merging of osteocyte lacunae White and Booth, 2014). Such a lack of microbial activity due to high density and protected location of the petrous pyramid has also been assumed to be partly related with decreased endogenous DNA decay (Gamba et al., 2014). However, the microstructure of four of the eight historical samples from Denmark that were histologically examined have amorphous, disintegrated, dark areas of bone (i.e. generalized destruction) with microcracking (Figure 12c-d) that has resulted in a considerable loss of collagen birefringence. Generalized destruction is assumed to be connected with loss of

the organic content (Collins et al., 2002; Garland, 1989; Jackes et al., 2001) and the presence of inclusions (Tjelldén et al., 2018).

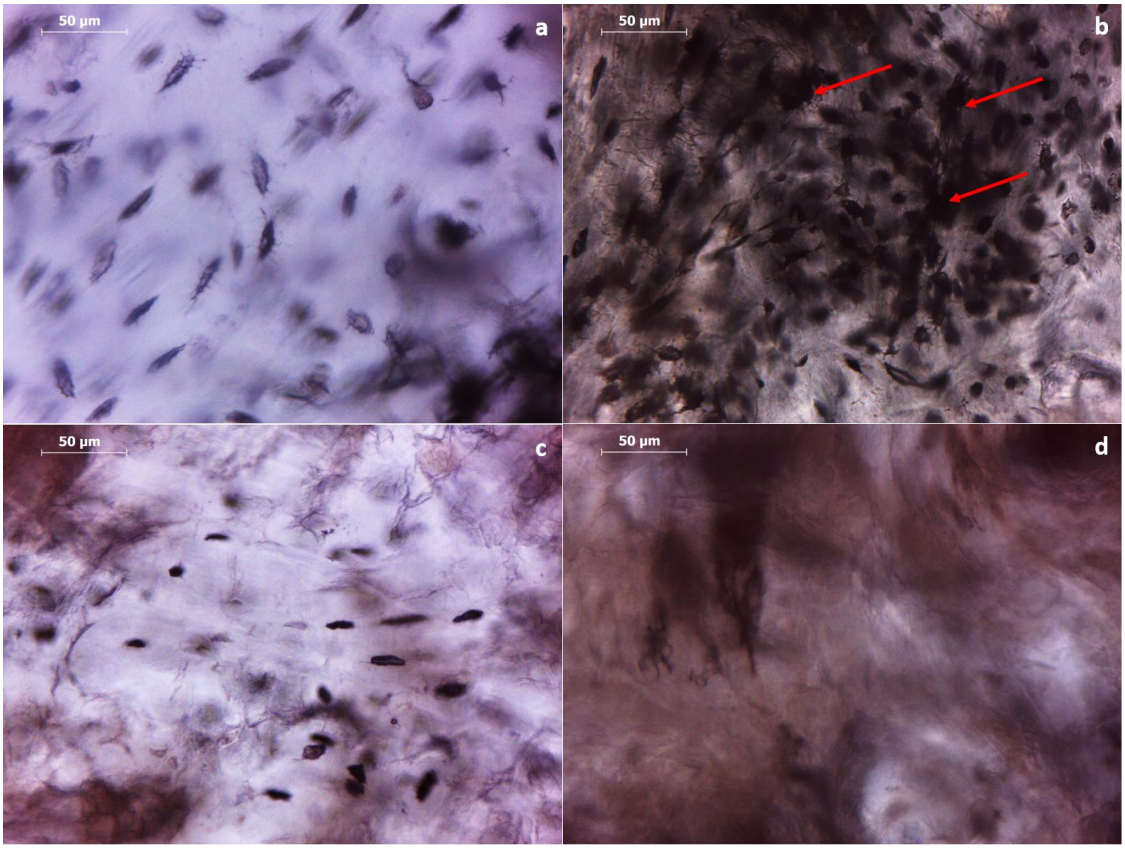

Figure 12. ***DEN4 Transverse PPL (a) and DEN2 Transverse PPL (b) 400x - Petrous bone***: Well-preserved area (a) versus possible microbial activity in (b) that appears as merged osteocyte lacunae (opaque/black holes indicated by red arrows).

DEN4 Transverse PPL (c) and (d) 400x - Petrous bone: Areas displaying degradation due to microcracking (c) that eventually leads to generalized destruction (d) characterized by loss of histological integrity (amorphous) as seen in PPL and a complete loss of collagen birefringence in XPL (dark appearance, hence no image).

Opaque features (inclusions) can be seen within pores of one specimen (Figure 13). Archaeological bone may be filled with detrital or other exogenous material that penetrates the pores (Bodzioch, 2015; Bodzioch and Kowal-Linka, 2012; Garland, 1989). Inclusions can fill up osteocyte lacunae, canaliculi and Haversian canals (Bodzioch, 2015; Hollund et al., 2012; Pfretzschner, 2004; Tjelldén et al., 2018; Turner-Walker, 1999) and can cause micro-cracks (Figure 13) that can accelerate the decay of the already degraded collagen, allowing the ionic exchange between water and bioapatite (Fernandez-Jalvo et al., 2010; Pfretzschner, 2004; Tjelldén et al., 2018).

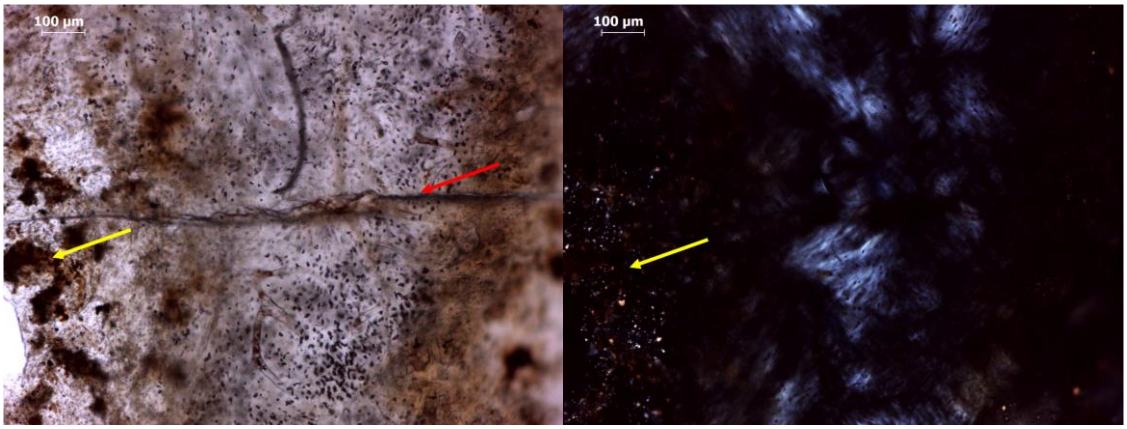

Figure 13. ***DEN2 Longitudinal PPL (left) and XPL (right) 100x - Petrous bone***: Inclusions (yellow arrow) in endosteal tissue close to a fissure (red arrow) that runs from the outer periosteal (red arrow) to the endosteal tissue that surrounds the semicircular canal.

Signs of microcracking (as seen on the walls of Haversian canals or others crossing the osteon boundaries in sample DEN1 (Figure 14)) are related to water uptake (Pfretzschner and Tütken, 2011), as microfissures near or within osteons relate to changes in density, collagen degradation and mineral dissolution (Bell, 1990; Pfretzschner and Tütken, 2011). However, cracking may also be attributed to physical stresses during sample preparation (Dal Sasso et al., 2014; Lander et al., 2014; Turner-Walker, 2012). Brown/orange staining seen in the outer periosteal surfaces of five Danish and two Central Asian specimens (Figure 14) could have been caused by the infiltration of iron oxides (Hollund et al., 2012; Pesquero et al., 2015) or other exogenouss substances that replace the osseous material and can be identified as stained sites with granular appearance (Garland, 1989).

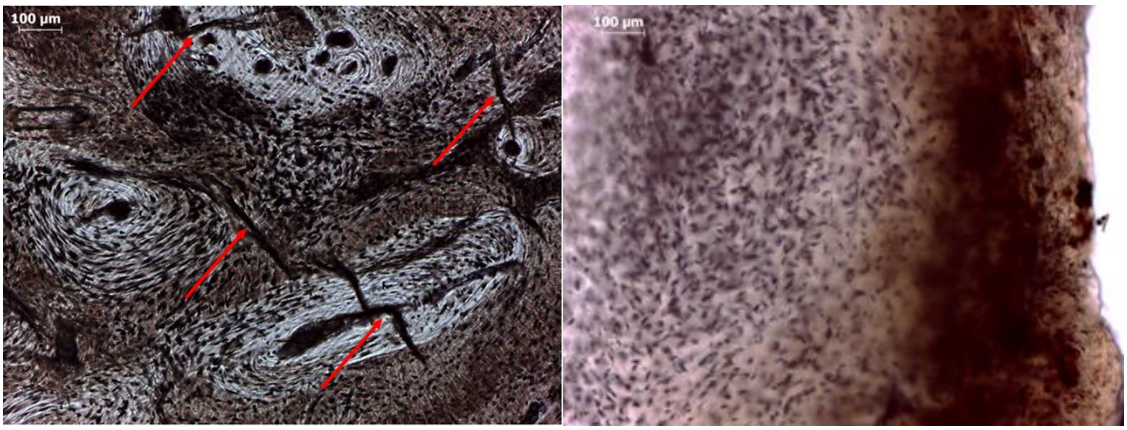

Figure 14. ***DEN1 Longitudinal PPL 100x - Petrous bone (left)***: Areas of inner periosteal bone exhibiting microcracking within and around osteons (red arrows).

DEN2 Transverse PPL 100x - Petrous bone (right): Brown staining of the outer periosteal tissue.

3.2. Bioapatite preservation

Changes in bioapatite composition occur as bone mineral is a relatively unstable and disordered form of hydroxyapatite, and this degree of disorder is responsible for the promotion of diagenetic modifications in BAp crystals (Asscher et al., 2011a; Trueman, 2013). Various ions (e.g. HPO_4^{2-}, PO_4^{3-}, CO_3^{2-}, Ca^{2+}, Mg^{2+}) can be incorporated into the bone-water system, enter the BAp hydrated layer, and subsequently, substitute other ions into the BAp core (Berna et al., 2004; Rey et al., 2009). The conditions of the burial environment (e.g. pH, local hydrology) are responsible for triggering a reorganization/growth of BAp crystals through dissolution (loss of less stable components) and recrystallization (formation of more stable structures) that is necessary for their survival post-mortem (e.g. Berna et al., 2004; Hedges and Millard, 1995; High et al., 2015).

In this study IRSF and C/P display the strong inverse relationship (R^2=0.78) reported in other works, with recrystallization driving the loss of carbonate from the apatite (Figure 15). The Danish and Central Asian samples display statistically significant differences both in IRSF values (U=3.000, p=0.003) and carbonate content (U=10.500, p=0.05). The petrous bones from Denmark have a lower average IRSF (IRSF=3.46±0.08) that is only slightly increased compared to modern human bone (IRSF=3.357±0.007), while the petrous bones from Central Asia (IRSF=4.04±0.1) show much stronger modifications. The infrared splitting factor (IRSF) reflects BAp crystal size and structural order/disorder, with the larger and/or more ordered crystals displaying higher IRSF values (e.g. Asscher et al., 2011a, 2011b). Thus, increased IRSF values here indicate an increase in average and/or maximum crystal length. This increase may be due to an increase of the size of the larger crystals at the expense of the smaller ones (i.e. Ostwald ripening), dissolution of the smaller crystals, or both (Kendall et al., 2018; Trueman, 2013; Weiner and Bar-Yosef, 1990).

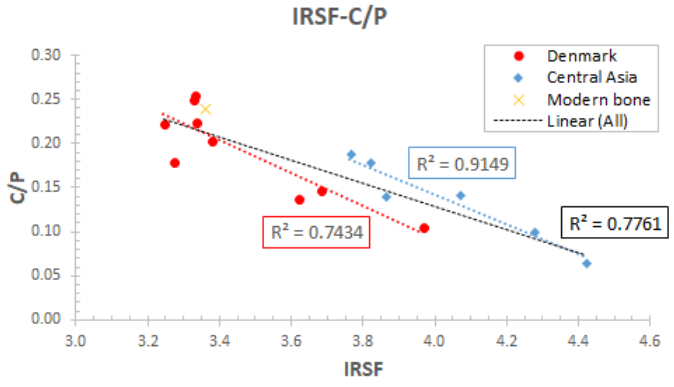

Figure 15. IRSF-to-C/P correlation that denotes site-specific variations. Increased IRSF values indicate an increase in average and/or maximum crystal length.

A loss of CO_3^{2-} content in our samples can be seen both in the Danish (C/P=0.19±0.02) and the Central Asian petrous bones (C/P=0.14±0.02) compared to modern human samples (C/P=0.240±0.003). Similarly to IRSF, the two assemblages exhibit site-specific differences in carbonate content (Figure 15), with the petrous bones from Denmark displaying a loss of about

20% of the initial carbonate, while the Central Asia bones have lost about the 40% of their initial CO_3^{2-}. The main driving factor in diagenetic alteration is the extent to which local conditions alter the mineral phase; the more stable the conditions the less altered is the bone. The longer time of exposure to the conditions of the burial environment for the Central Asian (i.e. Bronze Age) samples could also partly explain their differences in crystallinity and carbonate content. It is, generally, assumed that the longer the bone is exposed to the conditions of the burial environment, the greater is its dependency on external sources of phosphate (i.e. authigenic minerals) and other ions to fill in the pore space initially occupied by the organic component (Figueiredo et al., 2012; Trueman et al., 2004), although this also depends on other environmental factors.

Overall, the decreased CO_3^{2-} content observed in our samples promoted the formation of a more stable mineral phase (i.e. crystal size and lattice perfection) (Salesse et al., 2014). Carbonate ions (4-6 wt. %) can replace OH^- (type A) or PO_4^{3-} (type B) ions in the bioapatite crystal lattice (LeGeros, 1965; Wopenka and Pasteris, 2005). Type A substitutions take place at high temperatures (900-1000° C) with the exclusion of water, whereas type B substitutions can take place at much lower temperatures (25-100° C) (LeGeros, 1965).

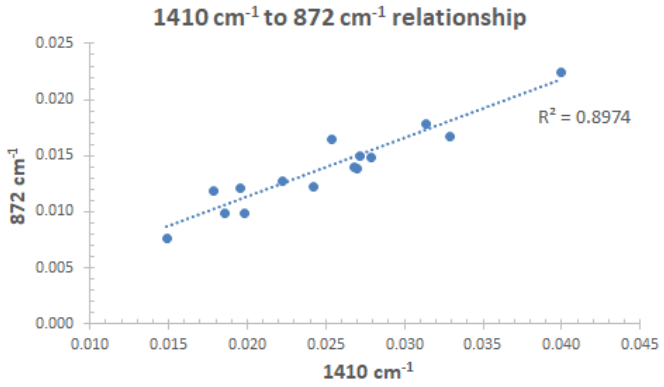

Figure 16. The very strong 1410-to-872 cm^{-1} peak height correlation indicative of the dominant role of type B carbonate in BAp crystal structure.

Here the peak height at c. 1410 cm^{-1} displays a very strong linear relationship (R^2=0.90) with this at c. 872 cm^{-1}(Figure 16). As both peaks reflect the type B carbonate environment in bioapatite crystals (Rey et al., 1989) it indicates that bone carbonate exchange during crystallinity increase (Figure 15) primarily occurs at the phosphate sites of the crystal lattice (i.e. type B) (LeGeros, 1965; Wopenka and Pasteris, 2005). An exchange of PO_4^{3-} for CO_3^{2-} alters the atomic-level bond spacings and orientations due to the differences in the O-O distances (LeGeros et al., 1969). A substitution of the smaller CO_3^{2-} by the larger PO_4^{3-} increases the unit cell dimensions of BAp crystals and forms more ordered crystal lattices (e.g. LeGeros, 1965; Wopenka and Pasteris, 2005). Consequently, our data prove that type B CO_3^{2-} is indeed the predominant form of carbonate that is replaced by exogenous phosphate or other ions on the sloping faces of BAp crystals (Fleet et al., 2004; LeGeros, 1965; Rey et al., 1989).

3.3. Collagen preservation

All samples exhibit very good collagen preservation, with collagen wt. % ranging from 7.42 to 17.84 (Table 8). Although there are no statistically significant differences (U=18.000, p=0.328) between the two sites, the Danish petrous bones show lower average collagen yields (12.49±1.04) than the Central Asia samples (14.67±1.1), despite being much younger. Collagen yields (wt. %) are commonly used to distinguish well-preserved from poorly-preserved collagen and currently c. 1 wt. % is considered a suitable threshold below which samples should not be used for isotopic and/or radiocarbon dating studies (Brock et al., 2010; Dobberstein et al., 2009; van Klinken, 1999).

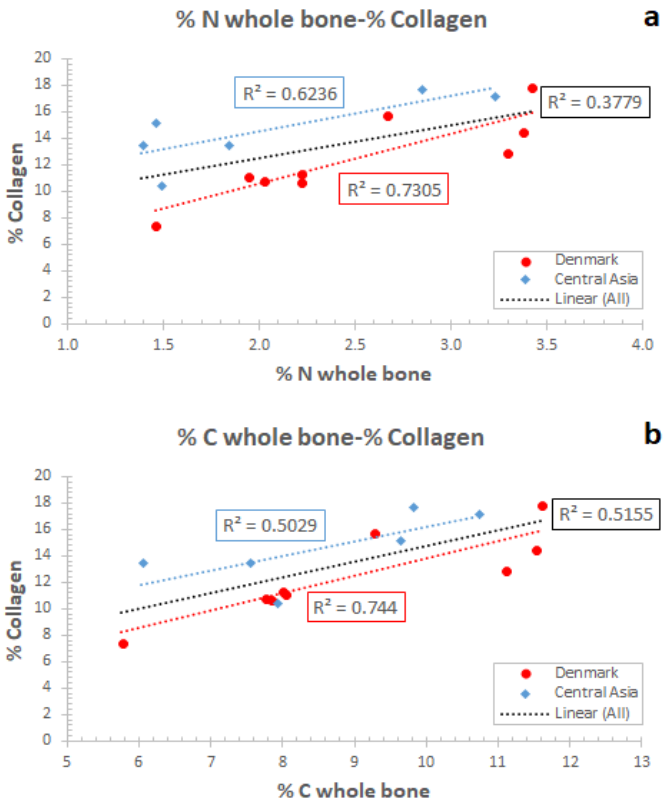

Figure 17. Data showing the reliability of N and C content in whole bone as indicators of collagen preservation.

A combined use of % C, % N and C/N ratio is assumed to significantly increase the successful screening of bones for collagen (Brock et al., 2012, 2010; Harbeck and Grupe, 2009). Starting with the % N in whole bone, which is c. 3.5 - 5.5 wt. % in modern bone (Baker et al., 1946; Eastoe and Eastoe, 1954), our values range from 1.39 to 3.42 (Table 8). It has been previously shown that % N is a reliable index to screen collagen preservation (Bocherens et al., 2005; Brock et al., 2010). Bocherens et al. (2005) support that a 0.4 % N threshold is adequate for samples in order to be further examined for stable isotopes and/or radiocarbon dating. Similarly, Brock et al. (2010) propose a cut-off point of 0.7 %, although when samples contain > 0.7 % N and give collagen yields < 1 wt. %, the nitrogen may be present as short-chain/degraded collagen or polypeptides, non-collagenous proteins, soil contaminants, or conservation treatments (Brock et al., 2012). The

Danish and the Central Asian samples show no statistically significant differences (U=14.500, p=0.145), while they both demonstrate strong, site-specific relationships between collagen wt. % and N wt. % (Figure 17a). The higher average % N in the Danish bones (2.51 versus 2.04 for Central Asian), which at the same time display lower collagen yields than the Central Asian bones, is noteworthy and could be possibly due to the presence of non-collagenous proteins in the former. Overall, it seems that our data are in agreement with past studies (e.g. Brock et al., 2012; Lebon et al., 2016) which claim that % N of whole bone can be a relatively good indicator of collagen preservation, although assessment of highly contaminated and/or degraded bones can be problematic.

Values range from 5.76 to 11.60% for the total amount of carbon (Table 8). Archaeological bone usually displays a significant decrease in carbon content compared to modern animal bone that have c. 15 wt. % C (Ambrose, 1990; Sillen and Parkington, 1996; van Klinken, 1999). While the two groups show no statistically significant differences (U=23.000, p=0.689), the samples from Central Asia display a moderate collagen wt. % - C wt. % correlation (R^2=0.50) while the petrous bones from Denmark exhibit a much stronger linear relationship (R^2=0.74) (Figure 17b). Thus, our data indicate that % C of whole bone can be an equally strong to % N of whole bone predictor of collagen content.

Collagen C/N ratio was also used as a quality indicator for collagen, with values ranging from 3.2 to 3.4 (Table 8) and samples from Denmark displaying no statistically significant differences from these of Central Asia (U=21.500, p=0.529). Values similar to modern bone (i.e. 2.9 to 3.6) are considered representative of good quality collagen, whereas much higher C/N ratios are linked to diagenesis (Ambrose, 1990; DeNiro, 1985; DeNiro and Weiner, 1988; Tuross, 2002). Post-mortem alterations in the carbon and nitrogen contents involve more than one mechanism (microbial attack and hydrolysis) (Ambrose, 1990; Balzer et al., 1997; Harbeck and Grupe, 2009; Turner-Walker, 2008; Tuross, 2002). A preferential loss of the hydrophobic amino acids during collagen hydrolysis and the amino acids with a higher number of carbons in microbial attack can affect the C/N ratio (Balzer et al., 1997; Grupe, 1995; Harbeck and Grupe, 2009; Masters, 1987; Turban-Just and Schramm, 1998; Tuross, 2002). Although the C/N ratios of whole bone powder could provide an alternative solution, the relationship with col. wt. % (Central Asia R^2=0.22 and Denmark R^2=0.48) does not seem to be sensitive enough to discriminate well- from poorly-preserved samples. Poor correlation between C/N of whole bone and collagen yields has also been reported by Brock et al. (2012) and Lebon et al. (2016).

The Am/P ratio can potentially provide valuable information on the relative amount of organic content in bone (Lebon et al., 2016; Trueman et al., 2008a, 2004). A strong to very strong correlation (Central Asia R^2=0.83, Denmark R^2=0.63) between Am/P and collagen wt. % can be seen in our data for both assemblages (Figure 18). The overall relationship between Am/P and collagen yields (R^2=0.33) however is weak, even if there are no statistically significant differences

in Am/P values between the two sites (U=14.500, p=0.145), due to changes in BAp crystals' relative phosphate amounts during dissolution/recrystallization (Figure 18).

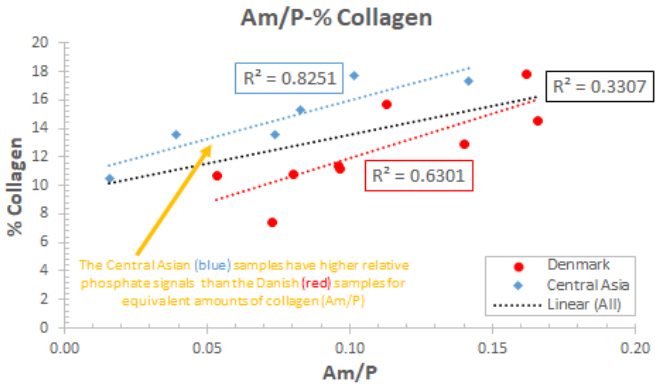

Figure 18. The effect of site-specific variations on the Am/P index. The lower intercept of the more recent (Danish) bones suggests that the phosphate for carbonate exchange (relative phosphate content), and vice versa, can affect the reliability of Am/P as a collagen predictor.

The application of the Am/P ratio as a quantitative approach to estimate collagen yields using the Lebon et al. (2016) equation (i.e. collagen wt. % = 113.13 Am/P + 1.69) can potentially provide reliable collagen content estimates (e.g. DEN2, DEN5, DEN8, CA3) with the average offset being -0.84±2.33% (Table 8). However, the collagen content estimates are affected by the relative phosphate content in the samples (Figure 18) that results to poor agreement with collagen yields in other specimens (e.g. DEN1, DEN6, CA4, CA5). The presence of overtones related to structural water (e.g. O-H stretch at 1640-1660 cm^{-1}) can also lead to increased values for specimens that contain less than c. 10 wt. collagen (Lebon et al., 2016; Trueman et al., 2008a). Further limitations include the significant effects of FTIR and collagen sample preparation strategies on Am/P (e.g. Kontopoulos et al., 2018) and collagen yields (e.g. Sealy et al., 2014), respectively.

Finally, our data are in agreement with other studies (e.g. Lebon et al., 2010; Weiner and Bar-Yosef, 1990) that support a lack of correlation between crystallinity (i.e. IRSF) and collagen content (Denmark R^2=0.19; Central Asia R^2=0.15). This observation might be unexpected as the mineral-organic relationship is considered very strong. The BAp crystals are located between the collagen fibrils (inter-fibrillar spaces) or on the surfaces of collagen fibrils (intra-fibrillar spaces), while their orientation and size are controlled by the fibril structure and organization (Boskey, 2003; Weiner and Price, 1986; Weiner and Traub, 1986). Hence the volume of bone matrix that is filled with collagen *in vivo* can be replaced post-mortem by exogenous ions until inter-crystallite porosity has been filled (Susini et al., 1988; Trueman et al., 2008b). Similar to IRSF, there is a very weak correlation between C/P and collagen wt. % for samples from Central Asia (R^2=0.05), while there is a moderate linear relationship (R^2=0.54) for samples from Denmark. We

have no good explanation of this difference, which would benefit from a larger study which might explore (for example) the selective leaching of proteins such as osteocalcin and osteonectin which may play a role in limiting the extent of recrystallisation.

3.4. DNA preservation

The survival of DNA in archaeological bone has been linked to mineral preservation as dissolution and recrystallization of BAp crystals leads to considerable loss of DNA (Allentoft et al., 2012; Götherström et al., 2002; Lindahl, 1993; Parsons and Weedn, 2006). Our data demonstrate that IRSF and C/P can be considered reliable predictors of DNA preservation as there is an overall strong inverse relationship (R^2=0.69) of crystallinity (IRSF) and an overall strong linear relationship (R^2=0.70) of C/P with endogenous DNA yields (Figure 19a-b). When samples are split into three groups based on their endogenous DNA yields (i.e. >10%, 1-10 %, and <1 %) to potentially enhance screening practices, samples with IRSF values similar to modern human bone (i.e. IRSF=3.357±0.007) display >10 % endogenous DNA (Figure 19c). When endogenous DNA yields drop below 10 %, samples display a very strong inverse relationship (R^2=0.93) with IRSF that increases to levels over 3.6 (Figure 19c). In tandem, samples with similar to modern bone C/P ratios (C/P=0.24±0.003) contain >10 % endogenous DNA (Figure 19d). When C/P decreases to the c. 0.15-0.18 level, this carbonate loss is accompanied by a significant loss of endogenous DNA to below 10 %, although contrariwise to IRSF, there is no strong correlation with DNA yields (Figure 19d). However, the small number of samples examined in this study does not allow any conclusion to be drawn on the possible thresholds.

Overall, the ionic exchanges in bioapatite crystals (phosphate for carbonate substitutions, and vice versa) of archaeological human petrous bone during dissolution/recrystallization can lead to a significant loss of DNA, although DNA molecules can be trapped and survive in archaeological timescales by adsorbing onto the surfaces of the crystals. The adsorption of DNA is controlled by environmental conditions (e.g. temperature, pH, local hydrology) (Grunenwald et al., 2014). At lower temperatures (i.e. 4 °C) the amount of DNA adsorbed onto crystals is significantly less than at higher temperatures (i.e. 22 or 37 °C), while in acidic environments adsorption increases compared to alkaline (Götherström et al., 2002; Grunenwald et al., 2014; Lindahl, 1993; Parsons and Weedn, 2006). Consequently, possible differences in their burial environments are responsible for the variations seen in the relationships between endogenous DNA content, crystallinity and carbonate content in our samples.

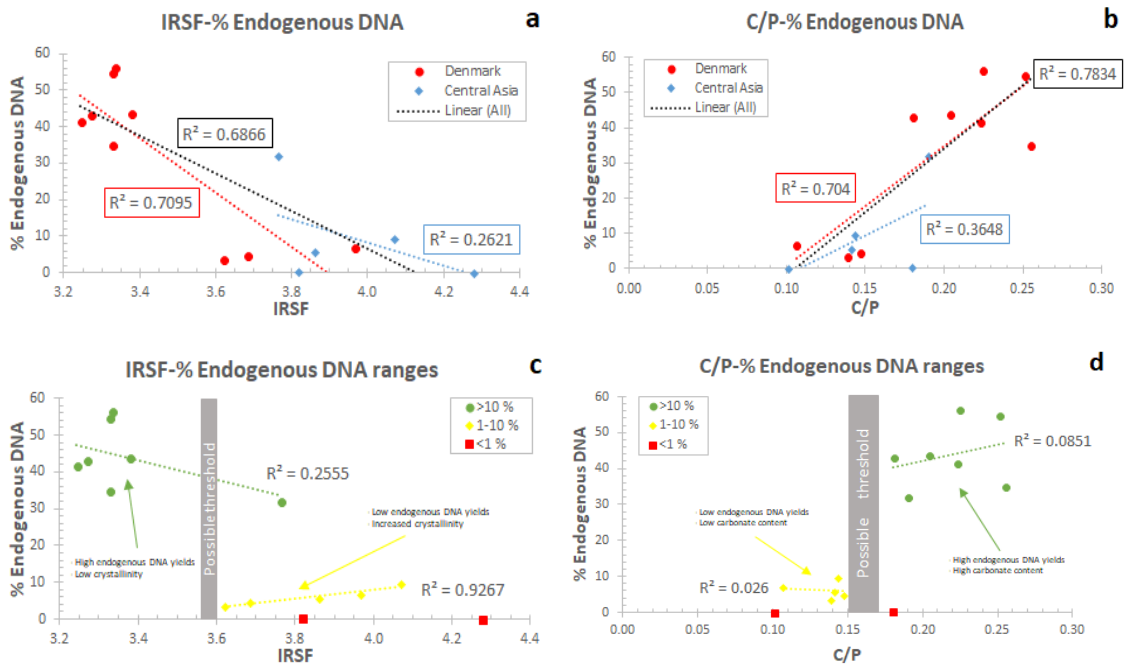

Figure 19. Correlation of crystallinity (a) and carbonate content (b) with endogenous DNA yields, and possible thresholds (c and d). Percentage endogenous DNA between the two sites were almost statistically significant different (U=8.000, p=0.06), and varied between 3.5 % and 56.3 % (average=32.2 %) in the Danish samples, and from 0.1 % to 32 % (average=9.6 %) in the Central Asian specimens.

Additionally, three of the Danish petrous bones (DEN4, DEN5, DEN9) that exhibit <10 % endogenous DNA also display poor histological preservation, with large areas suffering from generalized destruction. The DNA molecule is particularly prone to the interaction with water, which is also related to generalized destruction and ionic exchange in BAp crystals. Hydrolysis leads to breakage of the polynucleotide strands followed by chain breakage into shorter fragments (Bada et al., 1999; Hofreiter et al., 2001; Lindahl, 1993; Pääbo, 1989) and any variations in long-term DNA fragmentation are assumed to be caused by differences in temperature, pH and local hydrology (Allentoft et al., 2012; Burger et al., 1999; Lindahl, 1993; Lindahl and Nyberg, 1972).

Hydrolysis can cause deamination (i.e. loss of the amino -NH_2 group) and/or depurination (i.e. release the purines) with purines being more susceptible to hydrolysis than pyrimidines (Lindahl, 1993; Lindahl and Nyberg, 1972; Pääbo, 1989). Deamination of cytosine to uracil (C→T miscoding lesion) is the most common pathway and generates a C→T sequence error as the deaminated cytosine (now uracil) binds to adenine (Lindahl, 1993; Pääbo et al., 2004). Here, the increased C→T damage rates (Hansen et al., 2017) confirms such a scenario (0.27±0.04 average C→T mismatch for Denmark and 0.39±0.09 for Central Asia). However, correlation of C→T mismatch with the diagenetic parameters was weak (% DNA-C→T= 0.22; % Collagen-C→T= 0.14; IRSF-C→T= 0.18; C/P-C→T= 0.03; % N-C→T= 0.14; 0.02; % C-C→T= 0.00). While the methyl (-CH_3) group attached to cytosine can make them more susceptible to deamination (Brown and Brown, 2011; Hansen et al., 2001), increased methylation levels were not observed in our samples (see Hansen et al., 2017 for more information).

With regard to the collagen-DNA relationship, the crucial role of collagen loss in DNA degradation has been discussed in past studies (Campos et al., 2012; Götherström et al., 2002; Sosa et al., 2013), but our results demonstrate a lack of relationship between collagen and DNA preservation (Figure 20). As a result, collagen preservation is not always a good measure of endogenous DNA content as samples with good collagen preservation may not yield endogenous DNA, and vice versa.

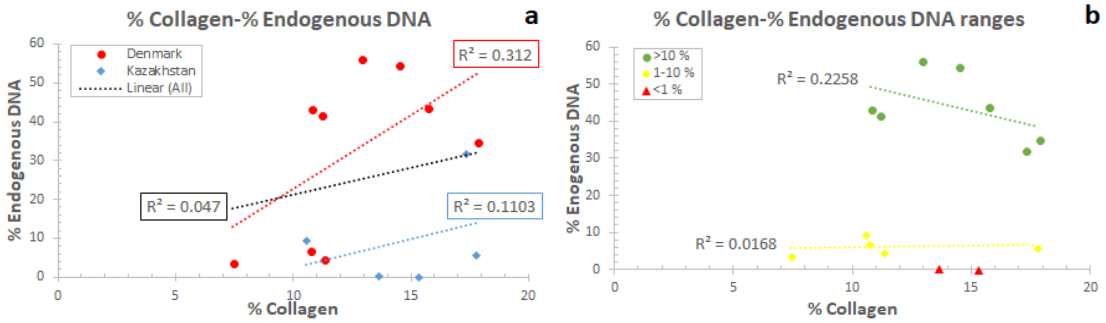

Figure 20. The relationship between collagen content and DNA preservation, indicating that at these levels of bone preservation, % collagen is not always a good indicator for successful aDNA recovery.

4. Conclusion

This study focused on human petrous bone diagenesis with the aim of providing new information which can potentially increase the success rates of some commonly used methods (e.g. histology, FTIR, elemental analysis, collagen wt. %) applied to screen petrous bone for DNA and collagen preservation. The analysis revealed:

- **Histomorphology**: the present findings confirm that the human petrous bone has unique microstructural characteristics with different types and arrangement of tissues compared to other adult skeletal elements. Woven and lamellar-like tissue distribution in outer periosteal, inner periosteal, and endosteal zones of the petrous pyramid is possibly controlled by the function and mechanical demands of each inner ear region. To our knowledge, this is the first report of the presence of osteons in both transverse and longitudinal sections in any skeletal element. However, it is difficult to arrive at any conclusions with regard to the effects of microstructure on the role of petrous bone as a repository of ancient biomolecules, although it is possible that its combined characteristics (woven tissue, lack of remodelling, protected location) may create microniches that allow DNA survival.
- **Diagenesis**: a) microscopic focal destructions were not observed in petrous bones. Only few merged osteocyte lacunae can possibly represent some limited microbial activity during early diagenetic stages; b) generalized destruction was linked with decreased levels of endogenous DNA content; c) dissolution and recrystallization of BAp crystals was associated with a significant loss of DNA but not collagen.

- **Screening methods**: a) GHI can be potentially used for collagen and DNA screening; b) Am/P, % N and % C content in whole bone are reliable indicators of collagen content; c) IRSF and C/P may potentially be used to identify bones with high (>10 %) endogenous DNA content.

Future research should further explore these initial histomorphological findings by examining a series of transverse and longitudinal thin sections to record changes across the entire petrous. That way any issues regarding the role of bioerosion in petrous bone degradation can be answered and susceptible areas can be identified. The potential effects of the burial environment on petrous bone diagenesis may also constitute the object of future studies as these may help pinpoint the critical degradation parameters. Another interesting research approach would also be the comparison of petrous bone with other skeletal elements to understand to what extent their histomorphological or even possible compositional differences increase DNA and collagen chances for postmortem survival in petrous bone. Multi-analytical approaches could provide deeper analyses of particular diagenetic mechanisms, while new proposals of different methods may further enhance screening practices.

Acknowledgements

We are indebted to Prof. Peter Zioupos for the two modern human samples (NHS REC approval 10/H0107/14) which were used as references in this study with the kind permission of the Department of Biology Ethics Committee (BEC) of the University of York. The Danish National Museum is thanked for allowing access to the skeletal material from Holmens Church (Denmark).

MJC was supported by Danish National Research Foundation (DNRF128) and KP from the Leverhulme Trust (PLP-2012-116). IK would like to thank Onassis Foundation (grant no. F ZL 047-1/2015-2016), Leventis Foundation and the Greek Archaeological Committee UK (GACUK).

References

Allentoft, M.E., Collins, M., Harker, D., Haile, J., Oskam, C.L., Hale, M.L., Campos, P.F., Samaniego, J.A., Gilbert, M.T.P., Willerslev, E., Zhang, G., Scofield, R.P., Holdaway, R.N., Bunce, M., 2012. The half-life of DNA in bone: measuring decay kinetics in 158 dated fossils. Proc. Biol. Sci. 279, 4724–4733. https://doi.org/10.1098/rspb.2012.1745

Ambrose, S.H., 1990. Preparation and characterization of bone and tooth collagen for isotopic analysis. J. Archaeol. Sci. 17, 431–451. https://doi.org/10.1016/0305-4403(90)90007-r

Asscher, Y., Regev, L., Weiner, S., Boaretto, E., 2011a. Atomic disorder in fossil tooth and bone mineral: An FTIR study using the grinding curve method. Archeosciences 135–141. https://doi.org/10.4000/archeosciences.3062

Asscher, Y., Weiner, S., Boaretto, E., 2011b. Variations in atomic disorder in biogenic carbonate hydroxyapatite using the infrared spectrum grinding curve method. Adv. Funct. Mater. 21, 3308–3313. https://doi.org/10.1002/adfm.201100266

Bada, J.L., Wang, X.S., Hamilton, H., Ambler, R.P., Finch, P., Grocke, D.R., Eglinton, G., Macko, S.A., 1999. Preservation of key biomolecules in the fossil record: current knowledge and future challenges (and discussion). Philos. Trans. R. Soc. Lond. B Biol. Sci. 354, 77–87.

Baker, S.L., Butterworth, E.C., Langley, F.A., 1946. The calcium and nitrogen content of

human bone tissue cleaned by micro-dissection. Biochem. J 40, 391–396.

Balzer, A., Gleixner, G., Grupe, G., Schmidt, H.L., Schramm, S., Turban-Just, S., 1997. In vitro decomposition of bone collagen by soil bacteria: The implications for stable isotope analysis in archaeometry. Archaeometry 39, 415–429.

Bell, L.S., 1990. Palaeopathology and diagenesis: an SEM evaluation of structural changes using backscattered electron imaging. J. Archaeol. Sci. 17, 85–102. https://doi.org/10.1016/0305-4403(90)90016-X

Bentley, A.R., 2006. Strontium Isotopes from the Earth to the Archaeological Skeleton: A Review. J Archaeol Method Theory 13, 135–187. https://doi.org/10.1007/s10816-006-9009-x

Berna, F., Matthews, A., Weiner, S., 2004. Solubilities of bone mineral from archaeological sites: the recrystalization window. J. Archaeol. Sci. 31, 867–882.

Bocherens, H., Drucker, D.G., Billiou, D., Moussa, I., 2005. Une nouvelle approche pour évaluer l'état de conservation de l'os et du collagène pour les mesures isotopiques (detation au radiocarbone, isotopes stables du carbone et de l'azote). Anthropologie 109, 557–567.

Bodzioch, A., 2015. Idealized model of mineral infillings in bones of fossil freshwater animals, on the example of Late Triassic metoposaurs from Krasiejów (Poland). Austin Journal of Earth Sciences 2, 1008.

Bodzioch, A., Kowal-Linka, M., 2012. Unraveling the origin of the Late Triassic multitaxic bone accumulation at Krasiejów (S Poland) by diagenetic analysis. Palaeogeogr. Palaeoclimatol. Palaeoecol. 346–347, 25–36. https://doi.org/10.1016/j.palaeo.2012.05.015

Boskey, A.L., 2003. Bone mineral crystal size. Osteoporos. Int. 14 Suppl 5, S16–20; discussion S20–1. https://doi.org/10.1007/s00198-003-1468-2

Brock, F., Higham, T., Ramsey, C.B., 2010. Pre-screening techniques for identification of samples suitable for radiocarbon dating of poorly preserved bones. J. Archaeol. Sci. 37, 855–865. https://doi.org/10.1016/j.jas.2009.11.015

Brock, F., Wood, R., Higham, T.F.G., Ditchfield, P., Bayliss, A., Ramsey, C.B., 2012. Reliability of nitrogen content (%N) and carbon:nitrogen atomic ratios (C:N) as indicators of collagen preservation Suitable for radiocarbon dating. Radiocarbon 54, 879–886. https://doi.org/10.1017/S0033822200047524

Brown, T.A., Barnes, I.M., 2015. The current and future applications of ancient DNA in Quaternary science. J. Quat. Sci. 30, 144–153. https://doi.org/10.1002/jqs.2770

Brown, T., Brown, K., 2011. Biomolecular archaeology An introduction. Wiley-blackwell, Sussex.

Buckley, M., Collins, M., Thomas-Oates, J., Wilson, J.C., 2009. Species identification by analysis of bone collagen using matrix-assisted laser desorption/ionisation time-of-flight mass spectrometry. Rapid Commun. Mass Spectrom. 23, 3843–3854. https://doi.org/10.1002/rcm.4316

Burger, J., Hummel, S., Herrmann, B., Henke, W., 1999. DNA preservation: A microsatellite-DNA study on ancient skeletal remains. Electrophoresis 20, 1722–1728. https://doi.org/3.0.CO;2-4">10.1002/(SICI)1522-2683(19990101)20:8<1722::AID-ELPS1722>3.0.CO;2-4

Campos, P.F., Craig, O.E., Turner-Walker, G., Peacock, E., Willerslev, E., Gilbert, M.T.P., 2012. DNA in ancient bone - where is it located and how should we extract it? Ann. Anat. 194, 7–16. https://doi.org/10.1016/j.aanat.2011.07.003

Cappellini, E., Prohaska, A., Racimo, F., Welker, F., Pedersen, M.W., Allentoft, M.E., de Barros Damgaard, P., Gutenbrunner, P., Dunne, J., Hammann, S., Roffet-Salque, M., Ilardo, M., Moreno-Mayar, J.V., Wang, Y., Sikora, M., Vinner, L., Cox, J., Evershed, R.P., Willerslev, E., 2018. Ancient biomolecules and evolutionary inference. Annu. Rev. Biochem. https://doi.org/10.1146/annurev-biochem-062917-012002

Caruso, V., Cummaudo, M., Maderna, E., Cappella, A., Caudullo, G., Scarpulla, V., Cattaneo, C., 2018. A comparative analysis of microscopic alterations in modern and ancient undecalcified and decalcified dry bones. Am. J. Phys. Anthropol. 165, 363–369. https://doi.org/10.1002/ajpa.23348

Collins, M.J., Nielsen–Marsh, C.M., Hiller, J., Smith, C.I., Roberts, J.P., Prigodich, R.V., Wess, T.J., Csapò, J., Millard, A.R., Turner–Walker, G., 2002. The survival of organic matter in bone: a review. Archaeometry 44, 383–394. https://doi.org/10.1111/1475-4754.t01-1-00071

Colonese, A.C., Farrell, T., Lucquin, A., Firth, D., Charlton, S., Robson, H.K., Alexander, M., Craig, O.E., 2015. Archaeological bone lipids as palaeodietary markers. Rapid Commun. Mass Spectrom. 29, 611–618. https://doi.org/10.1002/rcm.7144

Currey, J.D., 1999. The design of mineralised hard tissues for their mechanical functions. J. Exp. Biol. 202, 3285–3294.

Dal Sasso, G., Maritan, L., Usai, D., Angelini, I., Artioli, G., 2014. Bone diagenesis at the micro-scale: Bone alteration patterns during multiple burial phases at Al Khiday (Khartoum, Sudan) between the Early Holocene and the II century AD. Palaeogeogr. Palaeoclimatol. Palaeoecol. 416, 30–42. https://doi.org/10.1016/j.palaeo.2014.06.034

DeNiro, M.J., 1985. Postmortem preservation and alteration of in vivo bone collagen isotope ratios in relation to palaeodietary reconstruction. Nature 317, 806–809. https://doi.org/10.1038/317806a0T

DeNiro, M.J., Weiner, S., 1988. Chemical, enzymatic and spectroscopic characterization of “collagen” and other organic fractions from prehistoric bones. Geochim. Cosmochim. Acta 52, 2197–2206. https://doi.org/10.1016/0016-7037(88)90122-6

Dobberstein, R.C., Collins, M., Craig, O., Taylor, G.M., Penkman, K.E.H., Ritz-Timme, S., 2009. Archaeological collagen: Why worry about collagen diagenesis. Archaeol. Anthropol. Sci. 1, 31–42.

Doden, E., Halves, R., 1984. On the functional morphology of the human petrous bone. Am. J. Anat. 169, 451–462. https://doi.org/10.1002/aja.1001690407

Eastoe, J.E., Eastoe, B., 1954. The organic constituents of mammalian compact bone. Biochem. J 57, 453–459.

Fernandez-Jalvo, Y., Andrews, P., Pesquero, D., Smith, C.I., Marin-Monfort, D., Sanchez, B., Geigl, E.M., Alonso, A., 2010. Early bone diagenesis in temperate environments Part I: Surface features and histology. Palaeogeogr. Palaeoclimatol. Palaeoecol. 288, 62–81.

Figueiredo, M.M., Gamelas, J.A.F., Martins, A.G., 2012. Characterization of bone and bone-based graft materials using FTIR spectroscopy, in: Infrared Spectroscopy - Life and Biomedical Sciences. https://doi.org/10.5772/36379

Fleet, M.E., Liu, X., King, P.L., 2004. Accommodation of the carbonate ion in apatite: An FTIR and X-ray structure study of crystals synthesized at 2–4 GPa. Am. Mineral. 89, 1422–1432. https://doi.org/10.2138/am-2004-1009

Frisch, T., Sørensen, M.S., Overgaard, S., Bretlau, P., 2000. Estimation of volume referent bone turnover in the otic capsule after sequential point labeling. Ann. Otol. Rhinol. Laryngol. 109, 33–39. https://doi.org/10.1177/000348940010900106

Gamba, C., Jones, E.R., Teasdale, M.D., McLaughlin, R.L., Gonzalez-Fortes, G., Mattiangeli, V., Domboróczki, L., Kővári, I., Pap, I., Anders, A., Whittle, A., Dani, J., Raczky, P., Higham, T.F.G., Hofreiter, M., Bradley, D.G., Pinhasi, R., 2014. Genome flux and stasis in a five millennium transect of European prehistory. Nat. Commun. 5, 5257. https://doi.org/10.1038/ncomms6257

Garland, A.N., 1989. Microscopical analysis of fossil bone. Appl. Geochem. 4, 215–229. https://doi.org/10.1016/0883-2927(89)90021-8

Götherström, A., Collins, M.J., Angerbjörn, A., Lidén, K., 2002. Bone preservation and DNA

amplification. Archaeometry 44, 395–404. https://doi.org/10.1111/1475-4754.00072

Green, R.E., Krause, J., Briggs, A.W., Maricic, T., Stenzel, U., Kircher, M., Patterson, N., Li, H., Zhai, W., Fritz, M.H.-Y., Hansen, N.F., Durand, E.Y., Malaspinas, A.-S., Jensen, J.D., Marques-Bonet, T., Alkan, C., Prüfer, K., Meyer, M., Burbano, H.A., Good, J.M., Schultz, R., Aximu-Petri, A., Butthof, A., Höber, B., Höffner, B., Siegemund, M., Weihmann, A., Nusbaum, C., Lander, E.S., Russ, C., Novod, N., Affourtit, J., Egholm, M., Verna, C., Rudan, P., Brajkovic, D., Kucan, Ž., Gušic, I., Doronichev, V.B., Golovanova, L.V., Lalueza-Fox, C., de la Rasilla, M., Fortea, J., Rosas, A., Schmitz, R.W., Johnson, P.L.F., Eichler, E.E., Falush, D., Birney, E., Mullikin, J.C., Slatkin, M., Nielsen, R., Kelso, J., Lachmann, M., Reich, D., Pääbo, S., 2010. A draft sequence of the Neandertal genome. Science 328, 710–722. https://doi.org/10.1126/science.1188021

Grunenwald, A., Keyser, C., Sautereau, A.M., Crubézy, E., Ludes, B., Drouet, C., 2014. Adsorption of DNA on biomimetic apatites: Toward the understanding of the role of bone and tooth mineral on the preservation of ancient DNA. Appl. Surf. Sci. 292, 867–875. https://doi.org/10.1016/j.apsusc.2013.12.063

Grupe, G., 1995. Preservation of collagen in bone from dry, sandy soil. J. Archaeol. Sci. 22, 193–199.

Hackett, C.J., 1981. Microscopical focal destruction (tunnels) in exhumed human bones. Med. Sci. Law 21, 243–265. https://doi.org/10.1177/002580248102100403

Hansen, A., Willerslev, E., Wiuf, C., Mourier, T., Arctander, P., 2001. Statistical evidence for miscoding lesions in ancient DNA templates. Mol. Biol. Evol. 18, 262–265.

Hansen, H.B., Damgaard, P.B., Margaryan, A., Stenderup, J., Lynnerup, N., Willerslev, E., Allentoft, M.E., 2017. Comparing Ancient DNA Preservation in petrous bone and tooth cementum. PLoS One 12, e0170940. https://doi.org/10.1371/journal.pone.0170940

Harbeck, M., Grupe, G., 2009. Experimental chemical degradation compared to natural diagenetic alteration of collagen: implications for collagen quality indicators for stable isotope analysis. Archaeol. Anthropol. Sci. 1, 43–57. https://doi.org/10.1007/s12520-009-0004-5

Harvig, L., Frei, K.M., Price, T.D., Lynnerup, N., 2014. Strontium isotope signals in cremated petrous portions as indicator for childhood origin. PLoS One 9, e101603. https://doi.org/10.1371/journal.pone.0101603

Hedges, R.E.M., Millard, A.R., 1995. Bones and groundwater: Towards the modelling of diagenetic processes. J. Archaeol. Sci. 22, 155–164. https://doi.org/10.1006/jasc.1995.0017

Hedges, R.E.M., Millard, A.R., Pike, A.W.G., 1995. Measurements and relationships of diagenetic alteration of bone from three archaeological sites. J. Archaeol. Sci. 22, 201–209. https://doi.org/10.1006/jasc.1995.0022

Hendy, J., Welker, F., Demarchi, B., Speller, C., Warinner, C., Collins, M.J., 2018. A guide to ancient protein studies. Nat Ecol Evol 2, 791–799. https://doi.org/10.1038/s41559-018-0510-x

High, K., Milner, N., Panter, I., Penkman, K.E.H., 2015. Apatite for destruction: investigating bone degradation due to high acidity at Star Carr. J. Archaeol. Sci. 59, 159–168. https://doi.org/10.1016/j.jas.2015.04.001

Hill, C.A., 2011. Ontogenetic change in temporal bone pneumatization in humans. Anat. Rec. 294, 1103–1115. https://doi.org/10.1002/ar.21404

Hofreiter, M., Serre, D., Poinar, H.N., Kuch, M., Pääbo, S., 2001. Ancient DNA. Nat. Rev. Genet. 2, 353–359. https://doi.org/10.1038/35072071

Hollund, H.I., Jans, M.M.E., Collins, M.J., Kars, H., Joosten, I., Kars, S.M., 2012. What happened here? Bone hstology as a tool in decoding the postmortem histories of archaeological bone from Castricum, The Netherlands. Int. J. Osteoarchaeol. 22, 537–548. https://doi.org/10.1002/oa.1273

Jackes, M., Sherburne, R., Lubell, D., Barker, C., Wayman, M., 2001. Destruction of

microstructure in archaeological bone: a case study from Portugal. International Journal of Osteoarchaeology 11, 415–432.

Jeffery, N., Spoor, F., 2004. Prenatal growth and development of the modern human labyrinth. J. Anat. 204, 71–92. https://doi.org/10.1111/j.1469-7580.2004.00250.x

Jørkov, M.L.S., Heinemeier, J., Lynnerup, N., 2009. The petrous bone-a new sampling site for identifying early dietary patterns in stable isotopic studies. Am. J. Phys. Anthropol. 138, 199–209. https://doi.org/10.1002/ajpa.20919

Katić, V., Vujicić, G., Ivanković, D., Stavljenić, A., Vukicević, S., 1991. Distribution of structural and trace elements in human temporal bone. Biol. Trace Elem. Res. 29, 35–43.

Katzenberg, M.A., 2008. Stable isotope analysis: a tool for studying past diet, demography, and life history, in: Katzenberg, M.A., Saunders, S.R. (Eds.), Biological Anthropology of the Human Skeleton. John Wiley & Sons, pp. 413–441.

Kendall, C., Eriksen, A.M.H., Kontopoulos, I., Collins, M.J., Turner-Walker, G., 2018. Diagenesis of archaeological bone and tooth. Palaeogeogr. Palaeoclimatol. Palaeoecol. 491, 21–37. https://doi.org/10.1016/j.palaeo.2017.11.041

Kontopoulos, I., Nystrom, P., White, L., 2016. Experimental taphonomy: post-mortem microstructural modifications in Sus scrofa domesticus bone. Forensic Sci. Int. 266, 320–328. https://doi.org/10.1016/j.forsciint.2016.06.024

Kontopoulos, I., Presslee, S., Penkman, K., Collins, M.J., 2018. Preparation of bone powder for FTIR-ATR analysis: The particle size effect. Vib. Spectrosc. https://doi.org/10.1016/j.vibspec.2018.09.004

Lander, S.L., Brits, D., Hosie, M., 2014. The effects of freezing, boiling and degreasing on the microstructure of bone. Homo 65, 131–142. https://doi.org/10.1016/j.jchb.2013.09.006

Lebon, M., Reiche, I., Bahain, J.-J., Chadefaux, C., Moigne, A.-M., Fröhlich, F., Sémah, F., Schwarcz, H.P., Falguères, C., 2010. New parameters for the characterization of diagenetic alterations and heat-induced changes of fossil bone mineral using Fourier transform infrared spectrometry. J. Archaeol. Sci. 37, 2265–2276. https://doi.org/10.1016/j.jas.2010.03.024

Lebon, M., Reiche, I., Gallet, X., Bellot-Gurlet, L., Zazzo, A., 2016. Rapid quantification of bone collagen content by ATR-FTIR spectroscopy. Radiocarbon 58, 131–145. https://doi.org/10.1017/RDC.2015.11

Lee-Thorp, J.A., 2008. On isotopes and old bones. Archaeometry 50, 925–950. https://doi.org/10.1111/j.1475-4754.2008.00441.x

LeGeros, R.Z., 1965. Effect of carbonate on the lattice parameters of apatite. Nature 206, 403. https://doi.org/10.1038/206403a0

LeGeros, R.Z., Trautz, O.R., Klein, E., LeGeros, J.P., 1969. Two types of carbonate substitution in the apatite structure. Experientia 25, 5–7. https://doi.org/10.1007/BF01903856

Lindahl, T., 1993. Instability and decay of the primary structure of DNA. Nature 362, 709–715. https://doi.org/10.1038/362709a0

Lindahl, T., Nyberg, B., 1972. Rate of depurination of native deoxyribonucleic acid? Biochemistry 11, 3610–3618.

Longin, R., 1971. New method of collagen extraction for radiocarbon dating. Nature 230, 241–242.

Masters, P.M., 1987. Preferential preservation of noncollagenous protein during bone diagenesis: Implications for chronometric and stable isotopic measurements. Geochim. Cosmochim. Acta 51, 3209–3214. https://doi.org/10.1016/0016-7037(87)90129-3

Mazzoni, A., 1972. Internal auditory artery supply to the petrous bone. Ann. Otol. Rhinol. Laryngol. 81, 13–21. https://doi.org/10.1177/000348947208100103

Millard, A.R., 2001. Deterioration of bone, in: Brothwell, D R & Pollard, A M (Ed.), Handbook of Archaeological Sciences. Wiley, pp. 633–643.

Nielsen-Marsh, C., Gernaey, A., Turner-Walker, G., Hedges, R., Pike, A.W.G., Collins, M., 2000. The chemical degradation of bone, in: Cox, M., Mays, S. (Eds.), Human Osteology: In Archaeology and Forensic Science. Cambridge University Press, pp. 439–454.

Orlando, L., Cooper, A., 2014. Using ancient DNA to understand evolutionary and ecological processes. Annu. Rev. Ecol. Evol. Syst. 45, 573–598. https://doi.org/10.1146/annurev-ecolsys-120213-091712

Pääbo, S., 1989. Ancient DNA: extraction, characterization, molecular cloning, and enzymatic amplification. Proc. Natl. Acad. Sci. U. S. A. 86, 1939–1943.

Pääbo, S., Poinar, H., Serre, D., Jaenicke-Després, V., Hebler, J., Rohland, N., Kuch, M., Krause, J., Vigilant, L., Hofreiter, M., 2004. Genetic analyses from ancient DNA. Annu. Rev. Genet. 38, 645–679. https://doi.org/10.1146/annurev.genet.37.110801.143214

Parsons, T.J., Weedn, V.W., 2006. Preservation and recovery of DNA in postmortem specimens and trace samples, in: Forensic taphonomy: The postmortem fate of human remains. CRC Press.

Pesquero, M.D., Alcalá, L., Bell, L.S., Fernández-Jalvo, Y., 2015. Bacterial origin of iron-rich microspheres in Miocene mammalian fossils. Palaeogeogr. Palaeoclimatol. Palaeoecol. 420, 27–34. https://doi.org/10.1016/j.palaeo.2014.12.006

Pfretzschner, H.-U., 2004. Fossilization of Haversian bone in aquatic environments. C. R. Palevol 3, 605–616. https://doi.org/10.1016/j.crpv.2004.07.006

Pfretzschner, H.-U., Tütken, T., 2011. Rolling bones – Taphonomy of Jurassic dinosaur bones inferred from diagenetic microcracks and mineral infillings. Palaeogeogr. Palaeoclimatol. Palaeoecol. 310, 117–123. https://doi.org/10.1016/j.palaeo.2011.01.026

Pinhasi, R., Fernandes, D., Sirak, K., Novak, M., Connell, S., Alpaslan-Roodenberg, S., Gerritsen, F., Moiseyev, V., Gromov, A., Raczky, P., Anders, A., Pietrusewsky, M., Rollefson, G., Jovanovic, M., Trinhhoang, H., Bar-Oz, G., Oxenham, M., Matsumura, H., Hofreiter, M., 2015. Optimal ancient DNA Yields from the inner ear part of the human petrous bone. PLoS One 10, e0129102. https://doi.org/10.1371/journal.pone.0129102

Rey, C., Collins, B., Goehl, T., Dickson, I.R., Glimcher, M.J., 1989. The carbonate environment in bone mineral: a resolution-enhanced Fourier Transform Infrared Spectroscopy Study. Calcif. Tissue Int. 45, 157–164.

Rey, C., Combes, C., Drouet, C., Glimcher, M.J., 2009. Bone mineral: update on chemical composition and structure. Osteoporos. Int. 20, 1013–1021. https://doi.org/10.1007/s00198-009-0860-y

Salesse, K., Dufour, E., Lebon, M., Wurster, C., Castex, D., Bruzek, J., Zazzo, A., 2014. Variability of bone preservation in a confined environment: The case of the catacomb of Sts Peter and Marcellinus (Rome, Italy). Palaeogeogr. Palaeoclimatol. Palaeoecol. 416, 43–54. https://doi.org/10.1016/j.palaeo.2014.07.021

Sealy, J., Johnson, M., Richards, M., Nehlich, O., 2014. Comparison of two methods of extracting bone collagen for stable carbon and nitrogen isotope analysis: comparing whole bone demineralization with gelatinization and ultrafiltration. J. Archaeol. Sci. 47, 64–69. https://doi.org/10.1016/j.jas.2014.04.011

Sillen, A., Parkington, J., 1996. Diagenesis of bones from Eland's bay cave. J. Archaeol. Sci. 23, 535–542. https://doi.org/10.1006/jasc.1996.0050

Sørensen, M.S., 1994. Temporal bone dynamics, the hard way. Formation, growth, modeling, repair and quantum type bone remodeling in the otic capsule. Acta Otolaryngol. Suppl. 512, 1–22.

Sørensen, M.S., Bretlau, P., Josrgensen, M.B., 1992. Bone repair in the otic capsule of the rabbit. Acta Otolaryngol. 112, 968–975. https://doi.org/10.3109/00016489209137497

Sosa, C., Vispe, E., Nunez, C., Beata, M., Casalod, Y., Bolea, M., Hedges, R.E.M., Martinez-Jarreta, B., 2013. Association between ancient bone preservation and DNA yield: a multidisciplinary approach. Am. J. Phys. Anthropol. 151, 102–109.

Sponheimer, M., Lee-Thorp, J.A., 1999. Alteration of enamel carbonate environments during fossilization. J. Archaeol. Sci. 26, 143–150. https://doi.org/10.1006/jasc.1998.0293

Susini, A., Baud, C.A., Lacotte, D., 1988. Bone apatite crystals alterations in Neolithic skeletons and their relations to burial practices and soil weathering. Rivista di antropologia 66, 35–38.

Tjelldén, A.K.E., Kristiansen, S.M., Birkedal, H., Jans, M.M.E., 2018. The pattern of human bone dissolution--A histological study of Iron Age warriors from a Danish wetland site. International Journal of Osteoarchaeology.

Trueman, C.N., 2013. Chemical taphonomy of biomineralized tissues. Palaeontology 56, 475–486. https://doi.org/10.1111/pala.12041

Trueman, C.N.G., Behrensmeyer, A.K., Tuross, N., Weiner, S., 2004. Mineralogical and compositional changes in bones exposed on soil surfaces in Amboseli National Park, Kenya: diagenetic mechanisms and the role of sediment pore fluids. J. Archaeol. Sci. 31, 721–739. https://doi.org/10.1016/j.jas.2003.11.003

Trueman, C.N., Palmer, M.R., Field, J., Privat, K., Ludgate, N., Chavagnac, V., Eberth, D.A., Cifelli, R., Rogers, R.R., 2008b. Comparing rates of recrystallisation and the potential for preservation of biomolecules from the distribution of trace elements in fossil bones. C. R. Palevol 7, 145–158. https://doi.org/10.1016/j.crpv.2008.02.006

Trueman, C.N., Privat, K., Field, J., 2008a. Why do crystallinity values fail to predict the extent of diagenetic alteration of bone mineral? Palaeogeogr. Palaeoclimatol. Palaeoecol. 266, 160–167. https://doi.org/10.1016/j.palaeo.2008.03.038

Turban-Just, S., Schramm, S., 1998. Stable carbon and nitrogen isotope ratios of individual amino acids give new insights into bone collagen degradation. Bull. Soc. Geol. Fr. 169, 109–114.

Turner-Walker, G., 2012. Early bioerosion in skeletal tissues: persistence through deep time. Neues Jahrbuch fur Geologie und Paläontologie - Abhandlungen 265, 165–183. https://doi.org/10.1127/0077-7749/2012/0253

Turner-Walker, G., 2008. The chemical and microbial degradation of bones and teeth, in: Pinhasi, R., Mays, S. (Eds.), Advances in Human Palaeopathology. Wiley, West Sussex, pp. 1–29.

Turner-Walker, G., 1999. Pyrite Bone Diagenesis in Terrestrial Sediments. Bulletin of the Geological Society of Norfolk 48, 3–26.

Tuross, N., 2002. Alterations in fossil collagen. Archaeometry 44, 427–434. https://doi.org/10.1111/1475-4754.00075

van Klinken, G.J., 1999. Bone collagen quality indicators for palaeodietary and radiocarbon measurements. J. Archaeol. Sci. 26, 687–695. https://doi.org/10.1006/jasc.1998.0385

Weiner, S., Bar-Yosef, O., 1990. States of preservation of bones from prehistoric sites in the Near East: A survey. J. Archaeol. Sci. 17, 187–196. https://doi.org/10.1016/0305-4403(90)90058-D

Weiner, S., Price, P.A., 1986. Disaggregation of bone into crystals. Calcif. Tissue Int. 39, 365–375.

Weiner, S., Traub, W., 1986. Organization of hydroxyapatite crystals within collagen fibrils. FEBS Lett. 206, 262–266.

White, L., Booth, T.J., 2014. The origin of bacteria responsible for bioerosion to the internal bone microstructure: Results from experimentally-deposited pig carcasses. Forensic Sci. Int.

239, 92–102. https://doi.org/10.1016/j.forsciint.2014.03.024

Wopenka, B., Pasteris, J.D., 2005. A mineralogical perspective on the apatite in bone. Materials Science and Engineering: C 25, 131–143. https://doi.org/10.1016/j.msec.2005.01.008

Wright, L.E., Schwarcz, H.P., 1996. Infrared and isotopic evidence for diagenesis of bone apatite at Dos Pilas, Guatemala: Palaeodietary implications. J. Archaeol. Sci. 23, 933–944.

Zioupos, P., Currey, J.D., Casinos, A., 2000. Exploring the effects of hypermineralisation in bone tissue by using an extreme biological example. Connect. Tissue Res. 4, 229–248.

Abstract

This paper presents the characteristics of bone diagenesis in a secondary commingled Mycenaean burial in Kastrouli (Phocis, Greece) and explores how the different diagenetic pathways can act jointly or independently through histological (light microscopy), physical (FTIR-ATR) and biochemical (collagen) examination of human and animal bones. Post-mortem modifications in microstructure, bioapatite and collagen are characteristic of burial environments with groundwater fluctuation and high average temperatures. Within-site variations were defined by three main diagenetic pathways that exhibit differences in histological modifications, crystallinity, and collagen preservation. These differences were either related to different microenvironment conditions, and/or influenced by differences in the early taphonomic histories experienced by bones. Petrous bones display a lack of microbial activity and a generally better preserved microstructure but do not show any better bioapatite and collagen preservation compared to femora. The broader implications of bone diagenesis for isotopic studies that exploit collagen and carbon from bone carbonate are also underlined. Further, this study highlights the importance of IRSF, C/P and GHI for the qualitative assessment of archaeological bone, and the potential use of Am/P as collagen predictor.

Keywords: bone diagenesis; petrous bone; Mycenaean; secondary burial; commingled; histology; bioapatite; collagen

1. Introduction

Bone histology, bioapatite (BAp) and collagen can provide valuable information to the archaeologist and anthropologist. Bone histology can be used for the study of the age-at-death, pathology and to distinguish between human and non-human or burned and unburned bone (Assis et al., 2016; Cattaneo et al., 1999; Cuijpers, 2006; De Boer et al., 2013; Dominguez & Crowder, 2012; Hanson & Cain, 2007; Mulhern & Ubelaker, 2001; Stout & Teitelbaum, 1976). Bioapatite is important in archaeological research for the study of past human and animal movement (phosphate), dietary habits (carbonate) and environments (phosphate and carbonate) (Hedges, 2003; King et al., 2011; Lee-Thorp & van der Merwe, 1991; Wright & Schwarcz, 1996). Bone collagen is used to determine chronological age (i.e. ^{14}C dating), past lifeways (e.g. palaeodietary reconstruction, weaning practices), taxonomic identification, and occasionally for screening (e.g. amino acid racemization) (Ambrose, 1991; Asara et al., 2007; Buckley et al., 2009; Collins et al., 1999, 2009; DeNiro & Weiner, 1988; Douka et al., 2017; van Klinken, 1999; Poinar et al., 1996).

However, (a) microbial attack of the composite, (b) chemical deterioration of the inorganic matter (dissolution/recrystallization), and (c) chemical deterioration of the organic matter (hydrolysis), alter the microstructure and the biogenic chemical signals of bone post-mortem (Collins et al.,

2002; Kendall et al., 2018). Microbial activity can modify bone microstructure (Bell, 2012, 1990; Hackett, 1981; Hedges et al., 1995; Hollund et al., 2012; Kontopoulos et al., 2016; Turner-Walker & Jans, 2008; White & Booth, 2014), and in addition to the apparent modifications in bone histology, microbial attack can also enzymatically degrade collagen using collagenases, with temperature also having a profound effect on collagen degradation (Collins et al., 2002; Kendall et al., 2018; Nielsen-Marsh et al., 2000; Nielsen-Marsh & Hedges, 2000b). Any collagen preserved in archaeological bone can be protected by the bioapatite crystals (BAp) (Grupe, 1995), but post-mortem changes of the mineral phase can expose collagen to chemical hydrolysis (Collins et al., 2002). Such a reorganization or growth of BAp crystals occurs through dissolution and recrystallization when conditions are greatly under-saturated, primarily due to active hydrology (recharging with fresh water) or pH (Berna et al., 2004; Hedges, 2002; Hedges & Millard, 1995; High et al., 2015; Piepenbrink, 1989). Therefore, identifying the diagenetic pathway each bone has followed post-mortem can offer a unique insight into the preservation potential of bone in different burial environments and timescales which is of great importance to osteoarchaeological and forensic research.

1.1. The Mycenaean secondary burial in Kastrouli

The Mycenaean site of Kastrouli (38.40N 22.57E) is situated in the Mesokampos plateau of the Desfina peninsula (Phocis, Greece) at c. 550 m above sea level, and its position between the Itea and Antikyra gulfs was strategic for the control of the entire Desfina peninsula (Figure 21). The top of the Kastrouli hill is fortified with an ellipsoidal, relatively well-preserved wall, which is approximately 170 m in diameter north to south, c. 140 m in diameter east to west, with a maximum preserved height of c. 3 m (Sideris et al., 2017).

This Late Helladic IIIA2 to IIIC (c. 1350-1150 BC) site was systematically excavated in 2016 and among the several interesting finds was an undisturbed commingled burial within a hybrid rock-cut and built chamber tomb (Sideris et al., 2017). The tomb, which was partly made of limestone and partly carved into the bedrock, was oriented with its long axis in the W-E direction and consisted of a dromos in the W, an entrance with monumental lintel, a small chamber, and a niche or extension on the south side covered with a monumental limestone slab (Sideris et al., 2017).

The chamber from the floor bottom to the lower part of the roof slabs is c. 1.65 m, and although the upper c. 40 cm of sediment of the tomb was disturbed in antiquity and looted in the past decades, the lower c. 30 cm of the chamber deposits had not been disturbed since the Late Bronze Age. This layer was filled with macroscopically poorly-preserved commingled human bones (minimum number of fifteen adult individuals, two subadults, an infant and a fetus) (Figure 21), alongside numerous pottery sherds, few small finds, and few bones of domesticated animals (e.g.

Gallus gallus, *Bos taurus*, *Sus scrofa*, *Ovis aries*/*Capra hircus*) (Chovalopoulou et al., 2017; Sideris et al., 2017).

Figure 21. Top: The strategic position of Kastrouli between the Itea and Antikyra Gulfs at the heart of Desfina peninsula.
Bottom: The commingled skeletal remains from tomb A (locus 121) found at c. 1 m depth.

The information that can be retrieved through macroscopic analysis of commingled remains is mainly limited to the minimum number of individuals (MNI), sex, approximate age-at-death, stature or pathology (Adams & Byrd, 2014; Osterholtz et al., 2013). Although the application of other techniques (e.g. optical and scanning electron microscopy, ZooMS, DNA) can potentially answer several important archaeological questions (e.g. human vs non-human bone, species identification, kinship), such analyses can be obstructed through the partial or degraded condition of the skeletal remains (Adams & Byrd, 2014; Osterholtz et al., 2013).

As there is little evidence on bone diagenesis in commingled, disarticulated secondary burials (e.g. Booth & Madgwick, 2016) the aim of this study is to explore the characteristics of bone diagenesis in a secondary burial environment. Histological (light microscopy), physical (FTIR-ATR) and biochemical (collagen) analysis of human and animal bone structure were undertaken in order to explore how the different diagenetic pathways can act jointly or independently. The multiple layers of evidence can help elucidate why and how bone degrades in such conditions and shed light on within-site variations possibly related to different primary and secondary funerary treatments. These data have implications for future isotopic and biomolecular investigations.

2. Materials and Methods

Fifteen archaeological human femora, two human petrous bones and 7 animal bones were used in this study. Statistical analysis was carried out using IBM SPSS v.25 and the significance level was set at $p = 0.05$.Regression correlation (R^2) of 0-0.19 is regarded as very weak, 0.2-0.39 as weak, 0.40-0.59 as moderate, 0.6-0.79 as strong and 0.8-1 as very strong correlation, but these are rather arbitrary limits and should be considered in the context of the results.

2.1. Histology

Twenty-one transverse and two longitudinal thin sections of c. 200 μm from 15 human femora, 2 human petrous bones and 6 animal bones (Table 9) were prepared using an Exact 300 CL diamond band saw. Undecalcified thin sections of c. 200 μm were mounted onto glass microscope slides using Entellan New (Merck chemicals) for microscopy mounting medium and covered by a glass coverslip both cleaned with xylene before use. Thin sections were assessed under a Leica DM750 optical microscope using plane-polarized (PPL) and cross-polarized (XPL) transmitted light at a total magnification ranging from 40x to 400x. Digital images were captured by a Leica ICC50 HD camera for microscopy imaging with a capture resolution of 2048 x 1536 pixels. The general histological index (GHI) introduced by Hollund et al. (2012) was used as it is analogous to the Oxford histological index (OHI) as described by Millard (2001) but includes generalized destruction, cracking, and staining. A GHI value of 5 represents excellent microstructural preservation similar to modern bone (>95% intact microstructure), whereas a GHI value of 0 indicates poor microstructural preservation (<5% intact microstructure) with almost no original histological features observed.

2.2. FTIR

FTIR-ATR measurements were performed in triplicate on 15 human femora, 2 human petrous bones and 7 animal specimens (Table 9) using a Bruker Alpha Platinum [range: 4000-400 cm^{-1}; no. of scans: 144; zero filling factor: 4; resolution: 4 cm^{-1}; mode: absorbance]. Sample preparation and analysis was carried out using Kontopoulos et al. (2018)'s protocol. Bone samples were ground using an agate pestle and mortar following the mechanical cleaning of the outer and inner bone surfaces. About 2-3 mg of bone powder of 20-50 μm particle size were used for each

measurement, and after each measurement the crystal plate and the anvil of the pressure applicator were thoroughly cleaned using isopropyl alcohol.

The calculations of FTIR indices were conducted using OPUS 7.5 software as follows: a) infrared splitting factor (IRSF) was assessed after Weiner and Bar-Yosef (1990, p.191); b) carbonate-to-phosphate (C/P) ratio (Wright & Schwarcz, 1996, p.936); c) type B carbonate substitutions relative to phosphate (BPI) (Sponheimer & Lee-Thorp, 1999, p.145); and d) amide-to-phosphate (Am/P) (Trueman et al., 2004, p.726). The average values of two modern human femora and one modern bovine femur were used as reference throughout (Table 9). The 2nd derivatives were produced to explore the components of the amide I band, the ν_2 and ν_3 CO_3^{2-} bands using the OriginPro 2017 and the Savitzky-Golay filter with 13 smoothing points and a polynomial order of 4.

2.3. Collagen

Collagen was extracted from 15 human femora, 2 human petrous bones and 7 animal specimens (Table 9) using a modified Longin (1971) method. The exterior surfaces of bone samples were mechanically cleaned using a scalpel. Bone chunks of 300-500 mg were demineralized in 8 ml 0.6 M HCl at 4◦ C. Samples were agitated twice daily and acid solution was changed every two days. When demineralisation was completed, the supernatant was drained off and samples were rinsed three times with distilled water. Gelatinization was carried out by adding 8 ml pH3 HCl and samples were placed in hot blocks at 80◦ C for 48h. The supernatant liquor which contains the collagen was filtered off by using Ezee^{TM} filters and was freeze dried for 2 days in pre-weighed plastic tubes.

Extracted collagen was analyzed in duplicate. Tin capsules containing 0.9-1.1 mg of collagen were dropped into an oxygen rich combustion tube held at 1000° C. The tin capsules were ignited and burnt exothermally at 1800°C causing the sample to oxidise. The samples were carried through a layer of chromium oxide and copper oxide which ensure complete oxidation, followed by a layer of silver wool to remove unwanted sulphur and halides. The samples' gases pass into a second furnace containing copper held at 600°C where excess oxygen was removed and nitrogen oxides were reduced to elemental nitrogen. Any water was removed using a magnesium perchlorate trap. The samples then passed into a gas chromatography (GC) column held at 70°C which separates CO_2 and N_2 from each other. The resultant gases were then introduced into the Sercon 20-22 mass spectrometer where the samples were ionised, and the various masses separated in a magnetic field, focused into Faraday collector arrays and analysed.

3. Results and Discussion

3.1. Histological preservation

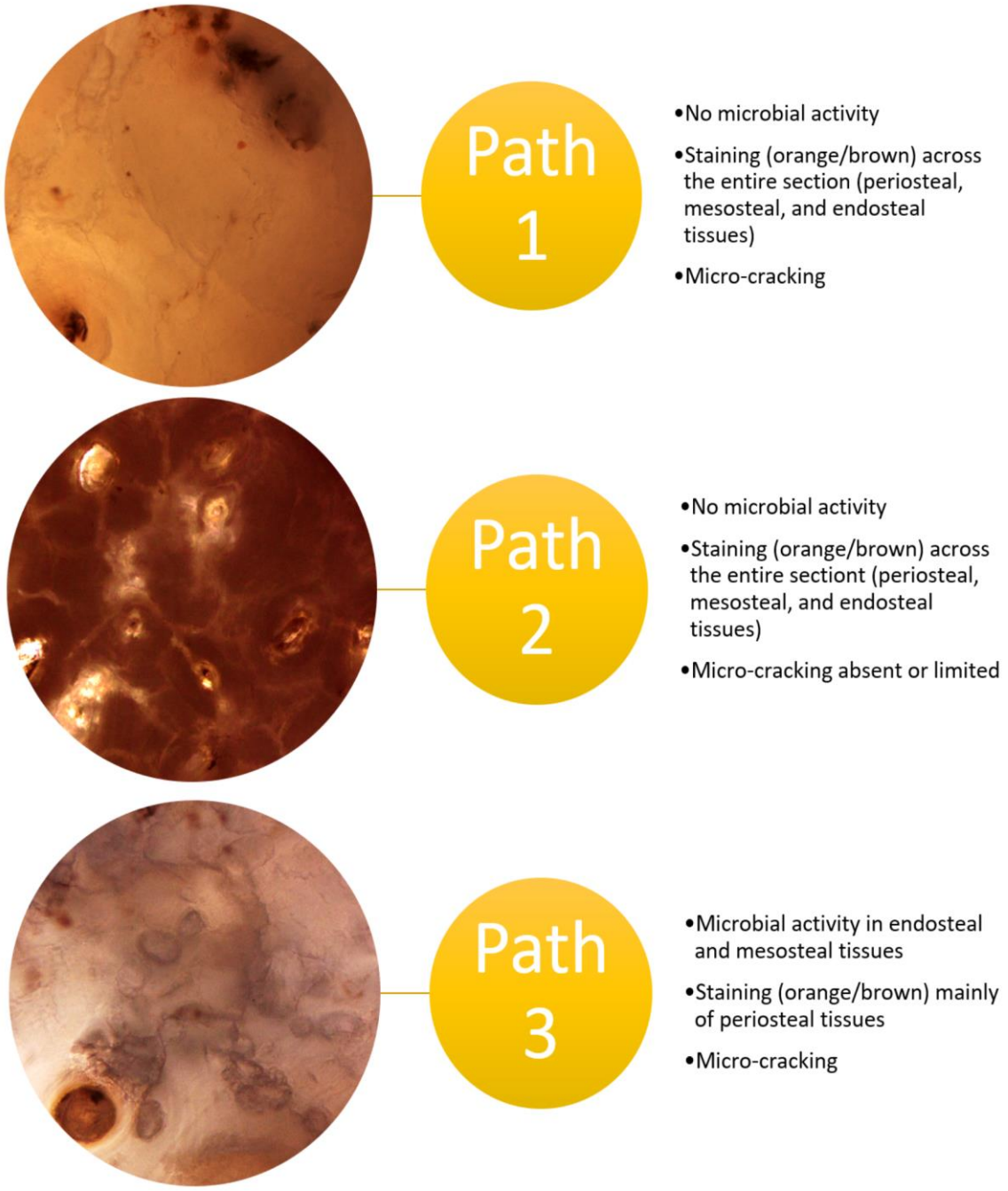

Figure 22. The three different diagenetic paths identified in Kastrouli (see also Table 9).

Histological preservation is very poor in Kastrouli (Table 9) with three distinct paths identified based on the presence/absence of microbial activity, micro-cracking and orange/brown staining (Figure 22). All human femora and animal bones appear microstructurally amorphous with sections often displaying disintegration, although some limited morphological features may still be recognizable (Figure 23a). Generalized destruction is accompanied by a loss of birefringence

in the amorphous areas under cross polarized light, linked to a loss of collagen (Caruso et al., 2018; Collins et al., 2002; Garland, 1989; Piepenbrink, 1986). The two human petrous bones also have many amorphous, disintegrated areas of bone (Figure 23b) accompanied by a loss of collagen birefringence, although the latter is still retained in many areas across the petrous thin sections. Their endosteal tissue that surrounds the cochlea and semicircular canal areas is considered more mineralized (Doden & Halves, 1984; Frisch et al., 2000; Jeffery & Spoor, 2004; Katić et al., 1991), however, it is unexpectedly more degraded than the periosteal tissue.

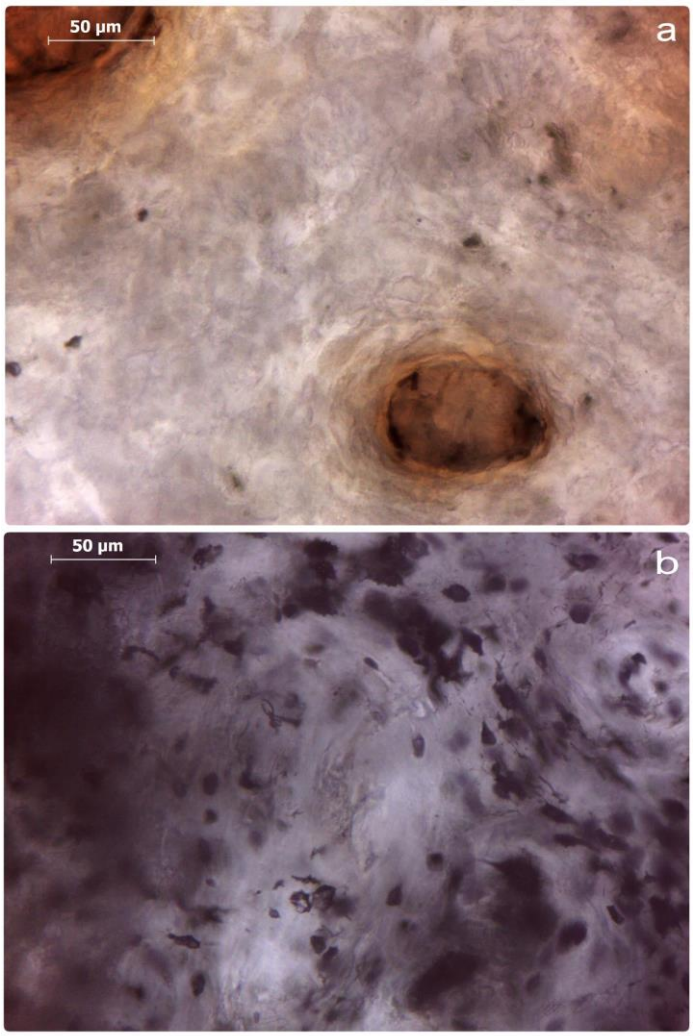

Figure 23. (a) **KAS2 Transverse PPL 400x - Human femur**: no histological features can be recognized, accompanied by a complete loss of birefringence (hence no image).
(b) **KAS16 Longitudinal PPL 400x - Human petrous bone**: osteocyte lacunae still preserved. Note the few merged lacunae which can be an indication of limited microbial activity.

Table 9. Summary of data (IRSF: Infrared splitting factor; C/P: carbonate-to-phosphate; BPI: carbonate type B-to-phosphate index; Am/P: amide-to-phosphate; GHI: general histological index). C/N collagen= % C/% N x atomic weight C/atomic weight N.
The symbols next to the GHI values indicate: * samples with transverse thin sections; ** samples with longitudinal thin sections.

[1]Collagen content estimates calculated using the equation *collagen wt. % = 113.13 Am/P + 1.69* presented in Lebon et al. (2016).

Sample	Skeletal Element	Species	IRSF	C/P	Am/P	BPI	Calcite	712 cm^{-1} Absorbance	GHI	Histological Pathway	Collagen wt. %	Collagen wt. % Estimates[1]	C/N
KAS1*	R. Femur (P)	Human	5.42 ±0.05	0.10 ±0.00	0.01 ±0.00	0.24 ±0.00	Present	0.00393	1	1	2.57	2.93	3.70
KAS2*	R. Femur (P)	Human	3.49 ±0.02	0.22 ±0.01	0.04 ±0.00	0.45 ±0.01	Absent	0.00	0	3	6.68	6.17	3.24
KAS3*	R. Femur (P)	Human	4.79 ±0.11	0.16 ±0.01	0.01 ±0.00	0.38 ±0.01	Present	0.00949	0	3	2.26	3.32	3.27
KAS4*	R. Femur (P)	Human	3.69 ±0.02	0.17 ±0.00	0.04 ±0.00	0.34 ±0.00	Absent	0.00	0	3	7.14	6.11	3.19
KAS5*	R. Femur (P)	Human	4.15 ±0.13	0.18 ±0.02	0.02 ±0.00	0.41 ±0.01	Present	0.00394	1	2	5.48	3.64	3.23
KAS6*	R. Femur (P)	Human	4.74 ±0.09	0.11 ±0.01	0.03 ±0.00	0.25 ±0.01	Absent	0.00	0	2	5.79	4.64	3.29
KAS7*	R. Femur (P)	Human	5.47 ±0.09	0.09 ±0.00	0.01 ±0.00	0.22 ±0.01	Present	0.00296	0	1	0.92	3.05	3.99
KAS8*	R. Femur (P)	Human	4.14 ±0.17	0.14 ±0.02	0.05 ±0.01	0.29 ±0.02	Absent	0.00	1	3	11.29	7.59	3.21
KAS9*	R. Femur (P)	Human	4.12 ±0.11	0.13 ±0.02	0.05 ±0.00	0.25 ±0.02	Absent	0.00	0	3	12.07	7.49	3.21
KAS10*	R. Femur (P)	Human	4.25 ±0.07	0.12 ±0.01	0.05 ±0.00	0.25 ±0.01	Absent	0.00	1	3	9.68	7.53	3.21
KAS11*	R. Femur (P)	Human	5.33 ±0.01	0.08 ±0.01	0.02 ±0.00	0.18 ±0.00	Absent	0.00	0	1	2.86	3.62	3.36
KAS12*	R. Femur (P)	Human	4.09 ±0.08	0.20 ±0.01	0.04 ±0.00	0.42 ±0.01	Present	0.00462	0	3	8.14	6.11	3.21
KAS13*	R. Femur (P)	Human	3.80 ±0.16	0.16 ±0.03	0.04 ±0.01	0.32 ±0.03	Absent	0.00	1	3	11.00	6.41	3.21
KAS14*	R. Femur (P)	Human	3.37 ±0.12	0.23 ±0.03	0.05 ±0.01	0.45 ±0.04	Absent	0.00	0	3	6.59	7.54	3.23
KAS15*	R. Femur (P)	Human	5.37 ±0.35	0.11 ±0.02	0.01 ±0.00	0.27 ±0.01	Present	0.00623	1	1	0.86	3.09	3.63
KAS16**	Petrous (L)	Human	4.12 ±0.12	0.15 ±0.01	0.04 ±0.00	0.28 ±0.02	Absent	0.00	3	Other	10.47	5.94	3.30
KAS17**	Petrous (R)	Human	4.07 ±0.08	0.16 ±0.01	0.03 ±0.00	0.34 ±0.01	Present	0.00129	3	Other	10.62	4.98	3.30
KAS18*	R. Carpometacarpus	Chicken	3.57 ±0.01	0.18 ±0.00	0.06 ±0.00	0.35 ±0.01	Present	0.00012	0	2	10.89	8.36	3.26
KAS19*	R. Carpometacarpus	Chicken	3.60 ±0.04	0.18 ±0.01	0.04 ±0.00	0.38 ±0.01	Absent	0.00	N/A	N/A	9.21	5.77	3.22
KAS22*	Phalanx	Cattle	3.52 ±0.06	0.25 ±0.01	0.03 ±0.00	0.54 ±0.01	Present	0.00192	0	2	5.28	5.30	3.27

Microbial activity (microscopic focal destruction; MFD) is present in 9 human femora, while the two human petrous bones and all animal bones show no signs of bacterial attack (Table 9). Possible microbial activity in the two human petrous bones appears as merged osteocyte lacunae, however, these are very sparse (Figure 23b). MFD in human femora appear as holes in the matrix of bone in transverse sections under plane polarized light and they are separated by hypermineralized tissue (or cuffing) (Figure 24a). Cuffing displays a dark coloration (brown/black) in plane polarized light (Figure 24a) and it appears denser than the unaffected areas (Bell, 1990; Hackett, 1981; Piepenbrink, 1989). It forms by mineral redeposition and waste products when microbes remove the inorganic matrix to attack collagen (Fernandez-Jalvo et al., 2010; Garland, 1989; Hackett, 1981; Hedges, 2002; Jackes et al., 2001). This explains why cuffing has higher concentrations of Ca and P compared to the unaltered and demineralized bone tissue (Pesquero et al., 2015). This hypermineralized tissue usually ranges from 3 to 6 μm in size, mostly surrounding the smaller non-Wedl MFD (Figure 24a) and it inhibits further expansion of the MFD (Hackett, 1981; Piepenbrink, 1986). The 'mosaic pattern' observed in several samples (Figure 24b) is also considered to be the final stage of bacterial attack, removing almost all microstructural features (Hackett, 1981; Piepenbrink, 1986; Turner-Walker & Jans, 2008).

Groundwater fluctuation in Kastrouli (see Moustris & Petrou, 2018 for weather data in region) due to hot and dry summers (desiccation, which causes the bone to shrink) followed by cold and humid winters (water uptake that swells bone collagen) is also likely to have contributed to the poor histological preservation (Hackett, 1981; Hedges & Millard, 1995; Nielsen-Marsh & Hedges, 2000b; Pfretzschner & Tütken, 2011; Turner-Walker, 2008; Turner-Walker & Jans,

2008). Desiccation is evidenced by micro-cracks observed centrally (Figure 24a; spread from the haversian canal outwards), peripherally (Figure 24a; spread from the cement line inwards), circumferentially and interstitially (Figure 24c; run across circumferential and interstitial lamellae) in several bones (Pfretzschner & Tütken, 2011). Additionally, the wet and dry (oxygen-rich environment) cycles in Kastrouli also favour the survival and activity of microorganisms in bone (Hackett, 1981; Reiche et al., 2003; Turner-Walker & Jans, 2008), while micro-cracking would further accelerate protein degradation and mineral transformation by increasing the flow of groundwater through the bone.

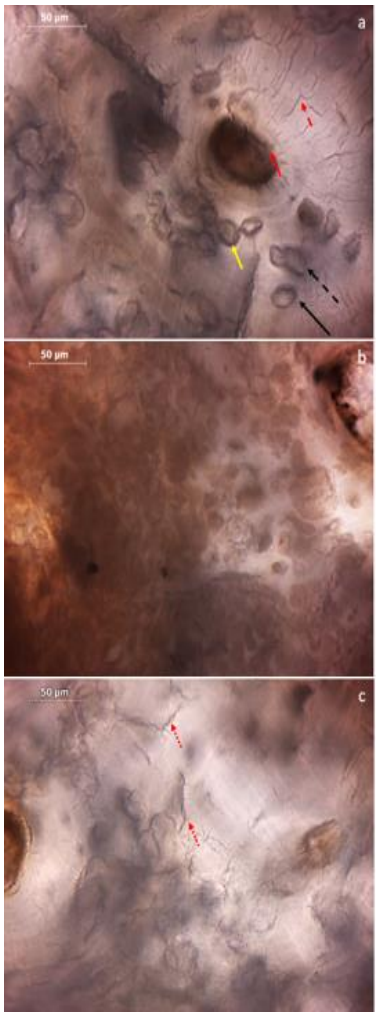

Figure 24. (a) **KAS9 Transverse PPL 400x - Human femur**: MFD in the form of linear-longitudinal (black arrow) and budded (dashed black arrow) tunnels surrounded by hypermineralized tissue (yellow arrow). Note the central (red arrow) and peripheral (dashed red arrows) micro-cracks.
(b) **KAS13 Transverse PPL 400x - Human femur**: The characteristic 'mosaic pattern' attributed to extensive bacterial activity.
(c) **KAS1 Transverse PPL 400x - Human femur**: Microcracking in degraded interstitial lamellae (dotted red arrows).

3.2. Bioapatite preservation

Bone mineral is a relatively unstable and disordered form of geologic hydroxyapatite (Asscher et al., 2011; LeGeros, 1965; LeGeros et al., 1967; Trueman, 2013). In the burial environment, local hydrology and soil pH are responsible for dissolution (loss of less stable components) and recrystallization (formation of more stable structure) of BAp crystals (Berna et al., 2004; Hedges, 2002; Hedges & Millard, 1995; High et al., 2015; Nielsen-Marsh et al., 2000; Nielsen-Marsh & Hedges, 2000a; Piepenbrink, 1989; Trueman, 2013). Ions present in the groundwater (e.g. HPO_4^{2-}, PO_4^{3-}, CO_3^{2-}, Ca^{2+}, Mg^{2+}) can be incorporated into the BAp hydrated layer, and subsequently, substitute other ions into the BAp core (Berna et al., 2004; Figueiredo et al., 2012; Lee-Thorp & van der Merwe, 1991; Rey & Combes, 2014; Stathopoulou et al., 2008; Trueman, 2013; Trueman et al., 2004). These alterations can be measured using the Infrared splitting factor (IRSF, also known as crystallinity) and the carbonate-to-phosphate (C/P) ratio (Brock et al., 2010; Hollund et al., 2013; Sponheimer & Lee-Thorp, 1999; Stathopoulou et al., 2008; Weiner & Bar-Yosef, 1990). The IRSF reflects BAp crystal size and structural order/disorder, with the larger and/or more ordered crystals displaying higher IRSF values (Surovell & Stiner, 2001; Termine & Posner, 1966; Weiner & Bar-Yosef, 1990; Weiner & Wagner, 1998; Wright & Schwarcz, 1996), while the C/P ratio reflects the carbonate content relative to phosphate content (Sponheimer & Lee-Thorp, 1999).

Dissolution/recrystallization of BAp crystals in Kastrouli is indicated by the histological appearance of many samples (e.g. microcracking, loss of birefringence). A recharge environment that is generated by wet and dry cycles (Hedges & Millard, 1995; Nielsen-Marsh et al., 2000) has clearly affected bioapatite preservation at this site. The seasonal or sporadic flow of unsaturated rainwater (Moustris & Petrou, 2018) through the bones situated near the ground surface (depth c. 1 m) has led to recrystallization of bioapatite crystals at increased rates (Grupe, 1995; Hedges & Millard, 1995; Nielsen-Marsh et al., 2000).

The IRSF values range from 3.37 to 5.47 (average=4.38±0.69) in human bones, and from 3.51 to 4.10 (average=3.69±0.23) in animal bones (Table 9). These crystallinity values are higher than modern bone IRSF (Figure 25a) and indicate an increase in average and/or maximum crystal length. This increase may be due to an increase of the size of the larger crystals at the expense of the smaller ones (i.e. Ostwald ripening), dissolution of the smaller crystals, or both (Nielsen-Marsh et al., 2000; Nielsen-Marsh & Hedges, 2000a; Reiche et al., 2002; Stiner et al., 1995; Trueman, 2013; Weiner & Bar-Yosef, 1990; Wright & Schwarcz, 1996).

Regarding carbonate content, C/P ranges from 0.23 to 0.08 (average=0.15±0.05) in humans, and from 0.25 to 0.15 (average=0.20±0.05) in animal bones (Table 9). A loss of CO_3^{2-} content during dissolution/recrystallization is thus observed in our samples compared to modern samples (Figure 25a). The human bones display an average loss of about 40 % of the initial carbonate and the

animal bones about the 20 % of their initial CO_3^{2-}, although there are differences in crystal size and atomic order between different animal species and hard tissues (Asscher et al., 2011).

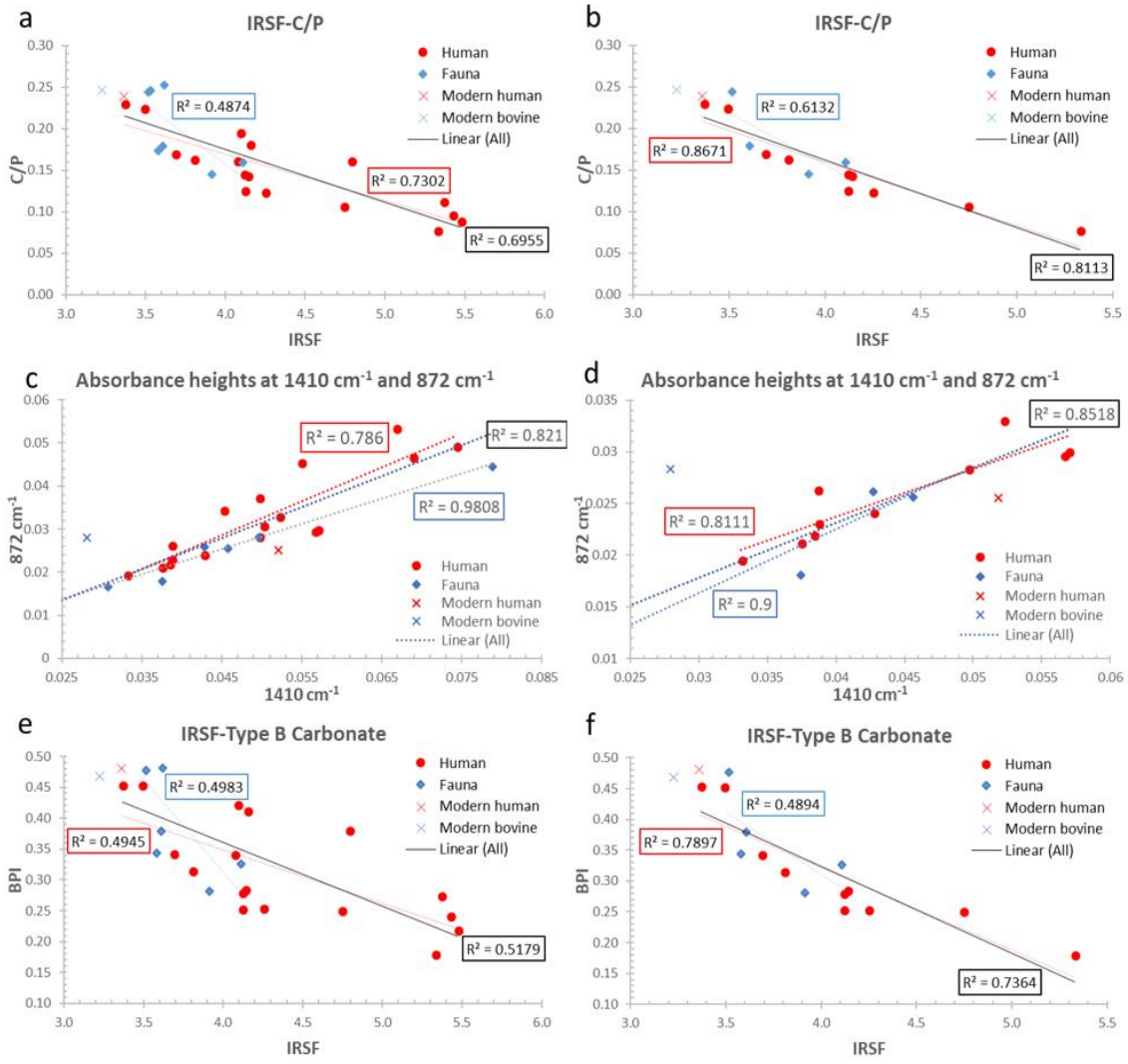

Figure 25. (a) The relationship between crystallinity (IRSF) and carbonate content (C/P) in BAp crystals (b) Same as (a), this time excluding samples containing calcite. (c) Correlation between 1410 cm^{-1} and 872 cm^{-1} showing that type B carbonate is the main CO_3^{2-} type reflected in C/P values. (d) Same as (c), this excluding samples containing calcite. (e) The relationship between crystallinity (IRSF) and type B CO_3^{2-}. (f) Same as (e), this time excluding samples containing calcite.

IRSF and C/P display very strong inverse relationship in humans (R^2=0.87) and strong in animals (R^2=0.61) which indicate that while recrystallization in bones results in loss of carbonate from the bioapatite crystals, this loss of CO_3^{2-} can vary intra-site and between species (Figure 25a-b). There are also statistically significant differences in crystallinity [x^2(2)=9.371, p=0.009] and C/P [x^2(2)=9.646, p=0.008] between the three different within-site diagenetic pathways. The *diagenetic path 1* (n=4) displays the poorest inorganic preservation with very high crystallinity values (IRSF=5.4±0.06) and very low carbonate content (C/P=0.09±0.01); the *diagenetic path 3* (n=9) shows intermediate values with lower crystallinity (IRSF=3.97±0.44) and slightly higher

CO_3^{2-} values (C/P=0.117±0.04), while the *diagenetic path 2* (n=8) demonstrates the best BAp preservation with IRSF=3.89±0.43 and C/P=0.19±0.05.

Carbonate ions (4-6 wt. %) can be exchanged with OH^- (type A) or PO_4^{3-} (type B) ions in the bioapatite crystal lattice (LeGeros, 1965; Wopenka & Pasteris, 2005). Type A substitutions require high temperatures (900-1000^o C) and the exclusion of water, while type B substitutions occur at much lower temperatures (25-100^o C) and are the dominant substitutions in bone (LeGeros, 1965). The very strong linear relationship (R^2=0.85; Figure 25c-d) between the c. 1410 cm^{-1} peak and the c. 872 cm^{-1} peak that is also assigned to type B carbonate (Elliott, 1964; LeGeros et al., 1969; Rey et al., 1989) shows that C/P (1410 cm^{-1}/1035 cm^{-1}) predominantly reflects the type B CO_3^{2-} environment (Sponheimer & Lee-Thorp, 1999). A substitution of CO_3^{2-} by PO_4^{3-} during recrystallization increases the unit cell dimensions of BAp crystals, as PO_4^{3-} O-O distances are longer than these in CO_3^{2-} (LeGeros et al., 1969), while it also results to more ordered crystal lattices (LeGeros, 1965; LeGeros et al., 1967; Rey et al., 2007; Wopenka & Pasteris, 2005). When crystallinity (IRSF) is plotted against type B CO_3^{2-} (BPI), however, it appears that the exchange of ions at the type B CO_3^{2-} site has less impact on BAp crystals of animal bones than in humans (Figure 25e-f), which implies differences in the diagenetic pathways followed by human and animal bones in Kastrouli.

Calcite ($CaCO_3$) is identified in 10 samples (see Table 9) primarily by the presence of a peak at 712 cm^{-1} (ν_4 carbon-oxygen in-plane bending) (Baxter et al., 1966; Hunt et al., 1950), while changes in the absorbance heights of the 872 cm^{-1} ν_2 carbon-oxygen out-of-plane bending and the 1410 cm^{-1} ν_3 carbon-oxygen asymmetric stretching (Baxter et al., 1966; Elliott, 1964; LeGeros et al., 1969; White, 1974) have also provided useful information. The strong linear relationship (R^2=0.71) between the ν_4 (712 cm^{-1}) and the ν_2 (872 cm^{-1}) vibration modes in our samples compared to the weak correlation (R^2=0.2) between the ν_3 (1410 cm^{-1}) and the ν_4 (712 cm^{-1}) suggests that the former modes are more sensitive indicators of calcite in archaeological bone. The 712 cm^{-1} is considered characteristic of the changes in the Ca-O distance during vibration which is three times larger for the ν_4 mode compared to the ν_2 mode (Gueta et al., 2007).

The carbonate moieties are coplanar, the O_1-O_2 distance affects the in-plane bending vibration (ν_4 mode) more than the out-of-plane bending vibration (ν_2 mode) (Gueta et al., 2007). This is important for the distinction between a rather amorphous bone calcium carbonate (lower order with greater Ca-O and O_1-O_2 distances) and exogenous calcite (higher order with smaller distances) (Gueta et al., 2007). The average IRSF=4.41±0.79 and C/P=0.17±0.06 for samples displaying calcite uptake compared to IRSF=4.01±0.53 and C/P=.016±0.05 in samples without calcite, and this difference in IRSF clearly demonstrates how the calcite uptake increases BAp crystal order.

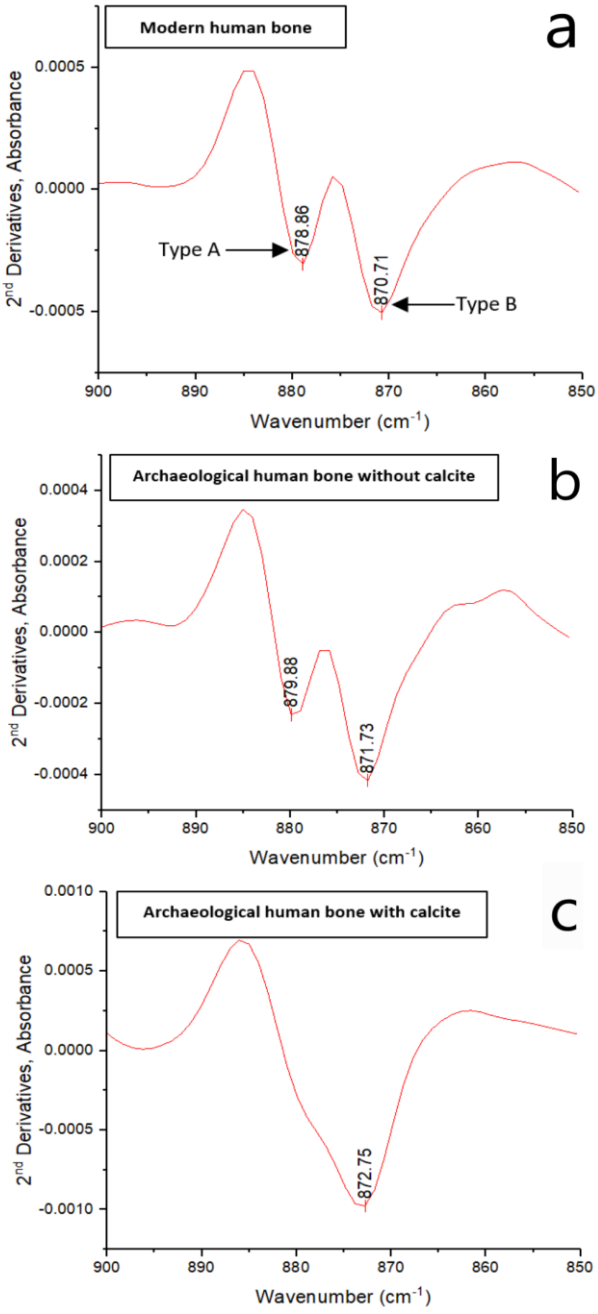

Figure 26. 2nd derivative spectra of the ν_2 carbonate band at c. 850-900 cm^{-1} of modern human bone (a), and archaeological bone with different calcite amounts (b and c). Note the effect on the 879 cm^{-1} component when there is an uptake of calcite (b vs c).

The ν_2 carbonate band at c. 850-900 cm^{-1} (which is considered free of organic constituents (Termine et al., 1973) and generally free of HPO_4^{2-} artifacts (Rey et al., 1989)) also offers useful information through 2nd derivative analysis (Figure 26). The two main carbonate bands in modern bone at c. 878 cm^{-1} and c. 871 cm^{-1}, which appear slightly shifted in archaeological bone, are frequently assigned to type A (stuffed) and type B (sloping faces) carbonates, respectively (Fleet, 2009; Fleet et al., 2004; Fleet & Liu, 2004; LeGeros, 1965; LeGeros et al., 1967; Rey et al., 1989). A gradual increase in the 872 cm^{-1} component is observed that is accompanied by a loss of the 879 cm^{-1} component with increasing calcite content (712 cm^{-1} absorbance height) in bones from

Kastrouli (Figure 26), likely due to small variations of the lattice dimensions of the substituents (Rey et al., 1989).

Therefore, the 2nd derivative analysis of the ν_2 CO_3^{2-} mode potentially indicates that an uptake of calcite may occur at the sloping faces of BAp crystals, replacing type B CO_3^{2-} during the interaction of bone with groundwater in the burial environment (Maurer et al., 2014; Wright & Schwarcz, 1996). This uptake may be either accompanied by a gradual loss of the type A carbonate (disappearance of the 878 cm^{-1} component) during severe dissolution of the crystal, and/or the exogenous carbonate vibration masks the c. 878 cm^{-1} component. As the CO_3^{2-} for OH^- substitution is achieved only with the exclusion of water, it is difficult for type A substitution to occur in bioapatite (LeGeros et al. 1969). Finally, a weak absorbance at c. 866 cm^{-1} that has been reported in modern bone and has been assigned to non-apatitic (labile) carbonate environment in amorphous calcium carbonate (Elliott, 1964; Rey et al., 1989) is not observed in Kastrouli bones and its absence from archaeological bone has been reported in other studies (Kontopoulos et al., 2018).

The spectra in the ν_3 carbon-oxygen asymmetric stretching mode (c. 1400-1500 cm^{-1}) are very complex (Figure 27a). The 2nd derivative analysis of this domain shows that the 1416 cm^{-1}, 1455 cm^{-1} and 1470 cm^{-1} site B CO_3^{2-} components (Brangule & Gross, 2015; Madupalli et al., 2017; Rey et al., 1989) decrease in archaeological bone compared to modern bone, a decrease which is higher in samples with calcite uptake (Figure 27). A decrease in the 1538 cm^{-1} component which is possibly related to type A carbonate (Madupalli et al., 2017; Rey et al., 1989) is also observed. On the other hand, the 1463 cm^{-1} that is often attributed to CO_3^{2-} site A (Madupalli et al., 2017; Rey et al., 1989) looks unchanged (Figure 27b-c). Nonetheless, a decrease of the 1538 cm^{-1}, the 1574 cm^{-1} and the 1556 cm^{-1} components (Figure 27b-c) may also be due to a loss of organic content (amide II) (Chadefaux et al., 2009; Paschalis et al., 2001). Furthermore, an increase in the 1505 cm^{-1} component (Figure 27c) in KAS12 (calcite uptake) which is indicative of ^{13}C enriched carbonate (Elliott, 1964) appears to be related to an uptake of environmental carbon from groundwater (Wright & Schwarcz, 1996). This observation has implications for isotopic studies that exploit the carbon content of bone structural carbonate (Lee-Thorp et al., 1989; Lee-Thorp & van der Merwe, 1991).

Therefore, it seems that there is a loss of some A site components both in the ν_3 and the ν_2 modes and a co-precipitation of exogenous carbonate and phosphate in B sites. An A-site carbonation in the apatitic c-axis channel would require much higher energy than B-site carbonation of phosphate sites (Madupalli et al., 2017); thus a loss of type A carbonate during BAp crystal dissolution is more probable. Additionally, exogenous carbonate may be positioned differently and these changes observed in the 2nd derivative components could be caused by the changes in carbonate orientation (Madupalli et al., 2017). It is also likely that the hypothesis of two carbonate

environments, each of which has its own characteristic absorption spectrum, might be an oversimplification (Elliott, 1964; Elliott et al., 1985).

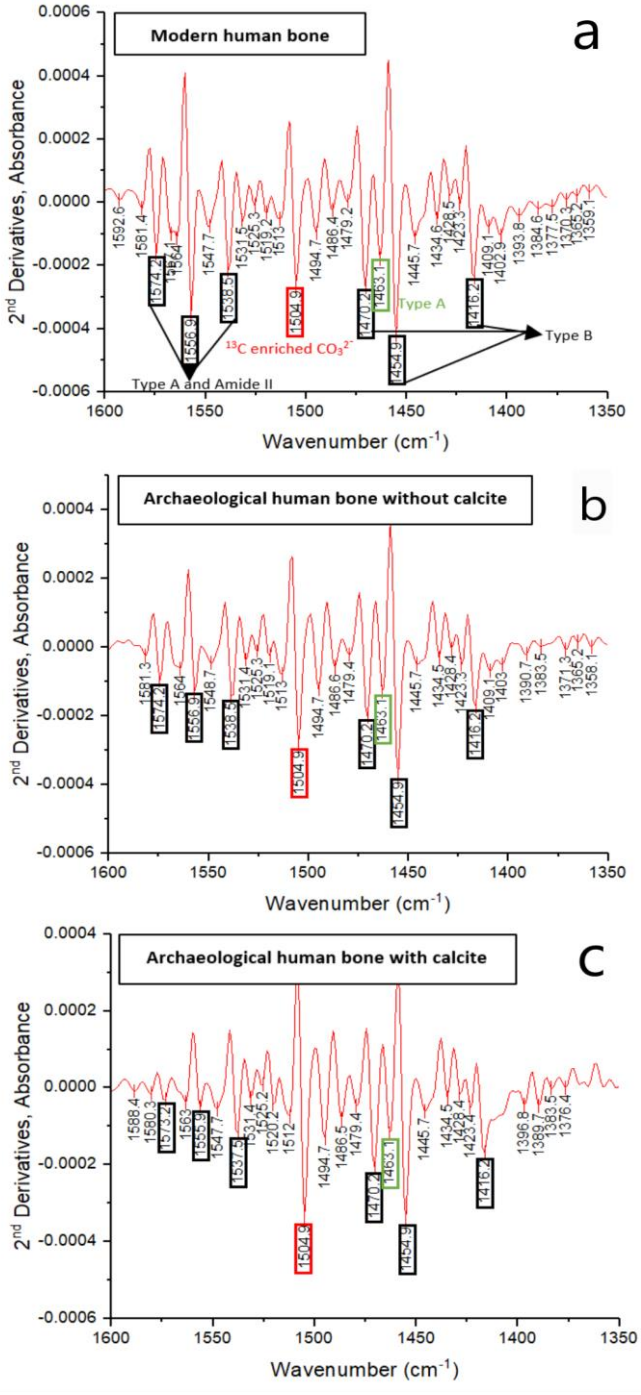

Figure 27. The complex 2nd derivative spectra of the ν_3 carbonate mode (c. 1400-1500 cm^{-1}) of modern human bone (a), and archaeological human bone with different calcite amounts (b and c). **Black boxes** highlight the components that decrease in archaeological bone; **green boxes** highlight the components that appear unchanged; **red boxes** highlight the component that appears slightly increased in c. Note that while c (calcite uptake) and b (no calcite) display similar crystallinity (IRSF), the former has much higher C/P ratio.

Consequently, it is difficult to make any safe assumptions on the location of exogenous CO_3^{2-} in the BAp crystal lattice due to the extensive overlapping and a variation in peak positions for the carbonate ion (Fleet & Liu, 2004). The many bands and shoulders displayed in these regions are

still not safely assigned to a specific CO_3^{2-} site (Elliott, 1964; LeGeros et al., 1969; Rey et al., 1989), and apart from carbonate, this domain also includes absorption from other bands (e.g. CH, CN, COO-, NH) that overlap with CO_3^{2-} (Elliott, 1964; Termine et al., 1973) and hinder further interpretation.

3.3. Collagen preservation

Collagen preservation displays within-site variations, ranging from 0.86 to 12.07 wt. % (average=6.73) in human specimens, and between 1.90 and 13.23 wt. % (average=8.35) in animal bones (Table 9). Collagen yields (wt. %) are commonly used to distinguish well-preserved from poorly-preserved collagen; here only KAS7 and KAS15 have collagen yields below the 1 wt. % that is currently considered the threshold for isotopic and/or radiocarbon dating studies (Brock et al., 2010, 2012; Dobberstein et al., 2009; van Klinken, 1999). The three different diagenetic paths also display statistically significant collagen yields [$x^2(2)=7.623$, $p=0.022$]. The *diagenetic path 1* displays very poor collagen preservation (collagen wt. %=1.8±1.06), the *diagenetic path 2* average collagen yields is 7.56±3.69, while *diagenetic path 3* displays slightly higher collagen yields (8.32±3.08).

Collagen C/N ratios used for quality assessment range from 3.19 to 3.99 (Table 9). Values similar to modern bone (i.e. 2.9 to 3.6) are considered representative of good quality collagen, while higher C/N ratios are related to diagenesis (Ambrose, 1990; DeNiro, 1985; DeNiro & Weiner, 1988; Tuross, 2002). Only three human specimens with *diagenetic path 1* characteristics (KAS1, KAS7, KAS15) exhibit C/N > 3.6 (Table 9), and these samples also show calcite uptake; thus collagen retained within these bones may not purely reflect original biochemical signals. Apart from the uptake of exogenous carbon, post-mortem alterations in the collagen carbon and nitrogen contents are affected by microbial attack and hydrolysis, both present in Kastrouli samples (Ambrose, 1990; Balzer et al., 1997; Harbeck & Grupe, 2009; Hedges et al., 1995; Turner-Walker, 2008; Tuross, 2002). Hydrophobic amino acids may have been hydrolyzed during wet periods in Kastrouli, whereas a microbial attack to the amino acids with a higher number of carbons may have also occurred in samples displaying MFD, altering the C/N ratio (Balzer et al., 1997; Grupe, 1995; Harbeck & Grupe, 2009; Masters, 1987; Turban-Just & Schramm, 1998; Tuross, 2002).

While bone may preserve its microstructure without preserving its collagen content due to hydrolysis (Collins et al., 2002; Hedges et al., 1995), in this secondary Mycenaean burial poor histological preservation is often accompanied by good collagen preservation (Table 9). This observation shows that many bones can still retain appreciable quantities of protein even after extensive histological alterations (Hedges et al., 1995) and highlights the limitations of GHI's use as collagen indicator.

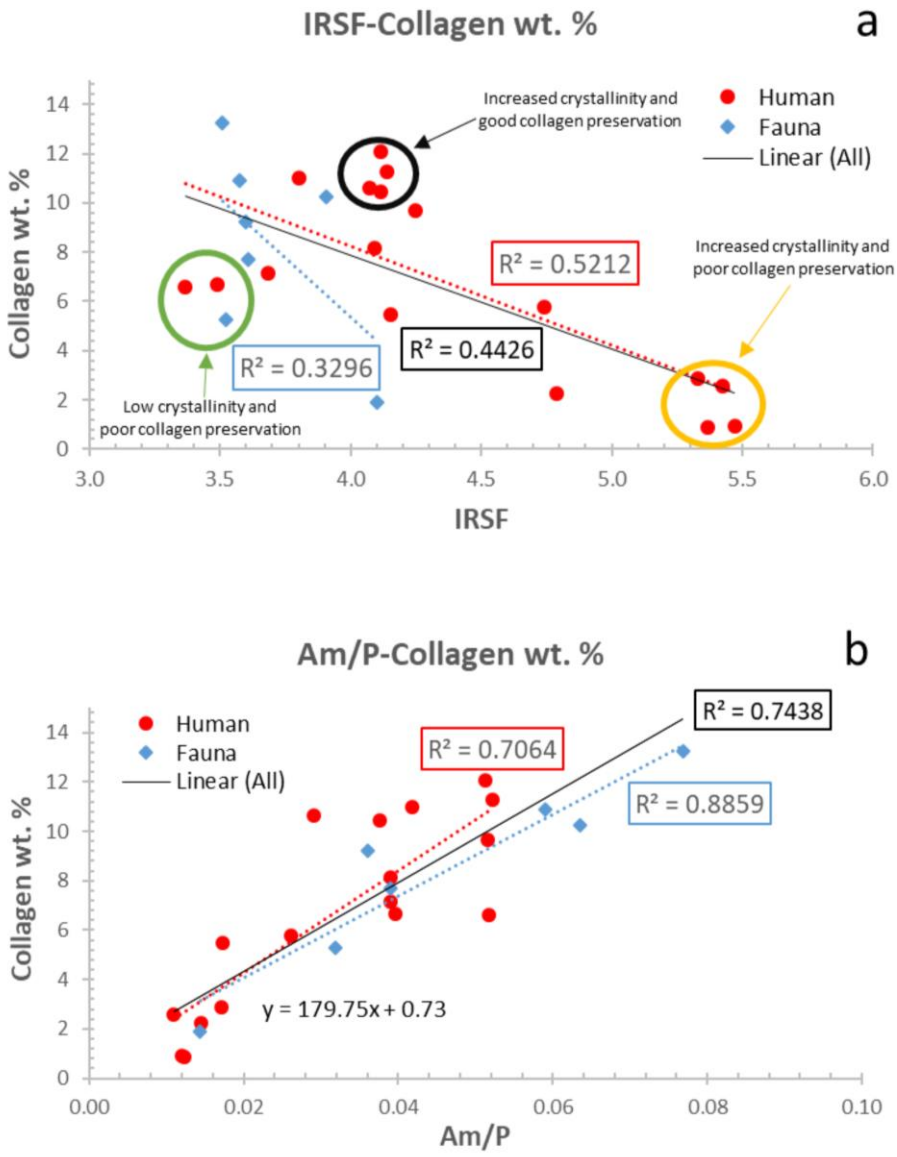

Figure 28. (a) The moderate relationship between IRSF-collagen wt. %. Note the group characterized by high IRSF and low collagen yields (yellow circle), a second group that displays low IRSF and low collagen yields (green circle) and a third group showing increased crystallinity and high collagen yields (black circle), indicative of the different combination of diagenetic pathways followed by these specimens. (b) The reliability of Am/P for predicting collagen content in archaeological bone.

The interaction between the mineral and organic fractions of bone is generally considered strong during diagenesis (Nielsen-Marsh et al., 2000; Person et al., 1995, 1996). This view is based on the fact that the orientation and size of BAp crystals *in vivo* are controlled by the fibril structure and organization as they are situated between (inter-fibrillar spaces) or on the surfaces (intra-fibrillar spaces) of collagen fibrils (Boskey, 2003; Weiner & Price, 1986; Weiner & Traub, 1986). However, in Kastrouli only a moderate correlation between crystallinity (IRSF) and collagen content (R^2= 0.44) is observed (Figure 28a), something that has also been reported in past studies (Hedges et al., 1995; Lebon et al., 2010; Weiner & Bar-Yosef, 1990). Thus, our data suggest that bioapatite recrystallization is possible even in the presence of reasonable amounts of collagen in

bone (Reiche et al., 2003), while within the same burial environment the volume of bone matrix that is filled with collagen *in vivo* can be replaced by BAp crystals of increased size (Pfretzschner, 2004; Susini et al., 1988; Trueman et al., 2008b).

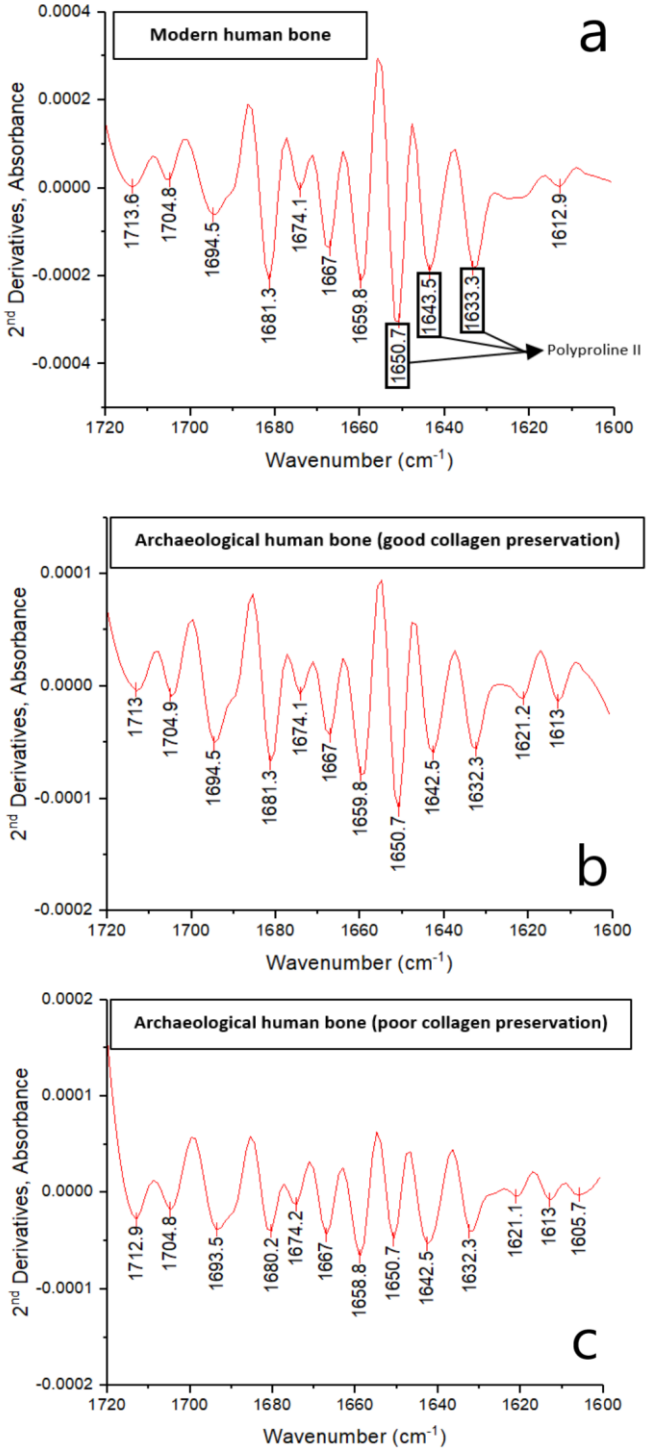

Figure 29. 2nd derivative spectra of the amide I band (c. 1600-1700 cm^{-1}) showing the disappearance of amide I components (black boxes) that accompany loss of collagen in archaeological bone (KAS8: c,d; KAS7: e,f).

The Am/P ratio shows a strong correlation (R^2=0.74) with collagen wt. % (Figure 28b) which highlights the potential of Am/P as collagen predictor for rapid screening. The application of the Am/P ratio as a quantitative approach to estimate collagen yields using the Lebon et al. (2016)

equation (i.e. collagen wt. % = 113.13 Am/P + 1.69), however, displays an average offset of -0.94±1.37% in Kastrouli. The relative phosphate content can lead to poor agreement of collagen estimates with collagen yields in some specimens (e.g. KAS8, KAS9), while overtones related to O-H stretching vibrations at 1640-1660 cm^{-1} (structural water) can also lead to increased values (Lebon et al., 2016; Trueman et al., 2008a). Further, any differences in collagen and FTIR protocols can also have significant effect on the collagen content estimates (e.g. Kontopoulos et al., 2018; Sealy et al., 2014).

Additional qualitative evidence can be obtained through the 2nd derivative analysis of the amide I band that shows a gradual decrease of the 1632, 1640, and 1650 cm^{-1} components assigned to the polyproline II helix (Lazarev et al., 1985) with decreasing collagen yields in archaeological bone (Figure 29). Cleavage of collagen cross-linking as seen from a decrease of the 1660 cm^{-1} and 1695 cm^{-1} components (Figure 29) (Paschalis et al., 2001) has led to a loss of the three-dimensional structure and breaking of the polypeptides into smaller peptides during hydrolysis (Adzhubei et al., 2013; Collins et al., 1995, 2002; Shoulders & Raines, 2009). High average temperatures (see Moustris & Petrou, 2018 for weather data in region) has also significantly affected the rate of collagen degradation in Kastrouli bones as the higher temperatures accelerate collagen loss with the thermal age in Kastrouli estimated to be approximately 3x the real age (Collins et al., 2002; Kendall et al., 2018).

4. Summary

Skeletal remains in this Mycenaean secondary burial have been seriously affected by diagenesis. Post-mortem modifications observed in microstructure, bioapatite and collagen are characteristic of burial environments with groundwater fluctuation and high average temperatures. Within-site differences may be related to different microenvironment conditions (e.g. groundwater, contact with limestone). However, as all bones were found within 30 cm of sediment, these bones have possibly experienced different early taphonomic histories. The death history and the effects of various factors (e.g. season of death, clothing, burial location) on bone degradation are often.overlooked in archaeology due to lack of relevant information. In secondary burials, the skeletal remains of a body (either exposed on the ground surface, interred in a coffin or buried directly into the soil) are retrieved and relocated once the soft tissue has decayed to some degree or excarnated. Therefore, future analyses may help understand the sequence of these alterations and shed light on past funerary practices such as disarticulation, primary and secondary treatment.

Key points

Histology

1. Three distinct pathways were identified based on the presence/absence of microbial activity, micro-cracking and orange/brown staining of bone tissue.

2. Generalized destruction was observed in all human femora and animal bones.
3. The two human petrous bones show better histological preservation than the femora, although the endosteal tissue that surrounds the cochlea and semicircular canal areas is unexpectedly more degraded than the other tissue zones.

Bioapatite

1. The seasonal and sporadic flow of unsaturated rainwater through the bones which were situated near the ground surface (depth c. 1 m) has led to the dissolution and recrystallization of bioapatite crystals (increased crystallinity, loss of carbonate, calcite uptake).
2. The two human petrous bones show poor bioapatite preservation with high crystallinity and loss of carbonate content.
3. 2nd derivative analysis of bone mid-IR spectra provides useful information on bioapatite carbonate environments (ν_2 carbonate band at c. 850-900 cm^{-1} and ν_3 carbonate mode at c. 1400-1500 cm^{-1}) and how they interact with calcite during recrystallization.

Collagen

1. Collagen yields do not show any strong correlation with crystallinity suggesting that bioapatite recrystallization is possible even in the presence of reasonable amounts of collagen in bone.
2. The two human petrous bones display good collagen preservation, with about half of the initial collagen content surviving.
3. The Am/P ratio can provide valuable information on the relative amount of collagen in bone, while GHI's use as collagen indicator is limited.
4. 2nd derivative analysis of the amide I band (c. 1600-1700 cm^{-1}) of bone mid-IR spectra can provide useful information on the components lost (e.g. polyproline II, cross-links) during collagen degradation.

Acknowledgements

Our warmest thanks go to Athanasios Sideris (fieldwork), Andreas Bertsatos and Marilena Chovalopoulou (osteological analysis and sampling). We are grateful to Prof. Peter Zioupos for the two modern human samples (NHS REC approval 10/H0107/14) which were used as references with the kind permission of the Department of Biology Ethics Committee (BEC) of the University of York. IK would like to thank Onassis Foundation (Grant no. F ZL 047-1/2015-2016), Leventis Foundation and the Greek Archaeological Committee UK (GACUK). KP thanks the Leverhulme Trust (PLP-2012-116) and MJC thanks the DNRF for the award of a Niels Bohr Professorship.

References

Adams B, Byrd J. 2014. *Commingled human remains: Methods in recovery, analysis and identification*. Elsevier Science & Technology: San Diego, United States.

Adzhubei AA, Sternberg MJE, Makarov AA. 2013. Polyproline-II helix in proteins: structure and function. *Journal of molecular biology* **425**: 2100–2132. DOI: 10.1016/j.jmb.2013.03.018

Ambrose SH. 1990. Preparation and characterization of bone and tooth collagen for isotopic analysis. *Journal of archaeological science* **17**: 431–451. DOI: 10.1016/0305-4403(90)90007-r

Ambrose SH. 1991. Effects of diet, climate and physiology on nitrogen isotope abundances in terrestrial foodwebs. *Journal of archaeological science* **18**: 293–317.

Asara JM, Schweitzer MH, Freimark LM, Phillips M, Cantley LC. 2007. Protein sequences from mastodon and Tyrannosaurus rex revealed by mass spectrometry. *Science* **316**: 280–285. DOI: 10.1126/science.1137614

Asscher Y, Regev L, Weiner S, Boaretto E. 2011. Atomic disorder in fossil tooth and bone mineral: An FTIR study using the grinding curve method. *ArchéoSciences* : 135–141. DOI: 10.4000/archeosciences.3062

Assis S, Santos A, Keenleyside A. 2016. Paleohistology and the study of human remains: past, present and future approaches. *Revista Argentina de antropología biológica* **18** DOI: 10.17139/raab.2016.0018.02.02

Balzer A, Gleixner G, Grupe G, Schmidt HL, Schramm S, Turban-Just S. 1997. In vitro decomposition of bone collagen by soil bacteria: The implications for stable isotope analysis in archaeometry. *Archaeometry* **39**: 415–429.

Baxter JD, Biltz RM, Pellegrino ED. 1966. The physical state of bone carbonate. A comparative infra-red study in several mineralized tissues. *The Yale journal of biology and medicine* **38**: 456–470.

Bell L. 2012. Histotaphonomy. In *Bone Histology*. CRC Press; 241–251. DOI: 10.1201/b11393-10

Bell LS. 1990. Palaeopathology and diagenesis: an SEM evaluation of structural changes using backscattered electron imaging. *Journal of archaeological science* **17**: 85–102. DOI: 10.1016/0305-4403(90)90016-X

Berna F, Matthews A, Weiner S. 2004. Solubilities of bone mineral from archaeological sites: the recrystalization window. *Journal of archaeological science* **31**: 867–882.

Booth TJ, Madgwick R. 2016. New evidence for diverse secondary burial practices in Iron Age Britain: A histological case study. *Journal of archaeological science* **67**: 14–24. DOI: 10.1016/j.jas.2016.01.010

Boskey AL. 2003. Bone mineral crystal size. *Osteoporosis international: a journal established as result of cooperation between the European Foundation for Osteoporosis and the National Osteoporosis Foundation of the USA* **14 Suppl 5**: S16–20; discussion S20–1. DOI: 10.1007/s00198-003-1468-2

Brangule A, Gross KA. 2015. Importance of FTIR spectra deconvolution for the analysis of amorphous calcium phosphates. *IOP Conference Series: Materials Science and Engineering* **77**: 012027. DOI: 10.1088/1757-899X/77/1/012027

Brock F, Higham T, Ramsey CB. 2010. Pre-screening techniques for identification of samples suitable for radiocarbon dating of poorly preserved bones. *Journal of archaeological science* **37**: 855–865. DOI: 10.1016/j.jas.2009.11.015

Brock F, Wood R, Higham TFG, Ditchfield P, Bayliss A, Ramsey CB. 2012. Reliability of nitrogen content (%N) and carbon:nitrogen atomic ratios (C:N) as indicators of collagen preservation suitable for radiocarbon dating. *Radiocarbon* **54**: 879–886. DOI: 10.1017/S0033822200047524

Buckley M, Collins M, Thomas-Oates J. 2009. Species identification by analysis of bone collagen using matrix-assisted laser desorption/ionisation time-of-flight mass spectrometry. *in mass spectrometry*

Caruso V, Cummaudo M, Maderna E, Cappella A, Caudullo G, Scarpulla V, Cattaneo C. 2018. A comparative analysis of microscopic alterations in modern and ancient undecalcified and decalcified dry bones. *American journal of physical anthropology* **165**: 363–369. DOI: 10.1002/ajpa.23348

Cattaneo C, DiMartino S, Scali S, Craig OE, Grandi M, Sokol RJ. 1999. Determining the human origin of fragments of burnt bone: a comparative study of histological, immunological and DNA techniques. *Forensic science international* **102**: 181–191.

Chadefaux C, Le Hô A-S, Bellot-Gurlet L, Reiche I. 2009. Curve-fitting micro-ATR-FTIR studies of the Amide I and II bands of type I collagen in archaeological bone materials. *e-PS* **6**: 129–137.

Chovalopoulou M-E, Bertsatos A, Manolis SK. 2017. Identification of skeletal remains from a Mycenaean burial in Kastrouli-Desfina, Greece. *Mediterranean Archaeology and Archaeometry* **17**: 265–269. DOI: 10.5281/zenodo.556353

Collins MJ, Nielsen–Marsh CM, Hiller J, Smith CI, Roberts JP, Prigodich RV, Wess TJ, Csapò J, Millard AR, Turner–Walker G. 2002. The survival of organic matter in bone: a review. *Archaeometry* **44**: 383–394. DOI: 10.1111/1475-4754.t01-1-00071

Collins MJ, Penkman KEH, Rohland N, Shapiro B, Dobberstein RC, Ritz-Timme S, Hofreiter M. 2009. Is amino acid racemization a useful tool for screening for ancient DNA in bone? *Proceedings. Biological sciences / The Royal Society* **276**: 2971–2977. DOI: 10.1098/rspb.2009.0563

Collins MJ, Riley MS, Child AM, Turner-Walker G. 1995. A basic mathematical simulation of the chemical degradation of ancient collagen. *Journal of archaeological science* **22**: 175–183. DOI: 10.1006/jasc.1995.0019

Collins MJ, Waite ER, van Duin ACT, Eglinton G. 1999. Predicting protein decomposition: The case of aspartic-acid racemization kinetics. *Philosophical transactions of the Royal Society of London. Series B, Biological sciences* **354**: 51–64.

Cuijpers AGFM. 2006. Histological identification of bone fragments in archaeology: telling humans apart from horses and cattle. *International Journal of Osteoarchaeology* **16**: 465–480. DOI: 10.1002/oa.848

De Boer HH, Van der Merwe AE, Maat GJR. 2013. The diagnostic value of microscopy in dry bone palaeopathology: A review. *International Journal of Paleopathology* **3**: 113–121. DOI: 10.1016/j.ijpp.2013.03.004

DeNiro MJ. 1985. Postmortem preservation and alteration of in vivo bone collagen isotope ratios in relation to palaeodietary reconstruction. *Nature* **317**: 806–809. DOI: 10.1038/317806a0T

DeNiro MJ, Weiner S. 1988. Chemical, enzymatic and spectroscopic characterization of "collagen" and other organic fractions from prehistoric bones. *Geochimica et cosmochimica acta* **52**: 2197–2206. DOI: 10.1016/0016-7037(88)90122-6

Dobberstein RC, Collins M, Craig O, Taylor GM, Penkman KEH, Ritz-Timme S. 2009. Archaeological collagen: Why worry about collagen diagenesis. *Archaeological and anthropological sciences* **1**: 31–42.

Doden E, Halves R. 1984. On the functional morphology of the human petrous bone. *The American journal of anatomy* **169**: 451–462. DOI: 10.1002/aja.1001690407

Dominguez VM, Crowder CM. 2012. The utility of osteon shape and circularity for differentiating human and non-human Haversian bone. *American journal of physical anthropology* **149**: 84–91. DOI: 10.1002/ajpa.22097

Douka K, Slon V, Stringer C, Potts R, Hübner A, Meyer M, Spoor F, Pääbo S, Higham T. 2017. Direct radiocarbon dating and DNA analysis of the Darra-i-Kur (Afghanistan) human temporal bone. *Journal of human evolution* **107**: 86–93. DOI: 10.1016/j.jhevol.2017.03.003

Elliott JC. 1964. *The crystallographic structure of dental enamel and related apatites*, Doctor of Philosophy, University of London, Faculty of Science

Elliott JC, Holcomb DW, Young RA. 1985. Infrared determination of the degree of substitution of hydroxyl by carbonate ions in human dental enamel. *Calcified tissue international* **37**: 372–375.

Fernandez-Jalvo Y, Andrews P, Pesquero D, Smith CI, Marin-Monfort D, Sanchez B, Geigl EM, Alonso A. 2010. Early bone diagenesis in temperate environments Part I: Surface features and histology. *Palaeogeography, palaeoclimatology, palaeoecology* **288**: 62–81.

Figueiredo MM, Gamelas JAF, Martins AG. 2012. Characterization of bone and bone-based graft materials using FTIR spectroscopy. In *Infrared spectroscopy - Life and biomedical sciences*. DOI: 10.5772/36379

Fleet ME. 2009. Infrared spectra of carbonate apatites: v2-Region bands. *Biomaterials* **30**: 1473–1481. DOI: 10.1016/j.biomaterials.2008.12.007

Fleet ME, Liu X. 2004. Location of type B carbonate ion in type A–B carbonate apatite synthesized at high pressure. *Journal of solid state chemistry* **177**: 3174–3182. DOI: 10.1016/j.jssc.2004.04.002

Fleet ME, Liu X, King PL. 2004. Accommodation of the carbonate ion in apatite: An FTIR and X-ray structure study of crystals synthesized at 2–4 GPa. *The American mineralogist* **89**: 1422–1432. DOI: 10.2138/am-2004-1009

Frisch T, Sørensen MS, Overgaard S, Bretlau P. 2000. Estimation of volume referent bone turnover in the otic capsule after sequential point labeling. *The Annals of otology, rhinology, and laryngology* **109**: 33–39. DOI: 10.1177/000348940010900106

Garland AN. 1989. Microscopical analysis of fossil bone. *Applied geochemistry: journal of the International Association of Geochemistry and Cosmochemistry* **4**: 215–229. DOI: 10.1016/0883-2927(89)90021-8

Grupe G. 1995. Preservation of collagen in bone from dry, sandy soil. *Journal of archaeological science* **22**: 193–199.

Gueta R, Natan A, Addadi L, Weiner S, Refson K, Kronik L. 2007. Local atomic order and infrared spectra of biogenic calcite. *Angewandte Chemie* **46**: 291–294. DOI: 10.1002/anie.200603327

Hackett CJ. 1981. Microscopical focal destruction (tunnels) in exhumed human bones. *Medicine, science, and the law* **21**: 243–265. DOI: 10.1177/002580248102100403

Hanson M, Cain CR. 2007. Examining histology to identify burned bone. *Journal of archaeological science* **34**: 1902–1913. DOI: 10.1016/j.jas.2007.01.009

Harbeck M, Grupe G. 2009. Experimental chemical degradation compared to natural diagenetic alteration of collagen: implications for collagen quality indicators for stable isotope analysis. *Archaeological and anthropological sciences* **1**: 43–57. DOI: 10.1007/s12520-009-0004-5

Hedges REM. 2002. Bone diagenesis: an overview of processes. *Archaeometry* **44**: 319–328. DOI: 10.1111/1475-4754.00064

Hedges REM. 2003. On bone collagen—apatite-carbonate isotopic relationships. *International Journal of Osteoarchaeology* **13**: 66–79. DOI: 10.1002/oa.660

Hedges REM, Millard AR. 1995. Bones and groundwater: Towards the modelling of diagenetic processes. *Journal of archaeological science* **22**: 155–164. DOI: 10.1006/jasc.1995.0017

Hedges REM, Millard AR, Pike AWG. 1995. Measurements and relationships of diagenetic alteration of bone from three archaeological sites. *Journal of archaeological science* **22**: 201–209. DOI: 10.1006/jasc.1995.0022

High K, Milner N, Panter I, Penkman KEH. 2015. Apatite for destruction: investigating bone degradation due to high acidity at Star Carr. *Journal of archaeological science* **59**: 159–168.

DOI: 10.1016/j.jas.2015.04.001

Hollund HI, Ariese F, Fernandes R, Jans MME, Kars H. 2013. Testing an alternative high-throughput tool for investigating bone diagenesis: FTIR in Attenuated Total Reflection (ATR) mode. *Archaeometry* **55**: 507–532. DOI: 10.1111/j.1475-4754.2012.00695.x

Hollund HI, Jans MME, Collins MJ, Kars H, Joosten I, Kars SM. 2012. What happened here? Bone histology as a tool in decoding the postmortem histories of archaeological bone from Castricum, The Netherlands. *International Journal of Osteoarchaeology* **22**: 537–548. DOI: 10.1002/oa.1273

Hunt JM, Wisherd MP, Bonham LC. 1950. Infrared absorption spectra of minerals and other inorganic compounds. *Analytical chemistry* **22**: 1478–1497. DOI: 10.1021/ac60048a006

Jackes M, Sherburne R, Lubell D, Barker C, Wayman M. 2001. Destruction of microstructure in archaeological bone: a case study from Portugal. *International Journal of Osteoarchaeology* **11**: 415–432.

Jeffery N, Spoor F. 2004. Prenatal growth and development of the modern human labyrinth. *Journal of anatomy* **204**: 71–92. DOI: 10.1111/j.1469-7580.2004.00250.x

Katić V, Vujicić G, Ivanković D, Stavljenić A, Vukicević S. 1991. Distribution of structural and trace elements in human temporal bone. *Biological trace element research* **29**: 35–43.

Kendall C, Eriksen AMH, Kontopoulos I, Collins MJ, Turner-Walker G. 2018. Diagenesis of archaeological bone and tooth. *Palaeogeography, palaeoclimatology, palaeoecology* **491**: 21–37. DOI: 10.1016/j.palaeo.2017.11.041

King CL, Tayles N, Gordon KC. 2011. Re-examining the chemical evaluation of diagenesis in human bone apatite. *Journal of archaeological science* **38**: 2222–2230. DOI: 10.1016/j.jas.2011.03.023

van Klinken GJ. 1999. Bone collagen quality indicators for palaeodietary and radiocarbon measurements. *Journal of archaeological science* **26**: 687–695. DOI: 10.1006/jasc.1998.0385

Kontopoulos I, Nystrom P, White L. 2016. Experimental taphonomy: post-mortem microstructural modifications in Sus scrofa domesticus bone. *Forensic science international* **266**: 320–328. DOI: 10.1016/j.forsciint.2016.06.024

Kontopoulos I, Presslee S, Penkman K, Collins MJ. 2018. Preparation of bone powder for FTIR-ATR analysis: The particle size effect. *Vibrational Spectroscopy* DOI: 10.1016/j.vibspec.2018.09.004

Lazarev YA, Grishkovsky BA, Khromova TB. 1985. Amide I band of IR spectrum and structure of collagen and related polypeptides. *Biopolymers* **24**: 1449–1478. DOI: 10.1002/bip.360240804

Lebon M, Reiche I, Bahain J-J, Chadefaux C, Moigne A-M, Fröhlich F, Sémah F, Schwarcz HP, Falguères C. 2010. New parameters for the characterization of diagenetic alterations and heat-induced changes of fossil bone mineral using Fourier transform infrared spectrometry. *Journal of archaeological science* **37**: 2265–2276. DOI: 10.1016/j.jas.2010.03.024

Lebon M, Reiche I, Gallet X, Bellot-Gurlet L, Zazzo A. 2016. Rapid quantification of bone collagen content by ATR-FTIR spectroscopy. *Radiocarbon* **58**: 131–145. DOI: 10.1017/RDC.2015.11

Lee-Thorp JA, van der Merwe NJ. 1991. Aspects of the chemistry of modern and fossil biological apatites. *Journal of archaeological science* **18**: 343–354. DOI: 10.1016/0305-4403(91)90070-6

Lee-Thorp J, Sealy JC, van der Merwe NJ. 1989. Stable carbon isotope ratio differences between bone collagen and bone apatite and their relationship to diet. *Journal of archaeological science* **16**: 585–599.

LeGeros RZ. 1965. Effect of carbonate on the lattice parameters of apatite. *Nature* **206**: 403.

DOI: 10.1038/206403a0

LeGeros RZ, Trautz OR, Klein E, LeGeros JP. 1969. Two types of carbonate substitution in the apatite structure. *Experientia* **25**: 5–7. DOI: 10.1007/BF01903856

LeGeros RZ, Trautz OR, LeGeros JP, Klein E, Shirra WP. 1967. Apatite crystallites: effects of carbonate on morphology. *Science* **155**: 1409–1411. DOI: 10.1126/science.155.3768.1409

Longin R. 1971. New method of collagen extraction for radiocarbon dating. *Nature* **230**: 241–242.

Madupalli H, Pavan B, Tecklenburg MMJ. 2017. Carbonate substitution in the mineral component of bone: Discriminating the structural changes, simultaneously imposed by carbonate in A and B sites of apatite. *Journal of solid state chemistry* **255**: 27–35. DOI: 10.1016/j.jssc.2017.07.025

Masters PM. 1987. Preferential preservation of noncollagenous protein during bone diagenesis: Implications for chronometric and stable isotopic measurements. *Geochimica et cosmochimica acta* **51**: 3209–3214. DOI: 10.1016/0016-7037(87)90129-3

Maurer A-F, Person A, Tütken T, Amblard-Pison S, Ségalen L. 2014. Bone diagenesis in arid environments: An intra-skeletal approach. *Palaeogeography, palaeoclimatology, palaeoecology* **416**: 17–29. DOI: 10.1016/j.palaeo.2014.08.020

Millard AR. 2001. Deterioration of bone. In *Handbook of Archaeological Sciences*, Brothwell, D R & Pollard, A M (ed). Wiley; 633–643.

Moustris A, Petrou J. 2018. Weather forecast for Greece. *meteo.gr - Weather forecast for Greece* [online] Available from: http://www.meteo.gr/index-en.cfm (Accessed 16 October 2018)

Mulhern DM, Ubelaker DH. 2001. Differences in osteon banding between human and nonhuman bone. *Journal of forensic sciences* **46**: 220–222.

Nielsen-Marsh C, Gernaey A, Turner-Walker G, Hedges R, Pike AWG, Collins M. 2000. The chemical degradation of bone. In *Human Osteology: In Archaeology and Forensic Science*, Cox M and Mays S (eds). Cambridge University Press; 439–454.

Nielsen-Marsh CM, Hedges REM. 2000a. Patterns of diagenesis in bone II: effects of acetic acid treatment and the removal of diagenetic CO23. *Journal of archaeological science* **27**: 1151–1159.

Nielsen-Marsh CM, Hedges REM. 2000b. Patterns of diagenesis in bone I: The effects of site environments. *Journal of archaeological science* **27**: 1139–1150. DOI: 10.1006/jasc.1999.0537

Osterholtz AJ, Baustian KM, Martin DL. 2013. *Commingled and disarticulated human remains: Working toward improved theory, method, and data*. Springer: New York, NY, UNITED STATES.

Paschalis EP, Verdelis K, Doty SB, Boskey AL, Mendelsohn R, Yamauchi M. 2001. Spectroscopic characterization of collagen cross-links in bone. *Journal of bone and mineral research: the official journal of the American Society for Bone and Mineral Research* **16**: 1821–1828. DOI: 10.1359/jbmr.2001.16.10.1821

Person A, Bocherens H, Mariotti A, Renard M. 1996. Diagenetic evolution and experimental heating of bone phosphate. *Palaeogeography, Palaeoclimatology, Palaeoeeology* **126**: 135–149.

Person A, Bocherens H, Saliege J-F, Paris F, Zeitoun V, Gerard M. 1995. Early diagenetic evolution of bone phosphate: An X-ray diffractometry analysis. *Journal of archaeological science* **22**: 211–221.

Pesquero MD, Alcalá L, Bell LS, Fernández-Jalvo Y. 2015. Bacterial origin of iron-rich microspheres in Miocene mammalian fossils. *Palaeogeography, palaeoclimatology, palaeoecology* **420**: 27–34. DOI: 10.1016/j.palaeo.2014.12.006

Pfretzschner H-U. 2004. Fossilization of Haversian bone in aquatic environments. *Comptes rendus. Palevol* **3**: 605–616. DOI: 10.1016/j.crpv.2004.07.006

Pfretzschner H-U, Tütken T. 2011. Rolling bones – Taphonomy of Jurassic dinosaur bones inferred from diagenetic microcracks and mineral infillings. *Palaeogeography, palaeoclimatology, palaeoecology* **310**: 117–123. DOI: 10.1016/j.palaeo.2011.01.026

Piepenbrink H. 1986. Two examples of biogenous dead bone decomposition and their consequences for taphonomic interpretation. *Journal of archaeological science* **13**: 417–430. DOI: 10.1016/0305-4403(86)90012-9

Piepenbrink H. 1989. Examples of chemical changes during fossilisation. *Applied geochemistry: journal of the International Association of Geochemistry and Cosmochemistry* **4**: 273–280. DOI: 10.1016/0883-2927(89)90029-2

Poinar HN, Höss M, Bada JL, Pääbo S. 1996. Amino acid racemization and the preservation of ancient DNA. *Science* **272**: 864–866.

Reiche I, Favre-Quattropani L, Vignaud C, Bocherens H, Charlet L, Menu M. 2003. A multi-analytical study of bone diagenesis: the Neolithic site of Bercy (Paris, France). *Measurement Science and Technology* **14**: 1608.

Reiche I, Vignaud C, Menu M. 2002. The crystallinity of ancient bone and dentine: new insights by transmission electron microscopy. *Archaeometry* **44**: 447–459. DOI: 10.1111/1475-4754.00077

Rey C, Collins B, Goehl T, Dickson IR, Glimcher MJ. 1989. The carbonate environment in bone mineral: a resolution-enhanced Fourier Transform Infrared Spectroscopy Study. *Calcified tissue international* **45**: 157–164.

Rey C, Combes C. 2014. What bridges mineral platelets of bone? *BoneKEy reports* **3**: 586. DOI: 10.1038/bonekey.2014.81

Rey C, Combes C, Drouet C, Sfihi H, Barroug A. 2007. Physico-chemical properties of nanocrystalline apatites: Implications for biominerals and biomaterials. *Materials Science and Engineering: C* **27**: 198–205. DOI: 10.1016/j.msec.2006.05.015

Sealy J, Johnson M, Richards M, Nehlich O. 2014. Comparison of two methods of extracting bone collagen for stable carbon and nitrogen isotope analysis: comparing whole bone demineralization with gelatinization and ultrafiltration. *Journal of archaeological science* **47**: 64–69. DOI: 10.1016/j.jas.2014.04.011

Shoulders MD, Raines RT. 2009. Collagen structure and stability. *Annual review of biochemistry* **78**: 929–958. DOI: 10.1146/annurev.biochem.77.032207.120833

Sideris A, Liritzis I, Liss B, Howland MD, Levy TE. 2017. At-risk cultural heritage: new excavations and finds from the Mycenaean site of Kastrouli, Phokis, Greece. *Mediterranean Archaeology and Archaeometry* **17**: 271–285. DOI: 10.5281/zenodo.163772

Sponheimer M, Lee-Thorp JA. 1999. Alteration of enamel carbonate environments during fossilization. *Journal of archaeological science* **26**: 143–150. DOI: 10.1006/jasc.1998.0293

Stathopoulou ET, Psycharis V, Chryssikos GD, Gionis V, Theodorou G. 2008. Bone diagenesis: New data from infrared spectroscopy and X-ray diffraction. *Palaeogeography, palaeoclimatology, palaeoecology* **266**: 168–174. DOI: 10.1016/j.palaeo.2008.03.022

Stiner MC, Kuhn SL, Weiner S, Bar-Yosef O. 1995. Differential burning, recrystallization, and fragmentation of archaeological bone. *Journal of archaeological science* **22**: 223–237.

Stout SD, Teitelbaum SL. 1976. Histological analysis of undecalcified thin sections of archeological bone. *American journal of physical anthropology* **44**: 263–269. DOI: 10.1002/ajpa.1330440208

Surovell TA, Stiner MC. 2001. Standardizing Infra-red measures of bone mineral crystallinity: an experimental approach. *Journal of archaeological science* **28**: 633–642. DOI:

10.1006/jasc.2000.0633

Susini A, Baud CA, Lacotte D. 1988. Bone apatite crystals alterations in Neolithic skeletons and their relations to burial practices and soil weathering. *Rivista di antropologia* **66**: 35–38.

Termine JD, Eanes ED, Greenfield DJ, Nylen MU, Harper RA. 1973. Hydrazine-deproteinated bone mineral. *Calcified tissue research* **12**: 73–90. DOI: 10.1007/BF02013723

Termine JD, Posner AS. 1966. Infra-red determination of the percentage of crystallinity in apatitic calcium phosphates. *Nature* **211**: 268–270. DOI: 10.1038/211268a0

Trueman CN. 2013. Chemical taphonomy of biomineralized tissues. *Palaeontology* **56**: 475–486. DOI: 10.1111/pala.12041

Trueman CNG, Behrensmeyer AK, Tuross N, Weiner S. 2004. Mineralogical and compositional changes in bones exposed on soil surfaces in Amboseli National Park, Kenya: diagenetic mechanisms and the role of sediment pore fluids. *Journal of archaeological science* **31**: 721–739. DOI: 10.1016/j.jas.2003.11.003

Trueman CN, Palmer MR, Field J, Privat K, Ludgate N, Chavagnac V, Eberth DA, Cifelli R, Rogers RR. 2008b. Comparing rates of recrystallisation and the potential for preservation of biomolecules from the distribution of trace elements in fossil bones. *Comptes rendus. Palevol* **7**: 145–158. DOI: 10.1016/j.crpv.2008.02.006

Trueman CN, Privat K, Field J. 2008a. Why do crystallinity values fail to predict the extent of diagenetic alteration of bone mineral? *Palaeogeography, palaeoclimatology, palaeoecology* **266**: 160–167. DOI: 10.1016/j.palaeo.2008.03.038

Turban-Just S, Schramm S. 1998. Stable carbon and nitrogen isotope ratios of individual amino acids give new insights into bone collagen degradation. *Bulletin de la Societe Geologique de France* **169**: 109–114.

Turner-Walker G. 2008. The chemical and microbial degradation of bones and teeth. In *Advances in human palaeopathology*, Pinhas R and Mays S (eds). Wiley: West Sussex; 1–29.

Turner-Walker G, Jans M. 2008. Reconstructing taphonomic histories using histological analysis. *Palaeogeography, palaeoclimatology, palaeoecology* **266**: 227–235. DOI: 10.1016/j.palaeo.2008.03.024

Tuross N. 2002. Alterations in fossil collagen. *Archaeometry* **44**: 427–434. DOI: 10.1111/1475-4754.00075

Weiner S, Bar-Yosef O. 1990. States of preservation of bones from prehistoric sites in the Near East: A survey. *Journal of archaeological science* **17**: 187–196. DOI: 10.1016/0305-4403(90)90058-D

Weiner S, Price PA. 1986. Disaggregation of bone into crystals. *Calcified tissue international* **39**: 365–375.

Weiner S, Traub W. 1986. Organization of hydroxyapatite crystals within collagen fibrils. *FEBS letters* **206**: 262–266.

Weiner S, Wagner HD. 1998. The material bone: Structure-mechanical function relations. *Annual Review of Materials Science* **28**: 271–298.

White L, Booth TJ. 2014. The origin of bacteria responsible for bioerosion to the internal bone microstructure: results from experimentally-deposited pig carcasses. *Forensic science international* **239**: 92–102. DOI: 10.1016/j.forsciint.2014.03.024

White WB. 1974. The carbonate minerals. In *The infrared spectra of minerals*, Farmer VC (ed). Mineralogical Society of Great Britain and Ireland; 227–284.

Wopenka B, Pasteris JD. 2005. A mineralogical perspective on the apatite in bone. *Materials Science and Engineering: C* **25**: 131–143. DOI: 10.1016/j.msec.2005.01.008

Wright LE, Schwarcz HP. 1996. Infrared and isotopic evidence for diagenesis of bone apatite at

Dos Pilas, Guatemala: Palaeodietary implications. *Journal of archaeological science* **23**: 933–944.

PERSONAL COMMUNICATION

Zioupos, P. 2017. Personal visit to the Cranfield Forensic Institute, Cranfield University, United Kingdom. May 2017.

REFERENCES

Adler, C. J. et al. (2011). Survival and recovery of DNA from ancient teeth and bones. *Journal of archaeological science*, 38 (5), pp.956–964. [Online]. Available at: doi:10.1016/j.jas.2010.11.010.

Adzhubei, A. A., Sternberg, M. J. E. and Makarov, A. A. (2013). Polyproline-II helix in proteins: Structure and function. *Journal of molecular biology*, 425 (12), pp.2100–2132. [Online]. Available at: doi:10.1016/j.jmb.2013.03.018.

Ajie, H. et al. (1990). AMS radiocarbon dating of bone osteocalcin. *Nuclear instruments & methods in physics research. Section B, Beam interactions with materials and atoms*, 52, pp.433–437.

Ajie, H. O. et al. (1992). Radiocarbon dating of bone osteocalcin: Isolating and characterizing a non-collagen protein. *Radiocarbon*, 34 (3), pp.296–305. [Online]. Available at: doi:10.1017/S0033822200063451 [Accessed 11 April 2017].

Ajie, H. O., Hauschka, P. V. and Kaplan, I. R. (1991). Comparison of bone collagen and osteocalcin for determination of radiocarbon ages and paleodietary reconstruction I. *Earth and planetary science letters*, 107, pp.380–388.

Allentoft, M. E. et al. (2012). The half-life of DNA in bone: measuring decay kinetics in 158 dated fossils. *Philosophical transactions of the royal society of London. Series B, Biological sciences*, 279 (1748), pp.4724–4733. [Online]. Available at: doi:10.1098/rspb.2012.1745.

Almany Magal, R. et al. (2014). Three-dimensional structure of minipig fibrolamellar bone: Adaptation to axial loading. *Journal of structural biology*, 186 (2), pp.253–264. [Online]. Available at: doi:10.1016/j.jsb.2014.03.007.

Ambrose, S. H. (1990). Preparation and characterization of bone and tooth collagen for isotopic analysis. *Journal of archaeological science*, 17 (4), pp.431–451. [Online]. Available at: doi:10.1016/0305-4403(90)90007-r.

Ambrose, S. H. (1991). Effects of diet, climate and physiology on nitrogen isotope abundances in terrestrial foodwebs. *Journal of archaeological science*, 18, pp.293–317.

Antonakos, A., Liarokapis, E. and Leventouri, T. (2007). Micro-Raman and FTIR studies of synthetic and natural apatites. *Biomaterials*, 28 (19), pp.3043–3054. [Online]. Available at: doi:10.1016/j.biomaterials.2007.02.028.

Ardizzoni, A. (2001). Osteocyte lacunar size-lamellar thickness relationships in human secondary osteons. *Bone*, 28 (2), pp.215–219. [Online]. Available at: doi:10.1016/s8756-3282(00)00417-8.

Asagiri, M. and Takayanagi, H. (2007). The molecular understanding of osteoclast differentiation. *Bone*, 40 (2), pp.251–264. [Online]. Available at: doi:10.1016/j.bone.2006.09.023.

Asara, J. M. et al. (2007). Protein sequences from mastodon and Tyrannosaurus rex revealed by mass spectrometry. *Science*, 316 (5822), pp.280–285. [Online]. Available at:

doi:10.1126/science.1137614.

Ascenzi, A. and Silvestrini, G. (1984). Bone-boring marine micro-organisms: An experimental investigation. *Journal of human evolution*, 13 (6), pp.531–536. [Online]. Available at: doi:10.1016/S0047-2484(84)80006-8.

Asscher, Y. et al. (2011). Atomic disorder in fossil tooth and bone mineral: An FTIR study using the grinding curve method. *ArchéoSciences*, (35), pp.135–141. [Online]. Available at: doi:10.4000/archeosciences.3062.

Asscher, Y., Weiner, S. and Boaretto, E. (2011). Variations in atomic disorder in biogenic carbonate hydroxyapatite using the infrared spectrum grinding curve method. *Advanced functional materials*, 21 (17), pp.3308–3313. [Online]. Available at: doi:10.1002/adfm.201100266.

Assis, S., Santos, A. and Keenleyside, A. (2016). Paleohistology and the study of human remains: past, present and future approaches. *Revista Argentina de antropología biológica*, 18 (2). [Online]. Available at: doi:10.17139/raab.2016.0018.02.02.

Bach-Gansmo, F. L. et al. (2016a). Immobilization and long-term recovery results in large changes in bone structure and strength but no corresponding alterations of osteocyte lacunar properties. *Bone*, 91, pp.139–147. [Online]. Available at: doi:10.1016/j.bone.2016.07.005.

Bach-Gansmo, F. L. et al. (2016b). Osteocyte lacunar properties and cortical microstructure in human iliac crest as a function of age and sex. *Bone*, 91, pp.11–19. [Online]. Available at: doi:10.1016/j.bone.2016.07.003.

Bada, J. L., Wang, X. S. and Hamilton, H. (1999). Preservation of key biomolecules in the fossil record: Current knowledge and future challenges. *Philosophical transactions of the royal society of London. Series B, Biological sciences*, 354 (1379), pp.77–86; discussion 86–87. [Online]. Available at: doi:10.1098/rstb.1999.0361.

Baker, S. L., Butterworth, E. C. and Langley, F. A. (1946). The calcium and nitrogen content of human bone tissue cleaned by micro-dissection. *Biochemical Journal*, 40 (3), pp.391–396. [Online]. Available at: https://www.ncbi.nlm.nih.gov/pubmed/16748020.

Bala, Y., Farlay, D. and Boivin, G. (2013). Bone mineralization: From tissue to crystal in normal and pathological contexts. *Osteoporosis international*, 24 (8), pp.2153–2166. [Online]. Available at: doi:10.1007/s00198-012-2228-y.

Balzer, A. et al. (1997). In vitro decomposition of bone collagen by soil bacteria: The implications for stable isotope analysis in archaeometry. *Archaeometry*, 39, pp.415–429.

Bartsiokas, A. and Middleton, A. P. (1992). Characterization and dating of recent and fossil bone by X-ray diffraction. *Science*, 19, pp.63–12.

Baxter, J. D., Biltz, R. M. and Pellegrino, E. D. (1966). The physical state of bone carbonate. A comparative infra-red study in several mineralized tissues. *The Yale journal of biology and medicine*, 38 (5), pp.456–470. [Online]. Available at: https://www.ncbi.nlm.nih.gov/pubmed/5957374.

Beasley, M. M. et al. (2014). Comparison of transmission FTIR, ATR, and DRIFT spectra: Implications for assessment of bone bioapatite diagenesis. *Journal of archaeological science*, 46 (0), pp.16–22. [Online]. Available at: doi:10.1016/j.jas.2014.03.008.

Bell, L. (2012). Histotaphonomy. In: *Bone histology*. Crowder, C. and Stout, S. (Eds). CRC Press. pp.241–251. [Online]. Available at: doi:10.1201/b11393-10.

Bell, L. S. (1990). Palaeopathology and diagenesis: An SEM evaluation of structural changes using backscattered electron imaging. *Journal of archaeological science*, 17 (1), pp.85–102. [Online]. Available at: doi:10.1016/0305-4403(90)90016-X.

Bell, L. S. and Elkerton, A. (2008). Unique marine taphonomy in human skeletal material recovered from the medieval warship Mary Rose. *International journal of osteoarchaeology*, 18 (5), pp.523–535. [Online]. Available at: doi:10.1002/oa.952.

Bell, L. S., Skinner, M. F. and Jones, S. J. (1996). The speed of post mortem change to the human skeleton and its taphonomic significance. *Forensic science international*, 82 (2), pp.129–140. [Online]. Available at: doi:10.1016/0379-0738(96)01984-6.

Bentley, A. R. (2006). Strontium isotopes from the earth to the archaeological skeleton: A review. *Journal of archaeological method and theory*, 13 (3), pp.135–187. [Online]. Available at: doi:10.1007/s10816-006-9009-x [Accessed 19 October 2016].

Berg, J. M. et al. (2015). *Biochemistry*. Macmillan Learning. [Online]. Available at: https://market.android.com/details?id=book-5bjzrQEACAAJ.

Berna, F., Matthews, A. and Weiner, S. (2004). Solubilities of bone mineral from archaeological sites: The recrystalization window. *Journal of archaeological science*, 31, pp.867–882.

Bloch, S. L., Kristensen, S. L. and Sørensen, M. S. (2012). The viability of perilabyrinthine osteocytes: A quantitative study using bulk-stained undecalcified human temporal bones. *The anatomical record: Advances in integrative anatomy and evolutionary biology*, 295 (7), Wiley Online Library., pp.1101–1108. [Online]. Available at: https://onlinelibrary.wiley.com/doi/abs/10.1002/ar.22492.

Bloch, S. L. and Sørensen, M. S. (2010). The viability and spatial distribution of osteocytes in the human labyrinthine capsule: A quantitative study using vector-based stereology. *Hearing research*, 270 (1-2), pp.65–70. [Online]. Available at: doi:10.1016/j.heares.2010.09.007.

Blumenschine, R. J. et al. (2007). Carnivore tooth-marks, microbial bioerosion, and the invalidation of Domínguez-Rodrigo and Barba's (2006) test of Oldowan hominin scavenging behavior. *Journal of human evolution*, 53 (4), pp.420–426. [Online]. Available at: doi:10.1016/j.jhevol.2007.01.011.

Bobroff, V. et al. (2016). What can infrared spectroscopy do for characterizing organic remnant in fossils? *Trends in analytical chemistry: TRAC*, 82 (C), Elsevier B.V., pp.443–456. [Online]. Available at: doi:10.1016/j.trac.2016.07.005.

Bocherens, H. et al. (1999). Palaeoenvironmental and palaeodietary implications of isotopic biogeochemistry of last interglacial Neanderthal and mammal bones in Scladina cave (Belgium). *Journal of archaeological science*, 26 (6), pp.599–607. [Online]. Available at: doi:10.1006/jasc.1998.0377.

Bocherens, H. et al. (2005). A new approach for assessing the preservation state of bone and collagen for isotopic analysis (radiocarbon dating, carbon and nitrogen stable isotopes). *L'anthropologie*, 109, pp.557–567. [Online]. Available at: doi:10.1016/j.anthro.2005.06.005.

Bocherens, H. et al. (2008). Grotte Chauvet (Ardèche, France): A 'natural experiment' for bone diagenesis in karstic context. *Palaeogeography, palaeoclimatology, palaeoecology*, 266 (3), pp.220–226. [Online]. Available at: doi:10.1016/j.palaeo.2008.03.023.

Bodzioch, A. and Kowal-Linka, M. (2012). Unraveling the origin of the Late Triassic multitaxic bone accumulation at Krasiejów (S Poland) by diagenetic analysis. *Palaeogeography, palaeoclimatology, palaeoecology*, 346–347, pp.25–36. [Online]. Available at: doi:10.1016/j.palaeo.2012.05.015.

Bohne, B. A. and Militchin, V. (2012). *Anatomy of the human temporal bone*. Department of Otolaryngology - Head and Neck Surgery, Washington University. [Online]. Available at: https://www.researchgate.net/publication/237838904_ANATOMY_of_HUMAN_TEMPORAL_BONE [Accessed 1 December 2018].

Boivin, G. and Meunier, P. J. (2003). The mineralization of bone tissue: A forgotten dimension in osteoporosis research. *Osteoporosis international*, 14 Suppl 3, pp.S19–S24. [Online]. Available at: doi:10.1007/s00198-002-1347-2.

Bollongino, R., Tresset, A. and Vigne, J.-D. (2008). Environment and excavation: Pre-lab impacts on ancient DNA analyses. *Comptes rendus. Palevol*, 7 (2–3), pp.91–98. [Online]. Available at: doi:10.1016/j.crpv.2008.02.002.

Booth, T. J. (2016). An investigation into the relationship between funerary treatment and bacterial bioerosion in European archaeological human bone. *Archaeometry*, 58 (3), pp.484–499. [Online]. Available at: doi:10.1111/arcm.12190.

Booth, T. J., Chamberlain, A. T. and Parker Pearson, M. (2015). Mummification in Bronze Age Britain. *Antiquity*, 89 (347), pp.1155–1173. [Online]. Available at: doi:10.15184/aqy.2015.111.

Booth, T. J. and Madgwick, R. (2016). New evidence for diverse secondary burial practices in Iron Age Britain: A histological case study. *Journal of archaeological science*, 67, pp.14–24. [Online]. Available at: doi:10.1016/j.jas.2016.01.010.

Booth, T. J., Redfern, R. C. and Gowland, R. L. (2016). Immaculate conceptions: Micro-CT analysis of diagenesis in Romano-British infant skeletons. *Journal of archaeological science*, 74, pp.124–134. [Online]. Available at: doi:10.1016/j.jas.2016.08.007.

Boskey, A. L. (2003). Bone mineral crystal size. *Osteoporosis international*, 14 Suppl 5, pp.S16–S20; discussion S20–S21. [Online]. Available at: doi:10.1007/s00198-003-1468-2.

Boyle, W. J., Simonet, W. S. and Lacey, D. L. (2003). Osteoclast differentiation and activation. *Nature*, 423 (6937), pp.337–342. [Online]. Available at: doi:10.1038/nature01658.

Brandt, E., Wiechmann, I. and Grupe, G. (2002). How reliable are immunological tools for the detection of ancient proteins in fossil bones? *International journal of osteoarchaeology*, 12, pp.307–316. [Online]. Available at: doi:10.1002/oa.624.

Brangule, A. and Gross, K. A. (2015). Importance of FTIR spectra deconvolution for the analysis of amorphous calcium phosphates. *IOP conference series: Materials science and engineering*, 77 (1), IOP Publishing., p.012027. [Online]. Available at: doi:10.1088/1757-899X/77/1/012027 [Accessed 16 May 2018].

Brock, F. et al. (2012). Reliability of nitrogen content (%N) and carbon:nitrogen atomic ratios (C:N) as indicators of collagen preservation suitable for radiocarbon dating. *Radiocarbon*, 54 (3-4), pp.879–886. [Online]. Available at: doi:10.1017/S0033822200047524.

Brock, F., Higham, T. and Ramsey, C. B. (2010). Pre-screening techniques for identification of samples suitable for radiocarbon dating of poorly preserved bones. *Journal of archaeological science*, 37 (4), pp.855–865. [Online]. Available at: doi:10.1016/j.jas.2009.11.015.

Bromage, T. G. et al. (2009). Lamellar bone is an incremental tissue reconciling enamel rhythms, body size, and organismal life history. *Calcified tissue international*, 84 (5), pp.388–404. [Online]. Available at: doi:10.1007/s00223-009-9221-2.

Bromage, T. G. et al. (2016). The scaling of human osteocyte lacuna density with body size and metabolism. *Comptes rendus. Palevol*, 15 (1), pp.32–39. [Online]. Available at: doi:10.1016/j.crpv.2015.09.001.

Brown, T. A. and Barnes, I. M. (2015). The current and future applications of ancient DNA in Quaternary science. *Journal of Quaternary Science*, 30 (2), pp.144–153. [Online]. Available at: doi:10.1002/jqs.2770.

Brown, T. and Brown, K. A. (2011). *Biomolecular archaeology: An Introduction*. 1st ed. Wiley-Blackwell. [Online]. Available at: http://www.worldcat.org/oclc/660539355?referer=xid.

Buckley, M. et al. (2008). Comparing the survival of osteocalcin and mtDNA in archaeological bone from four European sites. *Journal of archaeological science*, 35 (6), pp.1756–1764. [Online]. Available at: doi:10.1016/j.jas.2007.11.022.

Buckley, M. et al. (2009). Species identification by analysis of bone collagen using matrix-assisted laser desorption/ionisation time-of-flight mass spectrometry. *Rapid communications in mass spectrometry: RCM*, 23 (23), pp.3843–3854. [Online]. Available at: doi:10.1002/rcm.4316.

Buckley, M., Collins, M. and Thomas-Oates, J. (2008). A method of isolating the collagen (I) a2 chain carboxytelopeptide for species identification in bone fragments. *Analytical biochemistry*, 374, pp.325–334. [Online]. Available at: doi:10.1016/j.ab.2007.12.002.

Buckwalter, J. A. et al. (1995). Bone biology part I: structure, blood supply, cells, matrix, and mineralization. *The journal of bone and joint surgery*, (77), pp.1256–1275. [Online]. Available at: http://www.academia.dk/BiologiskAntropologi/Osteologi/PDF/BoneBiology_1995.pdf.

de Buffrenil, V., Dabin, W. and Zylberberg, L. (2004). Histology and growth of the cetacean petro-tympanic bone complex. *Journal of zoology*, 262 (4), pp.371–381. [Online]. Available at: doi:10.1017/S0952836903004758.

Burger, C. et al. (2008). Lateral packing of mineral crystals in bone collagen fibrils. *Biophysical journal*, 95 (4), pp.1985–1992. [Online]. Available at: doi:10.1529/biophysj.107.128355.

Burger, J. et al. (1999). DNA preservation: A microsatellite-DNA study on ancient skeletal remains. *Electrophoresis*, 20 (8), pp.1722–1728. [Online]. Available at: doi:3.0.CO;2-4">10.1002/(SICI)1522-2683(19990101)20:8<1722::AID-ELPS1722>3.0.CO;2-4.

Burr, D. B. (2002). The contribution of the organic matrix to bone's material properties. *Bone*, 31 (1), pp.8–11. [Online]. Available at: https://www.ncbi.nlm.nih.gov/pubmed/12110405.

Burr, D. B., Schaffler, M. B. and Frederickson, R. G. (1988). Composition of the cement line and its possible mechanical role as a local interface in human compact bone. *Journal of biomechanics*, 21 (11), pp.939–945. [Online]. Available at: https://www.ncbi.nlm.nih.gov/pubmed/3253280.

Busse, B. et al. (2010). Decrease in the osteocyte lacunar density accompanied by hypermineralized lacunar occlusion reveals failure and delay of remodeling in aged human bone. *Aging cell*, 9 (6), pp.1065–1075. [Online]. Available at: doi:10.1111/j.1474-9726.2010.00633.x.

Cadet, J. and Wagner, J. R. (2013). DNA base damage by reactive oxygen species, oxidizing agents, and UV radiation. *Cold Spring Harbor perspectives in biology*, 5 (2). [Online]. Available at: doi:10.1101/cshperspect.a012559.

Campos, P. F. et al. (2012). DNA in ancient bone - where is it located and how should we extract it? *Annals of anatomy = Anatomischer Anzeiger: official organ of the Anatomische Gesellschaft*, 194 (1), pp.7–16. [Online]. Available at: doi:10.1016/j.aanat.2011.07.003.

Canelón, S. P. and Wallace, J. M. (2016). β-aminopropionitrile-induced reduction in enzymatic crosslinking causes in vitro changes in collagen morphology and molecular composition. *PloS*

one, 11 (11), p.e0166392. [Online]. Available at: doi:10.1371/journal.pone.0166392.

Cappella, A. et al. (2015). The comparative performance of PMI estimation in skeletal remains by three methods (C-14, luminol test and OHI): analysis of 20 cases. *International journal of legal medicine*. [Online]. Available at: doi:10.1007/s00414-015-1152-z.

Cappellini, E. et al. (2018). Ancient biomolecules and evolutionary inference. *Annual review of biochemistry*. 87, pp.1029-1060. [Online]. Available at: doi:10.1146/annurev-biochem-062917-012002.

Carter, Y. et al. (2013). Variation in osteocyte lacunar morphology and density in the human femur-A synchrotron radiation micro-CT study. *Bone*, 52 (1), pp.126–132. [Online]. Available at: doi:10.1016/j.bone.2012.09.010.

Cattaneo, C. et al. (1999). Determining the human origin of fragments of burnt bone: A comparative study of histological, immunological and DNA techniques. *Forensic science international*, 102 (2-3), pp.181–191. [Online]. Available at: https://www.ncbi.nlm.nih.gov/pubmed/10464934.

Chadefaux, C. et al. (2009). Curve-fitting micro-ATR-FTIR studies of the Amide I and II bands of type I collagen in archaeological bone materials. *e-PS*, 6, pp.129–137.

Chalmers, J. M. (2010). Mid-infrared spectroscopy: The basics. In: Moss, D. (Ed). *Biomedical applications of synchrotron infrared microspectroscopy*. RSC Analytical Spectroscopy Series. RSC Publishing. pp.29–66. [Online]. Available at: doi:10.1039/9781849731997-00029 [Accessed 1 December 2018].

Cho, G., Wu, Y. and Ackerman, J. L. (2003). Detection of hydroxyl ions in bone mineral by solid-state NMR spectroscopy. *Science*, 300 (5622), pp.1123–1127. [Online]. Available at: doi:10.1126/science.1078470.

Clermont, Y., Lalli, M. and Bencsath-Makkai, Z. (2013). *Cartilage and bone*. [Online]. Available at: http://audilab.bmed.mcgill.ca/HA/html/bc_12_E.html [Accessed 14 September 2018].

Collins, M. et al. (2000). Slow rates of degradation of osteocalcin: Green light for fossil bone protein? *Geology*, 28, pp.1139–1142.

Collins, M. J. et al. (1995). A basic mathematical simulation of the chemical degradation of ancient collagen. *Journal of archaeological science*, 22 (2), pp.175–183. [Online]. Available at: doi:10.1006/jasc.1995.0019.

Collins, M. J. et al. (1999). Predicting protein decomposition: The case of aspartic-acid racemization kinetics [and discussion]. *Philosophical transactions of the royal society of London. Series B, Biological sciences*, 354 (1379), pp.51–64. [Online]. Available at: http://www.jstor.org/stable/56706.

Collins, M. J. et al. (2002). The survival of organic matter in bone: a review. *Archaeometry*, 44 (3), pp.383–394. [Online]. Available at: doi:10.1111/1475-4754.t01-1-00071.

Collins, M. J. et al. (2009). Is amino acid racemization a useful tool for screening for ancient DNA in bone? *Proceedings. Biological sciences / The royal society*, 276 (1669), pp.2971–2977. [Online]. Available at: doi:10.1098/rspb.2009.0563.

Collins, M. J. and Galley, P. (1998). Towards an optimal method of archaeological collagen extraction: The influence of pH and grinding. *Ancient biomolecules*, 2 (2/3), pp.209–223.

Colonese, A. C. et al. (2015). Archaeological bone lipids as palaeodietary markers. *Rapid*

communications in mass spectrometry: RCM, 29 (7), pp.611–618. [Online]. Available at: doi:10.1002/rcm.7144.

Cooper, A. (2011). *Biophysical chemistry*. Royal society of chemistry. [Online]. Available at: https://market.android.com/details?id=book-LQqaRoj78qIC.

Crescimanno, A. and Stout, S. D. (2012). Differentiating fragmented human and nonhuman long bone using osteon circularity. *Journal of forensic sciences*, 57 (2), pp.287–294. [Online]. Available at: doi:10.1111/j.1556-4029.2011.01973.x.

Cuijpers, A. G. F. M. (2006). Histological identification of bone fragments in archaeology: Telling humans apart from horses and cattle. *International journal of osteoarchaeology*, 16 (6), John Wiley & Sons, Ltd., pp.465–480. [Online]. Available at: doi:10.1002/oa.848.

Cuijpers, S. and Lauwerier, R. C. G. M. (2008). Differentiating between bone fragments from horses and cattle: A histological identification method for archaeology. *Environmental archaeology*, 13 (2), pp.165–179. [Online]. Available at: doi:10.1179/174963108X343281.

Cullinane, D. M. (2002). The role of osteocytes in bone regulation: Mineral homeostasis versus mechanoreception. *Journal of musculoskeletal & neuronal interactions*, 2 (3), pp.242–244. [Online]. Available at: http://www.ismni.org/jmni/pdf/7/Cullinane.pdf.

Currey, J. D. (1999). The design of mineralised hard tissues for their mechanical functions. *The journal of experimental biology*, 202 (Pt 23), pp.3285–3294. [Online]. Available at: https://www.ncbi.nlm.nih.gov/pubmed/10562511.

Currey, J. D. (2002). *Bones: Structure and mechanics*. Princeton University Press. [Online]. Available at: https://press.princeton.edu/titles/7313.html.

Currey, J. D. (2003). The many adaptations of bone. *Journal of biomechanics*, 36 (10), pp.1487–1495. [Online]. Available at: doi:10.1016/S0021-9290(03)00124-6.

Dalconi, M. C. et al. (2003). Structure of bioapatite in human foetal bones: An X-ray diffraction study. *Nuclear instruments & methods in physics research. Section B, Beam interactions with materials and atoms*, 200, pp.406–410. [Online]. Available at: doi:10.1016/S0168-583X(02)01730-5.

Dall'Ara, E. et al. (2015). Estimation of local anisotropy of plexiform bone: Comparison between depth sensing micro-indentation and Reference Point Indentation. *Journal of biomechanics*, 48 (15), pp.4073–4080. [Online]. Available at: doi:10.1016/j.jbiomech.2015.10.001.

Dal Sasso, G. et al. (2014). Bone diagenesis at the micro-scale: Bone alteration patterns during multiple burial phases at Al Khiday (Khartoum, Sudan) between the Early Holocene and the II century AD. *Palaeogeography, palaeoclimatology, palaeoecology*, 416, pp.30–42. [Online]. Available at: doi:10.1016/j.palaeo.2014.06.034.

Dal Sasso, G. et al. (2016). Bone diagenesis variability among multiple burial phases at Al Khiday (Sudan) investigated by ATR-FTIR spectroscopy. *Palaeogeography, palaeoclimatology, palaeoecology*, 463, pp.168–179. [Online]. Available at: doi:10.1016/j.palaeo.2016.10.005.

Daly, K. G. et al. (2018). Ancient goat genomes reveal mosaic domestication in the Fertile Crescent. *Science*, 361 (6397), pp.85–88. [Online]. Available at: doi:10.1126/science.aas9411.

De Boer, H. H. and Maat, G. J. R. (2012). The histology of human dry bone (a review). *CPAG*, 22, pp.49–65. [Online]. Available at: doi:2174-8063.

De Boer, H. H., Van der Merwe, A. E. and Maat, G. J. R. (2013). The diagnostic value of microscopy in dry bone palaeopathology: A review. *International journal of paleopathology*, 3 (2), pp.113–121. [Online]. Available at: doi:10.1016/j.ijpp.2013.03.004.

Demarchi, B. et al. (2016). Protein sequences bound to mineral surfaces persist into deep time. *eLife*, 5. [Online]. Available at: doi:10.7554/eLife.17092.

DeNiro, M. J. (1985). Postmortem preservation and alteration of in vivo bone collagen isotope ratios in relation to palaeodietary reconstruction. *Nature*, 317 (6040), pp.806–809. [Online]. Available at: doi:10.1038/317806a0T.

DeNiro, M. J. and Weiner, S. (1988). Chemical, enzymatic and spectroscopic characterization of 'collagen' and other organic fractions from prehistoric bones. *Geochimica et cosmochimica acta*, 52 (9), pp.2197–2206. [Online]. Available at: doi:10.1016/0016-7037(88)90122-6.

Deviese, T. et al. (2018). New protocol for compound-specific radiocarbon analysis of archaeological bones. *Rapid communications in mass spectrometry: RCM*, 32 (5), pp.373–379. [Online]. Available at: doi:10.1002/rcm.8047.

Dixon, R., Dawson, L. and Taylor, D. (2008). *The experimental degradation of archaeological human bone by anaerobic bacteria and the implications for recovery of ancient DNA*. In: 19 October 2008. Giannini Editore. pp.1–10. [Online]. Available at: http://eprints.lincoln.ac.uk/2660 [Accessed 1 December 2018].

Dobberstein, R. C. et al. (2009). Archaeological collagen: Why worry about collagen diagenesis? *Archaeological and anthropological sciences*, 1 (1), pp.31–42. [Online]. Available at: doi:10.1007/s12520-009-0002-7 [Accessed 4 September 2016].

Doden, E. and Halves, R. (1984). On the functional morphology of the human petrous bone. *The American journal of anatomy*, 169 (4), pp.451–462. [Online]. Available at: doi:10.1002/aja.1001690407.

Domínguez-Rodrigo, M. and Barba, R. (2006). New estimates of tooth mark and percussion mark frequencies at the FLK Zinj site: The carnivore-hominid-carnivore hypothesis falsified. *Journal of human evolution*, 50 (2), pp.170–194. [Online]. Available at: doi:10.1016/j.jhevol.2005.09.005.

Dominguez, V. M. and Crowder, C. M. (2012). The utility of osteon shape and circularity for differentiating human and non-human Haversian bone. *American journal of physical anthropology*, 149 (1), pp.84–91. [Online]. Available at: doi:10.1002/ajpa.22097.

Dong, P. et al. (2014). 3D osteocyte lacunar morphometric properties and distributions in human femoral cortical bone using synchrotron radiation micro-CT images. *Bone*, 60, pp.172–185. [Online]. Available at: doi:10.1016/j.bone.2013.12.008.

Douka, K. et al. (2017). Direct radiocarbon dating and DNA analysis of the Darra-i-Kur (Afghanistan) human temporal bone. *Journal of human evolution*, 107, pp.86–93. [Online]. Available at: doi:10.1016/j.jhevol.2017.03.003.

Ducy, P., Schinke, T. and Karsenty, G. (2000). The osteoblast: A sophisticated fibroblast under central surveillance. *Science*, 289 (5484), pp.1501–1504. [Online]. Available at: https://www.ncbi.nlm.nih.gov/pubmed/10968779.

Duer, M. and Veis, A. (2013). Bone mineralization: Water brings order. *Nature materials*, 12 (12), pp.1081–1082. [Online]. Available at: doi:10.1038/nmat3822.

Eastoe, J. E. and Eastoe, B. (1954). The organic constituents of mammalian compact bone. *Biochemical journal*, 57 (3), pp.453–459. [Online]. Available at:

https://www.ncbi.nlm.nih.gov/pubmed/13181859.

Eby, T. L. and Nadol, J. B., Jr. (1986). Postnatal growth of the human temporal bone. Implications for cochlear implants in children. *The Annals of otology, rhinology, and laryngology*, 95 (4 Pt 1), pp.356–364. [Online]. Available at: doi:10.1177/000348948609500407.

Elliott, J. C. (1964). *The crystallographic structure of dental enamel and related apatites*. Doctor of Philosophy, University of London, Faculty of Science. [Online]. Available at: https://qmro.qmul.ac.uk/xmlui/bitstream/handle/123456789/1562/ELLIOTTCrystallographicStructure1964.pdf?sequence=1.

Elliott, J. C., Holcomb, D. W. and Young, R. A. (1985). Infrared determination of the degree of substitution of hydroxyl by carbonate ions in human dental enamel. *Calcified tissue international*, 37 (4), pp.372–375. [Online]. Available at: https://www.ncbi.nlm.nih.gov/pubmed/3930033.

Eyre, D. (1987). Collagen cross-linking amino acids. In: Colowick, N. and Kaplan, N. (Eds). *Structural and contractile proteins, part D: Extracellular matrix*. Methods in Enzymology. 144. Academic Press. pp.115–139. [Online]. Available at: doi:10.1016/0076-6879(87)44176-1.

Eyre, D. R. (1995). The specificity of collagen cross-links as markers of bone and connective tissue degradation. *Acta orthopaedica Scandinavica. Supplementum*, 266, pp.166–170. [Online]. Available at: doi:10.3109/17453679509157685.

Fazekas, I. G. and Kósa, F. (1978). *Forensic fetal osteology*. Akadémiai Kiadó.

Fernandez-Jalvo, Y. et al. (2010). Early bone diagenesis in temperate environments Part I: Surface features and histology. *Palaeogeography, palaeoclimatology, palaeoecology*, 288, pp.62–81.

Figueiredo, M. M., Gamelas, J. A. F. and Martins, A. G. (2012). Characterization of bone and bone-based graft materials using FTIR spectroscopy. In: *Infrared spectroscopy - Life and biomedical sciences*. [Online]. Available at: doi:10.5772/36379.

Fleet, M. E. (2009). Infrared spectra of carbonate apatites: v2-Region bands. *Biomaterials*, 30 (8), pp.1473–1481. [Online]. Available at: doi:10.1016/j.biomaterials.2008.12.007.

Fleet, M. E. and Liu, X. (2004). Location of type B carbonate ion in type A–B carbonate apatite synthesized at high pressure. *Journal of solid state chemistry*, 177 (9), pp.3174–3182. [Online]. Available at: doi:10.1016/j.jssc.2004.04.002.

Fleet, M. E., Liu, X. and King, P. L. (2004). Accommodation of the carbonate ion in apatite: An FTIR and X-ray structure study of crystals synthesized at 2–4 GPa. *The American mineralogist*, 89 (10), pp.1422–1432. [Online]. Available at: doi:10.2138/am-2004-1009 [Accessed 14 January 2018].

Forbes, S. L., Stuart, B. H. and Dent, B. B. (2005). The effect of the burial environment on adipocere formation. *Forensic science international*, 154 (1), pp.24–34. [Online]. Available at: doi:10.1016/j.forsciint.2004.09.107.

Frisch, T. et al. (1998). Volume-referent bone turnover estimated from the interlabel area fraction after sequential labeling. *Bone*, 22 (6), pp.677–682. [Online]. Available at: doi:10.1016/S8756-3282(98)00050-7.

Frisch, T. et al. (2000). Estimation of volume referent bone turnover in the otic capsule after sequential point labeling. *The Annals of otology, rhinology, and laryngology*, 109 (1), pp.33–39. [Online]. Available at: doi:10.1177/000348940010900106.

Gamba, C. et al. (2014). Genome flux and stasis in a five millennium transect of European prehistory. *Nature communications*, 5, p.5257. [Online]. Available at: doi:10.1038/ncomms6257.

Gander, W. and von Matt, U. (1993). Smoothing filters. In: Gander, W. and Hřebíček, J. (Eds). *Solving problems in scientific computing using maple and Matlab®*. Springer Berlin Heidelberg, Berlin, Heidelberg, pp 121–139.

Garland, A. N. (1989). Microscopical analysis of fossil bone. *Applied geochemistry*, 4 (3), pp.215–229. [Online]. Available at: doi:10.1016/0883-2927(89)90021-8.

Garvie-Lok, S. J., Varney, T. L. and Katzenberg, M. A. (2004). Preparation of bone carbonate for stable isotope analysis: The effects of treatment time and acid concentration. *Journal of archaeological science*, 31 (6), pp.763–776. [Online]. Available at: doi:10.1016/j.jas.2003.10.014.

Gautieri, A. et al. (2011). Hierarchical structure and nanomechanics of collagen microfibrils from the atomistic scale up. *Nano letters*, 11 (2), pp.757–766. [Online]. Available at: doi:10.1021/nl103943u.

Gay, C. V., Gilman, V. R. and Sugiyama, T. (2000). Perspectives on osteoblast and osteoclast function. *Poultry science*, (79), pp.1005–1008. [Online]. Available at: https://pdfs.semanticscholar.org/c390/1215c3046ab3b19df3131a933b3fe885c543.pdf.

Gelse, K., Pöschl, E. and Aigner, T. (2003). Collagens—structure, function, and biosynthesis. *Advanced drug delivery reviews*, 55 (12), pp.1531–1546. [Online]. Available at: doi:10.1016/j.addr.2003.08.002.

Georgiadis, M., Müller, R. and Schneider, P. (2016). Techniques to assess bone ultrastructure organization: Orientation and arrangement of mineralized collagen fibrils. *Journal of the royal society, interface / The royal society*, 13 (119). [Online]. Available at: doi:10.1098/rsif.2016.0088.

Gerber, H. P. and Ferrara, N. (2000). Angiogenesis and bone growth. *Trends in cardiovascular medicine*, 10 (5), pp.223–228. [Online]. Available at: https://www.ncbi.nlm.nih.gov/pubmed/11282299.

Gilbert, M. T. P. et al. (2003). Distribution patterns of postmortem damage in human mitochondrial DNA. *American journal of human genetics*, 72 (1), pp.32–47. [Online]. Available at: doi:10.1086/345378.

Gilbert, M. T. P. et al. (2005). Assessing ancient DNA studies. *Trends in ecology & evolution*, 20 (10), pp.541–544. [Online]. Available at: doi:10.1016/j.tree.2005.07.005.

Gilbert, M. T. P. et al. (2006). Insights into the processes behind the contamination of degraded human teeth and bone samples with exogenous sources of DNA. *International Journal of Osteoarchaeology*, 16 (2), pp.156–164. [Online]. Available at: doi:10.1002/oa.832.

Giraud-Guille, M. M. (1988). Twisted plywood architecture of collagen fibrils in human compact bone osteons. *Calcified tissue international*, 42 (3), pp.167–180. [Online]. Available at: https://www.ncbi.nlm.nih.gov/pubmed/3130165.

Goggin, P. M. et al. (2016). High-resolution 3D imaging of osteocytes and computational modelling in mechanobiology: Insights on bone development, ageing, health and disease. *European cells & materials*, 31, pp.264–295. [Online]. Available at: https://www.ncbi.nlm.nih.gov/pubmed/27209400.

Goldring, S. R. (2015). The osteocyte: Key player in regulating bone turnover. *RMD open*, 1

(Suppl 1), p.e000049. [Online]. Available at: doi:10.1136/rmdopen-2015-000049.

Götherström, A. et al. (2002). Bone preservation and DNA amplification. *Archaeometry*, 44 (3), pp.395–404. [Online]. Available at: doi:10.1111/1475-4754.00072.

Gourion-Arsiquaud, S., West, P. A. and Boskey, A. L. (2008). Fourier transform-infrared microspectroscopy and microscopic imaging. *Methods in molecular biology* , 455, pp.293–303. [Online]. Available at: doi:10.1007/978-1-59745-104-8_20.

Gravlund, P. et al. (2012). Ancient DNA extracted from Danish aurochs (Bos primigenius): genetic diversity and preservation. *Annals of anatomy = Anatomischer Anzeiger: official organ of the Anatomische Gesellschaft*, 194 (1), pp.103–111. [Online]. Available at: doi:10.1016/j.aanat.2011.10.011.

Green, D. M. (1976). *An introduction to hearing*. Halsted Press.

Green, R. E. et al. (2010). A draft sequence of the Neandertal genome. *Science*, 328 (5979), pp.710–722. [Online]. Available at: doi:10.1126/science.1188021.

Greeves, N. (2018). *Chemtube3D*. [Online]. Available at: http://www.chemtube3d.com/solidstate/SShydroxyapatite.htm [Accessed 14 September 2018].

Grine, F. E. et al. (2015). Microbial osteolysis in an Early Pleistocene hominin (Paranthropus robustus) from Swartkrans, South Africa. *Journal of human evolution*, 85, pp.126–135. [Online]. Available at: doi:10.1016/j.jhevol.2015.05.004.

Grunenwald, A. et al. (2014). Adsorption of DNA on biomimetic apatites: Toward the understanding of the role of bone and tooth mineral on the preservation of ancient DNA. *Applied surface science*, 292, pp.867–875. [Online]. Available at: doi:10.1016/j.apsusc.2013.12.063.

Grupe, G. (1995). Preservation of collagen in bone from dry, sandy soil. *Journal of archaeological science*, 22, pp.193–199.

Grupe, G., Balzer, A. and Turban-Just, S. (2002). Modeling protein diagenesis in ancient bone: Towards a validation of stable isotope data. In: Ambrose, S. H. and Katzenberg, M. A. (Eds). *Biogeochemical approaches to paleodietary analysis*. Springer. pp.173–187. [Online]. Available at: doi:10.1007/0-306-47194-9_9.

Grupe, G. and Garland, A. N. (1993). *Histology of ancient human bone: Methods and diagnosis*. Springer-Verlag.

Guarino, F. M. et al. (2000). Detection of DNA in ancient bones using histochemical methods. *Biotechnic and histochemistry*, 75, pp.110–117.

Gueta, R. et al. (2007). Local atomic order and infrared spectra of biogenic calcite. *Angewandte Chemie* , 46 (1-2), pp.291–294. [Online]. Available at: doi:10.1002/anie.200603327.

Guo, D. and Bonewald, L. F. (2009). Advancing our understanding of osteocyte cell biology. *Therapeutic advances in musculoskeletal disease*, 1 (2), pp.87–96. [Online]. Available at: doi:10.1177/1759720X09341484.

Gupta, S. et al. (2015). Ancient DNA – Pitfalls and prospects. *Indian journal of science and technology*, 8 (13). [Online]. Available at: doi:10.17485/ijst/2015/v8i13/60073 [Accessed 25 May 2017].

Hackett, C. J. (1981). Microscopical focal destruction (tunnels) in exhumed human bones. *Medicine, science, and the law*, 21 (4), pp.243–265. [Online]. Available at:

doi:10.1177/002580248102100403.

Haglund, W. D. (2002). Recent mass graves, an introduction. *Advances in forensic taphonomy: Method, theory and archaeological perspectives*, CRC Press., pp.243–262. [Online]. Available at: https://books.google.com/books?hl=en&lr=&id=5q1rg9Xl9CEC&oi=fnd&pg=PA243&dq=Recent+mass+Graves+%CE%91n+Introduction+Haglund&ots=St2plVenfI&sig=xZsafCH78XezziSzf5WqynLu8Qc.

Hamed, E. and Jasiuk, I. (2012). Elastic modeling of bone at nanostructural level. *Materials science & engineering. R, Reports: a review journal*, 73 (3), pp.27–49. [Online]. Available at: doi:10.1016/j.mser.2012.04.001.

Hannah, K. M. et al. (2010). Bimodal distribution of osteocyte lacunar size in the human femoral cortex as revealed by micro-CT. *Bone*, 47 (5), pp.866–871. [Online]. Available at: doi:10.1016/j.bone.2010.07.025.

Hansen, A. et al. (2001). Statistical evidence for miscoding lesions in ancient DNA templates. *Molecular biology and evolution*, 18 (2), pp.262–265. [Online]. Available at: https://www.ncbi.nlm.nih.gov/pubmed/11158385.

Hansen, H. B. et al. (2017). Comparing ancient DNA preservation in petrous bone and tooth cementum. *PloS one*, 12 (1), p.e0170940. [Online]. Available at: doi:10.1371/journal.pone.0170940.

Hanson, D. B. and Buikstra, J. E. (1987). Histomorphological alteration in buried human bone from the lower Illinois Valley: Implications for palaeodietary research. *Journal of archaeological science*, 14 (5), pp.549–563. [Online]. Available at: doi:10.1016/0305-4403(87)90038-0.

Hanson, M. and Cain, C. R. (2007). Examining histology to identify burned bone. *Journal of archaeological science*, 34 (11), pp.1902–1913. [Online]. Available at: doi:10.1016/j.jas.2007.01.009.

Harbeck, M. and Grupe, G. (2009). Experimental chemical degradation compared to natural diagenetic alteration of collagen: implications for collagen quality indicators for stable isotope analysis. *Archaeological and anthropological sciences*, 1, pp.43–57. [Online]. Available at: doi:10.1007/s12520-009-0004-5.

Harvig, L. et al. (2014). Strontium isotope signals in cremated petrous portions as indicator for childhood origin. *PloS one*, 9 (7), p.e101603. [Online]. Available at: doi:10.1371/journal.pone.0101603.

Haynes, S. et al. (2002). Bone preservation and ancient DNA: The application of screening methods for predicting DNA survival. *Journal of archaeological science*, 29 (6), pp.585–592. [Online]. Available at: doi:10.1006/jasc.2001.0731.

Hedges, R. E. M. (2002). Bone diagenesis: An overview of processes. *Archaeometry*, 44 (3), pp.319–328. [Online]. Available at: doi:10.1111/1475-4754.00064.

Hedges, R. E. M. (2003). On bone collagen—apatite-carbonate isotopic relationships. *International journal of osteoarchaeology*, 13 (1-2), pp.66–79. [Online]. Available at: doi:10.1002/oa.660.

Hedges, R. E. M. and Millard, A. R. (1995). Bones and groundwater: Towards the modelling of diagenetic processes. *Journal of archaeological science*, 22 (2), pp.155–164. [Online]. Available at: doi:10.1006/jasc.1995.0017.

Hedges, R. E. M., Millard, A. R. and Pike, A. W. G. (1995). Measurements and relationships of diagenetic alteration of bone from three archaeological sites. *Journal of archaeological science*, 22 (2), pp.201–209. [Online]. Available at: doi:10.1006/jasc.1995.0022.

Hendy, J. et al. (2018). A guide to ancient protein studies. *Nature ecology & evolution*, 2 (5), pp.791–799. [Online]. Available at: doi:10.1038/s41559-018-0510-x.

Henmi, A. et al. (2016). Bone matrix calcification during embryonic and postembryonic rat calvarial development assessed by SEM-EDX spectroscopy, XRD, and FTIR spectroscopy. *Journal of bone and mineral metabolism*, 34 (1), pp.41–50. [Online]. Available at: doi:10.1007/s00774-014-0647-x.

Hernandez, C. J., Majeska, R. J. and Schaffler, M. B. (2004). Osteocyte density in woven bone. *Bone*, 35 (5), pp.1095–1099. [Online]. Available at: doi:10.1016/j.bone.2004.07.002.

High, K. et al. (2015). Apatite for destruction: Investigating bone degradation due to high acidity at Star Carr. *Journal of archaeological science*, 59, pp.159–168. [Online]. Available at: doi:10.1016/j.jas.2015.04.001.

Higham, T. F. G., Jacobi, R. M. and Ramsey, C. B. (2006). AMS radiocarbon dating of ancient bone using ultrafiltration. *Radiocarbon*, 48 (2), pp.179–195. [Online]. Available at: https://www.cambridge.org/core/journals/radiocarbon/article/ams-radiocarbon-dating-of-ancient-bone-using-ultrafiltration/5B9E8E83E9A0E74BFA2686B8371FB42C.

Hill, C. A. (2011). Ontogenetic change in temporal bone pneumatization in humans. *Anatomical record* , 294 (7), pp.1103–1115. [Online]. Available at: doi:10.1002/ar.21404.

Ho, S. P. et al. (2009). Structure, chemical composition and mechanical properties of human and rat cementum and its interface with root dentin. *Acta biomaterialia*, 5 (2), pp.707–718. [Online]. Available at: doi:10.1016/j.actbio.2008.08.013.

Hofmann, H., Fietzek, P. P. and Kühn, K. (1978). The role of polar and hydrophobic interactions for the molecular packing of type I collagen: a three-dimensional evaluation of the amino acid sequence. *Journal of molecular biology*, 125 (2), pp.137–165. [Online]. Available at: https://www.ncbi.nlm.nih.gov/pubmed/731689.

Hofmanová, Z. et al. (2016). Early farmers from across Europe directly descended from Neolithic Aegeans. *Proceedings of the national academy of sciences of the United States of America*, 113 (25), pp.6886–6891. [Online]. Available at: doi:10.1073/pnas.1523951113.

Hofreiter, M. et al. (2001). Ancient DNA. *Nature reviews. Genetics*, 2 (5), pp.353–359. [Online]. Available at: doi:10.1038/35072071.

Hollund, H. I. et al. (2012). What happened here? Bone histology as a tool in decoding the postmortem histories of archaeological bone from Castricum, the Netherlands. *International journal of osteoarchaeology*, 22 (5), pp.537–548. [Online]. Available at: doi:10.1002/oa.1273.

Hollund, H. I. et al. (2013). Testing an alternative high-throughput tool for investigating bone diagenesis: FTIR in Attenuated Total Reflection (ATR) mode. *Archaeometry*, 55 (3), pp.507–532. [Online]. Available at: doi:10.1111/j.1475-4754.2012.00695.x.

Hollund, H. I. et al. (2016). Pick the right pocket. Sub-sampling of bone sections to investigate diagenesis and DNA preservation. *International journal of osteoarchaeology*. [Online]. Available at: doi:10.1002/oa.2544.

Hollund, H. I., Blank, M. and Sjögren, K.-G. (2018). Dead and buried? Variation in post-mortem histories revealed through histotaphonomic characterisation of human bone from megalithic graves in Sweden. *PloS one*, 13 (10), p.e0204662. [Online]. Available at:

doi:10.1371/journal.pone.0204662.

Hunt, J. M., Wisherd, M. P. and Bonham, L. C. (1950). Infrared absorption spectra of minerals and other inorganic compounds. *Analytical chemistry*, 22 (12), pp.1478–1497. [Online]. Available at: doi:10.1021/ac60048a006.

Iliopoulos, G. (2004). *Microbial focal destruction in Late Miocene mammal bone from Kerassia (N. Euboea Island, Greece)* [Poster]. 5th International Symposium on Eastern Mediterranean Geology. Thessaloniki, Greece.

Jackes, M. et al. (2001). Destruction of microstructure in archaeological bone: A case study from Portugal. *International journal of osteoarchaeology*, 11, pp.415–432.

Janaway, R. C. (2002). Degradation of clothing and other dress materials associated with buried bodies of archaeological and forensic interest. In: Haglund, W. D. and Sorg, M. H. (Eds). *Advances in forensic taphonomy: method, theory, and archaeological perspectives*. books.google.com. pp.379–402. [Online]. Available at: https://books.google.com/books?hl=en&lr=&id=5q1rg9Xl9CEC&oi=fnd&pg=PA379&dq=Degradation+of+clothing+and+other+dress+materials+associated+with+buried+bodies+of+archaeological+and+forensic+interest&ots=St2plVdthD&sig=zxuMuPad_6RfAkIeyCDZ1MpaZoM.

Janaway, R. C. (2008). The decomposition of materials associated with buried cadavers. In: Tibbett, M. and Carter, D. O. (Eds.). *Soil analysis in forensic taphonomy*. CRC Press. pp.165–214. [Online]. Available at: https://www.taylorfrancis.com/books/e/9781420069921/chapters/10.1201%2F9781420069921-11.

Jans, M. M. E. et al. (2002). In situ preservation of archaeological bone: A histological study within a multidisciplinary approach. *Archaeometry*, 44 (3), pp.343–352. [Online]. Available at: doi:10.1111/1475-4754.t01-1-00067.

Jans, M. M. E. et al. (2004). Characterisation of microbial attack on archaeological bone. *Journal of archaeological science*, 31 (1), pp.87–95. [Online]. Available at: doi:10.1016/j.jas.2003.07.007.

Jeffery, N. and Spoor, F. (2004). Prenatal growth and development of the modern human labyrinth. *Journal of anatomy*, 204 (2), pp.71–92. [Online]. Available at: doi:10.1111/j.1469-7580.2004.00250.x.

Johnson, B. J. and Miller, G. H. (1997). Archaeological applications of amino acid racemization. *Archaeometry*, 19 (2), pp.265–287.

Jørkov, M. L. S., Heinemeier, J. and Lynnerup, N. (2007). Evaluating bone collagen extraction methods for stable isotope analysis in dietary studies. *Journal of archaeological science*, 34, p.1824. [Online]. Available at: doi:10.1016/j.jas.2006.12.020.

Jørkov, M. L. S., Heinemeier, J. and Lynnerup, N. (2009). The petrous bone: A new sampling site for identifying early dietary patterns in stable isotopic studies. *American journal of physical anthropology*, 138 (2), pp.199–209. [Online]. Available at: doi:10.1002/ajpa.20919.

Karkanas, P. et al. (1999). Mineral assemblages in Theopetra, Greece: A framework for understanding diagenesis in a prehistoric cave. *Journal of archaeological science*, 26 (9), pp.1171–1180. [Online]. Available at: doi:10.1006/jasc.1998.0354.

Karkanas, P. et al. (2000). Diagenesis in prehistoric caves: The use of minerals that form in situ to assess the completeness of the archaeological record. *Journal of archaeological science*, 27 (10), pp.915–929. [Online]. Available at: doi:10.1006/jasc.1999.0506.

Karkanas, P. (2010). Preservation of anthropogenic materials under different geochemical processes: A mineralogical approach. *Quaternary international*, 214, pp.63–69.

Katić, V. et al. (1991). Distribution of structural and trace elements in human temporal bone. *Biological trace element research*, 29 (1), pp.35–43. [Online]. Available at: https://www.ncbi.nlm.nih.gov/pubmed/1711360.

Katzenberg, M. A. (2008). Stable isotope analysis: A tool for studying past diet, demography, and life history. In: Katzenberg, M. A. and Saunders, S. R. (Eds). *Biological anthropology of the human skeleton*. John Wiley & Sons. pp.413–441. [Online]. Available at: https://edisciplinas.usp.br/pluginfile.php/4181236/mod_resource/content/1/Katzemberg%202008.pdf.

Kaya, M. et al. (2005). Effect of DNA structure on the formation of collagen-DNA complex. *International journal of biological macromolecules*, 35, pp.39–46.

Keenan, S. W. et al. (2015). Evaluating the consequences of diagenesis and fossilization on bioapatite lattice structure and composition. *Chemical geology*, 413, pp.18–27. [Online]. Available at: doi:10.1016/j.chemgeo.2015.08.005.

Keenan, S. W. and Engel, A. S. (2017). Early diagenesis and recrystallization of bone. *Geochimica et cosmochimica acta*, 196, pp.209–223. [Online]. Available at: doi:10.1016/j.gca.2016.09.033.

Keenan, S. W., Engel, A. S. and Elsey, R. M. (2013). The alligator gut microbiome and implications for archosaur symbioses. *Scientific reports*, 3, p.2877. [Online]. Available at: doi:10.1038/srep02877.

Keene, R. and Sakai, Y. (1991). Human bone contains type III collagen, type VI collagen, and fibrillin: Type III collagen is present on specific fibers that may mediate attachment of tendons, ligaments, and periosteum to calcified bone cortex. *Planning perspectives: PP*, 59, p.69.

Kendall, C. et al. (2018). Diagenesis of archaeological bone and tooth. *Palaeogeography, palaeoclimatology, palaeoecology*, 491, pp.21–37. [Online]. Available at: doi:10.1016/j.palaeo.2017.11.041.

King, C. L., Tayles, N. and Gordon, K. C. (2011). Re-examining the chemical evaluation of diagenesis in human bone apatite. *Journal of archaeological science*, 38 (9), pp.2222–2230. [Online]. Available at: doi:10.1016/j.jas.2011.03.023.

Kini, U. and Nandeesh, B. N. (2012). Physiology of bone formation, remodeling, and metabolism. In: Fogelman, I., Gnanasegaran, G. and van der Wall, H. (Eds). *Radionuclide and hybrid bone imaging*. Springer. pp.29–57. [Online]. Available at: doi:10.1007/978-3-642-02400-9_2 [Accessed 25 May 2017].

Kitamura, H. et al. (1997). Marked effect of DNA on collagen fibrillogenesis in vitro. *International journal of biological macromolecules*, 20, pp.241–244.

Klug, W. S. et al. (2012). *Concepts of genetics*. Pearson Education. [Online]. Available at: https://market.android.com/details?id=book-GL5zpwAACAAJ.

Kollmannsberger, P. et al. (2017). The small world of osteocytes: connectomics of the lacuno-canalicular network in bone. *New journal of physics*, 19 (7), IOP Publishing., p.073019. [Online]. Available at: doi:10.1088/1367-2630/aa764b [Accessed 16 May 2018].

Komori, T. (2013). Functions of the osteocyte network in the regulation of bone mass. *Cell and tissue research*, 352 (2), pp.191–198. [Online]. Available at: doi:10.1007/s00441-012-1546-x.

Kontopoulos, I. (2014). *Experimental histotaphonomy: Decoding diagenetic alterations in bone*. MSc, University of Sheffield, Sheffield, United Kingdom.

Kontopoulos, I. et al. (2018). Preparation of bone powder for FTIR-ATR analysis: The particle size effect. *Vibrational spectroscopy*, 99, pp.167–177. [Online]. Available at: doi:10.1016/j.vibspec.2018.09.004.

Kontopoulos, I., Nystrom, P. and White, L. (2016). Experimental taphonomy: Post-mortem microstructural modifications in Sus scrofa domesticus bone. *Forensic science international*, 266, pp.320–328. [Online]. Available at: doi:10.1016/j.forsciint.2016.06.024.

Koon, H. E. C., Nicholson, R. A. and Collins, M. J. (2003). A practical approach to the identification of low temperature heated bone using TEM. *Journal of archaeological science*, 30, pp.1393–1399. [Online]. Available at: doi:10.1016/S0305-4403(03)00034-7.

Koon, H. E. C., O'Connor, T. P. and Collins, M. J. (2010). Sorting the butchered from the boiled. *Journal of archaeological science*, 37 (1), pp.62–69. [Online]. Available at: doi:10.1016/j.jas.2009.08.015.

Kus, S., Marczenko, Z. and Obarski, N. (1996). Derivative UV-VIS spectrophotometry in analytical chemistry. *Chemia analityczna* (Warsaw), 41 (6), pp.899-929.

Lam, Y. M., Chen, X. and Pearson, O. M. (1999). Intertaxonomic variability in patterns of bone density and the differential representation of bovid, cervid, and equid elements in the archaeological record. *American antiquity*, 64 (2), pp.343–362. [Online]. Available at: doi:10.2307/2694283.

Lander, S. L., Brits, D. and Hosie, M. (2014). The effects of freezing, boiling and degreasing on the microstructure of bone. *Homo*, 65 (2), pp.131–142. [Online]. Available at: doi:10.1016/j.jchb.2013.09.006.

Landis, W. J. (1995). The strength of a calcified tissue depends in part on the molecular structure and organization of its constituent mineral crystals in their organic matrix. *Bone*, 16 (5), pp.533–544. [Online]. Available at: https://www.ncbi.nlm.nih.gov/pubmed/7654469.

Landis, W. J. and Jacquet, R. (2013). Association of calcium and phosphate ions with collagen in the mineralization of vertebrate tissues. *Calcified tissue international*, 93 (4), pp.329–337. [Online]. Available at: doi:10.1007/s00223-013-9725-7.

Lazarev, Y. A., Grishkovsky, B. A. and Khromova, T. B. (1985). Amide I band of IR spectrum and structure of collagen and related polypeptides. *Biopolymers*, 24 (8), pp.1449–1478. [Online]. Available at: doi:10.1002/bip.360240804.

Lebon, M. et al. (2010). New parameters for the characterization of diagenetic alterations and heat-induced changes of fossil bone mineral using Fourier transform infrared spectrometry. *Journal of archaeological science*, 37 (9), pp.2265–2276. [Online]. Available at: doi:10.1016/j.jas.2010.03.024.

Lebon, M. et al. (2011). Imaging fossil bone alterations at the microscale by SR-FTIR microspectroscopy. *Journal of analytical atomic spectrometry*, 26 (5), p.922. [Online]. Available at: doi:10.1039/c0ja00250j.

Lebon, M. et al. (2016). Rapid quantification of bone collagen content by ATR-FTIR spectroscopy. *Radiocarbon*, 58 (1), pp.131–145. [Online]. Available at: doi:10.1017/RDC.2015.11.

Lee Goff, M. (1992). Problems in estimation of postmortem interval resulting from wrapping of the corpse: A case study from Hawai'i. *Journal of agricultural entomology*, 9 (4), pp.237–243.

[Online]. Available at: http://scentsoc.org/Volumes/JAE/v9/4/00094237.pdf.

Lee–Thorp, J. (2002). Two decades of progress towards understanding fossilization processes and isotopic signals in calcified tissue minerals. *Archaeometry*, 44 (3), pp.435–446. [Online]. Available at: doi:10.1111/1475-4754.t01-1-00076.

Lee-Thorp, J. A. (2008). On isotopes and old bones. *Archaeometry*, 50 (6), pp.925–950. [Online]. Available at: doi:10.1111/j.1475-4754.2008.00441.x.

Lee-Thorp, J. A. and van der Merwe, N. J. (1991). Aspects of the chemistry of modern and fossil biological apatites. *Journal of archaeological science*, 18 (3), pp.343–354. [Online]. Available at: doi:10.1016/0305-4403(91)90070-6.

Lee-Thorp, J., Sealy, J. C. and van der Merwe, N. J. (1989). Stable carbon isotope ratio differences between bone collagen and bone apatite and their relationship to diet. *Journal of archaeological science*, 16, pp.585–599.

LeGeros, R. Z. (1965). Effect of carbonate on the lattice parameters of apatite. *Nature*, 206, p.403. [Online]. Available at: doi:10.1038/206403a0.

LeGeros, R. Z. et al. (1967). Apatite crystallites: Effects of carbonate on morphology. *Science*, 155 (3768), pp.1409–1411. [Online]. Available at: doi:10.1126/science.155.3768.1409.

LeGeros, R. Z. et al. (1969). Two types of carbonate substitution in the apatite structure. *Experientia*, 25 (1), pp.5–7. [Online]. Available at: doi:10.1007/BF01903856 [Accessed 17 January 2018].

LeGeros, R. Z. (1981). Apatites in biological systems. *Progress in crystal growth and characterization of materials*, 4 (1), Pergamon., pp.1–45.

Leng, H. et al. (2013). Effect of age on mechanical properties of the collagen phase in different orientations of human cortical bone. *Bone*, 55 (2), pp.288–291. [Online]. Available at: doi:10.1016/j.bone.2013.04.006.

Leventouri, T. (2006). Synthetic and biological hydroxyapatites: Crystal structure questions. *Biomaterials*, 27 (18), pp.3339–3342. [Online]. Available at: doi:10.1016/j.biomaterials.2006.02.021.

Light, N. and Bailey, A. J. (1985). Collagen cross-links: Location of pyridinoline in type I collagen. *FEBS letters*, 182 (2), pp.503–508. [Online]. Available at: doi:10.1016/0014-5793(85)80363-X.

Lindahl, T. (1993). Instability and decay of the primary structure of DNA. *Nature*, 362 (6422), pp.709–715. [Online]. Available at: doi:10.1038/362709a0.

Lindahl, T. (1996). The Croonian lecture, 1996: Endogenous damage to DNA. *Philosophical transactions of the royal society of London. Series B, Biological sciences*, 351 (1347), pp.1529–1538. [Online]. Available at: doi:10.1098/rstb.1996.0139.

Lindahl, T. and Nyberg, B. (1972). Rate of depurination of native deoxyribonucleic acid. *Biochemistry*, 11, pp.3610–3618.

Linderholm, A. (2016). Ancient DNA: The next generation – chapter and verse. *Biological journal of the Linnean Society. Linnean Society of London*, 117 (1), pp.150–160. [Online]. Available at: doi:10.1111/bij.12616.

Longin, R. (1971). New method of collagen extraction for radiocarbon dating. *Nature*, 230 (5291), pp.241–242. [Online]. Available at: https://www.ncbi.nlm.nih.gov/pubmed/4926713.

Luce, R. D. (2013). *Sound and hearing: A conceptual introduction*. Psychology Press. [Online]. Available at: https://www.taylorfrancis.com/books/9781317759805.

Mackie, E. J. et al. (2008). Endochondral ossification: how cartilage is converted into bone in the developing skeleton. *The international journal of biochemistry & cell biology*, 40 (1), pp.46–62. [Online]. Available at: doi:10.1016/j.biocel.2007.06.009.

Madupalli, H., Pavan, B. and Tecklenburg, M. M. J. (2017). Carbonate substitution in the mineral component of bone: Discriminating the structural changes, simultaneously imposed by carbonate in A and B sites of apatite. *Journal of solid state chemistry*, 255, pp.27–35. [Online]. Available at: doi:10.1016/j.jssc.2017.07.025.

Maggiano, C. et al. (2006). Spectral and photobleaching analysis using confocal laser scanning microscopy: a comparison of modern and archaeological bone fluorescence. *Molecular and cellular probes*, 20 (3-4), pp.154–162. [Online]. Available at: doi:10.1016/j.mcp.2005.11.009.

Mahamid, J. et al. (2008). Amorphous calcium phosphate is a major component of the forming fin bones of zebrafish: Indications for an amorphous precursor phase. *Proceedings of the national academy of sciences of the United States of America*, 105 (35), pp.12748–12753. [Online]. Available at: doi:10.1073/pnas.0803354105.

Mahamid, J. et al. (2010). Mapping amorphous calcium phosphate transformation into crystalline mineral from the cell to the bone in zebrafish fin rays. *Proceedings of the national academy of sciences of the United States of America*, 107 (14), pp.6316–6321. [Online]. Available at: doi:10.1073/pnas.0914218107.

Mahamid, J. et al. (2011). Bone mineralization proceeds through intracellular calcium phosphate loaded vesicles: A cryo-electron microscopy study. *Journal of structural biology*, 174 (3), pp.527–535. [Online]. Available at: doi:10.1016/j.jsb.2011.03.014.

Mamede, A. P. et al. (2018). Burned bones tell their own stories: A review of methodological approaches to assess heat-induced diagenesis. *Applied Spectroscopy Reviews*, 53 (8), pp.603–635. [Online]. Available at: doi:10.1080/05704928.2017.1400442.

Marchiafava, V., Bonucci, E. and Ascenzi, A. (1974). Fungal osteoclasia: A model of dead bone resorption. *Calcified tissue research*, 14 (3), pp.195–210. [Online]. Available at: http://www.ncbi.nlm.nih.gov/pubmed/4843788.

Mark, H. and Workman, J. Jr. (2003). Derivatives in spectroscopy: part III — computing the derivative. *Spectroscopy*, 18 (12), pp.106–111.

Martiniaková, M. et al. (2006). Differences among species in compact bone tissue microstructure of mammalian skeleton: Use of a discriminant function analysis for species identification. *Journal of forensic sciences*, 51 (6), pp.1235–1239. [Online]. Available at: doi:10.1111/j.1556-4029.2006.00260.x.

Martiniaková, M. et al. (2007). Histological study of compact bone tissue in some mammals: a method for species determination. *International journal of osteoarchaeology*, 17 (1), pp.82–90. [Online]. Available at: doi:10.1002/oa.856.

Martin, R. B. et al. (2015). *Skeletal tissue mechanics*. 2nd ed. Springer. [Online]. Available at: doi:10.1007/978-1-4939-3002-9.

Masters, P. M. (1987). Preferential preservation of noncollagenous protein during bone diagenesis: Implications for chronometric and stable isotopic measurements. *Geochimica et cosmochimica acta*, 51 (12), pp.3209–3214. [Online]. Available at: doi:10.1016/0016-7037(87)90129-3.

Maurer, A.-F. et al. (2014). Bone diagenesis in arid environments: An intra-skeletal approach. *Palaeogeography, palaeoclimatology, palaeoecology*, 416, pp.17–29. [Online]. Available at: doi:10.1016/j.palaeo.2014.08.020.

Mazzoni, A. (1972). Internal auditory artery supply to the petrous bone. *The Annals of otology, rhinology, and laryngology*, 81 (1), pp.13–21. [Online]. Available at: doi:10.1177/000348947208100103.

McClure, S. B. et al. (2011). Osteological and paleodietary investigation of burials from Cova de la Pastora, Alicante, Spain. *Journal of archaeological science*, 38 (2), pp.420–428. [Online]. Available at: doi:10.1016/j.jas.2010.09.023.

Memorang. *Bone (MSK) Flashcards*. [Online]. Available at: https://www.memorangapp.com/flashcards/194089/Bone/ [Accessed 14 September 2018].

Meneghini, C. et al. (2003). Rietveld refinement on x-ray diffraction patterns of bioapatite in human fetal bones. *Biophysical journal*, 84 (3), pp.2021–2029. [Online]. Available at: doi:10.1016/S0006-3495(03)75010-3.

Millard, A. R. (2001). Deterioration of bone. In: Brothwell, D R & Pollard, A M (Ed). *Handbook of archaeological sciences*. Wiley. pp.633–643.

Miszkiewicz, J. J. and Mahoney, P. (2016). Ancient human bone microstructure in medieval England: Comparisons between two socio-economic groups. *Anatomical record* , 299 (1), pp.42–59. [Online]. Available at: doi:10.1002/ar.23285.

Mitchell, D., Willerslev, E. and Hansen, A. (2005). Damage and repair of ancient DNA. *Mutation research*, 571 (1-2), pp.265–276. [Online]. Available at: doi:10.1016/j.mrfmmm.2004.06.060.

Moller, A. R. (2000). *Hearing: Its physiology and pathophysiology*. Academic Press. [Online]. Available at: https://market.android.com/details?id=book-fUDt6dXQY4YC.

Moussa, M. and Nasr, M. (2012). Histological analysis of the newly formed bone secondary to distraction osteogenesis of the mandible in goat. In: Rivas-Echeverria, C. and Carranca, C. (Eds). *Recent researches in medicine and medical chemistry*. 2012. WSEAS Press. pp.80–88. [Online]. Available at: http://www.wseas.us/e-library/conferences/2012/Kos/MEDICAL/MEDICAL-11.pdf.

Moustris, A. and Petrou, J. (2018). *Weather forecast for Greece*. [Online]. Available at: http://www.meteo.gr/index-en.cfm [Accessed 16 October 2018].

Mulhern, D. M. and Ubelaker, D. H. (2001). Differences in osteon banding between human and nonhuman bone. *Journal of forensic sciences*, 46 (2), pp.220–222. [Online]. Available at: https://www.ncbi.nlm.nih.gov/pubmed/11305421.

Müller, K. et al. (2011). Microbial attack of archaeological bones versus high concentrations of heavy metals in the burial environment. A case study of animal bones from a mediaeval copper workshop in Paris. *Palaeogeography, palaeoclimatology, palaeoecology*, 310 (1–2), pp.39–51. [Online]. Available at: doi:10.1016/j.palaeo.2011.03.023.

Nagaoka, T. and Kawakubo, Y. (2015). Using the petrous part of the temporal bone to estimate fetal age at death. *Forensic science international*, 248, pp.188.e1–e7. [Online]. Available at: doi:10.1016/j.forsciint.2015.01.009.

Nair, A. K. et al. (2013). Molecular mechanics of mineralized collagen fibrils in bone. *Nature communications*, 4, p.1724. [Online]. Available at: doi:10.1038/ncomms2720.

Nemzek, W. R. et al. (1996). Imaging findings of the developing temporal bone in fetal specimens. *American journal of neuroradiology*, 17 (8), pp.1467–1477. [Online]. Available at: https://www.ncbi.nlm.nih.gov/pubmed/8883642.

Neuman, W. F. and Neuman, M. W. (1953). The nature of the mineral phase of bone. *Chemical reviews*, 53 (1), pp.1–45. [Online]. Available at: doi:10.1021/cr60164a001.

Nielsen-Marsh, C. et al. (2000a). The chemical degradation of bone. In: Cox, M. and Mays, S. (Eds). *Human osteology: In archaeology and forensic science*. Cambridge University Press. pp.439–454. [Online]. Available at: http://eprints.soton.ac.uk/394456/ [Accessed 20 September 2016].

Nielsen-Marsh, C. M. et al. (2000b). A preliminary investigation of the application of differential scanning calorimetry to the study of collagen degradation in archaeological bone. *Thermochimica acta*, 365, pp.129–139.

Nielsen-Marsh, C. M. et al. (2002). Sequence preservation of osteocalcin protein and mitochondrial DNA in bison bones older than 55 ka. *Geology*, 30 (12), pp.1099–1102.

Nielsen-Marsh, C. M. and Hedges, R. E. M. (2000a). Patterns of diagenesis in bone I: The effects of site environments. *Journal of archaeological science*, 27 (12), pp.1139–1150. [Online]. Available at: doi:10.1006/jasc.1999.0537.

Nielsen-Marsh, C. M. and Hedges, R. E. M. (2000b). Patterns of diagenesis in bone II: effects of acetic acid treatment and the removal of diagenetic CO_3^{2-}. *Journal of archaeological science*, 27 (12), pp.1151–1159. [Online]. Available at: doi:10.1006/jasc.1999.0538.

Noble, B. S. (2008). The osteocyte lineage. *Archives of biochemistry and biophysics*, 473 (2), pp.106–111. [Online]. Available at: doi:10.1016/j.abb.2008.04.009.

Nyman, J. S. et al. (2006). Age-related effect on the concentration of collagen crosslinks in human osteonal and interstitial bone tissue. *Bone*, 39 (6), pp.1210–1217. [Online]. Available at: doi:10.1016/j.bone.2006.06.026.

Olesiak, S. E. et al. (2010). Nanomechanical properties of modern and fossil bone. *Palaeogeography, palaeoclimatology, palaeoecology*, 289 (1-4), pp.25–32. [Online]. Available at: doi:10.1016/j.palaeo.2010.02.006.

Orlando, L. and Cooper, A. (2014). Using Ancient DNA to Understand Evolutionary and Ecological Processes. *Annual review of ecology, evolution, and systematics*, 45 (1), pp.573–598. [Online]. Available at: doi:10.1146/annurev-ecolsys-120213-091712.

Ortner, D. J. and Turner-Walker, G. (2002). The biology of skeletal tissues. In: Ortner, D. J. (Ed). *Identification of pathological conditions in human skeletal remains*. 2nd ed. Elsevier. pp.11–35. [Online]. Available at: doi:10.1016/B978-0-12-528628-2.X5037-6.

Osipov, B. et al. (2013). Sexual dimorphism of the bony labyrinth: A new age-independent method. *American journal of physical anthropology*, 151 (2), pp.290–301. [Online]. Available at: doi:10.1002/ajpa.22279.

Ottani, V. et al. (2002). Hierarchical structures in fibrillar collagens. *Micron* , 33 (7-8), pp.587–596. [Online]. Available at: https://www.ncbi.nlm.nih.gov/pubmed/12475555.

Ottoni, C. et al. (2009). Preservation of ancient DNA in thermally damaged archaeological bone. *Die Naturwissenschaften*, 96 (2), pp.267–278. [Online]. Available at: doi:10.1007/s00114-008-0478-5.

Ou-Yang, H. et al. (2001). Infrared microscopic imaging of bone: Spatial distribution of CO_3^{2-}.

Journal of bone and mineral research, 16 (5), pp.893–900. [Online]. Available at: doi:10.1359/jbmr.2001.16.5.893.

Oxlund, H., Mosekilde, L. and Ortoft, G. (1996). Reduced concentration of collagen reducible cross links in human trabecular bone with respect to age and osteoporosis. *Bone*, 19 (5), pp.479–484. [Online]. Available at: https://www.ncbi.nlm.nih.gov/pubmed/8922646.

Pääbo, S. (1989). Ancient DNA: extraction, characterization, molecular cloning, and enzymatic amplification. *Proceedings of the national academy of sciences of the United States of America*, 86 (6), pp.1939–1943. [Online]. Available at: https://www.ncbi.nlm.nih.gov/pubmed/2928314.

Pääbo, S. et al. (2004). Genetic analyses from ancient DNA. *Annual review of genetics*, 38 (1), pp.645–679. [Online]. Available at: doi:10.1146/annurev.genet.37.110801.143214.

Parker Pearson, M. et al. (2005). Evidence for mummification in Bronze Age Britain. *Antiquity*, 79, pp.529–546. [Online]. Available at: https://www-cambridge-org.libproxy.york.ac.uk/core/services/aop-cambridge-core/content/view/E9B55A7BBEE01E4BA90B58911C9C370D/S0003598X00114486a.pdf/evidence_for_mummification_in_bronze_age_britain.pdf.

Parsons, T. and Weedn, V. W. (2006). Preservation and recovery of DNA in postmortem specimens and trace samples. In: Haglund, W. and Sorg, M. (Eds). *Forensic taphonomy: the postmortem fate of human remains*. CRC Press. pp.109–138.

Paschalis, E. P. et al. (1996). FTIR microspectroscopic analysis of human osteonal bone. *Calcified tissue international*, 59 (6), pp.480–487. [Online]. Available at: http://www.ncbi.nlm.nih.gov/pubmed/8939775.

Paschalis, E. P. et al. (2001). Spectroscopic characterization of collagen cross-links in bone. *Journal of bone and mineral research*, 16 (10), pp.1821–1828. [Online]. Available at: doi:10.1359/jbmr.2001.16.10.1821.

Pasteris, J. D. et al. (2004). Lack of OH in nanocrystalline apatite as a function of degree of atomic order: implications for bone and biomaterials. *Biomaterials*, 25 (2), pp.229–238. [Online]. Available at: doi:10.1016/S0142-9612(03)00487-3.

Pate, F. D., Hutton, J. T. and Norrish, K. (1989). Ionic exchange between soil solution and bone: toward a predictive model. *Applied geochemistry*, 4, pp.303–316.

Penkman, K. E. H. et al. (2011). A chronological framework for the British Quaternary based on Bithynia opercula. *Nature*, 476 (7361), pp.446–449. [Online]. Available at: doi:10.1038/nature10305.

Person, A. et al. (1995). Early diagenetic evolution of bone phosphate: An X-ray diffractometry analysis. *Journal of archaeological science*, 22, pp.211–221.

Person, A. et al. (1996). Diagenetic evolution and experimental heating of bone phosphate. *Palaeogeography, palaeoclimatology, palaeoeeology*, 126, pp.135–149. [Online]. Available at: https://ac-els-cdn-com.libproxy.york.ac.uk/S0031018297889067/1-s2.0-S0031018297889067-main.pdf?_tid=7f25a25c-2f3d-4506-a5cb-aafa217acfce&acdnat=1526427541_816de83888560752fcbd74257c9cd672.

Pesquero, M. D. et al. (2015). Bacterial origin of iron-rich microspheres in Miocene mammalian fossils. *Palaeogeography, palaeoclimatology, palaeoecology*, 420, pp.27–34. [Online]. Available at: doi:10.1016/j.palaeo.2014.12.006.

Pestle, W. J. and Colvard, M. (2012). Bone collagen preservation in the tropics: A case study from ancient Puerto Rico. *Journal of archaeological science*, 39 (7), pp.2079–2090. [Online].

Available at: doi:10.1016/j.jas.2012.03.008.

Petruska, J. A. and Hodge, A. J. (1964). A subunit model for the tropocollagen macromolecule. *Proceedings of the national academy of sciences of the United States of America*, 51, pp.871–876. [Online]. Available at: https://pdfs.semanticscholar.org/975a/da953d5e0b42dd9494d7510100c45f488a66.pdf.

Pfretzschner, H.-U. (2004). Fossilization of Haversian bone in aquatic environments. *Comptes rendus. Palevol*, 3 (6–7), pp.605–616. [Online]. Available at: doi:10.1016/j.crpv.2004.07.006.

Pfretzschner, H.-U. and Tütken, T. (2011). Rolling bones – Taphonomy of Jurassic dinosaur bones inferred from diagenetic microcracks and mineral infillings. *Palaeogeography, palaeoclimatology, palaeoecology*, 310 (1–2), pp.117–123. [Online]. Available at: doi:10.1016/j.palaeo.2011.01.026.

Piepenbrink, H. (1986). Two examples of biogenous dead bone decomposition and their consequences for taphonomic interpretation. *Journal of archaeological science*, 13 (5), pp.417–430. [Online]. Available at: doi:10.1016/0305-4403(86)90012-9.

Piepenbrink, H. (1989). Examples of chemical changes during fossilisation. *Applied geochemistry*, 4 (3), pp.273–280. [Online]. Available at: doi:10.1016/0883-2927(89)90029-2.

Piez, K. A. and Miller, A. (1974). The structure of collagen fibrils. *Journal of supramolecular structure*, 2 (2-4), pp.121–137. [Online]. Available at: doi:10.1002/jss.400020207.

Piga, G. et al. (2011). A multi-technique approach by XRD, XRF, FT-IR to characterize the diagenesis of dinosaur bones from Spain. *Palaeogeography, palaeoclimatology, palaeoecology*, 310 (1), pp.92–107. [Online]. Available at: doi:10.1016/j.palaeo.2011.05.018.

Piga, G. et al. (2016). Understanding the crystallinity indices behavior of burned bones and teeth by ATR-IR and XRD in the presence of bioapatite mixed with other phosphate and carbonate phases. *International journal of spectroscopy*, 2016, [Online]. Available at: doi:10.1155/2016/4810149 [Accessed 29 November 2017].

Pinhasi, R. et al. (2015). Optimal ancient DNA yields from the inner ear part of the human petrous bone. *PloS one*, 10 (6), p.e0129102. [Online]. Available at: doi:10.1371/journal.pone.0129102.

Pleshko, N., Boskey, A. and Mendelsohn, R. (1991). Novel infrared spectroscopic method for the determination of crystallinity of hydroxyapatite minerals. *Biophysical journal*, 60 (4), pp.786–793. [Online]. Available at: doi:10.1016/S0006-3495(91)82113-0.

Poinar, H. N. et al. (1996). Amino acid racemization and the preservation of ancient DNA. *Science*, 272 (5263), pp.864–866. [Online]. Available at: https://www.ncbi.nlm.nih.gov/pubmed/8629020.

Poinar, H. N. (2003). The top 10 list: criteria of authenticity for DNA from ancient and forensic samples. *International congress series / Excerpta Medica*, 1239, pp.575–579. [Online]. Available at: doi:10.1016/s0531-5131(02)00624-6.

Poinar, H. N. and Stankiewicz, B. A. (1999). Protein preservation and DNA retrieval from ancient tissues. *Proceedings of the national academy of sciences of the United States of America*, 96 (15), pp.8426–8431. [Online]. Available at: https://www.ncbi.nlm.nih.gov/pubmed/10411891.

Pokines, J. T. et al. (2016). The effects of experimental freeze-thaw cycles to bone as a component of subaerial weathering. *Journal of archaeological science: Reports*, 6, pp.594–602. [Online]. Available at: http://www.sciencedirect.com/science/article/pii/S2352409X16300931.

Ponce de León, M. S. et al. (2018). Human bony labyrinth is an indicator of population history and dispersal from Africa. *Proceedings of the national academy of sciences of the United States of America*, 115 (16), pp.4128–4133. [Online]. Available at: doi:10.1073/pnas.1717873115.

Posner, A. S. (1985). The structure of bone apatite surfaces. *Journal of biomedical materials research*, 19 (3), pp.241–250. [Online]. Available at: doi:10.1002/jbm.820190307.

Prats-Muñoz, G. et al. (2013). Human soft tissue preservation in the Cova des Pas site (Minorca Bronze Age). *Journal of archaeological science*, 40 (12), pp.4701–4710. [Online]. Available at: doi:10.1016/j.jas.2013.07.022.

Pruvost, M. et al. (2007). Freshly excavated fossil bones are best for amplification of ancient DNA. *Proceedings of the national academy of sciences of the United States of America*, 104 (3), pp.739–744. [Online]. Available at: doi:10.1073/pnas.0610257104.

Pruvost, M. et al. (2008). DNA diagenesis and palaeogenetic analysis: Critical assessment and methodological progress. *Palaeogeography, palaeoclimatology, palaeoecology*, 266 (3–4), pp.211–219. [Online]. Available at: doi:10.1016/j.palaeo.2008.03.041.

Quattropani, L. et al. (1999). Early Palaeolithic bone diagenesis in the Arago cave at Tautavel, France. *Mineralogical magazine*, 63 (6), pp.801–812.

Ramsey, C. B. et al. (2004). Improvements to the pretreatment of bone at Oxford. *Radiocarbon*, 46 (1), pp.155–163. [Online]. Available at: doi:10.1017/S0033822200039473 [Accessed 1 December 2018].

Raven, P. H. et al. (2016). *Biology*. McGraw-Hill Education. [Online]. Available at: https://market.android.com/details?id=book-VJxLjwEACAAJ.

Regev, L. et al. (2010). Distinguishing between calcites formed by different mechanisms using infrared spectrometry: Archaeological applications. *Journal of archaeological science*, 37 (12), pp.3022–3029. [Online]. Available at: doi:10.1016/j.jas.2010.06.027.

Reiche, I. et al. (2003). A multi-analytical study of bone diagenesis: The Neolithic site of Bercy (Paris, France). *Measurement science and technology*, 14 (9), p.1608. [Online]. Available at: http://stacks.iop.org/0957-0233/14/i=9/a=312.

Reiche, I. et al. (2011). Towards a better understanding of alteration phenomena of archaeological bone by a closer look at the organic/mineral association at micro-and nanoscale. Preliminary results on Neolithic samples from Chalain lake site 19, Jura, France. *ArcheoSciences. Revue d'archéométrie*, (35), pp.143–158. [Online]. Available at: https://journals.openedition.org/archeosciences/3075.

Reiche, I., Vignaud, C. and Menu, M. (2002). The crystallinity of ancient bone and dentine: New insights by transmission electron microscopy. *Archaeometry*, 44 (3), pp.447–459. [Online]. Available at: doi:10.1111/1475-4754.00077.

van der Rest, M. and Garrone, R. (1991). Collagen family of proteins. *FASEB J.*, 5 (13), pp.2814–2823. [Online]. Available at: https://www.ncbi.nlm.nih.gov/pubmed/1916105.

Rey, C. et al. (1989). The carbonate environment in bone mineral: A resolution-enhanced Fourier Transform Infrared Spectroscopy Study. *Calcified tissue international*, 45 (3), pp.157–164. [Online]. Available at: https://www.ncbi.nlm.nih.gov/pubmed/2505907.

Rey, C. et al. (2007). Physico-chemical properties of nanocrystalline apatites: Implications for biominerals and biomaterials. *Materials science and engineering: C*, 27 (2), pp.198–205. [Online]. Available at: doi:10.1016/j.msec.2006.05.015.

Reznikov, N. et al. (2015). The 3D structure of the collagen fibril network in human trabecular bone: relation to trabecular organization. *Bone*, 71, pp.189–195. [Online]. Available at: doi:10.1016/j.bone.2014.10.017.

Reznikov, N., Shahar, R. and Weiner, S. (2014a). Bone hierarchical structure in three dimensions. *Acta biomaterialia*, 10 (9), pp.3815–3826. [Online]. Available at: doi:10.1016/j.actbio.2014.05.024.

Reznikov, N., Shahar, R. and Weiner, S. (2014b). Three-dimensional structure of human lamellar bone: The presence of two different materials and new insights into the hierarchical organization. *Bone*, 59, pp.93–104. [Online]. Available at: doi:10.1016/j.bone.2013.10.023.

Rho, J. Y. et al. (1999). Variations in the individual thick lamellar properties within osteons by nanoindentation. *Bone*, 25 (3), pp.295–300. [Online]. Available at: http://www.ncbi.nlm.nih.gov/pubmed/10495133.

Rho, J. Y. et al. (2001). The anisotropic Young's modulus of equine secondary osteones and interstitial bone determined by nanoindentation. *The Journal of experimental biology*, 204 (Pt 10), pp.1775–1781. [Online]. Available at: https://www.ncbi.nlm.nih.gov/pubmed/11316498.

Rho, J. Y. et al. (2002). Microstructural elasticity and regional heterogeneity in human femoral bone of various ages examined by nano-indentation. *Journal of biomechanics*, 35 (2), pp.189–198. [Online]. Available at: https://www.ncbi.nlm.nih.gov/pubmed/11784537.

Ricard-Blum, S. (2011). The collagen family. *Cold Spring Harbor perspectives in biology*, 3 (1), p.a004978. [Online]. Available at: doi:10.1101/cshperspect.a004978.

Ricard-Blum, S. and Ruggiero, F. (2005). The collagen superfamily: From the extracellular matrix to the cell membrane. *Pathologie et biologie*, 53 (7), pp.430–442. [Online]. Available at: doi:10.1016/j.patbio.2004.12.024.

Richard, C. et al. (2010). New insight into the bony labyrinth: A microcomputed tomography study. *Auris, nasus, larynx*, 37 (2), pp.155–161. [Online]. Available at: doi:10.1016/j.anl.2009.04.014.

Roberts, S. J. et al. (2002). The taphonomy of cooked bone: Characterizing boiling and its physico-chemical effects. *Archaeometry*, 44, pp.485–494.

Robinson, N. E. and Robinson, A. B. (2001). Deamidation of human proteins. *Proceedings of the national academy of sciences of the United States of America*, 98 (22), pp.12409–12413. [Online]. Available at: doi:10.1073/pnas.221463198.

Rogers, K. D. and Zioupos, P. (1999). The bone tissue of the rostrum of a Mesoplodon Densirostris whale: A mammalian biomineral demonstrating extreme texture. *Journal of materials science letters*, 18, pp.651–654.

Ross, M. H. and Pawlina, W. (2011). *Histology: A text and atlas with correlated cell and molecular biology*. Wolters Kluwer/Lippincott Williams & Wilkins Health. [Online]. Available at: https://market.android.com/details?id=book-R65WDwAAQBAJ.

Rubin, M. A. et al. (2003). TEM analysis of the nanostructure of normal and osteoporotic human trabecular bone. *Bone*, 33 (3), pp.270–282. [Online]. Available at: doi:10.1016/S8756-3282(03)00194-7.

Saito, M. and Marumo, K. (2010). Collagen cross-links as a determinant of bone quality: a possible explanation for bone fragility in aging, osteoporosis, and diabetes mellitus. *Osteoporosis international*, 21 (2), pp.195–214. [Online]. Available at: doi:10.1007/s00198-009-1066-z.

Saito, M. and Marumo, K. (2015). Effects of collagen crosslinking on bone material properties in health and disease. *Calcified tissue international*, 97 (3), pp.242–261. [Online]. Available at: doi:10.1007/s00223-015-9985-5.

Salesse, K. et al. (2014). Variability of bone preservation in a confined environment: The case of the catacomb of Sts Peter and Marcellinus (Rome, Italy). *Palaeogeography, palaeoclimatology, palaeoecology*, 416, pp.43–54. [Online]. Available at: doi:10.1016/j.palaeo.2014.07.021.

Schaefer, M., Black, S. M. and Scheuer, L. (2009). *Juvenile osteology: a laboratory and field manual*. Elsevier, Academic Press.

Schafer, R. W. (2011). What is a Savitzky-Golay filter? [lecture notes]. *IEEE Signal Processing Magazine*, 28 (4), pp.111–117. doi: 10.1109/MSP.2011.941097.

Schaffler, M. B., Burr, D. B. and Frederickson, R. G. (1987). Morphology of the osteonal cement line in human bone. *The Anatomical record*, 217 (3), pp.223–228. [Online]. Available at: doi:10.1002/ar.1092170302.

Scheuer, L. and Black, S. (2000). *Developmental juvenile osteology*. Academic Press.

Schwartz, J. H. (2007). *Skeleton keys: An introduction to human skeletal morphology, development, and analysis*. Oxford University Press. [Online]. Available at: https://market.android.com/details?id=book-Y2xqQgAACAAJ.

Schweitzer, M. H. (2004). Molecular paleontology: some current advances and problems. *Annales de paléontologie*, 90 (2), pp.81–102. [Online]. Available at: doi:10.1016/j.annpal.2004.02.001.

Scorrano, G. et al. (2016). The tale of Henry VII: a multidisciplinary approach to determining the post-mortem practice. *Archaeological and anthropological sciences*, pp.1–8. [Online]. Available at: doi:10.1007/s12520-016-0321-4 [Accessed 11 April 2017].

Sealy, J. et al. (2014). Comparison of two methods of extracting bone collagen for stable carbon and nitrogen isotope analysis: comparing whole bone demineralization with gelatinization and ultrafiltration. *Journal of archaeological science*, 47, pp.64–69. [Online]. Available at: doi:10.1016/j.jas.2014.04.011.

Semal, P. and Orban, R. (1995). Collagen extraction from recent and fossil bones: Quantitative and qualitative aspects. *Journal of archaeological science*, 22 (4), pp.463–467. [Online]. Available at: doi:10.1006/jasc.1995.0045.

Senba, M., Kawai, K. and Mori, N. (2012). Pathogenesis of metastatic calcification and acute pancreatitis in adult T-cell leukemia under hypercalcemic state. *Leukemia research and treatment*, 2012, p.128617. [Online]. Available at: doi:10.1155/2012/128617.

Shin, J. Y. and Hedges, R. E. M. (2012). Diagenesis in bone and enamel apatite carbonate; the potential of density separation to assess the original composition. *Journal of archaeological science*, 39 (4), pp.1123–1130. [Online]. Available at: doi:10.1016/j.jas.2011.12.016.

Shoulders, M. D. and Raines, R. T. (2009). Collagen structure and stability. *Annual review of biochemistry*, 78, pp.929–958. [Online]. Available at: doi:10.1146/annurev.biochem.77.032207.120833.

Sillen, A. and Parkington, J. (1996). Diagenesis of Bones from Eland's Bay Cave. *Journal of archaeological science*, 23 (4), pp.535–542. [Online]. Available at: doi:10.1006/jasc.1996.0050.

Skedros, J. G. et al. (2005). Cement lines of secondary osteons in human bone are not mineral-

deficient: new data in a historical perspective. *The anatomical record. Part A, Discoveries in molecular, cellular, and evolutionary biology*, 286 (1), pp.781–803. [Online]. Available at: doi:10.1002/ar.a.20214.

Skedros, J. G., Grunander, T. R. and Hamrick, M. W. (2005). Spatial distribution of osteocyte lacunae in equine radii and third metacarpals: considerations for cellular communication, microdamage detection and metabolism. *Cells, tissues, organs*, 180 (4), pp.215–236. [Online]. Available at: doi:10.1159/000088938.

Skinner, H. C. W. (2013). Mineralogy of bones. In: Selinus, O. (Ed). *Essentials of medical geology: Revised edition*. Springer. pp.667–693. [Online]. Available at: doi:10.1007/978-94-007-4375-5_30.

Smith, C. I. et al. (2002). The strange case of Apigliano: early 'fossilization' of medieval bone in southern Italy. *Archaeometry*, 44 (3), pp.405–415. [Online]. Available at: doi:10.1111/1475-4754.t01-1-00073.

Smith, C. I. et al. (2005). Diagenesis and survival of osteocalcin in archaeological bone. *Journal of archaeological science*, 32 (1), pp.105–113. [Online]. Available at: doi:10.1016/j.jas.2004.07.003.

Smith, C. I. et al. (2007). Bone diagenesis in the European Holocene I: patterns and mechanisms. *Journal of archaeological science*, 34 (9), pp.1485–1493. [Online]. Available at: doi:10.1016/j.jas.2006.11.006.

Smith, J. W. (1960). Collagen fibre patterns in mammalian bone. *Journal of anatomy*, 94 (Pt 3), pp.329–344. [Online]. Available at: https://www.ncbi.nlm.nih.gov/pubmed/17105115.

Smith, M. J. et al. (2016). Holding on to the past: Southern British evidence for mummification and retention of the dead in the Chalcolithic and Bronze Age. *Journal of archaeological science: Reports*, 10, pp.744–756. [Online]. Available at: doi:10.1016/j.jasrep.2016.05.034.

Sørensen, M. S. (1994). Temporal bone dynamics, the hard way. Formation, growth, modeling, repair and quantum type bone remodeling in the otic capsule. *Acta oto-laryngologica. Supplementum*, 512, pp.1–22. [Online]. Available at: https://www.ncbi.nlm.nih.gov/pubmed/8191884.

Sørensen, M. S., Bretlau, P. and Jørgensen, M. B. (1990). Quantum type bone remodeling in the otic capsule of the pig. *Acta oto-laryngologica*, 110 (3-4), pp.217–223. [Online]. Available at: https://www.ncbi.nlm.nih.gov/pubmed/2239210.

Sørensen, M. S., Bretlau, P. and Jørgensen, M. B. (1992). Quantum type bone remodeling in the human otic capsule: Morphometric findings. *Acta oto-laryngologica*, 112 (sup496), pp.4–10. [Online]. Available at: doi:10.3109/00016489209136839.

Sørensen, M. S., Bretlau, P. and Josrgensen, M. B. (1992). Bone repair in the otic capsule of the rabbit. *Acta oto-laryngologica*, 112 (6), pp.968–975. [Online]. Available at: doi:10.3109/00016489209137497.

Sosa, C. et al. (2013). Association between ancient bone preservation and DNA yield: a multidisciplinary approach. *American journal of physical anthropology*, 151, pp.102–109.

Sponheimer, M. and Lee-Thorp, J. A. (1999). Alteration of enamel carbonate environments during fossilization. *Journal of archaeological science*, 26 (2), pp.143–150. [Online]. Available at: doi:10.1006/jasc.1998.0293.

Stathopoulou, E. T. et al. (2008). Bone diagenesis: New data from infrared spectroscopy and X-ray diffraction. *Palaeogeography, palaeoclimatology, palaeoecology*, 266 (3–4), pp.168–174.

[Online]. Available at: doi:10.1016/j.palaeo.2008.03.022.

Stevens, A. and Lowe, J. (2005). *Stevens & Lowe's human histology*. 3rd ed. Elsevier.

Stiner, M. C. et al. (1995). Differential burning, recrystallization, and fragmentation of archaeological bone. *Journal of archaeological science*, 22, pp.223–237.

Stiner, M. C. et al. (2001). Bone preservation in Hayonim cave (Israel): A macroscopic and mineralogical study. *Journal of archaeological science*, 28 (6), pp.643–659. [Online]. Available at: doi:10.1006/jasc.2000.0634.

Stock, S. R. (2015). The mineral–collagen interface in bone. *Calcified tissue international*, 97 (3), pp.262–280. [Online]. Available at: doi:10.1007/s00223-015-9984-6 [Accessed 13 September 2015].

Stout, S. D. (1978). Histological structure and its preservation in ancient bone. *Current anthropology*, 19, pp.601–604. [Online]. Available at: http://www.ncbi.nlm.nih.gov/pubmed/11630741.

Stout, S. D. and Teitelbaum, S. L. (1976). Histological analysis of undecalcified thin sections of archeological bone. *American journal of physical anthropology*, 44 (2), pp.263–269. [Online]. Available at: doi:10.1002/ajpa.1330440208.

Sun, D. Q. et al. (2018). Surgical management of tumors involving Meckel's cave and cavernous sinus: Role of an extended middle fossa and lateral sphenoidectomy approach. *Otology and neurotology*, 39 (1), pp.82–91. [Online]. Available at: doi:10.1097/MAO.0000000000001602.

Surovell, T. A. and Stiner, M. C. (2001). Standardizing infra-red measures of bone mineral crystallinity: An experimental approach. *Journal of archaeological science*, 28 (6), pp.633–642. [Online]. Available at: doi:10.1006/jasc.2000.0633.

Susini, A., Baud, C. A. and Lacotte, D. (1988). Bone apatite crystals alterations in Neolithic skeletons and their relations to burial practices and soil weathering. *Rivista di antropologia*, 66, pp.35–38.

Su, X. et al. (2003). Organization of apatite crystals in human woven bone. *Bone*, 32 (2), pp.150–162. [Online]. Available at: doi:10.1016/S8756-3282(02)00945-6.

Talsky, G. (1994). *Derivative spectrophotometry: low and higher order*. Wiley-VCH.

Termine, J. D. et al. (1973). Hydrazine-deproteinated bone mineral. *Calcified tissue research*, 12 (1), pp.73–90. [Online]. Available at: doi:10.1007/BF02013723.

Termine, J. D. and Posner, A. S. (1966). Infra-red determination of the percentage of crystallinity in apatitic calcium phosphates. *Nature*, 211 (5046), pp.268–270. [Online]. Available at: doi:10.1038/211268a0.

Teti, A. and Zallone, A. (2009). Do osteocytes contribute to bone mineral homeostasis? Osteocytic osteolysis revisited. *Bone*, 44 (1), pp.11–16. [Online]. Available at: doi:10.1016/j.bone.2008.09.017.

Thomas P. Gilbert, M. et al. (2005). Biochemical and physical correlates of DNA contamination in archaeological human bones and teeth excavated at Matera, Italy. *Journal of archaeological science*, 32 (5), pp.785–793. [Online]. Available at: doi:10.1016/j.jas.2004.12.008.

Thompson, T. J. U., Gauthier, M. and Islam, M. (2009). The application of a new method of Fourier transform infrared spectroscopy to the analysis of burned bone. *Journal of*

archaeological science, 36 (3), pp.910–914. [Online]. Available at: doi:10.1016/j.jas.2008.11.013.

Titorencu, I. et al. (2014). Osteoblast ontogeny and implications for bone pathology: An overview. *Cell and tissue research*, 355 (1), pp.23–33. [Online]. Available at: doi:10.1007/s00441-013-1750-3.

Tjelldén, A. K. E. et al. (2018). The pattern of human bone dissolution: A histological study of Iron Age warriors from a Danish wetland site. *International journal of osteoarchaeology.* 28 (4), pp.407-418. [Online]. Available at: https://onlinelibrary.wiley.com/doi/abs/10.1002/oa.2666.

Trueman, C. N. et al. (2008). Comparing rates of recrystallisation and the potential for preservation of biomolecules from the distribution of trace elements in fossil bones. *Comptes rendus. Palevol*, 7 (2–3), pp.145–158. [Online]. Available at: doi:10.1016/j.crpv.2008.02.006.

Trueman, C. N. (2013). Chemical taphonomy of biomineralized tissues. *Palaeontology*, 56 (3), pp.475–486. [Online]. Available at: doi:10.1111/pala.12041.

Trueman, C. N. G. et al. (2004). Mineralogical and compositional changes in bones exposed on soil surfaces in Amboseli National Park, Kenya: Diagenetic mechanisms and the role of sediment pore fluids. *Journal of archaeological science*, 31 (6), pp.721–739. [Online]. Available at: doi:10.1016/j.jas.2003.11.003.

Trueman, C. N. and Martill, D. M. (2002). The long–term survival of bone: The role of bioerosion. *Archaeometry*, 44 (3), pp.371–382. [Online]. Available at: doi:10.1111/1475-4754.t01-1-00070.

Trueman, C. N., Privat, K. and Field, J. (2008). Why do crystallinity values fail to predict the extent of diagenetic alteration of bone mineral? *Palaeogeography, palaeoclimatology, palaeoecology*, 266 (3–4), pp.160–167. [Online]. Available at: doi:10.1016/j.palaeo.2008.03.038.

Turban-Just, S. and Schramm, S. (1998). Stable carbon and nitrogen isotope ratios of individual amino acids give new insights into bone collagen degradation. *Bulletin de la Societe Geologique de France*, 169 (1), pp.109–114.

Turner, P. C. et al. (2005). *Molecular biology*, 3rd edition. Taylor and Francis. [Online]. Available at: https://market.android.com/details?id=book-6hGMQgAACAAJ.

Turner-Walker, G. (1999). Pyrite bone diagenesis in terrestrial sediments. *Bulletin of the geological society of Norfolk*, 48, pp.3–26.

Turner-Walker, G. et al. (2002). Sub-micron spongiform porosity is the major ultra-structural alteration occurring in archaeological bone. *International journal of osteoarchaeology*, 12 (6), pp.407–414. [Online]. Available at: doi:10.1002/oa.642.

Turner-Walker, G. (2008). The chemical and microbial degradation of bones and teeth. In: Pinhasi, R. and Mays, S. (Eds). *Advances in human palaeopathology*. John Wiley & Sons. pp.3–29.

Turner-Walker, G. (2012). Early bioerosion in skeletal tissues: persistence through deep time. *Neues jahrbuch für geologie und paläontologie - abhandlungen*, 265 (2), pp.165–183. [Online]. Available at: doi:10.1127/0077-7749/2012/0253.

Turner-Walker, G. and Jans, M. (2008). Reconstructing taphonomic histories using histological analysis. *Palaeogeography, palaeoclimatology, palaeoecology*, 266 (3–4), pp.227–235. [Online]. Available at: doi:10.1016/j.palaeo.2008.03.024.

Turner-Walker, G. and Mays, S. (2008). Histological studies on ancient bone. In: Pinhasi, R. and Mays, S. (Eds). *Advances in human palaeopathology*. John Wiley & Sons. pp.121–146.

Tuross, N. (2002). Alterations in fossil collagen. *Archaeometry*, 44 (3), pp.427–434. [Online]. Available at: doi:10.1111/1475-4754.00075.

Urbanová, P. and Novotný, V. (2004). Distinguishing human and non-human bones: Histometric method for forensic anthropology. *Anthropologie*, 42 (2), pp.175–183.

Väänänen, H. K. et al. (2000). The cell biology of osteoclast function. *Journal of cell science*, 113 (Pt 3), pp.377–381. [Online]. Available at: https://www.ncbi.nlm.nih.gov/pubmed/10639325.

Van de Vijver, K., Kinnaer, F. and Depuydt, S. (2018). St. Rombout's cemetery in Mechelen, Belgium (10th – 18th century AD): A typical urban churchyard? In: van Oosten, R. M. R. et al. (Eds). *The urban graveyard: Archaeological perspectives*. Sidestone Press. pp.239–287.

Van Doorn, N. L. et al. (2012). Site-specific deamidation of glutamine: A new marker of bone collagen deterioration. *Rapid communications in mass spectrometry: RCM*, 26 (19), pp.2319–2327. [Online]. Available at: doi:10.1002/rcm.6351.

Van Klinken, G. J. (1999). Bone collagen quality indicators for palaeodietary and radiocarbon measurements. *Journal of archaeological science*, 26 (6), pp.687–695. [Online]. Available at: doi:10.1006/jasc.1998.0385.

Van Klinken, G. J. and Hedges, R. E. M. (1995). Experiments on collagen–humic interactions: Speed of humic uptake, and effects of diverse chemical treatments. *Journal of archaeological science*, 22, pp.263–270.

Van Klinken, G. J., Richards, M. P. and Hedges, B. E. M. (2002). An overview of causes for stable isotopic variations in past European human populations: Environmental, ecophysiological, and cultural effects. In: Ambrose, S. H. and Katzenberg, M. A. (Eds). *Biogeochemical approaches to paleodietary analysis*. Springer. pp.39–63. [Online]. Available at: doi:10.1007/0-306-47194-9_3.

Van Oers, R. F. M. et al. (2008). Relating osteon diameter to strain. *Bone*, 43 (3), pp.476–482. [Online]. Available at: doi:10.1016/j.bone.2008.05.015.

Veis, A. (1997). Collagen fibrillar structure in mineralized and nonmineralized tissues. *Current opinion in solid state and materials science*, 2 (3), pp.370–378. [Online]. Available at: doi:10.1016/S1359-0286(97)80130-1.

Voss, S. C., Cook, D. F. and Dadour, I. R. (2011). Decomposition and insect succession of clothed and unclothed carcasses in Western Australia. *Forensic science international*, 211 (1-3), Elsevier., pp.67–75. [Online]. Available at: doi:10.1016/j.forsciint.2011.04.018.

Wadsworth, C. and Buckley, M. (2014). Proteome degradation in fossils: investigating the longevity of protein survival in ancient bone. *Rapid communications in mass spectrometry: RCM*, 28 (6), pp.605–615. [Online]. Available at: doi:10.1002/rcm.6821.

Wang, L. and Nilsen-Hamilton, M. (2013). Biomineralization proteins: from vertebrates to bacteria. *Frontiers in biology*, 8 (2), pp.234–246. [Online]. Available at: doi:10.1007/s11515-012-1205-3.

Wang, X. et al. (2002). Age-related changes in the collagen network and toughness of bone. *Bone*, 31 (1), pp.1–7. [Online]. Available at: https://www.ncbi.nlm.nih.gov/pubmed/12110404.

Wang, Y. et al. (2013). Water-mediated structuring of bone apatite. *Nature materials*, 12 (12),

pp.1144–1153. [Online]. Available at: doi:10.1038/nmat3787.

Waters, N. E. (1980). Some mechanical and physical properties of teeth. In: Vincent, J. F. V. and Currey, J. D. (Eds). *The mechanical properties of biological materials*. Symposia of the society for experimental biology. 34. Cambridge University Press. pp.99–135. [Online]. Available at: https://www.ncbi.nlm.nih.gov/pubmed/7020144.

Watson, J. D. and Crick, F. H. C. (1953). The structure of DNA. *Cold Spring Harbor Symposia on Quantitative Biology*, 18, pp.123–131. [Online]. Available at: doi:10.1101/SQB.1953.018.01.020.

Wedl, C. (1864). Über einen im zahnbein und knochen keimenden pilz. *Akademie der wissenschaften, mathematisch-naturwissenschaftliche classe, Vienna*, 50, pp.171–193.

Weiner, S. and Bar-Yosef, O. (1990). States of preservation of bones from prehistoric sites in the Near East: A survey. *Journal of archaeological science*, 17 (2), pp.187–196. [Online]. Available at: doi:10.1016/0305-4403(90)90058-D.

Weiner, S. and Price, P. A. (1986). Disaggregation of bone into crystals. *Calcified tissue international*, 39 (6), pp.365–375. [Online]. Available at: https://www.ncbi.nlm.nih.gov/pubmed/3026591.

Weiner, S. and Traub, W. (1986). Organization of hydroxyapatite crystals within collagen fibrils. *FEBS letters*, 206 (2), pp.262–266. [Online]. Available at: https://www.ncbi.nlm.nih.gov/pubmed/3019771.

Weiner, S. and Traub, W. (1992). Bone structure: from angstroms to microns. *FASEB J.*, 6 (3), pp.879–885. [Online]. Available at: https://www.fasebj.org/doi/10.1096/fasebj.6.3.1740237.

Weiner, S., Traub, W. and Wagner, H. D. (1999). Lamellar Bone: Structure–function relations. *Journal of structural biology*, 126 (3), pp.241–255. [Online]. Available at: doi:10.1006/jsbi.1999.4107.

Weiner, S. and Wagner, H. D. (1998). The material bone: Structure-mechanical function relations. *Annual review of materials science*, 28, pp.271–298.

White, L. and Booth, T. J. (2014). The origin of bacteria responsible for bioerosion to the internal bone microstructure: Results from experimentally-deposited pig carcasses. *Forensic science international*, 239, pp.92–102. [Online]. Available at: doi:10.1016/j.forsciint.2014.03.024.

White, T. D., Black, M. T. and Folkens, P. A. (2012). *Human osteology*. Elsevier. [Online]. Available at: https://www.sciencedirect.com/book/9780123741349/human-osteology [Accessed 30 November 2018].

White, W. B. (1974). The carbonate minerals. In: Farmer, V. C. (Ed). *The infrared spectra of minerals*. Mineralogical Society of Great Britain and Ireland. pp.227–284. [Online]. Available at: https://pubs.geoscienceworld.org/books/book/1871/chapter/106828104/the-carbonate-minerals [Accessed 13 June 2018].

Wiggins, K. and Drummond, P. (2007). Identifying a suitable mounting medium for use in forensic fibre examination. *Science and Justice*, 47 (1), pp.2–8. [Online]. Available at: doi:10.1016/j.scijus.2006.10.001.

Willerslev, E. and Cooper, A. (2005). Ancient DNA. *Proceedings. Biological sciences / The royal society*, 272 (1558), pp.3–16. [Online]. Available at: doi:10.1098/rspb.2004.2813.

Wilson, L. and Pollard, A. M. (2002). Here today, gone tomorrow? Integrated experimentation

and geochemical modeling in studies of archaeological diagenetic change. *Accounts of chemical research*, 35 (8), pp.644–651. [Online]. Available at: doi:10.1021/ar000203s.

Wittig, N. K. et al. (2016). Organ and tissue level properties are more sensitive to age than osteocyte lacunar characteristics in rat cortical bone. *Bone reports*, 4, pp.28–34. [Online]. Available at: doi:10.1016/j.bonr.2015.11.003.

Wopenka, B. and Pasteris, J. D. (2005). A mineralogical perspective on the apatite in bone. *Materials science and engineering: C*, 25 (2), pp.131–143. [Online]. Available at: doi:10.1016/j.msec.2005.01.008.

Wright, L. E. and Schwarcz, H. P. (1996). Infrared and isotopic evidence for diagenesis of bone apatite at Dos Pilas, Guatemala: Palaeodietary implications. *Journal of archaeological science*, 23, pp.933–944.

Yang, D. Y., Eng, B. and Saunders, S. R. (2003). Hypersensitive PCR, ancient human mtDNA, and contamination. *Human biology*, 75 (3), pp.355–364. [Online]. Available at: https://www.ncbi.nlm.nih.gov/pubmed/14527199.

Yang, D. Y. and Watt, K. (2005). Contamination controls when preparing archaeological remains for ancient DNA analysis. *Journal of archaeological science*, 32 (3), pp.331–336. [Online]. Available at: doi:10.1016/j.jas.2004.09.008.

Yerramshetty, J. S. and Akkus, O. (2008). The associations between mineral crystallinity and the mechanical properties of human cortical bone. *Bone*, 42 (3), pp.476–482. [Online]. Available at: doi:10.1016/j.bone.2007.12.001.

Yoshino, M. et al. (1991). Microscopical study on estimation of time since death in skeletal remains. *Forensic science international*, 49 (2), pp.143–158. [Online]. Available at: http://www.ncbi.nlm.nih.gov/pubmed/1855715.

Yost, W. A. (1994). *Fundamentals of hearing: An introduction*. 3rd ed. Academic Press.

Zangarini, S., Trombino, L. and Cattaneo, C. (2016). Micromorphological and ultramicroscopic aspects of buried remains: Time-dependent markers of decomposition and permanence in soil in experimental burial. *Forensic science international*, 263, pp.74–82. [Online]. Available at: doi:10.1016/j.forsciint.2016.03.052.

Zhang, Y.-R. et al. (2014). Review of research on the mechanical properties of the human tooth. *International journal of oral science*, 6 (2), pp.61–69. [Online]. Available at: doi:10.1038/ijos.2014.21.

Zioupos, P. et al. (1997). Mechanical properties of the rostrum of the whale Mesoplodon densirostris, a remarkably dense bony tissue. *Journal of zoology*, 241 (4), pp.725–737. [Online]. Available at: doi:10.1111/j.1469-7998.1997.tb05744.x.

Zioupos, P., Currey, J. D. and Casinos, A. (2000). Exploring the effects of hypermineralisation in bone tissue by using an extreme biological example. *Connective tissue research*, 4 (3), pp.229–248.

Zysset, P. K. et al. (1999). Elastic modulus and hardness of cortical and trabecular bone lamellae measured by nanoindentation in the human femur. *Journal of biomechanics*, 32 (10), pp.1005–1012. [Online]. Available at: https://www.ncbi.nlm.nih.gov/pubmed/10476838.